Aus dem Institut für Molekulare und Klinische Immunologie
der Medizinischen Fakultät der Otto-von-Guericke-Universität Magdeburg

Modulation der T-Zell-Aktivierung *in vitro* und *in vivo*

Habilitationsschrift

zur Erlangung des akademischen Grades

Dr. med. habil.
(doctor medicinae habilitatus)

an der Medizinischen Fakultät
der Otto-von-Guericke-Universität Magdeburg

Vorgelegt von Peter Reichardt
Aus Zwickau/Sachsen
Magdeburg 2013

Inhaltsverzeichnis

Abkürzungsverzeichnis

ADAP	adhesion- and degranulation-promoting adapter protein
APC	Antigen-präsentierende Zelle
ATP	adenosine triphosphate
CD	cluster of differentiation
CTL	cytotoxic T-lymphocyte
CTLA-4	cytotoxic T-lymphocyte-associated antigen 4 (CD152)
DAG	Diacylglycerol
DC	Dendritische Zelle
DNFB	2,4-Dinitro-1-Fluorbenzol
ERK	Extracellular-signal regulated kinases
iTreg	induzierte regulatorische T-Zelle
IL-#	Interleukin-#
IP_3	Inositol-1,4,5-Trisphosphat
IFNγ	Interferon gamma
ITAM	immunoreceptor tyrosine-based activation motif
IVIG	intravenöse Immunglobuline
KO	knock-out
LAT	linker for activation of T cells
LFA-1	lymphocyte function-associated antigen (LFA)-1
Lck	lymphocyte-specific protein tyrosine kinase (p56Lck)
mTOR	mammalian Target of Rapamycin
MAPK	mitogen-activated protein kinase
MHC	major histocompatibility complex, Haupthistokompatibilitätskomplex
NFAT	nuclear factor of activated T cells
NF-κB	nuclear factor-κB
PCB	Polychlorierte Biphenyle

PI3K	Phosphoinositol-3-Kinase
PIP2	Phosphoinositol-4,5-Bisphosphat
PIP3	Phosphoinositol-3,4,5-Trisphosphat
PKB	protein kinase B (Akt)
PLCγ	phospholipase C gamma
pMHC	Peptid-MHC (-Komplex)
PUFA	polyunsaturated fatty acid
SDF-1	stromal cell-derived factor-1
S1P1	Sphingosin-1-phosphat-Rezeptor-1
SKAP55	Src kinase−associated phosphoprotein of 55 kDa
SLP76	Src homology 2 (SH2) domain-containing leukocyte protein of 76 kDa
STED	Stimulated-Emission Depletion
STAT	signal-transducer-and-activator-of-transcription
TCR	T-Zell-Rezeptor
TNFα	Tumor-Nekrose-Faktor α
TDI	TGFβ Toluen-2,4-diisocyanate
TGFβ	transforming growth factor beta
Th	T-Helfer
Treg	Regulatorische T-Zelle
TIRF	total internal reflection fluorescence (Mikroskopie)
ZAP70	zeta-associated protein of 70 kDa

Zusammenfassung

Der adaptive Charakter des T-Zell-Rezeptor-Reservoirs bildet den Schlüssel für die Entwicklung eines immunologischen Gedächtnisses. Auf Umwelteinflüsse gezielt reagieren zu können stellt einen evolutionär Aufwand dar, der sich für den Menschen lohnt. Gleichzeitig bringt dieses neue Verteidigungskonzept eine Reihe von Problemfeldern mit sich. Intrinsische und extrinsische Einflussfaktoren können dazu führen, dass sich das Immunsystem funktionell so verändert, dass es dem Wirtsorganismus selbst Schaden zufügt. Die Gewährleistung effizienter und gleichzeitig sicherer T-Zell-Aktivierung besitzt daher höchste Relevanz für den Organismus.

Der Prozess der antigenspezifischen Aktivierung der T-Zelle wird im Zusammenspiel zwischen T-Zell-Rezeptor(TCR)- und costimulatorischen Signalen sowie unter Einbeziehung biophysikalischer Eigenschaften der Antigenpräsentation entscheidend moduliert. Die immunologische Synapse bildet dabei das morphologische Korrelat physiologischer T-Zell-Aktivierung an der Grenzfläche zwischen antigenpräsentierende Zelle und T-Zelle. Ein multimolekulares Netzwerk an Signalen von protrahierter Dauer und hoher Intensität innerhalb der Synapse kennzeichnet die Signalübermittlung während der T-Zell-Aktivierung. Um eine zentrale Akkumulation von TCR und phospho(p)-LAT bilden sich „signaling hotspots" mit zusätzlicher Anreicherung von pCD3ζ, pZAP70, pSLP76 und pPLCγ1. Eines der frühesten Ereignisse der T-Zell-Aktivierung ist die Aktivierung der Src-Kinase Lck. Dabei sind es vorrangig Konformationsänderungen und nicht Phosphorylierungen, welche Lck auf den Angriff am TCR-CD3-Komplex vorbereiten.

Die T-Zell-Migration durch den Organismus wird durch zeitlich und örtlich selektiv wirkende Signale gesteuert, um eine erfolgreiche Kontaktaufnahme mit antigenpräsentierenden Zellen und eine effiziente Immunantwort zu gewährleisten. Dazu gehört die Aktivierung von Integrinen wie LFA-1 beim Eintritt- und Austritt von T-Zellen aus Blut- und Lymphbahnen sowie die über Adaptermoleküle wie SLP76 vermittelte selektive Aktivierung von Integrinen

nach TCR- bzw. Chemokinrezeptor-Triggering. Gα-Proteine wie Gα12 und Gα13 spielen eine wichtige Rolle für Integrin-Signaling und korrekte T-Zell-Positionierung im Lymphknoten. Integrin-Signal-regulierende Proteine wie ADAP und SWAP70 sind dabei notwendig für intakte Motilität und Migration.

T-Zellen als Bestandteil des Organismus sind ständigem Kontakt mit der Umwelt ausgesetzt. Kovalente chemische Bindungen mit reaktiven Schadstoffen (elektrophile Xenobiotika) oder mit Medikamenten (β-Lactame) können das T-Zell-Signaling beeinflussen, myelotoxische Effekte die Reifung von Immunzellen stören. Nahrungsbestandteile wie langkettige Fettsäuren besitzen modulierenden Einfluss auf die T-Zell-Aktivierung und die Entwicklung allergischer Sensibilisierungen. Infektiöse Agenzien können das Immunsystem unterdrücken oder ungewöhnlich stark aktivieren (bakterielle Superantigene). Infektionen sind mögliche ungewollte Folge der Anwendung immunsuppressiver Medikamente (anti-TNFα). Genetische Defekte und Varianten (VHL-Gen) können zur Überforderung des Immunsystems und der Karzinom-Entwicklung führen.

Immuntherapeutische Ansätze umfassen sowohl die Anwendung von löslichen Substanzen (small molecules, altered peptide ligands, Biologicals wie anti-TNFα und anti-CD28) als auch zelltherapeutische Ansätze. Die Generierung von regulatorischen T-Zellen (Tregs) bildet dabei einen Schwerpunkt. Die Induktion von Tregs durch Antigenpräsentation mittels naiver B-Zellen stellt einen Ansatz mit möglichen Vorteilen für die reproduzierbare Umsetzbarkeit dar. Eine veränderte Balance des PI3K/Akt/mTOR-Signalwegs durch Akt-spezifische Phosphatasen scheint der Bildung dieser induzierten Tregs zugrunde zu liegen.

Für die medizinische Anwendung der T-Zell-Modulation, sei es zur Behandlung von immunpathologischen Zuständen oder zu deren Vermeidung, ist es sowohl notwendig, die molekularen Grundlagen der T-Zell-Aktivierung besser zu verstehen als auch die Mechanismen von deren Modulation sowie die gegenwärtigen Prinzipien gezielter Beeinflussung zu kennen. Diesem Ziel widmet sich diese zusammenfassende Darstellung.

1. Einleitung - Modulation der T-Zell-Aktivierung im Zentrum der adaptiven Immunantwort

Das adaptive Immunsystem entstand vor circa 500 Millionen Jahren, als mit Entwicklung der Wirbeltiere, Vertebraten, und insbesondere der kiefertragenden Wirbeltiere (Kiefermäuler, Gnathostomata, jawed vertebrates) die ersten T-Zell-Rezeptoren auf der Oberfläche von Abwehrzellen entstanden (*Forni 2013*).

Der adaptive Charakter des T- (und B-Zell)-Rezeptor-Reservoirs, d.h. die Möglichkeit der Anpassung an Umgebungsfaktoren und deren Nutzung innerhalb der Lebenszeit eines Organismus, bildet den Schlüssel für die Entwicklung eines immunologischen Gedächtnisses. Ein solches Gedächtnis verstärkt die Immunantwort beim erneuten Zusammentreffen mit einem „Aggressor" (z.B. Bakterium, Virus) um Größenordnungen. Es bildet die Voraussetzung für den Erfolg jeder Vakzinierung und erweitert die Verteidigungsfähigkeiten des hinsichtlich der Antigenspezifität „unflexiblen" angeborenen (engl. innate) Immunsystems wesentlich. Auf Umwelteinflüsse gezielt reagieren zu können stellt einen evolutionären Aufwand dar, der sich in Organismen mit relativ langer Lebensspanne wie dem Menschen offenbar lohnt (*Best 2013*).

Gleichzeitig bringt dieses neue, adaptive Verteidigungskonzept eine Reihe neuer Problemfelder mit sich. Umwelteinflüsse können dazu führen, dass sich das Immunsystem funktionell so verändert, dass es dem Wirtsorganismus selbst Schaden zufügt. T-Zellen sowie die funktionellen Partner der T-Zell-Rezeptoren, die MHC-(Major Histocompatibility Complex) Moleküle auf antigenpräsentierenden Zellen, sind nicht nur geeignet, die Antwort möglichst spezifisch gegen Infektionserreger zu lenken, sondern sie sind oft auch assoziiert mit immunologisch-vermittelten pathologischen Prozessen wie Neoplasien, Allergien und Autoimmunerkrankungen. Offenbar besteht eine evolutionäre Balance zwischen hohem Abwehrpotential und möglicher Selbstreaktivität, um die immunologische Reaktionsfähigkeit in notwendiger Stärke und Geschwindigkeit zu erhalten (*Thomas 2010*).

Deshalb besitzt die Gewährleistung einer effizienten und gleichzeitig sicheren T-Zell-Aktivierung höchste Relevanz für den Organismus.

Intrinsische, körpereigene Mechanismen der Steuerung der T-Zell-Aktivierung gehen dabei weit über effiziente T-Zell-Reifung im Thymus hinaus. So ist der Prozess der antigenspezifischen Aktivierung der T-Zelle an der immunologischen Synapse im Zusammenspiel zwischen T-Zell-Rezeptor(TCR)- und costimulatorischen Signalen sowie die resultierende Herausbildung eines Netzwerks intrazellulärer Signale ein komplexer und mannigfach modulierter Prozess (besprochen im Text anhand App. 04, 06, 07).

Intrinsisch gesteuert wird auch die T-Zell-Migration durch den Organismus. Ohne spezifische Signale, welche die Navigation innerhalb von Organkompartimenten sowie den Eintritt und das Verlassen von Blut- und Lymphgefäßen steuern, wäre eine rechtzeitige Kontaktaufnahme mit passenden antigenpräsentierenden Zellen und damit eine effiziente Immunantwort nicht möglich (App. 11, 9, 1, 10, 5).

Extrinsischen Einflüssen sind T-Zellen durch ständigen Kontakt des Organismus mit der Umwelt ausgesetzt. Dazu gehören Kontakte mit chemisch-reaktiven Substanzen (Schadstoffe, Medikamente) sowie Kontakte zu infektiösen Agenzien. Daneben beeinflussen genetische Varianten die T-Zell-Verteidigungsfunktionen des Individuums (siehe App. 15, 16, 20, 18, 17, 19).

Gezielt versucht der Mensch das adaptive Immunsystem zu beeinflussen durch Applikation pharmakologisch aktiver Immunmodulatoren sowie durch die Anwendung manipulierter Immunzellen zur Steuerung von T-Zellen und der Immunantwort (App. 12, 13, 8, 3, 14, 2).

Für die medizinische Anwendung der T-Zell-Modulation, sei es zur Behandlung immunpathologischer Zuständen oder zu deren Vermeidung, ist es zum einen notwendig, die molekularen Grundlagen der T-Zell-Aktivierung besser zu verstehen und zum anderen die Prinzipien experimenteller und klinischer Ansätze zu deren Modulation zu kennen und weiter zu entwickeln. Die vorliegende Arbeit fasst wichtige Elemente des gegenwärtigen Kenntnisstands zur T-Zell-Aktivierung und –Modulation mit Blick auf ihre potenzielle medizinische Relevanz zusammen und beschreibt die Resultate meiner Arbeit auf diesem Gebiet.

2. Die antigenspezifische T-Zell-Aktivierung erfolgt an der immunologischen Synapse

Das Immunsystem des Menschen wird regelmäßig in ein angeborenes (innate) Immunsystem und ein adaptives Immunsystem unterteilt. Das angeborene Immunsystem umfasst neben den wichtigsten professionellen antigenpräsentierenden Zellen (APC), den Dendritischen Zellen (DC), vor allem Fresszellen wie Makrophagen und neutrophile Granulozyten, daneben Natürliche Killerzellen (NK-Zellen) und andere. Ihnen gemeinsam ist, dass sie Untypisches, potentiell Fremdes (Gefährliches) anhand bestimmter molekularer Muster (molecular pattern) erkennen. Auch Epithelzellen können solche Mustererkennungsrezeptoren (pattern recognition receptors, PRR) tragen und damit in bestimmtem Maße an der frühen Immunerkennung teilnehmen. Die Signalübertragung über die PRR, darunter toll-like Rezeptoren (TLR), führen zur Aktivierung z.B. der Makrophagen, fördern deren Fähigkeit, aufgenommene Partikel abzutöten und zu zerstören und induzieren gleichzeitig „Gefahren"-Signale (danger signals), die an das adaptive Immunsystem weitergeleitet werden und deren Aktivierung dienen. Insoweit bildet das Triggering des angeborenen Immunsystems die funktionale Grundlage für die anschließende Aktivierung des adaptiven Immunsystems (*Kumar 2011, Jin 2012*).

Die zellulären Bestandteile des adaptiven Immunsystems sind vorrangig B- und T-Lymphozyten. B-Zellen sind für die Antikörperproduktion verantwortlich, sie verlangen in den meisten Fällen eine vorherige Lizensierung (Freischaltung) dieser Funktion durch CD4+ T-Zellen (T-Helfer-Zellen). Diese bilden beim Menschen die Mehrzahl der T-Zellen. Daneben kommen CD8+ T-Zellen vor, die direkte zytotoxische Funktionen wahrnehmen. CD4+ T-Zellen werden dagegen überwiegend durch die Produktion und Sekretion von löslichen Botenstoffen, z.B. Zytokinen, wirksam. Auf dem Muster sezernierter Zytokine basiert schwerpunktmäßig die funktionelle Unterteilung der T-Zellen und zwar zunächst dichotomal in Th1 und Th2-Zellen (Mosmann 1986). Dieses Konzept von vorrangig IFNγ/ IL-12 (Th1) bzw. IL-4/IL-10 (Th2) produzierenden T-Zell-Subtypen wurde

inzwischen wesentlich erweitert. Man unterscheidet eine Reihe anderer, distinkter Subtypen, darunter proinflammatorische Th17 (IL-17-produzierende)- und Th22-T-Zellen sowie Follikuläre Helferzellen (follicular helper T cells, wichtig für die Reifung antikörperproduzierender B-Zellen im Lymphknoten) sowie immunsupprimierende, regulatorische T-Zellen, Tregs. Die Balance dieser Subtypen im Verlauf einer Immunantwort ist von zentraler Bedeutung für den resultierenden biologischen Effekt der Immunantwort. Zunehmend wird erkannt, dass eine hohe funktionelle Plastizität zwischen einigen dieser Subtypen besteht und dass Übergänge auch noch in späten Entwicklungsstadien der Zellen auftreten können mit Konsequenzen für die anhaltende Immunantwort (*Magombedze 2013, Basu 2013*).

Die antigenspezifische T-Zell-Aktivierung erfolgt an der immunologischen Synapse. Keine Struktur verdeutlicht die Kooperation von angeborenem und adaptivem Immunsystem so eindrucksvoll wie diese multimolekulare Organisationsplattform an der Interaktionsfläche zwischen APC (z.B. einer DC als Vertreter der angeborenen Immunität) und T-Zelle (als Repräsentant des adaptiven Immunsystems). Die Synapse bildet die molekulare Matrix, über welche die T-Zelle im antigenspezifischen Kontext Signale empfängt. Hier wird bildlich gesprochen „der Staffelstab" der Immunantwort vom angeborenen an das adaptive Immunsystem übergeben (*Reichardt 2010*).
Mittels ihrer MHC-II-Moleküle präsentiert die APC ein Antigenbruchstück (in aller Regel ein Peptid) der T-Zelle. Diese interagiert mittels ihres TCR-CD3-Komplexes mit dem angebotenen Peptid-MHC (pMHC)-Liganden. Zusätzlich sichern Verbindungen zwischen Ankermolekülen wie dem Integrin LFA-1 (lymphocyte function-associated antigen-1) und ICAM-1 (Intercellular Adhesion Molecule 1) sowie costimulatorische Moleküle wie CD28 auf T-Zell-Seite mit z.B. B7.2 auf APC-Seite die Verbindung (*Bromley 2001).*
Der Kontakt des T-Zell-Rezeptors mit einem passenden pMHC-Komplex löst eine Plethora an Signalprozessen in der T-Zelle aus. Diese können zur vollständigen Aktivierung der T-Zelle führen, ihre funktionelle Prägung und die Ausübung ihrer Effektorfunktionen einleiten. Es ist wichtig zu betonen, dass eine immunologische Synapse nur ausgebildet wird, sofern ein Antigen-MHC-Komplex mit ausreichender Affinität zum T-Zell-Rezeptor präsentiert

wird. Unterhalb einer kritischen Schwelle kontaktieren sich die Zellen nur kurz ohne Einleitung einer T-Zell-Aktivierung. Ausreichend lange Kontakte mit ausreichend starken Signalen führen stattdessen zur Initiation der T-Zell-Aktivierung (Gunzer 2001, Henrickson 2008).
Erfolgreiches TCR-Triggering führt zu einer Kaskade an Signalprozessen. Zunächst werden Src-Kinasen wie die Lymphozyten-spezifische Tyrosinkinase p56(Lck) aktiviert, und diese phosphorylieren die ζ-Kette des TCR-CD3-Komplexes an ITAMS (immunoreceptor tyrosine-based activation motifs) (*Lin 2001*). Anschließend wird die Tyrosinkinase ZAP70 (zeta-associated protein of 70 kDa) zu den ITAMs rekrutiert und phosphoryliert ihrerseits Adapter wie LAT (linker for activation of T cells) und SLP76. Diese wiederum rekrutieren PLCγ1, einen Aktivator von Calciumströmen, und Vav1, einen Regulator der Aktin-Reorganisation. Dies führt u.a. zur Aktivierung von MAP–Kinasen und Transkriptionsfaktoren wie NFAT und NF-κB (Costello 1999, Smith-Garvin 2009). Allerdings besteht sowohl in Art und Umfang der notwendigen Zellkontakte als auch in der Qualität der eingeleiteten Aktivierung große Plastizität (*Reichardt 2007*). Daher ist, aufgrund ihrer sprichwörtlich zentralen Rolle bei der T-Zell-Aktivierung (ohne Synapse keine antigen-spezifische T-Zell-Aktivierung) die Entstehung, der molekularer Aufbau und das Signaling von Synapsen von großem Interesse (*Dustin 2010, Xie 2013*).

Um das komplexe Signaling-Netzwerk in immunologischen Synapsen zu untersuchen, entwickelten wir ein Multi-Parameter-Fluoreszenz-Mikroskopiesystem (Multi-Epitope Ligand Cartography, MELC) so weiter, dass es für die dreidimensionale Analyse der immunologischen APC-T-Synapse geeignet war **(App. 04, Philipsen 2013)**.
Wir charakterisierten die gleichzeitige räumliche Verteilung von 25 molekularen Markern über 2 Stunden auf dem Niveau einzelner stabiler Synapsen, darunter phosphorylierte und nichtphosphorylierte Signalproteine (wie phospho(p)ZAP70, pSLP76, pCD3 und pLAT sowie Proteine, welches die Struktur der Synapse beeinflussen wie F-Aktin, Tubulin, CD45 und ICAM-1.

Wir beobachteten die Bildung einer klassischen ringförmigen bull's eye Synapse (*Fooksman 2010*, *Reichardt 2007c*) mit einem zentralen

supramolekularen Bereich (cSMAC, central supramolecular activation cluster), der vorrangig eine Akkumulation von pLAT und TCR aufwies. Ein weiterer, peripherer Bereich (pSMAC) in welchem sich ebenfalls Signalmoleküle ansammelten, wurde distal von einem strukturbildenden F-Aktin-Ring begrenzt. Wir sahen anhaltendes TCR-Signaling während der gesamten Beobachtungszeit von 2 Stunden. Dabei folgte einer Phase intensiven TCR-Signalings unmittelbar nach dem Zellkontakt eine verstärkte Rekrutierung von Strukturproteinen gefolgt von einer anhaltenden Akkumulation von TCR und Signalproteinen (pLAT) im Zentrum der Synapse. Wir identifizierten diskrete Cluster (Signaling hotspots) im zentralen Synapsenbereich und fanden diese angereichert mit TCR, mit TCR-proximalen Signaling-Proteinen wie pLck und pZAP70 sowie Adapterproteinen wie pLAT und pSLP76.

Unsere Studie war die erste, die gleichzeitig eine größere Anzahl an Signalmolekülen während des Aufbaus der stabilen immunologischen Synapse verfolgen konnte. Die Tatsache, dass an der Synapse über Stunden dynamische Rekrutierung von Struktur- und Signalmolekülen erfolgt, führte auch Beobachtungen zusammen, die eine vollständige Aktivierung von T-Zellen erst nach einem Kontakt (oder einer sequentiellen Abfolge von Kontakten) über mehrere Stunden nahelegen (Iezzi 1998, Faroudi 2003).

Weiter offen ist, wie genau sich Synapsen von T-Zellen verschiedener Subtypen unterscheiden. Erste Hinweise auf z.B. verstärkte Rekrutierung von IFNγ-Rezeptor in Th1-Zellen bzw. ausbleibende Rekrutierung von Proteinkinase C Theta (PKCθ) in Tregs existieren (Maldonado 2009, Sumoza-Toledo 2006). Weiterhin gilt zu beachten, dass die Synapse nicht nur eine Struktur zum Austausch von Rezeptor-Liganden-Signalen sondern auch von Substrat ist. Die Untersuchung der Anordnung von membrannahen Vesikeln und deren intra- und interzellulären Transportwege sind neue, relevante Aspekt des Studiums der synaptischen Funktion (*Soares 2013*). Notwendig für solche Studien ist allerdings eine exzellente räumliche Zuordnung innerhalb der dreidimensionalen Synapsenstruktur. In der Zukunft werden geeignete technische Apparaturen, die eine verbesserte räumliche Anordnung von APC-T-Zell-Paaren ermöglichen, die Bildqualität verbessern (Biggs 2011). Hochauflösende Mikroskopie, die eine Betrachtung im Nanometer-Bereich erlaubt, wird weitere strukturelle Details zutage fördern und damit

mutmaßlich auch eine bessere Abschätzung funktioneller Zusammenhänge ermöglichen (Betzig 2006, Baddeley 2011).

Eine wichtige Frage im Kontext der antigeninduzierten T-Zell-Aktivierung ist die nach den frühesten molekularen Ereignissen auf der T-Zell-Oberfläche. Wie beschrieben weiß man, dass Lck unmittelbar nach Beginn des TCR-Triggerings Phosphorylierungen von ITAMS am TCR-CD3-Komplex vornimmt (*Lin 2001*). Allerdings ist Lck zu jeder Zeit bereits in großer Menge auf der Membranoberfläche von T-Zellen vorhanden. Wie wird Lck strukturell auf diesen „Angriff" am TCR vorbereitet?

In einem weiteren Projekt (**App. 06, Stirnweiss 2013)** gelang es uns, mittels unserer Multi-Epitop-Liganden-Cartographie, MELC, die räumliche und zeitliche Verteilung sowie den Phosphorylierungszustand verschiedener Kinasen, darunter Lck, gleichzeitig mit anderen Molekülen an der Membranoberfläche von (T-zell-ähnlichen) humanen Jurkat-Zellen zu messen. Durch vergleichende Betrachtung der Signalintensitäten der einzelnen Proteine auf Einzelzellebene war es uns möglich nachzuweisen, dass bei anti-CD3-getriggerter Aktivierung zwar TCR-Signaling-abhängige Moleküle wie CD3ε und ζ eine deutliche Phosphorylierung erfuhren, dass auf den identischen Zellen jedoch keine oder kaum Veränderungen der Lck-Phosphorylierung stattfanden. Dies war neben anderen Ergebnissen im Paper ein wichtiger Bestandteil der Beweisführung, dass es vorrangig Konformationsänderungen und nicht Phosphorylierungen waren, welche das Lck zum enzymatischen Angriff (Kinase-Aktivität) auf den TCR-Komplex vorbereitet. Diese Erkenntnis unterstrich frühere Beobachtungen (Nika 2010) und stellte ein zentrales Prinzip der T-Zell-Aktivierung in den Vordergrund (Paper wurde in Faculty of 1000, Immunology, gewählt).

Der Typ der beteiligten APC prägt wie beschrieben maßgeblich das Resultat der T-Zell-Aktivierung. Dies hängt (bei angenommen identischem kognaten TCR-Liganden (dem passenden Peptid-MHC-Komplex) vor allem von Art und Menge an costimulatorischen Signalen ab, welche zusätzlich auf die T-Zelle einwirken. Darüber hinaus kann auch die Beschaffenheit der Zelloberfläche

einen Einfluss haben. Große sphärische Oberflächen wie die einer ruhenden, runden B-Zelle treten großflächig mit T-Zellen in Kontakt zur Bildung einer symmetrischen, stukturell reifen (bull's eye) Synapse, während die eher kleinen, multimorphen Dendriten einer DC typischerweise nur punktuell (dafür oft multifokal) mit T-Zellen interagieren (Brossard 2005). Dass die Form der physikalischen Präsentation eines Stimulus eine Rolle bei der Signalinduktion spielt, konnten wir in einem anderen Zusammenhang zeigen. Erneut konnten wir mit Untersuchungen des T-Zell-Signalings durch multimolekulare Analyse auf Einzelzellebene beitragen **(App. 07, Arndt 2013)**. Bei der Analyse des Signalings nach T-Zell-Rezeptor-Stimulation humaner T-Zellen konnten wir charakteristische Unterschiede im Stimulationsmuster, hervorgerufen durch lösliche vs. (durch Anheftung an Microbeads) immobilisierte CD3-Antikörper, nachweisen. Wir fanden, dass lösliche Antikörper nur sehr kurzzeitige, wenngleich starke Signale auslösten, während immobilisierte Antikörper eher ein protrahiertes Signalmuster in T-Zellen erzeugten, was eher dem durch APC erzeugten Muster entsprach.
Diese Ergebnisse weisen (im begrenzten Umfang eines *in vitro*-Experiments) auf die Abhängigkeit des erzeugten Signalmusters von der räumlichen Anordnung eines ansonsten identischen Stimulus hin (in dem Fall anti-CD3-Antikörper). Sie verdeutlichen, dass die Anwendung immobilisierter Antikörper besser geeignet ist, die T-Zell-Aktivierung durch eine APC nachzustellen, da die induzierten Signalmuster wesentlich ähnlicher als nach der Anwendung löslicher Antikörper war. Zusammengefasst sind die Ergebnisse Indiz dafür, dass die biophysikalische Form, in welcher ein TCR-Trigger-Signal auf T-Zellen einwirkt, für das induzierte Signalmuster in T-Zellen wichtig ist. Auch das Konzept der Verbindung zwischen Signalstärke, Polarisation des Zytoskeletts und Zellkontaktarchitektur (eher rigide Synapse vs. eher fluide Kinapse) findet inzwischen breitere Anwendung (Dustin 2009, Moreau 2012).

3. T-Zell-Migration als *conditio sine qua non* der T-Zell-Aktivierung *in vivo*

Bis zur Ausbildung einer funktionalen immunologischen Synapse zwischen APC und T-Zelle müssen die Partner im Verlauf der Immunantwort weite Wege zurücklegen. Komplexe Migrationsvorgänge sind notwendig, denn typischerweise residieren beide Zelltypen zunächst an entfernten Punkten des Organismus. Diese *in vivo* Migration von Lymphozyten und anderen Immunzellen ist ein streng regulierter Prozess mit großem Einfluss auf die Immunantwort.
Die APC (z.B. eine Dendritische Zelle) nimmt das Antigen typischerweise im Gewebe der Haut, der Lunge, des Darms oder im Blutgefäßendothel auf und präsentiert Bruchstücke davon auf ihren MHC-Molekülen während die Zelle zum drainierenden Lymphknoten wandert. T-Zellen ruhen vorrangig in lymphatischen Organen, z.B. in der parakortikalen T-Zell-Zone des Lymphknotens. Residente und einwandernde DC präsentieren dort „ihre" prozessierten Antigene im Rahmen multipler Zellkontakte an zahlreiche T-Zellen. Im Parenchym wandern DCs vergleichsweise langsam (3 µm/min), kontaktieren jedoch mittels langer dendritischer Ausläufer innerhalb einer Stunde bis zu 5000 hochmotile T-Zellen, die sich mit der drei- bis vierfachen Geschwindigkeit bewegen (Miller 2004). Antigenspezifische Kontakte führen zu einer über Stunden anhaltenden Abfolge an Interaktionen mit wechselnder Beweglichkeit (phasenweise geringere Geschwindigkeiten teilweise bis hin zur Arretierung der T-Zellen) sowie veränderlichem Schwarmverhalten der T-Zellen (*Friedl 2002, Reichardt 2006, Reichardt 2010*).

Den unmittelbarsten Einblick in diese Abläufe einer Immunantwort und die dabei stattfindenden Zellkontakte gewinnt man durch moderne Methoden der Mikroskopie. Die Entwicklung hochsensitiver Bildgebungssysteme, welche bestimmte funktionelle Abläufe (wie z.B. Calcium-Signale) durch Reportersysteme visualisiert, die Beobachtung tief im lebenden Gewebe ermöglicht oder mit nanoskopischer Auflösung kleinste strukturelle Details erkennen lässt, hat in den letzten Jahren enorme Fortschritte gemacht (Reichardt 2009).

Um das dreidimensionale Milieu des Körpergewebes, in welchem die spezifischen immunologischen Zellkontakte stattfinden, bestmöglich *in vitro* nachzubilden, haben wir und andere experimentelle Systeme entwickelt, in welchen sich bestimmte biophysikalische Eigenschaften der Zellbewegung sehr ähnlich zu denen *in vivo* beobachten lassen (*Reichardt 2007b*).
Lebendzellbeobachtung in solchen Systemen erlaubte uns u.a. den Einfluss des Adaptermoleküls SLP76 auf die Chemokin-vermittelte Motilität humaner T-Zellen zu untersuchen. Es ist bekannt, dass als eine Konsequenz aus dem TCR-Triggering in der T-Zelle Integrine wie LFA-1 aktiviert werden. Integrine als Ankermoleküle auf der T-Zelle sind (neben der Funktion für die Stabilität der Synapse) auch für T-Zell-Motilität und Adhäsion wichtig (*Campbell 2003*). Neben den TCR-Signalen werden Integrine auch durch das Triggering von Chemokinrezeptoren wie CXCR4 (durch Stromal cell-derived factor-1, CXCL12) aktiviert und in ihrer Affinität und Avidität reguliert (Kinashi 2005). Das Adaptermolekül SLP76 ist ein wichtiger Bestandteil membrannaher Molekülkomplexe, seine Anwesenheit ist notwendig für den Anstieg an intrazellulärem Calcium und die Aktivierung des intrazellulären Ras/Raf/MAPK/ERK-Signalwegs (Yablonski 1998). Gleichzeitig sind Komponenten der SLP76-Signaling-Plattform an der Aktivierung von LFA-1 nach TCR-Triggering beteiligt (Bezman 2008).
Um den Einfluss von SLP76 nach Triggering von CXCR4 zu untersuchen, ermittelten wir (als ein Bestandteil des Papers) die basale und CXCR12-induzierte laterale Motilität (auf Fc-ICAM-1-beschichteten Oberflächen) von SLP76+/+ und SLP76-/- T-Zellen. Wie fanden vergleichbare Werte, d.h. die Zellen bewegten sich unabhängig von der Anwesenheit von SLP76 (wohingegen sie bei Fehlen des Adaptermoleküls Vav1 deutlich langsamer wurden) (**App. 11, Horn 2009**). Unsere Daten war im Kontext mit anderen Resultaten des Papers ein wichtiger Baustein für die Erkenntnis, dass eine differentielle Abhängigkeit von SLP76 im T-Zell-Signaling besteht und zwar dahingehend, dass SLP76 zwar für TCR-vermittelte Signale, nicht aber für das Chemokin-Rezeptor-Signaling (die CXCR4-Triggerung durch CXCL12) bei der Aktivierung des Integrin-Moleküls LFA-1 notwendig ist. Die komplexe Steuerung der Integrin-Affinität durch Chemokin-Rezeptor-Signale wurde

kürzlich erneut unterstrichen, als zwei räumlich getrennte, unabhängige (ADAP/SKAP55-)Molekülkomplexe in T-Zellen identifiziert wurden, die in Antwort auf CCR7-Triggering die LFA-1-Affinität regulieren (Kliche 2012).

Ferner, Lebendzellmikroskopie unter Verwendung von Kollagen-beschichteten Oberflächen gestattete uns, die Feinstrukturen der Oberflächenbeschaffenheit von APC wie DC genau zu beobachten und charakteristische Eigenschaft wie Dendritenanzahl und -länge zu quantifizieren. In einer solchen Studie ging es um die Charakterisierung der Rolle von SWAP70 auf die Sphingosin-1-Phosphat–induzierte Motilität von DC. SWAP70 ist ein Guanin-Nucleotid-Exchange-Faktor (GEF), der Signale von Tyrosinkinase-Rezeptoren wie Phosphatidylinositoltrisphosphat weiterleitet und so die Zytoskelettarchitektur und Membranbeschaffenheit beeinflusst (Shinoara 2002). Sphingosin-1-Phosphat ist ein bioaktives Lipid und ein Zellmembranbestandteil, der chemoattraktiv wirksam und am lymphozytären Egress aus Lymphknoten *in vivo* sowie an der Wanderung reifer DC beteiligt ist (*Rosen 2005*, Czeloth 2005).
Wir beobachteten (als ein Teil der Studie) in Abwesenheit von SWAP70 bei DC morphologische Auffälligkeiten (**App. 09, Ocaña-Morgner 2011**). Dazu zählten eine reduzierte Anzahl von Dendriten, deren geringere Kontraktion sowie ein eher elongierter Zellkörper mit dezentralem, rostralen Kernbereich. Diese Beobachtung lieferte ein morphologisches Korrelat welches die verminderte Motilität in 3D-Umgebungen und die verminderte Anreicherung im Lymphknoten in Abwesenheit von SWAP70 (parallel bestimmt in der Studie) zu erklären halfen. Die Bedeutung von SWAP70 für die T-Zell-Aktivierung wurde kürzlich erneut unterstrichen als bekannt wurde, dass ein SWAP70-intaktes Zytoskelett notwendig ist, einer u.a. durch Integrine (CD11b) vermittelten spontanen Reifung von DC entgegenzuwirken. Solche Reifungsprozesse fördern die Induktion von Immunprozessen beim DC-Kontakt mit T-Zellen und modulieren so deren Aktivität (Ocaña-Morgner 2013).

Zur Visualisierung der Zell-Zell-Distribution und -Kommunikation tief im lebenden Gewebe, im intakten Organ wie z.B. im Lymphknoten, ist vor allem die 2-Photon-Mikroskopie hervorragend geeignet. Diese Technik ermöglichte uns, in einer Reihe von Studien die *in vivo* Verteilung und Motilität von Lymphozyten an charakteristischen Strukturen des Lymphknotens der Maus zu untersuchen.

So konnten wir u.a. nachweisen, dass sich *in vivo* in Lymphknoten von ADAP (adhesion- and degranulation-promoting adapter protein)-defizienten Mäusen B- und T-Lymphozyten an lymphatischen Gefäßen ansammelten (**App. 01, Engelmann 2013**). ADAP ist ein zytosolisches Adapterprotein, welches u.a. in T-Zellen und myeloiden Zellen exprimiert wird (Dluzniewska 2007). ADAP ist beteiligt an der TCR- und Chemokin-vermittelten Aktivierung der Integrine, sein Fehlen führt zu verminderter T-Zell-Adhäsion und verminderter Konjugat-Formation mit APC (Burbach 2008).
Unsere Beobachtung war ein wichtiger Baustein im Paper und lieferte eine mögliche Erklärung für die parallel registrierte verminderte Induktion der Multiple-Sklerose-ähnlichen experimentellen autoimmunen Enzephalitis (EAE) bei Fehlen von ADAP. Unsere Daten demonstrierten, dass auch T-Zell-unabhängig (die adoptiv transferierten T-Zellen waren ADAP-kompetent) bei Fehlen von ADAP eine migratorische Defizienz bestand und dass diese selektiv war: während das Homing in den Lymphknoten normal blieb, wurde der Egress aus dem Lymphknoten vermindert, es bestand ein Hindernis im Überwinden der endothelialen Barrieren von lymphatischen Gefäßen. Die molekulare Ursache für das beobachtete intranodale Trapping sind derzeit allerdings unklar. Eine Defizienz im S1P-System wurde ausgeschlossen, weiterhin möglich wäre eine verstärkte Interaktion mit ICAM-1 *in vivo*. Weitere Experimente dazu sind von den Initiatoren der Studie geplant.

Die molekularen Grundlagen der integrinvermittelten T-Zell-Motilität waren der Fokus einer weiteren Studie, zu der wir durch Mikroskopie intakter Lymphknoten der Maus beitragen konnten. Bekanntermaßen vermitteln Integrine *in vivo* die Verankerung von T-Zellen im Gewebe und spielen eine zentrale Rolle beim Übertritt zwischen Blutgefäßen und z.B. lymphatischen

Organen (Hamann 1988, Berlin-Rufenach 1999). Entsprechend führen Störungen in der Aktivierung der Integrine zur Beeinträchtigung der Wanderwege von T-Zellen und damit zu Störungen der Immunantwort.
Elementar für die Integrin-Aktivierung ist das Signaling über Guanin-Nucleotid-bindende Gα-Proteine. Gegenstand der Studie war der Nachweis, dass die genetische Inaktivierung der G-Proteinuntereinheiten Gα12 und Gα13 zu einer erhöhten Aktivität von LFA-1 in CD4+ T-Zellen führt **(App. 10, Herroeder 2009).**
Speziell untersuchten wir (als Teil des Papers) die *in vivo* Verteilung von Gα12, Gα13-doppeldefizienten CD4+ T-Zellen im Lymphknoten der Maus. Wir fanden eine verstärkte Präsenz dieser T-Zellen in vaskularisierten Bereichen der T-Zell-Zone. Diese Anreicherung war, wie im Paper weiter gezeigt wurde, mit einer erhöhten T-Zell-Proliferation und einer verstärkten Suszeptibilität gegenüber immunvermittelten Erkrankungen (darunter Diabetes) verknüpft. Die Daten legten nahe, dass lokale Signale, die über Gα12- und Gα13-gekoppelte Rezeptoren vermittelt werden, eine Modulation der T-Zell–Wanderung bewirken können. Die Modulation der Migration über Gα-Rezeptoren ist auch Bestandteil der funktionellen Reifung von T-Zellen. Wie inzwischen gezeigt werden konnte, kommt es auf CD4+ T-Zellen im Verlauf ihrer Differenzierung zu einer selektiven Änderung des Gα-Repertoires, was eine spezifische Lokalisierung entsprechend ihres funktionalen Profils reflektiert (Foley 2010).

Einen neuartigen modulierenden Effekt durch Integrine auf T-Zell-Migration und –Funktion wiesen wir in einer weiteren, sehr umfangreichen Studie nach, welche sich mit dem Einfluss von LFA-1 auf die T-Zell-Migration beim Austritt aus dem Lymphknoten beschäftigte (**App. 05, Reichardt 2013**).
Zwar war wie oben beschrieben bekannt, dass LFA-1 essentiell für den Übertritt aus dem Blutgefäß in den Lymphknoten ist. Unklar war jedoch, ob Integrine auch beim Verlassen des Lymphknotens über die Lymphbahnen eine Rolle spielen. Bekannt war lediglich, dass T-Zellen den Lymphknoten über subkapsuläre Sinus, T-Zell-Zonen-nahe corticale Sinus und die Medulla verlassen können (Grigorova 2009, Sinha 2009) und dass der Egress vom Zusammenspiel zwischen zurückhaltenden Signalen (Chemokin-Rezeptor

CCR7) und egressfördernden Signalen (Sphingosin-1-Phosphat-Rezeptor-1, S1P1) (Pham 2008) abhängt.
Wir konnten mittels intravitaler Mikroskopie zeigen, dass auch LFA-1 eine Rolle bei der Entscheidung Egress vs. Retention im Lymphknoten spielt. Wir beobachteten ein differentielles Verhalten von LFA Wildtyp(WT)- und LFA-1-KO-T-Zellen beim Kontaktieren von ICAM-1-exprimierenden lymphatischen Netzwerken. Während WT-T-Zellen eher ins Lymphknotenparenchym zurückkehrten, verließen LFA-1-KO-T-Zellen den Knoten rascher. Offenbar spielt LFA-1 als Adhäsionsrezeptor bei der Entscheidungsfindung eine Rolle. Es ist noch unklar, welche T-Zell-Funktionen dabei beeinflusst werden. Der Effekt könnte aber die Immunantwort verstärken, indem die Anzahl an T-Zellen, welche im Verlauf einer Immunantwort aktiviert werden, erhöht wird. Dass der Kontakt zu lymphatischen Membranen zelluläre Aktivität beeinflussen kann wurde bereits früher für DC gezeigt (Podgrabinska 2009).
Unsere Ergebnisse verdeutlichten ein neues mechanistisches Prinzip, über welches LFA-1 die T-Zell-Migration und damit die T-Zell-Aktivierung beeinflussen kann.

Zusammengefasst unterstrichen unsere intravitalen und *ex vivo* Experimente mittels 2-Photon-Mikroskopie die Bedeutung eines intakten Migrationsverhalten von T-Zellen *in vivo*. Sie zeigen, dass die korrekte Wanderung durch lymphatisches Gewebe in wesentlicher Weise die Aktivierbarkeit und damit die Funktionsfähigkeit von T-Zellen bestimmt.

Wie kann diese Erkenntnis genutzt werden? Die immuntherapeutische Beeinflussung der T-Zell-Wanderung steht erst am Anfang. Sie hat jedoch mit der medikamentösen Gabe von FTY720, Sphingolimod, eines S1P-Rezeptor-Modulators, eine erste erfolgreiche Anwendung gefunden. FTY720 hemmt den Austritt von T-Zellen aus dem Lymphknoten und damit die T-Zell-vermittelte Inflammation. FTY720 wird bei der Prävention der Transplantatabstoßung und insbesondere bei der Behandlung bestimmter Formen der Multiplen Sklerose angewandt (Brinkmann 2001, Brinkmann 2009).

4. extrinsische Modulation der T-Zell-Aktivierung durch Umwelteinflüsse

Die T-Zell-Aktivierung läuft auch bei Angriff identischer Mengen identischen Antigens nicht in zwei Individuen gleich ab. Neben genetischen Voraussetzungen modulieren zahlreiche Umwelteinflüsse die auf T-Zellen einwirkenden Signale und beeinflussen damit die gesamte Immunantwort.

Das Immunsystem befindet sich in ständigem Austausch mit der Umwelt. Bereits intrauterin kommt es zum ersten Kontakt zwischen sich entwickelnden Bestandteilen des Immunsystems, darunter T-Zellen, mit von der Mutter aufgenommenen Substanzen wie Nahrungsbestandteilen (darunter komplexe Proteine aus Kuhmilch oder Fisch) oder Gräserpollen. Schwangerschaft und früheste Kindheit sind besonders sensible Phasen, in denen das Immunsystem geprägt wird (*Prescott 2009*). Das werdende Kind kann schon frühzeitig substanzspezifisch immunologische Toleranz oder allergische Sensibilisierungen entwickeln. Solchen Sensibilisierungen vorzubeugen bzw. sie frühzeitig zu entdecken ist von großer klinischer Bedeutung (Sausenthaler 2011, Leermakers 2013).
Eine der Hauptquellen für die Auseinandersetzung mit der Umwelt ist die Nahrung. Die Hauptnahrung für Neugeborene ist die Muttermilch. Ein Ansatz zur Untersuchung von Umweltfaktoren und immunologischen Erkrankungen ist daher der Vergleich der Zusammensetzung der Muttermilch mit späteren klinischen und paraklinischen Zeichen der allergischen Sensibilisierung.
Im Rahmen einer großen klinischen Studie zur Untersuchung der Entstehung allergische Sensibilisierungen bei Neugeborenen mit erhöhtem Allergierisiko (LARS, Leipziger Allergie-Risiko[kinder]-Studie) fanden wir eine Assoziation zwischen der Zusammensetzung der Muttermilch und der allergischen Sensibilisierung (**App. 15, Reichardt 2004**). Unter anderem fanden wir für Kinder mit vermindertem Geburtsgewicht eine Korrelation von hohen Spiegeln an Linolensäure (LA, 18:2n-6) mit hohem spezifischem IgE gegen Kuhmilch sowie von niedriger Docosapentaensäure (DPA, 22:5n-3) mit erhöhtem totalem Serum-IgE im Alter von 1 Jahr. Diese Daten stimmten überein mit der generellen Beobachtung, dass die langkettigen (mindestens

14 Kohlenstoffatome) n-6- (synonym Ω6-) Fettsäuren, insbesondere wie von uns gefunden LA, 18:2n-6, einen atopiefördernden Einfluss haben, während n3 (Ω3)-Fettsäuren eher schützen. Der Grund hierfür liegt darin, dass viele Vertreter der n6-Reihe, darunter Arachidonsäure (AA, 20:4n-6) und deren Metaboliten wie Leukotrien B4 proinflammatorische Eigenschaften haben (Ohtsuka 1997), während die n3-Reihe, z.B. Eicosapentaensäure (EPA, 20:5n-3) und Docosahexaensäure (DHA, 22:6n-3), eher als anti-inflammatorisch beschrieben werden. Insbesondere DPA, 22:5n-3, für welches wir niedrige Spiegel mit erhöhtem IgE verbunden sahen, ist als metabolischer Linker mit 20:5n-3 (EPA) und 22:6n-3 (DHA) verknüpft, und für diese beiden langkettigen Fettsäuren wurde anti-inflammatorische Kapazität beschrieben (*Calder 1998*). Für EPA wurde u.a. die Hemmung der T-Zell-Proliferation und der IL-2-Produktion sowie die Induktion von Apoptose in T-Zell-Blasten berichtet (Terada 2001). Inzwischen sind neuere Hinweise vorhanden die zeigen, dass n-3-Fettsäuren die proinflammatorische Entwicklung von Th17-T-Zellen unterdrücken bzw. die Entwicklung von regulatorischen T-Zellen fördern können (Han 2012, Monk 2013).

Langkettige Fettsäuren sind integrale Bestandteile der Zellmembran und beeinflussen die laterale Motilität von Signalmolekülen durch Veränderung der Zusammensetzung von lipid rafts. Eine n-3/n-6-Imbalance verändert das Signaling, auch von T-Zellen, darunter die Produktion des Calcium-second messengers Diacylglycerol (DAG) sowie die Rekrutierung und Aktivierung von PKCθ, MAPK und anderen Signalmolekülen (Kim 2010). Erst kürzlich wurde eine Arbeit veröffentlicht, welche (ähnlich zu dem von uns untersuchten Synapsensystem, s. App. 04) die Synapsenbildung zwischen B- und T-Zellen in Anwesenheit von Fischöl (reich an n-3 Fettsäuren) mittels TIRF-Mikroskopie (total internal reflection fluorescence) untersuchte (Rockett 2013). Die Zugabe von Fischöl verminderte die Anreicherung von MHC II und das Rekruitment von PKCθ an der Synapse. Wenngleich es sich um eine artifizielle Stimulation und ein *in vitro* System handelt, ist es doch interessant festzuhalten, dass dies ähnliche Resultate sind, wie sie bei der direkten Betrachtung von Synapsen von Tregs beobachtet wurden (Sumoza-Toledo 2006, Zanin-Zhorov 2010).

Unsere Daten aus der Muttermilchstudie ließen schlussfolgern, dass bestimmte Risikoneugeborene von einer frühzeitigen Supplementierung mit (n-3) langkettigen Fettsäuren profitieren könnten; ein Procedere, das damals nur für Neugeborene mit sehr niedrigem Geburtsgewicht empfohlen wurde (ESPGAN Committee 1990). In der Tat lassen inzwischen neuere Daten vermuten, dass die perinatale Supplementierung einen positiven Effekt auf die Atopievermeidung hat (*Klemens 2011*). Andere zusammenfassende Untersuchungen sehen hingegen keinen eindeutigen Zusammenhang (Sala-Vila 2008, Greer 2008). Da die Datenlage international nicht einheitlich ist, werden Kohortenstudien ähnlich zu unserer auch aktuell noch mit vergleichbarer Zielstellung durchgeführt. Erst kürzlich zeigte eine solche Studie erneut Resultate, die unseren Daten entsprachen, diesmal in der Korrelation von Fettsäuren der Muttermilch mit dem Risiko für allergisches Asthma (Soto-Ramirez 2012). Wahrscheinlich ist jedoch für eine aussagekräftige Risikoabschätzung aufgrund der multifaktoriellen Genese atopischer Erkrankungen eine deutlich umfangreichere Erhebung von klinischen und paraklinischen Parametern empfehlenswert (*Szefler 2012*). Die derzeitigen Empfehlungen zur Prävention von Allergie und Asthma beruhen weiterhin hauptsächlich auf dem ausschließlichen Stillen für 5 Monate bzw. der Gabe von stark hydrolysierter Formula-Milch (zur Vermeidung frühzeitigen Kontakts mit Allergenen) in dieser Zeit. Probiotika haben in bestimmten Konstellationen einen protektiven Effekt gezeigt. Noch offen ist der Effekt der Supplementierung mit Vitamin D und mit mikrobiellen Komponenten zur Steuerung intestinaler Inflammation (*Lau 2013*).

Neben Nahrungsbestandteilen werden Schadstoffe der Außenluft (reaktive Stickstoff- und Sauerstoffverbindungen aus Abgasen) sowie Innenraumschadstoffe (biologische Fremdstoffe wie Schimmelpilze oder reaktive Chemikalien in Farbstoffen, Kleber, Lösemittel) als wichtige Allergieauslöser angesehen (*D'Amato 2010, Jaakola 2013, Mendel 2007*).

Insbesondere die Beteiligung niedermolekularen Verbindungen (small molecules) wirft die Frage auf, ob und wie diese Substanzen gegenüber T-Zellen immunologisch wirksam werden können. Die TCR-Reaktivität ist

bekanntlich auf Peptide, wesentlich größere Moleküle, beschränkt. Neben toxischen Effekten wären auch epigenetische Einflüsse möglich (*Karmaus 2013*). Allerdings sind auch funktionelle Beeinflussungen des Signalings denkbar, z.B. von T-Zellen, wie nachfolgend gezeigt.

Seinerzeit viel beachtet waren die Studien (insbesondere die *Nature*-Publikation) von John Rhodes, welche einen wichtigen molekularen Mechanismus möglicher signalmodulierender Eigenschaften von Xenobiotika, chemisch reaktiven Fremdstoffen, beleuchteten (Rhodes 1989, Rhodes 1995). Er bewies die Fähigkeit von Xenobiotika aus der Gruppe der Aldehyde, Schiff-Basen mit Aminogruppen auf der Oberfläche von T-Zellen einzugehen. In Schiff-Basen (Imine) sind typischerweise Carbonylgruppen kleiner Moleküle (z.B. von Aldehyden) mit Aminogruppen (z.B. Lysyl-Reste von Aminosäuren) gekoppelt. Die so auf T-Zellen entstandenen Bindungen interferierten mit Clofilium-sensitiven Natrium- und Kaliumkanälen und beeinflussten dadurch das costimulatorische Signaling. Zudem zeigten die Daten, dass solche Bindungen offenbar auch integraler Bestandteil der molekularen Interaktion zwischen APC und T-Zellen waren.
Ausgehend von diesen Erkenntnissen führten wir eigene Untersuchungen zur Adduktbildung einer Reihe von umweltrelevanten Xenobiotika darunter von Aldehyden, Toluen-2,4-diisocyanat (TDI), 2,4-Dinitro-1-Fluorbenzol (DNFB) u.a. mit der ε-Aminogruppe von Modellpeptiden durch und quantifizierten die relative *in vitro*-Reaktivität der Xenobiotika (**App. 16, Reichardt 2003**).

Wir konnten regelmäßige und stabile Adduktbildungen nachweisen und damit zeigen, dass die Formation einfacher chemischer Bindungen wie Schiff-Basen nicht auf Aldehyde beschränkt ist, sondern auch bei anderen Klassen an Xenobiotika beobachtet werden kann. Solche elektrophilen Reaktionen bilden die molekulare Basis für die *in vivo*-Immuntoxizität und Immunmodulation zahlreicher Xenobiotika und reaktiver Metaboliten (*Pumford 1997*). Neben Aminogruppen sind häufig Thiole bevorzugte Angriffspunkte reaktiver Xenobiotika. Im Rahmen von intrazellulären Redoxreaktionen sind solche Prozesse auch bei der Entstehung posttranslationaler Modifikationen beteiligt (*Rudolph 2009*).

Im Detail zeigten unsere Daten, dass niedrig-aktive Substanzen kaum Tendenz haben, Bindungen einzugehen. Dies war zu erwarten. Wir beobachteten aber gleichzeitig, dass die von uns untersuchten Xenobiotika mit der strukturell höchsten Reaktivität ebenfalls nur geringe Adduktbildungen mit dem Modellpeptid eingingen. Offenbar werden sie in einem wässrigen Umgebungsmilieu, wie es im Organismus vorliegt, durch sofortige Reaktion mit dem Umgebungswasser in ihrer Reaktionsfähigkeit gegenüber Proteinen beschränkt. In der Folge wurden von uns die stärksten Effekte im physiologischen Milieu für Xenobiotika mit mittlerer chemischer Reaktivität beobachtet. Solche Zusammenhänge können Konsequenzen für die Einschätzung der Toxizität einer Substanz *in vivo* haben (Rotroff 2010). Inzwischen können mittels modernster Verfahren (Ultra-performance LC, UPLC, gekoppelt mit Time-of-Flight-Massenspektrometrie, TOF-MS) auch Substanzen mit hoher Reaktivität und kurzer Lebensdauer erfasst werden, für die *in vivo* bei Entstehung in unmittelbarer Nähe zu Proteinen oder DNA ebenfalls Adduktbildungen zu erwarten sind (Rousu 2009).

Die Bewertung gesundheitsschädlicher Arbeitsstoffe erfolgt in Deutschland maßgeblich durch die Ständige Senatskommission zur Prüfung gesundheitsschädlicher Arbeitsstoffe (MAK-Kommission) der Deutschen Forschungsgemeinschaft (DFG), und zwar hinsichtlich ihrer krebserzeugenden, keimzellmutagenen, sensibilisierenden, hautresorptiven und die Schwangerschaft beeinträchtigenden Eigenschaften. Entsprechend werden Grenzwerte wie maximale Arbeitsplatz-Konzentrationen (MAK-Werte) für flüchtige Chemikalien und Stäube, biologische Arbeitsstoff-Toleranzwerte (BAT-Werte), biologische Leitwerte (BLW) bzw. biologische Arbeitsstoff-Referenzwerte (BAR) festgelegt und jährlich aktualisierte Übersichten herausgegeben (MAK Collection 2013).

Immunmodulatorische Eigenschaften jenseits der Sensibilisierung werden nicht explizit berücksichtigt und die Klassifizierung orientiert sich an Einzelsubstanzen. Schwierig aber notwendig ist die Entwicklung geeigneter Systeme der experimentellen Testung bzw. der statistischen Erfassung komplexer klinischer und paraklinischer Daten, welche potentielle Effekte der Immunmodulation besser zu erkennen und zu beschreiben in der Lage sind (Rotroff 2010).

Die modulierenden Einflüsse von Xenobiotika auf Zellphysiologie und Immunantwort werden zunehmend besser verstanden. Eine wichtige Rolle spielen z.B. Xenobiotika-Rezeptoren wie der Aryl hydrocarbon Rezeptor (Ah Rezeptor), ein zytosolischer transkriptioneller Regulator, der seinen Namen aufgrund charakteristischer Interaktion mit aromatischen Kohlenwasserstoffen wie PCB (polychlorierten Biphenylen) und Dioxinen erhielt. Der Ah-Rezeptor ist in zahlreichen Immunzellen zu finden und besitzt u.a. modulierende Eigenschaften bei der T-Zell-Differenzierung (*Hao 2013*, Nakahama 2013).
Die Beeinflussung der T-Zell-Costimulation durch Xenobiotika wurde inzwischen auch der klinischen Anwendung zugeführt. So wurde die oben beschriebene costimulatorische Wirkung von Schiff-Base-formenden Substanzen erfolgreich zur Erzielung eines Adjuvans-Effekts bei einer Influenza-Vakzine angewandt (Charo 2004).

Fremdstoffe treten nicht immer nur zufällig bzw. ungewollt mit dem Organismus in Kontakt. Sie können auch durch den Arzt (iatrogen) gezielt zugeführt werden (als Medikamente). Teilweise geschieht dies mit dem expliziten Wunsch, das Immunsystem zu beeinflussen, teilweise auch mit anderer Zielstellung, in deren Rahmen sich die Beeinflussung des Immunsystems als Nebenwirkung ergibt.
Schon länger bekannt ist z.B. die Tatsache, dass Antibiotika, darunter Macrolide, Tetracycline und β-Lactam-Antibiotika, nicht nur eine spezifische bakterientötende oder -hemmende Wirkung besitzen sondern auch immunmodulatorische Effekte aufweisen. Allerdings sind viele Details zur Beeinflussung der Signalkaskade erst in den letzten Jahren zutage getreten (*Aminov 2013*). Rapamaycin, ein mTOR (mammalian Target of Rapamycin) - Inhibitor und ein potentes Immunsuppressivum, ist von seiner Struktur her ein Antibiotikum, ein Makrolid. Rapamycin und ein jüngeres Derivat der Gruppe, Everolimus, wird weitverbreitet bei Transplantationen von Herz-, Lunge, Leber und Niere eingesetzt (*Gunk-Turner 2012*). Mehr zur zentralen Rolle von mTOR für die Immunantwort und die Treg-Bildung weiter unten (App. 02, Etemire 2013).

Ein Beispiel für immunmodulierende Antibiotika aus der Gruppe der β-Lactam-Antibiotika ist die Kombination aus Piperacillin und Tazobactam. Dieses Antibiotikum wird vorrangig bei respiratorischen Infektionen angewendet. Piperacillin ist ein Penicillin-Derivat mit erweitertem Wirkungsspektrum, Tazobactam hemmt die Penicillin-abbauende Wirkung (Penicillinase) von Bakterien und verstärkt dadurch die Wirkung des Medikaments.

Wir beobachteten bei der klinischen Anwendung in einer Kinderklinik, dass überdurchschnittlich viele Patienten, die mit diesem Antibiotikum behandelt wurden, Fieber sowie Leukozytopenie und Thrombopenie entwickelten. Nach Absetzen des Medikaments sistierten diese Symptome (**App. 20, Reichardt 1999**). Unmittelbare allergische Reaktionen (IgE- und IgG-vermittelt) gegen Medikamente, darunter Penicilline, sind seit langem bekannt und stellen die am häufigsten berichteten Antibiotikaallergien dar (*Chang 2012*). Darüber hinaus wurden zirkulierende Benzylpenicillin-spezifische CD4+ T-Zellen nachgewiesen (Nhim 2013). Auch die kovalente Bindung an Albumin (ähnlich zu Xenobiotika) und die nachfolgende Beeinflussung der T-Zell-Funktion wurde für β-Lactam-Antibiotika vor kurzem gezeigt: Gene, die mit Th2- und Treg-Differenzierung verknüpft waren, wurden in T-Zellen nach Stimulation mit (dem β-Lactam-Antibiotikum) Cefuroxim herunterreguliert, während die Behandlung mit Ampicillin diese Gene aufregulierte (Mor 2013). Mithin können β-Lactame T-Zellen direkt immunmodulatorisch beeinflussen.

Der von uns beobachteten Nebenwirkung lag aber offenbar ein immunsuppressiver Effekt zugrunde, der schon im Knochenmark ansetzt (bone marrow suppression). Wahrscheinliche Ursache ist ein durch Piperacillin ausgelöster Reifungsdefekt (*Scheetz 2007*). Dies war zuvor bereits für eine Reihe von ß-Lactam-Antibiotika beobachtet worden und erklärt die bei unseren Patienten aufgetretene Erniedrigung der granulozytären und thrombozytären Zellreihe. Eine Schwierigkeit im klinischen Alltag besteht darin, mögliches medikamentenassoziiertes Fieber (Drug-related fever) von einer durch die Grundkrankheit (bakterielle Infektion) hervorgerufenen inflammatorischen Reaktion abzugrenzen. Deshalb ist es wichtig, Kenntnis von den molekularen Mechanismen zu haben, über die bestimmte Medikamente immunmodulatorische Effekte ausüben können, um klinische

und paraklinische (Labor-)Konstellationen rasch zu erkennen und richtig einordnen zu können. Unsere Studie konnte möglicherweise zu erhöhter Achtsamkeit bei der Anwendung von Piperacillin/Tazobactam beitragen. Unsere Schlussfolgerung, bei prolongierter Therapiedauer regelmäßiges Immunmonitoring / Blutbildkontrollen durchzuführen, wurde erst kürzlich erneut unterstützt [und unser Paper zitiert] (Lee 2009).

Die Anwendung von direkt immunmodulierenden Substanzen stellt den unmittelbarsten Eingriff in das Immunsystem dar. Sogenannte Biologicals (Biologics, Biopharmaka) sind bio- oder gentechnologisch hergestellte Proteine, die ganz oder teilweise körpereigenen Immunmediatoren entsprechen (z.B. Zytokine, -Rezeptoren, Antagonisten) bzw. diese gezielt blockieren sollen. Eine ganze Reihe solcher Substanzen ist den letzten Jahren entwickelt und z.T. mit großem Erfolg angewendet worden. Insbesondere monoklonale Anti-TNFα-Antikörper (darunter Infliximab) hat bei Rheumatoidarthritis und chronisch-entzündlichen Darmerkrankungen das Therapiespektrum wesentlich erweitert (Tambralli 2013, *Costa 2013*). Mechanistisch führt die Blockade des TNFα einerseits zu einer Verminderung der (intrazellulären) Abwehrleistung (von Makrophagen), andererseits wurde auf Jurkat-(T)-Zellen anti-inflammatorisches Signaling nach Kopplung von anti-TNFα an transmembranöses TNFα beobachtet, das zur Induktion von TGFβ und IL-10 führte (Mitoma 2005). *In vivo* wurde u.a. bei chronisch-entzündlichen Darmerkrankungen eine Suppression der inflammatorischen Zytokinproduktion sowie eine Induktion von Apoptose in T-Zellen der Lamina propria des Darmes beobachtet (Di Sabatino 2004, Dahlén 2013).
Allerdings ist zu beachten, dass immunsupprimierende Medikamente auch stets die Hauptaufgabe des Immunsystems, die Bekämpfung von Infektionen, erschweren. Infektionen unter anti-TNFα verlaufen z.T. schwer und gehören zu den gefürchtetsten Nebenwirkungen der Therapie (*Keystone 2011).* Bei einem 11-jährigen Patienten der Kinderklinik mit Morbus Crohn sahen wir 3 Tage nach Beginn einer Infliximab-Therapie eine massive Verschlechterung mit kardialer Dekompensation (**App. 18, Reichardt 2002b**). Es ergab sich, dass ein bis dahin klinisch nicht manifester intramyokardialer Abszess mit Absiedelung von *S. aureus* durch die immunsuppressive Therapie aktiviert

worden war und die Aortenklappe zerstörte. Die Infektion wurde antibiotisch rasch kontrolliert, die Aortenklappe musste aber operativ ersetzt werden. Solche und ähnliche Fälle machen deutlich, dass bei der Anwendung von anti-TNFα begleitende Infektionen weitgehend auszuschließen sind. Als eine Konsequenz wird inzwischen vor Therapiebeginn die routinemäßige Testung auf latente Tuberkulose empfohlen (Diel 2009).

Infektionen gehören zu den häufigsten Ereignissen, mit denen sich das Immunsystem auseinandersetzen muss, nicht selten mit hoher klinischer Relevanz. Nicht umsonst ist das Immunsystem evolutionär auf das Bekämpfen von Mikroorganismen ausgerichtet worden. Bakterien, Viren, Pilze und Protozoen verursachen akute Infektionen, denen das Immunsystem im Normalfall innerhalb von Stunden oder Tagen Herr wird. Allerdings versuchen viele Mikroorganismen mittels einer Unzahl an Strategien, der Zerstörung durch das Immunsystem zu entkommen und das Immunsystem herunterzuregulieren (immune evasion). Dies kann zu chronischen Infektionen führen.
Bekannte Beispiele sind chronische Infektionen durch Viren. Das HI-Virus befällt neben Endothelzellen, Makrophagen und DC nicht zuletzt auch CD4+ T-Zellen, deren Zahl im Verlauf der Erkrankung abnimmt. Unglücklicherweise sind Memory CD4+ T-Zellen als Hauptorganisatoren der Erkrankungsabwehr auch die Hauptbetroffenen der Infektion, weshalb eine vollständige Eradikation durch das Immunsystem so schwierig ist (*Zhang 2013*). Ein weiteres, in vieler Hinsicht prototypisches Beispiel für ein immunsupprimierendes Virus ist das Masern-Virus. Es infiziert DC und (wahrscheinlich über deren Kontakt) T-Zellen. In T-Zellen stören virale Glycoproteine die F-Aktin-Umlagerung und damit Signalprozesse. Die Folge ist eine Depletion der T-Zellen und eine klinisch relevante Immunsuppression (*Avota 2010*). Aus dem Spektrum bakterieller Infektionen mit Chronizität ist vor allem die Tuberkulose zu nennen. Sie gehört zu den häufigsten Infektionen weltweit und die Anzahl beobachteter Tuberkulose-Fälle bei Personen mit Risikofaktoren (darunter Patienten unter anti-TNFα-Therapie!) steigt in Deutschland (Diel 2009). Hinsichtlich einer zugrundeliegenden Immunmodulation wurde als direkter T-Zell-assoziierter Mechanismus die

präferentielle Induktion von regulatorischen T-Zellen nach Kontakt mit *M. tuberculosis* beobachtet, was die Ausbreitung der Infektion und deren Chronizität unterstützen soll (*Larson 2013*).

Neben immunsupprimierenden Effekten durch Infektionen kommt es teilweise auch zu einer sehr starken Aktivierung des Immunsystems mit z.T. fatalen Folgen. Dazu zählen u.a. allergische bzw. Überempfindlichkeitsreaktionen, bei denen (T-Zell-lizensiert) inadäquate Mengen an IgE- und IgG-Antikörpern von B-Zellen gebildet werden. Einen Sonderfall, der explizit T-Zellen betrifft, stellen sogenannte Superantigene dar. Diese Antigene (oft toxinähnliche Proteine bakteriellen oder viralen Ursprungs) sind in der Lage, TCR-unabhängig große Anteile der T-Zellen eines Organismus zu aktivieren. Die molekulare Grundlage dieser Eigenschaft besteht typischerweise darin, dass sie am MHC-Molekül einerseits und an der TCR-Seitenkette (z.B. β-Kette) andererseits binden können (*Marrack 1990, Li 1999*). Erkrankungen, die durch solche Superantigene ausgelöst werden, sind z.B. das Toxic-Shock-Syndrom sowie das mukokutane Lymphknotensyndrom oder auch Kawasaki-Syndrom (die Kawasaki-Erkrankung, engl. Kawasaki disease, KD).

KD ist eine akute systemische Vaskulitis des Kindesalters mutmaßlich infektiösen Ursprungs (*Jamieson 2013*). Zahlreiche Hinweise bestehen für die Beteiligung von Superantigenen, es ist jedoch nicht geklärt, ob diese überwiegend streptokokken- oder staphylokokkenassoziiert sind oder viralen Ursprungs. Die Krankheit führt infolge der (unbestrittenen) T-Zell-Aktivierung sowie systemischer Zytokinausschüttung (u.a. IL-1, IL-2, IL-6, TNFα, IFNγ) zu schweren generalisierten Symptomen (Lin 1993). KD kann unbehandelt in bis zu 25% zu koronaren Anomalien führen und ist eine der führenden Ursachen erworbener Herzerkrankungen im Kindesalter (Kato 1996, *Jamieson 2013*). Komplikationsrate und Folgen der Erkrankung können deutlich gemindert werden, wenn rasch hochdosierte intravenöse Immunglobuline (IVIG) verabreicht werden, mutmaßlich vor allem aufgrund einer toxin-neutralisierenden Wirkung (Durongpitsikul 1995).

Deshalb ist die frühzeitige Erkennung der Superantigenbeteiligung besonders wichtig. Um dies zu erreichen, untersuchten wir in einer klinischen Studie die TCR-Vβ-Ketten-Verteilung bei Kindern mit akutem fieberhaftem Infekt (**App. 17, Reichardt 2002**). Wir fanden bei Kindern, die im Verlauf die klinischen

Kriterien des KD erfüllten, einen höheren Prozentsatz an Vβ2 TCR als bei Patienten mit anderen Ursachen fieberhafter Erkrankungen bzw. ohne das klinische Bild von KD. Unsere Beobachtung zeigte eine Möglichkeit einer frühzeitigen Diagnose und damit gezielter Therapie von KD auf. Die Korrelation zwischen Vβ2 und KD ist von anhaltendem Interesse und wurde erst kürzlich erneut bestätigt (Natividad 2013). Therapeutisch begegnet man der proinflammatorischen T-Zell-Expansion, die mittlerweile als Th17/Treg–Dysbalance angesehen wird, jetzt neben der Anwendung von IVIG auch erfolgreich mit anti-TNFα (Mori 2012). Allerdings ist auch aktuell weder eine einheitliche infektiöse Ursache gefunden noch besteht eine einheitliche Meinung zur zwangsläufigen Beteiligung von Superantigenen in Patienten mit dem klinischem Bild von KD (Pinna 2008). Möglicherweise spielen individuelle genetische Faktoren eine entscheidende Rolle und können die uneinheitlichen klinischen Verläufe bei KD erklären helfen (*Onuchi 2012*).

Genetische Faktoren spielen neben den genannten Umwelt- und iatrogenen Einflüssen generell eine große Rolle bei der Modulation der T-Zell-Aktivierung bzw. der Immunantwort. Bekannt (aber glücklicherweise sehr selten) sind z.B. Defekte in der genetischen Information für die ζ-Kette des TCR-CD3-Komplexes oder der signal-transducer-and-activator-of-transcription (STAT)-Familie, die zu schweren kombinierten Immundefekten (SCID) führen können (*Hernandez-Trujillo 2013*). Wesentlich häufiger als diese T-Zell-Immundefekte sind dagegen Allergien und Autoimmunerkrankungen, für die ebenfalls genetische Risikofaktoren ermittelt wurden. Da viele dieser Erkrankungen wie z.B. Multiple Sklerose polygenetisch bedingt sind und multifaktorielle Auslöser besitzen, geschieht dies heutzutage nicht selten mit Hilfe systembiologischer Ansätze (*Stranger 2012, Liu 2012,* Baranzini 2013). Die rasche Entdeckung schwerer Defekte kann dazu beitragen, Therapien rasch einzuleiten und so die Prognose zu verbessern. Dazu gehören bei schwersten Immundefekten Knochenmarktransplantationen oder Gen-therapien insbesondere bei monogenetischen Erkrankungen (*Kelly 2013*).
Eine in immunologischer Hinsicht besonders interessante monogenetische Erkrankung, das von-Hippel-Lindau-Syndrom oder die retino-cerebelläre Angiomatose, beruht auf Punktmutationen im von-Hippel-Lindau-Gen (VHL)

(Neumann 1991). Dieses Tumor-Suppressor-Gen kodiert ein Protein mit Ubiquitin-Ligase-E3-Aktivität, das am Abbau des Hypoxie-induzierbaren Faktors (HIF) beteiligt ist (*Hsu 2012*). HIF spielt eine zentrale Rolle beim Signaling in Antwort auf den im Milieu verfügbaren Sauerstoff (oxygen sensing). Permanent hohe Aktivität von HIF im Kolon wird in Verbindung mit der Entwicklung von chronisch-entzündlichen Darmerkrankungen gebracht (Sha 2008). Die Inaktivierung des VHL-Gens kann zur verstärkten Expression des vaskulären endothelialen Wachstumsfaktors VEGF1 in DC führen. Auch oxidativer Stress, wie er u.a. in der Folge einer Tumorentwicklung entsteht, lässt VEGF1 ansteigen. VEGF1-high DC können immunsuppressive Eigenschaften entwickeln und die Proliferation von T-Zellen inhibieren (Kusmartsev 2008). Diese Zusammenhänge weisen auf eine mögliche Verbindung hin zwischen Oxygen-sensing, Immunsuppression und der Entwicklung von Karzinomen (als ultimative Form des Versagens des Immunsystems und der Immunüberwachung). Im Zentrum dieser Verbindung steht in diesem Beispiel das VHL-Gen.

Als Folge von sporadischen und hereditären Mutationen im HVL-Gen sind vor allem Nierenzellkarzinome bekannt. Aber auch Phäochromozytome und (multilokuläre) Paragangliome (alles Tumoren der chromaffinen Zellen der Nebenniere) sind damit assoziiert (*Bausch 2013*). Bei einem 9 Jahre alten Patienten einer Kinderklinik mit extraadrenalem Phäochromozytom fand sich nur 7 Monate nach Entfernung des ersten Tumors erneut ein Paragangliom, kontralateral gelegen. Da multifokale Paragangliome typisch für Syndrome wie die von-Hippel-Lindau-Erkrankung sind, leiteten wir umgehend die Untersuchung des VHL-Gens ein (**App. 19, Reichardt 2002c**). Statt einer der bis dato bekannten Mutationen ergab die Sequenzierung eine neue Punktmutation im VHL-Gen an Position 406 (VHL nt. 406 T→G). Der Patient wurde an dem histologisch gutartigen Tumor erfolgreich operiert und in ein Screening-Programm für VHL-Patienten übernommen.

Solche Anstrengungen, die Diagnose auf molekularer Ebene zu sichern, sind aus mehreren Gründen wichtig. Zum einen sicherte der Nachweis die Diagnose für den betreffenden Patienten. Die molekulare Zuordnung hatte zudem Konsequenzen hinsichtlich der Risikostratifizierung, hinsichtlich

Häufigkeit und Umfang des Follow-Up-Screenings sowie der Einbeziehung weiterer Familienmitglieder in das Screening.

Aus Sicht auf das adaptive Immunsystem noch interessanter ist ein erst kürzlich veröffentlichter Ansatz zum VHL-Gen: Patienten mit metastasierendem Nierenzellkarzinom wurden mit einer neuartigen Peptidvakzine behandelt. Das Besondere bestand darin, dass das verwendete Peptid auf Sequenzen des mutierten VHL-Gens beruhte. Ziel war es also, eine Immunreaktion gegen diese VHL-Peptide und damit gezielt gegen das Karzinom, in dem das VHL-Gen mutiert vorlag, zu induzieren (Rahma 2010). In jener Studie entwickelten vier der fünf so behandelten Patienten eine spezifische Immunreaktion (gemessen an der IFNγ-Produktion zytotoxischer T-Zellen) gegen das VHL-Peptid. Es ist vorstellbar, dass weiterentwickelte Verfahren dieser Immuntherapie zur Induktion von tumorspezifischen T-Zellen auch für unseren Patienten mit Paragangliom (die sich in bis zu 40% metastasierend entwickeln können) eines Tages nutzbar sein werden. Angiogenese-blockierende Medikamente werden bereits heute in der Therapie des metastasierenden Nierenkarzinoms eingesetzt und haben dessen Therapie revolutioniert (*Richard 2013*).

Das Beispiel unterstreicht gleichzeitig die Bedeutung eines weitläufigen Feldes der derzeitigen klinischen Immunologie: der gezielten Immuntherapie zur Verbesserung der Immunantwort gegen Tumoren.

5. Gezielte Modulation der T-Zell-Aktivierung durch Immuntherapie

Die T-Zell-Aktivierung erfordert einen passenden (kognaten) pMHC-Interaktionspartner. Aufgrund der exquisiten Spezifität dieser Interaktion hielt man die pMHC-TCR-Bindung lange Zeit für eine „all or none" Interaktion (Schlüssel-Schloss-Prinzip), d.h. entweder wird eine Aktivierung ausgelöst oder nicht. Dies ist aber nicht korrekt. Vielmehr gibt es eine Vielzahl von Abstufungen in der Aktivierung, ausgelöst durch in ihrer Struktur ähnliche (aber nicht identische) Peptide (Evavold 1991).
Die Synthese gezielt abgewandelter Peptidliganden (altered peptide ligands, APL) und ihre experimentelle Anwendung zur TCR-Stimulation erbrachte wichtige Erkenntnisse zu strukturellen Voraussetzungen und Hierarchie der Effektorfunktionen bei aberranter T-Zell-Stimulation (*Kilgore 2003*). So können bestimmte Peptide (partial agonists) selektiv Zellfunktionen wie Zytotoxizität auslösen aber keine Proliferation. Andere APL wirken als Antagonisten d.h. sie hemmen dominant die Stimulation durch kognate Peptidliganden (unterdrücken z.B. die Produktion von IFNγ). Wir konnten zeigen (**App. 12, Jones 2008**), dass ein antagonistischer Effekt an eine hohe TCR-Dichte gebunden ist. Offenbar benötigen Antagonisten eine kritische Menge an TCR damit ihr dominant negatives Signaling, welches sie in T-Zellen auslösen, wirksam wird. Antagonistische Peptide wurden *in vivo* als Varianten viraler zytotoxischer Peptide gefunden, welche die T-Zell-Antwort unterdrückten (im Sinne einer „immune evasion"-Strategie) und zur Persistenz von Infektionen beitragen können (Bertoletti 1994). Gleichzeitig erschienen solche Antagonisten als ideale Werkzeuge, um gezielt antigenspezifische Immunmodulation vorzunehmen (Vukmanović 2005). Die Hoffnung auf eine breite klinische Anwendung von APL hat sich bislang aber nicht erfüllt. In der klinischen Erprobung befinden sich derzeit (Treg-induzierende) APL u.a. im Tiermodell der Arthritis (Dominguez 2011).

Einer der weltweit meistbeachteten Fehlschläge der Immuntherapie fußt auf dem CD28-Superagonisten TGN1412. Dieses Molekül vermittelt ein so starkes Signal an CD28, dass die ansonsten essentielle Stimulation des TCR-CD3-

Komplexes nicht notwendig zur T-Zell-Aktivierung ist (Tacke 1997). In zahlreichen *in vitro*- und Tierversuchen hatte sich dabei geringe Toxizität und die präferentielle Induktion regulatorischer T-Zellen ergeben, weshalb das Molekül als erfolgversprechende immunmodulierende Substanz galt. Leider endete die Erstanwendung unglücklich; alle Probanden erkrankten schwer infolge eines ausgelösten Zytokinsturms (Suntharalingam 2006).
Auf der Suche nach einer Erklärung konnten wir zeigen, dass das durch TGN1412 induzierte Signalmuster sich von dem durch konventionellen CD28-Antikörper deutlich unterschied (**App. 13, Waibler 2008**). Speziell konnten wir (als ein Teil der Studie) mittels Lebendzell-Fluoreszenzmikroskopie zeigen, dass TGN1412 einen verzögerten aber extrem lang anhaltenden Calciumstrom in die Zelle initiiert. Dieses veränderte Signaling war in humanen CD4+ T-Zellen (naive und Memory-T-Zellen) zu beobachten aber nicht in T-Zellen von Cynomolgus-Affen (wie sie auch in vorangehenden Tierversuchen vor der klinischen Anwendung verwendet worden waren). Der verstärkte Calcium-Einstrom war auch notwendige Voraussetzung für die ferner nachgewiesene Aktivierung von Src- und Phospho-Inositol-3(PI3)-Kinasen sowie für die Produktion von IFNγ und IL-2. Unsere Daten lieferten einen wesentlichen molekularen Mechanismus für die unerwartet starke Immunantwort bei den Probanden. Der unterschiedlichen Reaktion auf den CD28-Superagonisten in Cynomolgus-Affe bzw. Mensch zugrundeliegend ist wahrscheinlich die selektive Expression inhibitorischer Siglec-Rezeptoren, die beim evolutionären Übergang vom Affen zum Menschen verlorenging (Nguyen 2006). Insgesamt hat das Drama um TGN1412 mehr zum Verständnis und zum Fortschritt der Immuntherapie beigetragen (und wichtige Veränderungen in den Regeln zur experimentellen Durchführung bewirkt) als viele Ansätze, die erfolgreicher verliefen (Hünig 2012). Allerdings unterstreichen die gemachten Erfahrungen die bestehenden komplexen Herausforderungen bei der Anwendung löslicher, synthetischer Moleküle.

Zelltherapeutische Ansätze repräsentieren einen noch komplexeren Ansatz und ein umfangreiches Feld der Immuntherapie, auf welchem große Anstrengungen unternommen werden um v.a. Autoimmunerkrankungen und Krebs zu behandeln. Insbesondere regulatorische T-Zellen, Tregs, sind in

Forschung und experimenteller Therapie von großem Interesse. Tregs können einerseits bereits im Thymus entstehen (natürliche Tregs) und andererseits auch in der Peripherie induziert werden (u.a. in Anwesenheit von TGFβ). Sie unterdrücken andere T-Zellen durch direkten Zellkontakt oder über lösliche Mediatoren (z.B. IL-10). Thymische Tregs zeigen stabile Expression des Transkriptionsfaktors Foxp3, der als Masterregulator für Tregs angesehen wird, während peripher induzierte Tregs diesen häufig nicht oder nicht stabil exprimieren (*Josefowicz 2012*).

In jüngster Zeit wurde deutlich, dass Tregs eine besondere Plastizität besitzen und im Verlauf der Immunantwort teilweise (wieder) klassische Effektorfunktionen annehmen können (*Kleinewietfeld 2013).* Entsprechend relevant sind Studien über die Unterschiede in der Signaltransduktion zwischen konventionellen T-Effektorzellen (Tcon) und Treg. Wir waren an einer derartigen Studie beteiligt (**App. 08, Schmidt 2011**), zu der wir mit Calcium-Imaging beitragen konnten. Im Paper konnte gezeigt werden, dass humane Treg (CD4+ CD25hi Foxp3+) bei Kokultur mit Tcon rasch Calcium-Ströme in Tcon unterdrückten und nachfolgend die Aktivierung der Transkriptionsfaktoren NFAT1 und NF-kB blockierten. Die Suppression erfolgte unterhalb des TCR-proximalen Signalingmoleküls PLCγ1, da dessen Aktivität unbeeinträchtigt blieb. Der exakte Angriffspunkt für die Unterdrückung des Calciumstroms blieb ungeklärt. Spekuliert werden kann über mögliche Modifikationen in der Interaktion von IP_3, das als second messenger für Calciumsignale fungiert, mit seinem Rezeptor (IP_3-Rezeptor). Unsere Daten offenbarten einen bis dato unbekannten, rasch einsetzenden intrazellulären signalmodulierenden Effekt der Treg-Suppression bei direktem Zellkontakt.

Wie aber wird der calcium-modulierende Effekt auf der T-Zelle überhaupt ausgelöst? Es gibt Hinweise, dass dafür der initiale sterische Kontakt zu bestimmten Oberflächenmolekülen auf Tregs verantwortlich ist, da eine intakte Membranbeschaffenheit für den suppressorischen Effekt bei ansonsten avitalen, Formaldehyd-fixierten Tregs notwendig war (Hagness 2012). Eine Reihe von selektiv bzw. bevorzugt auf natürlichen oder induzierten Tregs exprimierten regulatorischen Molekülankern ist beschrieben, darunter CTLA-4, OX40, Neuropilin und andere (*Yadav 2013*).

Allerdings war in der Studie von Hagness et. al. keiner der bekannten Inhibitoren zu ermitteln. Insgesamt muss angenommen werden, dass mehrere, voneinander unabhängige Mechanismen existieren, über welche (Foxp3+) Tregs ihre suppressive Aktivität *in vivo* ausüben (*Shevach 2009*). Eine differentielle Aktivierung (Phosphorylierung) von wenigen Kinasen (11 von 185 mittels Phosphoproteomics untersuchten Kinasen in eine Studie, König 2012) wurde als ein Korrelat für Besonderheiten im Signaling von Tregs im Vergleich zu konventionellen CD4+ T-Zellen ermittelt. Zu den differentiell erhöht gefundenen Kinasen zählten u.a. STK10 und STK4, was als Hinweis auf eine differenzielle Regulation LFA-vermittelter T-Zell-Adhäsion interpretiert wurde. Verminderte Aktivität zeigte AURKB, ein downstream target von AKT, welches involviert ist in die Kontrolle des Zellzyklus durch mTOR (König 2012).

Tregs sind auch an der physiologischen Aufrechterhaltung der perinatalen Toleranz beteiligt, die das Abstoßen des immunologisch teilweise fremden Embryos verhindert. Dies geschieht möglicherweise vor allem durch lokale, im Bereich des Uterus präsente Tregs (*Ernerudh 2011).* Offenbar sind Tregs dabei auch in einer sehr frühen Phase der Schwangerschaft, bei der Implantation der Blastozyste, von Bedeutung. Wir konnten mittels intravitaler 2-Photon-Mikroskopie zeigen (**App. 03, Teles 2013**), dass Tregs zyklusabhängig am Uterus gefunden werden. Ihre Zahl ist dynamischen Schwankungen unterworfen, die an hormonelle Regelkreise (insbesondere Estrogen-abhängig) gekoppelt sind. Die Anreicherung der Tregs ist dabei (ähnlich zum Lymphknoten) chemotaktisch über den (T-Zell-) Chemokinrezeptor CCR7 gesteuert. Solche Erkenntnisse können helfen, die immunologische Toleranz während der Schwangerschaft besser zu verstehen. Die physiologische Reduzierung der Anzahl gewebsspezifischer, inflammatorisch reaktiver T-Zellen am Uterus während der Schwangerschaft kann auch als Modell organbezogener Immuntoleranz verstanden werden und insofern generelle Hinweise zum Verständnis von T-Zell-Toleranzmechanismen liefern (*Erlebacher 2013*).

Zahlreiche Bestrebungen zielen darauf ab, die Bildung von Tregs zu fördern und klinisch nutzbar zu machen. Dies geschieht entweder durch Applikation Treg-fördernder Stimuli *in vivo* oder durch die *ex vivo*-Generierung, -Expansion und –genetische oder funktionelle Modulation von T-Zellen und/oder APC (*Tang 2013*, *McMurchy 2013*). Ebenfalls große Anstrengungen werden unternommen, *ex vivo* immunogene oder tolerogene DC zu generieren, um so gezielt inflammatorische Effektor-T-Zellen zu induzieren (z.B. in der Tumortherapie) bzw. um regulatorische T-Zellen zu erzeugen (z.B. bei Autoimmunerkrankungen, *Kalantari 2011*). Allerdings ist die Kultur von DC mit einer Reihe von Schwierigkeiten verbunden: Die Generierung aus Vorläuferzellen ist zeitaufwändig und die Erzielung des gewünschten Aktivierungszustands (immunogen vs. tolerogen) ist schwierig in dieser häufig heterogenen Zellpopulation (Gunzer 2011).

Die Verwendung von B-Zellen als APC würde eine Reihe von Vorteilen mit sich bringen. B-Zellen bilden eine im Vergleich zu DC homogene Zellgruppe, sie sind in großer Zahl aus peripherem Blut zu gewinnen. Zudem ist ihre *in vitro*-Kultur vergleichsweise einfach und kostengünstig. In der Tat wurden B-Zellen bereits in zelltherapeutischen Ansätzen als APC eingesetzt, allerdings vor allem unter maximaler Stimulation (mittels CD40-Aktiverung), damit sie als bestmögliche (starke) APC wirken (*Kondo 2009*).

Um die Aktivierung von T-Zellen durch naive B-Zellen genauer zu studieren, kultivierten wir naive B-Zellen, welche ein TCR-kognates Peptid MHC-restringiert präsentierten (hier ein Ovalbumin-Fragment), mit CD4+ T-Zellen. Wir fanden einen aberranten Phänotyp und immunregulatorische Eigenschaften bei den entstehenden T-Zellen und wiesen deren *in vivo*-Relevanz im (tierexperimentellen) Ansatz nach (**App. 14, Reichardt 2007**).

Wir beobachteten, dass es bei dem B-T-Kontakt zur Ausbildung einer reifen, strukturell vollständig ausgebildeten immunologischen Synapse kam. Dies war überraschend, da naive B-Zellen *in vivo* keine wesentliche Rolle bei der Initiierung der T-Zell–Antwort spielen (Epstein 1995). Zwar lagern sich lösliche Antigene (z.B. nach Immunisierung) auch auf B-Zellen an (Byersdorfer 2004), und B-Zellen können in bestimmten Situationen zur T-Zell-Aktivierung *in vivo* beitragen (Crawford 2006). Ferner sind B-Zellen in Abwesenheit anderer APC durchaus in der Lage, CD4+ T-Zellen effizient zu

stimulieren (Rodriguez-Pinto 2005). Allerdings resultiert die Antigen-präsentation durch B-Zellen vielfach nicht in T-Effektoren sondern in T-Zell-Toleranz (Raimondi 2006, Frommer 2008). Offenbar bestehen Besonderheiten in der T-Zell-Aktivierung durch B-Zellen im Vergleich zu DC.
In der Tat wiesen die von uns untersuchten B-Zell-induzierten T-Zellen (TofB) verglichen mit konventionellen (DC-induzierten) Effektor-T-Zellen einen aberranten Phänotyp und funktionelle Besonderheiten auf. Sie zeigten 72 h nach Aktivierung eine hohe Expression von L-Selectin, CD62L, was untypisch für aktivierte Zellen war. Ferner waren die TofB in der Lage, *in vitro* und *in vivo* im Tiermodell eine (ektope Herz-)Transplantatabstoßung zu verhindern (während konventionelle T-Zellen dies nicht taten). Die TofB agierten dabei über direkten Zellkontakt, waren aber Foxp3 negativ. Insofern unterschieden sie sich von bekannten Subtypen regulatorischer Zellen (*Yadav 2013*).
Unsere B-Zell-generierten Tregs bildeten daher eine neue Art induzierter Tregs, die aufgrund ihres Ursprungs eine Reihe von Vorteilen für die therapeutische Anwendung mit sich brachten. Tatsächlich waren B-Zellen bereits genutzt worden, um Mäuse gegen Epitope mit pathophysiologischer Relevanz zu tolerisieren (Lei 2005). Inzwischen werden B-Zellen auch direkt als APC zur Erzeugung von Tregs *in vitro* und *in vivo* verwendet (Sun 2012). Allerdings wurde in diesem Ansatz die immunsuppressorische Wirkung durch Kopplung des Antigens an Choleratoxin B (was die Expression von TGFβ und IL-10 in den B-Zellen induzierte) noch verstärkt.
Tatsächlich gibt es neben der toleranzinduzierenden Wirkung von B-Zellen als APC zahlreiche Hinweise auf indirekte, auf löslichen Faktoren (z.B. IL-10) beruhenden immunsuppressorischen Effekten von B-Zellen (die in diesem Zusammenhang dann auch häufig als regulatorische B-Zellen oder BiRegs bezeichnet werden) bei der Regulation von Autoimmunerkrankungen und der Antwort auf Infektionen (*Mauri 2010*).

Zusammengefasst hob unsere Arbeit zu B-Zell-induzierten Tregs eine Reihe von Besonderheiten beim Priming von CD4-Zellen durch naive B-Zellen hervor und unterstrich damit Eigenschaften von B-Zellen für die Immunantwort, die über die Antikörperproduktion hinausgehen (*Lund 2010*).

Die intrazellulären Signalwege, die mit diesem unerwarteten Phänotyp bei B-Zell-induzierten Tregs verknüpft waren, blieben zunächst unbekannt. Die molekularen Grundlagen zu erhellen gelang uns in einer weiteren Studie (**App. 02, Etemire 2013**).

Wir fanden Hinweise auf eine transiente Erniedrigung des PI3K/Akt/mTOR-Signalwegs in den regulatorischen T-Zellen. PI3-Kinasen (PI3K) (der Klasse IA bzw. IB) werden durch Signale vom TCR und Zytokin-Rezeptoren bzw. Chemokinrezeptoren aktiviert (*Han 2012*). Die PI3K phosphoryliert dann Phosphoinositol-4,5-bisphospat (PIP2) zu PIP3 an der inneren Zellmembran und leitet so eine Signalkaskade ein, welche die Aktivierung der Proteinkinase B (PKB oder auch Akt genannt) einschließt. Akt wird sowohl an Thr308 als auch (zur vollen Aktivierung) an S473 phosphoryliert (*Fayard 2010*). Aktives Akt phosphoryliert dann Substrate (v.a. Transkriptionsfaktoren der FOXO-Familie), fördert deren nukleäre Exclusion und beeinflusst so die Transkription zahlreicher immunologisch wichtiger Gene darunter IL-2 (*Hay 2011*). Gleichzeitig aktiviert Akt den mTOR-Komplex1 (mTORC1). mTOR ist eine Serin/Threonin-Kinase, die in Abhängigkeit vom Energiestatus der Zelle (Insulin, Glucose, ATP, Sauerstoff) in elementare Zellfunktionen wie Wachstum, Proliferation, Überleben und Transkription eingreift. Dabei spielt mTOR auch eine Schlüsselrolle bei Proliferation und Differenzierung von T-Zellen (Chi 2012). Phosphatasen wie PHLPP regulieren den PI3K/Akt-Signalweg negativ indem sie Akt dephosphorylieren (Gao 2005).

Konkret untersuchten wir die Signalmuster bei iTreg-Bildung nach Stimulation mit naiven B-Zellen bzw. mittels unreifer DC im Vergleich mit Effektor-T-Zellen nach Kontakt zu reifen (vollständig costimulierenden) DC. Wir fanden in den so induzierten Tregs (CD4+CD25+Foxp3-) zu frühen Zeitpunkten Signalmuster, die ähnlich zu denen in konventionellen Effektor-T-Zellen waren. Interessanterweise gehörte dazu eine initial effektive Aktivierung der Metalloprotease ADAM-17, die für das Abwerfen (Shedding) des CD62L verantwortlich war. Fehlende Downregulation des CD62L war die augenfälligste phänotypische Besonderheit der B-Zell-induzierten Tregs (TofB, App. 14, Reichardt 2007) gewesen. Wir sahen nun, dass es nach einer Phase effektiv downregulierten CD62L (bis 24 h nach Stimulationsbeginn) in den Tregs (nicht aber in konventionellen Effektor-T-Zellen) zu einer

Reexpression von CD62L kam, die zu der (ähnlich wie in naiven T-Zellen) früher von uns beobachteten hohen Expression zum Zeitpunkt 72 h führte. Parallel dazu beobachteten wir zum Zeitpunkt 24 h eine wesentlich niedrigere Phosphorylierungsrate von Akt-S473 in den Tregs. Dies ließ auf eine erniedrigte Aktivität des PI3K/Akt-Signalwegs zu diesem Zeitpunkt schließen. Weiterführend fanden wir als Ursache für die transiente phospho-Akt-Erniedrigung eine (nur in den Tregs stattfindende) Induktion von PHLPP1, einer Akt-spezifischen Phosphatase. Die iTregs wiesen regulatorische Kapazität *in vitro* und *in vivo* auf, die durch zusätzliche Applikation von costimulatorischen Signalen (CD28-Triggering im *in vitro*-System) aufgehoben wurde.

Unsere Daten zeigten, dass ähnlich zur Induktion von klassischen Foxp3+ Tregs auch für (durch schwache APC wie naive B-Zellen und unreife DC) induzierte Tregs die Intensität der PI3-Kinase-/Akt-Achse wichtig ist. Zudem legen unsere Ergebnisse nahe, dass für die Entwicklung von naiven T-Zellen zu Treg bzw. Effektor-Zellen ein kinetisches Fenster innerhalb der ersten 24 h besteht.

Insgesamt existieren inzwischen zahlreiche Hinweise, dass die Intensität des PI3K-mTOR-Signalings eine zentrale Rolle bei der T-Zell-Differenzierung in verschiedene Subtypen, darunter Tregs, spielt (Miskov-Zivanov 2013). Die genaue Rolle von PI3K-Signalen bei der Induktion von Treg ist jedoch nicht klar. Es gibt Berichte, dass PI3K-Aktivierung die Treg-Entwicklung sowohl hemmen (Littmann 2010) als auch fördern kann (Soond 2012). Unsere Daten könnten helfen, diese Diskrepanz zu erklären, indem sie nahelegen, dass PI3K-vermittelte Signale notwendig sind, dass es aber insbesondere erniedrigte Signalintensität ist, welche die Treg-Induktion begünstigt. In der Tat wurde verminderte Akt-S473-Phosphorylierung in Foxp3+ Tregs auch von anderen Arbeitsgruppe beobachtet (Crellin 2007, Oyang 2012). Mittlerweile hat sich die therapeutische Beeinflussung der PI3K/Akt-Signalings zu einem sehr umfangreichen immuntherapeutischen Feld bei der Bekämpfung von Neoplasien und Autoimmunerkrankungen entwickelt (*Foster 2012*).

6. Ausblick

So wie sich die Immunologie in den letzten Jahren rasant entwickelt hat sind auch zukünftig wesentliche Fortschritte im Verständnis und in der gezielten Anwendung der Immunmodulation zu erwarten. Die Modulation der T-Zell-Aktivierung wird dabei aller Voraussicht nach weiterhin einen elementaren Pfeiler moderner Immuntherapie bilden.

Grundlegendes Prinzip der sich abzeichnenden interventionellen Entwicklungen ist oft die direkte Modulation des an der T-Zelle eingehenden Musters aus TCR- und costimulatorischen Signalen. Eine etablierte Strategie ist dabei die direkte, antikörpervermittelte Blockade der costimulatorischen Rezeptoren CD28 sowie von deren Gegenspielern CTLA-4 (cytotoxic T-lymphocyte antigen-4) und PD-1 (programmed death-1) (*Bour-Jordan 2011, Iannone 2012*). Die wie beschrieben für die Treg-Entwicklung zentrale Achse PI3K/Akt/mTOR wird zum Gegenstand immuntherapeutischer Intervention unter Verwendung von komplett neuen Klassen an mTOR-Inhibitoren (*Bruno 2008, Benjamin 2011*).

Zelltherapeutische Ansätze werden dabei neben löslichen immunmodulierenden Faktoren (small molecule-drugs und biologicals) wahrscheinlich immer wichtiger (*Fischbach 2013*). Ein Schwerpunkt wird weiterhin die Induktion und gezielte Verwendung von regulatorischen T-Zellen sein (*Daniel 2011*). Moderne Methoden werden die Erzeugung, Identifizierung und Gewinnung von T-Zellen mit gewünschter Avidität und Spezifität erleichtern (Weissbrich 2013, Stärck 2013). Andere Ansätze trachten danach, den elementarsten Vorteil aber auch gleichzeitig die umfassendste Limitation des adaptiven Immunsystems, die Antigenspezifität, zu überwinden und antigen-unspezifische immunmodulierende Maßnahmen einzusetzen (*Monjazeb 2013*). Solche Arbeiten bilden bereits eine Brücke zur Anwendung von Komponenten des angeborenen, *per se* antigen-unspezifischen Immunsystems (*van den Boorn 2013*).

Eine vollständig neue Ebene der Modulation des Immunsystems wurde erst in den letzten Jahren deutlich: das Mikrobiom. Der menschliche Organismus teilt sich seinen „individuellen Lebensraum", seinen Körper, mit tausenden weiteren Arten an lebenden Organismen. Unsere Körperzellen sehen sich einer mehr als zehnfachen Menge co-existierender Zellen gegenüber, von Bakterien, Viren, Einzellern und möglichweise anderen Lebensformen. Viele von ihnen sind für unsere Gesundheit unentbehrlich, andere eher abträglich. Die Balance innerhalb dieses gemeinsamen Superorganismus beeinflusst unsere physischen und psychischen Regelkreise und Organfunktionen, darunter unser Immunsystem, offenbar in weit stärkerem Maße als bisher angenommen. Als ein konkretes Beispiel seien mikrobielle Stoffwechsel-produkte wie kurzkettige Fettsäuren genannt, welche die Homöostase intestinaler regulatorischer T-Zellen beeinflussen können (Smith 2013). Wie robust diese Aussagen tatsächlich sind, wird sich erst in Zukunft erweisen. Allerdings wird die Modulation der T-Zell-Aktivität über das Mikrobiom mit Sicherheit zu einem weiteren hochspannendes Feld der Immunbiologie darunter der T-Zell-Immunologie (Brerer 2011, *Strober 2013*).

Bildgebende Verfahren zum molekulare Studium des T-Zell-Signalings und der Synapse werden zunehmend auch die *in vivo*-Situation der T-Zell-Aktivierung besser erfassen können. Derzeit können intravital nur grobe Umrisse der Synapse sowie die räumliche Verteilung einiger weniger Proteine dargestellt werden (Barcia 2006, Azar 2010). Eine genauere Darstellung intakter Synapsen wird mit hochauflösender Mikroskopie, nanoskopischen Verfahren, wie z.B. STED (Stimulated-Emission Depletion) (Willig 2006) oder der Lokalisationsmikroskopie möglich sein (Cremer 2011). Die Verknüpfung dieser hochauflösenden Verfahren mit Intravitalmikroskopie befindet sich jedoch noch in ihren Anfängen (Eggeling 2009, Andresen 2012, Huber 2012).
Es kann erwartet werden, dass die Analyse von molekularen Wechselwirkungen (auch innerhalb der immunologischen Synapse) durch hochauflösende Darstellung bis hinunter zur Betrachtung von Einzelmolekülen im lebenden Organismus neue und faszinierende Einblicke in die Mechanismen der T-Zell-Aktivierung ermöglichen und neue Wege zu deren Modulation aufzeigen wird.

Literaturverzeichnis:

Reviews sind *kursiv* gekennzeichnet.

Aminov RI. Biotic acts of antibiotics. Front Microbiol. 2013 Aug 19;4:241.Review.

Andresen V, Pollok K, Rinnenthal JL, Oehme L, Günther R, Spiecker H, Radbruch H, Gerhard J, Sporbert A, Cseresnyes Z, Hauser AE, Niesner R. High-resolution intravital microscopy. PLoS One. 2012;7(12):e50915.

Arndt B, Mateusz Poltorak, Bhavani S. Kowtharapu, **Peter Reichardt**, Lars Philipsen, Jonathan A. Lindquist, Burkhart Schraven and Luca Simeoni. Analysis of TCR activation kinetics in primary human T cells upon focal or soluble stimulation. J Immunol Meth 2013; 387:276-83

Avota E, Gassert E, Schneider-Schaulies S. Measles virus-induced immunosuppression: from effectors to mechanisms. Med Microbiol Immunol. 2010 Aug;199(3):227-37. Review.

Azar GA, Lemaître F, Robey EA, Bousso P. Subcellular dynamics of T cell immunological synapses and kinapses in lymph nodes. Proc Natl Acad Sci U S A. 2010 Feb 23;107(8):3675-80. doi: 10.1073/pnas.0905901107. Epub 2010 Feb 4.

Baddeley, D. Crossman, D., Rossberger, S., Cheyne, J. E., Montgomery,J. M.,Jayasinghe, I. D., Cremer, C., Cannell, M. B., and Soeller, C. 4D super-resolution microscopy with conventional fluorophores and single wavelength excitation in optically thick cells and tissues. PLoS ONE(2011).6, e20645

Baranzini SE for the International Multiple Sclerosis Genetics Consortium. Collaborators (74). Network-Based Multiple Sclerosis Pathway Analysis with GWAS Data from 15,000 Cases and 30,000 Controls. Am J Hum Genet. 2013;92(6):854-65.

Barcia C, Thomas CE, Curtin JF, King GD, Wawrowsky K, Candolfi M, Xiong WD, Liu C, Kroeger K, Boyer O, Kupiec-Weglinski J, Klatzmann D, Castro MG, Lowenstein PR. *In vivo* mature immunological synapses forming SMACs mediate clearance of virally infected astrocytes from the brain. J Exp Med. 2006;203(9):2095-107

Basu R, Hatton RD, Weaver CT. The Th17 family: flexibility follows function. Immunol Rev. 2013 Mar;252(1):89-103. Review.

Bausch B, Jilg C, Gläsker S, Vortmeyer A, Lützen N, Anton A, Eng C, Neumann HP. Renal cancer in von Hippel-Lindau disease and related syndromes.Nat Rev Nephrol. 2013 Sep;9(9):529-38. Review.

Benjamin D, Colombi M, Moroni C, Hall MN. Rapamycin passes the torch: a new generation of mTOR inhibitors. Nat Rev Drug Discov. 2011;10(11):868-80. Review.

Berer K, Mues M, Koutrolos M, Rasbi ZA, Boziki M, Johner C, Wekerle H, Krishnamoorthy G. Commensal microbiota and myelin autoantigen cooperate to trigger autoimmune demyelination. Nature. 2011 Oct 26;479(7374):538-41.

Berlin-Rufenach C, Otto F, Mathies M, Westermann J, Owen MJ, Hamann A, Hogg N Lymphocyte migration in lymphocyte function-associated antigen (LFA)-1-deficient mice. J Exp Med 189(1999): 1467–1478

Bertoletti A, Sette A, Chisari FV, Penna A, Levrero M, De Carli M, Fiaccadori F, Ferrari C. Natural variants of cytotoxic epitopes are T-cell receptor antagonists for antiviral cytotoxic T cells. Nature. 1994 Jun 2;369(6479):407-10.

Best A, Hoyle A. The evolution of costly acquired immune memory. Ecol Evol. 2013 Jul;3(7):2223-32. Review.

Betzig, E., Patterson, G. H., Sougrat, R., Lindwasser, O. W., Olenych, S.,Bonifacino, J. S., Davidson, M. W., Lippincott-Schwartz, J., and Hess, H. F. (2006) Imaging intracellular fluorescent proteins at nanometer resolution. Science 313, 1642–1645

Bezman, N. A., L. Lian, C. S. Abrams, L. F. Brass, M. L. Kahn, M. S. Jordan,and G. A. Koretzky. 2008. Requirements of SLP76 tyrosines in ITAM and integrin receptor signaling and in platelet function *in vivo*. J. Exp. Med. 205:1775–1788.

Biggs, M. J., Milone, M. C., Santos, L. C., Gondarenko, A., and Wind, S. J. High-resolution imaging of the immunological synapse and T-cell receptor microclustering through microfabricated substrates. J. R. Soc. Interface (2011) 8(63):1462-71

Bour-Jordan H, Esensten JH, Martinez-Llordella M, Penaranda C, Stumpf M, Bluestone JA. Intrinsic and extrinsic control of peripheral T-cell tolerance by costimulatory molecules of the CD28/□B7 family. Immunol Rev. 2011 May;241(1):180-205.

Brinkmann V, Pinschewer DD, Feng L, Chen S.FTY720: altered lymphocyte traffic results in allograft protection. Transplantation. 2001;72:764-769.

Brinkmann V. FTY720 (fingolimod) in Multiple Sclerosis: therapeutic effects in the immune and the central nervous system. Br J Pharmacol. 2009 Nov;158(5):1173-82.

Bromley SK, Burack WR, Johnson KG, Somersalo K, Sims TN, Sumen C, Davis MM, Shaw AS, Allen PM, Dustin ML. The immunological synapse. Annu Rev Immunol. 2001;19:375-96. Review.

Brossard C, Feuillet V, Schmitt A, Randriamampita C, Romao M, Raposo G, Trautmann A.Multifocal structure of the T cell - dendritic cell synapse. Eur J Immunol. 2005 Jun;35(6):1741-53.

Bruno L, Merkenschlager M. Directing T cell differentiation and function with small molecule inhibitors. Cell Cycle. 2008 Aug;7(15):2296-8. Review.

Burbach, B. J., R. Srivastava, R. B. Medeiros, W. E. O'Gorman, E. J. Peterson, and Y. Shimizu. Distinct regulation of integrin-dependent T cell conjugate formation and NF-kB activation by the adapter protein ADAP. J. Immunol. 2008. 181:4840–4851.

Byersdorfer CA, Dipaolo RJ, Petzold SJ, Unanue ER. Following immunization antigen becomes concentrated in a limited number of APCs including B cells. J Immunol. 2004;173(11):6627-34.

Calder PC. Fat chance of immunomodulation. Immunol Today 1998;19:244–247. Review.

Campbell, D. J., C. H. Kim, and E. C. Butcher. 2003. Chemokines in the systemic organization of immunity. Immunol. Rev. 195: 58–71. Review.

Chang C, Mahmood MM, Teuber SS, Gershwin ME. Overview of penicillin allergy. Clin Rev Allergy Immunol. 2012 Aug;43(1-2):84-97. Review.

Charo J, Lindencrona JA, Carlson LM, Hinkula J, Kiessling R. Protective efficacy of a DNA influenza virus vaccine is markedly increased by the coadministration of a Schiff base-forming drug. J Virol. 2004;78(20):11321-6.

Costa J, Magro F, Caldeira D, Alarcão J, Sousa R, Vaz-Carneiro A. Infliximab reduces hospitalizations and surgery interventions in patients with inflammatory bowel disease: a systematic review and meta-analysis. Inflamm Bowel Dis. 2013;19(10):2098-110. Review.

Costello, P. S., Walters, A. E., Mee, P. J., Turner, M., Reynolds, L. F., Prisco, A., Sarner, N., Zamoyska, R., and Tybulewicz, V. L. The Rhofamily GTP exchange factor Vav is a critical transducer of T cell receptor signals to the calcium, ERK, and NF-kappaB pathways. Proc. Natl. Acad. Sci. U.S.A. (1999) 96, 3035–3040

Crawford A, Macleod M, Schumacher T, Corlett L, Gray D. Primary T cell expansion and differentiation *in vivo* requires antigen presentation by B cells. J Immunol. 2006;176(6):3498-506.

Crellin,N.K.,Garcia,R.V.,and Levings,M.K.(2007). Altered activation of AKT is required for the suppressive function of human CD4CCD25C T regulatory cells. Blood 109, 2014–2022.

Cremer C, Kaufmann R, Gunkel M, Pres S, Weiland Y, Müller P, Ruckelshausen T, Lemmer P, Geiger F, Degenhard S, Wege C, Lemmermann NA, Holtappels R, Strickfaden H, Hausmann M. Superresolution imaging of biological nanostructures by spectral precision distance microscopy. Biotechnol J. 2011 Sep;6(9):1037-51.

Czeloth, N., G. Bernhardt, F. Hofmann, H. Genth, and R. Förster. 2005. Sphingosine-1-phosphate mediates migration of mature dendritic cells. J. Immunol. 175: 2960–2967.

Dahlén R, Strid H, Lundgren A, Isaksson S, Raghavan S, Magnusson MK, Simrén M, Sjövall H, Öhman L. Infliximab inhibits activation and effector functions of peripheral blood T cells *in vitro* from patients with clinically active ulcerative colitis. Scand J Immunol. 2013;78(3):275-84.

D'Amato G, Cecchi L, D'Amato M, Liccardi G. Urban air pollution and climate change as environmental risk factors of respiratory allergy: an update. J Investig Allergol Clin Immunol. 2010;20(2):95-102. Review.

Daniel C, von Boehmer H. Extrathymic generation of regulatory T cells-chances and challenges for prevention of autoimmune disease. Adv Immunol. 2011;112:177-213. Review.

Diel, R., B. Hauer, R. Loddenkemper, B. Manger, K. Krüger. Empfehlungen für das Tuberkulosescreening vor Gabe von TNF-α-Inhibitoren bei rheumatischen Erkrankungen. Pneumologie 2009; 63:329–334

Di Sabatino A, Ciccocioppo R, Cinque B, Millimaggi D, Morera R, Ricevuti L, Cifone MG, Corazza GR. Infliximab Defective mucosal T cell death is sustainably reverted by infliximab in a caspase dependent pathway in Crohn's disease. Gut. 2004;53(1):70-7.

Dluzniewska, J., L. Zou, I. R. Harmon, M. T. Ellingson, and E. J. Peterson. Immature hematopoietic cells display selective requirements for adhesion- and degranulation-promoting adaptor protein in development and homeostatsis. Eur. J. Immunol. 2007. 37: 3208–3219.

Dominguez Mdel C, Lorenzo N, Barbera A, Darrasse-Jeze G, Hernández MV, Torres A, Hernández I, Gil R, Klatzmann D, Padrón G. An altered peptide ligand corresponding to a

novel epitope from heat-shock protein 60 induces regulatory T cells and suppresses pathogenic response in an animal model of adjuvant-induced arthritis. Autoimmunity. 2011;44(6):471-82

Durongpisitkul K, Gururaj VJ, Park JM,Martin CF: The prevention of coronary artery aneurysm in Kawasaki disease: a meta-analysis on the efficacy of aspirin and immunoglobulin treatment. Pediatrics 1995; 96: 1057–1061.

Dustin ML. Modular design of immunological synapses and kinapses. Cold Spring Harb Perspect Biol. 2009 Jul;1(1):a002873. Review.

Dustin ML, Chakraborty AK, Shaw AS. Understanding the structure and function of the immunological synapse. Cold Spring Harb Perspect Biol. 2010 Oct;2(10):a002311. Review.

Eggeling C, Ringemann C, Medda R, Schwarzmann G, Sandhoff K, Polyakova S, Belov VN, Hein B, von Middendorff C, Schönle A, Hell SW. Direct observation of the nanoscale dynamics of membrane lipids in a living cell. Nature. 2009 Feb 26;457(7233):1159-62.

Engelmann S, Togni M, Thielitz A, **Reichardt P**, Kliche S, Reinhold D, Schraven B, Reinhold A. T Cell-Independent Modulation of Experimental Autoimmune Encephalomyelitis in ADAP-Deficient Mice. J Immunol. 2013;191(10):4950-9.

Epstein MM, Di Rosa F, Jankovic D, Sher A, Matzinger P. Successful T cell priming in B cell-deficient mice.J Exp Med. 1995 Oct 1;182(4):915-22.

Erlebacher A. Mechanisms of T cell tolerance towards the allogeneic fetus. Nat Rev Immunol. 2013 Jan;13(1):23-33. Review.

Ernerudh J, Berg G, Mjösberg J. Regulatory T helper cells in pregnancy and their roles in systemic versus local immune tolerance.Am J Reprod Immunol. 2011 Jul;66 Suppl 1:31-43. Review.

ESPGAN Committee on Nutrition. Comment on the composition of cow's milk based follow-up formulas. Acta Paediatr Scand 1990;79:250–254.

Etemire E, Krull M , Hasenberg M, **Reichardt P** and M Gunzer. Transiently reduced PI3K/Akt activity drives the development of regulatory function in antigen-stimulated naïve T-cells. PLOS One Jul 11;8(7):e68378.

Evavold, B. D., and P. M. Allen. 1991. Separation of IL-4 production from Th cell proliferation by an altered T cell receptor ligand. Science 252: 1308–1310.

Faroudi M, Zaru R, Paulet P, Mu¨ ller S, Valitutti S. Cutting edge: T lymphocyte activation by repeated immunological synapse formation and intermittent signaling. J Immunol 2003;171:1128–1132.

Fayard,E.,Xue,G.,Parcellier,A.,Bozulic,L.,and Hemmings,B.A. ProteinkinaseB(PKB/Akt), a key mediator of the PI3K signaling pathway. Curr. Top. Microbiol. Immunol. (2010). 346, 31–56. Review.

Fischbach MA, Bluestone JA, Lim WA. Cell-based therapeutics: the next pillar of medicine. Sci Transl Med. 2013;5(179):179ps7. Review.

Foley JF, Singh SP, Cantu M, Chen L, Zhang HH, Farber JM. Differentiation of human T cells alters their repertoire of G protein alpha-subunits. J Biol Chem. 2010 Nov 12;285(46):35537-50.

Fooksman, D. R., Vardhana, S., Vasiliver-Shamis, G., Liese, J., Blair, D. A., Waite, J., Sacristan, C., Victora, G. D., Zanin-Zhorov, A., and Dustin, M. L. (2010) Functional anatomy of T cell activation and synapse formation. Annu. Rev. Immunol. 28, 79–105 Review.

Forni D, Cagliani R, Pozzoli U, Colleoni M, Riva S, Biasin M, Filippi G, De Gioia L, Gnudi F, Comi GP, Bresolin N, Clerici M, Sironi M. A 175 million year history of T cell regulatory molecules reveals widespread selection, with adaptive evolution of disease alleles. Immunity. 2013 Jun 27;38(6):1129-41. Review.

Foster JG, Blunt MD, Carter E, Ward SG. Inhibition of PI3K signaling spurs new therapeutic opportunities in inflammatory/autoimmune diseases and hematological malignancies. Pharmacol Rev. 2012 Oct;64(4):1027-54. Review.

Friedl P, Bröcker EB. TCR triggering on the move: diversity of T-cell interactions with antigen-presenting cells. Immunol Rev. 2002 Aug;186:83-9. Review.

Frommer F, Heinen TJ, Wunderlich FT, Yogev N, Buch T, Roers A, Bettelli E, Müller W, Anderton SM, Waisman A. Tolerance without clonal expansion: self-antigen-expressing B cells program self-reactive T cells for future deletion. J Immunol. 2008;181(8):5748-59.

Gao T, Furnari F, Newton AC. PHLPP: a phosphatase that directly dephosphorylates Akt, promotes apoptosis, and suppresses tumor growth. Mol Cell. 2005 Apr 1;18(1):13-24.

Greer FR, Sicherer SH, Burks AW; American Academy of Pediatrics Committee on Nutrition; American Academy of Pediatrics Section on Allergy and Immunology. Effects of early nutritional interventions on the development of atopic disease in infants and children: the role of maternal dietary restriction, breastfeeding, timing of introduction of complementary foods, and hydrolyzed formulas. Pediatrics. 2008;121(1):183-91. Review.

Grigorova IL, Schwab SR, Phan TG, Pham TH, Okada T, Cyster JG. Cortical sinus probing, S1P1-dependent entry and flowbased capture of egressing T cells. Nat Immunol (2009) 10: 58–65

Gunzer M, Janich S, Varga G, Grabbe S. Dendritic cells and tumor immunity. Semin Immunol. 2001;13:291-302. Review.

Gunzer M, Schäfer A, Borgmann S, Grabbe S, Zänker KS, Bröcker EB, Kämpgen E, Friedl P. Antigen presentation in extracellular matrix: interactions of T cells with dendritic cells are dynamic, short lived, and sequential. Immunity. 2000 Sep;13(3):323-32.

Gurk-Turner,C.,Manitpisitkul,W., and Cooper,M. Acomprehensive review of everolimus clinical reports: a new mammalian target of rapamycin inhibitor. Transplantation 2012: 94, 659–668. Review.

Hagness M, Henjum K, Landskron J, Brudvik KW, Bjørnbeth BA, Foss A, Taskén K, Aandahl EM. Kinetics and activation requirements of contact-dependent immune suppression by human regulatory T cells. J Immunol. 2012;188(11):5459-66.

Hamann A, Jablonski-Westrich D, Duijvestijn A, Butcher EC, Baisch H, Harder R, Thiele HGEvidence for an accessory role of LFA-1 in lymphocyte-high endothelium interaction during homing. J Immunol 1988;140: 693–699

Han, S.C.; Kang, G.J.; Ko, Y.J.; Kang, H.K.; Moon, S.W.; Ann, Y.S.; Yoo, E.S. Fermented fish oil suppresses T helper 1/2 cell response in a mouse model of atopic dermatitis via generation of CD4+CD25+Foxp3+ T cells. BMC Immunol. 2012, 13, 4

Han JM, Patterson SJ, Levings MK. The Role of the PI3K Signaling Pathway in CD4(+) T Cell Differentiation and Function. Front Immunol. 2012 Aug 13;3:245. Review.

Hao N, Whitelaw ML. The emerging roles of AhR in physiology and immunity. Biochem Pharmacol. 2013; 86(5):561-70.

Hay,N Interplay between FOXO, TOR, and Akt. Biochim.Biophys.Acta. 2011; 1813, 1965 -1970.

Henrickson SE, Mempel TR, Mazo IB, Liu B, Artyomov MN, Zheng H, Peixoto A, Flynn MP, Senman B, Junt T, Wong HC, Chakraborty AK, von Andrian UH. T cell sensing of antigen dose governs interactive behavior with dendritic cells and sets a threshold for T cell activation. Nat Immunol. 2008 Mar;9(3):282-91.

Hernandez-Trujillo V. New Genetic Discoveries and Primary Immune Deficiencies. Clin Rev Allergy Immunol. 2013 Jul 17. Review.

Herroeder S, **Reichardt P**, Sassmann A, Zimmermann B, Hogg N, Hollmann MW, Fischer KD, Vogt S, Grosse R, Gunzer M, Offermanns S, Wettschureck N. G-proteins of the G12/G13 family shape immune functions by controlling CD4+ T-cell adhesiveness. Immunity 2009;30:708-20.

Horn J, Wang X, **Reichardt P**, Stradal TE, Warnecke N, Simeoni L, Gunzer M, Yablonski D, Schraven B, Kliche S. Src homology 2-domain containing leukocyte-specific phosphoprotein of 76 kDa is mandatory for TCR-mediated inside-out signaling, but dispensable for CXCR4-mediated LFA-1 activation, adhesion, and migration of T cells. J Immunol. 2009;183(9):5756-67.

Hsu T. Complex cellular functions of the von Hippel-Lindau tumor suppressor gene: insights from model organisms. Oncogene. 2012 May 3;31(18):2247-57. Review.

Huber O, Brunner A, Maier P, Kaufmann R, Couraud PO, Cremer C, Fricker G. Localization microscopy (SPDM) reveals clustered formations of P-glycoprotein in a human blood-brain barrier model. PLoS One. 2012;7(9):e44776.

Hünig T. The storm has cleared: lessons from the CD28 superagonist TGN1412 trial. Nat Rev Immunol. 2012;12(5):317-8. Review.

Iannone F, Lapadula G. The inhibitor of costimulation of T cells: abatacept. J Rheumatol Suppl. 2012l;89:100-2. Review.

Iezzi G, Karjalainen K, Lanzavecchia A. The duration of antigenic stimulation determines the fate of naive and effector T cells. Immunity 1998;8:89–95.

Jaakkola MS, Quansah R, Hugg TT, Heikkinen SA, Jaakkola JJ. Association of indoor dampness and molds with rhinitis risk: A systematic review and meta-analysis. J Allergy Clin Immunol. 2013;132(5):1099-1110.e18.

Jamieson N, Singh-Grewal D. Kawasaki Disease: A Clinician's Update. Int J Pediatr. 2013;2013:645391. Review.

Jin B, Sun T, Yu XH, Yang YX, Yeo AE. The effects of TLR activation on T-cell development and differentiation. Clin Dev Immunol. 2012;2012:836485. Review.

Jones DS, **Reichardt P**, Ford ML, Edwards LJ, Evavold BD. TCR antagonism by peptide requires high TCR expression. J Immunol. 2008;181:1760-6.

Josefowicz SZ, Lu LF, Rudensky AY. Regulatory T cells: mechanisms of differentiation and function. Annu Rev Immunol. 2012;30:531-64. Review.

Kalantari T, Kamali-Sarvestani E, Ciric B, Karimi MH, Kalantari M, Faridar A, Xu H, Rostami A. Generation of immunogenic and tolerogenic clinical-grade dendritic cells. Immunol Res. 2011 Dec;51(2-3):153-60. Review.

Karmaus W, Ziyab AH, Everson T, Holloway JW. Epigenetic mechanisms and models in the origins of asthma. Curr Opin Allergy Clin Immunol. 2013 Feb;13(1):63-9. Review.

Kato H, Sugimura T, Akagi T, Sato N, Hashino K, Maeno Y, Kazue T, Eto G, Yamakawa R: Long term consequences of Kawasaki disease. A 10-21 year follow-up study of 594 patients. Circulation 1996; 94: 1379–1385.

Kelly BT, Tam JS, Verbsky JW, Routes JM. Screening for severe combined immunodeficiency in neonates. Clin Epidemiol. 2013 Sep 16;5:363-369. Review.

Keystone EC. Does anti-tumor necrosis factor-α therapy affect risk of serious infection and cancer in patients with rheumatoid arthritis?- a review of longterm data. J Rheumatol. 2011 Aug;38(8):1552-62.

Kim W, Khan NA, McMurray DN, Prior IA, Wang N, Chapkin RS. Regulatory activity of polyunsaturated fatty acids in T-cell signaling. Prog Lipid Res. 2010 Jul;49(3):250-61.

Kinashi, T. 2005. Intracellular signalling controlling integrin activation in lymphocytes. Nat. Rev. Immunol. 5: 546–559. Review.

Kleinewietfeld M, Hafler DA. The plasticity of human Treg and Th17 cells and its role in autoimmunity. Semin Immunol. 2013 S1044-5323(13)00090-0. Review.

Klemens CM, Berman DR, Mozurkewich EL. The effect of perinatal omega-3 fatty acid supplementation on inflammatory markers and allergic diseases: a systematic review. BJOG. 2011 Jul;118(8):916-25. Review.

Kliche S, Worbs T, Wang X, Degen J, Patzak I, Meineke B, Togni M, Moser M, Reinhold A, Kiefer F, Freund C, Förster R, Schraven B. CCR7-mediated LFA-1 functions in T cells are regulated by 2 independent ADAP/SKAP55 modules. Blood. 2012 Jan 19;119(3):777-85.

König S, Probst-Kepper M, Reinl T, Jeron A, Huehn J, Schraven B, Jänsch L. First insight into the kinome of human regulatory T cells. PLoS One. 2012;7(7):e40896.

Kondo E, Gryschok L, Klein-Gonzalez N, Rademacher S, Weihrauch MR, Liebig T, Shimabukuro-Vornhagen A, Kochanek M, Draube A, von Bergwelt-Baildon MS. CD40-activated B cells can be generated in high number and purity in cancer patients: analysis of immunogenicity and homing potential. Clin Exp Immunol. 2009 Feb;155(2):249-56

Kumar H, Kawai T, Akira S. Pathogen recognition by the innate immune system. Int Rev Immunol. 2011 Feb;30(1):16-34. Review.

Kusmartsev S, Eruslanov E, Kübler H, Tseng T, Sakai Y, Su Z, Kaliberov S, Heiser A, Rosser C, Dahm P, Siemann D, Vieweg J. Oxidative stress regulates expression of VEGFR1 in myeloid cells: link to tumor-induced immune suppression in renal cell carcinoma. J Immunol. 2008 Jul 1;181(1):346-53.

Larson RP, Shafiani S, Urdahl KB. Foxp3(+) regulatory T cells in tuberculosis.Adv Exp Med Biol. 2013;783:165-80. Review.

Lau S. What is new in the prevention of atopy and asthma? Curr Opin Allergy Clin Immunol. 2013 Apr;13(2):181-6.

Lei TC, Scott DW. Induction of tolerance to factor VIII inhibitors by gene therapy with immunodominant A2 and C2 domains presented by B cells as Ig fusion proteins. Blood. 2005;105: 4865-4870.

Lee KW, Chow KM, Chan NP, Lo AO, Szeto CC. Piperacillin/tazobactam Induced Myelosuppression. J Clin Med Res. 2009 Apr;1(1):53-5.

Leermakers ET, Sonnenschein-van der Voort AM, Heppe DH, de Jongste JC, Moll HA, Franco OH, Hofman A, Jaddoe VW, Duijts L. Maternal fish consumption during pregnancy and risks of wheezing and eczema in childhood: the Generation R Study. Eur J Clin Nutr. 2013 Apr;67(4):353-9.

Li H, Llera A, Malchiodi AE, Mariuzza RA. The structural basis of T cell activation by superantigens. Ann Rev Immunol 1999;17:435–466.

Lin CY, Lin CC,Hwang B, Chiang BN: Cytokines predict coronary aneurysm formation in Kawasaki disease patients. Eur J Pediatr 1993; 152: 309–312.

Lin J, Weiss A. T cell receptor signalling. J Cell Sci. 2001 Jan;114(Pt 2):243-4. Review.

Lin YC, Chang LY, Huang CT, Peng HM, Dutta A, Chen TC, Yeh CT, Lin CY. Effector/memory but not naive regulatory T cells are responsible for the loss of concomitant tumor immunity. J Immunol. 2009 May 15;182(10):6095-104.

Littman DR, Rudensky AY (2010) Th17 and regulatory T cells in mediating and restraining inflammation. Cell 140: 845–858.Review.

Lund FE, Randall TD. Effector and regulatory B cells: modulators of CD4+ T cell immunity. Nat Rev Immunol. 2010 Apr;10(4):236-47.

MAK Collection 2013. The MAK Collection for Occupational Health and Safety. http://onlinelibrary.wiley.com/book/10.1002/3527600418/topics

Magombedze G, Reddy PB, Eda S, Ganusov VV. Cellular and population plasticity of helper CD4(+) T cell responses. Front Physiol. 2013;4:206.

Maldonado RA, Soriano MA, Perdomo LC, Sigrist K, Irvine DJ, Decker T, Glimcher LH. Control of T helper cell differentiation through cytokine receptor inclusion in the immunological synapse. J Exp Med. 2009;206(4):877-92.

Marrack P, Kappler J: The staphylococcal enterotoxins and their relatives. Science 1990; 248: 705–711.Review.

Martini H, Enright V, Perro M, Workman S, Birmelin J, Giorda E, Quinti I, Lougaris V, Baronio M, Warnatz K, Grimbacher B. Importance of B cell co-stimulation in CD4(+) T cell differentiation: X-linked agammaglobulinaemia, a human model. Clin Exp Immunol. 2011 Jun;164(3):381-7.

Mauri C, Blair PA. Regulatory B cells in autoimmunity: developments and controversies. Nat Rev Rheumatol. 2010;6(11):636-43.

McMurchy AN, Levings MK. In vitro generation of human T regulatory cells: generation, culture, and analysis of FOXP3-transduced T cells. Methods Mol Biol. 2013;946:115-32. Review.

Mendell MJ. Indoor residential chemical emissions as risk factors for respiratory and allergic effects in children: a review. Indoor Air. 2007;17(4):259-77.

Miller MJ, Hejazi AS, Wei SH, Cahalan MD, Parker I. T cell repertoire scanning is promoted by dynamic dendritic cell behavior and random T cell motility in the lymph node.Proc Natl Acad Sci U S A. 2004;101(4):998-1003.

Miskov-Zivanov N, Turner MS, Kane LP, Morel PA, Faeder JR. The duration of T cell stimulation is a critical determinant of cell fate and plasticity. Sci Signal. 2013;6(300):ra97.

Mitoma H, Horiuchi T, Hatta N, Tsukamoto H, Harashima S, Kikuchi Y, Otsuka J, Okamura S, Fujita S, Harada M. Infliximab induces potent anti-inflammatory responses by outside-to-inside signals through transmembrane TNF-alpha. Gastroenterology. 2005;128(2):376-92.

Monjazeb AM, Zamora AE, Grossenbacher SK, Mirsoian A, Sckisel GD, Murphy WJ. Immunoediting and antigen loss: overcoming the achilles heel of immunotherapy with antigen non-specific therapies. Front Oncol. 2013;3:197. Review.

Monk JM, Hou TY, Turk HF, McMurray DN, Chapkin RS. n3 PUFAs reduce mouse CD4+ T-cell ex vivo polarization into Th17 cells. J Nutr. 2013;143(9):1501-8.

Mor F, Cohen IR. Beta-lactam antibiotics modulate T-cell functions and gene expression via covalent binding to cellular albumin. Proc Natl Acad Sci U S A. 2013;110(8):2981-6.

Moreau HD, Lemaître F, Terriac E, Azar G, Piel M, Lennon-Dumenil AM, Bousso P. Dynamic in situ cytometry uncovers T cell receptor signaling during immunological synapses and kinapses *in vivo*. Immunity. 2012;37(2):351-63.

Mori M, Imagawa T, Hara R, Kikuchi M, Hara T, Nozawa T, Miyamae T, Yokota S. Efficacy and limitation of infliximab treatment for children with Kawasaki disease intractable to intravenous immunoglobulin therapy: report of an open-label case series. J Rheumatol. 2012;39(4):864-7.

Mosmann TR, Cherwinski H, Bond MW, Giedlin MA, Coffman RL. Two types of murine helper T cell clone. I. Definition according to profiles of lymphokine activities and secreted proteins. J Immunol. 1986;136(7):2348-57.

Nakahama T, Hanieh H, Nguyen NT, Chinen I, Ripley B, Millrine D, Lee S, Nyati KK, Dubey PK, Chowdhury K, Kawahara Y, Kishimoto T. Aryl hydrocarbon receptor-mediated induction of the microRNA-132/212 cluster promotes interleukin-17-producing T-helper cell differentiation. Proc Natl Acad Sci U S A. 2013;110(29):11964-9.

Natividad MF, Torres-Villanueva CA, Saloma CP. Superantigen involvement and susceptibility factors in Kawasaki disease: profiles of TCR Vβ2+ T cells and HLA-DRB1, TNF-α and ITPKC genes among Filipino patients. Int J Mol Epidemiol Genet. 2013;4(1):70-6.

Neumann HPH, Wiestler OD. Clustering of features of von Hippel-Lindau syndrome: evidence for a complex genetic locus. Lancet 1991;337:1052–4.

Nguyen DH, Hurtado-Ziola N, Gagneux P, Varki A Loss of Siglec expression on T lymphocytes during human evolution. Proc Natl Acad Sci U S A 2006;103: 7765–7770.

Nhim C, Delluc S, Halgand F, de Chaisemartin L, Weaver RJ, Claude N, Joseph D, Maillère B, Pallardy M. Identification and frequency of circulating CD4(+) T lymphocytes specific to Benzylpenicillin in healthy donors. Allergy. 2013;68(7):899-905.

Nika K., C. Soldani, M. Salek,W. Paster, A. Gray, R. Etzensperger, L. Fugger, P. Polzella, V. Cerundolo, O. Dushek, T. Höfer, A. Viola, O. Acuto, Constitutively active Lck kinase in T cells drives antigen receptor signal transduction. Immunity 2010;32, 766–777

Ocaña-Morgner C, Götz A, Wahren C, Jessberger R. SWAP-70 restricts spontaneous maturation of dendritic cells. J Immunol. 2013;190(11):5545-58.

Ocaña-Morgner C, **Reichardt P**, Chopin M, Braungart S, Wahren C, Gunzer M, Jessberger R. Sphingosine 1-Phosphate-Induced Motility and Endocytosis of Dendritic Cells Is Regulated by SWAP-70 through RhoA. J Immunol. 2011;186(9):5345-55.

Ohtsuka Y, Yamashiro Y, Shimizu T, Nagata S, Igarashi J, Shinohara K et al. Reducing cell membrane n-6 fatty acids attenuates mucosal damage in food-sensitive enteropathy in mice. Pediatr Res 1997;42:835–839.

Onouchi Y. Genetics of Kawasaki disease: what we know and don't know.Circ J. 2012;76(7):1581-6. Review.

Ouyang W, Liao W, Luo CT, Yin N, Huse M, et al. Novel Foxo1-dependent transcriptional programs control T(reg) cell function. Nature 2012;491:554–559.

Pham TH, Okada T, Matloubian M, Lo CG, Cyster JG (2008) S1P1 receptor signaling overrides retention mediated by G alpha i-coupled receptors to promote T cell egress. Immunity 28:122–133

Philipsen L, Engels T, Schilling K, Gurbiel S, Fischer KD, Tedford K, Schraven B, Gunzer M, **Reichardt P**. Multimolecular analysis of stable immunological synapses reveals sustained recruitment and sequential assembly of signaling clusters. Mol Cell Proteomics. 2013;12(9):2551-67.

Pinna GS, Kafetzis DA, Tselkas OI, Skevaki CL. Kawasaki disease: an overview. Curr Opin Infect Dis. 2008;21(3):263-70. Review.

Podgrabinska S, Kamalu O, Mayer L, Shimaoka M, Snoeck H, Randolph GJ, Skobe M (2009) Inflamed lymphatic endothelium suppresses dendritic cell maturation and function via Mac-1/ICAM-1-dependent mechanism. J Immunol 183: 1767–1779

Prescott SL, Clifton V. Asthma and pr egnancy: emerging evidence of epigenetic interactions in utero. Curr Opin Allergy Clin Immunol. 2009;9(5):417-26. Review.

Pumford NR, Halmes NC. Protein targets of xenobiotic reactive intermediates. Annu Rev Pharmacol Toxicol. 1997;37:91-117. Review.

Rahma OE, Ashtar E, Ibrahim R, Toubaji A, Gause B, Herrin VE, Linehan WM, Steinberg SM, Grollman F, Grimes G, Bernstein SA, Berzofsky JA, Khleif SN. A pilot clinical trial testing mutant von Hippel-Lindau peptide as a novel immune therapy in metastatic renal cell carcinoma. J Transl Med. 2010;8:8.

Raimondi G, Zanoni I, Citterio S, Ricciardi-Castagnoli P, Granucci F. Induction of peripheral T cell tolerance by antigen-presenting B cells. I. Relevance of antigen presentation persistence. J Immunol. 2006;176(7):4012-20.

Reichardt, P, W. Handrick, A. Linke, R. Schille, W. Kiess. Leukocytopenia, thrombocytopenia and fever related to piperacillin/tazobactam treatment - a retrospective analysis in 38 children with cystic fibrosis. Infection.1999;27:355-6

Reichardt P, Apel TW, Domula M, Tröbs RB, Krause I, Bierbach U, Neumann HP, Kiess W. J Recurrent polytopic chromaffin paragangliomas in a 9-year-old boy resulting from a novel germline mutation in the von Hippel-Lindau gene. J Pediatr Hematol Oncol. 2002c ;24:145-8.

Reichardt, P; Dähnert, I.; Tiller, G.; Häusler, H.-J. Possible activation of an intra-myocardial inflammatory process (S. aureus) after treatment with infliximab in a boy with Crohn's disease.European Journal of Pediatrics. 2002b;161:281-3.

***Reichardt P**, Dornbach B, Gunzer M. APC, T cells and the immune synapse. Curr Top Microbiol Immunol 2010; 340:229-49. Review.*

***Reichardt P**, Dornbach B, Gunzer M. The molecular makeup and function of regulatory and effector synapses. Immunol Rev. 2007c;218:165-77. Review.*

Reichardt P, Dornbach B, Rong S, Beissert S, Gueler F, Loser K, Gunzer M. Naive B-cells generate regulatory T-cells in the presence of a mature immunologic synapse. Blood. 2007;110:1519-1529.

***Reichardt P**, Gunzer F, Gunzer M. Analyzing the physicodynamics of immune cells in a three-dimensional collagen matrix. Methods Mol Biol. 2007b;380:253-69. Review.*

***Reichardt P**, Gunzer M. The biophysics of T lymphocyte activation in vitro and in vivo. Results Probl Cell Differ. 2006;43:199-218. Review.*

***Reichardt P**, Hämmerling G, Gunzer M. Imaging Immunity. Eur J Immunol. 2009;39:3279-82. Review as Congress report*

Reichardt P, Lehmann I, Sierig G, Borte M. Analysis of T-cell receptor V-beta 2 in peripheral blood lymphocytes as a diagnostic marker for Kawasaki disease. Infection. 2002;30:360-4.

Reichardt P, Müller D, Posselt U, Vorberg B, Diez U, Schlink U, Reuter W, Borte M. Fatty acids in colostrum from mothers of children at high risk of atopy in relation to clinical and laboratory signs of allergy in the first year of life. Allergy. 2004 Apr;59(4):394-400.

Reichardt P.*, Patzak I.*, Jones K., Etemire E., Gunzer M., Hogg N. A role for LFA-1 in delaying T lymphocyte egress from lymph nodes. EMBO J. 2013;32(6):829-43.

Reichardt P, Schreiber A, Wichmann G, Metzner G, Efer J, Raabe F. Identification and quantification of *in vitro* adduct formation between protein reactive xenobiotics and a lysine-containing model peptide. Environ Toxicol. 2003;18:29-36.

Rhodes J. Evidence for an intercellular covalent reaction essential in antigen-specific T cell activation. J Immunol. 1989 Sep 1;143(5):1482-9.

Rhodes J, Chen H, Hall SR, Beesley JE, Jenkins DC, Collins P, Zheng B. Therapeutic potentiation of the immune system by costimulatory Schiff-base-forming drugs. Nature. 1995;377(6544):71-5.

Richard S, Gardie B, Couvé S, Gad S. Von Hippel-Lindau: how a rare disease illuminates cancer biology. Semin Cancer Biol. 2013;23(1):26-37. Review.

Rockett BD, Melton M, Harris M, Bridges LC, Shaikh SR. Fish oil disrupts MHC class II lateral organization on the B-cell side of the immunological synapse independent of B-T cell adhesion. J Nutr Biochem. 2013;24(11):1810-6

Rodríguez-Pinto D, Moreno J. B cells can prime naive CD4+ T cells *in vivo* in the absence of other professional antigen-presenting cells in a CD154-CD40-dependent manner. Eur J Immunol. 2005;35(4):1097-105.

Rosen, H., and E. J. Goetzl. 2005. Sphingosine 1-phosphate and its receptors: an autocrine and paracrine network. Nat. Rev. Immunol. 5: 560–570. Review.

Rotroff DM, Wetmore BA, Dix DJ, Ferguson SS, Clewell HJ, Houck KA, Lecluyse EL, Andersen ME, Judson RS, Smith CM, Sochaski MA, Kavlock RJ, Boellmann F, Martin MT, Reif DM, Wambaugh JF, Thomas RS. Incorporating human dosimetry and exposure into high-throughput *in vitro* toxicity screening. Toxicol Sci. 2010;117(2):348-58.

Rousu T, Pelkonen O, Tolonen A. Rapid detection and characterization of reactive drug metabolites *in vitro* using several isotope-labeled trapping agents and ultra-performance liquid chromatography/time-of-flight mass spectrometry. Rapid Commun Mass Spectrom. 2009;23(6):843-55.

Rudolph TK, Freeman BA. Transduction of redox signaling by electrophile-protein reactions. Sci Signal. 2009;2(90):re7.

Sala-Vila A, Miles EA, Calder PC. Fatty acid composition abnormalities in atopic disease: evidence explored and role in the disease process examined. Clin Exp Allergy. 2008;38(9):1432-50. Review.

Sausenthaler S, Heinrich J, Koletzko S; GINIplus and LISAplus Study Groups. Early diet and the risk of allergy: what can we learn from the prospective birth cohort studies GINIplus and LISAplus? Am J Clin Nutr. 2011;94(6 Suppl):2012S-2017S. Review.

Scheetz MH, McKoy JM, Parada JP, Djulbegovic B, Raisch DW, Yarnold PR, Zagory J. et al. Systematic review of piperacillin-induced neutropenia. Drug Saf. 2007;30(4):295–306. Review.

Schmidt A, Oberle M, EM Weiß, D Vobis, S Frischbutter, R Baumgrass, CS Falk, M Haag, B Brügger, H Lin, GW Mayr, **P Reichardt**, M Gunzer, E Suri-Payer and PH Krammer. Human regulatory T cells rapidly suppress T cel receptor-induced Ca2+s, NF-κB and NFAT signaling in conventional T cells. Sci Sign 2011;4(204):ra90.

Shinohara M, Terada Y, Iwamatsu A, Shinohara A, Mochizuki N, Higuchi M, Gotoh Y, Ihara S, Nagata S, Itoh H, Fukui Y, Jessberger R. SWAP-70 is a guanine-nucleotide-exchange factor that mediates signalling of membrane ruffling. Nature. 2002;416(6882):759-63.

Shah YM, Ito S, Morimura K, Chen C, Yim SH, Haase VH, Gonzalez FJ. Hypoxia-inducible factor augments experimental colitis through an MIF-dependent inflammatory signaling cascade. Gastroenterology. 2008;134(7):2036-48, 2048.e1-3.

Shevach EM. Mechanisms of foxp3+ T regulatory cell-mediated suppression. Immunity. 2009;30(5):636-45. Review.

Sinha RK, Park C, Hwang IY, Davis MD, Kehrl JH. B lymphocytes exit lymph nodes through cortical lymphatic sinusoids by a mechanism independent of sphingosine-1-phosphate-mediated chemotaxis. Immunity. 2009;30: 434–446

Smith PM, Howitt MR, Panikov N, Michaud M, Gallini CA, Bohlooly-Y M, Glickman JN, Garrett WS. The microbial metabolites, short-chain fatty acids, regulate colonic Treg cell homeostasis. Science. 2013;341(6145):569-73.

Smith-Garvin, J. E., Koretzky, G. A., and Jordan, M. S. T cell activation. Annu. Rev. Immunol. 2009; 27, 591–619. Review.

Soares H, Lasserre R, Alcover A. Orchestrating cytoskeleton and intracellular vesicle traffic to build functional immunological synapses. Immunol Rev. 2013;256(1):118-32. Review

Soond DR, Slack EC, Garden OA, Patton DT, Okkenhaug K Does the PI3K pathway promote or antagonize regulatory T cell development and function? Front Immunol 2012;3: 244. Review.

Soto-Ramírez N, Karmaus W, Zhang H, Liu J, Billings D, Gangur V, Amrol D, da Costa KA, Davis S, Goetzl L. Fatty acids in breast milk associated with asthma-like symptoms and atopy in infancy: a longitudinal study. J Asthma. 2012;49(9):926-34.

Stärck L, Popp K, Pircher H, Uckert W. Immunotherapy with TCR-Redirected T Cells: Comparison of TCR-Transduced and TCR-Engineered Hematopoietic Stem Cell-Derived T Cells. J Immunol. 2013 Nov 29. [Epub ahead of print]

Stirnweiss A, Hartig R, Gieseler S, Lindquist JA, **Reichardt P**, Philipsen L, Simeoni L, Poltorak M, Merten C, Zuschratter W, Prokazov Y, Paster W, Stockinger H, Harder T, Gunzer M, Schraven B. T cell activation results in conformational changes in the Src family kinase Lck to induce its activation. Sci Signal. 2013;6(263):ra13.

Stranger BE, De Jager PL. Coordinating GWAS results with gene expression in a systems immunologic paradigm in autoimmunity. Curr Opin Immunol. 2012;24(5):544-51. Review.

Strober W. Impact of the gut microbiome on mucosal inflammation. Trends Immunol. 2013;34(9):423-30.

Sumoza-Toledo A, Eaton AD, Sarukhan A. Regulatory T cells inhibit protein kinase C theta recruitment to the immune synapse of naive T cells with the same antigen specificity. J Immunol. 2006;176(10):5779-87.

Sun JB, Czerkinsky C, Holmgren J. B lymphocytes treated *in vitro* with antigen coupled to cholera toxin B subunit induce antigen-specific Foxp3(+) regulatory T cells and protect against experimental autoimmune encephalomyelitis. J Immunol. 2012;188(4):1686-97.

Suntharalingam G, Perry MR, Ward S, Brett SJ, Castello-Cortes A, et al. Cytokine storm in a phase 1 trial of the anti-CD28 monoclonal antibody TGN1412. N Engl J Med. 2006;355: 1018–1028.

Szefler SJ, Wenzel S, Brown R, Erzurum SC, Fahy JV, Hamilton RG, Hunt JF, Kita H, Liu AH, Panettieri RA Jr, Schleimer RP, Minnicozzi M. Asthma outcomes: biomarkers. J Allergy Clin Immunol. 2012;129(3 Suppl):S9-23. Review.

Tambralli A, Beukelman T, Weiser P, Atkinson TP, Cron RQ, Stoll ML. High doses of infliximab in the management of juvenile idiopathic arthritis. J Rheumatol. 2013;40(10):1749-55.

Tacke M, Hanke G, Hanke T, Hunig T (1997) CD28-mediated induction of proliferation in resting T cells *in vitro* and *in vivo* without engagement of the T cell receptor: evidence for functionally distinct forms of CD28. Eur J Immunol 27: 239–247.

Tang Q, Bluestone JA. Regulatory T-cell therapy in transplantation: moving to the clinic. Cold Spring Harb Perspect Med. 2013;3(11).

Teles A, Schumacher A, Kühnle MC, Linzke N, Thuere C, **Reichardt P**, Tadokoro CE, Hämmerling GJ, Zenclussen AC. Control of uterine microenvironment by foxp3(+) cells facilitates embryo implantation. Front Immunol. 2013;4:158.

Terada S, Takizawa M, Yamamoto S, Ezaki O, Itakura H, Akagawa KS. Suppressive mechanisms of EPA on human T cell proliferation. Microbiol Immunol. 2001;45(6):473-81.

Thomas R. The balancing act of autoimmunity: central and peripheral tolerance versus infection control. Int Rev Immunol. 2010;29(2):211-33. Review.

van den Boorn JG, Hartmann G. Turning tumors into vaccines: co-opting the innate immune system. Immunity. 2013;39(1):27-37. Review.

Vukmanović S, Santori FR. Self-peptide/MHC and TCR antagonism: physiological role and therapeutic potential. Cell Immunol. 2005;233(2):75-84.

Waibler Z, Sender LY, Merten C, Hartig R, Kliche S, Gunzer M, **Reichardt P**, Kalinke U, Schraven B. Signaling signatures and functional properties of anti-human CD28 superagonistic antibodies. PLoS One. 2008 Mar 5;3(3):e1708.

Weissbrich B, Nauerth M, Busch DH. Adoptive immunotherapy: New assay for the identification of T cells with optimal avidity. Oncoimmunology. 2013;2(10):e26199. Review.

Willig KI, Kellner RR, Medda R, Hein B, Jakobs S, Hell SW. Nanoscale resolution in GFP-based microscopy. Nat Methods. 2006;3(9):721-3.

Xie J, Tato CM, Davis MM. How the immune system talks to itself: the varied role of synapses. Immunol Rev. 2013;251(1):65-79. Review.

Yablonski, D., M. R. Kuhne, T. Kadlecek, and A. Weiss. Uncoupling of nonreceptor tyrosine kinases from PLC-1 in an SLP-76-deficient T cell. Science 1998, 81: 413–416.

Yadav M, Stephan S, Bluestone JA. Peripherally induced tregs - role in immune homeostasis and autoimmunity. Front Immunol. 2013;4:232. Review.

Zanin-Zhorov A, Ding Y, Kumari S, Attur M, Hippen KL, Brown M, Blazar BR, Abramson SB, Lafaille JJ, Dustin ML. Protein kinase C-theta mediates negative feedback on regulatory T cell function. Science. 2010;328(5976):372-6.

Zhang J, Crumpacker C. Eradication of HIV and Cure of AIDS, Now and How? Front Immunol. 2013;4:337.

Danksagung

Ich danke den Leitern der Einrichtungen, Teams und Abteilungen, bei denen ich die Möglichkeit hatte, mich über Jahre wissenschaftlich mit der T-Zell-Immunologie zu beschäftigen, für ihre anhaltende Unterstützung. Mein Dank gilt vor allem Professor Michael Borte, Professor Wieland Kiess, Professor Gerhard Metzner, Dr. Ferdinand Raabe, Professor Brian Evavold, Professor Matthias Gunzer, Professor Dirk Reinhold und nicht zuletzt Professor Burkhart Schraven.

Ich danke den zahlreichen Kollegen, Mitarbeitern und Freunden für viele fruchtbare Diskussionen und Anregungen. „Talking science" hat mir immer Freude bereitet und Inspiration gegeben, sehr oft mit Brian, Matthias, aber nicht zuletzt auch mit Dr. Gunnar Wichmann, Dr. Daniel Jones, Dr. Jon Lindquist und Dr. Stefanie Kliche, um einige wenige zu nennen.

Ich danke den Ingenieuren und Softwareentwicklern aus Jena. Gute Arbeit erfordert gutes Werkzeug und ihres hat in herauszuhebender Weise über Jahre funktioniert. Good job! Ferner danke ich den Technischen Assistenten an meiner Seite, die mir durch hervorragende Arbeit und angenehme Kommunikation die Arbeit wesentlich erleichtert haben, vornehmlich Birgit Labitzke und Guido Höbbel, sowie *last but not least* dem Master of MELC Dipl.-Ing. Lars Philipsen für hervorragende technische Fähigkeiten und Fertigkeiten. Der Erfolg ist immer ein Erfolg des gesamten Teams.

Ich danke Rotary International und der Deutschen Forschungsgemeinschaft (SFB854) für ihre finanzielle Unterstützung, die mir Teile meiner Arbeit erst ermöglichte.

Liste der in die kumulative Habilitation eingehenden Arbeiten

1. Engelmann S, Togni M, Thielitz A, **Reichardt P**, Kliche S, Reinhold D, Schraven B, Reinhold A. T Cell-Independent Modulation of Experimental Autoimmune Encephalomyelitis in ADAP-Deficient Mice. **J Immunol**. 2013 Oct 7. [Epub ahead of print]

2. Etemire E, Krull M, Hasenberg M, **P Reichardt P**#+ and M Gunzer#+. Transiently reduced PI3K/Akt activity drives the development of regulatory function in antigen-stimulated naïve T-cells. **PLOS One.** 2013: 8(7):e68378.
   +Corresponding Author, #Joint Senior Authors

3. Teles A, Schumacher A, Kühnle MC, Linzke N, Thuere C, **Reichardt P**, Tadokoro CE, Hämmerling GJ, Zenclussen AC. Control of uterine microenvironment by foxp3(+) cells facilitates embryo implantation. **Front Immunol.** 2013:4:158.

4. Philipsen L, Engels T, Schilling K, Gurbiel S, Fischer KD, Tedford K, Schraven B#, Gunzer M#, **Reichardt P**#+. Multi-molecular analysis of stable immunological synapses reveals sustained recruitment and sequential assembly of signaling clusters. **Mol Cell Proteomics**. 2013;12(9):2551-67. +Corresponding Author, #Joint Senior Authors

5. **Reichardt P.***, Patzak I.*, Jones K., Etemire E., Gunzer M., Hogg N. A role for LFA-1 in delaying T lymphocyte egress from lymph nodes. **EMBO J**. 2013;32(6):829-43.
   *Joint First authors

6. Stirnweiss A, Hartig R, Gieseler S, Lindquist JA, **Reichardt P**, Philipsen L, Simeoni L, Poltorak M, Merten C, Zuschratter W, Prokazov Y, Paster W, Stockinger H, Harder T, Gunzer M, Schraven B. T cell activation results in conformational changes in the Src family kinase Lck to induce its activation. **Sci Signal.** 2013; 6(263):ra13.

7. Arndt B, M Poltorak, BS. Kowtharapu, **Reichardt P**, L Philipsen, JA. Lindquist, B Schraven and L Simeoni. Analysis of TCR activation kinetics in primary human T cells upon focal or soluble stimulation. **J Immunol Meth** 2013; 387:276-83

8. Schmidt A, N Oberle, EM Weiß, D Vobis, S Frischbutter, R Baumgrass, CS Falk, M Haag, B Brügger, H Lin, GW Mayr, **Reichardt P**, M Gunzer, E Suri-Payer and PH Krammer. Human regulatory T cells rapidly suppress T cel receptor-induced Ca2+s, NF-κB and NFAT signaling in conventional T cells. **Sci Sign** 2011;4(204):ra90.

9. Ocaña-Morgner C, **Reichardt P**, Chopin M, Braungart S, Wahren C, Gunzer M, Jessberger R. Sphingosine 1-Phosphate-Induced Motility and Endocytosis of Dendritic Cells Is Regulated by SWAP-70 through RhoA. **J Immunol**. 2011;186(9):5345-55.

10. Herroeder S, **Reichardt P**, Sassmann A, Zimmermann B, Hogg N, Hollmann MW, Fischer KD, Vogt S, Grosse R, Gunzer M, Offermanns S, Wettschureck N. G-proteins of the G12/G13 family shape immune functions by controlling CD4+ T-cell adhesiveness. **Immunity** 2009;30:708-20.

11. Horn J, Wang X, **Reichardt P**, Stradal TE, Warnecke N, Simeoni L, Gunzer M, Yablonski D, Schraven B, Kliche S. Src homology 2-domain containing leukocyte-specific phosphoprotein of 76 kDa is mandatory for TCR-mediated inside-out signaling, but dispensable for CXCR4-mediated LFA-1 activation, adhesion, and migration of T cells. **J Immunol.** 2009 Nov 1;183(9):5756-67. Epub 2009 Oct 7.

12. Jones DS, **Reichardt P**, Ford ML, Edwards LJ, Evavold BD. TCR antagonism by peptide requires high TCR expression.
J Immunol. 2008;181:1760-6.

13. Waibler Z, Sender LY, Merten C, Hartig R, Kliche S, Gunzer M, **Reichardt P**, Kalinke U, Schraven B. Signaling signatures and functional properties of anti-human CD28 superagonistic antibodies. **PLoS ONE**. 2008;3:e1708.

14. **Reichardt P**, Dornbach B, Rong S, Beissert S, Gueler F, Loser K, Gunzer M. Naive B-cells generate regulatory T-cells in the presence of a mature immunologic synapse. **Blood**. 2007;110:1519-1529.

15. **Reichardt P+**, Müller D, Posselt U, Vorberg B, Diez U, Schlink U, Reuter W, Borte M. Fatty acids in colostrum from mothers of children at high risk of atopy in relation to clinical and laboratory signs of allergy in the first year of life. **Allergy**.2004;59(4):394-400.
+Corresponding author

16. **Reichardt P**, Schreiber A, Wichmann G, Metzner G, Efer J, Raabe F. Identification and quantification of *in vitro* adduct formation between protein reactive xenobiotics and a lysine-containing model peptide. **Environ Toxicol**.2003;18:29-36.

17. **Reichardt P**+, Lehmann I, Sierig G, Borte M. Analysis of T-cell receptor V-beta 2 in peripheral blood lymphocytes as a diagnostic marker for Kawasaki disease. **Infection**.2002;30:360-4.

18. **Reichardt, P**+; Dähnert, I.; Tiller, G.; Häusler, H.-J. Possible activation of an intra-myocardial inflammatory process (S. aureus) after treatment with infliximab in a boy with Crohn's disease. **European Journal of Pediatrics**.2002;161:281-3.
+Corresponding author

19. **Reichardt P**+, Apel TW, Domula M, Tröbs RB, Krause I, Bierbach U, Neumann HP, Kiess W. J Recurrent polytopic chromaffin paragangliomas in a 9-year-old boy resulting from a novel germline mutation in the von Hippel-Lindau gene. **J Pediatr Hematol Oncol**. 2002: 24:145-8.
+Corresponding author

20. **Reichardt, P**+, W. Handrick, A. Linke, R. Schille, W. Kiess. Leukocytopenia, thrombocytopenia and fever related to piperacillin/tazobactam treatment - a retrospective analysis in 38 children with cystic fibrosis. **Infection**.1999;27:355-6
+Corresponding author

- - -

Appendix 01

Engelmann S, Togni M, Thielitz A, **Reichardt P**, Kliche S, Reinhold D, Schraven B, Reinhold A.
T Cell-Independent Modulation of Experimental Autoimmune Encephalomyelitis in ADAP-Deficient Mice.
J Immunol. 2013 Oct 7. [Epub ahead of print]

IF: **5.5**

Published October 7, 2013, doi:10.4049/jimmunol.1203340

T Cell–Independent Modulation of Experimental Autoimmune Encephalomyelitis in ADAP-Deficient Mice

Swen Engelmann,*[,1] Mauro Togni,*[,1] Anja Thielitz,[†] Peter Reichardt,* Stefanie Kliche,* Dirk Reinhold,* Burkhart Schraven,*[,‡] and Annegret Reinhold*

The adhesion- and degranulation-promoting adaptor protein (ADAP), expressed in T cells, myeloid cells, and platelets, is known to regulate receptor-mediated inside-out signaling leading to integrin activation and adhesion. In this study, we demonstrate that, upon induction of active experimental autoimmune encephalomyelitis (EAE) by immunization with the myelin oligodendrocyte glycoprotein$_{35–55}$ peptide, ADAP-deficient mice developed a significantly milder clinical course of EAE and showed markedly less inflammatory infiltrates in the CNS than wild-type mice. Moreover, ADAP-deficient recipients failed to induce EAE after adoptive transfer of myelin oligodendrocyte glycoprotein–specific TCR-transgenic T cells (2D2 T cells). In addition, ex vivo fully activated 2D2 T cells induced significantly less severe EAE in ADAP-deficient recipients. The ameliorated disease in the absence of ADAP was not due to expansion or deletion of a particular T cell subset but rather because of a strong reduction of all inflammatory leukocyte populations invading the CNS. Monitoring the adoptively transferred 2D2 T cells over time demonstrated that they accumulated within the lymph nodes of ADAP-deficient hosts. Importantly, transfer of complete wild-type bone marrow or even bone marrow of 2D2 TCR–transgenic mice was unable to reconstitute EAE in the ADAP-deficient animals, indicating that the milder EAE was dependent on (a) radio-resistant nonhematopoietic cell population(s). Two-photon microscopy of lymph node explants revealed that adoptively transferred lymphocytes accumulated at lymphatic vessels in the lymph nodes of ADAP-deficient mice. Thus, our data identify a T cell–independent mechanism of EAE modulation in ADAP-deficient mice. ***The Journal of Immunology*****, 2013, 191: 000–000.**

Adaptor proteins play crucial roles in organizing molecular signaling complexes called signalosomes. They are subdivided in transmembrane adapter proteins and cytosolic adaptor proteins (1). The cytosolic adapter protein, adhesion- and degranulation-promoting adapter protein (ADAP), was originally identified on the basis of its association with SLP-76 (SLP-76–associated protein of 130 kDa also known as SLAP-130) (2) and with the Src family kinase Fyn (Fyn-binding protein called Fyb) (3). ADAP is expressed in T cells, NK cells, and myeloid cells but not in mature B cells (4). ADAP possesses a number of protein–protein interaction domains. These include a proline-rich region, tyrosine-based signaling motifs, two helical SH3 domains, two putative nuclear localization sites, and an Ena-Vasp homology (EVH1) domain binding site (5).

It is well established that ADAP couples TCR and chemokine receptor stimulation to the activation of integrins via a process called inside-out signaling. ADAP-deficient T cells display altered TCR-mediated adhesion, diminished LFA-1 activation (6, 7), and impaired conjugate formation with APCs (8). In addition to its role in TCR-mediated adhesion and T cell interaction with APCs, ADAP is also involved in chemokine receptor CCR7-mediated LFA-1 affinity/avidity regulation, adhesion, homing, as well as T cell motility within in the lymph nodes (9).

ADAP is also required for NF-κB activation in T cells (10). In this study, ADAP is critical for the assembly of the Carma1-Bcl10-Malt1-complex (11). Furthermore, ADAP associates with the adaptor molecule Nck (12). It has been shown that the functional cooperation between ADAP and Nck stabilizes the interaction of SLP-76 and the Wiskott–Aldrich syndrome protein (13). Thus, ADAP is also involved in the regulation of actin cytoskeleton rearrangement after TCR stimulation.

Recent work has established that ADAP may also play a role in outside-in signaling from integrins in T cells. Following LFA-1 stimulation of T cells, the ADAP-dependent formation of a ring-shaped actin reorganization called actin cloud was discovered (14). This LFA-1–mediated costimulation enhances IL-2 production, F-actin clustering, T cell polarization, and T cell motility (15). Besides its regulation of outside-in signaling in T cells, ADAP is also required for optimal CD11c integrin–mediated outside-in signaling in dendritic cells (DCs) (16).

ADAP-deficient mice have been studied in a limited number of disease models. In transplantation models, ADAP-deficient mice showed prolonged heart graft survival and ameliorated rejection of intestinal allografts (17, 18). In contrast, ADAP-deficient TCR-transgenic mice revealed an increased incidence of autoimmune diabetes (19). In platelets, loss of ADAP results in impaired $\alpha_{IIb}\beta_3$ integrin activation, leading to increased rebleeding of ADAP-deficient mice from tail wounds (20) and to instable thrombus

*Institute of Molecular and Clinical Immunology, Otto von Guericke University, 39120 Magdeburg, Germany; [†]Clinic of Dermatology and Venereology, Otto von Guericke University, 39120 Magdeburg, Germany; and [‡]Department of Immune Control, Helmholtz Center for Infection Research, Braunschweig, Germany

[1]S.E. and M.T. equally contributed.

Received for publication December 5, 2012. Accepted for publication September 9, 2013.

The work was supported by Deutsche Forschungsgemeinschaft Grants RE 2907/2-1 (to A.R.) and SFB854 TP12 (to B.S.).

Address correspondence and reprint requests to Prof. Burkhart Schraven, Institute of Molecular and Clinical Immunology, Medical Faculty, Otto von Guericke University, Leipziger Strasse 44, 39120 Magdeburg, Germany. E-mail address: schraven@med.ovgu.de

The online version of this article contains supplemental material.

Abbreviations used in this article: ADAP, adhesion- and degranulation-promoting adaptor protein; DC, dendritic cell; EAE, experimental autoimmune encephalomyelitis; MOG, myelin oligodendrocyte glycoprotein; MS, multiple sclerosis; S1P, sphingosine 1-phosphate.

formation after carotid artery injury in vivo (21). Recently, it was shown that loss of ADAP attenuated neutrophil recruitment in an ischemia–reperfusion-induced acute kidney injury model (22).

Experimental autoimmune encephalomyelitis (EAE) is a proinflammatory autoimmune disorder that targets the CNS and serves as an animal model for the human disease multiple sclerosis (MS). EAE can be induced in C57BL/6 mice by immunization with the encephalitogenic peptide myelin oligodendrocyte glycoprotein $(MOG)_{35–55}$. Historically, the disease is considered to be mediated by Thl cells because the adoptive transfer of activated brain-specific $CD4^+$ cells is sufficient to induce EAE in recipient animals. Recent evidence suggests that a proinflammatory cascade of Th17 cells, IL-6 and TGF-β1, in the CNS plays a critical role in the pathogenesis of EAE and MS (23, 24). The role of B cells and myelin-specific Abs is still controversial, because depending on the model, the presence of B cells is necessary or dispensable for the development of the disease (25, 26). However, it is clear that B cells are important in the relapsing phase by their production of the anti-inflammatory cytokine IL-10 (27).

During the past few years, an important immunological role of APCs, especially DCs and CNS-resident microglia, is emerging. In the normal CNS, microglia cells express low levels of MHC molecules. During EAE, the expression of costimulatory and MHC molecules on microglia increases, and this may play an important role in the reactivation of T cells that infiltrate the CNS (28). Bone marrow (BM)–derived DCs are the most potent APC population at priming naive T cells in secondary lymphoid organs. Indeed, it was shown that peripherally derived infiltrating DCs rather than radio-resistant CNS-resident microglia cells are involved in the pathogenesis of EAE (29).

In this paper, we report that ADAP-deficient mice undergo milder EAE. This is shown for active EAE as well as in a passive transfer EAE model. We further demonstrate that the ameliorated course of disease in the absence of ADAP is not primarily because of an intrinsic activation defect of T cells. Radiation-induced BM chimeras surprisingly reveal that the attenuated course of EAE is dependent on a radio-resistant nonhematopoietic compartment. We provide evidence that in ADAP-deficient hosts adoptively transferred T cells accumulate at $LYVE\text{-}1^+$ lymphatic vessels in the lymph nodes. Thus, it appears that trapping of T cells in the lymph nodes results in reduced infiltration of inflammatory cells into the CNS and consequently in strongly attenuated EAE.

Materials and Methods

Mice

ADAP-deficient mice (7) were backcrossed to C57BL/6JBom for at least 10 generations. Lck-deficient mice were provided by Dr. T. Mak (University of Toronto, Toronto, ON, Canada) (30). $MOG_{35–55}$-specific TCR transgenic mice (2D2 mice) were provided by Dr. V. Kuchroo (Harvard Medical School, Boston, MA) (31). Congenic C57/BL6-Ly 5.1 mice (B6.SJL) were purchased from Charles River Laboratories. The mice were bred and maintained under specific pathogen-free conditions in the central animal facility of the medical faculty of the University of Magdeburg. In all experiments, 8- to 12-wk-old littermate mice were used. All procedures were conducted according to protocols approved by the local authorities.

EAE induction

Induction of EAE was performed as described earlier (32). Briefly, active EAE was induced by immunization with 200 μg MOG p35–55 emulsified in CFA (Sigma-Aldrich) containing 800 μg heat-killed *Mycobacterium tuberculosis* (Difco Laboratories). The emulsion was administered s.c. as four 50-μl injections into the flanks of each leg. In addition, 200 ng pertussis toxin (List Biological Laboratories) dissolved in 200 μl PBS was injected i.p. on days 0 and 2 after immunization. Mice were monitored daily for clinical signs of EAE and graded on a scale of increasing severity from 0 to 5 as described earlier (33). Daily clinical scores were calculated as the average of all individual disease scores of each group, including mice not developing clinical signs of EAE.

For the adoptive transfer experiments, splenic T cells were isolated using a *Pan* T cell isolation kit and AutoMACS (Miltenyi Biotec). The indicated number of purified T cells in 100 μl PBS was injected into the tail vein. One week later, EAE was induced by immunization with MOG in CFA.

Passive induction of EAE by adoptive transfer of polarized MOG-specific Th1 cells was performed as described by Yang et al. (34). Briefly, splenocytes from 2D2 mice were cultured and stimulated with $MOG_{35–55}$ (20 μg/ml) in the presence of 5 μg/ml IL-2/IL-7 (Miltenyi Biotec) for 2 d. At the end of this incubation period, cells were expanded with IL-2 and IL-7 for another 4 d. Subsequently, cells were reactivated for 24 h with plate-bound anti-CD3 and anti-CD28 (1 μg/ml) in the presence of IL-12 (20 ng/ml; R & D Systems) and IL-18 (20 ng/ml; Biozol). Activated T cells were collected and washed, and $2–5 \times 10^6$ cells were transferred i.p. into recipient mice.

Ab-mediated depletion of host T cells was performed using anti-Thy1.2 Ab. Recipient mice were repeatedly injected i.p. with 500 μg anti-Thy1.2 mAb (clone 30H12; BioXCell) 2 d before transfer and on days 2, 6, and 10 after adoptive transfer of activated 2D2 T cells. Blood samples were taken on days 0, 2, 6, and 10 to control depletion of host T cells.

Immunohistological analysis

Mice were killed and cardially perfused with NaCl. Spinal cords were removed and fixed in 4% formaldehyde. Paraffin-embedded spinal cord longitudinal sections were stained with H&E for visualization of inflammatory infiltrates and evaluated in a blinded manner for the amount of inflammation as described previously (35).

ELISA

For the determination of specific anti-MOG Abs, plates were coated with $MOG_{35–55}$ (10 μg/ml) in bicarbonate buffer overnight at 37°C. After blocking with 1% BSA, the plates were incubated with serial dilutions of mouse serum overnight at 4°C. Specific binding was detected using alkaline phosphatase–labeled goat anti-mouse IgG (subclasses 1+2a+2b+3, Fcγ-fragment specific; Dianova, Hamburg, Germany).

Cytokine concentration

Levels of cytokines in plasma were determined using the Th1/Th2/Th17 cytometric bead array kit (BD Biosciences).

Isolation of leukocytes from spinal cord

Mice were killed with CO_2 and cardially perfused through the left ventricle using NaCl. Spinal cords were extruded by flushing the vertebral canal with PBS. CNS tissue was cut into pieces and treated with collagenase (2.5 mg/ml; Roche Diagnostics) and DNAse I (1 mg/ml; Sigma-Aldrich) for 45 min at 37°C. Tissue was ground through a cell strainer (70 μm), washed, resuspended in 37% Percoll, and layered onto 70% Percoll. After centrifugation (2000 rpm, 25 min), cells were removed from the interphase, washed, and stained for FACS analysis.

Flow cytometry

Flow cytometric analysis was performed on BD LSRFortessa using BD FACSDiva software (BD Biosciences). The following Abs were used for staining: anti-CD3, anti-CD4, anti-CD8, anti-Vα3.2, anti-CD11b, anti-CD11c, anti CD45, anti-CD45.1 and anti-CD45.2, anti-podoplanin (Gp38), and anti-CD31 (all BD Biosciences).

For staining of stromal cells, pooled lymph nodes were cut into pieces and digested with collagenase IV (final concentration, 4 mg/ml; Invitrogen) and DNAse (final concentration, 100 μg/ml; Sigma-Aldrich) for 25 min at 37°C. Cells were stained for podoplanin (Gp38) and CD31. For flow cytometric analysis, the CD45-negative cells were gated and analyzed for the expression of podoplanin, CD31, and ADAP. The polyclonal sheep anti-ADAP antiserum and the respective preimmune serum were provided by G. Koretzky (University of Pennsylvania, Philadelphia, PA) and were used for intracellular staining as described previously (4). The monoclonal anti-Fyb Ab was purchased from BD Biosciences.

Radiation-induced BM chimeric mice

BM donor mice were killed using CO_2, and BM cells were isolated by flushing femur and tibia bones with RPMI 1640 medium. BM cells were washed and resuspended in PBS. Anesthetized congenic recipient mice were lethally irradiated with 1200 rad using a BioBeam 8000 (STS Steuerungstechnik and Strahlenschutz), and 8×10^6 BM cells were administered by retro-orbital injection. Recipient mice were maintained on antibiotic-containing water (2 mg/ml neomycin sulfate; Sigma-Aldrich) for

1 wk after transplantation. Engraftment took place over 6–8 wk of recovery. Successful reconstitution was checked by flow cytometry using congenic markers CD45.1 and CD45.2.

Microglia function

Primary microglia cultures were prepared from wild-type and ADAP-deficient 1- to 3-d-old pups. The cerebral cortices and meninges were removed, and the brains of up to 10 mice were pooled. A single-cell suspension was generated by several rounds of enzymatic and mechanical digestion with the neural dissociation kit (Miltenyi Biotec). Subsequently, microglia cells were isolated using CD11b microbeads (Miltenyi Biotec) as described in the manufactures protocol (purity > 90%). Cells (5×10^4) were cultured in 96-well plates in DMEM (Life Technologies) supplemented with 10% FCS (Life Technologies), 1% gentamicin, 1% penicillin/streptomycin, and 0.5% glutamine. After resting for 24 h, microglia cells were stimulated with LPS from *Salmonella minnesota* (1 μg/ml; Sigma-Aldrich). Following stimulation for 24 h, supernatants were removed and stored for NO and cytokine measurement at −20°C. Concentration of TNF-α was determined using Mouse CBA Kit (BD Biosciences). NO production was quantified using Griess Reagent System (Promega) following the manufacturer's protocol.

Two-photon microscopy of inguinal lymph node explants

Splenic T cells and B cells from congenic B6.SJL mice were isolated by magnetic depletion (Miltenyi Biotec). Purified B cells were labeled with CFSE (5 μM), and purified T cells were labeled with Cell Tracker Orange (5 μM; both Molecular Probes). Approximately 10×10^6 cells (ratio 1:1) were administered i.v. by retro-orbital injection into each recipient mouse. Lymphatic vessels were visualized by Pacific Blue–labeled anti–LYVE-1 Ab (10 μg in 30 μl PBS) applied s.c. into the right flank 24 h before imaging. The left lymph node was left unstained and was used as control for FACS analysis. The inguinal lymph nodes of wild-type and ADAP-deficient recipients were imaged 48 h after adoptive transfer. Two-photon microscopy of explanted lymph nodes was performed as reported previously (36). The inguinal lymph node was surgically removed, immediately immersed in PBS, and placed with the medullary (hilar side) or the follicular (convex) side up, respectively, onto a glass slide. Imaging was performed at a 50 and 150 μm depth. Microscopy was performed using a ZeissLSM710 (Carl Zeiss, Jena, Germany) equipped with a MaiTai DeepSee Femtosecond-Laser (Spectra-Physics, Darmstadt, Germany) tuned to 850 nm on an AxioExaminer upright stage with a ×20, numerical aperture 1.0 (Carl Zeiss) water dipping lens. Image detection was done with three non-descanned detectors, typically equipped with emission detection filters of 565–610 nm (red), 500–500 nm (green), and ShortPass485 nm (blue). Individual red, green, blue, z-stacks of 606 × 606 μm images were recorded and tiled to combine up to 6 × 4 of such fields. Rendering of images was performed using Volocity software (version 4.3; Improvision, Waltham, MA). The number of LYVE-1–associated T cells and B cells was quantified in at least 20 defined areas of two-photon microscopic images.

Statistical analysis

Results are expressed as mean ± SEM. Student unpaired *t* test was used to assess the statistical significance of the differences. Statistical comparison of EAE disease severity between different two groups of animals was accomplished by performing nonparametric Wilcoxon matched pairs test using GraphPad Prism software (37). $p < 0.05$ was considered significant.

Results

ADAP-deficient mice developed milder EAE

EAE (the mouse model of MS) can be induced in C57BL/6 mice by s.c. immunization with $MOG_{35–55}$ peptide in mycobacteria-containing CFA. To assess the consequences of ADAP deficiency in this disease model, we induced EAE in ADAP-deficient mice and wild-type mice. Fig. 1A shows that ADAP-deficient mice undergo a significantly milder disease compared with wild-type mice.

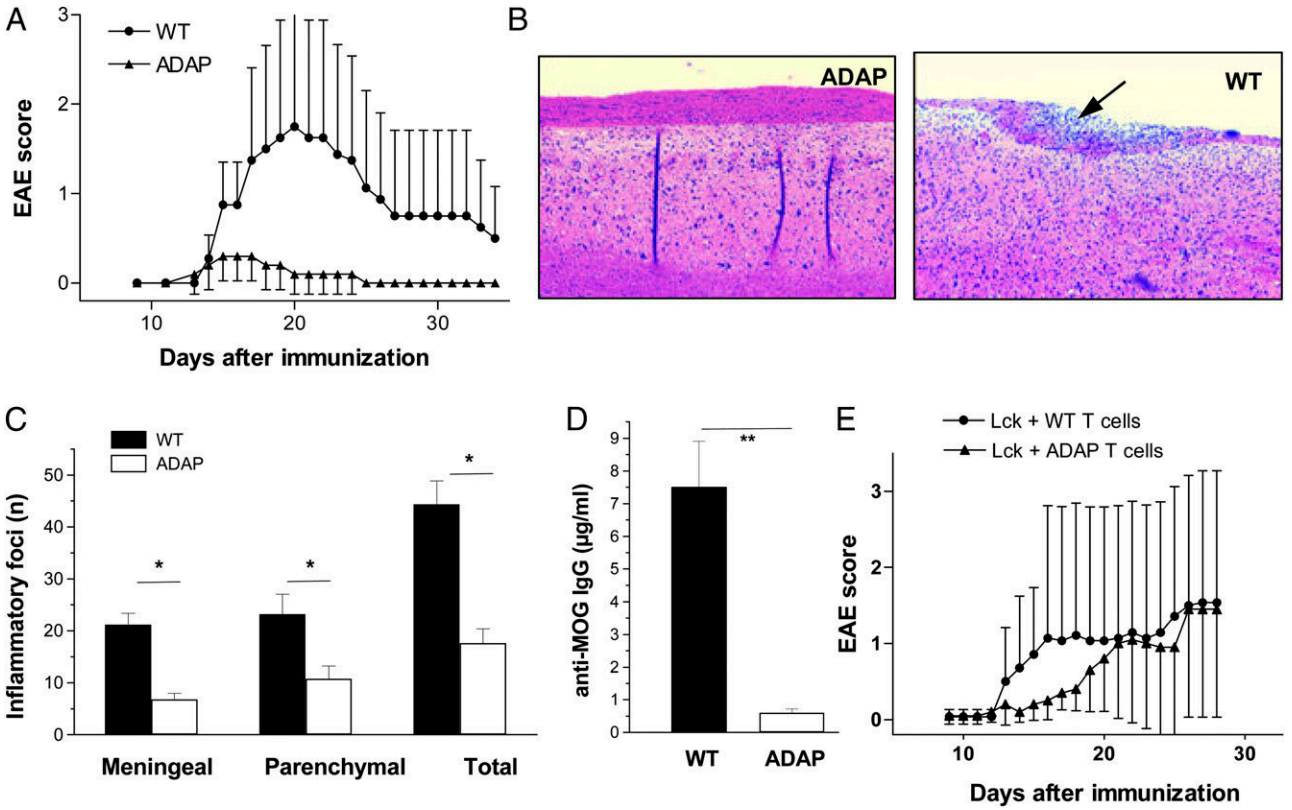

FIGURE 1. Milder EAE in ADAP-deficient mice. (**A**) EAE was induced following immunization with $MOG_{35–55}$ peptide in CFA. The clinical score of EAE was assessed for 35 d after immunization (mean ± SD; $n = 5$; $p < 0.05$ wild-type [WT] versus ADAP). (**B**) Representative histology of spinal cord longitudinal sections. Inflammatory infiltration was visualized by H&E staining. The arrowhead shows a typical heavy inflammatory cellular infiltration in WT animals. Original magnification ×200. (**C**) Histopathological analysis was performed, and meningeal, parenchymal, and total numbers of inflammatory foci were determined. Data represent mean number of inflammatory foci + SEM ($n = 5$; $p < 0.05$). (**D**) Serum levels of anti-$MOG_{35–55}$ specific IgG Abs were measured by ELISA ($n = 8$; $p < 0.01$). (**E**) WT T cells and ADAP-deficient T cells were adoptively transferred into Lck-deficient recipients. One week later, EAE was induced by immunization with $MOG_{35–55}$ peptide in CFA, and the animals were scored for clinical signs of disease (mean ± SD of at least five animals per group).

The milder clinical score of ADAP-deficient mice was further reflected by significantly reduced numbers of inflammatory foci in the spinal cord (Fig. 1B, 1C) where total inflammatory foci as well those in the meninges and the parenchyma were reduced. In addition, the levels of MOG-specific IgG Abs in the serum were significantly lower in ADAP-deficient-mice compared with wild-type mice (Fig. 1D). Taken together, these results suggest that loss of ADAP leads to a strongly attenuated clinical course of EAE, which is accompanied by lower inflammatory infiltrates in the CNS and reduced concentrations of anti-MOG Abs in the serum.

It has been reported previously that ADAP-deficient T cells show defective proliferation, IL-2 production, as well as impaired TCR-mediated LFA-1 clustering and adhesion (6, 7). To assess whether the observed amelioration of EAE in the absence of ADAP was due to impaired function of the ADAP-deficient T cell, we performed an adoptive transfer experiment in which wild-type T cells or ADAP-deficient T cells were transferred into Lck-deficient animals, which completely lack mature T cells. After 7 d, EAE was induced by immunization with $MOG_{35–55}$ peptide. The onset of EAE was delayed, although not statistically significant, when ADAP-deficient T cells were adoptively transferred into the Lck-deficient hosts compared with transferred wild-type T cells (Fig. 1E). This is possibly due to the well established defect in inside-out signaling of ADAP-deficient T cells (6, 7). However, both wild-type and ADAP-deficient T cells produced the same clinical score of disease at later time points of disease. These data indicate 1) that ADAP-deficient T cells are principally capable to induce EAE in T cell–deficient hosts and 2) that non-T cell–specific functions of ADAP are likely responsible for the blunted course of EAE in the absence of ADAP.

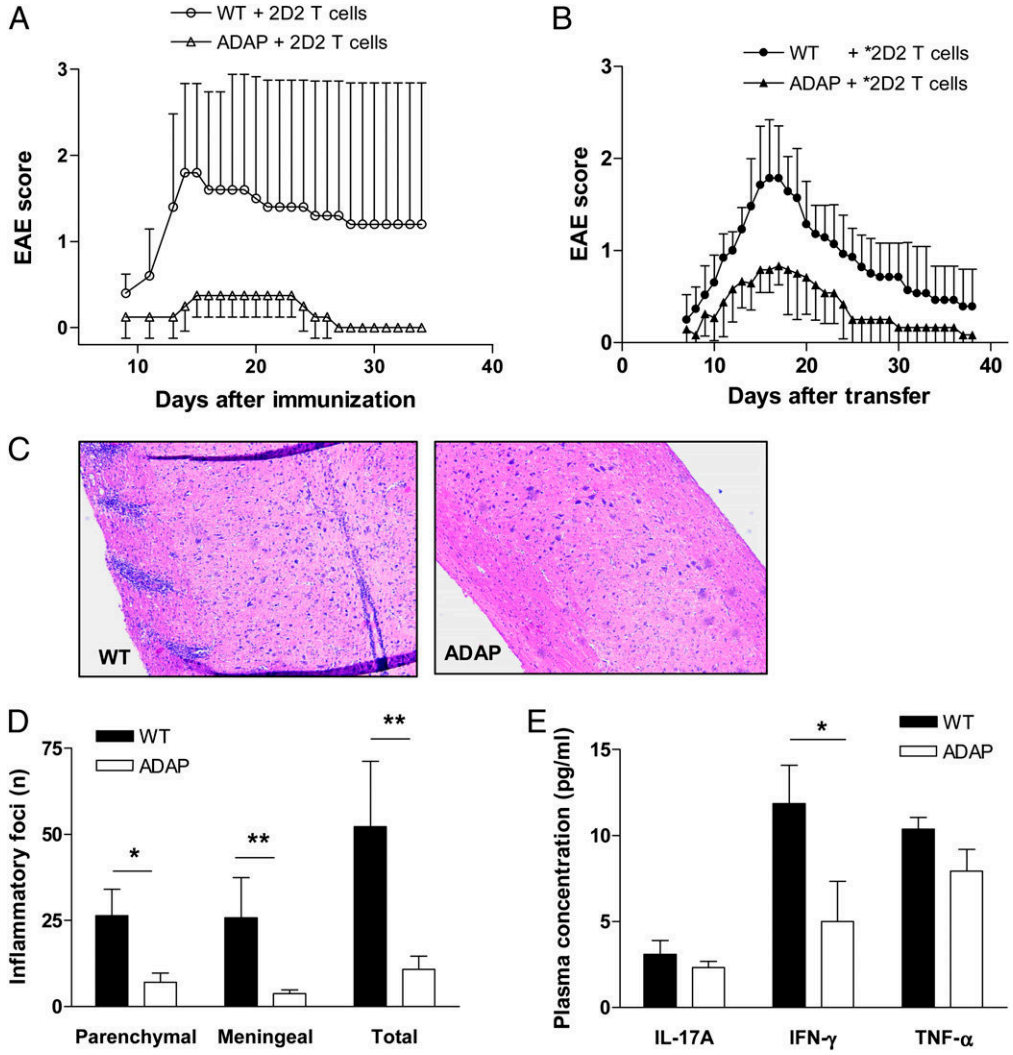

FIGURE 2. Reduced EAE severity in ADAP-deficient mice after adoptive transfer of 2D2-transgenic T cells. (**A**) Wild-type (WT) and ADAP-deficient mice were adoptively transferred with MOG-specific transgenic T cells (2D2). One week later, EAE was induced by immunization with $MOG_{35–55}$ peptide in CFA. The severity of EAE is presented as clinical score (mean ± SD; $n = 5$; $p < 0.05$ WT + 2D2 T cells versus ADAP + 2D2 T cells). (**B**) Splenic T cells of 2D2 mice were stimulated in vitro with $MOG_{35–55}$ in the presence of IL-2 and IL-7 and were reactivated with plate-bound anti-CD3 and anti-CD28 in the presence of IL-12 and IL-18. Fully activated transgenic *2D2 T cells were adoptively transferred into WT or ADAP-deficient recipients, and EAE course was monitored. Data are shown as mean ± SD of one representative experiment ($n = 13$ for WT and $n = 10$ for ADAP, respectively; $p < 0.05$ WT + *2D2 T cells versus ADAP + *2D2 T cells). (**C**) Representative images show longitudinal sections of spinal cords of ADAP-deficient and WT recipients adoptively transferred with *2D2 T cells (H&E staining, original magnification ×200). (**D**) Histopathological analysis was performed, and meningeal, parenchymal, and total numbers of inflammatory foci were determined. Data represent mean number of inflammatory foci + SEM ($n = 5$; $*p < 0.05$; $**p < 0.01$). (**E**) Mice adoptively transferred with *2D2 T cells were killed at day 14, and plasma concentrations of IL-17A, IFN-γ, and TNF-α were measured by cytometric bead array ($n = 9$, mean + SEM; $*p < 0.05$).

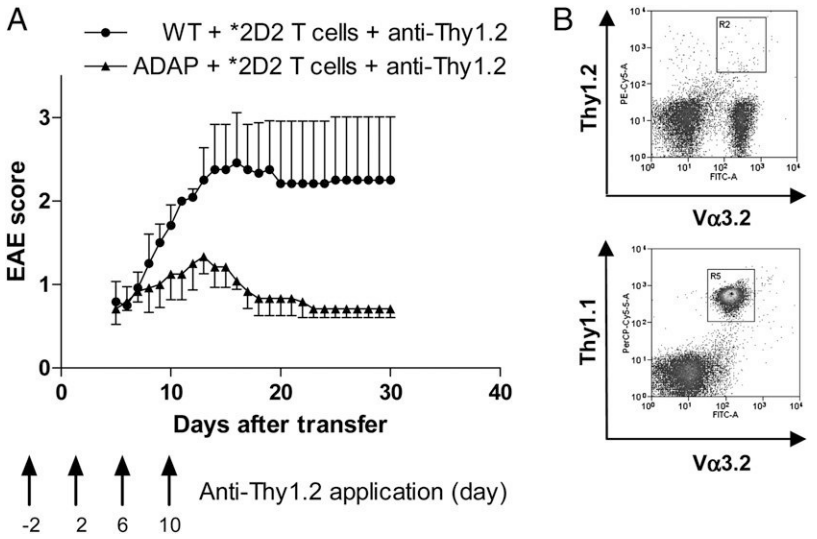

FIGURE 3. Reduced EAE severity in ADAP-deficient mice after adoptive transfer of 2D2-transgenic T cells and depletion of host T cells. (**A**) To deplete host T cells, recipient mice were repeatedly injected i.p. with 500 μg anti-Thy1.2 mAb 2 d before adoptive transfer and on days 2, 6, and 10 after transfer. Starting on day 5, the disease progression was monitored daily. Data are shown as mean ± SD of one representative out of two independent experiment ($n = 6$ mice/group; $p < 0.05$ wild-type [WT] + *2D2 T cells + anti-Thy1.2 versus ADAP + *2D2 T cells + anti-Thy1.2). (**B**) FACS plots demonstrate the depletion of endogenous T cells in peripheral blood taken on day 6 after transfer.

2D2 TCR–transgenic T cells do not reconstitute EAE in ADAP-deficient mice

To further substantiate this assumption we performed an additional adoptive transfer experiment where we transferred 2D2 TCR–transgenic T cells (the 2D2 T cells express a TCR that specifically recognizes the $MOG_{33–55}$ peptide) into either wild-type or ADAP-deficient recipient mice. Subsequently, we induced EAE in the two cohorts by immunization with $MOG_{35–55}$ peptide. As shown in Fig. 2A, even under these experimental conditions, ADAP-deficient mice display a significantly milder disease score compared with wild-type mice, thus corroborating that T cell–extrinsic functions of ADAP are responsible for the ameliorated disease in ADAP-deficient animals.

The blunted course of EAE even after transfer of MOG-specific 2D2 cells could be due to an impaired priming phase of the T cell response or due to an altered effector phase (or both). To distinguish between these possibilities, we by-passed the induction phase of the immune response in the peripheral lymphoid organs by transferring ex vivo–activated and polarized 2D2-transgenic T cells. To this end primary non-activated 2D2 TCR transgenic T cells were isolated and ex vivo activated for 2 rounds using $MOG_{35–55}$ peptide followed by one round of in vitro stimulation using anti-CD3/anti-CD28 Abs. This procedure resulted in the generation of fully activated *2D2 T cells. The *2D2 T cells were then transferred into either wild-type or ADAP-deficient hosts and the clinical score of the diseased animals was monitored over time. This experiment showed that even the ex vivo–activated *2D2 T cells induced significantly less severe EAE in ADAP-deficient recipients compared with wild-type recipients (Fig. 2B). Histological analysis of the spinal cords confirmed the clinical data by showing less cellular infiltration and significantly reduced numbers of meningeal, parenchymal, and total inflammatory foci in the ADAP-deficient recipients (Fig. 2C, 2D). Similarly, plasma concentration of the proinflammatory cytokine IFN-γ that plays a major pathophysiological role in EAE was significantly lower in ADAP-deficient mice. In contrast, no differences in the serum levels of IL-17A and TNF-α were observed between the two cohorts (Fig. 2E).

To exclude the possibility that endogenous ADAP-deficient T cells contribute to the milder EAE in ADAP-deficient mice, we performed Ab-mediated depletion of host T cells. Therefore, recipient mice were repeatedly injected with an anti-Thy1.2 Ab 2 d before adoptive transfer and on days 2, 6, and 10 after transfer. This Ab-mediated depletion of host T cells does not alter EAE severity in ADAP-deficient and wild-type recipient mice after adoptive transfer of fully activated 2D2-transgenic T cells (Fig. 3). In summary, the data shown in Figs. 2 and 3 clearly demonstrate that T cell–extrinsic functions of ADAP impair the inflammatory response in the ADAP-deficient animals.

ADAP-deficient mice showed reduced leukocyte infiltration in the spinal cord

We next attempted to characterize the immune cell populations that infiltrate the CNS during EAE in ADAP-deficient animals following transfer of *2D2 TCR–transgenic cells. Therefore, we

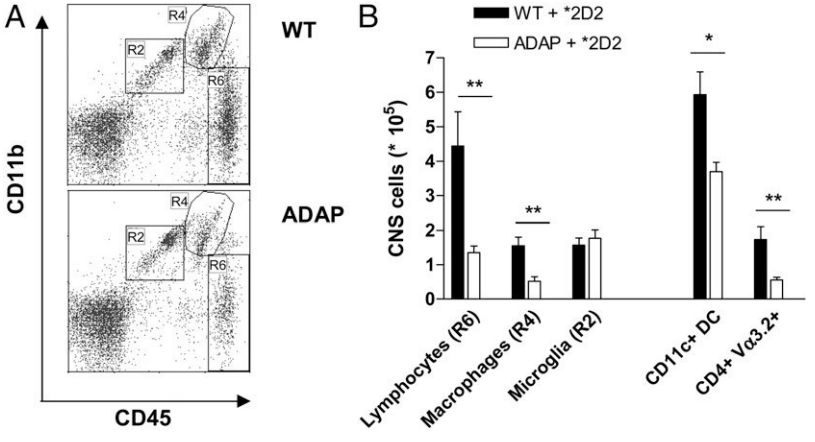

FIGURE 4. Less inflammatory cells in the spinal cord in ADAP-deficient mice. EAE was induced by adoptive transfer of fully activated MOG-specific *2D2-transgenic T cells. At day 14 after transfer, leukocytes were isolated from the spinal cord by Percoll gradient. (**A**) Cells were stained with Abs to CD45 and CD11b and analyzed by flow cytometry: R2, CNS-resident microglia; R4, invading macrophages and granulocytes; and R6, invading lymphocytes. (**B**) Absolute cell numbers of these CNS subpopulations are depicted. Transgenic *2D2 T cells were identified by the presence of the Vα3.2 TCR α-chain within the lymphocyte population. DCs were identified by $CD11c^+$ staining. Data show one representative out of five independent experiments (mean + SEM, $n = 6$). $*p < 0.05$, $**p < 0.01$.

isolated the leukocytes from the spinal cord at the clinical peak of disease and assessed their phenotypes by flow cytometry. Expression of CD45 was used to distinguish CNS-resident microglia (CD45 low) from invading leukocytes (CD45 high, R2; Fig. 4A). The CNS invading cell populations were further distinguished by the presence (macrophages and granulocytes) or absence (lymphocytes) of CD11b. This analysis revealed that ADAP-deficient mice showed consistently fewer invading leukocytes than their wild-type counterparts (regions R4 and R6; Fig. 4A). A deeper analysis of the leukocytes showed that significantly less lymphocytes, including TCR-transgenic Vα3.2 T cells, macrophages and DCs invaded the CNS of ADAP-deficient mice. In contrast, no difference in the number of resident microglia was observed (Fig. 4B). Further subtyping of the infiltrating $CD4^+$ T cells showed similar frequencies of FoxP3 regulatory T cells, IL-17^+ Th17 cells, IFN-γ^+ Th1 cells and IL-10–producing cells (data not shown). Thus, loss of ADAP leads to a globally impaired infiltration of leukocytes into the CNS without affecting a particular T cell or leukocyte subpopulation.

**2D2 T cells accumulate in the lymph nodes in ADAP-deficient mice*

After induction of passive EAE, activated encephalitogenic T cells home through the secondary lymphoid organs before they enter the CNS (38). To localize the ex vivo–activated inflammatory *2D2 cells over time, we isolated lymph nodes, spleen, blood, and spinal cord at days 7, 10, and 14 after adoptive transfer and quantified the transgenic T cells within the individual organs by flow cytometry. This approach revealed no significant differences between wild-type and ADAP-deficient recipients in the absolute number of *2D2 T cells in the spleen and the percentage of *2D2 T cells in the blood (Fig. 5A). However, at the same time, we recovered significantly more *2D2 T cells from the lymph nodes and significantly less *2D2 T cells from the spinal cord of ADAP-deficient recipients. This indicates that in the absence of ADAP the activated *2D2-transgenic T cells are retained within the peripheral lymph nodes.

Next, we investigated whether the accumulation of T cells within the lymph nodes was a specific property of the ex vivo–activated *2D2 T cells. Therefore, we repeated the adoptive transfer experiments this time using nonactivated 2D2 T cells (Fig. 5B). Also under these experimental conditions, we found an increased percentage of nonactivated 2D2 T cells in the lymph nodes of ADAP-deficient recipients. At the same time, similar numbers of nonactivated 2D2 T cells were recovered from the blood and the spleen of both ADAP-deficient and wild-type mice. Collectively, these results demonstrate that in ADAP-deficient recipients, T cells accumulate in the peripheral lymph nodes independent of their activation state.

Nonhematopoietic radio-resistant cells partially mediate the milder course of EAE in ADAP-deficient mice

To dissect whether the accumulation of T cells in the lymph nodes of ADAP-deficient mice was mediated by cells of the hematopoietic system or by nonhematopoietic cells (e.g., stromal cells of the lymph node), we generated radiation BM chimeras and reconstituted the hematopoiesis of ADAP-deficient recipients with wild-type BM. To track the reconstituted cells, we used the B6.SJL congenic mouse strain carrying the CD45.1 (Ly-5.1) allele. Eight weeks after reconstitution, EAE was induced by immunization with $MOG_{35–55}$ peptide in CFA. As shown in Fig. 6A, even after transfer of whole B6.SJL BM into ADAP-deficient recipients, the severity of EAE was much lower in ADAP-deficient recipients compared with wild-type recipients. To confirm this result using a different experimental setup, we reconstituted both wild-type and ADAP-deficient recipients with complete BM of 2D2 TCR–transgenic mice. After reconstitution, EAE was induced by two injections of pertussis toxin. As shown in Fig. 6B, wild-type recipients developed severe disease whereas ADAP-deficient recipients did not. These data show that the attenuated EAE in ADAP-deficient mice is mediated via a radio-resistant nonhematopoietic mechanism.

Microglia is the CNS-resident radio-resistant macrophage, critical for the development of EAE by the release of cytokines as well as reactive oxygen species (39). To assess whether ADAP deficiency might result in diminished function of radio-resistant microglia cells, we investigated functional activity of wild-type and ADAP-deficient primary microglia. For this purpose, NO production and

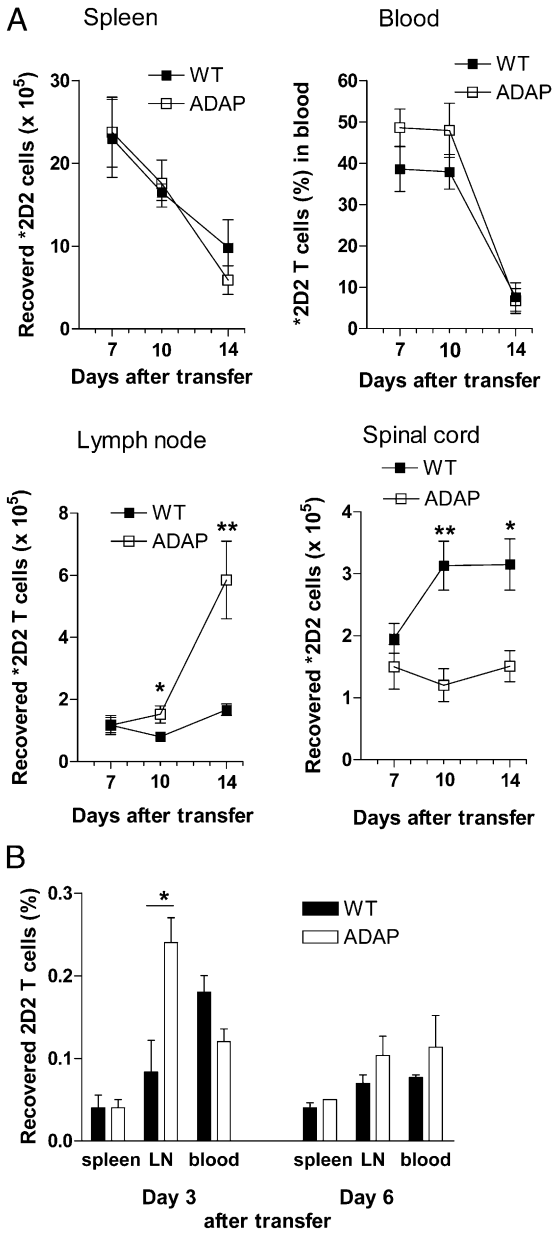

FIGURE 5. Accumulation of adoptively transferred T cells in the lymph nodes of ADAP-deficient mice. (**A**) Wild-type (WT) and ADAP-deficient recipients were adoptively transferred with fully activated *2D2-transgenic T cells. At days 7, 10, and 14 after transfer, the number of activated *2D2 T cells (gated on $CD4^+V\alpha3.2^+$) in spleen, lymph nodes, spinal cord, and blood was analyzed (mean ± SEM, $n = 6$; $^*p < 0.05$; $^{**}p < 0.01$). (**B**) WT and ADAP-deficient recipients were adoptively transferred with nonactivated transgenic 2D2 T cells. At days 3 and 6 after transfer, the recovery of transgenic T cells (gated on $CD4^+V\alpha3.2^+$) in the lymphoid organs was determined by flow cytometry (mean + SEM, $n = 3$; $^*p < 0.05$).

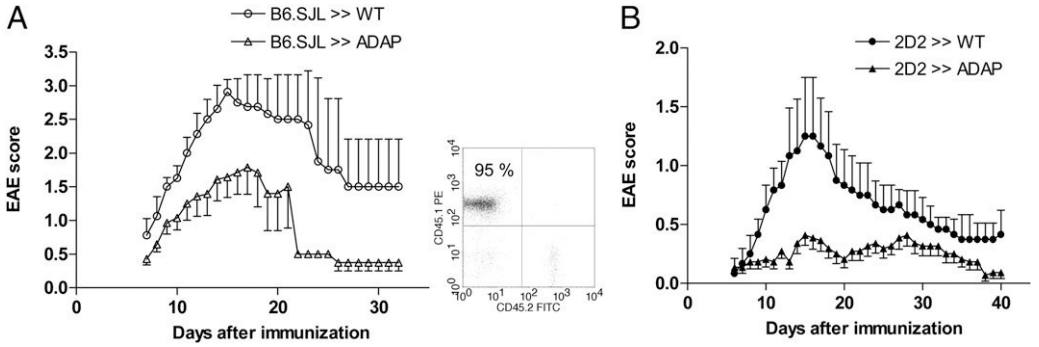

FIGURE 6. Milder EAE in mice with ADAP deficiency in the radio-resistant nonhematopoietic compartment. (**A**) Radiation BM chimeras were generated by reconstitution of ADAP-deficient mice and wild-type (WT) mice with congenic WT BM (B6.SLJ). Eight weeks after successful reconstitution, EAE was induced by immunization with $MOG_{35–55}$ in CFA. Data represent one of two independent experiments ($n = 8$ for WT recipients and $n = 7$ for ADAP recipients; mean EAE score ± SD; $p < 0.05$; B6.SJL > > WT versus B6.SJL > > ADAP). The representative FACS plot shows ablation of CD45.2 cells in chimeras reconstituted with B6.SJL (CD45.1) BM. (**B**) Lethally irradiated ADAP-deficient mice and WT mice were reconstituted with 2D2 BM cells. After reconstitution, EAE was induced by two doses of pertussis toxin on days 0 and 2. Results of one representative out of two independent experiments are shown as mean EAE score ± SD ($n = 6$; $p < 0.05$; 2D2 > > WT versus 2D2 > > ADAP).

cytokine secretion after LPS stimulation were measured. Comparison of wild-type and ADAP-deficient microglia revealed similar amounts of NO and TNF-α in response to LPS stimulation (Supplemental Fig. 1). Therefore, we can exclude the possibility that hypofunctional radio-resistant microglia cells contribute to the milder EAE in ADAP-deficient mice.

Next, we asked the question whether non–BM-derived radio-resistant lymph node stromal cells would express ADAP. Stromal cells of the lymph nodes can be divided into two categories: follicular DCs are prominent stromal cell constituents of the B cell follicles, and fibroblastic reticular cells associate with the T cells areas. Marginal reticular cells are also known as sinus-lining cells. The other nonhematopoietic cells in the lymph node include blood endothelial cells and lymphatic endothelial cells (40). To distinguish these different subsets within the CD45-negative cell population of the lymph nodes, we performed FACS analysis of collagenase-digested lymph nodes and stained the cells for CD31 and podoplanin (Gp38). All four subsets were subsequently analyzed by flow cytometry for their expression of ADAP using a polyclonal anti-ADAP antiserum (4). This approach revealed that none of the stromal cell populations expresses ADAP (Fig. 7A). The same result was achieved when we used a monoclonal anti-ADAP Ab (data not shown). These results indicate that ADAP is not expressed in lymph node stromal cells and thus exclude the possibility that impaired stromal cell functions ameliorate the clinical course of EAE in ADAP-deficient animals.

Adoptively transferred lymphocyte accumulate on LYVE-1$^+$ structures in the lymph node

To further elucidate the reason for the accumulation of T cells within the lymph nodes of ADAP-deficient animals, we applied two-photon microscopy and studied the localization of adoptively transferred and differentially labeled T and B cells within the inguinal lymph nodes. To identify the lymphatic vessels an anti–LYVE-1 Ab was applied s.c. in the flank and the tail base 24 h before imaging. Fig. 7B depicts that inguinal lymph nodes were structurally normal and that the transferred T cells and B cells properly homed to the T cell zone and to the B cell follicles, respectively. Further analysis of the images and quantification of the numbers of T cells and B cells associated with LYVE-1$^+$ lymphatic vessels revealed significantly higher numbers of adoptively transferred T and B lymphocytes on LYVE-1$^+$ lymphatic vessels in ADAP-deficient recipients compared with wild-type recipients (Fig. 7B). In contrast, there was no such increase in T and B cell areas (data not shown). These results demonstrate that the adoptively transferred lymphocytes localize within the lymph nodes of ADAP-deficient mice at lymphatic vessels. Thus, it appears that ADAP-deficient hosts undergo a much milder EAE course because the encephalitogenic T cells are retained at LYVE-1$^+$ lymphatic vessels within the lymph nodes.

Discussion

To determine the role of the cytosolic ADAP in an autoimmune mouse model we induced EAE in wild-type and ADAP-deficient mice by immunization with $MOG_{35–55}$ peptide. This approach revealed that the loss of ADAP strongly attenuates the clinical course of EAE. In line with the lower EAE score, we observed reduced inflammatory infiltrates in the spinal cord of ADAP-deficient mice and lower levels of MOG-specific Abs in the serum.

It is well established that loss of ADAP impairs the function of T cells (6, 7). Therefore, we expected that the ameliorated EAE in ADAP-deficient animals is to a large extent because of an altered T cell function. Surprisingly, however, when transferred into a T cell–deficient background ($Lck^{-/-}$ hosts), ADAP-deficient T cells displayed a similar capability of inducing EAE as wild-type T cells. Thus, it appears that despite altered inside-out signaling capability and impaired NF-κB activation (which might be responsible for the delayed onset of disease that we observed in our experiment), ADAP-deficient T cells are capable of exerting similar effector functions as wild-type T cells, at least in the EAE model.

To gain further insights into the mechanisms underlying the blunted EAE in the ADAP-deficient mice, we applied a passive transfer EAE model using ADAP-proficient transgenic T cells expressing the $MOG_{35–55}$-specific TCR 2D2. Unexpectedly, adoptive transfer of either nonprimed 2D2 T cells or even ex vivo–activated *2D2 T cells also failed to induce EAE in ADAP-deficient recipients. This finding strongly suggests that the ameliorated clinical course of EAE in the ADAP-deficient hosts is indeed not mediated by functionally altered T cells but rather via a T cell–independent mechanism. Moreover, it shows that the described immunological dysfunction of ADAP-deficient mice (e.g., with regard to vesicular stomatis virus infection or transplantation models) very likely has a much more complex cellular basis as thought previously (6, 17, 18).

During induction of EAE, activated encephalitogenic T cells are the first immune cells that enter the CNS (38). In this study, they induce an inflammatory response that, among other pathophysio-

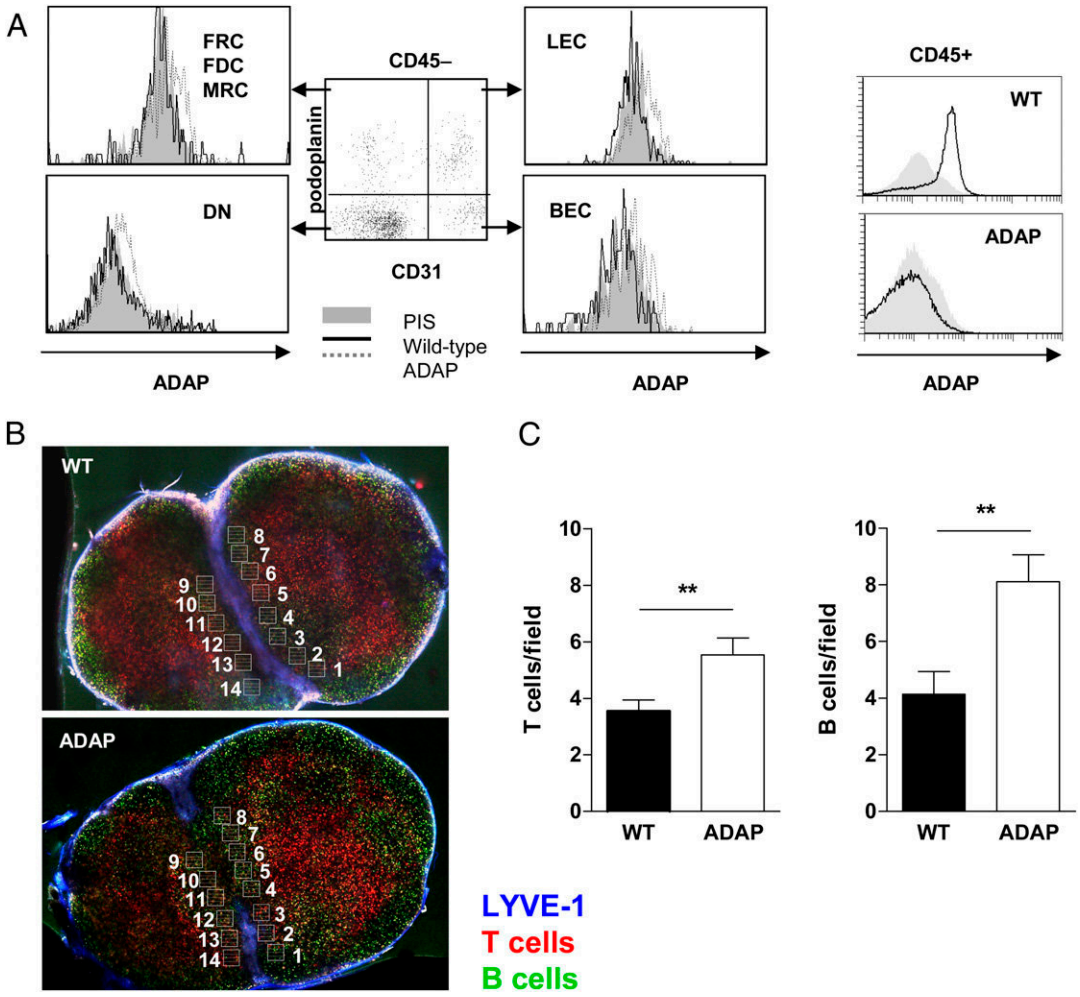

FIGURE 7. Association of adoptively transferred lymphocytes with LYVE-1$^+$ structure in the lymph nodes of ADAP-deficient mice. (**A**) Lymph nodes were digested with collagenase and stromal cell subsets were identified by FACS analysis. The CD45-negative cells were gated, and staining with podoplanin and CD31 identified the stromal cell subset in the four quadrants. Histograms show staining for ADAP in these four quadrants. Dot plot and histograms of one representative FACS analysis are shown. The control for intracellular ADAP staining was performed on CD45$^+$ lymph node cells from wild-type (WT) and ADAP-deficient mice (*right panel*). (**B**) Inguinal lymph nodes of WT and ADAP-deficient recipients were imaged 48 h after adoptive transfer of WT CFSE-labeled B cells and Cell Tracker Orange–labeled T cells using two-photon laser scanning microscopy (original magnification ×200). Lymphatic vessels were visualized by Pacific blue–labeled anti–LYVE-1 Ab applied s.c. 24 h before imaging. The figure shows representative images from the follicular side of WT and ADAP-deficient inguinal lymph nodes at 150-μm depths. The counting grids were used for quantitative analysis. (**C**) LYVE-1–associated T cells and B cells were counted. The graphic plots represent the cell number (mean + SEM; $^{**}p < 0.01$) from 20 counting grids. Results show one representative out of three independent experiments. BEC, Blood endothelial cell; DN, double-negative cell; FDC, follicular DC; FRC, fibroblastic reticular cell; LEC, lymphatic endothelial cell; MRC, marginal reticular cell.

logical consequences, leads to recruitment of additional inflammatory cells such as macrophages, B cells, and DCs. Flow cytometric analysis of the cellular populations in the inflamed CNS showed a strong reduction of invading T cells in the absence of ADAP. Importantly, however, the percentages of CNS-infiltrating Tregs, Th1, and Th17 cells were found to be equal in wild-type versus ADAP-deficient hosts, indicating that the ameliorated disease in the absence of ADAP is not due to expansion or deletion of a particular T cell subset.

However, analysis of the CNS-invading cell populations revealed that loss of ADAP affected all leukocyte populations (T cells, macrophages, and DCs) that invade the CNS. On the basis of the above thoughts that activated T cells recruit inflammatory immune cells to the CNS, we hypothesized that the globally reduced inflammatory response within the CNS was primarily because of the reduced recruitment of encephalitogenic T cells into the brain. In line with this idea, a FACS-based analysis of hematopoietic tissues clearly revealed that in ADAP-deficient hosts the transferred T cells do not reach the CNS because they accumulate within the lymph nodes. It is tempting to assume that as a consequence other inflammatory cells that normally drive the clinical course of EAE do not become activated as well, thereby causing the generally reduced EAE response in ADAP-deficient mice.

It is well known that ADAP is not only expressed in T cells but also in a variety of other hematopoietic cells (DC, mast cells, and platelets) that have been shown to influence the course of EAE. Thus, it was necessary to investigate whether an impaired function of one of these cell populations might be responsible for the blunted inflammatory response and the accumulation of T cells in the lymph nodes of ADAP-deficient animals. However, to our great surprise, analysis of BM chimeras revealed that neither transfer of complete wild-type BM nor of BM of 2D2 TCR–transgenic mice reconstituted the clinical course of EAE in the ADAP-deficient recipients. This finding strongly suggests that not impaired functions of hematopoietic cells but rather altered functions of (a) nonhematopoietic cell population(s) prevent(s) the induction of

EAE in the absence of ADAP. However, flow cytometry analysis of isolated wild-type lymph nodes as well as analysis of publicly available mRNA expression data (previously assembled by the Immunological Genome Project Consortium, www.immgen.org) (41) did not provide evidence for expression of ADAP in stromal cell populations. Hence, we conclude that loss of ADAP in lymph node stromal cells also does not account for blunted course of EAE in ADAP-deficient mice.

We are aware of the possibility that the persistence of ADAP-deficient radio-sensitive cells caused by incomplete BM ablation could exert an inhibitory effect on encephalitogenic cells. In addition, ADAP-deficient radio-resistant BM-derived APCs might be responsible for attenuated EAE severity. Langerhans cells of host origin remain for months in lethally irradiated mice that had received BM transplants (42). Microglia cells (which express ADAP) might inhibit the development and maintenance of inflammation in the CNS (39). However, we believe it unlikely that altered functions of microglia in the absence of ADAP are responsible for the ameliorated recruitment of inflammatory T cells for the following reasons. First, it has been reported that in the normal CNS microglia express low levels of MHC molecules and thus are poor activators of naive T cells (43). Second, using BM chimeras, it has been shown that infiltrating hematopoietic DCs rather than radio-resistent CNS-resident microglia cells are sufficient to induce EAE (29). Third, it was reported that eradicating part of the myeloid compartment or blocking specific signaling capacity of DCs/APCs (in the periphery as well as in the CNS) reduces the severity of EAE (44–46). Fourth, intracerebral application of MOG-loaded DCs results in exacerbation of EAE (47). Finally, our own data show that TNF-α secretion and NO production after LPS stimulation was similar in wild-type and ADAP-deficient microglia cells. These data suggest that DCs rather than microglia cells are involved in the onset of EAE.

Insights into the mechanism that leads to the accumulation of T cells in the ADAP-deficient hosts were provided by two-photon microscopy of ADAP-deficient lymph nodes following adoptive transfer of fluorescence-labeled T cells. This analysis showed that in ADAP-deficient hosts the wild-type T cells (as well as transferred wild-type B cells, which both properly homed to the lymph nodes) accumulated at LYVE-1^+ lymphatic vessels within the lymph nodes. We interpreted this observation in the way that in the absence of ADAP T cells can enter the lymph nodes but are unable to egress the lymph node.

What could be the mechanism(s) that lead(s) to the trapping of T cells in lymph nodes in the absence of ADAP? Most obviously an alteration of the sphingosine 1-phosphate system could account for such a phenotype. However, ex vivo analysis of 2D2 T cells recovered from the lymph nodes of wild-type or ADAP-deficient recipients did not show differences in the expression of the sphingosine 1-phosphate receptor 1 (S. Engelmann and A. Reinhold, unpublished observations). Moreover, it seems unlikely that the serum levels of sphingosine 1-phosphate (S1P) themselves are affected by the loss of ADAP because blood-borne S1P is primarily produced by erythrocytes and vascular endothelial cells, which do not express ADAP (48). In addition, replacement of the ADAP-deficient hematopoietic system by the wild-type hematopoietic system did not rescue the clinical course of EAE in the ADAP-deficient animals. Hence, an alteration of the S1P system as the reason for the lymph node trapping of the T cells in the ADAP-deficient animals seems unlikely.

It is known that ADAP is expressed in platelets that have been suggested to be involved in the blood-lymphatic vascular separation during embryonic development (49). Although ADAP-deficient platelets have an altered function and ADAP-deficient mice show prolonged bleeding after injury (20), we so far do not have convincing evidence that the blood and the lymphatic vessels are not properly separated from each other in the ADAP-deficient animals. However, we cannot rule out the possibility that very minor alterations in the separation process between blood and lymphatic vessels account for the observed phenotype. Further studies are required to evaluate this possibility.

Finally, it could be that via direct or indirect mechanisms loss of ADAP leads to an enhanced expression of ICAM-1, the ligand for the T cell integrin LFA-1 on lymphatic endothelial cells. This might induce a stronger adhesion of the T cells to the lymphatic endothelial cells, thereby preventing their egress from the lymph node. Indeed, we recently observed that the interaction between LFA-1 expressed by lymph node T cells and ICAM-1 expressed by lymphatic vessels determines the egress rate of T cells from the lymph nodes (50). We are currently setting up the experimental systems to evaluate this possibility.

In summary, we demonstrate that loss of ADAP promotes resistance of EAE in mice, likely by trapping encephalitogenic T cells in the peripheral lymph nodes on LYVE-1^+ lymphatic structures. Further studies using lineage-specific ADAP-deficient mice are needed to precisely dissect which nonhematopoietic cell population is responsible for the observed phenotype and also to identify the functional role of ADAP in, for example, microglia. Nevertheless, our data show that altered immune functions in ADAP-deficient mice have a complex cellular basis that goes beyond impaired functions of the T cells and likely also involves nonhematopoietic cells.

Disclosures

The authors have no financial conflicts of interest.

References

1. Kliche, S., J. A. Lindquist, and B. Schraven. 2004. Transmembrane adapters: structure, biochemistry and biology. *Semin. Immunol.* 16: 367–377.
2. Musci, M. A., L. R. Hendricks-Taylor, D. G. Motto, M. Paskind, J. Kamens, C. W. Turck, and G. A. Koretzky. 1997. Molecular cloning of SLAP-130, an SLP-76-associated substrate of the T cell antigen receptor-stimulated protein tyrosine kinases. *J. Biol. Chem.* 272: 11674–11677.
3. da Silva, A. J., Z. Li, C. de Vera, E. Canto, P. Findell, and C. E. Rudd. 1997. Cloning of a novel T-cell protein FYB that binds FYN and SH2-domain-containing leukocyte protein 76 and modulates interleukin 2 production. *Proc. Natl. Acad. Sci. USA* 94: 7493–7498.
4. Dluzniewska, J., L. Zou, I. R. Harmon, M. T. Ellingson, and E. J. Peterson. 2007. Immature hematopoietic cells display selective requirements for adhesion- and degranulation-promoting adaptor protein in development and homeostatsis. *Eur. J. Immunol.* 37: 3208–3219.
5. Menasche, G., S. Kliche, N. Bezman, and B. Schraven. 2007. Regulation of T-cell antigen receptor-mediated inside-out signaling by cytosolic adapter proteins and Rap1 effector molecules. *Immunol. Rev.* 218: 82-91.
6. Griffiths, E. K., C. Krawczyk, Y. Y. Kong, M. Raab, S. J. Hyduk, D. Bouchard, V. S. Chan, I. Kozieradzki, A. J. Oliveira-Dos-Santos, A. Wakeham, et al. 2001. Positive regulation of T cell activation and integrin adhesion by the adapter Fyb/Slap. *Science* 293: 2260–2263.
7. Peterson, E. J., M. L. Woods, S. A. Dmowski, G. Derimanov, M. S. Jordan, J. N. Wu, P. S. Myung, Q. H. Liu, J. T. Pribila, B. D. Freedman, et al. 2001. Coupling of the TCR to integrin activation by Slap-130/Fyb. *Science* 293: 2263–2265.
8. Burbach, B. J., R. Srivastava, R. B. Medeiros, W. E. O'Gorman, E. J. Peterson, and Y. Shimizu. 2008. Distinct regulation of integrin-dependent T cell conjugate formation and NF-κB activation by the adapter protein ADAP. *J. Immunol.* 181: 4840–4851.
9. Kliche, S., T. Worbs, X. Wang, J. Degen, I. Patzak, B. Meineke, M. Togni, M. Moser, A. Reinhold, F. Kiefer, et al. 2012. CCR7-mediated LFA-1 functions in T cells are regulated by 2 independent ADAP/SKAP55 modules. *Blood* 119: 777–785.
10. Medeiros, R. B., B. J. Burbach, K. L. Mueller, R. Srivastava, J. J. Moon, S. Highfill, E. J. Peterson, and Y. Shimizu. 2007. Regulation of NF-κB activation in T cells via association of the adapter proteins ADAP and CARMA1. *Science* 316: 754–758.
11. Srivastava, R., B. J. Burbach, and Y. Shimizu. 2010. NF-κB activation in T cells requires discrete control of IκB kinase α/β (IKKα/β) phosphorylation and IKKγ ubiquitination by the ADAP adapter protein. *J. Biol. Chem.* 285: 11100–11105.
12. Sylvester, M., S. Kliche, S. Lange, S. Geithner, C. Klemm, A. Schlosser, A. Grossmann, U. Stelzl, B. Schraven, E. Krause, and C. Freund. 2010. Adhesion

and degranulation promoting adapter protein (ADAP) is a central hub for phosphotyrosine-mediated interactions in T cells. *PLoS ONE* 5: e11708.
13. Pauker, M. H., B. Reicher, S. Fried, O. Perl, and M. Barda-Saad. 2011. Functional cooperation between the proteins Nck and ADAP is fundamental for actin reorganization. *Mol. Cell. Biol.* 31: 2653–2666.
14. Suzuki, J., S. Yamasaki, J. Wu, G. A. Koretzky, and T. Saito. 2007. The actin cloud induced by LFA-1-mediated outside-in signals lowers the threshold for T-cell activation. *Blood* 109: 168–175.
15. Wang, H., B. Wei, G. Bismuth, and C. E. Rudd. 2009. SLP-76-ADAP adaptor module regulates LFA-1 mediated costimulation and T cell motility. *Proc. Natl. Acad. Sci. USA* 106: 12436–12441.
16. Togni, M., S. Engelmann, D. Reinhold, B. Schraven, and A. Reinhold. 2012. The adapter protein ADAP is required for selected dendritic cell functions. *Cell Commun. Signal.* 10: 14.
17. Tian, J., O. Pabst, D. Römermann, S. Skubich, R. Förster, J. Beckmann, J. H. Chen, and M. W. Hoffmann. 2007. Inactivation of T-cell receptor-mediated integrin activation prolongs allograft survival in ADAP-deficient mice. *Transplantation* 84: 400–406.
18. Tian, J., J. I. Rodriguez-Barbosa, O. Pabst, D. Roemermann, R. Foerster, J. Beckmann, and M. W. Hoffmann. 2010. ADAP deficiency combined with costimulation blockade synergistically protects intestinal allografts. *Transpl. Int.* 23: 71–79.
19. Zou, L., F. Mendez, N. Martin-Orozco, and E. J. Peterson. 2008. Defective positive selection results in T cell lymphopenia and increased autoimmune diabetes in ADAP-deficient BDC2.5-C57BL/6 mice. *Eur. J. Immunol.* 38: 986–994.
20. Kasirer-Friede, A., B. Moran, J. Nagrampa-Orje, K. Swanson, Z. M. Ruggeri, B. Schraven, B. G. Neel, G. Koretzky, and S. J. Shattil. 2007. ADAP is required for normal alphaIIbbeta3 activation by VWF/GP Ib-IX-V and other agonists. *Blood* 109: 1018–1025.
21. Kasirer-Friede, A., Z. M. Ruggeri, and S. J. Shattil. 2010. Role for ADAP in shear flow-induced platelet mechanotransduction. *Blood* 115: 2274–2282.
22. Block, H., J. M. Herter, J. Rossaint, A. Stadtmann, S. Kliche, C. A. Lowell, and A. Zarbock. 2012. Crucial role of SLP-76 and ADAP for neutrophil recruitment in mouse kidney ischemia-reperfusion injury. *J. Exp. Med.* 209: 407–421.
23. Korn, T., J. Reddy, W. Gao, E. Bettelli, A. Awasthi, T. R. Petersen, B. T. Bäckström, R. A. Sobel, K. W. Wucherpfennig, T. B. Strom, et al. 2007. Myelin-specific regulatory T cells accumulate in the CNS but fail to control autoimmune inflammation. *Nat. Med.* 13: 423–431.
24. Veldhoen, M., R. J. Hocking, R. A. Flavell, and B. Stockinger. 2006. Signals mediated by transforming growth factor-β initiate autoimmune encephalomyelitis, but chronic inflammation is needed to sustain disease. *Nat. Immunol.* 7: 1151–1156.
25. Hjelmström, P., A. E. Juedes, J. Fjell, and N. H. Ruddle. 1998. B-cell-deficient mice develop experimental allergic encephalomyelitis with demyelination after myelin oligodendrocyte glycoprotein sensitization. *J. Immunol.* 161: 4480–4483.
26. Lyons, J. A., M. J. Ramsbottom, and A. H. Cross. 2002. Critical role of antigen-specific antibody in experimental autoimmune encephalomyelitis induced by recombinant myelin oligodendrocyte glycoprotein. *Eur. J. Immunol*. 32: 1905–1913.
27. Fillatreau, S., C. H. Sweenie, M. J. McGeachy, D. Gray, and S. M. Anderton. 2002. B cells regulate autoimmunity by provision of IL-10. *Nat. Immunol.* 3: 944–950.
28. Chastain, E. M., D. S. Duncan, J. M. Rodgers, and S. D. Miller. 2011. The role of antigen presenting cells in multiple sclerosis. *Biochim. Biophys. Acta* 1812: 265–274.
29. Greter, M., F. L. Heppner, M. P. Lemos, B. M. Odermatt, N. Goebels, T. Laufer, R. J. Noelle, and B. Becher. 2005. Dendritic cells permit immune invasion of the CNS in an animal model of multiple sclerosis. *Nat. Med.* 11: 328–334.
30. Molina, T. J., K. Kishihara, D. P. Siderovski, W. van Ewijk, A. Narendran, E. Timms, A. Wakeham, C. J. Paige, K. U. Hartmann, A. Veillette, et al. 1992. Profound block in thymocyte development in mice lacking p56lck. *Nature* 357: 161–164.
31. Bettelli, E., M. Pagany, H. L. Weiner, C. Linington, R. A. Sobel, and V. K. Kuchroo. 2003. Myelin oligodendrocyte glycoprotein-specific T cell receptor transgenic mice develop spontaneous autoimmune optic neuritis. *J. Exp. Med.* 197: 1073–1081.
32. Togni, M., K. D. Swanson, S. Reimann, S. Kliche, A. C. Pearce, L. Simeoni, D. Reinhold, J. Wienands, B. G. Neel, B. Schraven, and A. Gerber. 2005. Regulation of in vitro and in vivo immune functions by the cytosolic adaptor protein SKAP-HOM. *Mol. Cell. Biol.* 25: 8052–8063.
33. Steinbrecher, A., D. Reinhold, L. Quigley, A. Gado, N. Tresser, L. Izikson, I. Born, J. Faust, K. Neubert, R. Martin, et al. 2001. Targeting dipeptidyl peptidase IV (CD26) suppresses autoimmune encephalomyelitis and up-regulates TGF-β1 secretion in vivo. *J. Immunol.* 166: 2041–2048.
34. Yang, K., J. L. Vega, M. Hadzipasic, J. P. Schatzmann Peron, B. Zhu, Y. Carrier, S. Masli, L. V. Rizzo, and H. L. Weiner. 2009. Deficiency of thrombospondin-1 reduces Th17 differentiation and attenuates experimental autoimmune encephalomyelitis. *J. Autoimmun.* 32: 94–103.
35. Preller, V., A. Gerber, S. Wrenger, M. Togni, D. Marguet, J. Tadje, U. Lendeckel, C. Röcken, J. Faust, K. Neubert, et al. 2007. TGF-β1-mediated control of central nervous system inflammation and autoimmunity through the inhibitory receptor CD26. *J. Immunol.* 178: 4632–4640.
36. Reichardt, P., B. Dornbach, S. Rong, S. Beissert, F. Gueler, K. Loser, and M. Gunzer. 2007. Naive B cells generate regulatory T cells in the presence of a mature immunologic synapse. *Blood* 110: 1519–1529.
37. Fleming, K. K., J. A. Bovaird, M. C. Mosier, M. R. Emerson, S. M. LeVine, and J. G. Marquis. 2005. Statistical analysis of data from studies on experimental autoimmune encephalomyelitis. *J. Neuroimmunol.* 170: 71–84.
38. Flügel, A., T. Berkowicz, T. Ritter, M. Labeur, D. E. Jenne, Z. Li, J. W. Ellwart, M. Willem, H. Lassmann, and H. Wekerle. 2001. Migratory activity and functional changes of green fluorescent effector cells before and during experimental autoimmune encephalomyelitis. *Immunity* 14: 547–560.
39. Heppner, F. L., M. Greter, D. Marino, J. Falsig, G. Raivich, N. Hövelmeyer, A. Waisman, T. Rülicke, M. Prinz, J. Priller, et al. 2005. Experimental autoimmune encephalomyelitis repressed by microglial paralysis. *Nat. Med.* 11: 146–152.
40. Roozendaal, R., and R. E. Mebius. 2011. Stromal cell-immune cell interactions. *Annu. Rev. Immunol.* 29: 23–43.
41. Heng, T. S., M. W. Painter, and Immunological Genome Project Consortium. 2008. The Immunological Genome Project: networks of gene expression in immune cells. *Nat. Immunol.* 9: 1091–1094.
42. Merad, M., M. G. Manz, H. Karsunky, A. Wagers, W. Peters, I. Charo, I. L. Weissman, J. G. Cyster, and E. G. Engleman. 2002. Langerhans cells renew in the skin throughout life under steady-state conditions. *Nat. Immunol.* 3: 1135–1141.
43. Miller, S. D., E. J. McMahon, B. Schreiner, and S. L. Bailey. 2007. Antigen presentation in the CNS by myeloid dendritic cells drives progression of relapsing experimental autoimmune encephalomyelitis. *Ann. N. Y. Acad. Sci.* 1103: 179–191.
44. Isaksson, M., B. Ardesjö, L. Rönnblom, O. Kämpe, H. Lassmann, M. L. Eloranta, and A. Lobell. 2009. Plasmacytoid DC promote priming of autoimmune Th17 cells and EAE. *Eur. J. Immunol.* 39: 2925–2935.
45. King, I. L., M. A. Kroenke, and B. M. Segal. 2010. GM-CSF-dependent, $CD103^+$ dermal dendritic cells play a critical role in Th effector cell differentiation after subcutaneous immunization. *J. Exp. Med.* 207: 953–961.
46. Skarica, M., T. Wang, E. McCadden, D. Kardian, P. A. Calabresi, D. Small, and K. A. Whartenby. 2009. Signal transduction inhibition of APCs diminishes th17 and Th1 responses in experimental autoimmune encephalomyelitis. *J. Immunol.* 182: 4192–4199.
47. Zozulya, A. L., S. Ortler, J. Lee, C. Weidenfeller, M. Sandor, H. Wiendl, and Z. Fabry. 2009. Intracerebral dendritic cells critically modulate encephalitogenic versus regulatory immune responses in the CNS. *J. Neurosci.* 29: 140–152.
48. Gräler, M. H. 2010. Targeting sphingosine 1-phosphate (S1P) levels and S1P receptor functions for therapeutic immune interventions. *Cell. Physiol. Biochem.* 26: 79–86.
49. Bertozzi, C. C., P. R. Hess, and M. L. Kahn. 2010. Platelets: covert regulators of lymphatic development. *Arterioscler. Thromb. Vasc. Biol.* 30: 2368–2371.
50. Reichardt, P., I. Patzak, K. Jones, E. Etemire, M. Gunzer, and N. Hogg. 2013. A role for LFA-1 in delaying T-lymphocyte egress from lymph nodes. *EMBO J.* 32: 829–843.

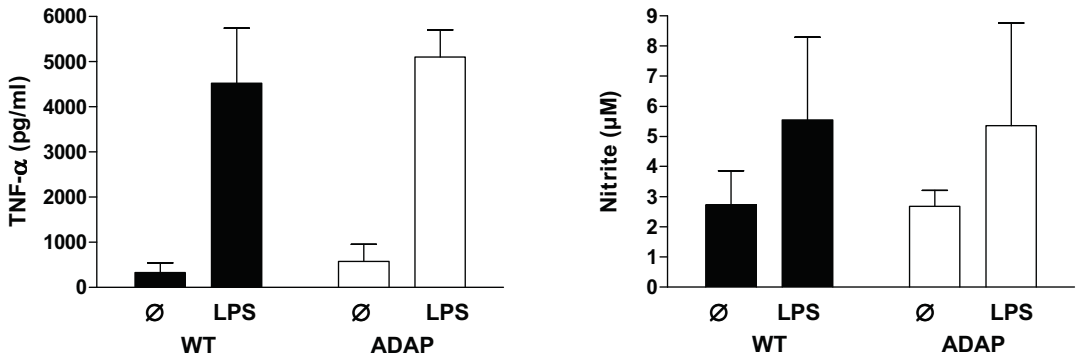

Figure S1

Unaltered function of ADAP-deficient primary microglia.

Microglia cells were isolated from neonatal wild type and ADAP-deficient mice by magnetic separation, and were stimulated with LPS for 24 h. (A) TNF-α secretion was measured by cytometric bead array. (B) NO production was determined by quantification of nitrite using Griess assay. Values are given as mean + SEM (n=6).

Appendix 02

Eloho Etemire, Marco Krull, Mike Hasenberg, **Peter Reichardt#+** and Matthias Gunzer#+.
Transiently reduced PI3K/Akt activity drives the development of regulatory function in antigen-stimulated naïve T-cells
PLOS One. 2013: 8(7):e68378.
+Corresponding Author, #Joint Senior Authors

IF: 4.1

OPEN ACCESS Freely available online

PLOS ONE

Transiently Reduced PI3K/Akt Activity Drives the Development of Regulatory Function in Antigen-Stimulated Naïve T-Cells

Eloho Etemire[1¶], Marco Krull[2¶], Mike Hasenberg[1], Peter Reichardt[2*¶], Matthias Gunzer[1*¶]

1 University Duisburg-Essen, University Hospital, Institute for Experimental Immunology and Imaging, Essen, Germany, **2** Otto von Guericke University, Institute of Molecular and Clinical Immunology, Magdeburg, Germany

Abstract

Regulatory T-cells (T_{regs}) are central for immune homeostasis and divided in thymus-derived natural T_{regs} and peripherally induced iT_{reg}. However, while phenotype and function of iT_{regs} are well known, a remarkable lack exists in knowledge about signaling mechanisms leading to their generation from naïve precursors in peripheral tissues. Using antigen specific naïve T-cells from mice, we investigated CD4+ CD25+ FoxP3- iT_{reg} induction during antigen-specific T-cell receptor (TCR) stimulation with weak antigen presenting cells (APC). We show that early signaling pathways such as ADAM-17-activation appeared similar in developing iT_{reg} and effector cells (T_{eff}) and both initially shedded CD62-L. But iT_{reg} started reexpressing CD62-L after 24 h while T_{eff} permanently downmodulated it. Furthermore, between 24 and 72 hours iT_{reg} presented with significantly lower phosphorylation levels of Akt-S473 suggesting lower activity of the PI3K/Akt-axis. This was associated with a higher expression of the Akt hydrophobic motif-specific phosphatase PHLPP1 in iT_{reg}. Importantly, the lack of costimulatory signals via CD28 from weak APC was central for the development of regulatory function in iT_{reg} but not for the reappearance of CD62-L. Thus, T-cells display a window of sensitivity after onset of TCR triggering within which the intensity of the PI3K/Akt signal controls entry into either effector or regulatory pathways.

Citation: Etemire E, Krull M, Hasenberg M, Reichardt P, Gunzer M (2013) Transiently Reduced PI3K/Akt Activity Drives the Development of Regulatory Function in Antigen-Stimulated Naïve T-Cells. PLoS ONE 8(7): e68378. doi:10.1371/journal.pone.0068378

Editor: Ari Waisman, Johannes Gutenberg University of Mainz, Germany

Received May 7, 2013; **Accepted** May 27, 2013; **Published** July 11, 2013

Funding: This work was supported by the German Research Foundation (DFG, SFB854 to M.G. and P.R.). http://www.dfg.de. The funders had no role in study design, data collection and analysis, decision to publish, or preparation of the manuscript.

Competing Interests: The authors have declared that no competing interests exist.

* E-mail: Matthias.gunzer@uni-due.de (MG); peter.reichardt@med.ovgu.de (PR)

¶ These authors contributed equally to this work.

Introduction

Following T-cell receptor (TCR) triggering, naïve T-cells have multiple possibilities into which type of effector phenotype they develop [1]. Current concepts describe the effector lineages, Th1, Th2, Th17, T_{FH} and T_{reg} and variations of these, where the status of "lineage" is still debated [2]. For these T-cell types master regulators have been identified driving the expression of lineage-identifying functions [3]. Meanwhile evidence is accumulating that T-cells can express more than one "master regulator" and thereby acquiring new functions even after initial differentiation [4]. T_{regs} are a special lineage as they downregulate the activity of all other lines [5] and are divided into naturally occurring nT_{reg} generated from T-cell precursors in the thymus and induced iT_{reg}, which form in the periphery by conversion of effector T-cells or by appropriate *de novo* activation of naïve T-cells [6]. T_{regs} can also be viewed based on their expression of the specific transcription factor FoxP3 as either $FoxP3^+$ or $FoxP3^-$ T_{regs} [7,8].

Master regulators and functional capacities of established T-cell lineages are well understood [9] and very recently also the differences in signaling of established T_{reg} in response to TCR triggers have being elucidated in great detail [10]. However, much less is known about initial signaling events that lead to the generation of defined cell lineages. This is despite the fact that differentiation starts from a specific TCR trigger on naïve T-cells as common signal and only differs in "environmental conditions" such as the type of cytokines present or the APC present during triggering. Thus, next to TCR signaling the impact of environmental factors should trigger additional distinct events that can modulate the overall outcome of the effector function. In a way analogous to the identification of master regulators in stably established lineages [11] it should therefore be possible to identify the earliest signaling events differing in TCR-triggered T-cells on their way to specific lineages by investigating signaling pathways downstream of the TCR under distinct inducing conditions. Environmental conditions transforming naïve T-cells into specific lineages *in vitro* are well known. Next to TCR-triggering they require specific lineage inducing cytokines [11]. *In vitro* conditions for iT_{reg} induction typically involve TGFβ [12,13] and iT_{regs} can be induced *in vivo* from naïve T-cells by targeting cognate antigens to immature dendritic cells (DC) [14,15].

We previously demonstrated the induction of CD4+ CD25+ Foxp3- T_{reg} cells from TCR-transgenic T-cells *in vitro* without lineage-modifying cytokines using TCR-triggers by weak antigen presenting cells (i.e. non-professional APCs with low levels of costimulation such as naïve B-cells [16]). This approach allowed the transformation of naïve T-cells within 3 days of co-culture into $FoxP3^-$ iT_{regs} that potently inhibited transplanted heart rejection

in vivo. In contrast, when using mature DC as APC the cells developed into Th2-type effector cells (T_{eff}) [16,17]. In this model iT_{regs} demonstrated proliferation and expression of the activation markers CD25/CD69, yet in contrast to T_{eff} retained high surface levels of CD62-L [16]. Since these distinct phenotypes developed from a population of naïve T-cells within 72 hours of co-incubation, we reasoned that this model would allow studying the immediate signaling events leading to the generation of either T_{eff} or iT_{reg}.

We report here that naïve T-cells on their way to iT_{regs} display remarkably similar signaling mechanisms compared to T-cells on their way to T_{effs}. However, after an initial CD62-L loss similarly to T_{eff}, iT_{reg} start re-expressing CD62-L 24 hours after onset of TCR-triggering. Low co-stimulatory levels from weak APC resulted in defective activation of the phosphatidyl-inositol-3-kinase (PI3K) pathway inducing a transiently lower activity of Akt accompanied with increased expression of the Akt-hydrophobic motif-specific phosphatase PHLPP1 in iT_{regs}. The regulatory phenotype could be overridden by external CD28 stimulation. Importantly, later PI3K signaling in iT_{reg} reached again effectivity levels of T_{eff}. Thus, transiently reduced PI3K activity in the first 24 hours of TCR triggering appears to be decisive in the lineage decision of iT_{regs} in this model.

Results

Transient Downregulation of CD62-L is Mediated by TACE

iT_{regs} generated by antigen specific activation of naïve T-cells through naïve B-cells (TofB) were identified by high expression of CD62-L despite proliferation and expression of the activation markers CD25 and CD69 [16]. This was in contrast to T_{effs} generated from activating naïve T-cells by DC (TofDC) that showed permanent downregulation of CD62-L and effector functions of conventionally activated T-cells [16]. This system provided a model for investigating the molecular mechanisms driving T-cell differentiation from naïve T-cells as common starting point.

To clarify when loss of CD62-L on T-cells started relative to the onset of APC contact we observed the levels of surface CD62-L on T-cells following co-incubation with naïve B-cells or DC. Interestingly, under both conditions we observed initial CD62-L shedding that was more extensive in TofDC at 6 hours after contact formation but reached almost the same level in TofDC and TofB after 12 hours (Figure 1A). However starting at 24 hours after contact formation, TofB re-expressed CD62-L, and at 72 hours the number of CD62-L expressing cells was undistinguishable from naïve T-cells cultured alone. In contrast, CD62-L in TofDC was lost from most T-cells at 12–72 hours of observation (Figure 1A). It is pertinent to note that based on gating strategy and morphological analysis, we can exclude differential apoptosis kinetics as driving this difference in CD62-L kinetics (data not shown). Thus, CD62-L shows distinct kinetics in T-cells developing into iT_{reg} or T_{eff} cells.

CD62-L shedding marks T-cell activation and is mediated by the matrix metalloprotease TACE on the cell surface [18]. To clarify if TACE was involved in early CD62-L loss here, we blocked TACE with the specific inhibitor TAPI-2. Indeed TAPI-2 significantly reduced CD62-L shedding in TofB and TofDC at 6 and 24 hours of co-incubation but importantly not at 72 hours (Figure 1B–C).

TACE activity is linked to TCR triggering by the signaling effector MEK, which in turn activates the kinase Erk. Erk phosphorylates the inactive endoplasmatic TACE leading to its extracellular expression [19,20]. To test, whether Erk was also involved in CD62-L shedding here we inhibited MEK using PD184352. Confirming an important role of TACE in the early but not late loss of CD62-L we observed that MEK-inhibition induced a significant block of CD62-L shedding during the "shedding phases" at 6 and 24 hours of T-APC co-incubation (Figure 1 D–E). Taken together, CD62-L shedding in the first 6–24 hours of T-cell activation is a TACE mediated pERK driven event requiring antigen specific activation but being independent of the APC strength.

Sustained Downregulation of CD62-L Mediated by PI3K and mTOR

The observation that TACE drives only the initial regulation of CD62-L required to identify pathways responsible for the long-term regulation of CD62-L in TofB and TofDC. The PI3K/mTOR pathway is involved in regulating CD62-L following TCR triggering by sequestration of the transcription factor Foxo1 from the nucleus. This leads to decreased expression of the transcription factor KLF2 which binds the promoter of CD62-L [10,21,22]. Having seen the different long-term expression of CD62-L in TofB and TofDC we hypothesized that differences in PI3K/mTOR signaling might provide a mechanism for this dichotomy. We thus investigated the involvement of both pathways on protein and mRNA levels of CD62-L and KLF-2.

The addition of the PI3K inhibitor Ly294002 (10 μM) to both co-culture systems had no effect on early CD62-L regulation. However, at 24 hours CD62-L surface expression was significantly increased in TofB and TofDC. Importantly, at 72 hours, PI3K inhibition significantly increased CD62-L in TofDC but not in TofB (Figure 2 A–B). The addition of the mTOR inhibitor Rapamycin (100 nM) partially mirrored the effects of PI3K inhibition in TofDC, but not in TofB. We saw no significant effect of Rapamycin on CD62-L surface expression at any time in TofB while in TofDC the inhibitor significantly increased the expression at 24 and 72 hours, albeit to a lower extent as the PI3K-inhibitor (Figure 2 C–D). The effects of Rapamycin and LY2924002 were titratable but both inhibitors showed toxic effects when used at supra-effective doses during long-term exposure (Figure S1A and Figure S1B).

Re-expression of CD62-L is dependent on protein neo synthesis [22]. Consequently we measured significantly higher levels of mRNA for both, CD62-L (Figure 2E) and KLF-2 (Figure 2F) in TofB as opposed to TofDC by qPCR. Already detectable as a trend at 24 hours, it was more pronounced at 72 hours. The inhibition of PI3K (Figure 2G) or mTOR (Figure 2H) also led to a pronounced increase of mRNA for CD62-L and KLF-2 in both TofB and TofDC at 24 hours after initiation of activation.

Collectively this suggests that the induction of TofB and TofDC is similar at the level of initial CD62-L shedding but shows differences with respect to PI3K/mTOR signaling culminating in high versus low levels of CD62-L at later time points.

T-cells Triggered by iDC Replicate CD62-L Expression and Regulatory Behavior of TofB

While naïve B-cells are able to activate naïve T-cells in culture, it is unlikely that this happens in lymph nodes *in vivo*. Here, B-cells are localized in follicles and the majority of naïve T-cells localize in T-cell zones enriched in DC [23]. While DC are the most efficient APC under inflammatory conditions, their lack leads to autoimmunity rather than immune suppression [24]. Thus, without inflammation DC serve as gate keepers of self tolerance [14,25]. Here DC reside in a resting or immature state in the middle of T-

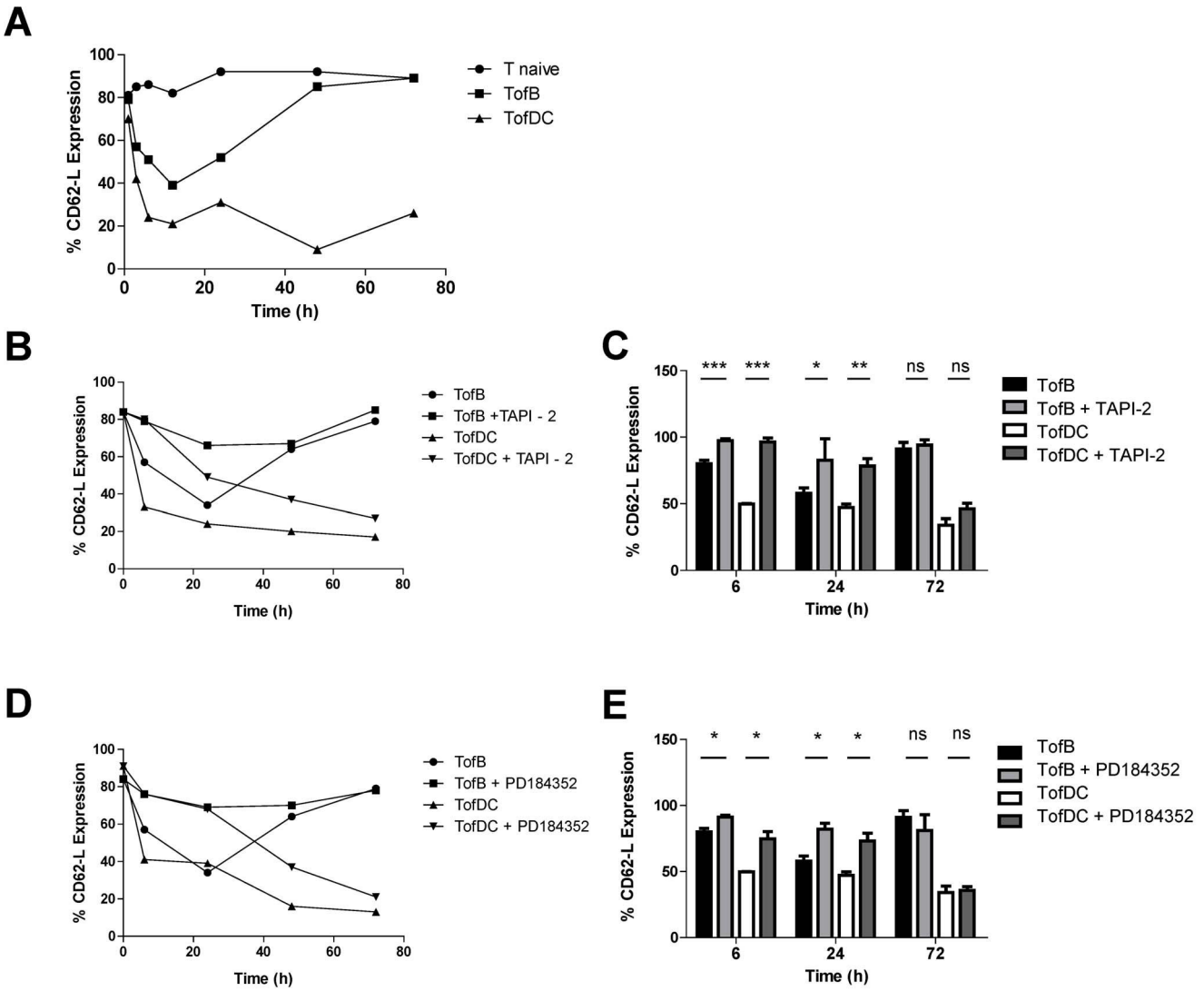

Figure 1. Downregulation of CD62-L is mediated by TACE. Naïve antigen specific T-cells were either left untreated (T naïve) or stimulated with either naïve B-cells (TofB) or activated dendritic cells (TofDC), both loaded with a cognate peptide of chicken ovalbumin, for different periods of time and in the absence or presence of inhibitors. Subsequently the number of cells expressing CD62-L was measured by flow cytometry. (A) one representative Kinetic of CD62-L expression on naïve and differentially activated T-cells over a 72 hour incubation time (representative experiment of 5) (B) Kinetics of CD62-L expression in the presence of the TACE sheddase inhibitor, TAPI-2. (C) The inhibition of TACE shows a significant interference with CD62-L shedding up to 24 hours after the initiation of T-cell priming. (D) Kinetics of CD62-L expression in the presence of the MEK-inhibitor PD184352 (E) Inhibition of MEK blocks CD62-L shedding in the first 24 hours of T-cell activation while the long term regulation of CD62-L expression is independent of MEK-TACE driven regulation. (C) and (E) show mean values+SEM of three independent experiments.
doi:10.1371/journal.pone.0068378.g001

cell zones maintaining self tolerance by the generation of iT_{regs} [26] *in vivo*. Thus, immature DC (iDC) should be a more physiological weak APC to investigate the plasticity of T-cell responses in our model.

Therefore we generated iDC by culturing non-adherent bone marrow cells in the presence of GM-CSF alone as described [27]. iDC in comparison to DC expressed comparable levels of MHC II but far lower levels of CD11c and the co-stimulatory molecules CD80 and CD86 (Figure S2).

Next we measured CD62-L expression in T-cells primed by iDC (TofiDC). Remarkably we found a transient downregulation and re-expression of CD62-L in TofiDC in a fashion almost identical to that seen with TofB. Furthermore, TofiDC always showed a higher expression of CD62-L as compared to TofDC (Figure 3A–B). Thus it was important to test whether TofiDC would also functionally equal TofB. We therefore decided to test, whether TofiDC were functionally T_{regs}. *In vitro* inhibitory tests indeed confirmed that TofiDC possessed regulatory activity of the same potency as TofB (Figure 3C–D). In addition, the characterization of TofiDC showed them to be Foxp3 negative just as TofB (data not shown).

The analysis of the PI3K/mTOR pathway had suggested that an incomplete triggering of this mechanism mediated the inability to permanently downregulate CD62-L in TofB and TofDC. We therefore asked, whether the blockade of this pathway would also functionally change the activity of TofDC. Thus we generated TofDC in the presence of Ly294002 and Rapamycin. When tested in *in vitro* inhibitory assays, indeed PI3K inhibited cells (TofDC+Ly) presented with a regulatory capacity equal to TofiDC and TofB (Figure 3 C–D). Interestingly, the blockade of mTOR

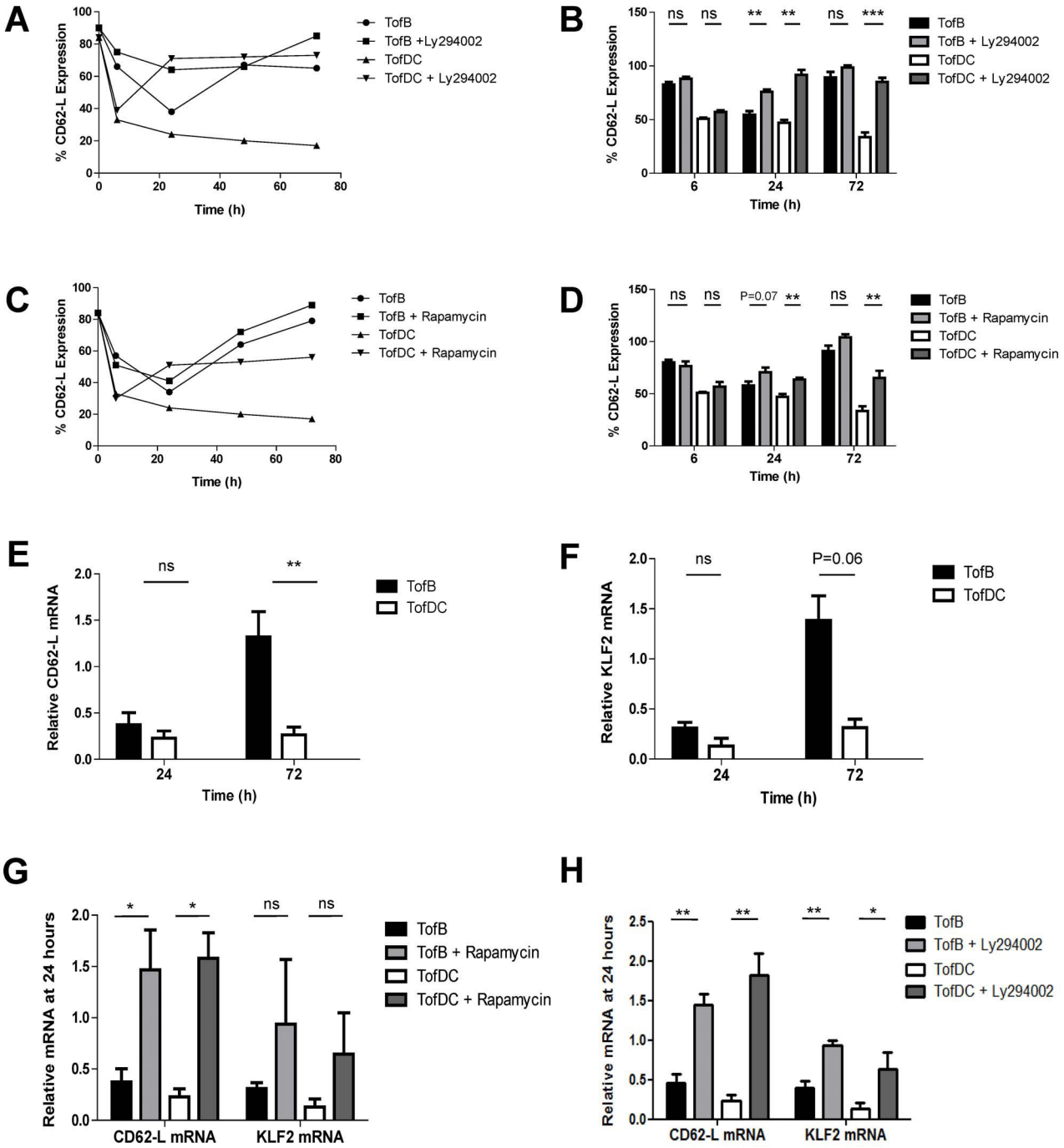

Figure 2. Sustained downregulation of CD62-L is mediated by PI3K and mTOR signaling. For FACS analysis, cells were treated and analyzed as described in Figure 1, while for qPCR analysis T-cells were recovered/enriched from co-cultures by MACS depletion. (A) Kinetics of CD62-L expression in the presence of the PI3K inhibitor, LY294002. (B) LY294002 has no effect on CD62-L loss in the first 6 hours after onset of T-cell activation but induces significant upregulation of CD62-L at later time points. (C) Kinetics of CD62-L expression in the presence of the mTOR inhibitor, Rapamycin. (D) Rapamycin has no effect on CD62-L loss in the first 6 hours after onset of T-cell activation but induces upregulation of CD62-L at later time points. (E) qPCR analysis of CD62-L mRNA expression level in TofB and TofDC at 24 and 72 hours. (F) qPCR analysis of KLF2 mRNA expression levels in TofB and TofDC at 24 and 72 hours. (G) qPCR analysis of CD62-L mRNA induction in both TofB and TofDC by Rapamycin and a detectable yet non-significant induction of KLF2 mRNA. (H) qPCR analysis of CD62-L and KLF2 mRNA induction in TofB and TofDC in the presence or absence of Ly294002. Data in B and D-H are means+SEM of 3–5 independent experiments.
doi:10.1371/journal.pone.0068378.g002

could not significantly induce a regulatory phenotype in TofDC (Figure 3C–D) despite its pronounced effect on CD62-L expression. Thus, incomplete PI3K- but not mTOR-activation was responsible for the induction of iT_{regs} in this system.

Sub-optimal Co-stimulation Induces Regulatory Function but does not Influence CD62-L

Naïve B-cells and iDC both lack costimulatory molecules, especially CD80 and CD86 (Figure S2 and [16]). These molecules

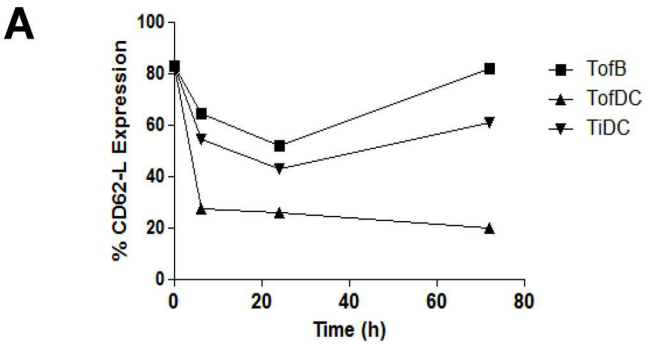

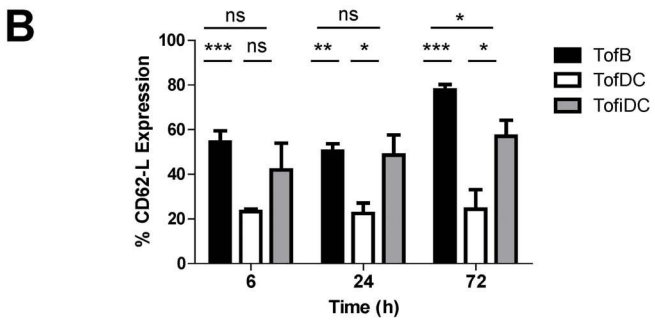

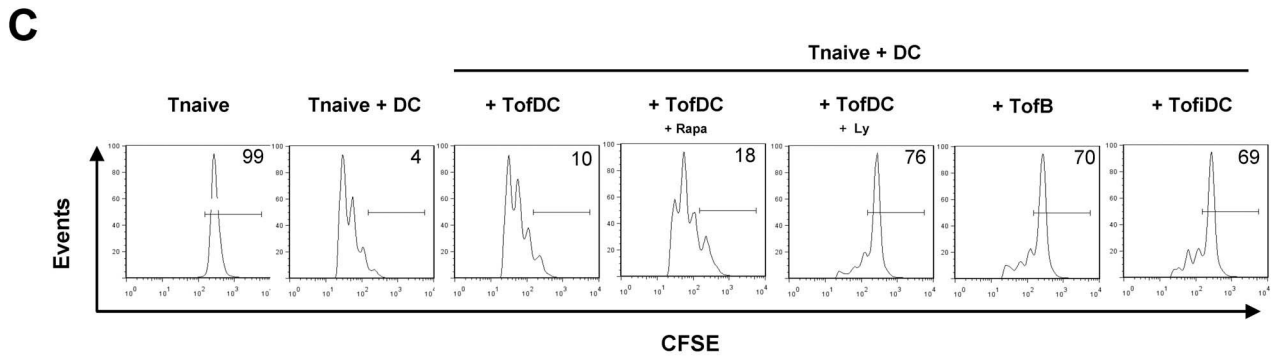

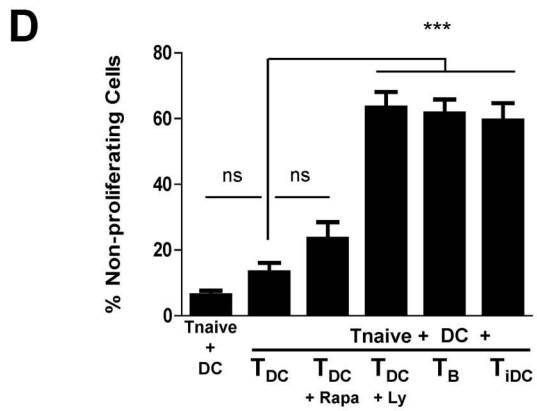

Figure 3. T-cells triggered by immature DC replicate CD62-L expression signature and regulatory behavior of TofB. Naïve antigen specific T-cells were treated as described in Figure 1 except for priming with immature DC (TofiDC), which was additionally run in a separate culture. For *in vitro* inhibitory assays, naïve T-cells were stained with CFSE and incubated alone or in the presence of mature dendritic cells loaded with cognate peptide. To the same type of culture we also added various types of CFSE-negative activated T-cells for modulation of T-cell proliferation. The proliferation of the naïve T-cells was measured by CFSE-dilution after 72 hours of co-incubation (A) Kinetics of CD62-L dynamics in TofiDC with respect to the TofB and TofDC (B) CD62-L levels in naive T-cells primed with iDC, B-cells or mature DC. (C) Regulatory capacity of the various activated T-cells (representative experiment). (D) Statistical analysis shows that TofB, $TofDC_{Ly}$ and TofiDC induce significant inhibition of naive T-cell proliferation relative to TofDC while $TofDC_{Rapa}$ induce no significant inhibition. Data are means+SEM of 4–5 experiments.
doi:10.1371/journal.pone.0068378.g003

are triggers for CD28 on T-cells which in turn is a prominent activator of the PI3K pathway [28]. The lack of costimulation might thus underly the inability of naïve B-cells or iDC to induce effector T-cells.

To study this we generated TofB, TofDC and TofiDC in the absence or presence of artificial CD28-signals provided by soluble antibodies. In an *in vitro* test for T-cell activation we observed that TofB and TofiDC generated in the presence of CD28 antibodies showed significantly less inhibition of T-cell proliferation as compared to TofB or TofiDC generated without additional co-stimulation (Figure 4 A–B). TofDC generated with additional CD28 triggering had the same effect on T-cell proliferation as the regular TofDC indicating the level of stimulation in DC could not be further augmented by the addition of CD28. However, opposed to the fundamental change in functional activity induced by CD28 co-ligation we only observed a mild effect of this treatment on CD62-L loss at 6 hours in TofB while at later time points CD62-L expression returned to its high levels seen before with naïve B-cells or iDC (Figure 4 C).

Together these results suggest that defective CD28 co-stimulation plays a key role in the induction of regulatory function in naïve T-cells but has no discernible influence on CD62-L dynamics.

Defective Akt Signaling Following T-cell Triggering by Weak APCs

Analysis so far had suggested suboptimal PI3K/mTOR signaling as basis for the induction of iT_{regs} by weak APC. However, TofB and TofiDC were viable proliferating cells expressing levels of CD25 equivalent to TofDC (not shown). Proliferation of T-cells requires nutrient production. This is dependent on a functional PI3K/mTOR pathway and mediated by the downstream effector Akt [22]. Thus the question was how a low activity of the PI3K/mTOR pathway would be consistent with active cell proliferation.

Therefore we tested the activity of Akt via the phosphorylation status of its activation loop at Thr308 and the hydrophobic motif at Ser473. Differences at the phosphorylation of Ser473 can be found in T_{regs} [10,29]. As expected, in all three T-cell types total levels of Akt were mostly unchanged over the observation period of 72 hours (Figure 5A and Figure S3). However, also Thr308-phosphorylation was always identical in all cells (Figure 5B and Figure S3). But we did detect defective phosphorylation of Ser473 in TofB and TofiDC compared to TofDC starting at 6 hours after contact initiation and being highly significant at 24 hours (Figure 5C/D). Both, the number pAkt Ser473-expressing cells as well as their amount of pAkt Ser473 (by MFI) were lower in TofB/TofiDC as compared to TofDC (Figure 5D). However, at 72 hours the reduced phosphorylation of Ser473 was mostly lost again (Figure 5C and Figure S3B). Thus during generation, TofB and TofiDC have a phase of reduced Akt-Ser473 phosphorylation that is gradually abrogated again.

What mechanism could drive this phospho-site specific defect in TofB and TofiDC? We measured the phosphatase PHLPP1 which can induce regulatory properties in T-cells and is associated with the defective phosphorylation of pAkt Ser473 [12]. Indeed, PHLPP1 mRNA was significantly increased in TofB and TofiDC as compared to TofDC. This was highly significant at 6 hours and still maintained as a trend at 24 and 72 hours (Figure 5E). These levels of PHLPP1 fit with the temporal downregulation of pAkt Ser473. Collectively these data show that during the generation of iT_{regs} by weak APC there was an initial phase of weak PI3K/mTOR induction leading to transiently defective Akt activity and the re-expression of CD62-L coincided with this period of weak Akt activity.

Discussion

By virtue of their unique activity as suppressors of all other T-cell types T_{regs} occupy a special niche in adaptive immunity. There are several studies exploring their biology ranging from their development/induction to the mechanisms of action [30,31]. However, despite the extensive knowledge we have about these issues of T_{reg} biology there is a remarkable dearth of information regarding early signaling events driving the induction of iT_{regs} from naïve CD4 T-cells despite the central role of this mechanism in adaptive immunity.

To bridge this gap, we present in this report a kinetic study examining early signaling events that lead to the production of CD4+ CD25+ Foxp3- iT_{regs} from naïve CD4 T-cells. Thereby we took advantage of our previously reported model of naïve CD4 T-cell co-culture with naïve B-cells as APC [16]. In addition, we incorporated a well-known second type of weak APC in our system, immature DC, which also provides a physiologically relevant means of T-cell activation *in vivo*. Furthermore we performed experiments on 2 different strains of mice, with both showing similar results and trends thus negating the possibility of our observations been a strain specific effect.

We were surprised to find that the induction of T_{regs} in this model was achieved via triggering of remarkably similar pathways as that of T_{effs}. We only found a transiently reduced activity of the PI3K/Akt pathway between 6–24 hours post-activation as a characteristic sign for the induction of a T_{reg} phenotype. This was accomplished by the transient induction of PHLPP1, an Akt hydrophobic motif-specific phosphatase, selectively in T_{regs}. It is very interesting to see that a recent report found very similar defects in signaling (namely low Akt473 phosphorylation) in fully established FoxP3-expressing Tregs [10]. Thus, the signaling defect seen in T_{regs} might also be the same initial defect that leads to T_{reg} induction from naïve T-cells.

The role of the PI3K pathway in T_{reg} development is presently controversial as there are reports that PI3K activation inhibits T_{reg} development [32] while others claim the opposite [33]. Our data indicate that PI3K activation is necessary for and compatible with iT_{reg} development but only when being attenuated at the beginning of the T-cell stimulation. In our model, this is achieved by weak APCs such as naïve B-cells and immature DC via their characteristically low co-stimulatory input derived from sub-optimal surface levels of co-stimulatory molecules. Interestingly, while not a downstream effector molecule of the TCR complex, CD28 co-stimulation is known to be vitally involved in producing robust PI3K activation [34,35]. Adding CD28 to the weak APC-T-cell co-culture led to the restoration of the effector phenotype and abrogation of regulatory function. This shows that a low degree of CD28 signaling at the onset of TCR triggering can lead to a signal sufficiently high to drive T-cell activation and differentiation but favoring the development of a regulatory phenotype, a conclusion also reached by others [36]. As PI3K activity reached levels similar to those in T_{effs} at timepoints later than 24 hours, early signaling events up to 24 hours after the initial TCR trigger appear to occur in a window of sensitivity in a T-cell, where the activity of the PI3K pathway is decisive in determining the later effector phenotype.

A characteristic peculiarity of iT_{reg} in our model was the high expression of CD62-L despite effective activation and proliferation of the cells. We found that CD62-L in iT_{reg} followed a pattern of initial TACE-mediated loss, as in T_{eff}. Then, however, the cellular

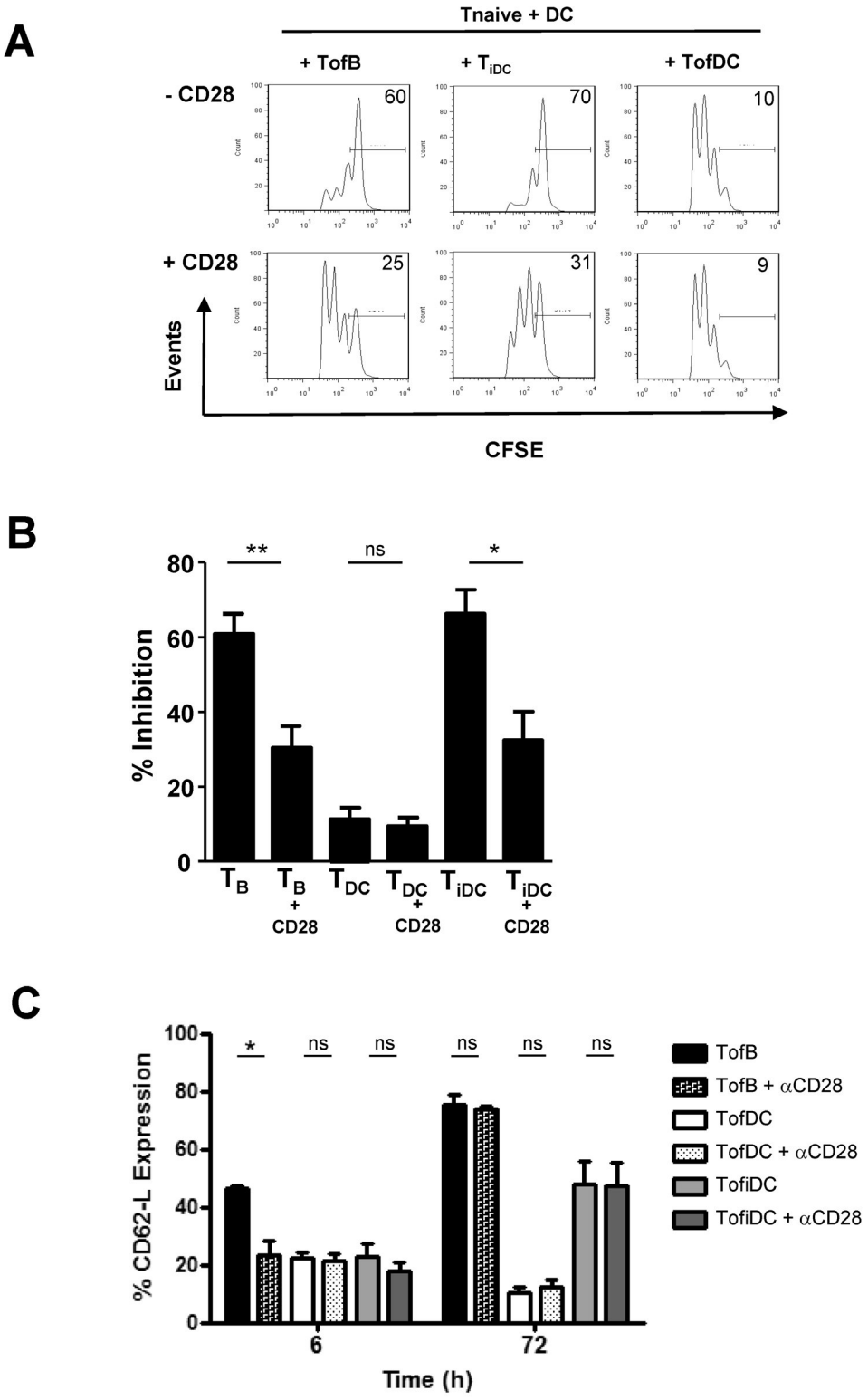

Figure 4. Sub-optimal co-stimulation drives acquisition of regulatory function but exerts negligible influence on CD62-L dynamics. Co-stimulation was augmented by the addition of CD28 antibodies to cultures during the generation of TofB, TofiDC or TofDC for their use in downstream studies. The obtained activated cells were then tested for their inhibitory capacity against naïve T-cells. (A) Representative FACS analysis of *in vitro* proliferation assays of CFSE stained naïve T-cells in the presence of various activated T-cells showing that the addition of CD28 antibodies during the generation of TofB and TofiDC strongly reduces their regulatory capacity. (B) Statistical analysis of the effect of increased co-stimulation on the regulatory capacity of TofB and TofiDC. (C) CD62-L expression levels in T-cells generated with or without additional CD28 antibodies. Data are means+SEM of 3–4 experiments.

doi:10.1371/journal.pone.0068378.g004

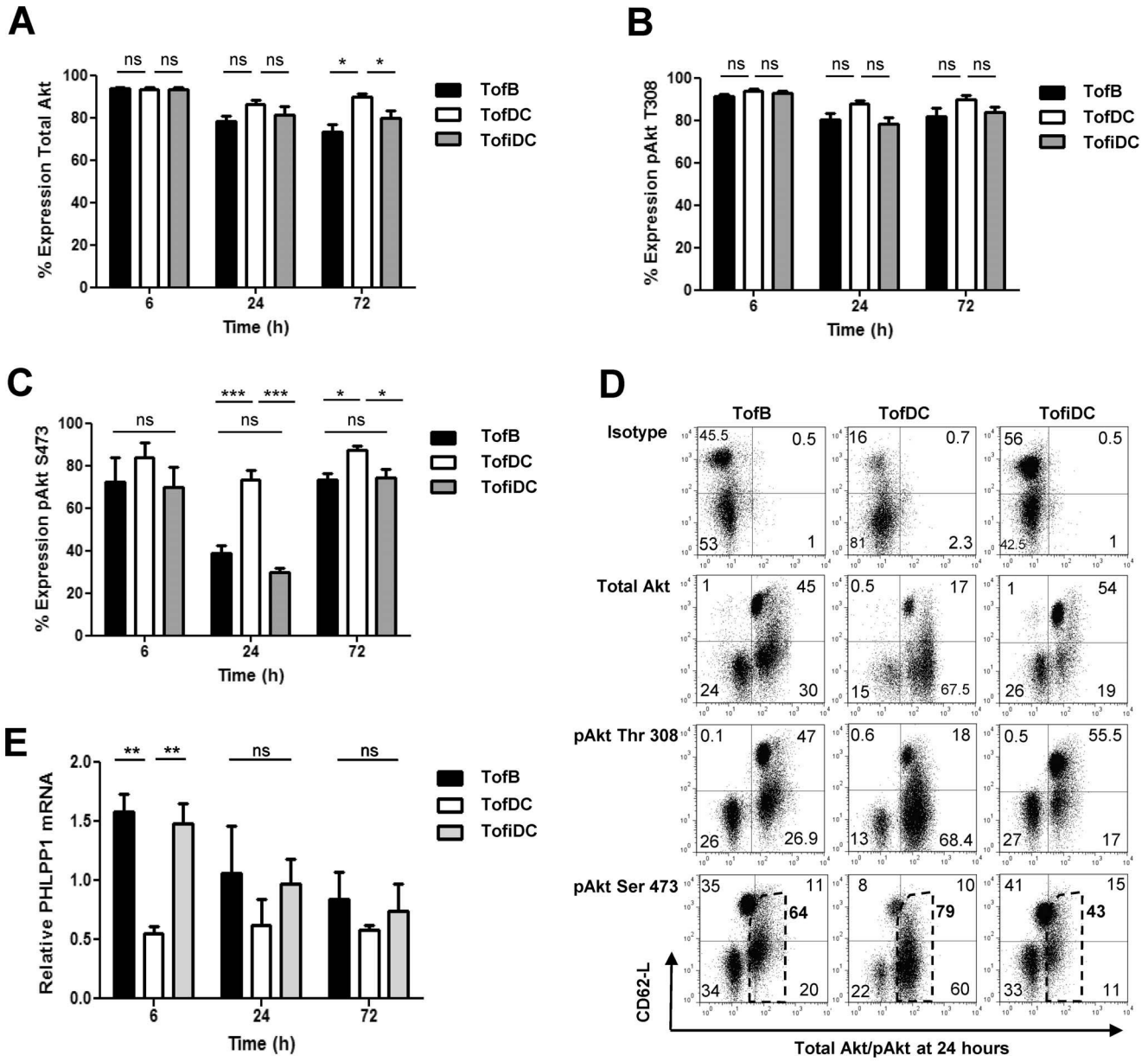

Figure 5. Phospho-site specific defective Akt signaling observed following T-cell triggering by weak APCs. Cells were treated as described in Figure 3 including priming with immature DC (TofiDC) and intracellular FACS staining of total Akt and phopho-forms was performed at indicated time points. For qPCR analysis, T cells were recovered/enriched from co-cultures by MACS depletion. (A) Time course of the number of cells expressing total Akt. (B) Time course of the number of cells expressing pAkt Thr308. (C) Time course of the number of cells expressing pAkt Ser473. (D) One representative FACS blot showing reduced pAkt Ser473 activation in TofB and TofiDC at 24 hours. Numbers in quadrants denominate the percentage of cells. The dashed region indicates the pSer473 positive fraction analyzed for its MFI value (fat number on the right of the dashed region). (E) qPCR readout of PHLPP1 levels in TofB and TofiDC compared to TofDC. Data are means+SEM of 3–4 experiments. Data in D are representative of 4 independent experiments.
doi:10.1371/journal.pone.0068378.g005

development deviated and iT_{reg} re-expressed CD62-L while T_{eff} maintained low levels of the molecule. Again we observed that CD62-L re-expression coincided with the timing of defective PI3K/Akt activity. Attenuation of PI3K signaling during T_{reg} differentiation/development has been put forward by Okkenhaug and coworkers as allowing for the nuclear return and subsequent binding of the transcription factor Foxo on the promoter region of the Foxp3 locus in the nucleus [33]. We extend this position by suggesting that Foxo on return possibly also binds onto the promoter for KLF2 thereby leading to increased CD62-L transcription and its re-expression in the iT_{reg} but not the T_{eff} in our model. The latter showed consistently high PI3K activity. It was possible that CD62L was additionally modulated by the selective presence of microRNAs as recently reported [37]. However, we could not confirm a role for the miRNA let7-b in inducing CD62-L re-expression as we found it to be equally downregulated in both TofB and TofDC (unpublished data). Also of interest was the observation that both T_{regs} in our model were $Foxp3^{-}$. While we previously showed that the TofB developed independent of IL-10 presence in B cells, the Roncarolo group have shown that immature DCs produce $Foxp3^{-}$ $CD25^{low}$ Tr1

like T_{regs} under allogeneic sub-optimal T cell activation conditions under the influence of IL-10 [38].

Having observed the re-expression of CD62-L on the iT_{regs} in our model we asked whether the re-expression of CD62-L was always associated with the acquisition of regulatory function. This question is pertinent as there are several studies linking the CD62-L transcription factor Foxo with T_{reg} induction [39–42] or function [10]. However, CD62-L aside its requirement for homing to lymph nodes has also been related with the acquisition and maintenance of memory in central memory T-cells [43,44] as well as with the development of effector function such as lytic activity in human tumor-infiltrating T lymphocytes [45]. Our data indeed showed independence of the development of lymphatic homing capacity and regulatory activity since Ly294002-treated T_{eff} with high CD62-L did show regulatory properties when tested functionally while Rapamycin-treated TofDC with high CD62-L showed no inhibitory function. Furthermore, our data also show that increased co-stimulation via CD28 has no discernible effect on CD62-L regulation while at same time inducing a complete loss of regulatory function.

Together these data suggest a compartmentalization in the signaling pathways controlling the acquisition of regulatory activity and homing. Obviously, only PI3K but not mTOR inhibition is able to upregulate CD62-L together with the acquisition of a regulatory phenotype in naïve T-cells. This unexpected finding is interesting given that administration of the mTOR-inhibiting drug Rapamycin is an established means of inducing T_{reg} expansion from $CD4^+$ $CD25^+$ cells [46]. Furthermore, Rapamycin was reported to induce T_{regs} from naïve T-cells [47]. In said study however, naïve $CD4^+$ T-cells were co-cultured with B-cells as APC in the presence of Rapamycin. Based on similarities with our study, it is tempting to speculate that the resultant regulatory behavior might have been conferred by the presence of the B-cell, as in our system. However, even in the absence of B-cells, naïve T-cells triggered with CD3 antibodies in the presence of Rapamycin or Ly294002 do acquire a T_{reg} phenotype [48]. This disparity in results might be indicative that antigen specific activation by weak APC can trigger more delicate pathways of T-cell activation as opposed to the very strong stimulus coming from polyclonal CD3 crosslinking. The nature of these triggers has, however, remains elusive so far.

In summary, we present data showing that remarkably similar signaling pathways drive the generation of iT_{regs} and T_{eff} from naïve T-cells and iT_{reg} inducing signaling features are again very similar to those active in established T_{reg} [10]. The key difference between the induction of a T_{reg} and a T_{eff} phenotype appears to be signaling thresholds combined with carefully timed signal intensity modulation in the PI3K/Akt pathway. At the same time separate mechanisms exist, that control the expression of specific homing markers. A better understanding of these mechanisms might help to provide means for a selective generation and tissue specific recruitment of T-cell effector phenotypes in the future.

Materials and Methods

Ethics

All cells used in this study were isolated from organs of mice. Before organ harvest the mice were sacrificed painlessly by deep narcosis followed by cervical dislocation according to institutional guidelines and no invasive procedures were carried out using live animals. According to the German Tierschutzgesetz (TSchG) the use of animal tissue following painless sacrifice and without any further treatment of live animals is not considered an animal experiment and therefore does not require ethical approval. However, the animal welfare officer of both institutions, where the experiments were performed, was informed and had to collect information on the number of animals used for tissue donation. This information was forwarded to the local authorities (Landesverwaltungsamt Sachsen-Anhalt and LANUV, Nordrhein Westfalen).

Mice

DO11.10 [49] and OT-II mice [50] with transgenic TCRs recognising a peptide of chicken-ovalbumin (pOVA AA323–339) were used for T-Cells while B-cells and bone marrow DCs (DCs) were obtained from C57BL/6 and BALB/c mice. Animals were housed and bred in an animal facility of the Otto-von Guericke University and the University Duisburg-Essen, Germany, under SPF-conditions and treated according to institutional guidelines.

Cell Preparation

Naive $CD4^+$ T-cells from spleens of DO11.10 or OT-II mice, splenic B-cells BALB/c or C57BL/6 and mature bone marrow derived DC were all generated as previously described [16] while immature DC (iDC) were generated using the same technique as DC but with absence of IL-4 as described [51]. All cells were cultured at 37°C with 5% CO_2.

T-cell Activation Assays

Naïve T-cells were co-cultured with OVA-peptide loaded LPS stimulated DC, iDC or naive B-cells at a ratio of 10:1/10:1 or 1:1, respectively. The cell culture medium was RPMI-based and supplemented with 10% fetal calf serum (Gibco, Los Angeles, USA). After 72 hours co-cultures underwent immunomagnetic depletion of non-CD4 cells using the MACS system as described [16]. B-cell (TofB), iDC (TofiDC) or DC (TofDC)–primed T-cells (with or without pharmacological modulators) were extensively washed with PBS after immunomagnetic recovery to deplete any inhibitors and assayed to test their inhibitory capacity on naïve T-cells primed with pOVA loaded DCs (10:1) at a ratio of 1:1 (T primed: T naïve). To measure T-cell proliferation, naïve DO11.10 or OT-II T-cells were stained with 5,6-carboxyfluorescein-diacetate-succinimidyl-ester (CFSE, 0.5 μM; Molecular Probes, Leiden, Netherlands). Readouts for proliferation or activation markers were taken at indicated timepoints. T-cell activation was modulated pharmacologically using TAPI-2 (Calbiochem, Darmstadt, Germany, 100 μM), Ly294002 (Promega, Mannheim, Germany, 10 μM), PD184352 (Selleck Chemicals, Munich, Germany, 2 μM) [22] and Rapamycin (Calbiochem, 100 nM) [52]. Anti-CD28 (Beckton Dickinson, Heidelberg, Germany) mediated co-stimulation was provided at 10 μg/ml.

Flow Cytometry

For surface staining, all antibodies were purchased from BD except for CD11c (Caltag, Burlingame, USA), MHCII (eBioscience, Frankfurt, Germany) and CD80/86 (Abcam, Cambridge, UK). For intracellular staining, FITC conjugated pan Akt, pAkt Thr308 and pAkt Ser473 with isotype controls were from Cell Signalling Technology (Frankfurt, Germany) and used with the BD cytoperm/cytofix with GolgiPlug kit. Events were acquired on a BD FACSCalibur™ and LSRFortessa™.

Real-Time PCR

T-cells co-incubated with B-cells, iDC or DC were recovered via the MACS system to an average purity of 88%. Total RNA was isolated and cDNA synthesized using the RNeasy kit and the Quantitect Reverse-Transcriptase-kit (Qiagen, Cologne, Germany). Primers were reagent kits from Qiagen. Real-time PCR

was performed on either the Qiagen RotorGene or ABI prism 7000, using the QuantiTect SYBR Green PCR Kit (Qiagen) or the Maxima SYBR Green/ROX qPCR Master Mix (2×) kit (Fermentas, St. Leon-Rot, Germany) in duplicates. C_t values were averaged and normalized against C_t values of β-Actin. Results were derived using the comparative Ct method ($\Delta\Delta C_t$).

Statistical Analysis

Statistical significance was evaluated with student's t-test using GraphPad Prizm 5 (GraphPad Software, San Diego, CA, USA). P-values <0.05 were considered significant. Data were expressed as means +/− SEM with 3 or more independent experiments performed.

Supporting Information

Figure S1 Effect of inhibitor Titration on CD62-L levels. Naïve antigen specific T-cells were stimulated with either naïve B-cells (TofB) or activated dendritic cells (TofDC), both loaded with a cognate peptide of chicken ovalbumin, for different periods of time and in the absence or presence of inhibitors. Subsequently, CD62-L expression levels on T cells were measured by flow cytometry. (A) One representative FACS blot showing the dose dependent regulation of CD62-L in T cells by the PI3K inhibitor LY294002. (B) One representative FACS blot showing the dose dependent regulation of CD62-L in T cells by the mTOR inhibitor Rapamycin. Data are representative of 3 independent experiments.
(PDF)

Figure S2 Characterization of Immature DCs against mature DCs. Immature DC were characterized with respect to expression levels of relevant lineage and stimulatory marker molecules.(A) Representative FACS histogram showing expression levels of the indicated surface molecules. Dashed lines represent isotypes and solid lines indicate expression level of quantified molecules (B) Comparison of % surface expression of MHC II, CD11c, CD80 and CD86 between both cell phenotypes. (C) On a per cell basis, DC express more CD11c than immature DC while both cells possess equal amounts of MHC II. (D) On a per cell basis, DC express more co-stimulatory molecules than immature DC. Data are means+SEM of 2 experiments.
(TIF)

Figure S3 Akt signaling profile at 6 and 72 hours. Cells were treated as described in Figure 5. (A) Representative FACS blots showing Akt/pAkt levels in TofB, TofiDC and TofDC at 6 h (B) Representative FACS blots showing Akt/pAkt levels in TofB, TofiDC and TofDC at 72 hours.
(TIF)

Acknowledgments

We thank Jochen Hühn (HZI, Braunschweig, Germany) and Burkhart Schraven (Otto-von-Guericke University, Magdeburg) for critical reading of the manuscript.

Author Contributions

Conceived and designed the experiments: MG PR. Performed the experiments: EE MK MH. Analyzed the data: EE MK MG. Wrote the paper: MG EE.

References

1. Kanno Y, Vahedi G, Hirahara K, Singleton K, O'Shea JJ (2012) Transcriptional and epigenetic control of T helper cell specification: molecular mechanisms underlying commitment and plasticity. Annu Rev Immunol 30: 707–731.
2. Zhu J, Yamane H, Paul WE (2010) Differentiation of effector CD4 T cell populations. Annu Rev Immunol 28: 445–489.
3. Weaver CT, Hatton RD, Mangan PR, Harrington LE (2007) IL-17 family cytokines and the expanding diversity of effector T cell lineages. Annu Rev Immunol 25: 821–852.
4. Oestreich KJ, Weinmann AS (2012) Master regulators or lineage-specifying? Changing views on CD4(+) T cell transcription factors. Nat Rev Immunol 12: 799–804.
5. Sakaguchi S, Miyara M, Costantino CM, Hafler DA (2010) FOXP3+ regulatory T cells in the human immune system. Nat Rev Immunol 10: 490–500.
6. Wood KJ, Bushell A, Hester J (2012) Regulatory immune cells in transplantation. Nat Rev Immunol 12: 417–430.
7. Passerini L, Di NS, Gregori S, Gambineri E, Cecconi M, et al. (2011) Functional type 1 regulatory T cells develop regardless of FOXP3 mutations in patients with IPEX syndrome. Eur J Immunol 41: 1120–1131.
8. Vieira PL, Christensen JR, Minaee S, O'Neill EJ, Barrat FJ, et al. (2004) IL-10-secreting regulatory T cells do not express Foxp3 but have comparable regulatory function to naturally occurring CD4+CD25+ regulatory T cells. J Immunol 172: 5986–5993.
9. O'Shea JJ, Paul WE (2010) Mechanisms underlying lineage commitment and plasticity of helper CD4+ T cells. Science 327: 1098–1102.
10. Ouyang W, Liao W, Luo CT, Yin N, Huse M, et al. (2012) Novel Foxo1-dependent transcriptional programs control T(reg) cell function. Nature 491: 554–559.
11. Szabo SJ, Kim ST, Costa GL, Zhang X, Fathman CG, et al. (2000) A novel transcription factor, T-bet, directs Th1 lineage commitment. Cell 100: 655–669.
12. Patterson SJ, Han JM, Garcia R, Assi K, Gao T, et al. (2011) Cutting edge: PHLPP regulates the development, function, and molecular signaling pathways of regulatory T cells. J Immunol 186: 5533–5537.
13. Semple K, Nguyen A, Yu Y, Wang H, Anasetti C, et al. (2011) Strong CD28 costimulation suppresses induction of regulatory T cells from naive precursors through Lck signaling. Blood 117: 3096–3103.
14. Kretschmer K, Apostolou I, Hawiger D, Khazaie K, Nussenzweig MC, et al. (2005) Inducing and expanding regulatory T cell populations by foreign antigen. Nat Immunol 6: 1219–1227.
15. Apostolou I, von Boehmer H (2004) In vivo instruction of suppressor commitment in naive T cells. J Exp Med 199: 1401–1408.
16. Reichardt P, Dornbach B, Song R, Beissert S, Gueler F, et al. (2007) Naive B cells generate regulatory T cells in the presence of a mature immunological synapse. Blood 110: 1519–1529.
17. Reichardt P, Dornbach B, Gunzer M (2007) The molecular makeup and function of regulatory and effector synapses. Immunol Rev 218: 165–177.
18. Moreau HD, Lemaitre F, Terriac E, Azar G, Piel M, et al. (2012) Dynamic In Situ Cytometry Uncovers T Cell Receptor Signaling during Immunological Synapses and Kinapses In Vivo. Immunity 37: 351–363.
19. Diaz-Rodriguez E, Montero JC, Esparis-Ogando A, Yuste L, Pandiella A (2002) Extracellular signal-regulated kinase phosphorylates tumor necrosis factor alpha-converting enzyme at threonine 735: a potential role in regulated shedding. Mol Biol Cell 13: 2031–2044.
20. Soond SM, Everson B, Riches DW, Murphy G (2005) ERK-mediated phosphorylation of Thr735 in TNFalpha-converting enzyme and its potential role in TACE protein trafficking. J Cell Sci 118: 2371–2380.
21. Fabre S, Carrette F, Chen J, Lang V, Semichon M, et al. (2008) FOXO1 regulates L-Selectin and a network of human T cell homing molecules downstream of phosphatidylinositol 3-kinase. J Immunol 181: 2980–2989.
22. Sinclair LV, Finlay D, Feijoo C, Cornish GH, Gray A, et al. (2008) Phosphatidylinositol-3-OH kinase and nutrient-sensing mTOR pathways control T lymphocyte trafficking. Nat Immunol 9: 513–521.
23. Gerner MY, Kastenmuller W, Ifrim I, Kabat J, Germain RN (2012) Histo-Cytometry: A Method for Highly Multiplex Quantitative Tissue Imaging Analysis Applied to Dendritic Cell Subset Microanatomy in Lymph Nodes. Immunity 37: 1–13.
24. Ohnmacht C, Pullner A, King SB, Drexler I, Meier S, et al. (2009) Constitutive ablation of dendritic cells breaks self-tolerance of CD4 T cells and results in spontaneous fatal autoimmunity. J Exp Med 206: 549–559.
25. Steinman RM, Nussenzweig MC (2002) Inaugural Article: Avoiding horror autotoxicus: The importance of dendritic cells in peripheral T cell tolerance. Proc Natl Acad Sci U S A 99: 351–358.
26. Dudziak D, Kamphorst AO, Heidkamp GF, Buchholz VR, Trumpfheller C, et al. (2007) Differential antigen processing by dendritic cell subsets in vivo. Science 315: 107–111.
27. Gunzer M, Schäfer A, Borgmann S, Grabbe S, Zänker KS, et al. (2000) Antigen presentation in extracellular matrix: interactions of T cells with dendritic cells are dynamic, short lived, and sequential. Immunity 13: 323–332.
28. Riha P, Rudd CE (2010) CD28 co-signaling in the adaptive immune response. Self Nonself 1: 231–240.
29. Crellin NK, Garcia RV, Levings MK (2007) Altered activation of AKT is required for the suppressive function of human CD4+CD25+ T regulatory cells. Blood 109: 2014–2022.

30. Josefowicz SZ, Lu LF, Rudensky AY (2012) Regulatory T cells: mechanisms of differentiation and function. Annu Rev Immunol 30: 531–564.
31. Bilate AM, Lafaille JJ (2012) Induced CD4+Foxp3+ regulatory T cells in immune tolerance. Annu Rev Immunol 30: 733–758.
32. Littman DR, Rudensky AY (2010) Th17 and regulatory T cells in mediating and restraining inflammation. Cell 140: 845–858.
33. Soond DR, Slack EC, Garden OA, Patton DT, Okkenhaug K (2012) Does the PI3K pathway promote or antagonize regulatory T cell development and function? Front Immunol 3: 244.
34. Powell JD, Pollizzi KN, Heikamp EB, Horton MR (2012) Regulation of immune responses by mTOR. Annu Rev Immunol 30: 39–68.
35. Garcon F, Patton DT, Emery JL, Hirsch E, Rottapel R, et al. (2008) CD28 provides T-cell costimulation and enhances PI3K activity at the immune synapse independently of its capacity to interact with the p85/p110 heterodimer. Blood 111: 1464–1471.
36. Pletinckx K, Dohler A, Pavlovic V, Lutz MB (2011) Role of dendritic cell maturity/costimulation for generation, homeostasis, and suppressive activity of regulatory T cells. Front Immunol 2: 39.
37. Guenin-Mace L, Carrette F, Asperti-Boursin F, Le Bon A, Caleechurn L, et al. (2011) Mycolactone impairs T cell homing by suppressing microRNA control of L-selectin expression. Proc Natl Acad Sci U S A 108: 12833–12838.
38. Levings MK, Gregori S, Tresoldi E, Cazzaniga S, Bonini C, et al. (2005) Differentiation of Tr1 cells by immature dendritic cells requires IL-10 but not CD25+CD4+ Tr cells. Blood 105: 1162–1169.
39. Harada Y, Harada Y, Elly C, Ying G, Paik JH, et al. (2010) Transcription factors Foxo3a and Foxo1 couple the E3 ligase Cbl-b to the induction of Foxp3 expression in induced regulatory T cells. J Exp Med.
40. Kerdiles YM, Stone EL, Beisner DR, McGargill MA, Ch'en IL, et al. (2010) Foxo transcription factors control regulatory T cell development and function. Immunity 33: 890–904.
41. Ouyang W, Beckett O, Ma Q, Paik JH, Depinho RA, et al. (2010) Foxo proteins cooperatively control the differentiation of Foxp3+ regulatory T cells. Nat Immunol 11: 618–627.
42. Hedrick SM, Michelini RH, Doedens AL, Goldrath AW, Stone EL (2012) FOXO transcription factors throughout T cell biology. Nat Rev Immunol 12: 649–661.
43. Dang X, Raffler NA, Ley K (2009) Transcriptional regulation of mouse L-selectin. Biochim Biophys Acta 1789: 146–152.
44. Roberts AD, Ely KH, Woodland DL (2005) Differential contributions of central and effector memory T cells to recall responses. J Exp Med 202: 123–133.
45. Yang S, Liu F, Wang QJ, Rosenberg SA, Morgan RA (2011) The shedding of CD62L (L-selectin) regulates the acquisition of lytic activity in human tumor reactive T lymphocytes. PLoS ONE 6: e22560.
46. Battaglia M, Stabilini A, Tresoldi E (2012) Expanding human T regulatory cells with the mTOR-inhibitor rapamycin. Methods Mol Biol 821: 279–293.
47. Chen JF, Gao J, Zhang D, Wang ZH, Zhu JY (2010) CD4+Foxp3+ regulatory T cells converted by rapamycin from peripheral CD4+CD25(−) naive T cells display more potent regulatory ability in vitro. Chin Med J (Engl) 123: 942–948.
48. Sauer S, Bruno L, Hertweck A, Finlay D, Leleu M, et al. (2008) T cell receptor signaling controls Foxp3 expression via PI3K, Akt, and mTOR. Proc Natl Acad Sci U S A 105: 7797–7802.
49. Murphy KM, Heimberger AB, Loh DY (1990) Induction by antigen of intrathymic apoptosis of $CD4^{+}CD8^{+}TCR^{lo}$ thymocytes in vivo. Science 250: 1720–1723.
50. Barnden MJ, Allison J, Heath WR, Carbone FR (1998) Defective TCR expression in transgenic mice constructed using cDNA-based alpha- and beta-chain genes under the control of heterologous regulatory elements. Immunol Cell Biol 76: 34–40.
51. Labeur MS, Roters B, Pers B, Mehling A, Luger TA, et al. (1999) Generation of tumor immunity by bone marrow-derived dendritic cells correlates with dendritic cell maturation stage. J Immunol 162: 168–175.
52. Procaccini C, De Rosa V, Galgani M, Abanni L, Cali G, et al. (2010) An Oscillatory Switch in mTOR Kinase Activity Sets Regulatory T Cell Responsiveness. Immunity 33: 929–941.

Appendix 03

Teles A, Schumacher A, Kühnle MC, Linzke N, Thuere C, **Reichardt P**, Tadokoro CE, Hämmerling GJ, Zenclussen AC.
Control of uterine microenvironment by foxp3(+) cells facilitates embryo implantation.
Front Immunol. 2013:4:158.

IF [neu], seit 2011 offizielles Organ der International Union of Immunological Societies

frontiers in
IMMUNOLOGY

ORIGINAL RESEARCH ARTICLE
published: 20 June 2013
doi: 10.3389/fimmu.2013.00158

Control of uterine microenvironment by Foxp3$^+$ cells facilitates embryo implantation

Ana Teles[1,2], Anne Schumacher[1], Marie-Cristine Kühnle[3], Nadja Linzke[1], Catharina Thuere[1], Peter Reichardt[4], Carlos Eduardo Tadokoro[5], Günter J. Hämmerling[3] and Ana Claudia Zenclussen[1]*

[1] *Experimental Obstetrics and Gynecology, Medical Faculty, Otto-von-Guericke University Magdeburg, Magdeburg, Germany*
[2] *PDBEB, Center for Neuroscience and Cell Biology, University of Coimbra, Coimbra, Portugal*
[3] *Molecular Immunology, German Cancer Research (Center DKFZ), Heidelberg, Germany*
[4] *Institute for Molecular and Clinical Immunology, Medical Faculty, Otto-von-Guericke University, Magdeburg, Germany*
[5] *Instituto Gulbenkian de Ciências, Oeiras, Portugal*

Edited by:
Donata Medaglini, University of Siena, Italy

Reviewed by:
Ali M. Harandi, University of Gothenburg, Sweden
Charles Kelly, King's College London, UK

****Correspondence:***
Ana Claudia Zenclussen, Experimental Obstetrics and Gynecology, Medical Faculty, Otto-von-Guericke University Magdeburg, 39108 Magdeburg, Germany
e-mail: ana.zenclussen@med.ovgu.de

Günter J. Hämmerling and Ana Claudia Zenclussen are co-senior authors.

Implantation of the fertilized egg into the maternal uterus depends on the fine balance between inflammatory and anti-inflammatory processes. Whilst regulatory T cells (Tregs) are reportedly involved in protection of allogeneic fetuses against rejection by the maternal immune system, their role for pregnancy to establish, e.g., blastocyst implantation, is not clear. By using 2-photon imaging we show that Foxp3$^+$ cells accumulated in the mouse uterus during the receptive phase of the estrus cycle. Seminal fluid further fostered Treg expansion. Depletion of Tregs in two Foxp3.DTR-based models prior to pairing drastically impaired implantation and resulted in infiltration of activated T effector cells as well as in uterine inflammation and fibrosis in both allogeneic and syngeneic mating combinations. Genetic deletion of the homing receptor CCR7 interfered with accumulation of Tregs in the uterus and implantation indicating that homing of Tregs to the uterus was mediated by CCR7. Our results demonstrate that Tregs play a critical role in embryo implantation by preventing the development of a hostile uterine microenvironment.

Keywords: regulatory T cells, implantation, pregnancy, fibrosis, inflammation

INTRODUCTION

Normal pregnancy is a physiological state during which distinct processes take place at different stages. Pregnancy begins with the fertilization of the ovum, followed by implantation of the blastocyst in the maternal uterus. To implant, the blastocyst needs to adhere to the endometrium so that it can be provided with oxygen and nutrients. For these changes to occur tissue remodeling and inflammatory processes in the uterus are required. It has been observed that ablation of immunoregulatory molecules such as transforming growth factor beta (TGF-β) or heme oxygenase-1 (*Hmox1*) negatively interferes with implantation (McLennan and Koishi, 2004; Zenclussen et al., 2011). Thus, a balance between pro- and anti-inflammatory molecules is assumed to support successful implantation. Cells of the innate immune system present in the uterus are known to be critical for implantation. For example, uterine natural killer cells (uNK cells) produce IFN-γ, which contributes to the initiation of vascular modification and decidual integrity (Ashkar et al., 2000). Macrophages present in the uterus secrete IL-1, which is reportedly involved in implantation (Houser et al., 2011). Ablation of uterine dendritic cells (DC) causes implantation failure due to perturbed angiogenesis (Plaks et al., 2008) while the absence of uterine mast cells (MCs) leads to defective implantation and spiral artery remodeling (Woidacki et al., 2013).

Once implantation is established, a period of maintenance follows, during which the maternal immune system actively tolerates the foreign paternal antigens expressed by the fetus (Tafuri et al., 1995) while being fully active against potential infections. Maternal CD4$^+$CD25$^+$ regulatory T cells (Tregs) have been reported to contribute to the maintenance of tolerance during pregnancy by suppressing maternal alloreactive immune responses against paternal structures in fetal cells (Zenclussen et al., 2005; Shima et al., 2010; Rowe et al., 2012; Samstein et al., 2012). It has been speculated the Tregs also participate at initial stages of pregnancy, e.g., implantation (Zenclussen et al., 2005; Schumacher et al., 2007), at which inflammatory processes and innate cell populations play an important role. However, conclusive experimental proof that Tregs are important for implantation was missing. The present study addresses this question and by using specific models shows that Foxp3$^+$ Tregs are needed for successful implantation because they prevent the development of a hostile uterine microenvironment. In their absence, inflammation and fibrosis occur, both negatively interfering with embryo implantation.

MATERIALS AND METHODS

STUDY APPROVAL

All studies were conducted according to governmental and institutional regulations (AZ 42502-2-868, Magdeburg; AZ 35-9185.81/G-98/08, Heidelberg; AO 10/2010, Oeiras).

MICE AND TREG DEPLETION

Foxp3^{DTR} (Kim et al., 2007) and *Foxp3*^{GFP} knock-in mice (Fontenot et al., 2005) were kindly provided by Alexander Rudensky (Washington, DC, USA) and Jocelyne Demengeot (Oeiras, Portugal) and bred in our facilities. CCR7$^{-/-}$ mice were purchased from Jackson Laboratories; C57BL/6 and BALB/c (intact, vasectomized, and seminal vesicle-deficient) mice from Charles River, Germany. BAC transgenic Foxp3.LuciDTR-4 mice (Suffner et al., 2010) were generated and maintained at the DKFZ, Heidelberg. Mated females were checked daily for vaginal plugs; its appearance indicates day 0 of pregnancy. Females were mated and checked daily for vaginal plugs, its appearance indicates day 0.5 of pregnancy. Vaginal lavage was performed with 20 μL of 0.9% sodium chloride. Cycle stage was defined after observation of the cellular components under light microscopy (Axiovert C, Carl Zeiss, Germany; magnification ×200), and was confirmed by hematoxylin/Eosin. Treg depletion in Foxp3^{DTR} mice was performed by i.p. application of 15 ng/g body weight diphtheria toxin (DT) every fourth day. In Foxp3Luci.DTR mice, DT was applied daily beginning at day −2. Control mice received PBS or DT. Implantations sites at day 5 of pregnancy were identified after i.v. injection of 0.5% Chicago Blue dye.

2-PHOTON *IN VIVO* MICROSCOPY

Imagining of uterine *Foxp3*^{GFP} cells during the estrus cycle was performed as follows. Animals were anesthetized by i.p. injection of ketamine and xylazine, 120 or 16 μg/g of mouse weight, respectively, and kept on a heating pad at 37°C. One of the uterine horns was carefully exposed and 0.1 M caffeine (Sigma-Aldrich, USA) was applied to decrease uterine contractions. For maternal blood visualization, animals were intravenously injected with 100 μl of Rhodamine B isothiocyanate-Dextran (RhoB-Dex) 70,000 KDa (Sigma-Aldrich, Inc., USA) before acquiring images in a multiphoton laser scanning microscope (MPLSM). We used a Prairie Ultima 2-photon microscope (Prairie Technologies, Inc.). The microscope was equipped with a Chameleon Ti:Sapphire laser (Coherent, Inc., USA), four top PMTs for simultaneous up to four channel acquisitions and a 20× water immersion objective (Olympus, Inc., USA). The laser was tuned to 880 nm to allow for concomitant excitation of RhoB-Dex and GFP^{+}-Treg. The wavelength emission for RhoB-Dex and GFP is 590 and 509 nm, respectively. Sequential images were acquired for observation of Treg in the uterus. For analysis of uterine Treg images, we have developed our own software algorithms based on endogenous tissue markers information (e.g., location of blood vessels) from consecutive z-stacks acquisitions for stabilization of Treg movies. Once the images were stabilized, we used Imaris software (Bitplane AG, Inc.) for reconstruction of three-dimensional models in order to determine distribution in the uterus. For more detail, please see Zenclussen et al. (2013).

FLOW CYTOMETRY

The following fluorescence-conjugated antibodies were purchased from BD Biosciences or eBioscience: CD4 (RM-4 or RM4-5), CD8 (53-6.7), Foxp3 (FJK-16s or NRRF-30), Ki67 (B56), CD44 (IM7), CD62L (Mel-14). Samples were processed as described (Zenclussen et al., 2005; Woidacki et al., 2013), measured in a FACSCalibur or FACSCanto II (BD Biosciences) and analyzed with CellQuest Pro software (BD Biosciences).

HISTOLOGY AND IMMUNOFLUORESCENCE

Analysis of uterine tissue was performed after staining with Hematoxylin/Eosin. The slides were dewaxed and left in Hematoxylin (Fluka Biochemika, Germany) for 1–2 min followed by rinse with tap water and a further incubation in Eosin (Fluka Biochemika, Germany) for 1–2 min and finally dehydrated to xylol and covered. Fibrosis extent was evaluated by Masson's trichrome and Picrosirius red stainings. For the first, the dewaxed slides were left in picrosirius red stain solution (Sigma) for 1 h and rinsed in 10 dips of water before being dehydrated to xylol and covered. For Masson's trichrome staining it was proceed as follows: after dewaxing, the slides were placed in Bouin's solution (Sigma) overnight (ON) for mordating and washed in running tap water before staining for 5 min in working Weigert's iron Hematoxylin solution (Sigma). After washing in running tap water, the samples were stained in Biebrich Scarlet-acid Fuchsin (Sigma) for 5 min and rinsed in distilled water. The slides were placed in Phosphomolybdic/Phosphotungstic acid solution (Sigma) for 10 min and the solution was discarded and substituted by aniline blue solution for five more min. Finally, the slides were placed in 1% acetic acid solution for 3 min and dehydrated to xylol before being covered.

Connective tissue growth factor (CtGF) in uterine tissue was studied by immunofluorescence**.** For this, tissue sections were dewaxed and blocked for 30 min with 3% bovine serum albumin (BSA) in PBS at room temperature (RT). The slides were then washed in PBS and incubated with anti-CTGF primary antibody (Abcam ab6992) in 2% BSA at a dilution of 1:200 ON at 4°C. After further washing the slides with PBS they were incubated with Alexa Fluor 488 goat anti-Rabbit IgG secondary antibody (Abcam) at a dilution of 1:200 for 45 min at RT. Sections were washed and the slides were covered with Dapi Vecta Shield mounting medium.

IN VITRO PROLIFERATION

MACS-sorted Treg or effector T cells were stained with carboxyfluorescein diacetate succinimidyl ester (CFSE, Molecular Probes, Leiden, Netherlands), cultured with rmIL-2 (R & D systems) and treated with freshly prepared seminal vesicle fluid (SVF) from BALB/c males. Anti-TGF-β1 mAb was kindly provided by Hideo Yagita (Juntendo University, Tokyo, Japan).

QUANTITATIVE REAL TIME PCR

mRNA was isolated using Trizol® and cDNA synthesis was done using reverse transcriptase (Invitrogen, Karlsruhe, Germany). Real time PCR was performed with the help of an iCycler (BIORAD, Munich, Germany) using SYBR Green (Applied Biosystems, Germany). Initial denaturation was done at 95°C for 5 min followed by a denaturation step of 40 cycles of 45 s at 95°C. Annealing step followed at 59°C for 30 s 72°C for 30 s extension. The amount of cDNA was standardized with the reference gene β-actin. Primers are available upon request.

STATISTICAL ANALYSIS

Statistical analyses were performed with Prism software (GraphPad). Normality in the distribution of the data was analyzed by

the D'Agostino and Pearson omnibus normality test. Differences in the percentage of $CD4^+Foxp3^{GFP+}$, $CD8^+$ $KI67^+$, $CD44^+$, and $CD62L^+$ cells between groups were analyzed by Mann–Whitney-*U* test. The *in vitro* experiments using cells cultured with SVF were analyzed by two-way ANOVA test. Implantation numbers were measured at day 5, data are expressed as medians of % of implanted females and analyzed by Fisher's exact test. Levels of molecules measured by qPCR [IL-15, CCR5, CCL19, CXCL3, IL-1b, gp130, TNF-α, RORγτ, CCL5, CtGF, CXCL9, urokinase-type plasminogen activator (uPA), prostaglandin F receptor (Ptgfr), IL-9, Gal-1, leukemia inhibitory factor (LIF), p. 53] were analyzed by Mann–Whitney-*U* test. Number of animals used for each experiment is included in the Figure legends.

RESULTS

UTERINE Foxp3$^+$ TREGS ACCUMULATE DURING THE FERTILE PHASE OF THE CYCLE AT THE ANTIMESOMETRIAL REGION

First, we determined the frequencies of $CD4^+Foxp3^+$ Tregs in samples from *Foxp3^{gfp}* female animals at each stage of the estrus cycle (diestrus, proestrus, estrus, metestrus, **Figure 1A**) by flow cytometry (**Figure 1B**). We observed substantial fluctuation in Treg frequency in the vaginal lavage, with Tregs peaking at the receptive phase, namely estrus, and decreasing toward metestrus. *In vivo* 2-photon microscopy in *Foxp3^{gfp}* animals impressively demonstrated a clustering of Tregs in uterine tissue during estrus (**Figure 1C**; Movie S1 in Supplementary Material) that was not observed during the other phases of the estrus cycle, e.g., diestrus

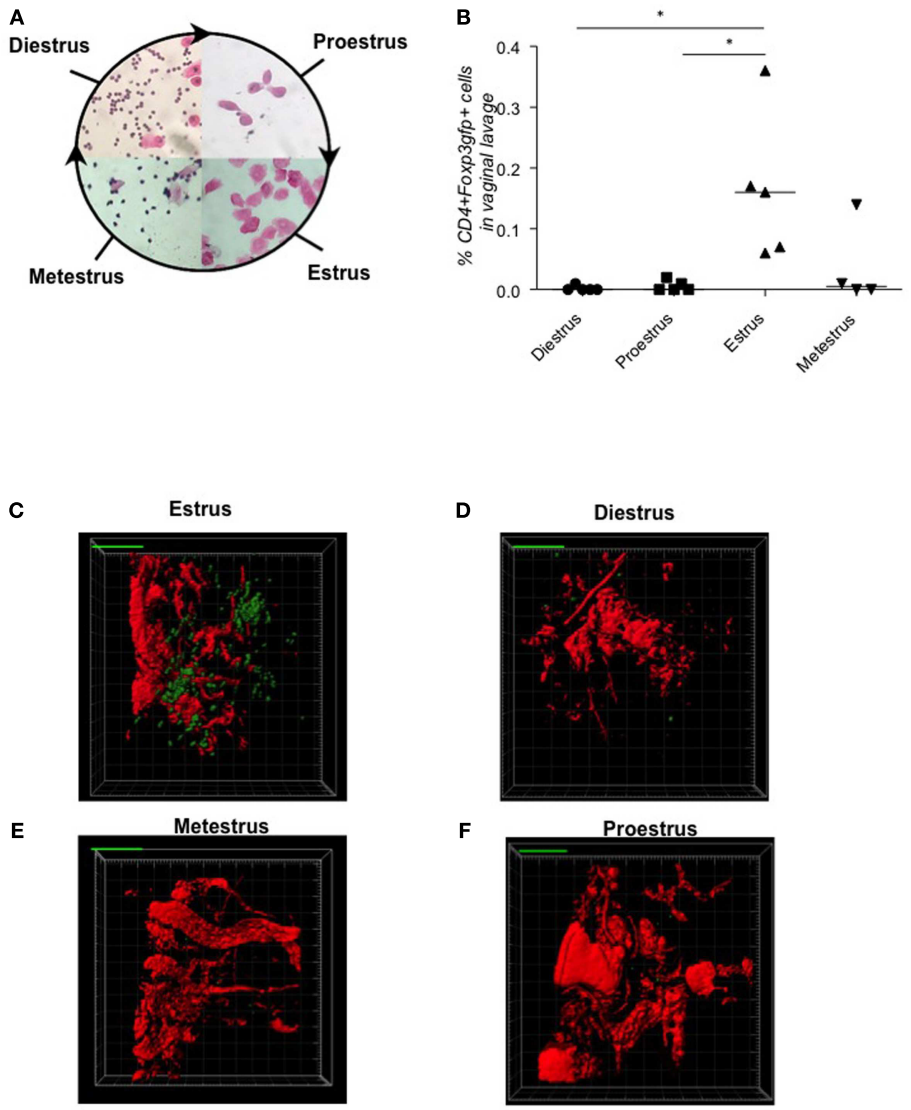

FIGURE 1 | Tregs fluctuate during estrus cycle peaking at estrus, time point of sexual receptivity. Determination of the estrus cycle in non-pregnant females according to cell types in vaginal smears **(A)**. Percentage of $CD4^+Foxp3^{GFP+}$ cells of female $Foxp3^{GFP}$ mice ($n = 5$/cycle stage) was analyzed in vaginal lavage **(B)**. Data are expressed as single dot plots with medians and were analyzed by Mann–Whitney-*U* test ($^*P \leq 0.05$). Snap shots of two-photon microscopy videos of $Foxp3^{GFP}$ positive cells in uterus performed at different phases of the cycle **(C)** estrus phase; **(D)** diestrus phase; **(E)** metestrus phase; **(F)** proestrus phase.

[**Figure 1D**; metestrus (**Figure 1E**) or proestrus (**Figure 1F**); Movies S2–S4 in Supplementary Material]. In agreement with these findings, previous work has suggested oscillations in uterine Foxp3 mRNA expression levels during the estrus cycle (Kallikourdis and Betz, 2007; Guerin et al., 2011). According to the 2-photon studies, Tregs seem to accumulate preferentially in the perivascular space close to small blood vessels at the antimesometrial region during estrus (Movie S1 in Supplementary Material).

SEMINAL FLUID FOSTERS THE EXPANSION OF UTERINE Foxp3$^+$ TREGS

Next, we paired females with seminal vesicle-deficient, vasectomized, or intact allogeneic males. When compared to virgin mice, an expansion of Tregs was observed in the uterine draining lymph nodes from females paired with intact or vasectomized males, whereas no expansion was found in females mated with seminal vesicle-deficient males (**Figure 2A**). Hence, seminal fluid has a proliferative effect on Tregs *in vivo*. These results could be reproduced *in vitro* with CSFE-labeled $CD4^+CD25^+$ Tregs isolated by magnetic cell sorting, which were stimulated to proliferate by addition of seminal fluid and this was partially inhibited by addition of anti-TGF β (**Figure 2B**), whereas conventional T cells were not affected (**Figure 2C**). Thus, the accumulation of Tregs at sexual receptivity is followed by an expansion triggered by seminal fluid, most likely by TGF-β contained herein.

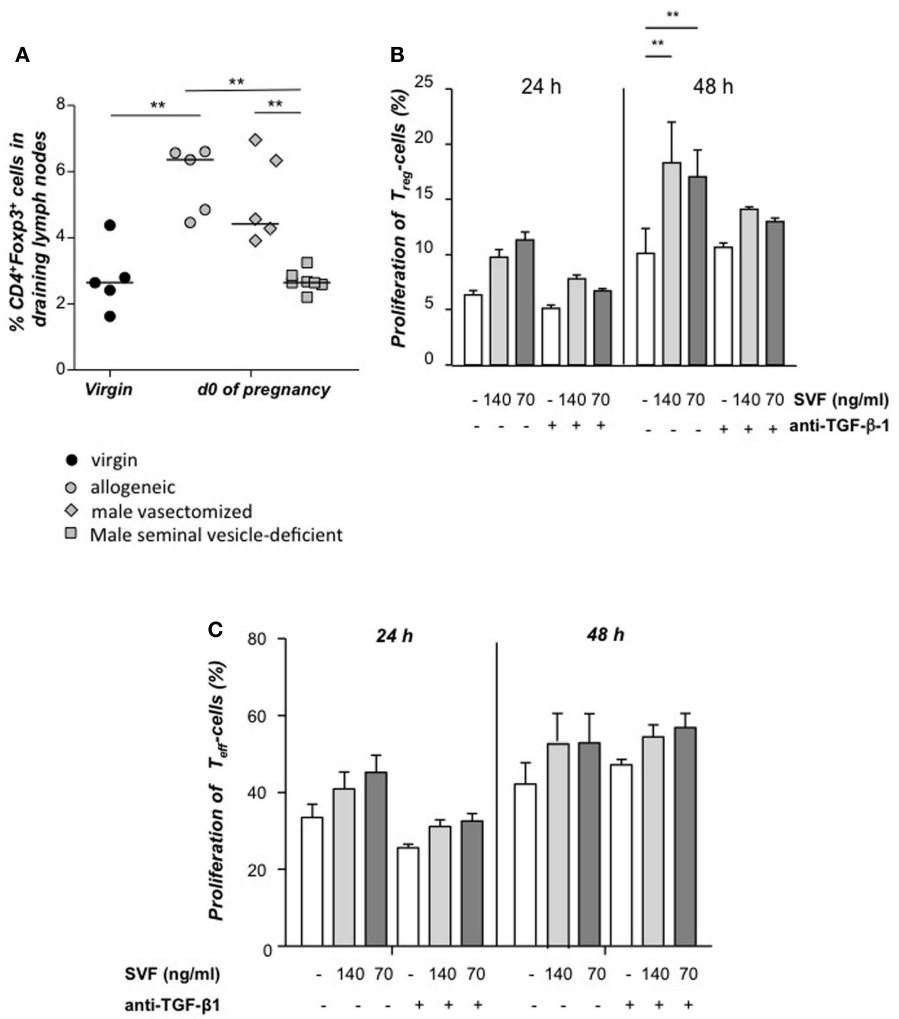

FIGURE 2 | Tregs expand *in vivo* and *in vitro* in presence of seminal fluid. Percentage of $CD4^+Foxp3^+$ cells in the uterine draining lymph nodes of CBA/J females mated with seminal vesicle-deficient, vasectomized, or intact BALB/c males was analyzed at day of conception (day 0.5) and compared to virgin CBA/J females ($n = 4$–7) **(A)**. Statistical analysis were performed by Mann–Whitney-*U* test (**$P \leq 0.01$). **(B)** Tregs were isolated from non-pregnant CBA/J females by magnetic cell sorting, stained with CFSE and cultured with seminal vesicle fluid (SVF) from BALB/c males. TGF-β1 was blocked with anti-TGF-β1 antibody, and proliferation of Treg determined after 24 h by using FACScan Calibur. Data are representative of four experiments and expressed as mean with SEM. Analysis was performed by two-way ANOVA test (**$P \leq 0.01$). **(C)** Conventional T effector cells were isolated from non-pregnant CBA/J females by magnetic cell sorting, stained with CFSE and cultured with seminal vesicle fluid (SVF) from BALB/c males. TGF-β1 was blocked with anti-TGF-β1 antibody, and proliferation of Treg determined after 24 h by using FACScan Calibur. Data are representative of four experiments and expressed as mean with SEM. Analysis was performed by two-way ANOVA test and no statistically significant differences were found among the groups.

DEPLETION OF Foxp3$^+$ TREGS PRIOR TO MATING RESULTED IN UTERINE INFLAMMATION AND FIBROSIS THAT IMPAIRED IMPLANTATION

As Treg accumulation at receptivity suggested a role for embryo implantation, we investigated the effect of CD4$^+$Foxp3$^+$ Treg depletion on implantation by using two distinct strains of Foxp3.DTR mice, namely Foxp3^{DTR} knock-in mice (Fontenot et al., 2005), and BAC-transgenic Foxp3.LuciDTR-4 mice (Suffner et al., 2010). Upon application of DT, at least 90% of CD4$^+$Foxp3$^+$ Tregs were specifically depleted in both strains. Thus, for Treg depletion Foxp3.DTR mice are superior to the frequently used anti-CD25 antibodies, which deplete only about 70% of CD4$^+$Foxp3$^+$ Treg, owing to limited expression of CD25 on Foxp3$^+$ T cells (Shima et al., 2010). Moreover, Foxp3 represents a highly selective marker for Tregs, whereas CD25 is also expressed on a fraction of other leukocytes (Shima et al., 2010). Treg depletion was performed during various time intervals before mating, namely from day 9 to 5 of pregnancy, and from day 2 to 5. To confirm the occurrence of implantations at day 5, Chicago Blue was utilized (**Figure 3A**) Treg depletion beginning at day 9 in *Foxp3^{DTR}* mice provoked a failure of the embryos to implant, whereas PBS- and DT-treated control mice displayed normal implantation (**Figures 3B,C**). When Foxp3.LuciDTR mice were used, syngeneic matings were included in order to elucidate whether the mechanisms leading to implantation failure were dependent on potentially present paternal alloantigens (**Figure 3C**). Treg ablation from day 2 to 5 resulted in severely impaired implantation not only in biologically relevant allogeneic pregnancies but also in syngeneic matings (**Figure 3C**). We speculated that at this early time point Tregs may counteract pro-inflammatory events occurring during implantation. Without Tregs, inflammation may be too strong and hinder the nidation of the embryo. Indeed, we observed that Treg depletion resulted in accumulation of CD8$^+$ T cells in the uterus (**Figure 3D**) and the presence of activated T cells in lymph nodes draining the uterus, as indicated by the increased expression of KI67, CD44, and down-regulation of CD62L in CD4$^+$Foxp3$^-$ effector cells (**Figures 3E–G**). Additionally, the uterine tissue was inflamed and thickened after DT treatment. mRNA expression of the inflammatory mediators IL-15, CCR5, CCL19, and CXCL3, all inflammatory was upregulated (**Figures 4A–D**). Levels of IL-1β, gp130, TNF-α, ROR-gamma-t, or CCL5 were not significantly modified (**Figures 5A–E**). We also observed the appearance of fibrosis in the uterus of mice depleted of Treg as indicated by elevated levels of CtGF and CXCL9 mRNA (**Figures 6A,B**), important regulators of fibrosis (Gressner and Gressner, 2008; Zeremski et al., 2011). Fibrosis was further confirmed histologically in mice devoid of Tregs by means of Hematoxylin-Eosin (**Figure 6Cii**), Picrosirius (**Figure 6Civ**), and the Masson's trichrome staining (**Figure 6Cv**) as well as by means of CtGF immunofluorescence (**Figure 6Cviii**) as compared to DT-treated control mice (**Figures 6Ci,iii,v,vii**). The levels of uPA, known to positively influence tissue remodeling and whose absence leads to infertility (Carmeliet et al., 1994), were downregulated and almost undetectable in the absence of Tregs (**Figure 6D**). It is of interest that Ptgfr was also upregulated (**Figure 6E**) as prostaglandin is routinely given to provoke therapeutic abortions (Wagner et al., 2011). No changes were found in the levels of the immunosuppressive factors IL-9 and Gal-1 (**Figures 7A,B**). LIF and p53, known to define fertility (Hu et al., 2007), were also not modified after Treg depletion (**Figures 7C,D**). Inflammation and fibrosis were only investigated in syngeneic matings in order to investigate the effects of Treg depletion independent of allogenicity. Together, the data indicate that depletion of Tregs prior to mating leads to a hostile uterine environment that is characterized by the occurrence of inflammation and fibrosis, thereby interfering with implantation.

CCR7 MEDIATED THE HOMING OF TREG TO THE UTERUS AND ITS GENETIC ABLATION IMPAIRED IMPLANTATION

The chemokine receptor CCR7 has been identified as a homing receptor on Tregs required for migration to lymph nodes and spleen (Worbs and Förster, 2007). In order to explore a role for CCR7 in Treg homing into the uterus and for embryo implantation, we employed CCR7-deficient mice. The number of CD4$^+$Foxp3$^+$ Treg in the uterus was drastically reduced in CCR7$^{-/-}$ mice (**Table 1**), whereas the frequency of conventional CD4$^+$Foxp3$^-$ T cells was only partially reduced (data not shown). Consistent with the absence of uterine Treg, CCR7 deficiency resulted in implantation failure (**Table 1**). Supporting our findings on the importance of CCR7 on Treg for implantation, Guerin et al. (2011) reported the presence of CCL19, the ligand for CCR7, in glandular and luminal uterine epithelial cells, however a role for this chemokine for the recruitment of Treg into the uterus was not investigated. We show here that CCR7 mediates the homing of Treg to the uterus and that its absence hampers implantation.

DISCUSSION

The presence of Foxp3$^+$ Tregs in uterus during early pregnancy has already been reported (Schumacher et al., 2007; Thuere et al., 2007). Here, by employing flow cytometry, we confirm that these cells are present in the uterus in the non-pregnant state and that they further fluctuate during the different phases of the estrous cycle. It seems that this fluctuation occurs in response to hormones, as has been proposed after observing variations in the Foxp3 mRNA levels (Kallikourdis and Betz, 2007; Guerin et al., 2011). *In vivo* 2-photon microscopy in *Foxp3^{gfp}* animals impressively confirmed oscillations in the frequency of Treg in the uterus and further revealed a clustering of Tregs in uterine tissue during the receptive phase of the cycle, the estrus. This may be interpreted as an accumulation of these cells at the future implantation niches and preparation of the uterus for implantation.

We further observed that Foxp3$^+$ Tregs expanded immediately after copulation at day 0 of pregnancy. The expansion occurred after mating females with intact or vasectomized males but not after mating with males lacking seminal vesicles, suggesting that components of the seminal fluid are active in expanding Tregs which is in accordance with other reports (Robertson et al., 2009; Guerin et al., 2011). Treg expansion by seminal fluid could be confirmed by *in vitro* experiments that further indicated TGF-β as a possible modulator of Treg expansion. Hence, Treg presence at the moment of pairing and their further expansion by paternal components implies a role for embryo implantation.

To investigate the potential role of CD4$^+$Foxp3$^+$ Tregs we employed two distinct strains of Foxp3.DTR mice for Treg depletion, namely Foxp3^{DTR} knock-in mice and BAC-transgenic Foxp3.LuciDTR-4 mice. We observed that depletion of Tregs

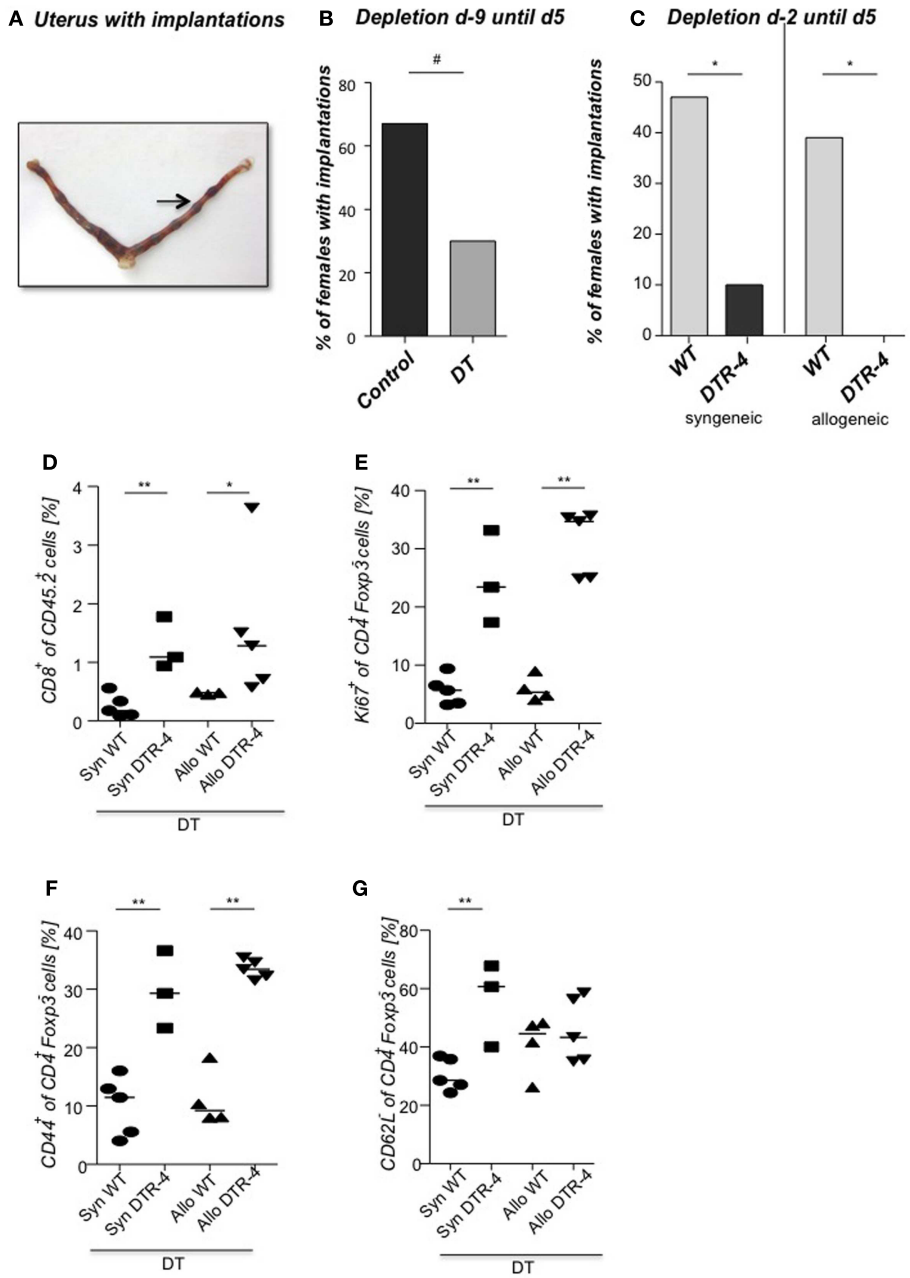

FIGURE 3 | Embryo implantation is impaired after Treg depletion. Foxp3$^+$ Treg were depleted in *Foxp3^{DTR}* mice by application of DT every fourth day, starting 9 days before mating (day 9) with BALB/c males. Control groups received PBS. **(A)** shows a representative picture of a uterus stained at day 5 post conception with Chicago Blue dye application. The arrow indicates a representative implantation site. The percentage of females presenting implantations was analyzed on day 5 after mating [**(B)**, $n = 5$–12]. Foxp3$^+$ Treg were depleted in Foxp3.LuciDTR-4 mice by daily application of DT, starting on day 2 with allogeneic (CBAJ) or syngeneic (C57/BL6) males. Control groups were wt C57/BL6 females treated with DT. Implantation numbers were measured at day 5 [**(C)**, $n = 15$–21]. For **(B,C)**, data are expressed as medians of % of implanted females and analyzed by Fisher's exact test (#$P < 0.1$, *$P < 0.05$). Not all plugged animals became pregnant. In samples from animals shown in Figure 3B, the percentage of CD8$^+$ cells was analyzed in the uterus by flow cytometry **(D)**, and the percentage of KI67$^+$, CD44$^+$, and CD62L$^+$ **(E–G)** determined in uterine draining lymph nodes ($n = 5$/group). Data are expressed as medians and were analyzed by Mann–Whitney-*U* test (*$P < 0.05$; **$P < 0.01$).

prior to mating resulted in a dramatic impairment of implantation. In line with this, it was recently reported that diminished endometrial Foxp3 mRNA was associated with infertility in women (Jasper et al., 2006). We speculated that at this early time point Tregs may counteract pro-inflammatory events occurring during implantation and facilitate a uterine environment that

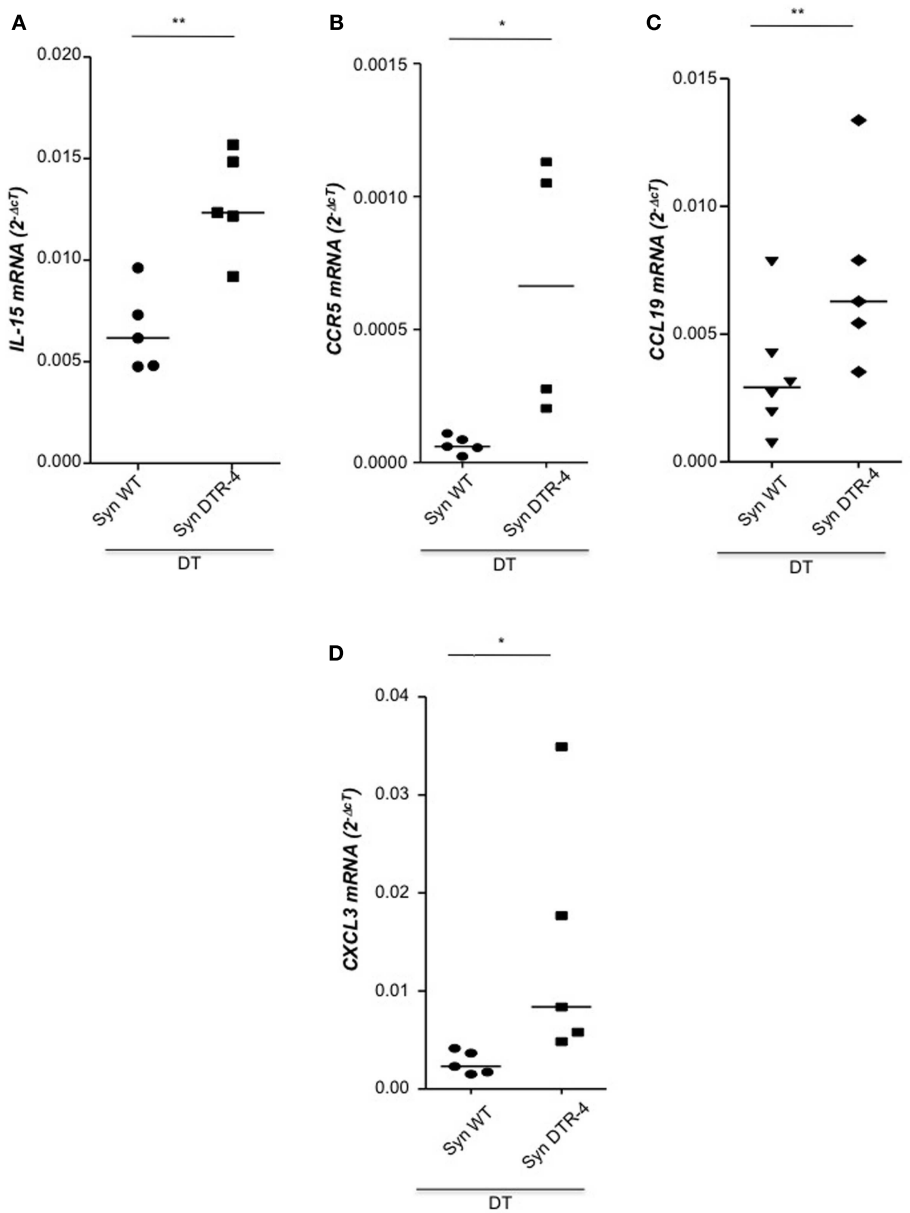

FIGURE 4 | Depletion of Tregs creates an inflammatory uterine milieu. In samples from Foxp3.LuciDTR-4 or wild type animals treated with DT by daily application starting on day 2 and further mated syngeneically, inflammation markers were measured ($n = 4$–6/group) in uterine tissue by qPCR. Levels of IL-15 **(A)**, CCR5 **(B)**, CCL19 **(C)**, and CXCL3 **(D)** were significantly elevated in mice depleted of Tregs as compared to DT-treated controls. Data are expressed as single dots with medians and were analyzed by Mann–Whitney-*U* test (#$P < 0.1$, $P < 0.05$; **$P < 0.01$).

supports implantation. Without Tregs, inflammation may be too strong and may favor a hostile uterine microenvironment that would hinder nidation of the embryo. Indeed, we observed a strong upregulation of the pro-inflammatory mediators IL-15, CCR5 CCL19 and CXCL3. We also found augmented levels of $CD8^+$ cells and activated $CD4^+$ cells in uterus. These findings are supported by studies showing that Treg depletion in Foxp3.DTR mice leads to T cell activation and pro-inflammatory modulation of the microenvironment of sites where Tregs accumulate, such as tumors (Li et al., 2010). Besides inflammation and accumulation of effector cells, we observed swollen uteruses that were devoid of implantations. The development of uterine fibrosis was indicated by the upregulation of CtGF and CXCL9. uPA, a positive regulator of tissue remodeling in the uterus was almost undetectable in the absence of Treg, which is in line with impaired infertility of uPA deficient animals (Carmeliet et al., 1994). Our data reveals that the lack of Tregs results in uterine conditions that are hostile for the embryo to implant. The levels of the known fertility factors LIF and p53 (Hu et al., 2007) were not modified in the absence of Treg.

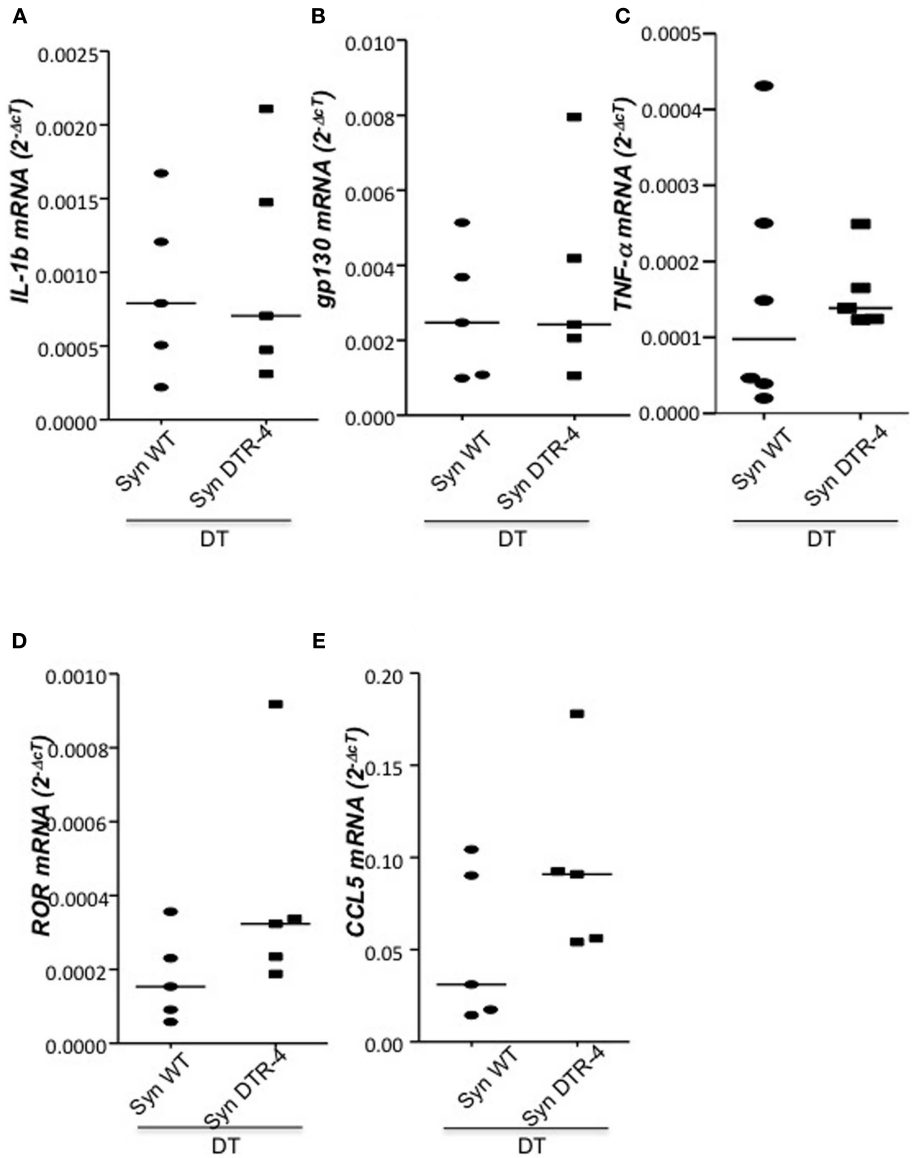

FIGURE 5 | Depletion of Tregs does not provoke changes in the levels of IL-1b, gp130, TNF-α, ROR-γτ, or CCL5. In samples from Foxp3.LuciDTR-4 or wild type animals treated with DT by daily application starting on day 2 and further mated allogeneically, inflammation markers were measured ($n = 4$–6/group) in uterine tissue by qPCR. Levels of IL-1b **(A)**, gp130 **(B)**, TNF-α **(C)**, RORγτ **(D)**, and CCL5 **(E)** mRNA were comparable in mice depleted of Tregs and DT-treated controls. Data are expressed as single dot plots with medians and were analyzed by Mann–Whitney-*U* test. No statistically significant differences were observed between both groups in any of the molecules.

We conclude that Treg are pivotal for implantation as they control the uterine microenvironment needed for the blastocyst to attach and grow in the uterus. Many of the effects seen here after Treg depletion are reminiscent of clinical parameters associated with infertility. Pathologies like endometritis, endometriosis, inflammatory pelvic diseases, and fallopian tube blockage associated with inflammatory processes cause the metamorphosis of reproductive tract tissues and vaginal fluid and are often a cause of infertility by hindering nidation (Shah et al., 2005; He et al., 2010; Braundmeier et al., 2012). Likewise, it is known that, e.g., pelvic inflammation, uterine swelling, and intraluminal occluding fibrosis of the oviduct after infections with Chlamydia sp. are associated with infertility (Weiss et al., 2009; Wiesenfeld et al., 2012). Thus, it seems that the specific depletion of Treg mimics alterations induced by pathogens that lead to infertility, specifically an inflammatory milieu and fibrosis, thereby hindering successful implantation.

The targets for regulation by uterine Tregs are not clear, but as T cell-deficient mice such as RAG mutant mice lack

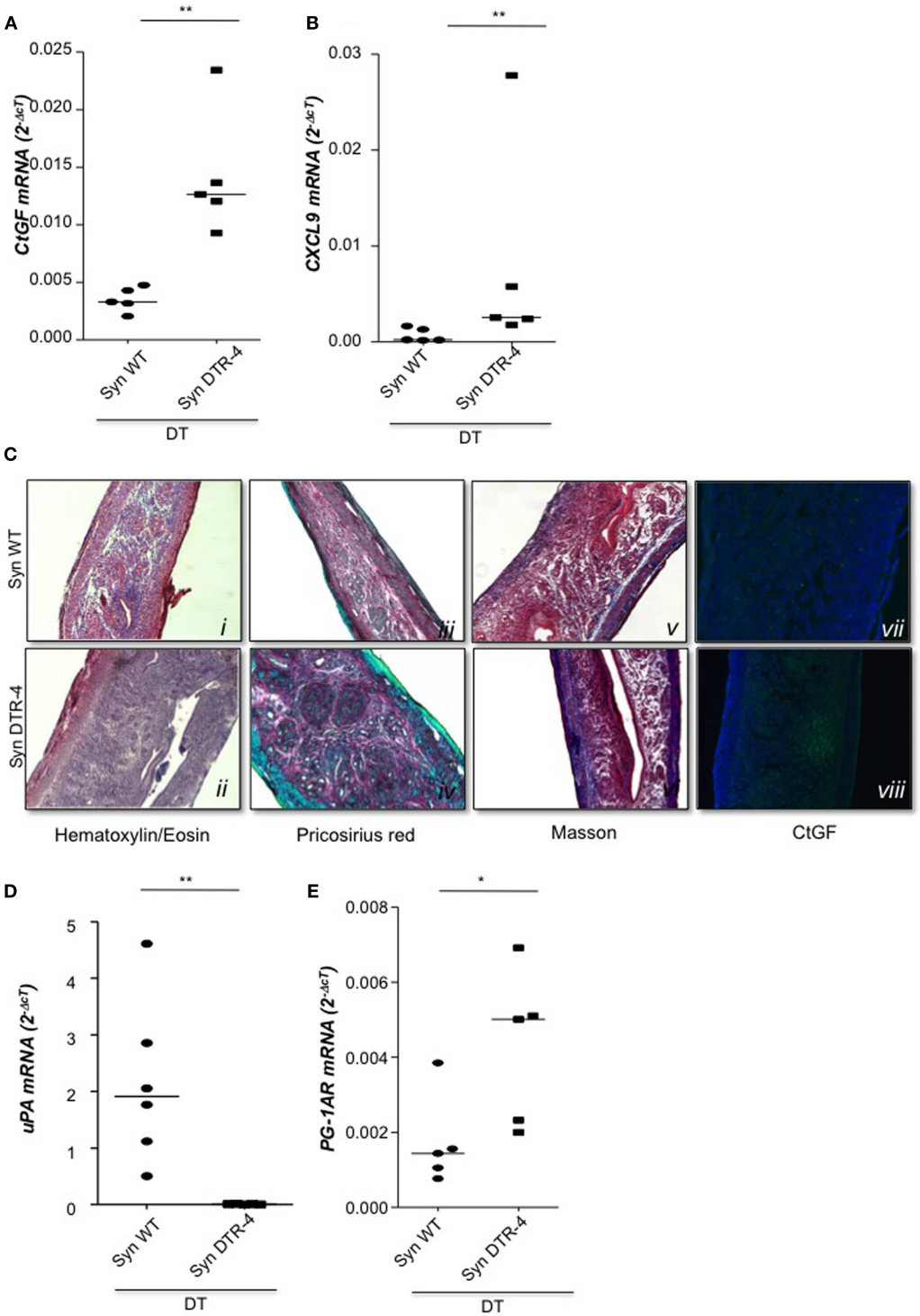

FIGURE 6 | Treg depletion leads to uterine fibrosis. In samples from Foxp3.LuciDTR-4 or wild type animals treated with DT by daily application starting on day 2 and further mated syngeneically, fibrosis markers were measured ($n = 4$–6/group) in uterine tissue by qPCR. Levels of CtGF **(A)** and CXCL9 **(B)** were significantly elevated in mice depleted of Tregs as compared to DT-treated controls. Data are expressed as single dots with medians and were analyzed by Mann–Whitney-*U* test (#$P < 0.1$, **$P < 0.01$). Additionally, staining with Hematoxylin/Eosin revealed fibrosis areas with disorganized collagen fibers in animals without Tregs compared to wild type controls (**C ii** vs. **i**). Pricosirius red staining revealed a higher amount of green/blue-stained thin collagen fibers that confirms fibrosis in mice devoid of Tregs vs. controls (**C iv** vs. **iii**). Further, Masson's staining manifested larger areas of collagen fibers in blue/violet in DT-treated Foxp3.Luci.DTR animals compared to DT-treated controls (**C vi** vs. **v**). Finally in (**C vii, viii**), immunofluorescence staining for CtGF confirmed accumulation of CtGF positive cells in mice depleted in Tregs as compared to the controls. All pictures were taken with a 10× objective. Analysis of uPA mRNA revealed that animals depleted in Tregs presented very low, almost undetectable levels of this molecule as compared to DT-treated controls **(D)**. Treg depletion further provoked an augmentation of prostaglandin 1A mRNA **(E)**.

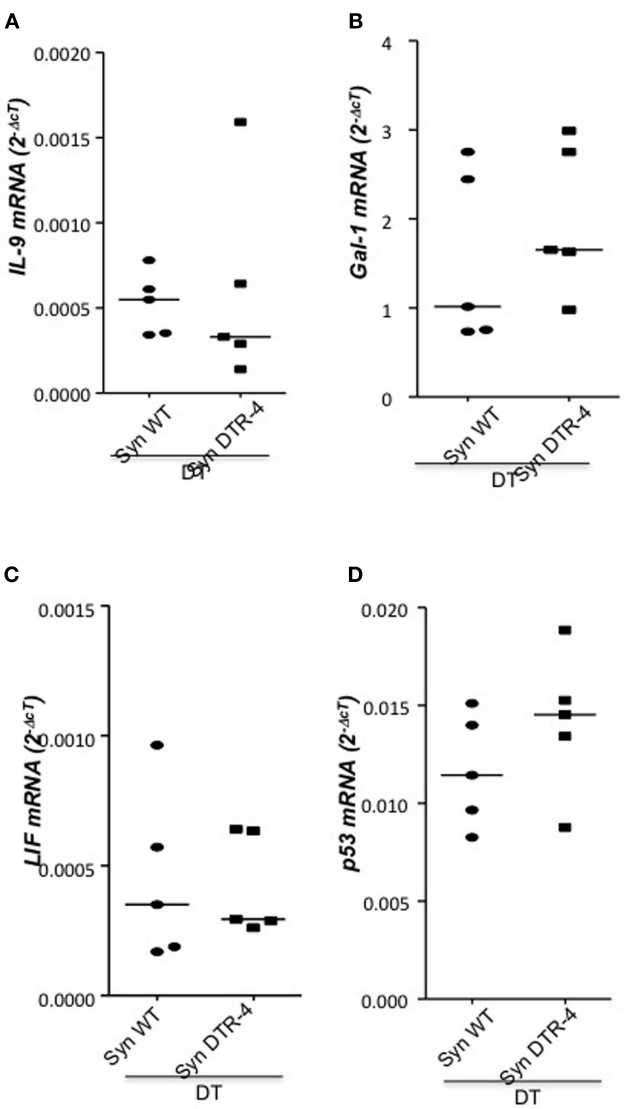

FIGURE 7 | Treg depletion does not provoke changes in IL-9, Gal-1, LIF, or p53. In samples from Foxp3.LuciDTR-4 or wild type animals treated with DT by daily application starting on day 2 and further mated allogeneically, inflammation markers were measured ($n = 4$–6/group) in uterine tissue by qPCR. Levels of IL-9 **(A)**, Gal-1 **(B)**, LIF **(C)**, and p53 **(D)** mRNA were comparable in mice depleted of Tregs and DT-treated controls. Data are expressed as single dot plots with medians and were analyzed by Mann–Whitney-*U* test. No statistically significant differences were observed between both groups in any of the molecules.

both Tregs and effector T cells, but present normal implantation rates, it seems reasonable to assume that effector T cells are major targets and that uterine Tregs serve to control excessive production of inflammatory cytokines. We also demonstrated that homing of Tregs to the uterus depends on CCR7 and that CCR7 deficiency resulted in implantation failure. In support of this finding, Guerin et al. (2011) described the presence of CCL19, the ligand for CCR7, in glandular and luminal uterine epithelial cells.

Table 1 | Consequences of CCR7 deficiency in number of uterine Tregs and implantation rate.

	% of uterine Foxp3$^+$ cells within CD4 cells	Implantation rate
Wild type controls ($n = 5$)	11.97 (4.48–21.1)	100%
CCR7$^{-/-}$ animals ($n = 5$)	0 (0–0.01)	55%
Statistical significance	<0.05	<0.05

In another study it was reported that Treg depletion with anti-CD25 antibody at day 2.5 post conception would hinder implantation only in allogeneic but not syngeneic mating combinations (Shima et al., 2010). At first sight this appears to be at disagreement with our findings that Treg depletion in Foxp3.DTR mice causes implantation failure also in syngeneic matings. However, in view of the fact that Foxp3.DTR allow more efficient and more specific depletion of Tregs the above authors themselves have suggested the use of Foxp3.DTR mice for respective studies, as has been done here (Shima et al., 2010).

Once pregnancy is established, the embryo expressing paternal antigens needs to be protected against the maternal immune system. In several reports Tregs have been shown to be important for this process (Zenclussen et al., 2005; Schumacher et al., 2007; Samstein et al., 2012). Using the same Foxp3.DTR knock-in mice employed here, Samstein et al. (2012) have shown that the *de novo* conversion of Treg in the periphery contributes to embryo protection. However, as only 10% of all embryos are rejected in the absence of Foxp3$^+$ Tregs their protective role for maintaining the integrity of the fetus appears to be limited as compared to the strong effect of Treg on implantation observed here. Additional and multiple mechanisms must exist to ensure maternal tolerance toward the fetus. Several distinct tolerance mechanisms have been reported, such as awareness of maternal T cells for paternal alloantigens and acquisition of a transient state of tolerance during pregnancy (Tafuri et al., 1995), ignorance of fetus-specific T cells, epigenetic silencing in decidual tissue of chemokines that attract T cells (Nancy et al., 2012), and others.

In view of the importance of pregnancy for survival of a species; its first phase, namely embryo implantation, must be tightly controlled. Our data reveal the importance of Treg for this process, likely by suppressing excessive inflammation in the uterine microenvironment. The results are relevant for human pregnancies, especially when designing protocols for improving fertility.

ACKNOWLEDGMENTS

We are thankful to David N. Olivieri and Iván Gómez-Conde for stabilizing the intravital microscopy movies, to Sabine Schmitt and Markus Scharm for technical assistance, to Katja Woidacki and Federico Jensen for the assistance with the immunohistology, and to Birgit Vey for manuscript editing. This work was supported by DFG grants to Ana Claudia Zenclussen (ZE 526/4-2 and SFB 854 TP7), and by grants from the Wilhelm Sander Stiftung Germany (grant 2009.022.1) and Helmholtz Alliance for Immunotherapy to Günter J. Hämmerling. Ana Teles was supported by the FCT Foundation, Portugal and a PhD grant from the Medical Faculty, Otto-von-Guericke University, Magdeburg.

SUPPLEMENTARY MATERIAL

The Supplementary Material for this article can be found online at: http://www.frontiersin.org/Mucosal_Immunity/10.3389/fimmu.2013.00158/abstract

Movie S1 | Estrus: 3D reconstruction of live 2-photon-microscopy of uterus from a representative Foxp3^{gfp} animal during the estrus phase oft he estrus cycle. The green cells are Tregs clustered at the mesometrial region. Animals were anesthetized by i.p. injection of ketamine and xylazine, 120 or 16 μg/g of mouse weight, respectively, and kept on a heating pad at 37°C. One of the uterine horns was carefully exposed and 0.1 M caffeine (Sigma-Aldrich, USA) was applied to decrease uterine contractions. For maternal blood visualization, animals were intravenously injected with 100 μl of Rhodamine B isothiocyanate-Dextran (RhoB-Dex) 70,000 KDa (Sigma-Aldrich, Inc., USA) before acquiring images in a multiphoton laser scanning microscope (MPLSM). We used a Prairie Ultima 2-photon microscope (Prairie Technologies, Inc.). The microscope was equipped with a Chameleon Ti:Sapphire laser (Coherent, Inc., USA), four top PMTs for simultaneous up to four channel acquisitions and a 20× water immer sion objective (Olympus, Inc., USA). The laser was tuned to 880 nm to allow for concomitant excitation of RhoB-Dex and GFP$^+$-Treg. The wavelength emission for RhoB-Dex and GFP is 590 and 509 nm, respectively. Sequential images were acquired for observation of Treg in the uterus. For analysis of uterine Treg images, we have developed our own software algorithms based on endogenous tissue markers information (e.g., location of blood vessels) from consecutive z-stacks acquisitions for stabilization of Treg movies. Once the images were stabilized, we used Imaris software (Bitplane AG, Inc.) for reconstruction of three-dimensional models in order to determine distribution in the uterus.

Movie S2 | Diestrus: depicts a 3D reconstruction of representative live 2-photon-microscopy of uterus from a Foxp3^{gfp} animal at diestrus. Green Tregs are scarce. Animals were anesthetized by i.p. injection of ketamine and xylazine, 120 or 16 μg/g of mouse weight, respectively, and kept on a heating pad at 37°C. One of the uterine horns was carefully exposed and 0.1 M caffeine (Sigma-Aldrich, USA) was applied to decrease uterine contractions. For maternal blood visualization, animals were intravenously injected with 100 μl of Rhodamine B isothiocyanate-Dextran (RhoB-Dex) 70,000 KDa (Sigma-Aldrich, Inc., USA) before acquiring images in a multiphoton laser scanning microscope (MPLSM). We used a Prairie Ultima 2-photon microscope (Prairie Technologies, Inc.). The microscope was equipped with a Chameleon Ti:Sapphire laser (Coherent, Inc., USA), four top PMTs for simultaneous up to four channel acquisitions and a 20× water immersion objective (Olympus, Inc., USA). The laser was tuned to 880 nm to allow for concomitant excitation of RhoB-Dex and GFP$^+$-Treg. The wavelength emission for RhoB-Dex and GFP is 590 and 509 nm, respectively. Sequential images were acquired for observation of Treg in the uterus. For analysis of uterine Treg images, we have developed our own software algorithms based on endogenous tissue markers information (e.g., location of blood vessels) from consecutive z-stacks acquisitions for stabilization of Treg movies. Once the images were stabilized, we used Imaris software (Bitplane AG, Inc.) for reconstruction of three-dimensional models in order to determine distribution in the uterus.

Movie S3 | Metestrus: shows a video from a 3D reconstruction of live 2-photon microscopy showing almost undetectable green Tregs within the uterus. Animals were anesthetized by i.p. injection of ketamine and xylazine, 120 or 16 μg/g of mouse weight, respectively, and kept on a heating pad at 37°C. One of the uterine horns was carefully exposed and 0.1 M caffeine (Sigma-Aldrich, USA) was applied to decrease uterine contractions. For maternal blood visualization, animals were intravenously injected with 100 μl of Rhodamine B isothiocyanate-Dextran (RhoB-Dex) 70,000 KDa (Sigma-Aldrich, Inc., USA) before acquiring images in a multiphoton laser scanning microscope (MPLSM). We used a Prairie Ultima 2-photon microscope (Prairie Technologies, Inc.). The microscope was equipped with a Chameleon Ti:Sapphire laser (Coherent, Inc., USA), four top PMTs for simultaneous up to four channel acquisitions and a 20× water immersion objective (Olympus, Inc., USA). The laser was tuned to 880 nm to allow for concomitant excitation of RhoB-Dex and GFP$^+$-Treg. The wavelength emission for RhoB-Dex and GFP is 590 and 509 nm, respectively. Sequential images were acquired for observation of Treg in the uterus. For analysis of uterine Treg images, we have developed our own software algorithms based on endogenous tissue markers information (e.g., location of blood vessels) from consecutive z-stacks acquisitions for stabilization of Treg movies. Once the images were stabilized, we used Imaris software (Bitplane AG, Inc.) for reconstruction of three-dimensional models in order to determine distribution in the uterus.

Movie S4 | Proestrus: distribution of green Foxp3^{gfp+} cells (Tregs) inside the uterus during proestrus. Animals were anesthetized by i.p. injection of ketamine and xylazine, 120 or 16 μg/g of mouse weight, respectively, and kept on a heating pad at 37°C. One of the uterine horns was carefully exposed and 0.1 M caffeine (Sigma-Aldrich, USA) was applied to decrease uterine contractions. For maternal blood visualization, animals were intravenously injected with 100 μl of Rhodamine B isothiocyanate-Dextran (RhoB-Dex) 70,000 KDa (Sigma-Aldrich, Inc., USA) before acquiring images in a multiphoton laser scanning microscope (MPLSM). We used a Prairie Ultima 2-photon microscope (Prairie Technologies, Inc.). The microscope was equipped with a Chameleon Ti:Sapphire laser (Coherent, Inc., USA), four top PMTs for simultaneous up to four channel acquisitions and a 20× water immersion objective (Olympus, Inc., USA). The laser was tuned to 880 nm to allow for concomitant excitation of RhoB-Dex and GFP$^+$-Treg. The wavelength emission for RhoB-Dex and GFP is 590 and 509 nm, respectively. Sequential images were acquired for observation of Treg in the uterus. For analysis of uterine Treg images, we have developed our own software algorithms based on endogenous tissue markers information (e.g., location of blood vessels) from consecutive z-stacks acquisitions for stabilization of Treg movies. Once the images were stabilized, we used Imaris software (Bitplane AG, Inc.) for reconstruction of three-dimensional models in order to determine distribution in the uterus.

REFERENCES

Ashkar, A. A., Di Santo, J. P., and Croy, B. A. (2000). Interferon gamma contributes to initiation of uterine vascular modification, decidual integrity, and uterine natural killer cell maturation during normal murine pregnancy. *J. Exp. Med.* 192, 259–270. doi:10.1084/jem.192.2.259

Braundmeier, A., Jackson, K., Hastings, J., Koehler, J., Nowak, R., and Fazleabas, A. (2012). Induction of endometriosis alters the peripheral and endometrial regulatory T cell population in the non-human primate. *Hum. Reprod.* 27, 1712–1722. doi:10.1093/humrep/des083

Carmeliet, P., Schoonjas, L., Kieckens, L., Ream, B., Degen, J., Bronson, R., et al. (1994). Physiological consequences of loss of plasminogen activator gene function in mice. *Nature* 368, 419–424. doi:10.1038/368419a0

Fontenot, J. D., Rasmunssen, J. P., Gavin, M. A., and Rudensky, A. Y. (2005). A function for interleukin-2 in Foxp3-expressing regulatory T cells. *Nat. Immunol.* 6, 1142–1151. doi:10.1038/ni1263

Gressner, O. A., and Gressner, A. M. (2008). Connective tissue growth factor: a fibrogenic master switch in fibrotic liver diseases. *Liver Int.* 28, 1065–1079. doi:10.1111/j.1478-3231.2008.01826.x

Guerin, L. R., Moldenhauer, L. M., Prins, J. R., Bromfield, J. J., Hayball, J. D., and Robertson, S. A. (2011). Seminal fluid regulates accumulation of FOXP3+ regulatory T cells in the preimplantation mouse uterus through expanding the FOXP3+ cell pool and CCL19-mediated recruitment. *Biol. Reprod.* 85, 397–408. doi:10.1095/biolreprod.110.088591

He, Q., Tsang, L. L., Ajonuma, L. C., and Chan, H. C. (2010). Abnormally up-regulated cystic fibrosis transmembrane conductance regulator expression and uterine fluid accumulation contribute to *Chlamydia trachomatis*-induced female infertility. *Fertil. Steril.* 93, 2608–2614. doi:10.1016/j.fertnstert.2010.01.040

Houser, B. L., Tilburgs, T., Hill, J., Nicotra, M. L., and Strominger, J. L. (2011). Two unique human decidual macrophage populations. *J. Immunol.* 186, 2633–2642. doi:10.4049/jimmunol.1003153

Hu, W., Feng, Z., Teresky, A. K., and Levine, A. J. (2007). p53 regulates maternal reproduction through LIF. *Nature* 450, 721–724. doi:10.1038/nature05993

Jasper, M. J., Tremellen, K. P., and Robertson, S. A. (2006). Primary unexplained infertility is associated with reduced expression of the T-regulatory cell transcription factor Foxp3 in endometrial tissue. *Mol. Hum. Reprod.* 12, 301–308. doi:10.1093/molehr/gal032

Kallikourdis, M., and Betz, A. G. (2007). Periodic accumulation of regulatory T cells in the uterus: preparation for the implantation of a semi-allogeneic fetus? *PLoS ONE* 2:e382. doi:10.1371/journal.pone.0000382

Kim, J. M., Rasmussen, J. P., and Rudensky, A. Y. (2007). Regulatory T cells prevent catastrophic autoimmunity throughout the lifespan of mice. *Nat. Immunol.* 8, 191–197. doi:10.1038/ni1428

Li, X., Kostareli, E., Suffner, J., Garbi, N., and Hämmerling, G. J. (2010). Efficient Treg depletion induces T-cell infiltration and rejection of large tumors. *Eur. J. Immunol.* 40, 3325–3335. doi:10.1002/eji.201041093

McLennan, I. S., and Koishi, K. (2004). Fetal and maternal transforming growth factor-beta 1 may combine to maintain pregnancy in mice. *Biol. Reprod.* 70, 1614–1618. doi:10.1095/biolreprod.103.026179

Nancy, P., Tagliani, E., Tay, C. S., Asp, P., Levy, D. E., and Erlebacher, A. (2012). Chemokine gene silencing in decidual stromal cells limits T cell access to the maternal-fetal interface. *Science* 336, 1317–1321. doi:10.1126/science.1220030

Plaks, V., Birnberg, T., Berkutzki, T., Sela, S., BenYashar, A., Kalchenko, V., et al. (2008). Uterine DCs are crucial for decidua formation during embryo implantation in mice. *J. Clin. Invest.* 118, 3954–3965. doi:10.1172/JCI36682

Robertson, S. A., Guerin, L. R., Bromfield, J. J., Branson, K. M., Ahlström, A. C., and Care, A. S. (2009). Seminal fluid drives expansion of the CD4+CD25+ T regulatory cell pool and induces tolerance to paternal alloantigens in mice. *Biol. Reprod.* 80, 1036–1045. doi:10.1095/biolreprod.108.074658

Rowe, J. H., Ertelt, J. M., Xin, L., and Way, S. S. (2012). Pregnancy imprints regulatory memory that sustains anergy to fetal antigen. *Nature* 490, 102–106. doi:10.1038/nature11462

Samstein, R. M., Josefowicz, S. Z., Arvey, A., Treuting, P. M., and Rudensky, A. Y. (2012). Extrathymic generation of regulatory T cells in placental mammals mitigates maternal-fetal conflict. *Cell* 150, 29–38. doi:10.1016/j.cell.2012.05.031

Schumacher, A., Wafula, P. O., Bertoja, A. Z., Sollwedel, A., Thuere, C., Wollenberg, I., et al. (2007). Mechanisms of action of regulatory T cells specific for paternal antigens during pregnancy. *Obstet. Gynecol.* 110, 1137–1145. doi:10.1097/01.AOG.0000284625.10175.31

Shah, A. A., Schripsema, J. H., Imtiaz, M. T., Sigar, I. M., Kasimos, J., Matos, P. G., et al. (2005). Histopathologic changes related to fibrotic oviduct occlusion after genital tract infection of mice with *Chlamydia muridarum*. *Sex. Transm. Dis.* 32, 49–56. doi:10.1097/01.olq.0000148299.14513.11

Shima, T., Sasaki, Y., Itoh, M., Nakashima, A., Ishii, N., Sugamura, K., et al. (2010). Regulatory T cells are necessary for implantation and maintenance of early pregnancy but not late pregnancy in allogeneic mice. *J. Reprod. Immunol.* 85, 121–129. doi:10.1016/j.jri

Suffner, J., Hochweller, K., Kühnle, M. C., Li, X., Kroczek, R. A., Garbi, N., et al. (2010). Dendritic cells support homeostatic expansion of Foxp3+ regulatory T cells in Foxp3.LuciDTR mice. *J. Immunol.* 184, 1810–1820. doi:10.4049/jimmunol.0902420

Tafuri, A., Alferink, J., Möller, P., Hämmerling, G. J., and Arnold, B. (1995). T cell awareness of paternal alloantigens during pregnancy. *Science* 270, 630–633. doi:10.1126/science.270.5236.630

Thuere, C., Zenclussen, M. L., Schumacher, A., Langwisch, S., Schulte-Wrede, U., Teles, A., et al. (2007). Kinetics of regulatory T cells during murine pregnancy. *Am. J. Reprod. Immunol.* 58, 514–523. doi:10.1111/j.1600-0897.2007.00538.x

Wagner, N., Abele, H., Hoopmann, M., Grischke, E. M., Blumenstock, G., Wallwiener, D., et al. (2011). Factors influencing the duration of late first and second-trimester termination of pregnancy with prostaglandin derivates. *Eur. J. Obstet. Gynecol. Reprod. Biol.* 155, 75–78. doi:10.1016/j.ejogrb.2010.10.019

Weiss, G., Goldsmith, L. T., Taylor, R. N., Bellet, D., and Taylor, H. S. (2009). Inflammation in reproductive disorders. *Reprod. Sci.* 16, 216–229. doi:10.1177/1933719108330087

Wiesenfeld, H. C., Hillier, S. L., Meyn, L. A., Amortegui, A. J., and Sweet, R. L. (2012). Subclinical pelvic inflammatory disease and infertility. *Obstet. Gynecol.* 120, 37–43. doi:10.1097/AOG.0b013e31825a6bc9

Woidacki, K., Popovic, M., Metz, M., Schumacher, A., Linzke, N., Teles, A., et al. (2013). Mast cells rescue implantation defects caused by c-kit deficiency. *Cell Death Dis.* 4, e462. doi:10.1038/cddis.2012.214

Worbs, T., and Förster, R. (2007). A key role for CCR7 in establishing central and peripheral tolerance. *Trends Immunol.* 28, 274–280. doi:10.1016/j.it.2007.04.002

Zenclussen, A. C., Gerlof, K., Zenclussen, M. L., Sollwedel, A., Bertoja, A. Z., Ritter, T., et al. (2005). Abnormal T cell reactivity against paternal antigens in spontaneous abortion: adoptive transfer of pregnancy-induced CD4+CD25+ T regulatory cells prevents fetal rejection in a murine abortion model. *Am. J. Pathol.* 166, 811–822. doi:10.1016/S0002-9440(10)62302-4

Zenclussen, A. C., Olivieri, D. N., Dustin, M. L., and Tadokoro, C. E. (2013). In vivo multiphoton microscopy technique to reveal the physiology of the mouse uterus. *Am. J. Reprod. Immunol.* 69, 281–289. doi:10.1111/aji.12066

Zenclussen, M. L., Casalis, P. A., El-Mousleh, T., Rebelo, S., Langwisch, S., Linzke, N., et al. (2011). Haem oxygenase-1 dictates intrauterine fetal survival in mice via carbon monoxide. *J. Pathol.* 225, 293–304. doi:10.1002/path.2946

Zeremski, M., Dimova, R., Astemborski, J., Thomas, D. L., and Talal, A. H. (2011). CXCL9 and CXCL10 chemokines as predictors of liver fibrosis in a cohort of primarily African-American injection drug users with chronic hepatitis C. *J. Infect. Dis.* 204, 832–836. doi:10.1093/infdis/jir424

Conflict of Interest Statement: The authors declare that the research was conducted in the absence of any commercial or financial relationships that could be construed as a potential conflict of interest.

Received: 30 April 2013; paper pending published: 05 June 2013; accepted: 08 June 2013; published online: 20 June 2013.

*Citation: Teles A, Schumacher A, Kühnle M-C, Linzke N, Thuere C, Reichardt P, Tadokoro CE, Hämmerling GJ and Zenclussen AC (2013) Control of uterine microenvironment by Foxp3$^+$ cells facilitates embryo implantation. Front. Immunol. **4**:158. doi: 10.3389/fimmu.2013.00158*

This article was submitted to Frontiers in Mucosal Immunity, a specialty of Frontiers in Immunology.

Appendix 04

Philipsen L, Engels T, Schilling K, Gurbiel S, Fischer KD, Tedford K, Schraven B#, Gunzer M#, **Reichardt P#+.**
Multi-molecular analysis of stable immunological synapses reveals sustained recruitment and sequential assembly of signaling clusters.
Mol Cell Proteomics. 2013;12(9):2551-67.
+Corresponding Author, #Joint Senior Authors

IF: 7.4

This paper is available on line at http://www.mcponline.org

Multimolecular Analysis of Stable Immunological Synapses Reveals Sustained Recruitment and Sequential Assembly of Signaling Clusters*[S]

Lars Philipsen‡, Thomas Engels‡, Kerstin Schilling§, Slavyana Gurbiel‡, Klaus-Dieter Fischer¶, Kerry Tedford§, Burkhart Schraven‡¶¶, Matthias Gunzer‡‖¶¶, and Peter Reichardt‡¶¶

The formation of the immunological synapse between T cells and antigen-presenting cells (APC) begins within minutes of contact and can take hours for full T-cell activation. Although early phases of the synapse have been extensively studied for a select number of proteins, later phases have not yet been examined in detail. We studied the signaling network in stable synapses by measuring the simultaneous localization of 25 signaling and structural molecules over 2 h at the level of individual synapses using multi-epitope ligand cartography (MELC). Signaling proteins including phospho(p)ZAP70, pSLP76, pCD3ζ, and pLAT, along with proteins that influence synapse structure such as F-actin, tubulin, CD45, and ICAM-1, were localized in images of synapses and revealed the multidimensional construction of a mature synapse. The construction of the stable synapse included intense early TCR signaling, a phase of recruitment of structural proteins, and a sustained increase in signaling molecules and colocalization of TCR and pLAT signaling clusters in the center of the synapse. Consolidation of TCR and associated proteins resulted in formation of a small number of discrete synaptic microclusters. Development of synapses and cSMAC composition was greatly affected by the absence of Vav1, with an associated loss in PLCγ1 recruitment, pSLP76, and increased CXCR4. Together, these data demonstrate the use of multi-epitope ligand cartography to quantitatively analyze synapse formation and reveal successive recruitment of structural and signaling proteins and sustained phosphorylation at the mature synapse. ***Molecular & Cellular Proteomics 12: 10.1074/mcp.M112.025205, 2551–2567, 2013.***

Adaptive immune responses are initiated by the meeting of a T cell and an antigen-presenting cell (APC)[1] bearing peptide-MHC (pMHC) complexes that are a specific fit for the T-cell receptor (TCR) on the T-cell surface. Within seconds, TCR signaling starts with a sequence of phosphorylation and de-phosphorylation events of membrane-proximal and -distal TCR-signaling molecules and their spatial reorganization into protein multiclusters (1). Together with the rearrangement of structural molecules at the cell–cell interface, these signals lead to the formation of a supramolecular structure termed the immunological synapse (1–3). The synapse can differ substantially in size and composition, but comprises several common structural motifs (4–6). In the classical synapse, these structural motifs are organized in domains that form a target

From the ‡Otto von Guericke University, Institute of Molecular and Clinical Immunology, Leipziger Str. 44, 39120 Magdeburg, Germany; §Otto von Guericke University, Center of Cellular Signaling and Disease Models (ZEBIK), Division of Functional Genomics and Medical Toponomics, Leipziger Str. 44, 39120 Magdeburg, Germany; ¶Otto von Guericke University, Institute of Biochemistry and Cell Biology, Leipziger Str. 44, 39120 Magdeburg, Germany; ‖University Duisburg-Essen, University Hospital, Institute of Experimental Immunology and Imaging, Hufelandstraβe 55, 45147 Essen, Germany

Received October 31, 2012, and in revised form, May 13, 2013

Published, MCP Papers in Press, June 10, 2013, DOI 10.1074/mcp.M112.025205

[1] The abbreviations used are: APC, Antigen-presenting cell; 3D, Three-dimensional; AA, Amino acid; BIRT377, (R)-5-(4-bromophenyl)-3-(3,5-dichlorophenyl)-1,5-dimethylimidazolidine-2,4-dione. A small molecule and integrin antagonist, BT B cell-T cell; Ca, Calcium; CMP, Combinatorial molecular phenotype, syn. combinatorial molecular pattern; cSMAC, Central supramolecular activation cluster; CXCR4, C-X-C chemokine receptor type 4; ERK, Extracellular signal-related kinase; FCS, Fetal calf serum; IS, Immunological Synapse; KO, Knock-out; LAT, Linker for the Activation of T cells; LCK, Lymphocyte-Specific Protein Tyrosine Kinase; MAPK, Mitogen-activated protein kinase; MELC. Multi-Epitope Ligand Cartography; MFI, Median fluorescence intensity; NA, Numerical aperture; NFAT, Nuclear factor of activated T cells; NF-κB, Nuclear Factor kappa B; PBS, Phosphate-buffered saline; pOVA, Peptide [of the AA sequence 323–339] of the Ovalbumin protein, cognate ligand for OT-II TCR transgene CD4+ T cells; pPLCγ1, Phospho-Protein kinase C γ1; pSMAC, Peripheral supramolecular activation cluster; pTyr, Phospho-Tyrosine; pZAP70, Phospho-Zeta-chain-associated protein kinase [with molecular weight of 70 kDa]; RhoGEF, Rho guanine nucleotide exchange factor; RPMI, A cell culture medium first developed at Roswell Park Memorial Institute; SH2, Src homology-2 *domain* ; SLP76, SH2-containing leukocyte protein [with molecular weight of 76 kDa]; TCR, T cell receptor; WT, Wildtype.

pattern. Two signaling areas form the middle of the synapse: the bullseye in the center is the central supramolecular activation cluster (cSMAC), dominated by TCR and associated signaling molecules, and the ring around it is called the peripheral (p)SMAC, dominated by the presence of stabilizing integrins (1, 6). The outermost ring, the distal (d)SMAC, is composed of F-actin important for structural integrity of the synapse. The purpose of the synapse, and its dynamic precursor the kinapse, is to translate information obtained from the APC on amount and quality of peptide and presence of coreceptors into T-cell actions such as proliferation or secretion (1).

TCR triggering activates a cascade of signaling events. First, Src kinases such as LCK are activated and phosphorylate the TCR-complexed CD3ζ chain on intracellular tyrosine-based activation motifs (ITAMs). Next, ZAP70 is recruited to ITAMs and phosphorylates adaptors such as LAT and SLP76. These in turn recruit PLCγ1, an activator of calcium flux, and Vav1, a regulator of actin reorganization, leading to activation of MAPKs and transcription factors such as NFAT and NF-kB (7, 8). The early TCR signaling leading to calcium flux takes place in seconds, followed by the appearance of the synapse within minutes. Recruitment and assembly of preformed complexes of signaling proteins facilitate structural formation of synapse and TCR signal amplification (9–11). For example, TCR and LAT are found in separate protein islands in the membrane, or in subsynaptic vesicles, and are brought together at the membrane to initiate signaling in microclusters (12–15). Microclusters are small aggregates of signaling proteins, adaptors, and TCR that change location in the synapse over time. Microclusters originate in the dSMAC and migrate in an actin-dependent manner through the pSMAC toward the center of the cSMAC (16, 17).

Current views on the formation and functions of the cSMAC are evolving with ongoing research. Because the cSMAC contains an accumulation of TCR, it was originally posited to serve as a platform for TCR signaling (2, 3). However, further investigations revealed that the centrally located TCR are not signaling-active and are down-regulated for recycling or degradation (17–20). The cSMAC is not uniform in composition but contains at least two different zones: a central zone where TCR signaling terminates, encompassed by a zone enriched with actively-signaling TCR, F-actin and associated coreceptors and kinases (9–12, 16, 21). It was proposed that the cSMAC modulates receptor degradation and signaling by regulating association of TCR with phospho-tyrosine proteins (22, 23).

Multi-epitope ligand cartography (MELC) is a microscopy-based technology that was developed to study the simultaneous locations of dozens of proteins in a single sample of fixed cells or tissue (24). The MELC system consists of a microscope, a CCD camera and a robotic transfer device enabling an automated sequence of delivering washing fluid and staining solution to the sample—all controlled by a computer. To perform MELC, the sample is stained with a fluorescent reagent, imaged, photo-bleached to completely remove fluorescence, washed, and then stained again with a subsequent fluorescent reagent until all detection reagents have been applied in sequence. The image data can be analyzed directly as raw fluorescence intensity or converted to binary data for each pixel confirming presence or absence of fluorescence for each protein. This resulting mathematical data can then be used to analyze colocalizations of all the proteins studied in the sample at a network-level scale (24–27).

We report here the results of using MELC technology to study the co-localizations of 25 molecules (24 proteins and DNA) in T cell–APC conjugates that were imaged at different time points to monitor synapse formation. To investigate the roles of these molecules in synapse formation for longer than the few minutes it takes to form the outlines of the cSMAC, cells were imaged over 2 h. MELC revealed a layered construction of the synapse with sequential recruitment of structural proteins and signaling molecules and a consolidation of LAT and TCR complexes that ultimately formed the mature synapse at late time points (60 min). Synapses contained a limited number of microclusters consisting of TCR associated with phosphorylated CD3ζ and signaling proteins in the cSMAC. Furthermore, MELC was used to analyze synapse formation in T cells from Vav1 knockout mice, and identified key differences in synapse signaling in the mutant T cells. Our results show that MELC technology is valuable in analyzing the large-scale translocation of many proteins in individual T cell–APC contacts simultaneously and thus can deliver new insights into the function and dynamics of formation of the immunological synapse.

EXPERIMENTAL PROCEDURES

Mice—OT-II mice carrying a transgenic TCR recognizing peptide of chicken ovalbumin (AA 323–339) peptide, pOVA, in the context of I-A^b have been described (28) and were used as a source of T cells. C57Bl/6 (H-2^b) mice (from Harlan Germany) were used as a B cell source. Vav1$^{-/-}$ mice (29) were provided by Dr. Klaus-Dieter Fischer, University of Magdeburg, Germany. Animals were housed under specific pathogen-free conditions and treated according to institutional guidelines. All animal experiments were approved by the animal protection committee of the local authorities.

Cell Preparation, Pair Formation—Cell preparation and induction of B cell-T cell (BT) pair formation were performed as previously described (5). In brief, naïve CD4$^+$ T cells from spleens of OT-II mice were enriched to over 90% purity (as assessed by expression of Vα2 TCR transgene) by negative isolation via immunomagnetic depletion (Miltenyi, Bergisch Gladbach, Germany). Naïve splenic B cells from C57Bl/6 mice were obtained by the same procedure with purities between 90 and 95%. For T cell activation, B cells were loaded with 100 μg/ml pOVA for 24 h and washed. Freshly isolated T cells were then mixed in a 1:1 ratio with B cells and co-incubated in an RPMI-based, FCS-supplemented media (Invitrogen, Los Angeles, CA). To synchronize pair formation, cells were centrifuged shortly at 260 $\times$ *g* and incubated at 37 °C, 5% CO_2. Cells were used for subsequent analysis at indicated time points.

Slide Preparation for MELC—T and B cell mixtures were fixed with 2% paraformaldehyde for 15 min and adhered to poly-L-Lysine-coated glass slides. Two to three different cell-coated areas per slide (reflecting different time points of pair formation or different biological samples, *e.g.* KO *versus* WT) were created by applying single droplets of cell suspension. Slides were stored in PBS at 4 °C until imaged by MELC.

MELC—

Antibody Library—We established a MELC library of 24 fluorescence tags (plus propidium iodide) as listed in Table I. We performed a stepwise selection process to judge specificity and usability of each antibody in our system. In brief, we first chose antibody products and clones based on evidence of previous successful and specific usage, ideally by multiple methods, as documented in peer-reviewed literature (see Table I). We then tested the performance of their directly immunofluorescent dye-coupled derivatives in our system by assessing the spatial distribution of the resulting signals (T cell-/B cell-specific, synaptic enrichment) as well as the signal quality (signal-to-noise ratio; details in Table I and supplemental Fig. S3). Most of the antibodies tested performed well in our system. However, several molecules of interest to the study of immune synapses (such as LFA-1) could not be included in the library as the signals delivered by the antibodies were not reliable, too weak or too unspecific in our system. Such, in the case of CD11a (LFA-1), the antibody did not deliver a T-cell specific pattern or synaptic enrichment in our hands. This was possibly due to effects of fixation and/or permeabilization in our protocol, which for technical reasons had to be identical for all markers. Wherever possible such molecules were replaced with stains for surrogate markers, *e.g.* the stain for LFA-1 was replaced by a stain for its main ligand ICAM-1, CD54. The appropriate working dilutions, incubation times and positions within the MELC run were worked-out in a series of pilot experiments based on previous conditions found to be generally suitable to MELC (24) and adapted to our system. During build-up of the MELC library, MELC runs were performed with varying and cumulative numbers and positions of the individual markers to ensure consistency of fluorescence signals in our system.

Image Recording by Toponome Imaging Cycler (TIC)—The sample was placed on the stage of an inverted wide-field fluorescence microscope (Leica DM IRE2; 63 × oil lens NA 1.40). For each of the two or three conditions defined by application of individual droplets of cell solution, one or two suitable fields of view were defined manually, and the corresponding XYZ-positions and a transmitted light reference image was acquired. A fully automated cyclic robotic process started with the incubation of the first fluorescently labeled antibody. After a washing step, the fluorescence signals and a corresponding phase contrast image were acquired by a cooled charge-coupled device camera (Apogee KX4; Apogee Instruments, Roseville, CA, USA). We performed z-stacks to investigate the three-dimensional (3D) structure of the synapse (32 z-planes with a distance of 300 nm and 2× binning resulting in three-dimensional image stacks of 1024 × 1024 × 32 voxels, with a corresponding object space of 292 × 292 × 9.3 μm^3; final voxel size 286 × 286 × 300 nm^3). To eliminate specific signal from a given tag before the addition of the next tag, a bleaching step was performed. A following image of postbleaching fluorescence signals was recorded before the subsequent incubation-imaging-bleaching-cycle started. These cycles were processed until all tags were applied to the sample.

Image Analysis—The fluorescence and post-bleaching fluorescence images produced by each tag were automatically aligned voxel-wise using the corresponding phase contrast images reaching an alignment accuracy of 1 pixel in all dimensions. Fluorescence images were corrected for illumination faults using flat-field correction. Post-bleaching images were subtracted from the following fluorescence tag images. Finally, cases of section artifacts were excluded as invalid by a mask-setting process.

3D Reconstruction and Visualization—To improve the resolution of the 3D image stacks of wide field fluorescent images, we performed a deconvolution/deblurring using the XCOSM software package (an interface to Computational Optical Sectioning Microscopy algorithms for removing out-of focus light in 3D image volumes, Washington University St. Louis, MO, USA; www.essrl.wustl.edu/~preza/xcosm/). Volocity software was used for rendering and visualization (Version 4.0.1, Perkin Elmer, Improvision). *Definition of synapse in 3D space*: We visualized the synapse with multicolor overlays using the deblurred fluorescence images of the CD3ε, CD45R, F-actin and pLAT markers and recorded the positions (*x,y,z*) of the cSMAC, the diameters of the synapse and the angles of the virtual plane through the synapse in relation to the *xy*-plane and the *xz*-planes for each individual synapse. Regions of interest, ROIs, were calculated for the SMAC and derived p- and cSMAC in relation to these coordinates as depicted in supplemental Fig. S4. Compartments for B cell, T cell and the distal pole (uropod) of the T cell in the BT pair were manually defined for each synapse.

CMP Analysis—The preprocessed image data were subjected to binarization as described previously (24). Briefly, the thresholds automatically generated by the system were validated and adjusted manually for each fluorescence signal. The expression of an epitope was set to the value of "0" for a signal below the threshold and to "1" for a signal above the threshold in projection to a pixel. CMP matrices were generated by superimposing binarized images where each pixel in the visual field was coded with a 1/0 code of *n* epitope expression. Specific combinations of a selection of markers, termed CMP motifs, were also analyzed. These CMP motifs were defined using a 1/0/* code to signify if the signal was present (1), absent (0), or undetermined (*). We calculated the relative frequency of CMPs or CMP motifs either by dividing the number of positive pixels for the individual molecule by the total pixels within the ROI (subcompartment, *e.g.* cSMAC) analyzed (the resulting motif was then called a "base motif") or by the total number of valid pixels within the BT pair analyzed.

Flow Cytometry—Antibodies against surface markers (CD4, CD19) were from BD Pharmingen, San José, CA, USA and antibodies for intracellular staining of total tyrosine-phosphorylated signaling molecules (anti-pTyr-Alexa488, clone PY20) were from Biolegend, San Diego, CA, USA. The integrin inhibitor BIRT377 was a kind gift from Terence Kelly (Boehringer Ingelheim). Staining procedure was performed using the BD Fix&Perm Kit as indicated by manufacturer. Flow cytometry was performed at a BD Fortessa. BT pair formation was quantified as the percentage of all live $CD4^+$ T cells in contact with B cells (CD19). Median fluorescence intensity (MFI) of signaling proteins was calculated and the signal from the identically labeled isotype control subtracted.

Western Blot—For analysis of pERK in cell pairs: co-incubation of T and B cells was stopped at 30 min. To some samples, anti-CD3 (2C11, 5 μg/ml) was added to boost signal. Cells were lysed as described previously (30) to obtain cytoplasmic extracts. Protein lysate (20 μg) was separated on a 10% SDS-PAGE and transferred to PVDF membranes. Proteins were detected with primary antibodies to phospho-ERK1/2 (S202/Y204, Cell Signaling) and beta-actin (Sigma), followed by HRP-coupled anti-rabbit and anti-rat secondary antibodies (BD Pharmingen) respectively, and analyzed with the Rotilumin detection system (Roth, Karlsruhe, Germany).

For ERK, Vav1, and SLP76 expression in WT and $Vav1^{-/-}$ OT-II T cells, purified T cells were activated by CD3-crosslinking and analyzed using anti-p-ERK (E4), ERK1 (K23) (both from Santa Cruz, Santa Cruz, CA, USA), Anti-Vav, sheep anti-human SLP76 (all from Upstate, Lake Placid, NY, USA), and purified mouse anti-SLP (pY128) (BD Pharmingen). Total ERK and beta-actin served as loading controls.

Statistical Analysis—Student's *t* test or a nonparametrical test where indicated in the results section were applied to assess statistical significance. Significance levels and symbols employed were $p < 0.05$ (*), $p < 0.01$ (**); and $p < 0.001$(***). Statistical analysis and plotting was done with GraphPad Prism 5.01 (Graphpad Software, La Jolla, CA, USA) or MATLAB (The Mathworks Inc., Natick, MA, USA).

RESULTS

Establishment of the MELC System to Study the Immunological Synapse—The MELC system displays the location of many proteins simultaneously in fixed cells. This large-scale mapping of proteins makes it possible to do statistical analysis of protein co-localizations in subdomains of a cell. Here we used MELC to study the formation of the immunological synapse over a 2 h time course by following 25 molecules (24 proteins and DNA) in BT pairs. Murine OT-II TCR transgenic CD4+ naïve T cells (28) were stimulated with naïve primary B lymphocytes from C57/Bl6 mice as APC. B cells were loaded with saturating concentrations (100 μg/ml, $\sim$ 105 nM) of a full agonist peptide (pOVA, AA 323–339, the cognate ligand to the OT-II TCR) (5). T cells and B cells were co-incubated, centrifuged to initiate conjugate formation, plated, and then fixed and permeabilized at various time points. The MELC system was programmed to subject the T cell–B cell pairs to 25 rounds of an automated sequence of staining and image collection, followed by bleaching of the fluorescence. The resulting microscopic images were then processed with algorithms to compensate for systemic artifacts such as lateral shift or residual, nonspecific fluorescence signals (24).

A representative field of view for BT pairs with stainings for 5 proteins (CD3ε, CD45R, pLCK, pLAT, pSLP76) is shown in Fig. 1*A*, with insets of magnifications of 4 selected pairs (labeled I-IV). Serial stainings of a BT pair show the cumulative appearance of fluorescence with pseudocolor applied to each stain to distinguish between the molecules (Fig. 1*B*). To confirm that the signaling protein localizations studied were specific to the APC - T cell synapse, we used T cell–T cell pairs as controls (Fig. 1*C*). In the upper block showing BT pairs and the lower block showing T cell–T cell pairs, F-actin, tubulin and DNA were similarly stained in both B cells and T cells. T cell marker CD3ε, total (t)-LCK, and CD45 stained T cells only whereas CD45R stained specifically B cells. Importantly, punctate staining of pLAT, pLCK, pSLP76, and pZAP70 was specific to the interface of the BT pairs. Further confirmation of the restriction of signaling to specific antigen-loaded BT pairs was provided by Western blot of activated ERK MAPK and by FACS analysis of phospho-tyrosine (supplemental Fig. S1*A* and S1*B*). The final library of antibodies and stains to target 25 molecules simultaneously is shown in Table I. A complete sequence of all 25 individual fluorescence signals within one representative BT pair is shown in supplemental Fig. S2.

We first compared the cell-type specificities and strengths of the 25 signals generated with the panel of antibodies and stains. We recorded the fluorescence signal intensities for each reagent stain at 30 min after conjugation in B cells alone, T cells alone, and T cell–B cell pairs. The resulting numerical values of signal intensity were displayed graphically (Fig. 1*D*, supplemental Fig. S3). The cell-type and BT-pair-specific expression pattern was statistically distinct for the majority of molecules and cellular entities. Several markers such as the co-stimulatory protein CD86, the integrin-ligand CD54, the chemokine receptor CXCR4 and phosphorylated signaling molecules such as pPLCγ1 were represented by very weak or undefined signals when referenced to the total cell bodies. However, enrichment of these markers at the cell-cell interface forming the APC–T-cell synapse could be clearly visualized. Thus, measurements within the synaptic subregion of the cell pairs (as employed in Figs. 2ff) resulted in statistically distinct and specific patterns for all 25 molecules used in the study (supplemental Fig. S2). Together, these data demonstrate the imaging acquisition of signals from 25 molecules involved in TCR signaling simultaneously at the level of individual BT pairs.

Sustained Antigen-specific TCR Signaling During a Two-hour Process of Physical Maturation of the Synapses—TCR activation triggers an immediate burst of signaling in TCR microclusters and subsequent organization of SMACs into central and peripheral zones within minutes. Subsequently, productive signaling through the T-cell synapse can last for hours. To determine the optimal time window for synapse formation, we evaluated pair formation and associated synaptic signaling in BT pairs in our system.

To more specifically allocate the signals detected in the BT pairs, we defined synaptic subregion based on the well-established division into central and peripheral signaling clusters (Fig. 2*A*–2*C*). The p- and cSMAC borders are generally defined by the presence of specific molecules such as LFA-1 or TCR respectively (2, 31, 32), but we chose instead to use spatial orientation and the location of pLAT to define these domains in the *x*-, *y*- and *z*-planes. pLAT was chosen as a marker for the center of the synapse and to define the ideal *z*-plane because pLAT was consistently found at the BT interface from 5 min after pair formation to the last time point and was typically found at the center of the synapse in a small number of discrete points. The F-actin ring around the synapse in the dSMAC was used to define the outer border of the pSMAC. We then developed an algorithm to use these F-actin and pLAT coordinates to calculate the position and alignment of the synapse in the x, y and z axes. The areas encircled by the actin ring ranged in diameter between 4 and 5 μm, and we defined the inner third of the areas as the cSMAC (Fig. 2*A*–*C*, Fig. S4).

Using this spatial synaptic definition we followed the kinetics of localization of key synaptic molecules within the pSMAC and cSMAC, respectively, in MELC. We observed (supplemental Fig. S1*C*) a gradual accumulation of F-actin in the peripheral subregion of the synapse with a peak at 60 min followed by a plateau. Similarly, CD3ε, an integral component

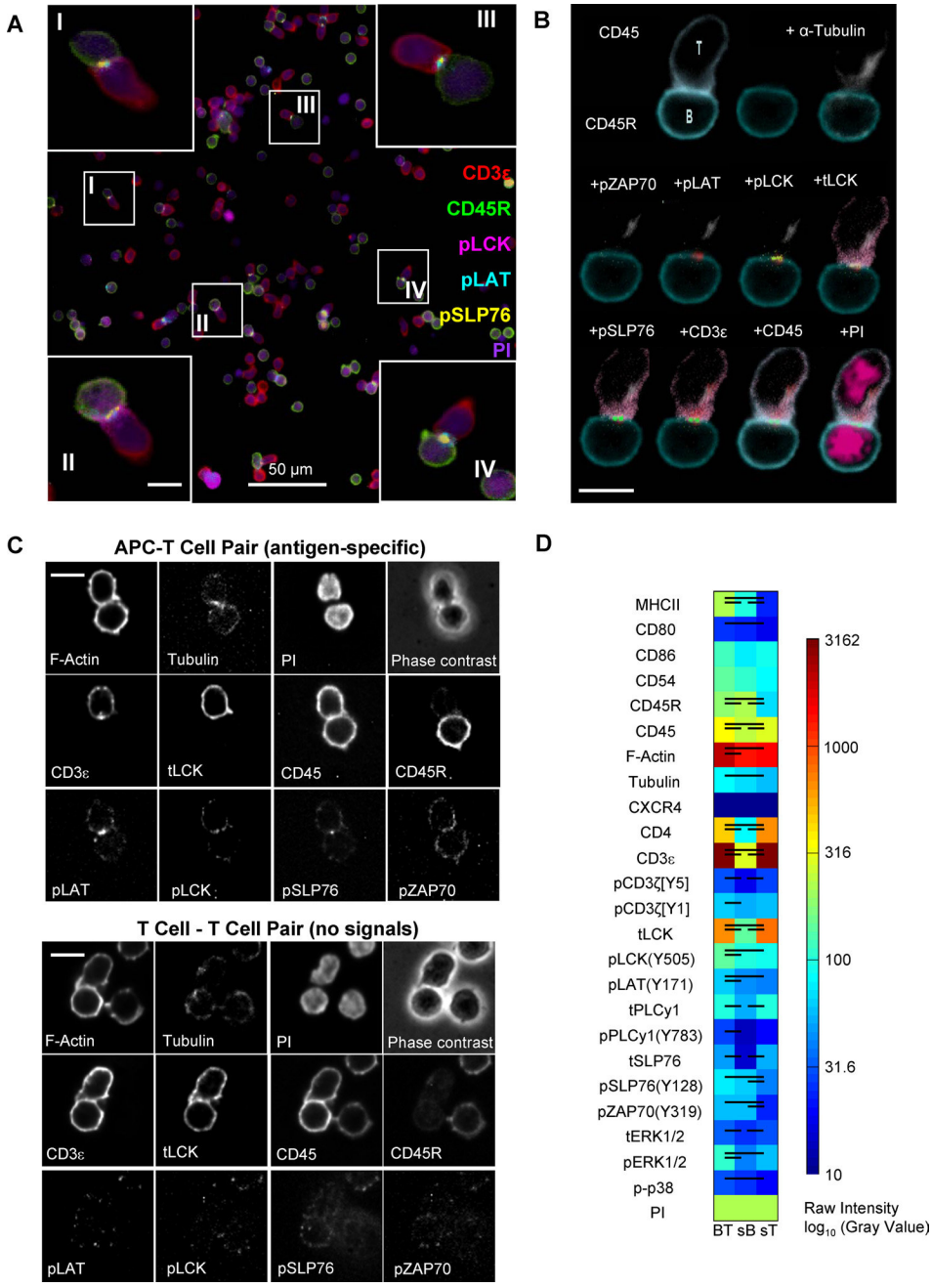

FIG. 1. **Establishment of the MELC system.** Sequential imaging of 25 molecules in synapse formation during *in vitro* activation of naïve CD4+ T-cells (OT-II) with specific antigen (100 μg/ml pOVA peptide)-loaded primary B cells as APC. *A*, Representative field of view in MELC imaging. Overlay image of the field of view acquired in individual fluorescence channels generated from 5 channels: CD3ε: red; CD45R: green; pLCK: pink; pLAT: cyan; pSLP76: yellow; PI (propidium iodide, nuclear marker): purple. Magnified insets (I-IV) demonstrate typical T-cell-B cell (BT) pairs. Scale bar in insets: 10 μm. *B*, Magnified, cumulative, multicolor overlay image of selected individual signals in one specific BT-cell pair with a characteristic synapse. For visual clarity, the CD45 signal is only depicted in the first and in the last two images. Scale bar: 10 μm. *C*, Phospho-signaling proteins at the synapse are limited to antigen-specific BT pairs. Upper panels: BT pair displaying a characteristic synapse. Top Row: F-actin, tubulin, PI, phase contrast image of cell pair. Middle row: CD3ε, tLCK, CD45, CD45R, to show T or B cells. Bottom row: synapse-localized pLAT, pLCK, pSLP76 and pZAP70 signals. Lower block: Absence of signals in T-cell-T-cell pairs. Scale bar: 10 μm. *D*, Comparison of levels of fluorescence obtained from all 25 markers in BT pairs (BT), single B (sB) and single T-cells (sT). Intensity of raw fluorescent signals at the 30 min time point is shown was converted to a color scale to visually illustrate cell type-specific expression. Statistically significant expression ($p < 0.05$ or lower) is indicated by bars. Note that the raw intensity approach here fails to resolve small differences in expression for several markers demonstrating medium to very low intensity (CD86, CD54, CD3ζ[Y1]). This formed the basis for the subsequent use of BT (synaptic) subregions and a pixel-based analysis (Figs 2ff). Analysis was performed in 32 BT pairs, 40 single B cells and 40 single T-cells in four independent experiments.

TABLE I

List of 25 molecules and epitopes detected by 24 specific antibodies (plus propidium iodide) used in MELC analysis. Specificity and Quality Control Criteria:

Methods/Lit: Key publications are listed where the actual product or the exact clone was employed by the methods indicated. Reports on the biology of the target protein with only indirect, not clone-specific evidence for antibody specificity were termed accordingly (Biology). More details can be found on the manufacturer's website. IB, Immunoblot; FC, Flow Cytometry; IHC, Immunohistochemistry; Biol., Biology.

Distribution: Predominant spatial distribution of the molecule based on the mean fluorescence intensity in the respective compartment: T cell (if single T [sT] > single B [sB]; t test, see all individual graphs and statistics in Fig. S3); B cell (if sT < sB); T and B (if sT not > sB and sT not < sB); Synapse (if Synapse [cS, central Synapse, cSMAC] > sT and sT ≤ sB).

S/N Ratio: Signal-to-Noise Ratio: Mean (mean fluorescence intensity in the respective compartment); S.D. (standard deviation); p, *p* value in the G test likelihood ratio to differ from an arbitrary threshold of 1.5.

Molecule	Phospho site	Clone	Fluorophore	Source	Cat. no	Methods/Lit	Distribution	S/N Ratio (mean, S.D., p)		
IA-IE (I-A/I-E)	2G9	FITC	BD Pharmingen		553623	IF[55], IB[56]	B cell	6,4360	1,2158	0,000
CD80		16-10A1	Alexa488	Biolegend	104716	IB[57], IHC[58]	Synapse	1,6733	0,0961	0,001
CD86		GL-1	Alexa488	Biolegend	105018	IB[59], IHC[58]	Synapse	2,7400	1,0622	0,000
CD54 (ICAM-1)		YN1/1.7.4	FITC	Biolegend	116112	IHC[60], IB[61]	Synapse	3,3510	0,8439	0,000
CD45R		RA3–6B2	Alexa488	BD Pharmingen	557669	FC[62], IF[63]	B cell	7,0420	1,9092	0,000
CD45		30-F11	FITC	BD Pharmingen	553080	FC, IF[64], FC, IB[65]	T cell	4,5800	0,8806	0,000
F-actin		C4	Alexa488	BD Pharmingen	558623	IF, IB[66], WB[67]	Synapse	5,9470	0,6657	0,000
α-Tubulin		TU-01	FITC	Acris	BM753	IB[68], IB, IF[69]	Synapse	2,8340	0,3413	0,000
CD184 (CXCR4)		2B11	FITC	BD Pharmingen	551967	FC[70] IB, IF, FC[71]	Synapse	1,6210	0,1753	0,015
CD4		RM4-5	Alexa488	BD Pharmingen	557667	IP[72] FC[73]	T cell	3,6280	0,4174	0,000
CD3ϵ		17A2	Alexa488	Biolegend	100210	IB, IHC[74], IF[75]	T cell	6,3510	1,3455	0,000
pCD3ζ [Y5]	ITAM 5, pY142	K25-407.69	Alexa488	BD Pharmingen	558486	FC[76] IB[77]	T cell	2,8600	0,4193	0,000
pCD3ζ [Y1]	ITAM 1	EM-26	Alexa488	SYBILLA[a]		IB[78], IB[79]	Synapse	1,5650	0,0545	0,008
tLCK		MOL-171	Alexa488	BD Pharmingen	558504	IB[80], IB[81]	T cell	3,5660	0,3203	0,000
pLCK	p505	4	Alexa488	BD Pharmingen	557879	Biol.[82], FC[76]	Synapse	1,8610	0,2861	0,000
pLAT	p171	158–1169	Alexa488	BD Pharmingen	558519	Biol.[83]	Synapse	2,9040	0,8116	0,000
tPLCγ1		10	Alexa488	BD Pharmingen	558566	Biol.[84]	T cell	2,2600	0,1511	0,000
pPLCγ1	pY783	27	Alexa488	BD Pharmingen	557884	Biol.[85] FC[86]	Synapse	1,8160	0,2890	0,000
tSLP76		H3	Alexa488	BD Pharmingen	560056	IB[87], IB[88]	T cell	2,3830	0,2939	0,000
pSLP76	pY128	J141	Alexa488	BD Pharmingen	558439	IB [89], IF[90]	Synapse	3,3450	0,6042	0,000
pZap70/Syk	pY319/pY352 Syk	17A	Alexa488	BD Pharmingen	557818	Biol.[91], Biol.[92]	Synapse	1,7820	0,2446	0,000
tERK1/2		G263-7	Alexa488	BD Pharmingen	612592	IB, FC[93], FC[76]	T and B	5,3420	0,5224	0,000
pERK1/2	pT202/pY204	20A	Alexa488	BD Pharmingen	612594	Biol.[94], FC[95]	T cell	2,5110	0,3598	0,000
p-p38	pT180/pY182	36	Alexa488	BD Pharmingen	612594	Biol.[96], FC[97]	T cell	1,5533	0,0306	0,001
PI (propidium iodide, nuclear marker)				Sigma	P4170		Nucleus	2,7450	0,4333	0,000

[a] The pCD3ζ[Y1] antibody was generously provided by Dr. J. Lindquist and the SYBILLA (Systems Biology of T-cell activation in Health and Disease) consortium.

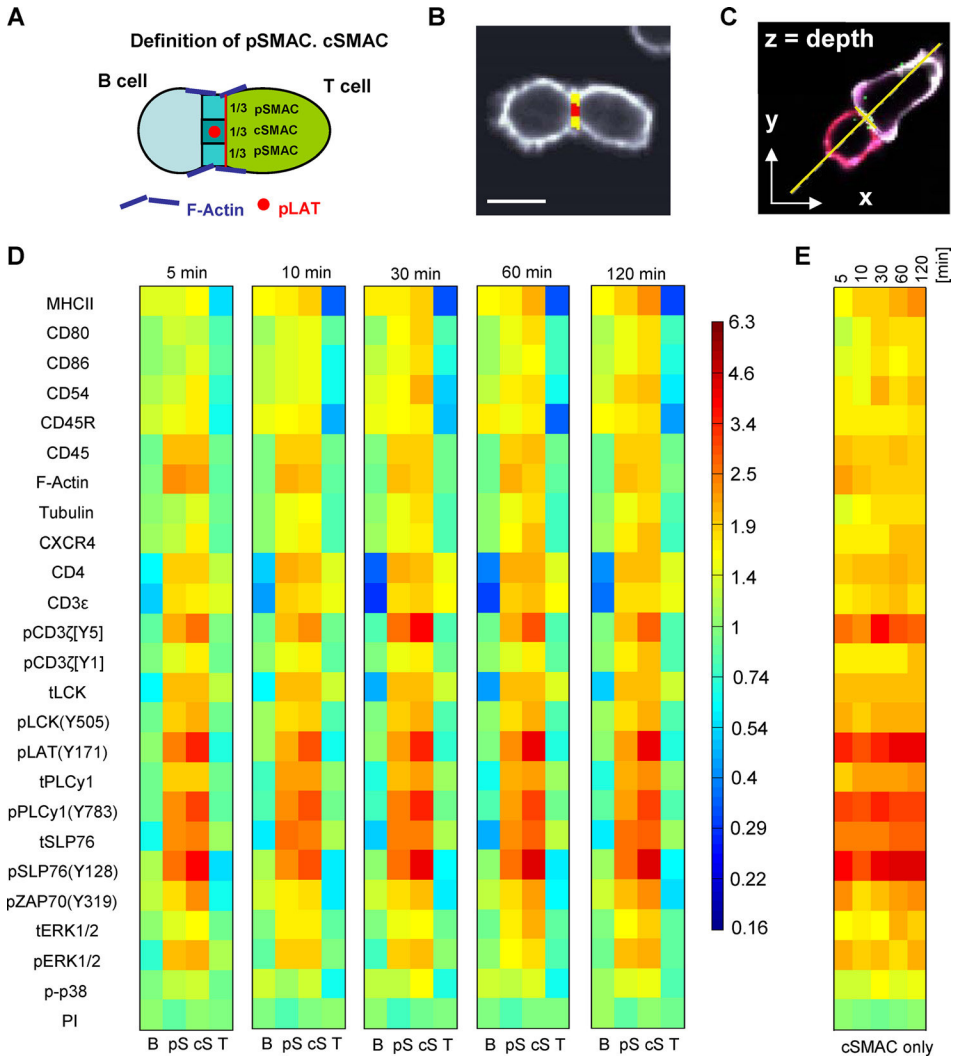

FIG. 2. **Sustained antigen-specific TCR signaling during a two-hour process of forming physically mature immunological synapses.** *A*, Graphical illustration of the spatial definition of the synapse. The synaptic area peripherally bordered by an F-actin perimeter was divided into thirds centered on pLAT as marker for cSMAC (cS) and flanked by pSMAC (pS). Adjacent to the synapse was the B cell (B) and T-cell (T) body defined as further compartments used in the subsequent analysis. *B*, Representative micrograph of a BT pair with the cSMAC (red) and pSMAC (yellow). Scalebar: 10 μm. *C*, Defining synaptic position in x,y direction and optimal z-plane (z) for analysis from the 3D image stack. MATLAB tool developed by us (for more details see supplemental Fig. S4 and Methods Section) *D*, Signal enrichment at the synapse. Relative signal intensity for all markers studied within the four compartments, T-cell body, B cell body and the synaptic subregions cSMAC (cS) and pSMAC (pS), over time. Fluorescent signal intensities of markers in each compartment were normalized to the mean intensity of signal over all four subregions at each time point. The color scale represents the intensity of each marker (1 = mean intensity over all four subregions). *E*, Density map of signals in the cSMAC (cS) subregion only. The sequence of markers is identical to Fig. 2D. Data represent the mean of 130 synapses analyzed in four (at 5 min, three) independent experiments per time point.

of the TCR-CD3 complex, continuously accumulated and reached high levels at 120 min for most of the synapses in the population. As CD3ε accumulation in the cSMAC is considered to represent structural maturation of the synapse, we concluded that the physical maturation of the synapse in our system was completed after 120 min. In addition, we observed pLAT to be consistently enriched at the cSMAC throughout the entire observation period, which suggested ongoing signaling activity. Likewise, using conventional flow cytometry measuring signals of an anti-phospho-tyrosine monoclonal antibody (PY20) we observed high signaling activity in APC-T cells pairs exceeding the levels found in single T cells at early (5 min) and late (120 min) time points (supplemental Fig. S1*D*). Of note, onset of pair formation was immediate after the synchronized APC-T-cell contact. Most BT pairs had formed already after 5 min and were strictly dependent on the presence of specific antigen and integrins (supplemental Fig. S1*E*).

Based on these kinetic evaluations, we decided to use MELC to study T-cell signaling events at various time points

up till 2 h (at 5, 10, 30, 60, and 120 min). For each time point, we calculated the intensities of the stains in the four compartments T-cell body (T), B cell body (B), pSMAC (pS), and cSMAC(cS) relative to the total intensity of the stain in the entire BT pair. We chose this form of graphical display to better visualize the enrichment over time of structural and signaling molecules at the synaptic interface of the BT pair. The relative intensities are depicted graphically with a color scale (Fig. 2*D*). The majority of signaling proteins and phosphorylated signaling proteins relocated to the synapse within 5 min and remained there for the entire observation period. The values for the cSMAC alone from each time point were aligned for a direct comparison, and showed a rapid and sustained influx of signaling proteins to the synapse (Fig. 2*E*).

The two most enriched proteins at the cSMAC were pLAT and pSLP76, followed by many other signaling proteins such as t- and pLCK, t- and pPLCγ1, tSLP76, and moderate levels of pERK1/2. The TCR, represented by CD3ζ, CD3ε, and its co-receptor CD4, also enriched at the synapse (Fig. 2*D*, 2*E*). Additionally, the intensities of structural/adhesive proteins were enhanced. For example, we observed a strong increase in F-actin in the pSMAC and a more moderate increase in tubulin, predominantly in the cSMAC, reflecting the reorganization of the cytoskeleton during synapse formation (5, 33, 34). There was a corresponding synaptic enrichment in the chemokine receptor CXCR4 which contributes to LFA-1 activation and thus mediates signal amplification at the synapse (35, 36), and a slow increase in CD54 (ICAM-1), the main ligand for the LFA-1 integrin—the prototypic marker for the pSMAC. Enrichment of B cell-specific proteins also took place at the synapse. We saw increased fluorescent signals at the synapse of MHC II (the ligand for the TCR), CD86 (a ligand for T-cell co-stimulation marker CD28), and CD45R (B220, a marker for the B cell membrane). In addition to the clear trend of gradual synaptic enrichment of different proteins, some of which peaked at 60 min whereas others peaked at 120 min, one important observation was the rapid high signaling activity by 5 min. In fact, several phosphorylated signaling proteins, notably pLAT, pSLP76, and pZAP70, were already declining toward 10 min (only the decline for pZAP70 in the cSMAC reached statistical significance, $p < 0.05$, see supplemental Table S2). It is possible that this decline represents a property of the experimental system, where the T and B cells are mixed by centrifugation to trigger conjugation. The force with which the cells are brought together might initiate a burst of TCR signaling (37, 38), followed by a lull as the T-cell deformation is corrected and the T cell begins to adhere normally to the APC. Because the APC are homogenously coated with the TCR-specific peptide, the T cells can then immediately and synchronously begin again to signal to the formation of the synapse. A period of re-orientation and resetting of the synapse before proper formation of a cSMAC was described before (39). Indeed, the subsequent rise of synaptic enrichment at 30 min and later is paralleled by an increase in CD3 accumulation in the cSMAC (Fig. S1*C*). Thus, a constant stream of synaptic signaling accompanies the proper physical maturation of the synapse, which, in our system, following a brief stage of SMAC resetting, starts at 10 min and is completed by 120 min of BT pair formation.

Distinct Phases of Molecular Recruitment and Colocalization Define Kinetic Changes in the Signaling Signature of the Synapse and Reveal a Delayed "Signaling Maturation"—Given the known centripetal movement of TCR microclusters through the pSMAC to the cSMAC (12, 40), we sought to analyze the location frequencies of our set of TCR signaling proteins in these individual compartments. As TCR signaling efficiency relies on coordinated spatial arrangement of a network of molecules we also aimed at looking into specific colocalizations of signaling proteins in the stable synapse.

As the fluorescent signals obtained for phosphorylated signaling proteins at the synapse were relatively low (Fig. 1*D*) we applied a threshold algorithm that transformed the 16-bit intensity signal into binary information for each protein at a pixel: either present (1) or absent (0) (supplemental Fig. S2). This approach also facilitated collection of signals of phospho-proteins from small subregions of the cells that measured only a few pixels in diameter. The amount of pixels positive for each signal within a subregion was then recorded and compared with the total number of pixels in this subregion to obtain the relative frequency of each protein in a given compartment of the synapse.

Using this approach, we analyzed the location of individual signaling proteins in the subcompartments of the immune synapse with MELC. Characteristic changes are illustrated as an archetypal graphical display of synapse formation in Fig. 3*A* (complete list in supplemental Table S1). The analysis revealed several layers in the synaptic buildup based on the consecutive recruitment of groups of proteins.

First, the kinetics of signaling in the synapse showed the previously mentioned high signaling levels at 5 min and subsequent decline at 10 min likely reflecting a period of resetting following the forced onset of pair formation. The decline of active signaling molecules toward 10 min in the cSMAC was significant for pZAP70 but pSLP76, pLAT, pLCK, pCD3ζ[Y5] and pCD3ζ [Y1] also showed a decline (supplemental Table S1). In contrast, other molecules like F-actin showed no decrease but rather increased toward 10 min.

Second, between 10 and 30 min key components of TCR signaling including pZAP70, pSLP76, and pPLCγ1 increased strongly and remained high from then on. These dynamic changes likely reflected consistent TCR signaling via the now evolving structurally stable synapse following the resetting and reorientation phase.

Third, between 30 and 60 min, the data showed a rise in the recruitment of molecules supportive for TCR signaling such as tERK in the cSMAC and the chemokine receptor CXCR4 in the pSMAC. This suggested an increased build-up of the physical structure and binding strength of the T-cell–B-cell pair during

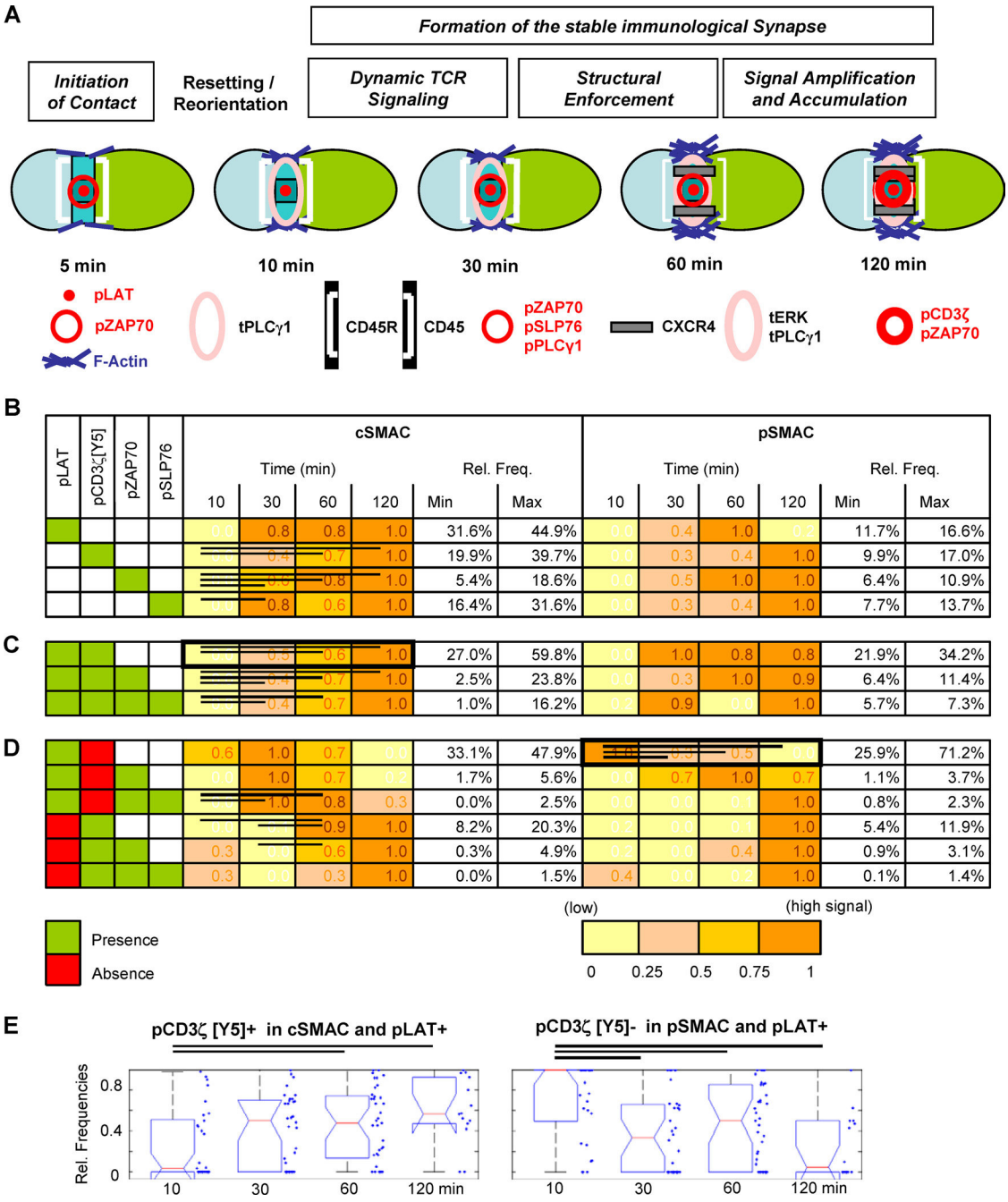

FIG. 3. **Distinct phases of molecular recruitment and co-localization in pSMAC and cSMAC during buildup of the mature synapse.** *A*, Sequential molecular assembly of the synapse with phases of earls TCR signaling, structural enforcement and delayed accumulation of signaling molecules. Data obtained in MELC. Characteristic changes in positioning and amount of molecules are indicated by symbols. A complete list of numerical data is given in supplemental Table S1. *B*, Localization of selected signaling molecules pLAT, pCD3ζ[Y5], pZAP70, and pSLP76 in synaptic subcompartments during stepwise formation of the stable synapse between 10 and 120 min. Graphical Tables illustrate the relative frequencies of pixels positive for the indicated proteins over time in the cSMAC and pSMAC subcompartment A color-coded scale in shades of orange enables a visual scan of data to detect trends: Color shades and numbers in the orange-colored boxes represent relative frequencies of a protein (0.0, minimum, yellow; 1.0, maximum, orange) relative to minimum and maximum frequencies (% of positive pixels in compartment) of that protein (white boxes, Rel. Freq.: Min, Max). Green squares identify protein represented by row. Visualized is an continuous increase of signaling molecules in the cSMAC toward 60 to 120 min (identical trend in pSMAC). Statistical significance is shown using bars (thin line, $p < 0.05$; thick line, $p < 0.01$). *C*, Co-localization of signaling molecules confined to synaptic areas positive for pLAT- and CD3ε. Graphical Tables illustrate CMPs and their relative frequencies over time using the orange color-coded scale. The increase in signaling molecules in cSMAC appears more pronounced (16-fold for areas with co-localizing pLAT, CD3ζ, pZAP70, and pSLP76) than for single molecules alone. Bars indicate statistical significances (thin line: 0.05; thick line: $p < 0.01$). *D*, Opposed kinetics of co-localization

this period. Supporting this, we previously described an increase in binding forces between T cell–APC conjugates after 30 min (41). In addition, the presence of the CD45 phosphatase and its splicing form CD45R in the pSMAC decreased between 30 and 60 min of synapse formation. These changes all suggested a critical phase of molecular recruitment favoring binding and prolonged TCR signaling.

Finally, between 60 and 120 min, we observed a continuous rise of active signaling molecules such as pCD3ζ and pZAP70 in the cSMAC and recruitment of tPLCγ1 toward the center and of F-actin toward the periphery of the synapse. These events occurred at timepoints accompanying the final structural maturation of the synaptic population studied (Fig. 2) and indicated a delayed TCR signal amplification and change in TCR signaling signature.

Next, to analyze the kinetics and distribution of TCR signaling in more depth, we focused on selected signaling proteins and their colocalizations during the period of the proper formation of the stable synapse in our system, *i.e.* between 10 and 120 min. We initially analyzed the presence of pLAT, pCD3ζ[Y5], pZAP70, and pSLP76, in cSMAC and pSMAC, respectively (Fig 3*B*). We found that all three molecules displayed a gradual increase of the frequencies of these individual molecules in both cSMAC and pSMAC (between 1.4-fold, pSLP76 in cSMAC; and 3.5-fold, pZAP70 in cSMAC). Highest levels were reached at 60 and 120 min, respectively, suggesting ongoing recruitment of signaling molecules at delayed time points.

We next wanted to analyze the frequencies of co-localizations of these synaptic molecules (Fig. 3*C*). We tested the frequencies of co-localization of pZAP70 and pSLP76 in synaptic areas that were also positive for pLAT and CD3 (pCD3ζ[Y5]). The use of binarized imaging data resulting from the thresholding of fluorescent signals was not only useful in evaluating low-intensity signals of individual markers, but could also be used to generate and quantify CMP motifs (25, 42, 43), patterns of localizations of several markers within one spot (pixel). Although it is conceptually easier to think of a CMP motif as a protein complex, MELC analysis does not provide data on actual binding between proteins—only on shared locations. Using such colocalization CMPs for analysis, the accumulation of signaling molecules in the cSMAC over time became more obvious. For example, the frequency of pixels positive for pLAT, pCD3ζ[Y5], and pZAP70 increased 9.5-fold (from 2.5% to 23.8%) and the frequency of colocalizations of pLAT, pCD3ζ[Y5], pZAP70, and pSLP76 increased 16.2-fold (from 1.0% to 16.2%) (Fig. 3*C*).

Finally, we studied the frequency of synaptic areas distinctively characterized by the presence or absence of pLAT and pCD3ζ, respectively (Fig. 3*D*). pLAT is considered to mainly correspond to membrane domains or vesicles, and CD3 primarily localizes with TCR in domains separate from those containing pLAT (12). During the course of synapse formation, we found that the frequencies of CMPs containing pLAT but not pCD3ζ peaked very early in the pSMAC (at 10 min) and at 30 min in the cSMAC and then strongly decreased over time (in the pSMAC by approximately two-thirds, from 71.2% to 25.9%). In contrast, (TCR)-areas containing pCD3ζ but not pLAT showed an increase in both pSMAC and cSMAC peaking at 120 min (in the cSMAC from 8.2% to 20.3%). Both pCD3ζ+pLAT- areas and pCD3ζ+pLAT+ areas (Fig. 3*C*) were found at higher frequencies in the cSMAC than in the pSMAC (20.3 *versus* 11.9%, and 59.8 *versus* 34.2%, respectively). However, the area of the pSMAC was 8 times that of the cSMAC according to our definition of the cSMAC as 1/3 of the radius of the pSMAC. The continuous increase of CD3ζ was consistent with the CD3ζ enrichment observed earlier and paralleled the general recruitment toward the synapse (supplemental Fig. S1*C*). Our observation of an increase of pLAT clusters (Fig. 3*B*), and increase of pLAT+pCD3ζ+ (Fig. 3*C*) yet decrease of pLAT+pCD3ζ- (Fig. 3*D*) suggests that the TCR and pLAT clusters became confluent over time in both pSMAC and cSMAC. Indeed, the merging of LAT with TCR/CD3 clusters during T-cell activation has been described to start within minutes after onset of synapse formation (14). Here we observe this process on a multiprotein level for longer time periods, up to 120 min.

In summary, these findings suggest that sustained TCR signaling within the synapse is accompanied by a gradual accumulation of distinct clusters of signaling molecules and a delayed change in signaling that we would call synaptic "signaling maturation."

Molecular Composition of Microclusters at the Center of the Synapse—TCR signaling in T cells on planar lipid bilayers takes place in numerous microclusters that take between 70 and 140 nm (14) and vary from 10 to close to a 100 TCR molecules per cluster while in transit to the cSMAC (44). Studies of T cell–APC conjugates immobilized in an upright position on grids showed that larger microclusters measuring about 1.5 μm^2 form in these synapses and coalesce in the center by 60 min (45). To study the distribution of microclusters in late-stage synapses in the BT pairs, we applied three-dimensional graphical rendering to selected synapses. TCR signaling proteins at the interface of the cell pairs were local-

of signaling molecules in synaptic subcompartments with distinctive presence or absence of pLAT and CD3ζ[Y5]. Green and red color code for the presence or absence of the protein markers indicated. pLAT cluster (in absence of CD3ζ) peak early in pSMAC (10 min) and then disappear. In contrast, signaling-associated pLAT cluster (pLAT+, CD3ζ-, ZAP70+, SLP76+) and CD3ζ-cluster increase toward 60 to 120 min in the cSMAC (identical trend in pSMAC). Bars indicate statistical significances (thin line: 0.05; thick line: $p < 0.01$). *E*, shows two of the characteristic CMP motifs illustrated (and highlighted by frame) in *D* as box plots. Bars indicate statistical significances (thin: 0.05; thick: $p < 0.01$). pLAT and CD3ζ were used as base motifs to define the subregion for analysis in *C* and *D*, respectively. CMP analysis of 130 synapses.

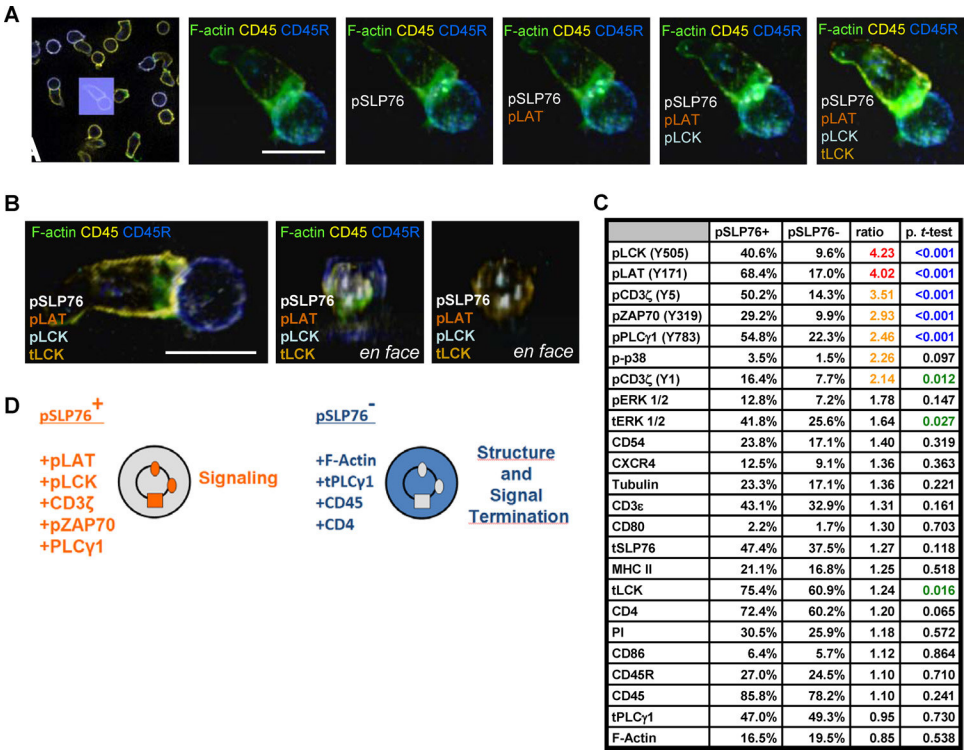

	pSLP76+	pSLP76-	ratio	p. *t*-test
pLCK (Y505)	40.6%	9.6%	4.23	<0.001
pLAT (Y171)	68.4%	17.0%	4.02	<0.001
pCD3ζ (Y5)	50.2%	14.3%	3.51	<0.001
pZAP70 (Y319)	29.2%	9.9%	2.93	<0.001
pPLCγ1 (Y783)	54.8%	22.3%	2.46	<0.001
p-p38	3.5%	1.5%	2.26	0.097
pCD3ζ (Y1)	16.4%	7.7%	2.14	0.012
pERK 1/2	12.8%	7.2%	1.78	0.147
tERK 1/2	41.8%	25.6%	1.64	0.027
CD54	23.8%	17.1%	1.40	0.319
CXCR4	12.5%	9.1%	1.36	0.363
Tubulin	23.3%	17.1%	1.36	0.221
CD3ε	43.1%	32.9%	1.31	0.161
CD80	2.2%	1.7%	1.30	0.703
tSLP76	47.4%	37.5%	1.27	0.118
MHC II	21.1%	16.8%	1.25	0.518
tLCK	75.4%	60.9%	1.24	0.016
CD4	72.4%	60.2%	1.20	0.065
PI	30.5%	25.9%	1.18	0.572
CD86	6.4%	5.7%	1.12	0.864
CD45R	27.0%	24.5%	1.10	0.710
CD45	85.8%	78.2%	1.10	0.241
tPLCγ1	47.0%	49.3%	0.95	0.730
F-Actin	16.5%	19.5%	0.85	0.538

FIG. 4. **Molecular composition of microclusters at the synapse.** *A*, Localization of pSLP76^{+} clusters around the center of the synapse. Micrographs of a representative BT-cell pair (first panel) show the cumulative overlay of images of structural molecules (F-actin, CD45, CD45R) with signaling molecules (pSLP76, pLAT, pLCK, tLCK) in the indicated colors (next 5 panels). *B*, *En face* view of a representative synapse at a B cell-T-cell pair. Original image stained for the same proteins as in (*A*) (left image) and 2 axial *en face* views (middle and right image) through the synapse showing all molecules (middle image) or signaling molecules only (right image). Note the presence of discrete microclusters around the cSMAC. Scale bar: 10 μm. *C*, Molecular composition of pSLP76^{+} clusters in the synapse at 60 min. CMP analysis shows percentage of pixels positive for the given protein colocalizing with pSLP76 (pSLP76^{+}) compared with the percentage of pixels in areas (pixels) that do not contain pSLP76 (pSLP76^{-}). These values are compared in the ratio column (pSLP76^{+}/pSLP76^{-}). Highest ratios are colored (red: ratio>4; orange: ratio>2.) Significant *p* values are colored (green: $p < 0.05$; blue: $p < 0.01$). *D*, Graphical illustration of the composition of SLP76^{+} clusters in the cSMAC and the surrounding area, respectively. Red bars point to the projected locations of the molecules listed. Potential functions of the respective clusters are indicated (signaling *versus* structure/signaling termination).

ized predominantly in several microclusters ~2–3 pixels (600–900 nm) in diameter. These microclusters surrounded the center of the synapse and contained activated signaling molecules including pSLP76, pLAT, and pLCK (Fig. 4*A*, 4*B*). We used CMP analysis to contrast the molecular composition of signaling clusters containing pSLP76^{+} areas *versus* pSLP76^{-} areas (Fig. 4*C*). pSLP76 was chosen from among the signaling molecules as its staining showed a high signal-to-noise ratio and clearly revealed the location and shape of the signaling clusters. CMP analysis showed that pSLP76 was strongly and significantly colocalized with pLCK, pLAT, pCD3ζ, pZAP70, and pPLCγ1. In contrast, CD4, CD86, CD45, and total signaling proteins such as tPLCγ1 showed little or no tendency to accumulate in these clusters. Also notable, F-actin was found more frequently outside these clusters than in them (Fig. 4*C*). Thus, signaling in the synapse is concentrated in a few microclusters of active TCR signaling (including pSLP76, pLAT, pLCK, pCD3ζ, pZAP70, and PLCγ1) whereas the surrounding area is dominated by molecules more important for the integrity of structure (F-actin) and signal termination (such as CD45) (Fig. 4*D*).

Altered Molecular Composition of Synapses in T Cells from Vav1$^{-/-}$ Mice—An important application of MELC technology to the study of the synapse would be to use it to characterize signaling defects in T cells from mutant mice such as Vav1 knockout mice (Vav1$^{-/-}$). Vav1 is required for T-cell development and activation by mediating signals leading to calcium fluxing, MAPK activation and actin polymerization (46). Vav1 can act as a scaffold protein through its many protein interaction domains and as an enzyme that activates Rho GTPases (47). Studies on mutants of Vav1 lacking GEF activity have shown that Vav1 acts through recruitment of signaling proteins to activate PLCγ1 (47) and regulate calcium signaling. Vav1 is also recruited to and stabilizes SLP76 microclusters (48), (49). To investigate the molecular composition of synapses in the absence of Vav1, we applied a MELC analysis to T-cell synapses from Vav1-mutant mice.

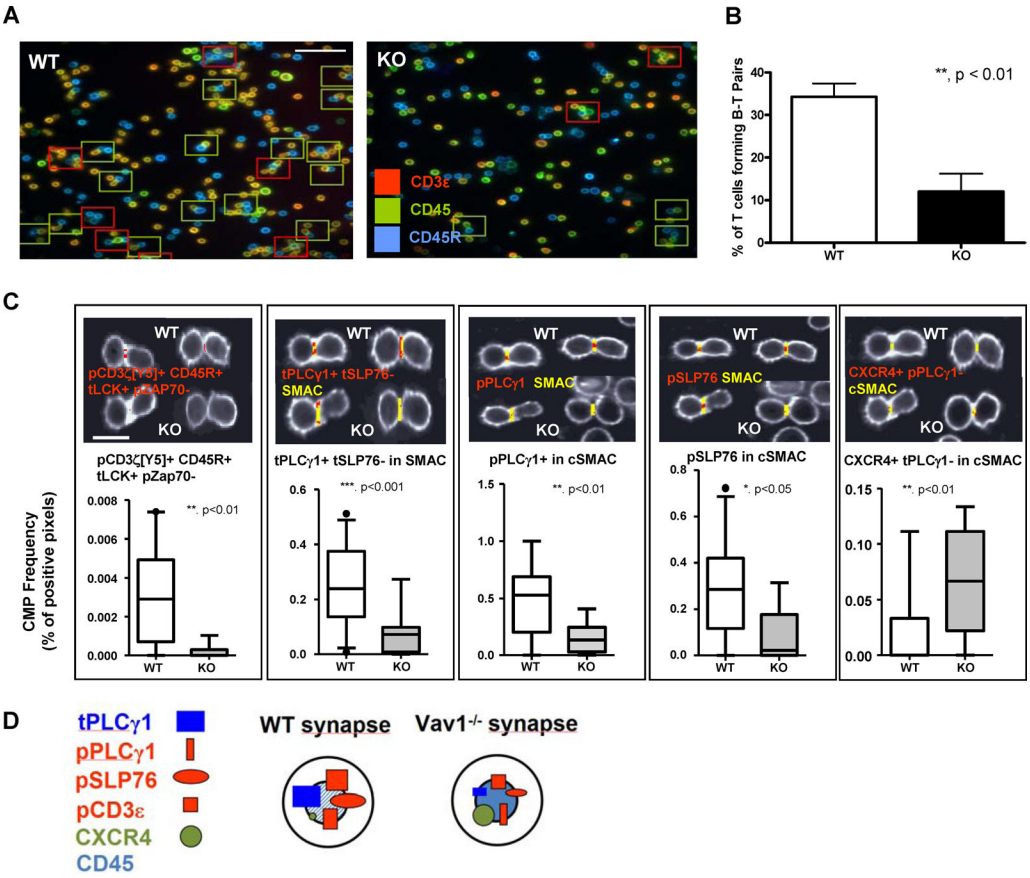

FIG. 5. **Synapse formation and signaling is impaired in the absence of Vav1.** *A*, Representative field of view WT *versus* Vav1$^{-/-}$ T-cell–B-cell pairs. Selected synaptic pairs indicated by rectangles: green: used for analysis; red: excluded from analysis because of interference by neighboring cells. Left: WT T-cells. Right: Vav1$^{-/-}$ T-cells. Note that very few pairs are formed with Vav1$^{-/-}$ T-cells. Scale bar: 50 μm. *B*, Quantification of pair formation. Mean ± S.E. from two independent experiments each with more than 50 WT and 50 KO T-cells analyzed. *C*, Significant differences in molecular composition of WT *versus* Vav1$^{-/-}$ synapses. Micrographs displaying signals of specific molecule/co-localization motif (red) and synapse areas (SMAC or cSMAC, yellow) in synapses of two characteristic T-cell-B cell pairs. Box plots and statistical significance of relative frequencies of the indicated molecules in the cSMAC. Whiskers show 5–95% confidence interval. Scale bar: 10 μm. *D*, Graphical illustration of the principal differences in composition between WT and Vav1$^{-/-}$ synapses based on data obtained from MELC CMP analysis.

We first quantified the overall capacity of Vav1$^{-/-}$ T cells to stably bind to APC and to form synapses. The numbers of conjugates formed was strongly reduced in BT pairs with T cells from Vav1$^{-/-}$ mice (from 31.1 ± 4.9% for WT to 11.2 ± .2% for Vav1$^{-/-}$) (Fig. 5*A*, 5*B*). Similar data were obtained by flow cytometry (supplemental Fig. S5*A*). The overall signaling in Vav1$^{-/-}$ T cells was defective as shown conventionally by Western blot demonstrating greatly reduced activation of pERK in total cell extracts (supplemental Fig. S5*B*), however tSLP76 expression was normal in these cells (supplemental Fig. S5*C*). ERK and SLP76 were chosen because Vav1 is known to induce ERK activation (46) and to influence stability of the SLP76 complex (49). CMP analysis of individual synapses formed by Vav1$^{-/-}$ T cells revealed significant shifts in groups of proteins when compared with synapses by WT T cells (supplemental Table S2). First, in WT synapses (supplemental Table S2, Part A) TCR-associated molecules CD4, pCD3ε, and pCD3ζ were much more likely to be found in WT synapses than in Vav1$^{-/-}$ synapses. Second, structural and costimulatory proteins CD80/86, CXCR4 and F-actin were all present at lower frequencies in WT synapses than in Vav1$^{-/-}$ synapses. These differences are more obvious when directly looking at the CMP motifs found be higher in Vav1$^{-/-}$ synapses (Table S2, Part B). Third, several signaling molecules were mislocalized in Vav1$^{-/-}$ synapses. For example, CD45 was found enriched in Vav1$^{-/-}$ synapses suggesting failure in synaptic exclusion. Most notably, total PLCγ1 was greatly reduced in Vav1$^{-/-}$ synapses and consequently also pPLCγ1. Given the importance of Vav1 to SLP76 microclusters (49), we expected to find reductions in tSLP76 at the synapse but tSLP76 was unexpectedly less enriched in WT synapses. However, motifs containing pSLP76 were clearly expressed at lower frequencies in Vav1$^{-/-}$ synapses again suggesting inadequate signaling in Vav1$^{-/-}$ synapses. In contrast, no or only minor differences were found in localization of LCK, pLAT, pZAP70, CD54, p38 and ERK, indicating that

localization of these proteins does not primarily depend on Vav1. Images of selected CMP motifs and quantitative comparisons of their occurrence in WT and Vav1$^{-/-}$ synapses are shown in Fig. 5*C*. A graphical summary of the signaling profile in the Vav1$^{-/-}$ T cells illustrates these alterations in signaling clusters, showing the impaired recruitment of tPLCγ1, pPLCγ1 and pSLP76 (Fig. 5*D*). These data confirm that Vav1 regulates PLCγ1 localization, either directly or indirectly through protein complex formation, SLP76 activation, and reveal a novel defect in CXCR4 localization. These results represent the first large-scale imaging data on Vav1$^{-/-}$ T-cell synapses and validate the use of MELC to detect and quantify molecular signaling defects at the level of the individual synapses.

DISCUSSION

Current imaging technologies directed at the study of the synapse are limited in the number of proteins that can be tracked simultaneously. MELC technology has been used to map multiple proteins in the same sample of fixed cells or tissues. In this report, we used MELC for the first time to study 25 molecules at the immune synapse over an extended period of time. We evaluated individual reagent stains over five time points and performed quantitative analysis of co-localizations of proteins and the relationships between different classes of proteins at the synapse. We used the resulting data to characterize the layered construction of the synapse, the composition of late-stage microclusters, and the structure of Vav1 mutant synapses.

Signaling at the synapse takes place in microclusters of proteins containing TCR, phosphorylated TCR-proximal signaling proteins including pLCK and pZAP70 and adapter proteins including pLAT and pSLP76. Studies on live T cells immobilized on lipid planar bilayers demonstrated that microclusters originate in the dSMAC and migrate in an actin-dependent manner to the center of the cSMAC (12, 40). We analyzed images of signaling changes over 2 h at the synapse of fixed cell pairs to identify trends in synapse formation. We used primary mouse naïve T cells and naïve B cells, a homogenous APC population that display lower levels of co-stimulatory and danger signals than macrophages and dendritic cells. With these cells, central localization of TCR clusters took between 30 and 60 min, and TCR signaling, as measured by the appearance of phosphorylated proteins, peaked at 60–120 min, consistent with previous observations (3, 17, 19). While individual signaling molecules have been followed at the synapse for over an hour (50), MELC enabled us to analyze network-scale numbers of signaling proteins in this time period.

Results from MELC revealed that the construction of the synapse occurred in overlapping layers of proteins classes. Based on recruitment of F-actin toward the periphery and of CD3 toward the center of the synapse we observed the structural maturation in our synaptic population to be complete after 120 min. Already at 5 min, we observed high levels of phosphorylated molecules suggesting a rapid burst of signaling from the sudden contact of T cell and B cells after centrifugation, along with an appearance of pLAT and pZAP70, but little F-actin or SLP76. This initial jolt of signaling tapered off by 10 min, probably as T cells re-oriented to build a stable synapse. The proper buildup of the mature synapse including formation of a cSMAC (central CD3ε accumulation) then started at 10 min when intense TCR signaling (re-) started and continued throughout. This was supported by processes of consolidation and structural reinforcement that ranged from 30 to 60 min. At this time, costimulatory proteins like CD86 and CXCR4 began to appear and nonactivated signaling proteins such as tERK were recruited. These events indicated a period of structural enforcement and increased binding strength of the cell-cell contact. In accordance with this, we have previously observed a rise in binding forces between APC-T-cell pairs after ~30 min of APC-T-cell contact (41). Furthermore, CD45R and CD45 were reduced in the synapse area likely resulting in a release of TCR signaling from phosphatase inhibition, further indicating that a platform for signaling was being assembled. A last, protracted stage of strong TCR signaling accumulation and coalescence was apparent at the timepoints 60 min and 120 min. The overall levels of signaling molecules present in pSMAC and cSMAC further increased compared with earlier timepoints. Signals by pLAT in the pSMAC peaked at 60 min, although signaling continued to rise in the central synapse area toward 120 min. Thus, synapses were built in stages with a structural platform that accompanied a gradual increase in signaling by pCD3ζ, pZAP70, pLAT, pSLP76 over the entire 2 h and a prolonged and gradual shift from pSMAC to cSMAC signaling.

To parse the numerical data derived from our MELC analysis of synapses, we compared CMPs containing pLAT and/or TCR (CD3ζ) over the time course of the study. pLAT was chosen as a marker of membrane domains that are initially distinct from TCR membrane domains. It has recently been shown that LAT is recruited to the membrane in subsynaptic vesicles where it becomes phosphorylated at SLP76 microclusters, and that when LAT domains couple to TCR domains they become microclusters (12, 15). LAT and TCR are also located in separate protein islands that concatenate on activation (14). Analysis of CMP featuring pLAT alone *versus* CMP with TCR alone revealed that they exhibited dynamics consistent with the merging of LAT and TCR into clusters. As the CMP containing pLAT alone without TCR declined in the pSMAC, they increased in the cSMAC together with CMP containing both pLAT and TCR, suggestive of a merging of two different clusters to make a functional signaling TCR microcluster (14). In addition, the high frequency of colocalized signaling mediators at delayed time points underlines the potential importance of these late stages of synapse formation for T-cell activation. Indeed, the time point of 120

min coincides with the minimum time needed for a B-cell–T-cell contact to ensure full T-cell activation (3).

We found that signaling within the synapse culminated in a small number of large microclusters at the border between the pSMAC and cSMAC. Within these microclusters the proteins most specifically co-localized were active pSLP76 (used to define the clusters), pLAT, pLCK, pZAP70, and pCD3ζ. This cluster composition corresponds to that described for proper microclusters (signalosomes consisting of CD3ζ, pZAP70, pSLP76, pLAT, pPLCγ1, and others) and their surrounding area (consisting of CD3ε, pERK, CD45, and others) as previously reported (40). Surprisingly, F-actin was negatively associated with these microclusters. It is possible that these microclusters (rendered at 60 min onset of pair formation) represent late-stage signaling in a mature, fully developed synapse. The large size of the microclusters, the small number of them, the location and the negative association with F-actin are all consistent with the possibility that these microclusters have coalesced, moved toward the center of the synapse and are detaching from actin, but can nonetheless still actively signal.

MELC was also used to analyze synapse formation in Vav1 mutant T cells. We observed that loss of Vav1 resulted in an approximate two-thirds decrease in the number of synapses formed, which represents a challenge in conventional biochemical analysis of signaling in synapses. However, MELC assessment of mass protein localization at single T-cell level could still point to defects in Vav1 KO T cells that might lead to insights into development of mutant cells. Given that Vav1 is mutated in the T-cell germline of the mice used here, we reasoned that it is possible that any signaling-active T-cells were selected during development for the ability to overcome the loss of Vav1, possibly by having greater levels of proteins that would make TCR signaling easier (51) and that MELC might be helpful in detecting them. For example, our CMP array showed that CXCR4 is significantly increased in the synapses of Vav1 T cells. CXCR4 is associated with TCR, recruited to synapses and signals through ZAP70 (52). It is possible that increased levels of CXCR4 at the synapse generate enough additional signaling through ZAP70 to partially compensate for lower levels of TCR and higher levels of CD45, leading to signaling-active Vav1 KO T cells. However, the severe decrease in PLCγ1 recruitment to the synapse we observed would hinder normal TCR signaling to calcium-dependent targets such as NF-kB or NFAT. In contrast, we observed normal localization and activation of the critical adaptor LAT, indicating that some of the main TCR signaling events can still occur without Vav1.

In the future, MELC results can be expanded by using new techniques such as using grids to hold conjugate pairs in place to enable clear imaging of the interface planes (45), or using super-resolution imaging technologies (53, 54) to improve resolution to low nm scales. We demonstrated here the use of MELC as a tool to analyze the architecture of the synapse over 2 h, the composition of microclusters, and the synapse composition following loss of a key TCR signaling protein, Vav1. This report highlights the advantages of using MELC to perform network-scale studies to shed light on the complex functions of the immune synapse.

Acknowledgments—We thank Guido Höbbel and Susanne Bonifatius for excellent technical support, and Ursula Bommhardt, Jon Lindquist, Tilo Beier, Stefanie Kliche, and Luca Simeoni for most helpful discussions. We thank BD Pharmingen for generously providing several of their antibodies and Dr. J. Lindquist with the SYBILLA program (Systems Biology of T-cell activation in Health and Disease) for providing the pCD3ζ[Y1] antibody.

* This work was supported by the German Research Foundation (SFB) by grant SFB854 to K.D.F., B.S., M.G., and P.R. and by the SPP1468 (Immunobone) to M.G.

S This article contains supplemental Figs. S1 to S5 and Tables S1 and S2.

** To whom correspondence should be addressed: Otto von Guericke University, Institute of Molecular and Clinical Immunology, Leipziger Str. 44, 39120 Magdeburg, Germany. Tel.: +49 391 67 17888; Fax: +49 391 67 15852; E-mail: peter.reichardt@med.ovgu.de.

B.S. is also Head of the Department of Immune Control, Helmholtz Centre for Infection Research, Braunschweig, Germany.

¶¶ Joint Senior Authors.

REFERENCES

1. Fooksman, D. R., Vardhana, S., Vasiliver-Shamis, G., Liese, J., Blair, D. A., Waite, J., Sacristan, C., Victora, G. D., Zanin-Zhorov, A., and Dustin, M. L. (2010) Functional anatomy of T cell activation and synapse formation. *Annu. Rev. Immunol.* **28,** 79–105
2. Monks, C. R., Freiberg, B. A., Kupfer, H., Sciaky, N., and Kupfer, A. (1998) Three-dimensional segregation of supramolecular activation clusters in T cells. *Nature* **395,** 82–86
3. Grakoui, A., Bromley, S. K., Sumen, C., Davis, M. M., Shaw, A. S., Allen, P. M., and Dustin, M. L. (1999) The immunological synapse: a molecular machine controlling T cell activation. *Science* **285,** 221–227
4. Friedl, P., den Boer, A. T., and Gunzer, M. (2005) Tuning immune responses: diversity and adaptation of the immunological synapse. *Nat. Rev. Immunol.* **5,** 532–545
5. Reichardt, P., Dornbach, B., Rong, S., Beissert, S., Gueler, F., Loser, K., and Gunzer, M. (2007) Naive B cells generate regulatory T cells in the presence of a mature immunologic synapse. *Blood* **110,** 1519–1529
6. Reichardt, P., Dornbach, B., and Gunzer, M. (2007) The molecular makeup and function of regulatory and effector synapses. *Immunol. Rev.* **218,** 165–177
7. Costello, P. S., Walters, A. E., Mee, P. J., Turner, M., Reynolds, L. F., Prisco, A., Sarner, N., Zamoyska, R., and Tybulewicz, V. L. (1999) The Rho-family GTP exchange factor Vav is a critical transducer of T cell receptor signals to the calcium, ERK, and NF-kappaB pathways. *Proc. Natl. Acad. Sci. U.S.A.* **96,** 3035–3040
8. Smith-Garvin, J. E., Koretzky, G. A., and Jordan, M. S. (2009) T cell activation. *Annu. Rev. Immunol.* **27,** 591–619
9. Hartman, N. C., Nye, J. A., and Groves, J. T. (2009) Cluster size regulates protein sorting in the immunological synapse. *Proc. Natl. Acad. Sci. U.S.A.* **106,** 12729–12734
10. Hashimoto-Tane, A., Yokosuka, T., Sakata-Sogawa, K., Sakuma, M., Ishihara, C., Tokunaga, M., and Saito, T. (2011) Dynein-driven transport of T cell receptor microclusters regulates immune synapse formation and T cell activation. *Immunity* **34,** 919–931
11. Reichardt, P., Dornbach, B., and Gunzer, M. (2010) APC, T cells, and the immune synapse. *Curr. Top Microbiol. Immunol.* **340,** 229–249
12. Purbhoo, M. A., Liu, H., Oddos, S., Owen, D. M., Neil, M. A., Pageon, S. V., French, P. M., Rudd, C. E., and Davis, D. M. (2010) Dynamics of subsynaptic vesicles and surface microclusters at the immunological synapse. *Sci. Signal* **3,** ra36
13. Varma, R., Campi, G., Yokosuka, T., Saito, T., and Dustin, M. L. (2006) T cell

receptor-proximal signals are sustained in peripheral microclusters and terminated in the central supramolecular activation cluster. *Immunity* **25,** 117–127
14. Lillemeier, B. F., Mortelmaier, M. A., Forstner, M. B., Huppa, J. B., Groves, J. T., and Davis, M. M. (2010) TCR and Lat are expressed on separate protein islands on T cell membranes and concatenate during activation. *Nat. Immunol.* **11,** 90–96
15. Williamson, D. J., Owen, D. M., Rossy, J., Magenau, A., Wehrmann, M., Gooding, J. J., and Gaus, K. (2011) Pre-existing clusters of the adaptor Lat do not participate in early T cell signaling events. *Nat. Immunol.* **12,** 655–662
16. Yokosuka, T., Kobayashi, W., Sakata-Sogawa, K., Takamatsu, M., Hashimoto-Tane, A., Dustin, M. L., Tokunaga, M., and Saito, T. (2008) Spatiotemporal regulation of T cell costimulation by TCR-CD28 microclusters and protein kinase C theta translocation. *Immunity* **29,** 589–601
17. Dustin, M. L. (2008) T cell activation through immunological synapses and kinapses. *Immunol. Rev.* **221,** 77–89
18. Lee, K. H., Dinner, A. R., Tu, C., Campi, G., Raychaudhuri, S., Varma, R., Sims, T. N., Burack, W. R., Wu, H., Wang, J., Kanagawa, O., Markiewicz, M., Allen, P. M., Dustin, M. L., Chakraborty, A. K., and Shaw, A. S. (2003) The Immunological Synapse Balances T Cell Receptor Signaling and Degradation. *Science* **302,** 1218–1222
19. Lee, K. H., Holdorf, A. D., Dustin, M. L., Chan, A. C., Allen, P. M., and Shaw, A. S. (2002) T cell receptor signaling precedes immunological synapse formation. *Science* **295,** 1539–1542
20. Carrasco, Y. R., Fleire, S. J., Cameron, T., Dustin, M. L., and Batista, F. D. (2004) LFA-1/ICAM-1 Interaction Lowers the Threshold of B Cell Activation by Facilitating B Cell Adhesion and Synapse Formation. *Immunity* **20,** 589–599
21. Sanchez-Lockhart, M., Graf, B., and Miller, J. (2008) Signals and sequences that control CD28 localization to the central region of the immunological synapse. *J. Immunol.* **181,** 7639–7648
22. Cemerski, S., Das, J., Giurisato, E., Markiewicz, M. A., Allen, P. M., Chakraborty, A. K., and Shaw, A. S. (2008) The balance between T cell receptor signaling and degradation at the center of the immunological synapse is determined by antigen quality. *Immunity* **29,** 414–422
23. Cemerski, S., Das, J., Locasale, J., Arnold, P., Giurisato, E., Markiewicz, M. A., Fremont, D., Allen, P. M., Chakraborty, A. K., and Shaw, A. S. (2007) The stimulatory potency of T cell antigens is influenced by the formation of the immunological synapse. *Immunity* **26,** 345–355
24. Schubert, W., Bonnekoh, B., Pommer, A. J., Philipsen, L., Bockelmann, R., Malykh, Y., Gollnick, H., Friedenberger, M., Bode, M., and Dress, A. W. (2006) Analyzing proteome topology and function by automated multidimensional fluorescence microscopy. *Nat. Biotechnol.* **24,** 1270–1278
25. Linke, B., Pierre, S., Coste, O., Angioni, C., Becker, W., Maier, T. J., Steinhilber, D., Wittpoth, C., Geisslinger, G., and Scholich, K. (2009) Toponomics analysis of drug-induced changes in arachidonic acid-dependent signaling pathways during spinal nociceptive processing. *J. Proteome. Res.* **8,** 4851–4859
26. Pierre, S., Maeurer, C., Coste, O., Becker, W., Schmidtko, A., Holland, S., Wittpoth, C., Geisslinger, G., and Scholich, K. (2008) Toponomics analysis of functional interactions of the ubiquitin ligase PAM (Protein Associated with Myc) during spinal nociceptive processing. *Mol. Cell Proteomics.* **7,** 2475–2485
27. Berndt, U., Philipsen, L., Bartsch, S., Hu, Y., Rocken, C., Bertram, W., Hammerle, M., Rosch, T., and Sturm, A. (2010) Comparative Multi-Epitope-Ligand-Cartography reveals essential immunological alterations in Barrett's metaplasia and esophageal adenocarcinoma. *Mol. Cancer* **9,** 177
28. Barnden, M. J., Allison, J., Heath, W. R., and Carbone, F. R. (1998) Defective TCR expression in transgenic mice constructed using cDNA-based alpha- and beta-chain genes under the control of heterologous regulatory elements. *Immunol. Cell Biol.* **76,** 34–40
29. Fischer, K. D., Kong, Y. Y., Nishina, H., Tedford, K., Marengere, L. E., Kozieradzki, I., Sasaki, T., Starr, M., Chan, G., Gardener, S., Nghiem, M. P., Bouchard, D., Barbacid, M., Bernstein, A., and Penninger, J. M. (1998) Vav is a regulator of cytoskeletal reorganization mediated by the T-cell receptor. *Curr. Biol.* **8,** 554–562
30. Patra, A. K., Na, S. Y., and Bommhardt, U. (2004) Active protein kinase B regulates TCR responsiveness by modulating cytoplasmic-nuclear localization of NFAT and NF-kappa B proteins. *J. Immunol.* **172,** 4812–4820
31. Vardhana, S., Choudhuri, K., Varma, R., and Dustin, M. L. (2010) Essential role of ubiquitin and TSG101 protein in formation and function of the central supramolecular activation cluster. *Immunity* **32,** 531–540
32. Storim, J., Brocker, E. B., and Friedl, P. (2010) A dynamic immunological synapse mediates homeostatic TCR-dependent and -independent signaling. *Eur. J. Immunol.* **40,** 2741–2750
33. Dustin, M. L., and Cooper, J. A. (2000) The immunological synapse and the actin cytoskeleton: molecular hardware for T cell signaling. *Nat. Immunol.* **1,** 23–29
34. Stinchcombe, J. C., Majorovits, E., Bossi, G., Fuller, S., and Griffiths, G. M. (2006) Centrosome polarization delivers secretory granules to the immunological synapse. *Nature* **443,** 462–465
35. Horn, J., Wang, X., Reichardt, P., Stradal, T. E., Warnecke, N., Simeoni, L., Gunzer, M., Yablonski, D., Schraven, B., and Kliche, S. (2009) Src homology 2-domain containing leukocyte-specific phosphoprotein of 76 kDa Is mandatory for TCR-mediated inside-out signaling, but dispensable for CXCR4-mediated LFA-1 activation, adhesion, and migration of T cells. *J. Immunol.* **183,** 5756–5767
36. Shamri, R., Grabovsky, V., Gauguet, J. M., Feigelson, S., Manevich, E., Kolanus, W., Robinson, M. K., Staunton, D. E., von Andrian, U. H., and Alon, R. (2005) Lymphocyte arrest requires instantaneous induction of an extended LFA-1 conformation mediated by endothelium-bound chemokines. *Nat. Immunol.* **6,** 497–506
37. Li, Y. C., Chen, B. M., Wu, P. C., Cheng, T. L., Kao, L. S., Tao, M. H., Lieber, A., and Roffler, S. R. (2010) Cutting Edge: mechanical forces acting on T cells immobilized via the TCR complex can trigger TCR signaling. *J. Immunol.* **184,** 5959–5963
38. Kim, S. T., Takeuchi, K., Sun, Z. Y., Touma, M., Castro, C. E., Fahmy, A., Lang, M. J., Wagner, G., and Reinherz, E. L. (2009) The alphabeta T cell receptor is an anisotropic mechanosensor. *J. Biol. Chem.* **284,** 31028–31037
39. Freiberg, B. A., Kupfer, H., Maslanik, W., Delli, J., Kappler, J., Zaller, D. M., and Kupfer, A. (2002) Staging and resetting T cell activation in SMACs. *Nat. Immunol.* **3,** 911–917
40. Saito, T., Yokosuka, T., and Hashimoto-Tane, A. (2010) Dynamic regulation of T-cell activation and co-stimulation through TCR-microclusters. *FEBS Lett.* **584,** 4865–4871
41. Hosseini, B. H., Louban, I., Djandji, D., Wabnitz, G. H., Deeg, J., Bulbuc, N., Samstag, Y., Gunzer,M., Spatz, J. P., and Hammerling, G. J. (2009) Immune synapse formation determines interaction forces between T cells and antigen-presenting cells measured by atomic force microscopy. *Proc. Natl. Acad. Sci. U.S.A.* **106,** 17852–17857
42. Schubert, W. (2007) A three-symbol code for organized proteomes based on cyclical imaging of protein locations. *Cytometry A.* **71,** 352–360
43. Schubert, W., Gieseler, A., Krusche, A., and Hillert, R. (2009) Toponome mapping in prostate cancer: detection of 2000 cell surface protein clusters in a single tissue section and cell type specific annotation by using a three symbol code. *J. Proteome. Res.* **8,** 2696–2707
44. Yokosuka, T., Sakata-Sogawa, K., Kobayashi, W., Hiroshima, M., Hashimoto-Tane, A., Tokunaga, M., Dustin, M. L., and Saito, T. (2005) Newly generated T cell receptor microclusters initiate and sustain T cell activation by recruitment of Zap70 and SLP-76. *Nat. Immunol.* **6,** 1253–1262
45. Biggs, M. J., Milone, M. C., Santos, L. C., Gondarenko, A., and Wind, S. J. (2011) High-resolution imaging of the immunological synapse and T-cell receptor microclustering through microfabricated substrates. *J. R. Soc. Interface*
46. Tybulewicz, V. L. (2005) Vav-family proteins in T-cell signalling. *Curr. Opin. Immunol.* **17,** 267–274
47. Saveliev, A., Vanes, L., Ksionda, O., Rapley, J., Smerdon, S. J., Rittinger, K., and Tybulewicz, V. L. (2009) Function of the nucleotide exchange activity of vav1 in T cell development and activation. *Sci. Signal* **2,** ra83
48. Pauker, M. H., Hassan, N., Noy, E., Reicher, B., and Barda-Saad, M. (2012) Studying the Dynamics of SLP-76, Nck, and Vav1 Multimolecular Complex Formation in Live Human Cells with Triple-Color FRET. *Sci. Signal* **5,** rs3
49. Sylvain, N. R., Nguyen, K., and Bunnell, S. C. (2011) Vav1-mediated scaffolding interactions stabilize SLP-76 microclusters and contribute to antigen-dependent T cell responses. *Sci. Signal* **4,** ra14
50. Huppa, J. B., Gleimer, M., Sumen, C., and Davis, M. M. (2003) Continuous T cell receptor signaling required for synapse maintenance and full

effector potential. *Nat. Immunol.* **4,** 749–755
51. Charvet, C., Canonigo, A. J., Billadeau, D. D., and Altman, A. (2005) Membrane localization and function of Vav3 in T cells depend on its association with the adapter SLP-76. *J. Biol. Chem.* **280,** 15289–15299
52. Kumar, A., Humphreys, T. D., Kremer, K. N., Bramati, P. S., Bradfield, L., Edgar, C. E., and Hedin, K. E. (2006) CXCR4 physically associates with the T cell receptor to signal in T cells. *Immunity* **25,** 213–224
53. Betzig, E., Patterson, G. H., Sougrat, R., Lindwasser, O. W., Olenych, S., Bonifacino, J. S., Davidson, M. W., Lippincott-Schwartz, J., and Hess, H. F. (2006) Imaging intracellular fluorescent proteins at nanometer resolution. *Science* **313,** 1642–1645
54. Baddeley, D. Crossman, D., Rossberger, S., Cheyne, J. E., Montgomery, J. M., Jayasinghe, I. D., Cremer, C., Cannell, M. B., and Soeller, C. (2011) 4D super-resolution microscopy with conventional fluorophores and single wavelength excitation in optically thick cells and tissues. *PLoS ONE* **6,** e20645
55. Tezel, A., Paliwal, S., Shen, Z., and Mitragotri, S. (2005) Low-frequency ultrasound as a transcutaneous immunization adjuvant. *Vaccine* **23,** 3800–3807
56. Marios-Frankiskos, S., Panagiota, M., Katerina, B., and Athanassakis, I. (2010) Serum-derived MHC class II molecules: potent regulators of the cellular and humoral immune response. *Immunobiology* **215,** 194–205
57. Razi-Wolf, Z., Freeman, G. J., Galvin, F., Benacerraf, B., Nadler, L., and Reiser, H. (1992) Expression and function of the murine B7 antigen, the major costimulatory molecule expressed by peritoneal exudate cells. *Proc. Natl. Acad. Sci. U.S.A.* **89,** 4210–4214
58. Herold, K. C., Vezys, V., Koons, A., Lenschow, D., Thompson, C., and Bluestone, J. A. (1997) CD28/B7 costimulation regulates autoimmune diabetes induced with multiple low doses of streptozotocin. *J. Immunol.* **158,** 984–991
59. Hathcock, K. S., Laszlo, G., Dickler, H. B., Bradshaw, J., Linsley, P., and Hodes, R. J. (1993) Identification of an alternative CTLA-4 ligand costimulatory for T cell activation. *Science* **262,** 905–907
60. Burns, A. R., and Doerschuk, C. M. (1994) Quantitation of L-selectin and CD18 expression on rabbit neutrophils during CD18-independent and CD18-dependent emigration in the lung. *J. Immunol.* **153,** 3177–3188
61. Takei, F. (1985) Inhibition of mixed lymphocyte response by a rat monoclonal antibody to a novel murine lymphocyte activation antigen (MALA-2). *J. Immunol.* **134,** 1403–1407
62. Allman, D. M., Ferguson, S. E., and Cancro, M. P. (1992) Peripheral B cell maturation. I. Immature peripheral B cells in adults are heat-stable antigenhi and exhibit unique signaling characteristics. *J. Immunol.* **149,** 2533–2540
63. Lang, H., Ebihara, Y., Schmiedt, R. A., Minamiguchi, H., Zhou, D., Smythe, N., Liu, L., Ogawa, M., and Schulte, B. A. (2006) Contribution of bone marrow hematopoietic stem cells to adult mouse inner ear: mesenchymal cells and fibrocytes. *J. Comp. Neurol.* **496,** 187–201
64. Lagasse, E., Connors, H., Al-Dhalimy, M., Reitsma, M., Dohse, M., Osborne, L., Wang, X., Finegold, M., Weissman, I. L., and Grompe, M. (2000) Purified hematopoietic stem cells can differentiate into hepatocytes in vivo. *Nat. Med.* **6,** 1229–1234
65. McNeill, L., Cassady, R. L., Sarkardei, S., Cooper, J. C., Morgan, G., and Alexander, D. R. (2004) CD45 isoforms in T cell signalling and development. *Immunol. Lett.* **92,** 125–134
66. Lessard, J. L. (1988) Two monoclonal antibodies to actin: one muscle selective and one generally reactive. *Cell Motil. Cytoskeleton* **10,** 349–362
67. Schmitz, S., Grainger, M., Howell, S., Calder, L. J., Gaeb, M., Pinder, J. C., Holder, A. A., and Veigel, C. (2005) Malaria parasite actin filaments are very short. *J. Mol. Biol.* **349,** 113–125
68. Lukas, J., Mazna, P., Valenta, T., Doubravska, L., Pospichalova, V., Vojtechova, M., Fafilek, B., Ivanek, R., Plachy, J., Novak, J., and Korinek, V. (2009) Dazap2 modulates transcription driven by the Wnt effector TCF-4. *Nucleic Acids Res.* **37,** 3007–3020
69. Kukharskyy, V., Sulimenko, V., Macurek, L., Sulimenko, T., Draberova, E., and Draber, P. (2004) Complexes of gamma-tubulin with nonreceptor protein tyrosine kinases Src and Fyn in differentiating P19 embryonal carcinoma cells. *Exp. Cell. Res.* **298,** 218–228
70. Bleul, C. C., Wu, L., Hoxie, J. A., Springer, T. A., and Mackay, C. R. (1997) The HIV coreceptors CXCR4 and CCR5 are differentially expressed and regulated on human T lymphocytes. *Proc. Natl. Acad. Sci. U.S.A.* **94,** 1925–1930
71. Forster, R., Kremmer, E., Schubel, A., Breitfeld, D., Kleinschmidt, A., Nerl, C., Bernhardt, G., and Lipp, M. (1998) Intracellular and surface expression of the HIV-1 coreceptor CXCR4/fusin on various leukocyte subsets: rapid internalization and recycling upon activation. *J. Immunol.* **160,** 1522–1531
72. Bosselut, R., Zhang, W., Ashe, J. M., Kopacz, J. L., Samelson, L. E., and Singer, A. (1999) Association of the adaptor molecule LAT with CD4 and CD8 coreceptors identifies a new coreceptor function in T cell receptor signal transduction. *J. Exp. Med.* **190,** 1517–1526
73. Zhang, M., Zhang, J., Rui, J., and Liu, X. (2010) p300-mediated acetylation stabilizes the Th-inducing POK factor. *J. Immunol.* **185,** 3960–3969
74. Miescher, G. C., Schreyer, M., and MacDonald, H. R. (1989) Production and characterization of a rat monoclonal antibody against the murine CD3 molecular complex. *Immunol. Lett.* **23,** 113–118
75. Fleige, H., Haas, J. D., Stahl, F. R., Willenzon, S., Prinz, I., and Forster, R. (2012) Induction of BALT in the absence of IL-17. *Nat. Immunol.* **13,** 1
76. Flores-Borja, F., Jury, E. C., Mauri, C., and Ehrenstein, M. R. (2008) Defects in CTLA-4 are associated with abnormal regulatory T cell function in rheumatoid arthritis. *Proc. Natl. Acad. Sci. U.S.A.* **105,** 19396–19401
77. Yudushkin, I. A., and Vale, R. D. (2010) Imaging T-cell receptor activation reveals accumulation of tyrosine-phosphorylated CD3zeta in the endosomal compartment. *Proc. Natl. Acad. Sci. U.S.A.* **107,** 22128–22133
78. Dopfer, E. P., Schopf, B., Louis-Dit-Sully, C., Dengler, E., Hohne, K., Klescova, A., Prouza, M., Suchanek, M., Reth, M., and Schamel, W. W. (2010) Analysis of novel phospho-ITAM specific antibodies in a S2 reconstitution system for TCR-CD3 signalling. *Immunol. Lett.* **130,** 43–50
79. Borroto, A., Arellano, I., Dopfer, E. P., Prouza, M., Suchanek, M., Fuentes, M., Orfao, A., Schamel, W. W., and Alarcon, B. (2013) Nck recruitment to the TCR required for ZAP70 activation during thymic development. *J. Immunol.* **190,** 1103–1112
80. Tani-ichi, S., Maruyama, K., Kondo, N., Nagafuku, M., Kabayama, K., Inokuchi, J., Shimada, Y., Ohno-Iwashita, Y., Yagita, H., Kawano, S., and Kosugi, A. (2005) Structure and function of lipid rafts in human activated T cells. *Int. Immunol.* **17,** 749–758
81. Tamura, T., Igarashi, O., Hino, A., Yamane, H., Aizawa, S., Kato, T., and Nariuchi, H. (2001) Impairment in the expression and activity of Fyn during differentiation of naive CD4+ T-cells into the Th2 subset. *J. Immunol.* **167,** 1962–1969
82. Abraham, N., Miceli, M. C., Parnes, J. R., and Veillette, A. (1991) Enhancement of T-cell responsiveness by the lymphocyte-specific tyrosine protein kinase p56lck. *Nature* **350,** 62–66
83. Lin, J., and Weiss, A. (2001) Identification of the minimal tyrosine residues required for linker for activation of T cell function. *J. Biol. Chem.* **276,** 29588–29595
84. Chen, P., Murphy-Ullrich, J. E., and Wells, A. (1996) A role for gelsolin in actuating epidermal growth factor receptor-mediated cell motility. *J. Cell Biol.* **134,** 689–698
85. Yu, H., Fukami, K., Itoh, T., and Takenawa, T. (1998) Phosphorylation of phospholipase Cgamma1 on tyrosine residue 783 by platelet-derived growth factor regulates reorganization of the cytoskeleton. *Exp. Cell Res.* **243,** 113–122
86. Levytskyy, R. M., Hirve, N., Guimond, D. M., Min, L., Andreotti, A. H., and Tsoukas, C. D. (2012) In Vivo Consequences of Disrupting SH3-Mediated Interactions of the Inducible T-Cell Kinase. *J. Signal. Transduct.* **2012,** 694386
87. Bonilla, F. A., Fujita, R. M., Pivniouk, V. I., Chan, A. C., and Geha, R. S. (2000) Adapter proteins SLP-76 and BLNK both are expressed by murine macrophages and are linked to signaling via Fcgamma receptors I and II/III. *Proc. Natl. Acad. Sci. U.S.A.* **97,** 1725–1730
88. Bubeck Wardenburg J., Fu, C., Jackman, J. K., Flotow, H., Wilkinson, S. E., Williams, D. H., Johnson, R., Kong, G., Chan, A. C., and Findell, P. R. (1996) Phosphorylation of SLP-76 by the ZAP-70 protein-tyrosine kinase is required for T-cell receptor function. *J. Biol. Chem.* **271,** 19641–19644
89. Adachi, K. and Davis, M. M. (2011) T-cell receptor ligation induces distinct signaling pathways in naive vs. antigen-experienced T cells. *Proc. Natl. Acad. Sci. U.S.A.* **108,** 1549–1554
90. Lasserre, R., Cuche, C., Blecher-Gonen, R., Libman, E., Biquand, E., Danckaert, A., Yablonski, D., Alcover, A., and Di Bartolo, V. (2011) Release of serine/threonine-phosphorylated adaptors from signaling microclusters down-regulates T cell activation. *J. Cell Biol.* **195,** 839–853

91. Di Bartolo, V, Mege, D., Germain, V., Pelosi, M., Dufour, E., Michel, F., Magistrelli, G., Isacchi, A., and Acuto, O. (1999) Tyrosine 319, a newly identified phosphorylation site of ZAP-70, plays a critical role in T cell antigen receptor signaling. *J. Biol. Chem.* **274,** 6285–6294
92. Iwashima, M., Irving, B. A., van Oers, N. S., Chan, A. C., and Weiss, A. (1994) Sequential interactions of the TCR with two distinct cytoplasmic tyrosine kinases. *Science* **263,** 1136–1139
93. Anand, S., Stedham, F., Gudgin, E., Campbell, P., Beer, P., Green, A. R., and Huntly, B. J. (2011) Increased basal intracellular signaling patterns do not correlate with JAK2 genotype in human myeloproliferative neoplasms. *Blood* **118,** 1610–1621
94. Boulton, T. G., and Cobb, M. H. (1991) Identification of multiple extracellular signal-regulated kinases (ERKs) with antipeptide antibodies. *Cell Regul.* **2,** 357–371
95. Krutzik, P. O., and Nolan, G. P. (2003) Intracellular phospho-protein staining techniques for flow cytometry: monitoring single cell signaling events. *Cytometry A.* **55,** 61–70
96. Brunet, A., and Pouyssegur, J. (1996) Identification of MAP kinase domains by redirecting stress signals into growth factor responses. *Science* **272,** 1652–1655
97. Srivastava, N., Brennan, J. S., Renzi, R. F., Wu, M., Branda, S. S., Singh, A. K., and Herr, A. E. (2009) Fully integrated microfluidic platform enabling automated phosphoprofiling of macrophage response. *Anal. Chem.* **81,** 3261–3269

Appendix 05

Reichardt P.*, Patzak I.*, Jones K., Etemire E., Gunzer M., Hogg N.
A role for LFA-1 in delaying T lymphocyte egress from lymph nodes
EMBO J. 2013;32(6):829-43.
*Joint First authors

IF: 9.8

The EMBO Journal (2013) 32, 829–843
www.embojournal.org

TRANSPARENT PROCESS

THE EMBO JOURNAL

A role for LFA-1 in delaying T-lymphocyte egress from lymph nodes

Peter Reichardt[1,4], Irene Patzak[2,4], Kristian Jones[2], Eloho Etemire[3], Matthias Gunzer[1,3,5] and Nancy Hogg[2,5,*]

[1]Institute of Molecular and Clinical Immunology, Otto von Guericke University Magdeburg, Magdeburg, Germany, [2]Leukocyte Adhesion Laboratory, Cancer Research UK London Research Institute, London, UK and [3]University Duisburg/Essen, Universitätsklinikum Essen, Institute of Experimental Immunology and Imaging, Hufelandstraße 55, Essen, Germany

Lymphocytes use the integrin leukocyte function-associated antigen-1 (LFA-1) to cross the vasculature into lymph nodes (LNs), but it has been uncertain whether their migration within LN is also LFA-1 dependent. We show that LFA-1 mediates prolonged LN residence as *LFA-1*$^{-/-}$ CD4 T cells have significantly decreased dwell times compared with *LFA-1*$^{+/+}$ T cells, a distinction lost in hosts lacking the major LFA-1 ligand ICAM-1. Intra-vital two-photon microscopy revealed that *LFA-1*$^{+/+}$ and *LFA-1*$^{-/-}$ T cells reacted differently when probing the ICAM-1-expressing lymphatic network. While *LFA-1*$^{+/+}$ T cells returned to the LN parenchyma with greater frequency, *LFA-1*$^{-/-}$ T cells egressed promptly. This difference in exit behaviour was a feature of egress through all assessed lymphatic exit sites. We show that use of LFA-1 as an adhesion receptor amplifies the number of T cells returning to the LN parenchyma that can lead to increased effectiveness of T-cell response to antigen. Thus, we identify a novel function for LFA-1 in guiding T cells at the critical point of LN egress when they either exit or return into the LN for further interactions.

The EMBO Journal (2013) **32,** 829–843. doi:10.1038/emboj.2013.33; Published online 26 February 2013
Subject Categories: signal transduction; immunology
Keywords: LFA-1; lymphatics; lymph node; migration; T cells

Introduction

The integrin leukocyte function-associated antigen-1 (LFA-1; αLβ2; CD11a/CD18) contributes to lymphocyte adhesion and migration in two major ways. It orchestrates adhesive interactions between T and B lymphocytes and their antigen-presenting cells (APC) thereby lowering the threshold for stimulation during immune responses (Grakoui *et al*, 1999; Carrasco *et al*, 2004). LFA-1 is also vital for the continual migration of lymphocytes across high endothelial venules (HEVs) into lymph nodes (LNs) and into other tissues during an infection (Hamann *et al*, 1988; Berlin-Rufenach *et al*, 1999). Entering an LN is a multistep process that includes signalling into lymphocytes by endothelial-tethered chemokines (von Andrian and Mempel, 2003; Bajenoff *et al*, 2007; Evans *et al*, 2009; Girard *et al*, 2012). This initiates the process of LFA-1 activation, firm binding of lymphocytes and their subsequent migration across the vasculature into the LN parenchyma. An unresolved question is whether LFA-1 exclusively mediates immigration into the LN or, in the absence of antigen, also has a role in leukocyte trafficking within the node itself. In favour of integrin-independent migration are studies with 'integrin nude' dendritic cells (DCs) that migrate normally *in vivo* (Lammermann *et al*, 2008). In contrast, *CD18*$^{-/-}$ T cells move in the T zone of the LN with 15% lower velocity than WT T cells (Woolf *et al*, 2007).

T lymphocytes continually leave the circulation and spend 6–12 h within an LN where they may encounter APC in keeping with their role in immune surveillance (Smith and Ford, 1983; Tomura *et al*, 2008). The LN is a lymphocyte-filled structure consisting of dense T and B cell-dominated areas, each with a network of potentially antigen-loaded conduits and presenting cells along which the lymphocytes migrate (Gretz *et al*, 2000; Sixt *et al*, 2005; Bajenoff *et al*, 2006). T cells exit the LN via the lymphatic vessel (LV) network composed of the subcapsular sinus that connects with the T zone adjacent cortical sinuses and the macrophage-rich medulla. Recent reports show that T cells can exit into the LVs from all these locations within the node (Grigorova *et al*, 2009; Sinha *et al*, 2009). Their departure from the LN depends on competition between the CCL19/CCL21 chemokine receptor CCR7 that delivers a retention signal and the sphingosine 1-phosphate receptor-1 (S1P1) that increases in expression over time that the T cells spend in the LN (Lo *et al*, 2005; Pham *et al*, 2008). Interaction of S1P1 with its ligand sphingosine 1-phosphate (S1P) on the lymphatic endothelium is considered to constitute a directional signal for T-cell egress (Grigorova *et al*, 2009). As a final step, the lymphocytes are transported by the lymphatic drainage into blood via the thoracic duct (Gowans, 1957).

We show by adoptive transfer and intra-vital two-photon microscopy that *LFA-1*$^{-/-}$ T cells pass through the LN more rapidly than *LFA-1*$^{+/+}$ T cells and that LFA-1 is not essential for T-cell egress. In contrast, LFA-1-expressing T cells are restrained on the lymphatic vasculature and re-visit the LN parenchyma with greater frequency rather than exiting immediately. This leads to a more effective priming of adoptively transferred T cells in WT LNs, compared with *ICAM-1*$^{-/-}$ LNs. Thus, we identify LFA-1 as a critical adhesion factor influencing the fate of T cells at the point of LN exiting.

*Corresponding author. Cancer Research UK London Research Institute, Leukocyte Adhesion Laboratory, 44 Lincoln's Inn Fields, London WC2A 3LY, UK. Tel.: +44 207 269 3255; Fax: +44 207 269 3417;
E-mail: nancy.hogg@cancer.org.uk
[4]Joint First Authors.
[5]Joint Senior Authors.

Received: 20 August 2012; accepted: 31 January 2013; published online: 26 February 2013

Results

Transit of LFA-1$^{-/-}$ and LFA-1$^{+/+}$ T lymphocytes through the inguinal LN

To assess whether the major subset of recirculating CD4 T cells use LFA-1 as they travel through a LN, we compared the intra-nodal behaviour of *LFA-1*$^{-/-}$ and *LFA-1*$^{+/+}$ T cells. The two CD4 T-cell populations expressed comparable proportions of CD44^{lo} and CD62L^{high} markers typical of recirculating naïve cells that have not been exposed to antigen (WT, 68.5 ± 3.66%; KO, 75.63 ± 3.02% (mean ± s.e.m.), $n = 6$ mice, $P = 0.163$), with the remainder representing a more mature CD44^{high} and CD62L$^{lo\text{-}int}$ CD4 T-cell phenotype (Supplementary Figure 1A). Thus, lack of LFA-1 did not affect T-cell maturation in terms of proportions of naïve and non-naïve CD4 T cells.

Following differential labelling using either fluorescent green CSFE or orange SNARF-1 dyes, we injected purified CD4 T cells in equivalent numbers into the tail vein of host WT mice as previously described (Berlin-Rufenach *et al*, 1999). The adoptively transferred CD4 T cells revealed a uniform phenotype of CD44^{lo} and CD62L^{int}, typical of intra-nodal naïve T cells (WT, 93.2 ± 0.92%; KO, 95.2 ± 0.95% (mean ± s.e.m.), $n = 4$ mice/group, $P = 0.335$) (Supplementary Figure 1B; Klinger *et al*, 2009). Pre-sorting CD4 and CD44^{lo} T cells yielded a similar result (data not shown).

At 6 h when both entry into and egress from the inguinal LN was occurring, the ratio of *LFA-1*$^{+/+}$ over *LFA-1*$^{-/-}$ CD4 T cells was ~7:1 (WT/KO, 6.8 ± 1.5) (mean ± s.d.) (Figure 1A; Smith and Ford, 1983; Tomura *et al*, 2008). To focus exclusively on the behaviour of T cells already in the LN, we blocked further entry at 6 h using a combination of MEL-14 and PS2/3 mAbs specific for L-selectin and α4 integrin, adhesion receptors that have critical roles in lymphocyte LN entry along with LFA-1. In control contemporaneous experiments, we showed that the mAb-blocking regime equivalently prevented entry of *LFA-1*$^{+/+}$ and *LFA-1*$^{-/-}$ T cells into the inguinal LN (WT block—98.9 ± 0.4%, KO block—99.4 ± 0.3% (mean ± s.e.m.), $n = 3$ mice per group) (Supplementary Figure 1C). Following this blockade, the WT/KO ratio was altered 4–6 h later to ~16:1 (10 h: WT/KO, 15.7 ± 5.0; 12 h: WT/KO, 17.5 ± 4.5) (mean ± s.d.) (Figure 1A). It was important to establish that the adoptively transferred *LFA-1*$^{+/+}$ and *LFA-1*$^{-/-}$ T cells were equally viable between 6 and 10 h (Annexin V staining, data not shown). Thus, the 2.3-fold increase in WT/KO ratio suggested that *LFA-1*$^{-/-}$ T cells passed through the LN at a faster rate than *LFA-1*$^{+/+}$ T cells.

To further confirm that it was absence of LFA-1 itself that was responsible for the altered LN trafficking, we decreased the advantage of *LFA-1*$^{+/+}$ over *LFA-1*$^{-/-}$ CD4 T cells by transferring both T-cell types into host mice deficient in the most widespread LFA-1 ligand, ICAM-1 (Figure 1B). In this situation, the initial ratio of *LFA-1*$^{+/+}$ to *LFA-1*$^{-/-}$ T cells was similar to the WT hosts as *LFA-1*$^{+/+}$ T cells can make use of a second LFA-1 ligand, ICAM-2, to cross the HEV (Boscacci *et al*, 2010). Following mAb blockade at 6 h of further T-cell LN entry into *ICAM-1*$^{-/-}$ host mice, the WT/KO ratio did not however significantly change at 10 h (6 h: WT/KO, 5.4 ± 1.2; 10 h: WT/KO, 3.5 ± 0.2 (mean ± s.d.)) unlike the situation in the WT host (Figure 1B). This provided more evidence that it was lack of LFA-1 and not some other developmental feature of *LFA-1*$^{-/-}$ T cells that was responsible for the accelerated journey of the T cells through the LN.

We next asked whether T-cell access to the different compartments of the LN was LFA-1 dependent and would provide an explanation for the more rapid LN journey of *LFA-1*$^{-/-}$ T cells. Adoptively transferred *LFA-1*$^{+/+}$ and *LFA-1*$^{-/-}$ CD4 T cells were both observed to be widespread in the T-cell parenchymal areas at 6 h after T-cell transfer, ranging from the peripheral areas bordering the B-cell follicles (inset 1) to the dense T-cell zone (inset 2) (Figure 1C). An average of 95.7 ± 16.6 *LFA-1*$^{+/+}$ and *LFA-1*$^{-/-}$ 16.7 ± 2.8 T cells was counted in LN sections of the T-cell zone (mean ± s.e.m. of individual LN tissue slices from 7 host mice) giving a ratio of 7/1, which is identical to the ratio obtained by flow cytometry of whole LNs.

Although lack of LFA-1 expression did not prevent T cells from accessing the T-cell zone, it might influence the characteristics of their migration. Investigating the motility of the two types of cells using intra-vital two-photon microscopy within the T zone, we found that *LFA-1*$^{+/+}$ T cells were 11% faster than *LFA-1*$^{-/-}$ T cells (WT, 12.30 ± 0.49 μm/min versus KO, 10.82 ± 0.44 μm/min (mean ± s.e.m), $P < 0.02$) (Figure 1D). There was no significant difference in their migration in *ICAM-1*$^{-/-}$ hosts (WT, 9.84 ± 0.55 μm/min versus KO, 8.62 ± 0.41 μm/min, $P = 0.08$) (Figure 1D). This further confirmed that the effect on migration was LFA-1 regulated by binding of LFA-1 to ICAM-1.

In summary, *LFA-1*$^{-/-}$ CD4 T cells had a shorter dwell time in the LN than *LFA-1*$^{+/+}$ T cells implying that the latter cells were being restrained through interaction via LFA-1. The fact that *LFA-1*$^{+/+}$ T cells had slightly increased speed compared with *LFA-1*$^{-/-}$ T cells in the T zone did not obviously account for their apparently longer time in the LN. Importantly, the difference in travel time was abolished when *LFA-1*$^{+/+}$ T cells were adoptively transferred into *ICAM-1*$^{-/-}$ hosts where they behaved like *LFA-1*$^{-/-}$ T cells.

Accumulation of LFA-1$^{+/+}$ T cells compared with LFA-1$^{-/-}$ T cells at LYVE-1-expressing LVs

A possible explanation for the difference between *LFA-1*$^{+/+}$ and *LFA-1*$^{-/-}$ T cells in the timing of LN residence might depend on a differential ability to leave the LN via the draining lymphatic vasculature. To directly test this possibility, we investigated T-cell associations with the LV by intra-vital two-photon imaging of the inguinal LN from its hilar side towards the follicular side up to a depth of ~150 μm. It was possible to compare areas of the T zone that were LV free as well as distinct LV-containing areas. Within the latter, we observed centrally located, T zone-adjacent LV areas (central, cLV) where the network of LV was tubular in shape and without any macrophage association and more peripherally located LV areas (peripheral, pLV) towards the medullary region, where the tubular LV became increasingly lined with macrophages (Miller *et al*, 2002; Matheu *et al*, 2011) (Figure 2A; Supplementary Figure S2A).

The overall density of adoptively transferred T cells in these two areas was similar (cLV, 26.8 ± 6.4 total T cells/field of view; pLV, 29.0 ± 12.9 total T cells/field of view). However, the important finding was that the ratio of *LFA-1*$^{+/+}$/*LFA-1*$^{-/-}$ T cells in both of the LV-dominated regions was enhanced by ~50% compared with the proper T zone (ratio in T zone set at 1:0 for comparison purposes) (Figure 2B). This greater

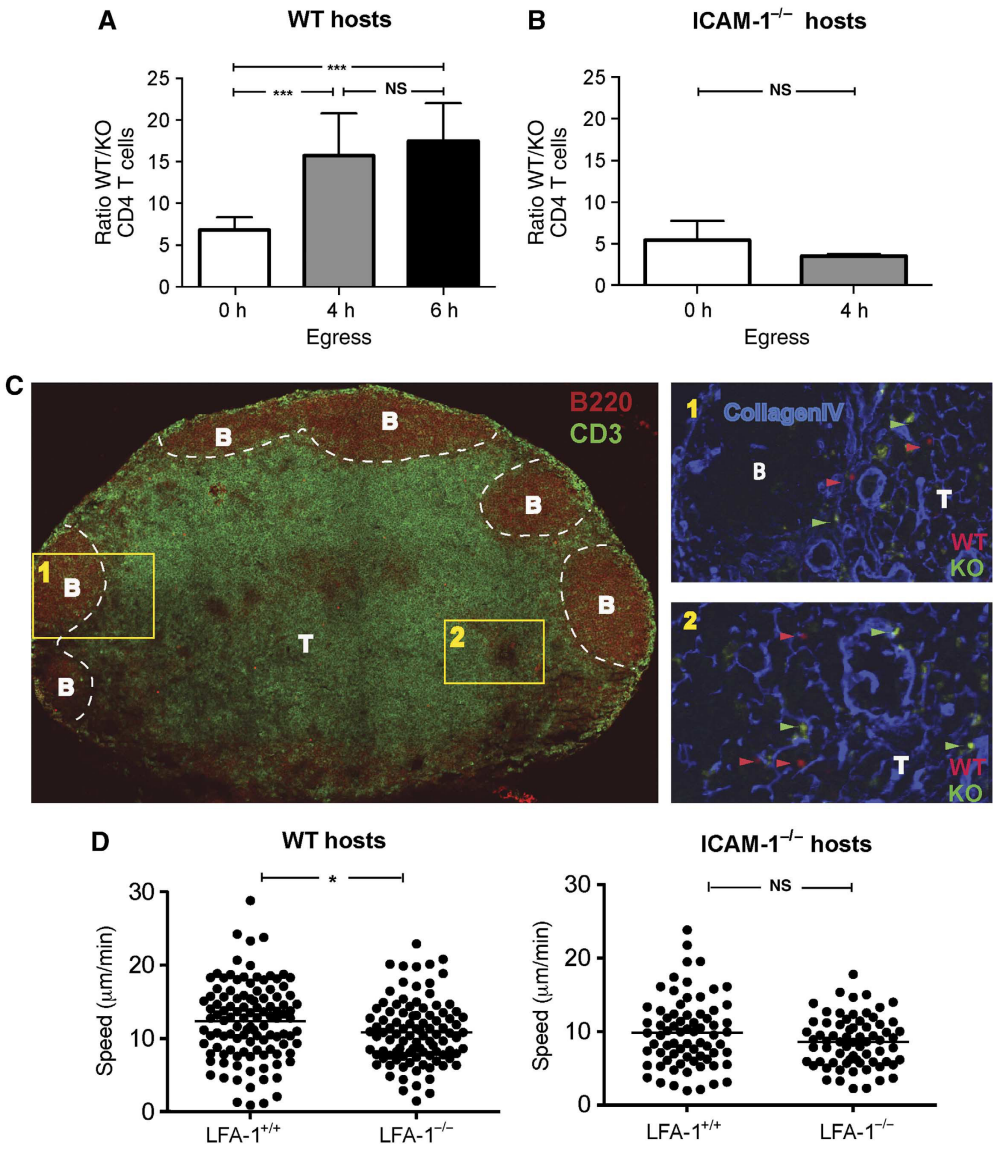

Figure 1 Comparison of non-stimulated *LFA-1*$^{+/+}$ and *LFA-1*$^{-/-}$ CD4 T-lymphocyte behaviour in the inguinal LN. (**A**) The numbers of CD4 T cells in host mice expressed as a ratio of *LFA-1*$^{+/+}$ (WT) to *LFA-1*$^{-/-}$ (KO) over time; CFSE and SNARF-1-labelled CD4 T cells (5×10^6 per cell type) were adoptively transferred into WT host mice and the T cells present in the LN at 6, 10 and 12 h were quantified; further entry was blocked from 6 h onwards with anti-L-selectin and α4 mAbs; each data point represents ⩾7 mice. (**B**) Experimental set-up as in (**A**), but with *ICAM-1*$^{-/-}$ mice used as adoptive transfer hosts. The ratio of WT/KO CD4 T cells at 6 and 10 h is shown; $n = 9$ mice per time point. (**C**) Tiled image showing immunostained CD3$^+$ T-cell area (green) and B220$^+$ B-cell follicles (red). Insets show the distribution at 6 h following transfer of *LFA-1*$^{+/+}$ T cells (WT, red), *LFA-1*$^{-/-}$ T cells (KO, green) and collagen IV (blue) at the T-/B-cell boundary (inset 1) and the deep T-cell zone (inset 2). The images are representative of six tissue slices from three mice. (**D**) Motility of *LFA-1*$^{-/-}$ and *LFA-1*$^{+/+}$ CD4 cells in T-cell zone in WT and *ICAM-1*$^{-/-}$ host mice in the T zone at 150 μm depth; velocity data from intra-vital two-photon imaging combined from three experiments with >100 cells analysed per host mouse strain.

LV-associated accumulation of *LFA-1*$^{+/+}$ T cells was lost when *ICAM-1*$^{-/-}$ mice were used as hosts further confirming a key role for LFA-1 in this skewed distribution (Figure 2C).

Collectively, the analysis of T-cell distribution within the LN revealed that *LFA-1*$^{+/+}$ T cells were more extensively represented than *LFA-1*$^{-/-}$ T cells in the regions where LV pre-dominated. As this effect was dependent on ICAM-1, LFA-1 appeared to affect the behaviour of T cells at the LV via ICAM-1 interactions.

Expression of ICAM-1 by LVs

An important issue was whether LYVE-1$^+$ LV directly expressed the most widespread LFA-1 interaction partner, ICAM-1, under non-inflammatory conditions. A broad pattern of ICAM-1 staining was observed on LN tissue sections with labelling of macrophages, DCs, fibroblastic cells, and endothelial cells as previously described (Katakai *et al*, 2004; Westermann *et al*, 2005; Woolf *et al*, 2007). We also observed significant ICAM-1$^+$ staining that colocalised with LYVE-1$^+$ LV in both the central (*inset 1*) and peripheral (*inset 2*) regions of the LN (Figure 3A). To quantify the coincidence in expression of LYVE-1 and ICAM-1 on the LVs, we randomly selected LV and performed pixel-by-pixel comparison of LYVE-1 and ICAM-1 staining (Figure 3B). The overlap in staining indicated substantial co-expression (central LV: 72.93 ± 1.75%; peripheral LV: 80.26 ± 3.0%; isotype control: 1.2 ± 0.4% (mean ± s.d.)).

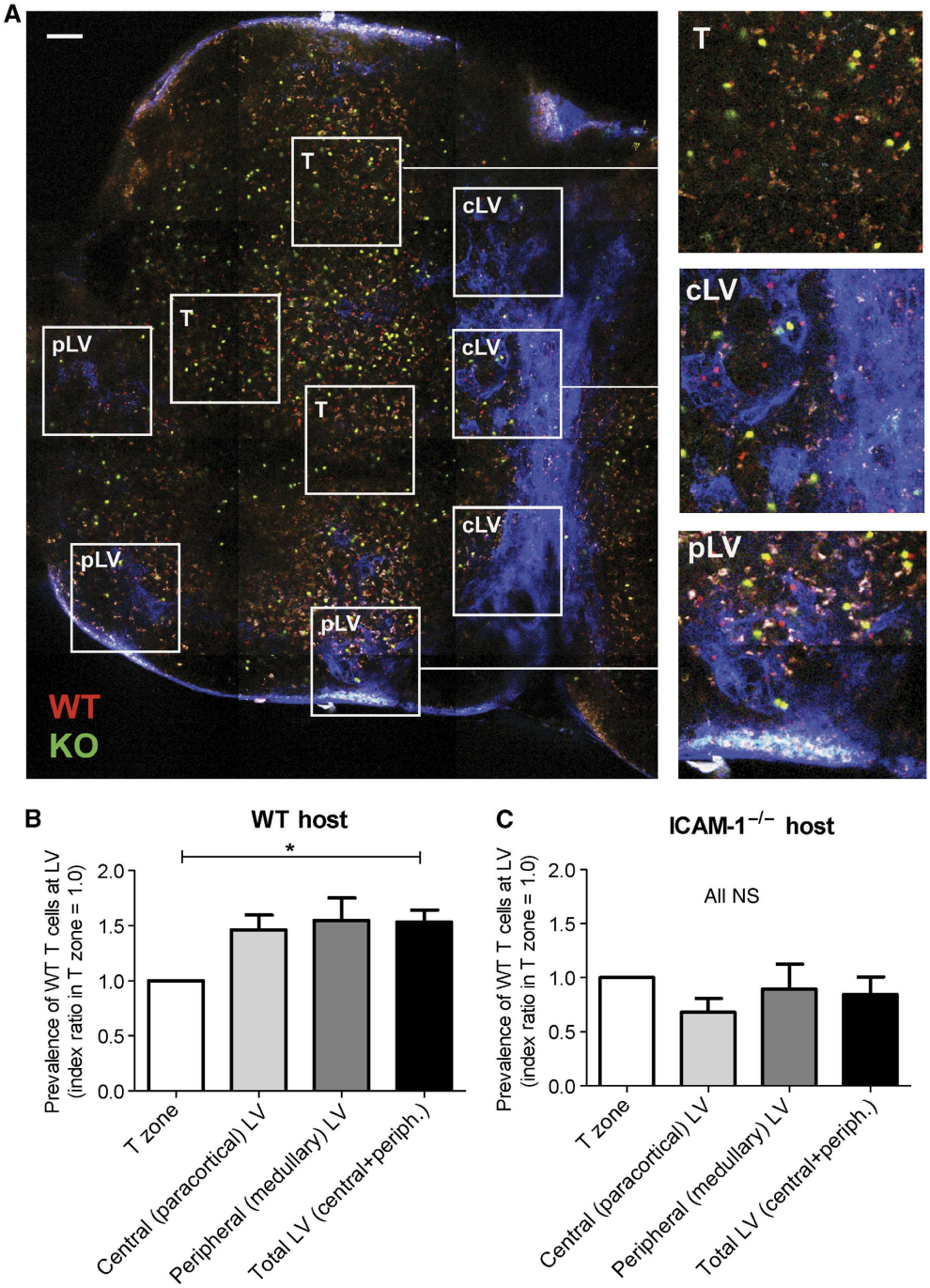

Figure 2 Distribution of *LFA-1*$^{+/+}$ and *LFA-1*$^{-/-}$ T cells in T zone and peripheral regions of the LN. (**A**) Tiled image of an explanted inguinal LN showing three distinct zones used for quantification of the *LFA-1*$^{+/+}$/*LFA-1*$^{-/-}$ T cell (WT/KO) ratio; scale bar = 100 μm. Insets for each zone as typically quantified for analysis are shown: the T-cell zone (T zone, >150 μm depth); central zone (cLV) at 80–150 μm depth showing LYVE-1^{+} lymphatic vessels (blue); peripheral medullary region (pLV) at 50–80 μm depth showing LYVE-1^{+} LV (blue) ± associated autofluorescent macrophages (white). (**B**) Increased prevalence of *LFA-1*$^{+/+}$ over *LFA-1*$^{-/-}$ T cells in the central and peripheral LV-associated regions over the T zone (set at an index ratio of 1.0) in WT host mice; data are averaged from four experiments with a total of >600 T cells analysed. (**C**) Lack of increased prevalence of *LFA-1*$^{+/+}$ over *LFA-1*$^{-/-}$ T cells in central and peripheral type LV-associated regions over T zone in host *ICAM-1*$^{-/-}$ mice; data are averaged from three experiments with >500 T cells analysed.

These findings established that the LV of unimmunised mice expresses the LFA-1 ligand ICAM-1 *in situ*, thus providing interaction opportunities for LFA-1-expressing T cells.

LFA-1$^{+/+}$ *and LFA-1*$^{-/-}$ *T cells differ in terms of ICAM-1-dependent migration to chemokine CCL21 and S1P*

As critical interplay between receptors CCR7 and S1P1 governs T-cell exit into the LV (Lo *et al*, 2005; Pham *et al*, 2008; Grigorova *et al*, 2009), a difference in migratory response to the key mediators CCL21 and S1P might explain the behaviour of *LFA-1*$^{-/-}$ compared with *LFA-1*$^{+/+}$ T cells. Western blotting indicated that their receptors S1P1 and CCR7 were equally expressed in terms of total receptor amounts by the two T cell types (Figure 4A) and CCR7 was detected equivalently at membrane level as determined by FACS analysis (WT, 4745 ± 2285 versus KO, 4482 ± 2264

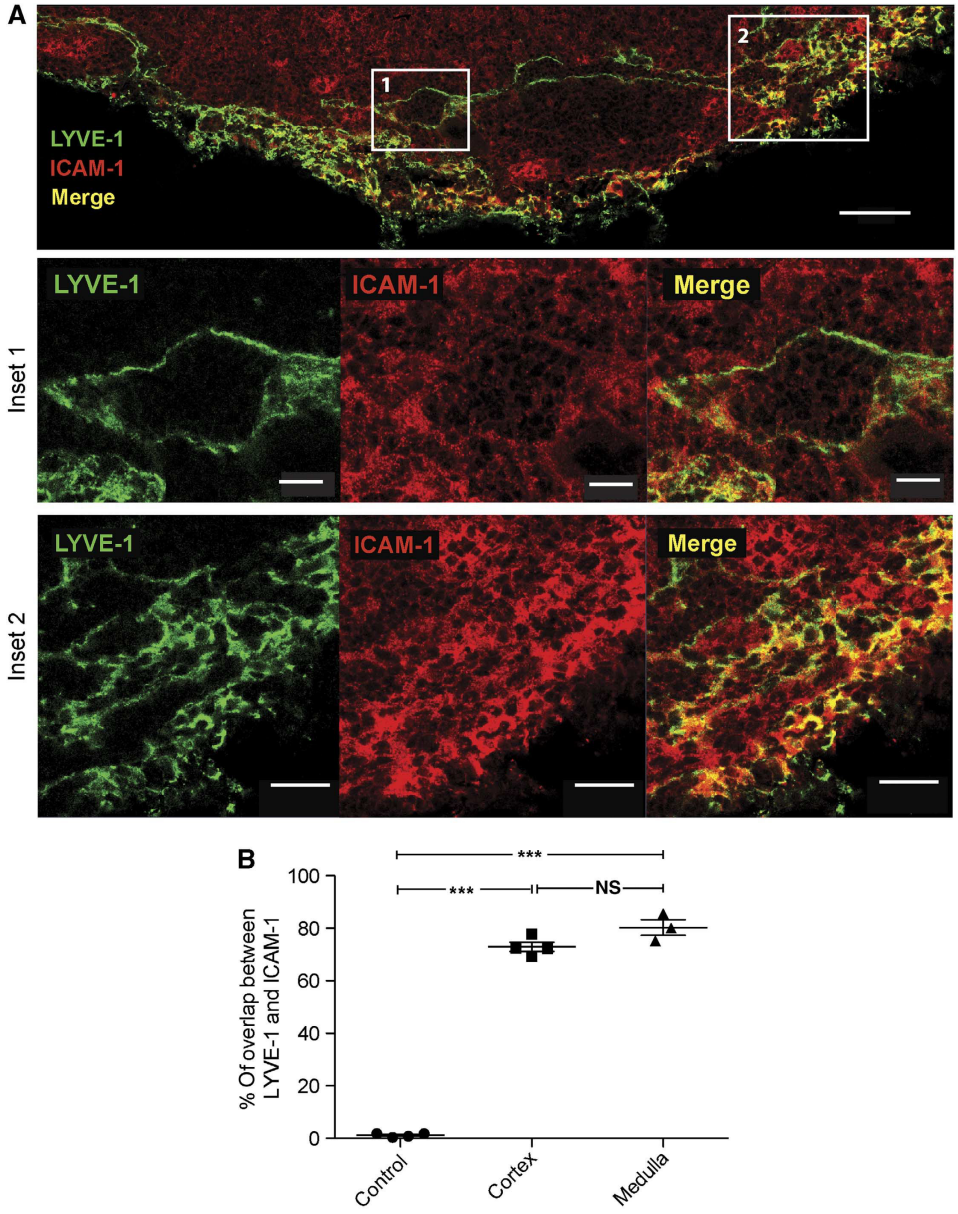

Figure 3 Co-expression of ICAM-1 and LYVE-1 on the lymphatic vasculature. (**A**) Immunohistochemical images of an unstimulated inguinal pLN tissue section comparing LYVE-1 (green) LV with ICAM-1 (red) and merged (yellow) staining; scale bar = 50 μm. Shown enlarged below: inset 1 indicates a T zone-associated LV and inset 2, a peripheral LV region; scale bars 10 and 20 μm, respectively. (**B**) Pixel-by-pixel determination of the overlap in staining between LYVE-1 and ICAM-1 on LV; data were generated from tissue sections of seven LNs. An isotype control mAb for ICAM-1 was also compared with LYVE-1 mAb and showed no staining or overlap; tissue sections from three LNs.

(mean fluorescence intensity ± s.d.)) (Figure 4B). We next tested the T cells for their ability to undergo migration to S1P and CCL21 using a transwell chemotaxis assay under ICAM-1-independent (Figure 4C) or ICAM-1-dependent conditions (Supplementary Figure 3). Under these circumstances, *LFA-1*$^{-/-}$ as well as *LFA-1*$^{+/+}$ T cells responded positively to the mediators and in a similar fashion whether or not ICAM-1 was present. Finally, we measured the response to S1P and CCL21 in a shear flow assay where engaging immobilised ICAM-1 and stimulants was necessary for adhesion and migration. Under these conditions only *LFA-1*$^{+/+}$ T cells, but not *LFA-1*$^{-/-}$ T cells, were able to attach and migrate to both S1P and CCL21 (Figure 4D).

Although these *in vitro* experiments showed *LFA-1*$^{-/-}$ and *LFA-1*$^{+/+}$ T cells to be migrating similarly in response to S1P, a question was whether the motility difference observed *in vivo* was dependent upon responsiveness toward S1P within the node. However, treatment of mice with FTY720, the general downregulator of S1P receptor that causes blockade of T-cell egress from the pLN, did not alter the velocity differential between *LFA-1*$^{+/+}$ and *LFA-1*$^{-/-}$ CD4 T-cell motility within the LN (Supplementary Figure 4).

These experiments showed that signalling through CCR7 and S1P1 on the CD4 T cells was not altered by LFA-1 deficiency. Additionally, both mediators had the ability to activate LFA-1 adhesion/migration under shear flow conditions. This differential adhesion to ICAM-1 could also be a factor determining T-cell behaviour *in vivo* and, when happening at ICAM-1-expressing LV, might be expected to influence their egress.

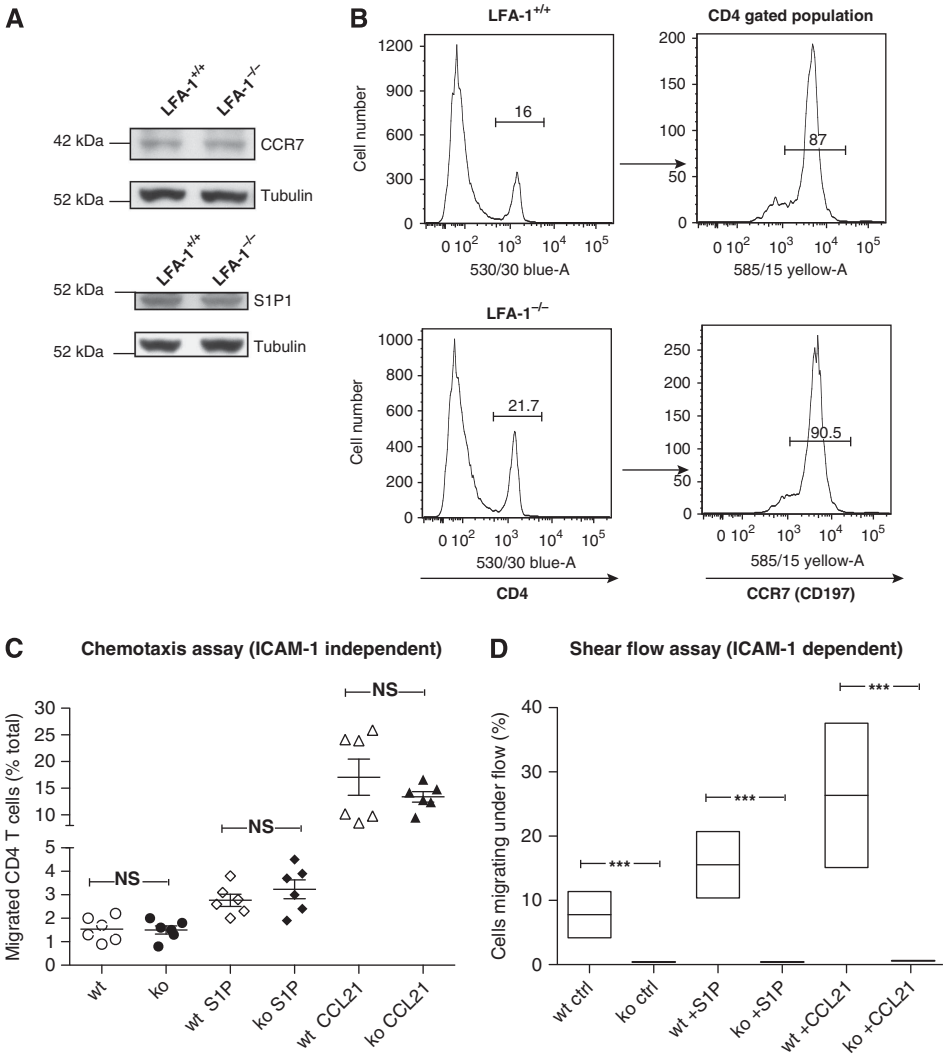

Figure 4 Responses of *LFA-1*$^{+/+}$ and *LFA-1*$^{-/-}$ CD4 T cells to S1P and CCL21. (**A**) Western blotting analysis of CCR7 and S1P1 (EDG-1) levels in CD4 T cells with α-tubulin serving as a sample loading control; data are typical for $n = 2$ experiments. (**B**) Flow cytometry analysis indicating the proportions of *LFA-1*$^{+/+}$ and *LFA-1*$^{-/-}$ CD4 lymphocytes in LN and splenocyte sample and the proportion of each that expressed CCR7; typical result of $n = 2$. (**C**) Transwell assay on uncoated filters showing the percentage of total input T cells that responded to 25 nM S1P and 6 μM CCL21 in the lower chamber; data averaged from $n = 6$ assays. (**D**) Shear flow assay showing proportion of total T cells in contact with ICAM-1 that adhered and migrated under flow conditions of 1 dyne cm^2 in response to S1P and CCR7 as above; $n = 90$–120 T cells were analysed per condition; $n = 3$ experiments.

LFA-1$^{+/+}$ *and LFA-1*$^{-/-}$ *T-cell associations with central LVs adjacent to the T zone*

We next studied the motile behaviour of T cells in regions with LYVE-1$^+$ LVs. In general, the T cells within the paracortical region were observed to migrate with higher motility than the T cells at the periphery of the T zone (Supplementary Video 1). The spread of high MW FITC dextran indicated that the flow of lymphatic fluid throughout the network was intact during the investigation (Supplementary Figure S2B; Gretz *et al*, 2000). This was further corroborated by observing persistent lymphatic flow during the whole imaging period as detected in an efferent vessel over 2 h (Supplementary Video 2).

The LVs in the paracortical area were characteristically tubular shaped and devoid of associated macrophages (Figure 5A). The velocity of the T cells associated with these LVs resembled their average speed in the T zone with *LFA-1*$^{+/+}$ T cells migrating faster than the *LFA-1*$^{-/-}$ T cells (WT, 12.47 ± 0.53 μm/min versus KO, 8.54 ± 0.55 μm/min) (Figure 5B). Towards the periphery of the T zone, the tubular LVs gradually became sparsely associated with auto-fluorescing macrophages (white) (Supplementary Figure 5). The speed of the more peripheral *LFA-1*$^{+/+}$ T cells also decreased to the extent that they now migrated more slowly than the *LFA-1*$^{-/-}$ T cells (WT, 4.45 ± 0.43 μm/min versus KO, 6.48 ± 0.41 μm/min).

In spite of these differences in speed between *LFA-1*$^{+/+}$ and *LFA-1*$^{-/-}$ T cells in the T zone regions, similar proportions contacted and probed the LV membranes (WT, 65.79 ± 5.22% versus KO, 65.23 ± 8.47% (mean ± s.e.m)) (Figure 5C). However, the outcome of this contact was substantially different when the two types of T cells were compared in that a higher proportion of *LFA-1*$^{-/-}$ than *LFA-1*$^{+/+}$ T cells crossed into the LV sinuses (WT,

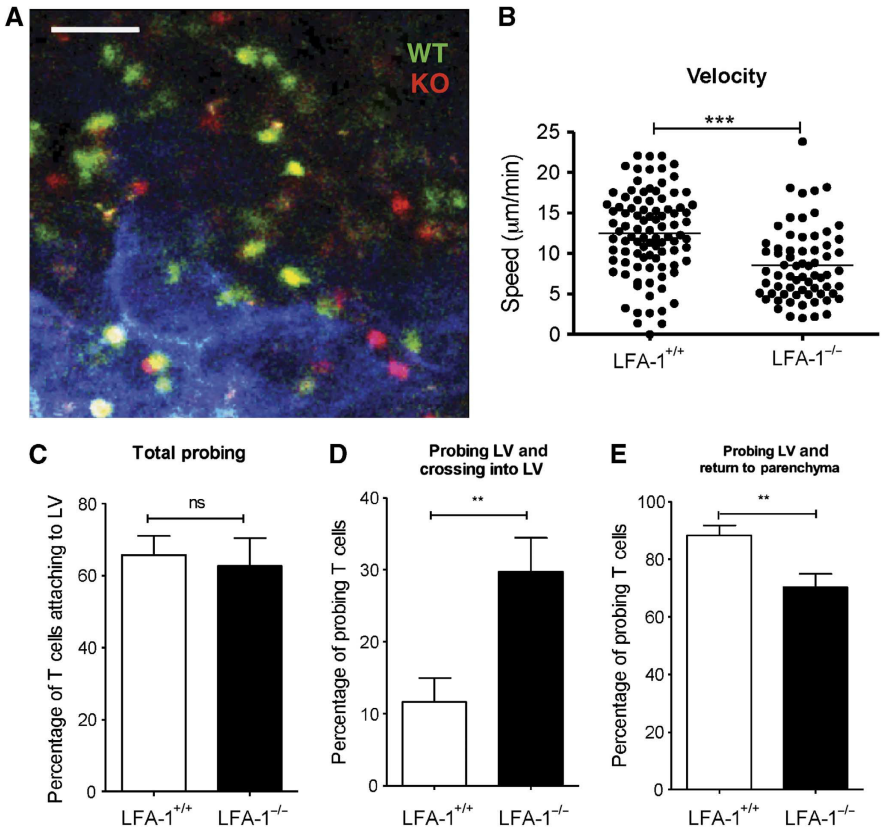

Figure 5 Association of *LFA-1*$^{+/+}$ and *LFA-1*$^{-/-}$ T cells with the lymphatic vessels in the central LV region. (**A**) Intra-vital microscope image of *LFA-1*$^{-/-}$ and *LFA-1*$^{+/+}$ CD4 cells interacting with cortical LV located at 80–150 μm depth from the hilar region where LV (LYVE-1^{+}, blue) appears tubular and macrophage free; scale bar = 50 μm. (**B**) Quantification data for T-cell velocity in areas with x–y axis length of 250 μm encompassing tubular cLV; a total of >150 cells were analysed (WT, 94 cells; KO, 67 cells) combined from 3 experiments. (**C**) Frequency of probing on outer LV walls by both T-cell types. (**D**) Proportion of T cells that crossed into the LV following probing of LV walls. (**E**) Proportion of T cells that returned to T-cell parenchyma following probing behaviour; (**C**–**E**) data combined from $n = 5$ experiments with >400 T cells analysed; T-cell probing and crossing in LV was recorded during an observation time of 30 min.

11.62 ± 3.34% versus KO, 29.73 ± 4.70% (mean ± s.e.m)) (Figure 5D; Supplementary Video 3). Correspondingly, higher numbers of *LFA-1*$^{+/+}$ than *LFA-1*$^{-/-}$ T cells returned to the T-cell parenchyma after making LV contact (WT, 88.37 ± 3.34% versus KO, 70.25 ± 4.71% (mean ± s.e.m)) (Figure 5E).

A question was whether the 2.3-fold decrease in LN dwell time of *LFA-1*$^{-/-}$ compared with *LFA-1*$^{+/+}$ T cells (Figure 1A) could be accounted for by the use of LFA-1 to reverse migrate back into the LN. To investigate this issue, the comparative proportion of *LFA-1*$^{+/+}$ or *LFA-1*$^{-/-}$ T cells leaving the LN at 6 h was determined by calculating the percentage of each T-cell type in contact with LV that subsequently exited over 30 min following adoptive transfer (WT—11.62 × 0.65 = 7.55%; KO—29.73 × 0.65 = 19.32%). Over this time period 2.6-fold more *LFA-1*$^{-/-}$ than *LFA-1*$^{+/+}$ T cells left the LN indicating that their distinctive behaviour at the point of LV contact could account for the effect of LFA-1 on T-cell LN dwell time. This is a rough estimate as it is unknown whether the rate of reverse migration versus exiting is the same at all time points and at all LV contacts within the LN.

In summary, *LFA-1*$^{-/-}$ T cells were able to cross into the LV and did so with almost three times the frequency of *LFA-1*$^{+/+}$ T cells which preferentially reverse migrated back to the node parenchyma following LV contact.

LFA-1$^{+/+}$ *and LFA-1*$^{-/-}$ *T-cell interactions with the distal LV network vessels in the medulla region of the LN*

The final option for exit from the LN is in the medulla although many fewer T cells exited in this region compared with the more centrally located LVs. Immunohistochemical staining showed the medullary LVs to have the appearance of an open meshwork of interconnecting LYVE-1^{+} sinuses (green) intimately associated with numerous MOMA-1^{+} (CD169, sialoadhesin) macrophages (blue) some of which also expressed LYVE-1 (Gordon *et al*, 2010; Figure 6A, *inset*). Both LVs and associated macrophages expressed ICAM-1 (Supplementary Figure 6).

Furthermore, because of the dominance of the meshwork-like LV network in this region it was easier to observe the shape of the T cells, but more difficult to identify individual LV and T-cell entry and exit events. T cells extensively probed the interconnected LV structures by crawling over and adhering to them. *LFA-1*$^{+/+}$ T cells migrated at an average lower velocity than the *LFA-1*$^{-/-}$ T cells (WT, 3.83 ± 0.37 μm/min versus KO, 5.93 ± 0.40 μm/min, $P < 0.001$ (mean ± s.e.m)) (Figure 6B and C; Supplementary Video 4). *LFA-1*$^{+/+}$ T cells frequently appeared elongated, whereas many of the *LFA-1*$^{-/-}$ T cells maintained a rounder morphology. Measurement of the cells' longest versus shortest dimensions indicated that 38.5% of *LFA-1*$^{+/+}$ T cells had axis ratios of

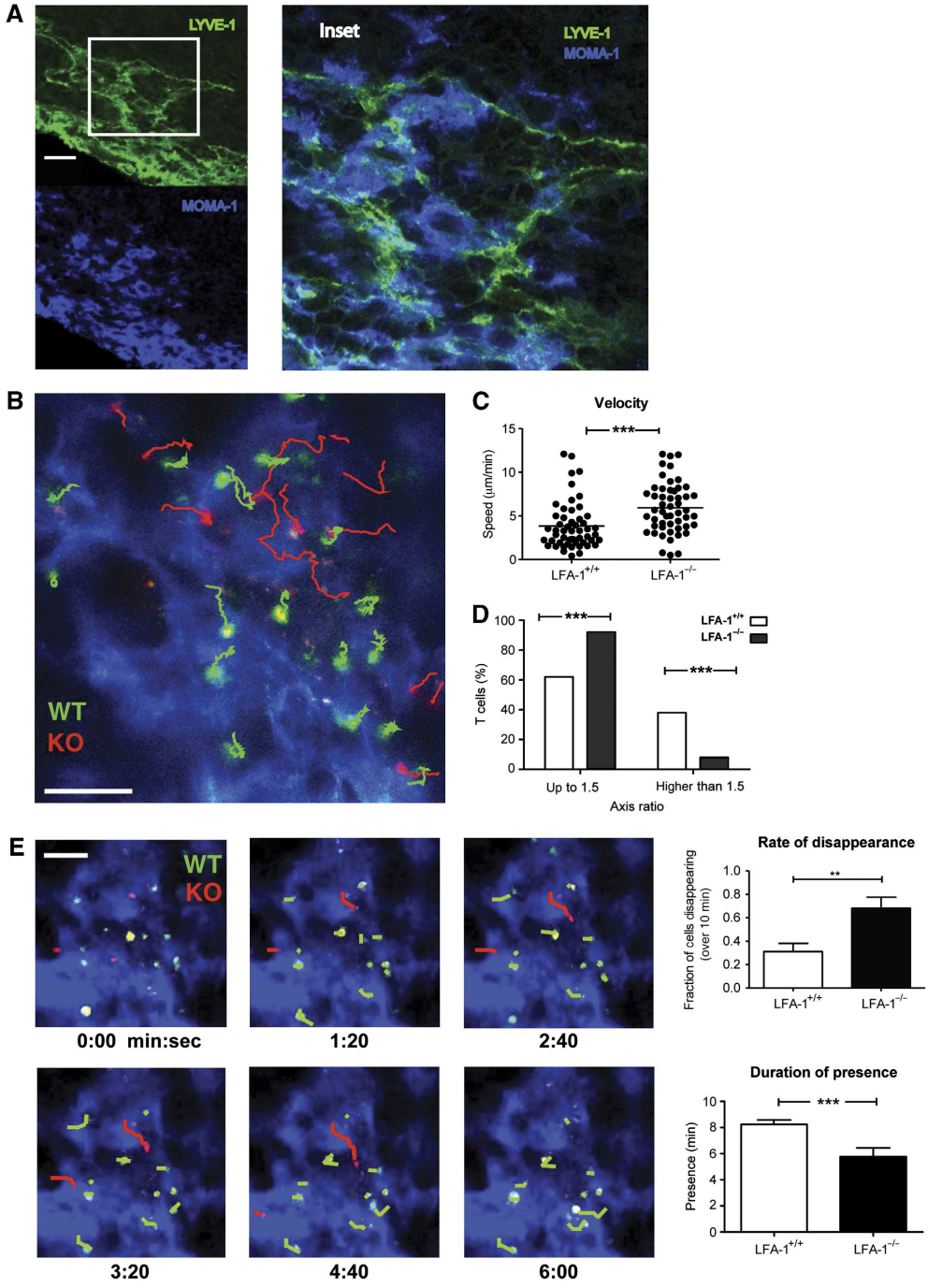

Figure 6 Association of *LFA-1*$^{+/+}$ and *LFA-1*$^{-/-}$ T cells with the LV network in the medulla. (**A**) LYVE-1^{+} LV and MOMA-1/CD169^{+} macrophages in the medulla area. Tissue section of inguinal LN was stained for LYVE-1 (green) and MOMA-1/CD169 (blue) and analysed by confocal microscopy, scale bar = 30 μm; inset shows detail of close association of LV and macrophages; image typical of sections from $n = 3$ LN. (**B**) Migratory behaviour of *LFA-1*$^{+/+}$ (WT, green tracks) and *LFA-1*$^{-/-}$ (KO, red tracks) CD4 T cells on the LYVE-1 network of vessels (blue) viewed from the hilar region at 50 μm depth, scale bar = 50 μm. (**C**) Quantification of velocity is shown for both *LFA-1*$^{+/+}$ and *LFA-1*$^{-/-}$ cells; data combined from two characteristic experiments each with >50 T cells analysed/group. (**D**) Axis ratio of *LFA-1*$^{+/+}$ and *LFA-1*$^{-/-}$ T-cell shape; quantification of the relative proportion of each cell type with a length/width ratio of <1.5 compared with proportion that were >1.5; data combined from three experiments with a total of >100 T cells/type analysed are shown. (**E**) T cells in contact with LYVE-1^{+} LV in the medulla (blue); kinetics of *LFA-1*$^{+/+}$ and *LFA-1*$^{-/-}$ T-cell migration across the LV of the medulla into the efferent lymphatic drainage; paths taken by the T cells over 6 min are indicated (WT: green; KO: red), scale bar = 50 μm; upper right panel: proportion of each T-cell type disappearing into lymphatic drainage and lower right panel: duration of presence or dwell time of each T-cell type during the observation period; data represent the mean ± s.e.m. of two characteristic experiments (45 WT and 25 KO T cells analysed) each observed over a 10-min period.

>1.5 compared with only 7.7% *LFA-1*$^{-/-}$ T cells (Figure 6D). This difference in morphology suggested that the elongated *LFA-1*$^{+/+}$ T cells, unlike the *LFA-1*$^{-/-}$ T cells, were attached and adhesive. Swapping the fluorescent dyes between *LFA-1*$^{+/+}$ and *LFA-1*$^{-/-}$ T cells yielded the same result (Supplementary Figure 7).

Supporting their adhesive appearance, *LFA-1*$^{+/+}$ T cells displayed a more sessile behaviour, while *LFA-1*$^{-/-}$ moved more rapidly over the LV network and disappeared faster from the imaging field. Over a 10-min period, 68% *LFA-1*$^{-/-}$ T cells left the tissue compared with 31% of the *LFA-1*$^{+/+}$ T cells which continued their probing interactions on the LV network (Figure 6E). Correspondingly, the *LFA-1*$^{-/-}$ T cells disappeared quickly with an average lymphatic contact time of 5.7 ± 0.67 min, whereas the *LFA-1*$^{+/+}$ T cells took 8.24 ± 0.33 min to cross the LVs (Figure 6E).

In summary in the medulla the *LFA-1*$^{+/+}$ T cells migrated more slowly than *LFA-1*$^{-/-}$ T cells which correlated with greater adhesive contact with the LV network of cells. In contrast, *LFA-1*$^{-/-}$ T cells were observed to be less adherent and more motile, with the consequence that they exited more rapidly than the *LFA-1*$^{+/+}$ T cells after they had engaged the LV membrane.

An assessment of directionality of T-cell migration at the lymphatic vasculature and its functional implications

As a further measure of the effect of LFA-1 on exiting behaviour, we measured the T-cell migratory angle in association with the LVs in the central paracortical region (Figure 7A). As the LVs were frequently branched and curvaceous, we defined a default exit angle for each individual imaging field according to its planar orientation to the LV and quantified the path length travelled by the T cell within a range of 90° around the specified exit angle. *LFA-1*$^{-/-}$ T cells followed a more direct trajectory compared with *LFA-1*$^{+/+}$ T cells (Figure 7B). This suggested that LFA-1 interactions were dictating the deviation from the most straightforward exit route. The difference disappeared in *ICAM-1*$^{-/-}$ hosts further confirming the role of LFA-1 in the migration pattern at the point of making the exit decision (Figure 7C).

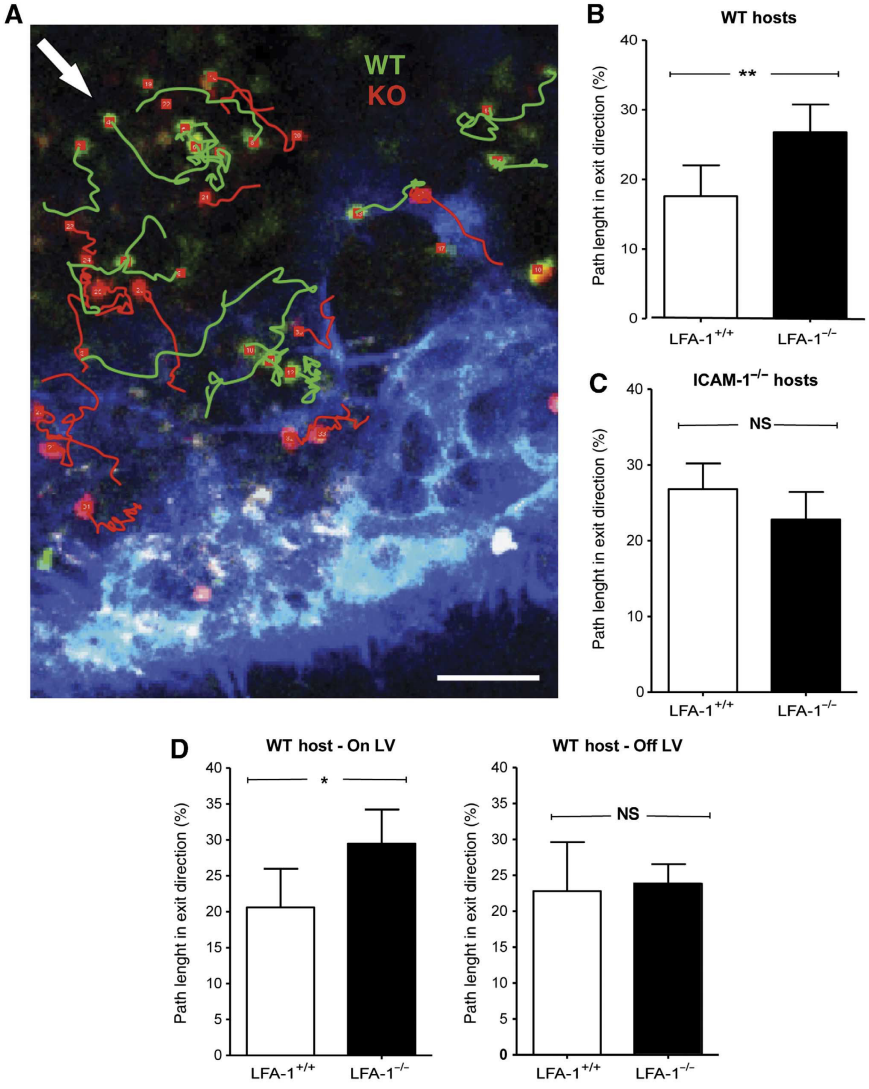

Figure 7 Measurement of directionality of T-cell migration at LV exit structures. (**A**) Migratory behaviour of *LFA-1*$^{+/+}$ and *LFA-1*$^{-/-}$ T cells showing their individual tracks adjacent to LYVE-1+ lymphatic vasculature (blue); exit angle as defined for this field of view indicated by arrow (white); scale bar = 50 μm. (**B**) Quantification of all cumulative path length and orientation data: proportion of *LFA-1*$^{+/+}$ and *LFA-1*$^{-/-}$ T cells in WT hosts migrating in exit direction (within a 90° angle around defined exit angle). (**C**) As (**B**) but in *ICAM-1*$^{-/-}$ hosts. (**D**) A comparison of T cells migrating directly on the LV versus T cells within this area without LV contact during the time of analysis. Data represent the mean of $n = 3$ experiments with >150 cells total analysed in each experimental group during an observation time of 30 min.

To test whether the direction of migration was influenced by the LV directly or alternatively by closely associated cells in the immediate microenvironment, we looked at directionality of T cells both on and off the LV. *LFA-1*$^{+/+}$ T cells displayed a more random directionality compared with *LFA-1*$^{-/-}$ T cells when in direct contact with LV, whereas their migratory behaviour did not differ when not in contact (Figure 7D). Thus, the more random migration of *LFA-1*$^{+/+}$ T cells at the point of LV exit is dictated by direct contact with LV.

A role for ICAM-1-expressing LV in increased immune responsiveness

It was important to clarify whether prolonged T-cell contact with ICAM-1-expressing LVs might be an epi-phenomenon without biological significance or would directly affect T-cell function. A reasonable hypothesis was that such contact aiding reverse migration back into the LN would allow T cells further opportunities to encounter any antigen-laden APC thus enhancing an immune response. To discriminate between the use of LFA-1/ICAM-1 for optimal antigen presentation and LV egress behaviour, we adoptively transferred equal numbers of WT DCs pre-incubated or not with ovalbumin peptide (pOVA) into the footpads of *ICAM-1*$^{-/-}$ and WT hosts as previously described (Mempel *et al*, 2004; Lammermann *et al*, 2008). CFSE-labelled OVA-TCR transgenic OT-2 CD4 T cells were injected i.v. 16 h later. Previous studies have shown overlapping roles for ICAM-1 and ICAM-2 in LN homing, suggesting that OT-2 T cells would not be significantly delayed in entry into the LN of *ICAM-1*$^{-/-}$ host mice (Lehmann *et al*, 2003; Boscacci *et al*, 2010) and we observed this to be the case (WT, 3315 ± 843 versus KO, 2270 ± 551 homing OT-2 T cells; $n = 3$ experiments). In this context, the OT-2 T cells should have an equivalent opportunity for stimulation in each host. When proliferation of the T cells isolated from ipsilateral LNs was assessed at 72 h, proliferation in the nodes of *ICAM-1*$^{-/-}$ hosts was significantly reduced compared with WT hosts (Figure 8A and B). There was also a trend for ongoing proliferation in the contralateral LN of the WT host, suggesting that stimulated T cells had already left the directly stimulated LN. These experiments indicate that LFA-1 contributes to an immune response not only via the well-described interaction between T cells and DCs but also at the level of the LVs.

Discussion

It is well established that T-cell migration across the high endothelial vasculature into LN relies on the integrin LFA-1 (Hamann *et al*, 1988; Berlin-Rufenach *et al*, 1999). In this study, we have asked whether LFA-1 plays any role within the LN during the trafficking of T cells that continually circulate between blood and the LNs. We found that *LFA-1*$^{-/-}$ CD4 T cells spend less time in the LN than *LFA-1*$^{+/+}$ lymphocytes yet show similar behaviour in *ICAM-1*$^{-/-}$ host mice. Intravital microscopy revealed that after probing the surface of LVs, *LFA-1*$^{+/+}$ T cells more frequently returned back into the LN, whereas *LFA-1*$^{-/-}$ T cells had a greater tendency to exit. Thus, T cells did not require LFA-1 to exit, but rather LFA-1-mediated adhesion to the LV contributed to reverse migration back into the LN parenchyma.

We first verified that the reduced dwell time of *LFA-1*$^{-/-}$ T cells in the LN was not accounted for by lack of niche access nor speed of migration within the T zone. In fact, *LFA-1*$^{-/-}$ T cells migrated somewhat more slowly than *LFA-1*$^{+/+}$ T cells, a deficit also observed in *CD18*$^{-/-}$ T cells (Woolf *et al*, 2007). This difference was lost in host mice lacking the LFA-1 ligand ICAM-1. Comparison of the migration in different areas of the LN revealed a gradual decrease in T cell speed from central T zone to the peripheral and medullary regions, that predominantly affected *LFA-1*$^{+/+}$ T cells. The slower speed in the medulla has previously also been noted by others (Wei *et al*, 2005; Sanna *et al*, 2006; Nombela-Arrieta *et al*, 2007; Grigorova *et al*, 2009, 2010).

The speed of T-cell migration may be influenced by locally regulated LFA-1 activation and deactivation brought about through contacts in the densely cellular LN microenvironment where ICAM-1 varies. A feature of DC migration, for example, is chemokine-induced adhesion to ICAM-1-expressing stromal cells (Schumann *et al*, 2010). However, the use of knock-in T cells expressing LFA-1 in a primed intermediate affinity conformation suggests that regulated LFA-1 activity is not involved in motility within the LN parenchyma (Park *et al*, 2010). It is currently difficult to reconcile these conflicting data.

However, the varying speeds of migration within the T zone do not provide an explanation for a faster exit rate of *LFA*$^{-/-}$ T cells from the LN. A clue to this different behaviour was the finding that *LFA-1*$^{+/+}$ CD4 T cells had increased presence over *LFA-1*$^{-/-}$ cells in regions of the LN where LVs were most concentrated. A key finding was that the *LFA-1*$^{+/+}$ T cells reverse migrated back into the LN more frequently than *LFA-1*$^{-/-}$ T cells after probing the LV walls. An observation was that the paths of the *LFA-1*$^{-/-}$ T cells on the LV were straighter than those of the *LFA-1*$^{+/+}$ T cells which displayed more random trajectories correlating with frequency of in migration back into the node parenchyma. As this LFA-1-mediated activity took place on the LV walls, it was relevant to demonstrate that the ligand ICAM-1 was expressed by the non-stimulated LV for which there has previously been both positive and negative evidence (Johnson *et al*, 2006; Link *et al*, 2007). In addition, the differences in the T-cell trajectories disappeared in *ICAM-1*$^{-/-}$ host mice.

The arrival of T cells at the point of egress occurs stochastically as a balance of responsiveness to retaining factors such as CCL21 and factors influencing egress such as S1P. Our study indicates that adhesion through LFA-1 is another factor determining egress potential. In *in vitro* chemotaxis assays, the state of LFA-1 expression had no impact on the response to CCL21 and S1P whether the assays were ICAM-1 dependent or independent. In seeming conflict is our data indicating that the LFA-1/ICAM-1 interaction dictates how T cells migrate on the LV. The requirement for shear flow conditions to activate LFA-1 on recirculating primary T cells has been reported by Woolf *et al* (2007) and we show that *LFA-1*$^{+/+}$ CD4 T cells, but not *LFA-1*$^{-/-}$ T cells, adhered and migrated under shear flow conditions on ICAM-1 in response to both immobilised S1P and CCL21. The LVs display fluid flow, but the parenchyma of the LN is considered to be shear free at least in terms of fluid. We show that T cells are adhering in an LFA-1-dependent way on the LV but not in the adjacent areas. One explanation is that the expression or organisation of ICAM-1 on LV surface activates LFA-1. Alternatively, T cells

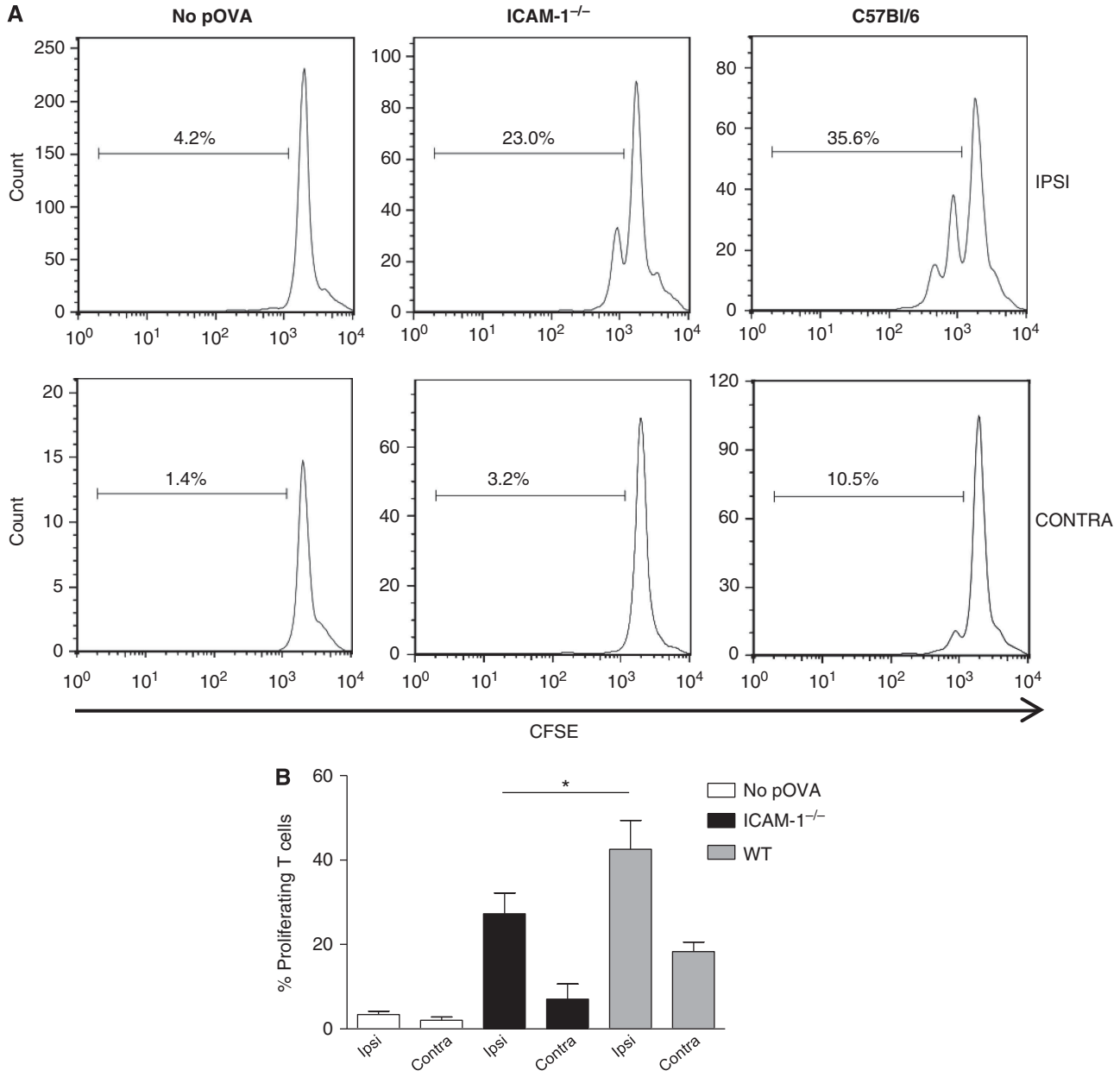

Figure 8 Response of OT-2 transgenic T cells in WT and ICAM-1 host mice. (**A**) The proportion of proliferating CFSE-labelled OT-2 T cells exposed to WT dendritic cells pre-incubated or not with pOVA in either WT or *ICAM-1*$^{-/-}$ host mice; dendritic cells were injected into hind foot pad and both ipsilateral (IPSI) and contralateral (CONTRA) lymph nodes were examined at 72 h following i.v. injection of OT-2 CD4 T cells; (**B**) combined data from $n = 3$ experiments showing the extent of proliferation in both ipsilateral and contralateral nodes as in (**A**).

interacting with HEV bear filipodia expressing LFA-1 that extend into the HEV from the leading edge (Shulman *et al*, 2009; Heasman *et al*, 2010). This might provide another possible means of LFA-1 activation if a similar process occurs when T cells interact with LVs.

These data are consistent with reports that the interaction of S1P1 with its ligand S1P causes integrin activation (Paik *et al*, 2001; Ledgerwood *et al*, 2008) and that *S1P1*$^{-/-}$ T cells are deficient in firm adhesion to LN HEVs under flow conditions, an LN entry step that is integrin mediated (Halin *et al*, 2005). In terms of distribution, S1P is LV associated as well as being present in lymph and therefore in position to influence LFA-1 activity on the T cells (Pham *et al*, 2008; Grigorova *et al*, 2009). Although the initial lymphatics express CCL21 (Tal *et al*, 2011), it is not yet established whether chemokines within the LN are LV tethered (Randolph *et al*, 2005). Thus, it is tempting to speculate that local concentration of LV-associated S1P might be responsible for stimulating the random migratory trajectory of *LFA-1*$^{+/+}$ T cells at the LV membrane via its LFA-1 activating function.

Our study provides evidence that LFA-1-mediated migration on the LV contributes to the balance of factors determining whether or not a T cell will leave the LN. A key issue is what T-cell functions might be influenced by this behaviour. Contact of DCs with LVs can suppress their activation, suggesting a role for lymphatic membranes in influencing the state of leukocyte activation (Podgrabinska *et al*, 2009).

However, revisiting of the T zone parenchyma gives T cells further opportunity to scan for antigen-loaded presenting cells and to subsequently become activated. This might be a particularly decisive mechanism for effective immune activation when the numbers of cognate APC in an LN or the amount of presented antigen on their surface are low. We provide evidence that such a mechanism does indeed function *in vivo*. Stimulation of OT-2 transgenic T cells by ovalbumin-laden ICAM-1-expressing DCs in a WT host was 30% more efficient compared with the same situation in an *ICAM-1*$^{-/-}$ host. Collectively, these data show that intranodal T-cell activation is not only dependent on the LFA-1-ICAM-1 axis during T-cell/APC interaction, but also during migration on and contact formation with LVs.

Our data add to previous reports that T cells engage in one or more rounds of shuttling between T zone parenchyma and the LV prior to finally exiting (Grigorova *et al*, 2009, 2010). LFA-1-mediated adhesion contributes to this reverse migration back into the node parenchyma. We propose that this behaviour increases the probability on a per T-cell basis of encountering APC-associated antigen. In contrast, according to the concept of immune surveillance, T cells enhance their opportunities of encountering foreign antigen by recirculating around the body and entering into and exiting from many LNs. However, this LFA-1-mediated shuttling of T cells may make an additional contribution to immune surveillance at the level of the individual LN.

In terms of LN entry across the HEV, LFA-1 supplies adhesive support for the T cells enabling them to withstand the force of blood flow and to migrate across the HEV into the node. Conversely, at the point of leaving the LN, LFA-1-mediated T cell contacts with LV membranes represent a critical contribution in shaping whether or not T cells exit. Thus, LFA-1 contributes to the functions that T cells perform both at the beginning and end of their LN journey.

Materials and methods

Mice

LFA-1$^{-/-}$ mice were bred on the C57BL/6JCrl to backcross generation 12 (Berlin-Rufenach *et al*, 1999). *ICAM-1*$^{-/-}$ mice (C57BL/6J) were obtained from Drs Britta Engelhardt and Urban Deutsch (Theodor Kocher Institute, Bern, Switzerland) with the permission of Dr Arthur Beaudet (Baylor College, Houston, TX, USA) (Bullard *et al*, 2007). Sex-matched 5- to 12-week-old mice were used in the experiments. Mice transgenic for 3A9 TCR specific for I-A^{k}/HEL$^{46\text{-}71}$ were on a B10.BR background (Jackson Laboratory, Bar Harbor, ME, USA) and bred at LRI (Ho *et al*, 1994). All animal experiments were approved by the Landesverwaltungsamt Sachsen-Anhalt (file number: 203.h-42502-2-874 Uni MD) and the United Kingdom Home Office.

Purification of CD4+ T lymphocytes

CD4 splenic and LN T cells were enriched by negative isolation via immunomagnetic depletion using a mouse CD4+ T cell Isolation kit (MACS Miltenyi Biotech) with purity of >95% as assessed by flow cytometry. In some experiments, naïve CD4 T cells were isolated by FACS through gating on the CD4 T cells and sorting the CD44^{lo} cell population.

Flow cytometry

Leukocytes (5×10^5) were incubated on ice in 50 μl of PBS/0.1% BSA containing the following directly conjugated mAbs at optimal dilution: CD4-APC or -FITC (RM4-5, eBioscience or BD Biosciences); CD44-FITC or -BrilliantViolet421 (IM7, PharMingen or Biolegend); CD62L-APC-eFluor780 (MEL-14, eBioscience); CD69-PE (eBioscience). In some experiments, intact LNs were cultured under appropriate conditions, then fluorochrome-labelled CD4 T cells were tested for state of apoptosis using biotinylated Annexin V (Invitrogen) detected with Streptavidin-Pacific Blue.

Immunoblotting

Cell lysates, prepared as previously described (Svensson *et al*, 2009), were separated using pre-cast 3–8% SDS–PAGE gels (Invitrogen) and transferred onto PVDF membrane (Immobilon-P, Millipore). Blots were probed with rabbit anti-S1P1 (EDG-1, H-60, Santa Cruz), rat CCR7 mAb (4B12, eBioscience) and mouse anti-α-tubulin mAb (Sigma Aldrich Ltd), followed by secondary Abs: goat anti-rabbit Ig-HRP, rabbit anti-rat Ig-HRP, and sheep anti-mouse Ig-HRP (all Dako Ltd) and ECL detection reagents (GE Healthcare).

Chemotaxis

Splenocytes were washed twice in 0.1% fatty acid-free BSA (Sigma Aldrich Ltd) and incubated for 1 h at 37°C prior to incubation at 1×10^6 cells/100 μl in 5 μm pore Transwell insert wells (Corning) that were either uncoated or coated overnight with mouse ICAM-1-Fc at 1 μg/ml. The lower wells contained either 600 μl RPMI-1640/0.1% fatty acid-free BSA, medium plus 25 nM S1P (Biomol/Enzo Life Sciences) or 6 μM CXCL21 (PeproTech EC Ltd) with dose level determined by titration. After incubation at 37°C for 2.5 h on uncoated filters or the shorter time of 1.5 h on ICAM-1-coated wells (to detect rapid migration), the chambers were rested on ice for 20 min, inserts discarded and the migrated cells recovered using ice-cold 5 mM EDTA/PBS. CD4 T cells were identified by flow cytometry and enumerated with the aid of counting beads (CountBright absolute counting beads, Invitrogen).

Shear flow assay

ibiTreat μ-slide VI flow chambers (Ibidi) were coated overnight with protein A (0.5 mg/ml, Sigma-Aldrich Ltd), then incubated with 2% fatty acid-free BSA for 30 min at RT followed by mouse ICAM-1Fc (1 μg/ml), S1P (1 μM), or CCL21 (6 μM). Purified CD4 T cells (5×10^5 cells/ml) were allowed to attach for 15 min at 37°C in 20 mM HEPES pH 7 in HBSS, then flow conditions of 1 dyn cm^2 were implemented using an automated syringe pump (KDS model 200; Linton Instrumentation) as previously reported (Evans *et al*, 2011). The adhesion/migration characteristics of T cells were recorded using a 20× lens on a Nikon Diaphot 300 microscope, a Sony XCD-X700 camera and AQM^{2001} Kinetic Acquisition Manager software (Kinetic Imaging Ltd, Bromborough, UK). Images were taken every 2 s for 3 min.

Immunofluorescence: in vitro and in vivo labelling

For immunohistology, snap-frozen inguinal LNs were cut in 10 μm sections, fixed in 4% paraformaldehyde, blocked in 1% BSA and 10% rabbit serum and stained for 1 h at RT with various mAbs and pAbs: FITC-CD3, PE-B220 (eBioscience); ICAM-1-Biotin (YN1/1.7.4, eBioscience). Biotinylated primary mAbs were detected using Streptavidin-AlexaFluor555 (Invitrogen). LYVE-1 (clone 223322, R&D Systems, Europe) was directly labelled with AlexaFluor488, AlexaFluor546 or Pacific Blue (Molecular Probes) and MOMA-1 (CD169, Bachem or Acris) was directly labelled with AlexaFluor680 or Pacific blue. Sections were assessed using LSM 510 and 710 confocal microscopes using 20×/0.8 Plan-Apochromat and 40×/1.3 Plan-NEOFLUAR DIC oil objectives and capturing images using, respectively, LSM 510 software and Software Zen 2009 (Zeiss).

Pixel-by-pixel determination of overlap between ICAM-1 and LYVE-1 staining was analysed using ImageJ software. Each fluorescence channel was treated separately by giving a value of 1.0 to each pixel to indicate positive staining and then the two values derived from ICAM-1 and LYVE-1 staining were multiplied. Staining of LYVE-1 was set at 100% to obtain percentages for co-staining with ICAM-1.

Adoptive transfer of T cells for homing and intra-vital studies

For adoptive transfer studies, CD4 T cells from *LFA-1*$^{-/-}$ and *LFA-1*$^{+/+}$ control C57BL/6JCrl mice at 5×10^6 cells/ml in 5% FCS/RPMI were labelled as described (Berlin-Rufenach *et al*, 1999). Briefly, T cells were incubated with either 0.5 μM CFSE or 5 μM SNARF-1 (all Molecular Probes) according to manufacturer's protocol at 37°C for 45 min. The differentially labelled T-cell preparations were mixed at 5×10^6 cells each to achieve a 1:1 ratio of *LFA-1*$^{+/+}$ and

LFA-1$^{-/-}$ cells for i.v. injection into recipient mice. For quantification of the entry ratio, a correction factor was applied to the subsequent data if the injected lymphocyte ratio was not 1:1.

To block further lymphocyte entry, 100 μg each of purified rat mAbs MEL 14 (L-selectin, CD62L) and PS2/3 (α4, CD47d) per mouse were injected i.v. at 6 h post T-cell transfer. To test the efficiency of this blockade while simultaneously mimicking the LN trafficking experiments, endotoxin-free L-selectin mAb MEL-14 and α4 integrin mAb PS2/3 or PBS as a control were injected 30 min prior to the fluorochrome-labelled T cells (5×10^6 per cell type), then LN T-cell numbers were assessed 4 h later (see text). PS2/3 was prepared by the CR UK Monoclonal Antibody Service; MEL-14 was a kind gift of Dr Alf Hamann, Charite Universitaetsmedizin Berlin, Germany and purchased from eBioscience.

For two-photon imaging, T cells were stained with 5 μm CFSE, 5 μM Cell Tracker Orange (CTO) or 5 μM Cell Tracker Blue (CTB) (all from Molecular Probes) according to manufacturer's protocols and as previously described (Reichardt *et al*, 2007b). Colours were routinely swapped between experiments. For *in vivo* labelling of LV, anti-mouse LYVE-1 labelled with Alexa 546 or Pacific Blue at 5–10 μg in 30 μl PBS was injected s.c. in the mouse flank 24 h before imaging. To visualise dynamics of lymph flow, FITC dextran (2 MDa, Sigma-Aldrich Ltd) was applied s.c. into the right footpad at 2 h and 30 min before imaging.

Two-photon microscopy

Fluorescently labelled, purified CD4 T cells (1:1 ratio, 5×10^6 per cell type) were injected i.v. into the tail vein of 5- to 6-week-old C57BL/6 mice at 6 h before imaging as previously described (Gunzer *et al*, 2004; Reichardt *et al*, 2007a, b). For some experiments, the KO:WT ratio was increased up to 5:1 cells to compensate for the deficiency of LN entry of *LFA-1*$^{-/-}$ T cells. The ratio or time of natural homing, without the use of blocking antibodies, in the time window chosen had no effect on viability or motility behaviour of the T cells imaged.

For intra-vital microscopy, anaesthesia of mice was initiated with i.p. application of 30 mg/kg ketamine (Inresa, Freiburg, Germany) plus 3 mg/kg xylazine (Bayer Health Care, Leverkusen, Germany) followed by intra-tracheal intubation and ventilation with oxygen-isoflurane (Deltaselect, Pfullingen, Germany). The inguinal LN was exposed by surgically removing surrounding tissue carefully sparing blood and lymph vessels. Quality of regional perfusion and oxygenation under anaesthesia was monitored oxymetrically (O2C, LEA, Giessen, Germany), and temperature maintained at 37°C. For *ex vivo* imaging of explanted LN, organs were kept in PBS and imaged immediately after being explanted. Single scan fields of typically 303×303 μm were imaged, which in some experiments were tiled to combine up to 3636×3636 μm combined fields.

Two-photon microscopy was performed using a ZeissLSM710 microscope (Carl Zeiss, Jena, Germany) equipped with a MaiTai DeepSee Femtosecond-Laser (Spectra-Physics, Darmstadt, Germany) typically tuned to 800 nm on an AxioExaminer upright stage with a 20×, NA 1.0 (Zeiss) water dipping lens. Image detection was done with three non-descanned (NDD) detectors typically equipped with emission detection filters of 565–610 nm (red), 500–500 (green), and ShortPass485 (blue). Individual RGB z-stacks of max 606×606 μm images were recorded in single plane or multiple z-planes as indicated, for time-lapse sequences typically every 4–20 s and lasting typically 15–30 min. Image rendering was performed using Volocity 4.3 (Improvision, Waltham, MA, USA). Cell tracking was done using the ImageJ Plugin ManualTracker and the computer-assisted manual tracking software CellTracker as described before (Reichardt *et al*, 2007b).

CellTracker software was also used for computing path length within exit angles. For each path of movement of individual cells as recorded by the software between two observation points, a directional xy angle was automatically assigned. This allowed quantification of the summary path lengths in each directional angle for each T-cell population. When comparing with the exit angle defined for the field of view based on its positioning in the LN, the percentage of path length in exit direction (exit angle ±90°) could be quantified and allowed a measure of the propensity to exit for this cell type. Data were plotted with Prism 4 (GraphPad Software, San Diego, CA, USA).

Adoptive transfer of dendritic and T cells for testing immune responsiveness

DCs were prepared as previously reported (Gunzer *et al*, 2000; Reichardt *et al*, 2007a). Briefly, bone marrow-derived cells (BMDCs) were differentiated in RPMI-based media with IL-4 and GM-CSF for 7 days and treated with 20 ng/ml LPS (*E. coli* 0111, B4; Sigma, Deisenhofen, Germany) on day 7. On day 8, OVA peptide (pOVA, AS 323-339 from chicken ovalbumin, Peptide Core facility, HZI, Braunschweig, Germany) was added at 20 ng/ml to the culture. After 4 h of co-incubation with pOVA, non-adherent DC was harvested, extensively washed to remove excess peptide and injected (0.5×10^6 in 20 μl PBS) into the right hind footpad of age-matched C57/BL6 WT or *ICAM-1*$^{-/-}$ hosts as in Mempel *et al* (2004) and Lammermann *et al* (2008). As a control, DC from the same culture (but not peptide loaded) was injected into the right hind footpad of WT hosts. After 16 h, CD4 T cells from OVA TCR-transgenic OT-2 mice (Barnden *et al*, 1998) were obtained by negative isolation. All OT-2 cells were stained with 10 μM CFSE as described (Reichardt *et al*, 2007a) and 5×10^6 cells were injected retro-orbitally into each host. Seventy-two hours later ipsilateral and contralateral popliteal nodes were prepared separately and the contained leukocytes were labelled with fluorochrome-conjugated antibodies against CD4 and analysed for proliferation by CFSE dilution using flow cytometry on a MCAS-Quant system (Miltenyi, Bergisch-Gladbach, Germany).

Statistical analysis

The statistical package within GraphPad Prism 4 was used for analysing data. Student's *t*-test or a non-parametric test (Mann–Whitney) or Fisher's Exact Test (for analysis of a contingency table) was applied to assess statistical significance. Significance levels employed are indicated in Results; **P*-value <0.05; ***P*-value <0.01; ****P*-value <0.001 were considered as significant.

Supplementary data

Supplementary data are available at *The EMBO Journal* Online (http://www.embojournal.org).

Acknowledgements

We are most grateful for the help of CRUK colleagues Emma Nye, Experimental Pathology for immunohistochemistry technology; Stuart Horswell, Bioinformatics and Biostatistics; Andy Filby, FACS Laboratory; Frederic Bollet-Quivogne, Light Microscopy; Katie Bentley, Vascular Biology for computational help; Neil Rogers and Caetano Reis e Sousa for transgenic mice. We also thank Alf Hamann, Berlin for generous supplies of mAb MEL-14. This work was supported by Cancer Research UK (NH and IP), C. J. Martin Fellowship (KJ) and by the German Research Foundation through grant SFB854 (PR and MG) and SPP1468 (to MG).

Author contributions: IP, PR, EE and KJ performed the experiments, compiled data and commented on the manuscript, MG supervised intra-vital technology, T cell proliferation experiments and helped with the manuscript, NH directed the project and wrote the manuscript.

Conflict of interest

The authors declare that they have no conflict of interest.

References

Bajenoff M, Egen JG, Koo LY, Laugier JP, Brau F, Glaichenhaus N, Germain RN (2006) Stromal cell networks regulate lymphocyte entry, migration, and territoriality in lymph nodes. *Immunity* **25:** 989–1001

Bajenoff M, Egen JG, Qi H, Huang AY, Castellino F, Germain RN (2007) Highways, byways and breadcrumbs: directing lymphocyte traffic in the lymph node. *Trends Immunol* **28:** 346–352

Barnden MJ, Allison J, Heath WR, Carbone FR (1998) Defective TCR expression in transgenic mice constructed using cDNA-based alpha- and beta-chain genes under the control of heterologous regulatory elements. *Immunol Cell Biol* **76:** 34–40

Berlin-Rufenach C, Otto F, Mathies M, Westermann J, Owen MJ, Hamann A, Hogg N (1999) Lymphocyte migration in lymphocyte function-associated antigen (LFA)-1-deficient mice. *J Exp Med* **189:** 1467–1478

Boscacci RT, Pfeiffer F, Gollmer K, Sevilla AI, Martin AM, Soriano SF, Natale D, Henrickson S, von Andrian UH, Fukui Y, Mellado M, Deutsch U, Engelhardt B, Stein JV (2010) Comprehensive analysis of lymph node stroma-expressed Ig superfamily members reveals redundant and nonredundant roles for ICAM-1, ICAM-2, and VCAM-1 in lymphocyte homing. *Blood* **116:** 915–925

Bullard DC, Hu X, Schoeb TR, Collins RG, Beaudet AL, Barnum SR (2007) Intercellular adhesion molecule-1 expression is required on multiple cell types for the development of experimental autoimmune encephalomyelitis. *J Immunol* **178:** 851–857

Carrasco YR, Fleire SJ, Cameron T, Dustin ML, Batista FD (2004) LFA-1/ICAM-1 interaction lowers the threshold of B cell activation by facilitating B cell adhesion and synapse formation. *Immunity* **20:** 589–599

Evans R, Lellouch AC, Svensson L, McDowall A, Hogg N (2011) The integrin LFA-1 signals through ZAP-70 to regulate expression of high affinity LFA-1 on T lymphocytes. *Blood* **117:** 3331–3342

Evans R, Patzak I, Svensson L, De Filippo K, Jones K, McDowall A, Hogg N (2009) Integrins in immunity. *J Cell Sci* **122:** 215–225

Girard JP, Moussion C, Forster R (2012) HEVs, lymphatics and homeostatic immune cell trafficking in lymph nodes. *Nat Rev Immunol* **12:** 762–773

Gordon EJ, Rao S, Pollard JW, Nutt SL, Lang RA, Harvey NL (2010) Macrophages define dermal lymphatic vessel calibre during development by regulating lymphatic endothelial cell proliferation. *Development* **137:** 3899–3910

Gowans JL (1957) The effect of the continuous re-infusion of lymph and lymphocytes on the output of lymphocytes from the thoracic duct of unanaesthetized rats. *Br J Exp Pathol* **38:** 67–78

Grakoui A, Bromley SK, Sumen C, Davis MM, Shaw AS, Allen PM, Dustin ML (1999) The immunological synapse: a molecular machine controlling T cell activation. *Science* **285:** 221–227

Gretz JE, Norbury CC, Anderson AO, Proudfoot AE, Shaw S (2000) Lymph-borne chemokines and other low molecular weight molecules reach high endothelial venules via specialized conduits while a functional barrier limits access to the lymphocyte microenvironments in lymph node cortex. *J Exp Med* **192:** 1425–1440

Grigorova IL, Panteleev M, Cyster JG (2010) Lymph node cortical sinus organization and relationship to lymphocyte egress dynamics and antigen exposure. *Proc Natl Acad Sci USA* **107:** 20447–20452

Grigorova IL, Schwab SR, Phan TG, Pham TH, Okada T, Cyster JG (2009) Cortical sinus probing, S1P1-dependent entry and flow-based capture of egressing T cells. *Nat Immunol* **10:** 58–65

Gunzer M, Schafer A, Borgmann S, Grabbe S, Zanker KS, Brocker EB, Kampgen E, Friedl P (2000) Antigen presentation in extracellular matrix: interactions of T cells with dendritic cells are dynamic, short lived, and sequential. *Immunity* **13:** 323–332

Gunzer M, Weishaupt C, Hillmer A, Basoglu Y, Friedl P, Dittmar KE, Kolanus W, Varga G, Grabbe S (2004) A spectrum of biophysical interaction modes between T cells and different antigen-presenting cells during priming in 3-D collagen and *in vivo*. *Blood* **104:** 2801–2809

Halin C, Scimone ML, Bonasio R, Gauguet JM, Mempel TR, Quackenbush E, Proia RL, Mandala S, von Andrian UH (2005) The S1P-analog FTY720 differentially modulates T-cell homing via HEV: T-cell-expressed S1P1 amplifies integrin activation in peripheral lymph nodes but not in Peyer patches. *Blood* **106:** 1314–1322

Hamann A, Jablonski-Westrich D, Duijvestijn A, Butcher EC, Baisch H, Harder R, Thiele HG (1988) Evidence for an accessory role of LFA-1 in lymphocyte-high endothelium interaction during homing. *J Immunol* **140:** 693–699

Heasman SJ, Carlin LM, Cox S, Ng T, Ridley AJ (2010) Coordinated RhoA signaling at the leading edge and uropod is required for T cell transendothelial migration. *J Cell Biol* **190:** 553–563

Ho WY, Cooke MP, Goodnow CC, Davis MM (1994) Resting and anergic B cells are defective in CD28-dependent costimulation of naive CD4+ T cells. *J Exp Med* **179:** 1539–1549

Johnson LA, Clasper S, Holt AP, Lalor PF, Baban D, Jackson DG (2006) An inflammation-induced mechanism for leukocyte transmigration across lymphatic vessel endothelium. *J Exp Med* **203:** 2763–2777

Katakai T, Hara T, Sugai M, Gonda H, Shimizu A (2004) Lymph node fibroblastic reticular cells construct the stromal reticulum via contact with lymphocytes. *J Exp Med* **200:** 783–795

Klinger A, Gebert A, Bieber K, Kalies K, Ager A, Bell EB, Westermann J (2009) Cyclical expression of L-selectin (CD62L) by recirculating T cells. *Int immunol* **21:** 443–455

Lammermann T, Bader BL, Monkley SJ, Worbs T, Wedlich-Soldner R, Hirsch K, Keller M, Forster R, Critchley DR, Fassler R, Sixt M (2008) Rapid leukocyte migration by integrin-independent flowing and squeezing. *Nature* **453:** 51–55

Ledgerwood LG, Lal G, Zhang N, Garin A, Esses SJ, Ginhoux F, Merad M, Peche H, Lira SA, Ding Y, Yang Y, He X, Schuchman EH, Allende ML, Ochando JC, Bromberg JS (2008) The sphingosine 1-phosphate receptor 1 causes tissue retention by inhibiting the entry of peripheral tissue T lymphocytes into afferent lymphatics. *Nat Immunol* **9:** 42–53

Lehmann JC, Jablonski-Westrich D, Haubold U, Gutierrez-Ramos JC, Springer T, Hamann A (2003) Overlapping and selective roles of endothelial intercellular adhesion molecule-1 (ICAM-1) and ICAM-2 in lymphocyte trafficking. *J Immunol* **171:** 2588–2593

Link A, Vogt TK, Favre S, Britschgi MR, Acha-Orbea H, Hinz B, Cyster JG, Luther SA (2007) Fibroblastic reticular cells in lymph nodes regulate the homeostasis of naive T cells. *Nat Immunol* **8:** 1255–1265

Lo CG, Xu Y, Proia RL, Cyster JG (2005) Cyclical modulation of sphingosine-1-phosphate receptor 1 surface expression during lymphocyte recirculation and relationship to lymphoid organ transit. *J Exp Med* **201:** 291–301

Matheu MP, Cahalan MD, Parker I (2011) Immunoimaging: studying immune system dynamics using two-photon microscopy. *Cold Spring Harb Protoc* **2011:** 147–155

Mempel TR, Henrickson SE, Von Andrian UH (2004) T-cell priming by dendritic cells in lymph nodes occurs in three distinct phases. *Nature* **427:** 154–159

Miller MJ, Wei SH, Parker I, Cahalan MD (2002) Two-photon imaging of lymphocyte motility and antigen response in intact lymph node. *Science* **296:** 1869–1873

Nombela-Arrieta C, Mempel TR, Soriano SF, Mazo I, Wymann MP, Hirsch E, Martinez AC, Fukui Y, von Andrian UH, Stein JV (2007) A central role for DOCK2 during interstitial lymphocyte motility and sphingosine-1-phosphate-mediated egress. *J Exp Med* **204:** 497–510

Paik JH, Chae S, Lee MJ, Thangada S, Hla T (2001) Sphingosine 1-phosphate-induced endothelial cell migration requires the expression of EDG-1 and EDG-3 receptors and Rho-dependent activation of alpha vbeta3- and beta1-containing integrins. *J Biol Chem* **276:** 11830–11837

Park EJ, Peixoto A, Imai Y, Goodarzi A, Cheng G, Carman CV, von Andrian UH, Shimaoka M (2010) Distinct roles for LFA-1 affinity regulation during T-cell adhesion, diapedesis, and interstitial migration in lymph nodes. *Blood* **115:** 1572–1581

Pham TH, Okada T, Matloubian M, Lo CG, Cyster JG (2008) S1P1 receptor signaling overrides retention mediated by G alpha i-coupled receptors to promote T cell egress. *Immunity* **28:** 122–133

Podgrabinska S, Kamalu O, Mayer L, Shimaoka M, Snoeck H, Randolph GJ, Skobe M (2009) Inflamed lymphatic endothelium suppresses dendritic cell maturation and function via Mac-1/ICAM-1-dependent mechanism. *J Immunol* **183:** 1767–1779

Randolph GJ, Angeli V, Swartz MA (2005) Dendritic-cell trafficking to lymph nodes through lymphatic vessels. *Nat Rev Immunol* **5:** 617–628

Reichardt P, Dornbach B, Rong S, Beissert S, Gueler F, Loser K, Gunzer M (2007a) Naive B cells generate regulatory T cells in the presence of a mature immunologic synapse. *Blood* **110:** 1519–1529

Reichardt P, Gunzer F, Gunzer M (2007b) Analyzing the physicodynamics of immune cells in a three-dimensional collagen matrix. *Methods Mol Biol* **380:** 253–269

Sanna MG, Wang SK, Gonzalez-Cabrera PJ, Don A, Marsolais D, Matheu MP, Wei SH, Parker I, Jo E, Cheng WC, Cahalan MD, Wong CH, Rosen H (2006) Enhancement of capillary leakage and restoration of lymphocyte egress by a chiral S1P1 antagonist *in vivo*. *Nat Chem Biol* **2:** 434–441

Schumann K, Lammermann T, Bruckner M, Legler DF, Polleux J, Spatz JP, Schuler G, Forster R, Lutz MB, Sorokin L, Sixt M (2010) Immobilized chemokine fields and soluble chemokine gradients cooperatively shape migration patterns of dendritic cells. *Immunity* **32:** 703–713

Shulman Z, Shinder V, Klein E, Grabovsky V, Yeger O, Geron E, Montresor A, Bolomini-Vittori M, Feigelson SW, Kirchhausen T, Laudanna C, Shakhar G, Alon R (2009) Lymphocyte crawling and transendothelial migration require chemokine triggering of high-affinity LFA-1 integrin. *Immunity* **30:** 384–396

Sinha RK, Park C, Hwang IY, Davis MD, Kehrl JH (2009) B lymphocytes exit lymph nodes through cortical lymphatic sinusoids by a mechanism independent of sphingosine-1-phosphate-mediated chemotaxis. *Immunity* **30:** 434–446

Sixt M, Kanazawa N, Selg M, Samson T, Roos G, Reinhardt DP, Pabst R, Lutz MB, Sorokin L (2005) The conduit system transports soluble antigens from the afferent lymph to resident dendritic cells in the T cell area of the lymph node. *Immunity* **22:** 19–29

Smith ME, Ford WL (1983) The recirculating lymphocyte pool of the rat: a systematic description of the migratory behaviour of recirculating lymphocytes. *Immunology* **49:** 83–94

Svensson L, Howarth K, McDowall A, Patzak I, Evans R, Ussar S, Moser M, Metin A, Fried M, Tomlinson I, Hogg N (2009) Leukocyte adhesion deficiency-III is caused by mutations in KINDLIN3 affecting integrin activation. *Nat Med* **15:** 306–312

Tal O, Lim HY, Gurevich I, Milo I, Shipony Z, Ng LG, Angeli V, Shakhar G (2011) DC mobilization from the skin requires docking to immobilized CCL21 on lymphatic endothelium and intralymphatic crawling. *J Exp Med* **208:** 2141–2153

Tomura M, Yoshida N, Tanaka J, Karasawa S, Miwa Y, Miyawaki A, Kanagawa O (2008) Monitoring cellular movement *in vivo* with photoconvertible fluorescence protein "Kaede" transgenic mice. *Proc Natl Acad Sci USA* **105:** 10871–10876

von Andrian UH, Mempel TR (2003) Homing and cellular traffic in lymph nodes. *Nat Rev Immunol* **3:** 867–878

Wei SH, Rosen H, Matheu MP, Sanna MG, Wang SK, Jo E, Wong CH, Parker I, Cahalan MD (2005) Sphingosine 1-phosphate type 1 receptor agonism inhibits transendothelial migration of medullary T cells to lymphatic sinuses. *Nat Immunol* **6:** 1228–1235

Westermann J, Bode U, Sahle A, Speck U, Karin N, Bell EB, Kalies K, Gebert A (2005) Naive, effector, and memory T lymphocytes efficiently scan dendritic cells *in vivo*: contact frequency in T cell zones of secondary lymphoid organs does not depend on LFA-1 expression and facilitates survival of effector T cells. *J Immunol* **174:** 2517–2524

Woolf E, Grigorova I, Sagiv A, Grabovsky V, Feigelson SW, Shulman Z, Hartmann T, Sixt M, Cyster JG, Alon R (2007) Lymph node chemokines promote sustained T lymphocyte motility without triggering stable integrin adhesiveness in the absence of shear forces. *Nat Immunol* **8:** 1076–1085

Appendix 06

Stirnweiss A, Hartig R, Gieseler S, Lindquist JA, **Reichardt P**, Philipsen L, Simeoni L, Poltorak M, Merten C, Zuschratter W, Prokazov Y, Paster W, Stockinger H, Harder T, Gunzer M, Schraven B. T cell activation results in conformational changes in the Src family kinase Lck to induce its activation.
Sci Signal. 2013; 6(263):ra13.

IF: 7.6

IMMUNOLOGY

T Cell Activation Results in Conformational Changes in the Src Family Kinase Lck to Induce Its Activation

Anja Stirnweiss,[1]* Roland Hartig,[1] Steffi Gieseler,[1]† Jonathan A. Lindquist,[1] Peter Reichardt,[1] Lars Philipsen,[1] Luca Simeoni,[1] Mateusz Poltorak,[1] Camilla Merten,[1] Werner Zuschratter,[2] Yury Prokazov,[2] Wolfgang Paster,[3]‡ Hannes Stockinger,[3] Thomas Harder,[1] Matthias Gunzer,[1]§ Burkhart Schraven[1,4]‖

The lymphocyte-specific Src family protein tyrosine kinase p56^{Lck} (Lck) is essential for T cell development and activation and, hence, for adaptive immune responses. The mechanism by which Lck activity is directed toward specific substrates in response to T cell receptor (TCR) activation remains elusive. We used fluorescence lifetime imaging microscopy to assess the activation-dependent spatiotemporal changes in the conformation of Lck in live human T cells. Kinetic analysis of the fluorescence lifetime of Lck biosensors enabled the direct visualization of the dynamic local opening of 20% of the total amount of Lck proteins after activation of T cells with antibody against CD3 or by superantigen-loaded antigen-presenting cells. Parallel biochemical analysis of TCR complexes revealed that the conformational changes in Lck correlated with the induction of Lck enzymatic activity. These data show the dynamic, local activation through conformational change of Lck at sites of TCR engagement.

INTRODUCTION

Src family tyrosine kinases (SFKs) trigger numerous cellular processes, including proliferation, differentiation, adhesion, and migration. The SFK family member p56^{Lck} (referred to as Lck) critically induces T cell responses after activation of cell surface receptors. Lck-deficient peripheral T cells cannot be activated through the T cell receptor (TCR). Consequently, T cell development is severely impaired in the absence of Lck (*1*). Phosphorylation of immunoreceptor tyrosine-based activation motifs (ITAMs) within the TCR-associated CD3 and ζ chains by Lck is one of the earliest detectable events after TCR stimulation, and it initiates multiple signaling cascades that culminate in T cell activation and proliferation (*2*); however, despite years of research, the molecular events preceding ITAM phosphorylation are poorly understood. Changes in the accessibility of ITAM-containing substrates and in the catalytic activity of Lck have been proposed to contribute to the initiation of signaling after TCR stimulation.

The activity of SFKs is tightly controlled by structural dynamics that are highly conserved between members and across species (*3*). Accordingly, the activity of Lck is controlled by conformational changes that arise from phosphorylation and dephosphorylation of two critical tyrosine residues, Tyr^{394} and Tyr^{505} (*4*). When phosphorylated by the C-terminal Src kinase (Csk), the C-terminal tyrosine residue Tyr^{505} inhibits Lck activity (*5*, *6*). Phosphorylation of the inhibitory tyrosine induces an intramolecular association with the Src homology 2 (SH2) domain, causing the kinase to adopt a closed, "inactive" conformation (*3*, *7*), which is stabilized by an additional interaction between the SH3 domain and a polyproline helix within the linker region (*7*, *8*). The plasma membrane–localized tyrosine phosphatase CD45 counteracts Csk by dephosphorylating Tyr^{505}, thereby generating a pool of Lck in an open, "primed" conformation (*9*, *10*). Ligand binding to the SH2 and SH3 domains of Lck may additionally contribute to its activation (*11*–*13*). Activation of Lck is thought to depend on the autophosphorylation of Tyr^{394} within the activation loop of the kinase domain (*14*). Only Lck molecules phosphorylated on Tyr^{394} show enhanced enzymatic activity and facilitate substrate phosphorylation (*15*, *16*).

Nika *et al*. demonstrated that in resting T lymphocytes, as well as in nonstimulated Jurkat cells (a human CD4$^+$ leukemic T cell line), a substantial amount of Lck exists in a constitutively active (Tyr^{394}-phosphorylated) form (*17*). The authors described four pools of Lck in resting T cells: (i) closed, inactive Lck (Tyr^{505}-phosphorylated); (ii) primed (nonphosphorylated); (iii) active Lck (Tyr^{394}-phosphorylated); and (iv) active, doubly phosphorylated (DPho) Lck (phosphorylated on both Tyr^{394} and Tyr^{505}). In Jurkat cells, each pool constitutes about 25% of the total amount of Lck, whereas in resting human T cells, about 50% of the total Lck protein is primed (*17*). Nika *et al*. did not observe changes in the enzymatic activity of Lck upon stimulation of the TCR. The authors concluded that the Lck-dependent tyrosine phosphorylation of ITAMs does not result from TCR-mediated de novo activation of Lck, but rather from other mechanisms, such as the relocalization of active Lck within the cell or from ligand-mediated conformational changes within the TCR (*18*, *19*).

[1]Institute of Molecular and Clinical Immunology, Otto von Guericke University, Leipziger Strasse 44, 39120 Magdeburg, Germany. [2]Leibniz Institute for Neurobiology, Brenneckestrasse 6, 39118 Magdeburg, Germany. [3]Molecular Immunology Unit, Institute for Hygiene and Applied Immunology, Center for Physiology, Pathophysiology, and Immunology, Medical University of Vienna, Lazarettgasse 19, A-1090 Vienna, Austria. [4]Department of Immune Control, Helmholtz Centre for Infection Research, 38124 Braunschweig, Germany.
*Present address: Division of Children's Leukaemia and Cancer Research, Telethon Institute for Child Health Research, 100 Roberts Road, Subiaco, WA 6008, Australia.
†Present address: Children's Hospital, Otto von Guericke University, Leipziger Strasse 44, 39120 Magdeburg, Germany.
‡Present address: T Cell Signalling Laboratory, Sir William Dunn School of Pathology, University of Oxford, South Parks Road, Oxford OX1 3RE, UK.
§Present address: Institute for Experimental Immunology and Imaging, University Hospital, University of Duisburg/Essen, Universitätsstraße 2, 45117 Essen, Germany.
‖To whom correspondence should be addressed. E-mail: Burkhart.Schraven@med.ovgu.de

To assess the potential role of the conformational dynamics of Lck in T cell activation, Paster *et al.* constructed a biosensor consisting of the complete Lck backbone flanked by enhanced cyan fluorescent protein (ECFP) and enhanced yellow fluorescent protein (EYFP) (*20*), which act respectively as donor and acceptor fluorophores for Förster resonance energy transfer (FRET). When the Lck biosensor molecule is in the active, open conformation, FRET is low, whereas a closed enzyme (inactive, Tyr^{505}-phosphorylated) produces a strong FRET signal. With this Lck biosensor, the authors measured FRET with intensity-based detection techniques and observed no substantial changes in the FRET efficiency of the biosensor upon TCR-mediated activation of Jurkat cells (*20*, *21*).

We investigated the conformational dynamics of Lck in response to TCR activation with an alternative technique to monitor FRET. FRET affects the mean lifetime for which the donor fluorophore molecules remain in the excited state before they relax back to the ground state and release a photon. Through the use of fluorescence lifetime imaging microscopy (FLIM) (*22*, *23*), we recorded, at microscopic resolution, donor fluorescence decay kinetics, which enabled the measurement of FRET independently of fluorophore concentrations. We used a new time domain FLIM strategy to follow the conformational dynamics of the Lck biosensor of Paster *et al.* The greatly improved signal-to-noise ratio obtained with our strategy enabled us to directly measure and visualize the conformational opening of Lck upon TCR activation in live T cells. Moreover, in vitro kinase assays revealed that the opening of Lck correlated with the enhanced enzymatic activity of the kinase.

RESULTS

A fluorescence-based Lck biosensor rescues signaling in Lck-deficient Jurkat cells

To identify changes in the conformational states of Lck in live cells, we used a unimolecular biosensor consisting of the complete Lck backbone flanked by ECFP and EYFP, which acted as donor and acceptor fluorophores, respectively (CLckY-1; Fig. 1A) (*20*). To assess the function of the biosensor, we expressed it in the Lck-deficient Jurkat cell line JCam1.6, which is unresponsive to TCR-mediated signals (*24*). Expression of CLckY-1 in JCam1.6 cells reconstituted global tyrosine phosphorylation (Fig. 1B) and Ca^{2+} flux in response to soluble stimulation with a monoclonal antibody against CD3 (αCD3) similar to that in Jurkat cells that express wild-type Lck (Fig. 1, C and D).

Spectral measurements reveal the FRET behavior of the CLckY-1 biosensor

To distinguish the true FRET events of the biosensor from other excited state reactions, we recorded intensity spectra with a time-resolved,

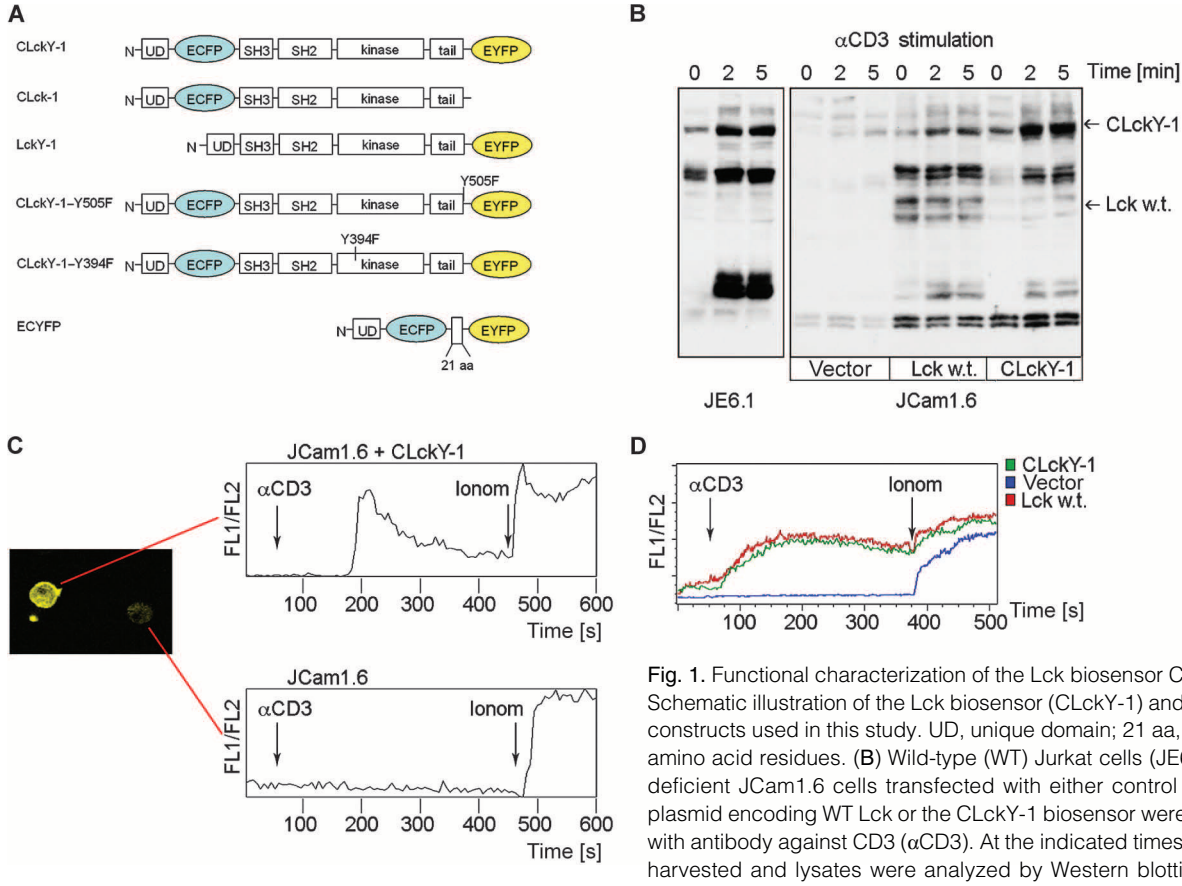

Fig. 1. Functional characterization of the Lck biosensor CLckY-1. (**A**) Schematic illustration of the Lck biosensor (CLckY-1) and the control constructs used in this study. UD, unique domain; 21 aa, linker of 21 amino acid residues. (**B**) Wild-type (WT) Jurkat cells (JE6.1) or Lck-deficient JCam1.6 cells transfected with either control plasmid or plasmid encoding WT Lck or the CLckY-1 biosensor were stimulated with antibody against CD3 (αCD3). At the indicated times, cells were harvested and lysates were analyzed by Western blotting for total tyrosine phosphorylation with the antibody 4G10. A typical result from one of three independent experiments is shown. (**C** and **D**) JCam1.6 cells transfected as described in (B) were loaded with the Ca^{2+}-sensitive dye Indo-1 AM. Ca^{2+} mobilization of cells after treatment with αCD3 or ionomycin (Ionom) was measured either (C) by confocal microscopic analysis of individual cells, which showed that only transfected cells responded to antibody stimulation, or (D) by bulk analysis by flow cytometry measured at a flow rate of 300 cells s^{-1}. Representative results out of three (for confocal analysis) or five (for flow cytometric analysis) independent experiments are shown.

microspectroscopic delay line (DL) detector. To generate a FRET-positive control, we transfected cells with a plasmid encoding a plasma membrane–anchored fusion protein in which the donor and acceptor fluorophores were separated by 21 amino acid residues (ECYFP; Fig. 1A). Because of the close proximity of the fluorophores, ECYFP reports on the maximal possible FRET signal. We also used a variant of CLckY-1 in which Tyr^{394} was mutated to phenylalanine (CLckY-1–Y394F; Fig. 1A). This Y394F mutation induces formation of the closed conformation of Lck (*20*); hence, the FRET of CLckY-1–Y394F reports on a fraction of the Lck biosensor that is in the constitutively closed conformation, which is expected to be greater than that of CLckY-1. As a FRET-negative control, we generated CLckY-1–Y505F, in which the C-terminal negative regulatory residue Tyr^{505} was mutated to phenylalanine (Fig. 1A). This mutation prevents the intramolecular interaction between the C terminus and the SH2 domain of Lck, thus generating a constitutively open conformation that exhibits a low FRET efficiency (*20*).

At an excitation wavelength of 420 nm, which excites the donor ECFP only, the intensity spectra of all constructs showed a first peak at 475 nm (Fig. 2A). This peak represents the characteristic emission spectrum of the donor (ECFP). A prominent second peak at 525 nm indicates the FRET-induced fluorescence of the acceptor (EYFP) and marks the FRET signal of the positive control (ECYFP). The peak at 525 nm was also observed in the biosensor molecules (Fig. 2A). As expected, the peak intensity was highest in the spectrum of the Lck Y394F biosensor, lower in the wild-type Lck biosensor (CLckY-1), and undetectable in cells with the FRET-negative control (CLckY-1–Y505F), consistent with the constitutively open conformation of this mutant Lck.

To differentiate between inter- and intramolecular FRET, we compared the fluorescence spectra of JCam1.6 cells expressing the CLckY-1 biosensor with those of cells expressing a version that contained only ECFP (donor-tagged Lck, CLck-1; Fig. 1A) and cells that coexpressed donor-only (CLck-1) and acceptor-only (LckY-1) tagged biosensors (Fig. 1A). A FRET-specific peak at 525 nm was not detectable in cells expressing CLck-1 alone or in those coexpressing CLck-1 and LckY-1 (Fig. 2B). Hence, the FRET signals measured in cells expressing Lck biosensor variants were caused by intramolecular energy transfer and correlated with the conformational states of the Lck biosensors.

FLIM discriminates between the individual kinetic components of ECFP fluorescence

For unknown molecular reasons, not all ECFP molecules mediate FRET (*25*). Thus, a subfraction of the ECFP molecules that undergo a change in FRET may escape detection against a background of fluorescence signal from molecules that do not undergo FRET. To tackle these inherent problems of the low signal-to-noise ratio in FRET measurements,

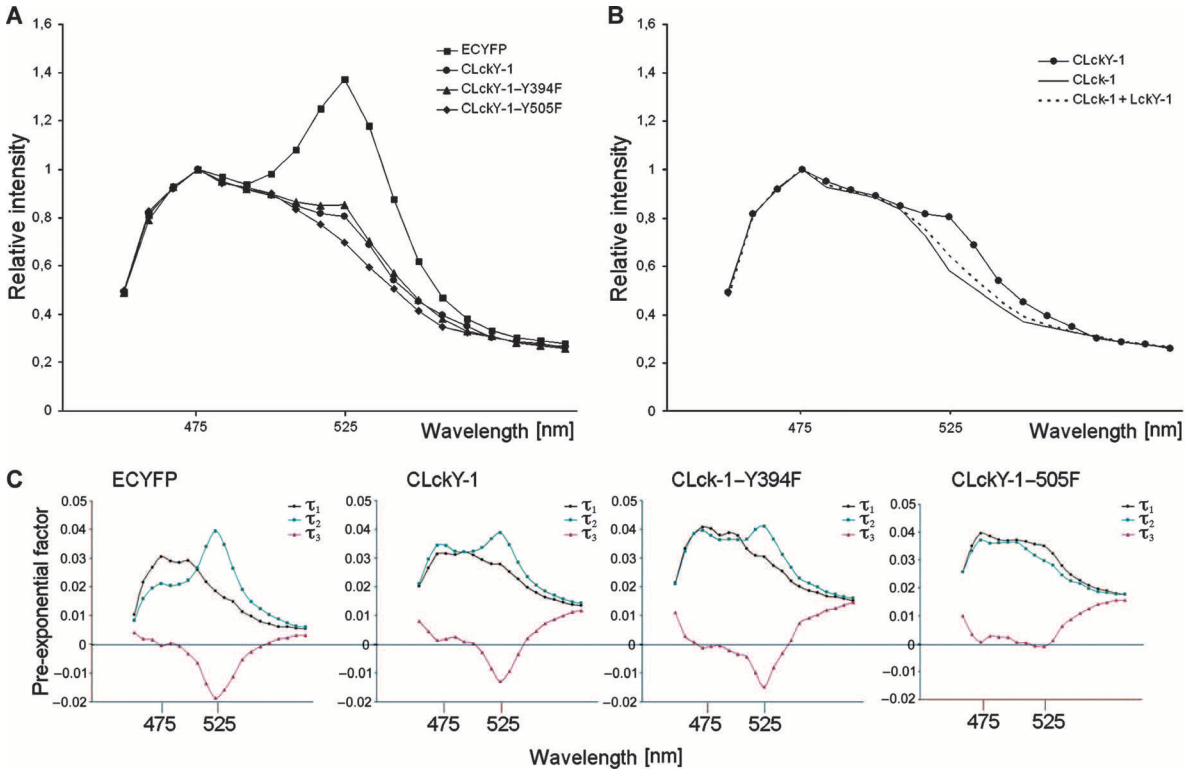

Fig. 2. Microspectroscopic characterization of CLckY-1 and different control constructs. (**A** and **B**) Spectral emissions along a wavelength range of 460 to 650 nm were resolved and collected by the DL detector after excitation at 420 nm. Represented are the relative fluorescence intensities against the emission wavelength of five independent measurements for JCam1.6 cells transfected with the appropriate plasmids encoding (A) ECYFP, CLckY-1, CLckY-1–Y394F, or CLckY-1–Y505F or (B) CLckY-1, CLck-1, or CLck-1 and LckY-1. (**C**) DAS spectra of the measurements shown in (A) and (B) of ECFP subpopulations that were identified by a three-exponential fit of the experimental data with individual characteristic lifetimes of τ_1 (3.2 ns), τ_2 (1.4 ns), and τ_3 (0.8 ns), respectively. Diagrammed are the changes in the pre-exponential factors of the three lifetimes as a function of the wavelengths for ECYFP, the Lck-biosensor CLckY-1, CLckY-1–Y394, and CLckY-1–Y505F. Negative pre-exponential factors result from FRET between the donor and acceptor.

we made use of detailed characterizations of the decay kinetics of ECFP fluorescence. Our work and that of others showed that in an ECFP-EYFP FRET pair, the mean decay of ECFP fluorescence, described by the mean lifetime τ_{mean}, can be fitted with three exponential decay components. These kinetic components are defined by three individual decay lifetimes: τ_1, τ_2, and τ_3, which characterize individual subpopulations of fluorophore pairs that can be individually selected for FRET measurements (*26–31*). We applied a Levenberg-Marquardt nonlinear, least-squares algorithm to dissect the decay kinetics of ECFP fluorescence in the Lck biosensor into individual lifetimes. A three-exponential fit resulted in a precise ($\chi^2 < 1.3$) description of the experimental data and revealed three individual τ values of ECFP within the biosensor of 3.2 ns (τ_1), 1.4 ns (τ_2), and 0.8 ns (τ_3), respectively. The fractional distributions of the individual lifetimes were calculated as 40% (τ_1), 35% (τ_2), and 25% (τ_3).

Analysis of decay-associated spectra identifies the ECFP subpopulation of the Lck biosensor involved in FRET

Plotting the pre-exponential factors of the individual lifetimes against the emission wavelength yielded the decay-associated spectra (DAS) (Fig. 2C), which were used to identify those ECFP molecules engaged in FRET. When the component undergoes FRET, the pre-exponential factor of an individual lifetime acquires a more negative value relative to the baseline at the emission wavelength of the acceptor. At the acceptor emission maximum of 525 nm, only τ_3 acquired negative values in Jurkat cells expressing ECYFP, CLckY-1, or CLckY-1–Y394F (Fig. 2C). Comparing the FRET signals of these constructs led to the following arrangement of FRET signals: ECYFP > CLckY-1–Y394F > CLckY-1. No negative value for τ_3 was found in cells expressing the constitutively open CLckY-1–Y505F, which indicated that among the three components contributing to the mean fluorescence decay of ECFP, only τ_3 was affected by FRET. In addition, τ_3 contributed to 25% of

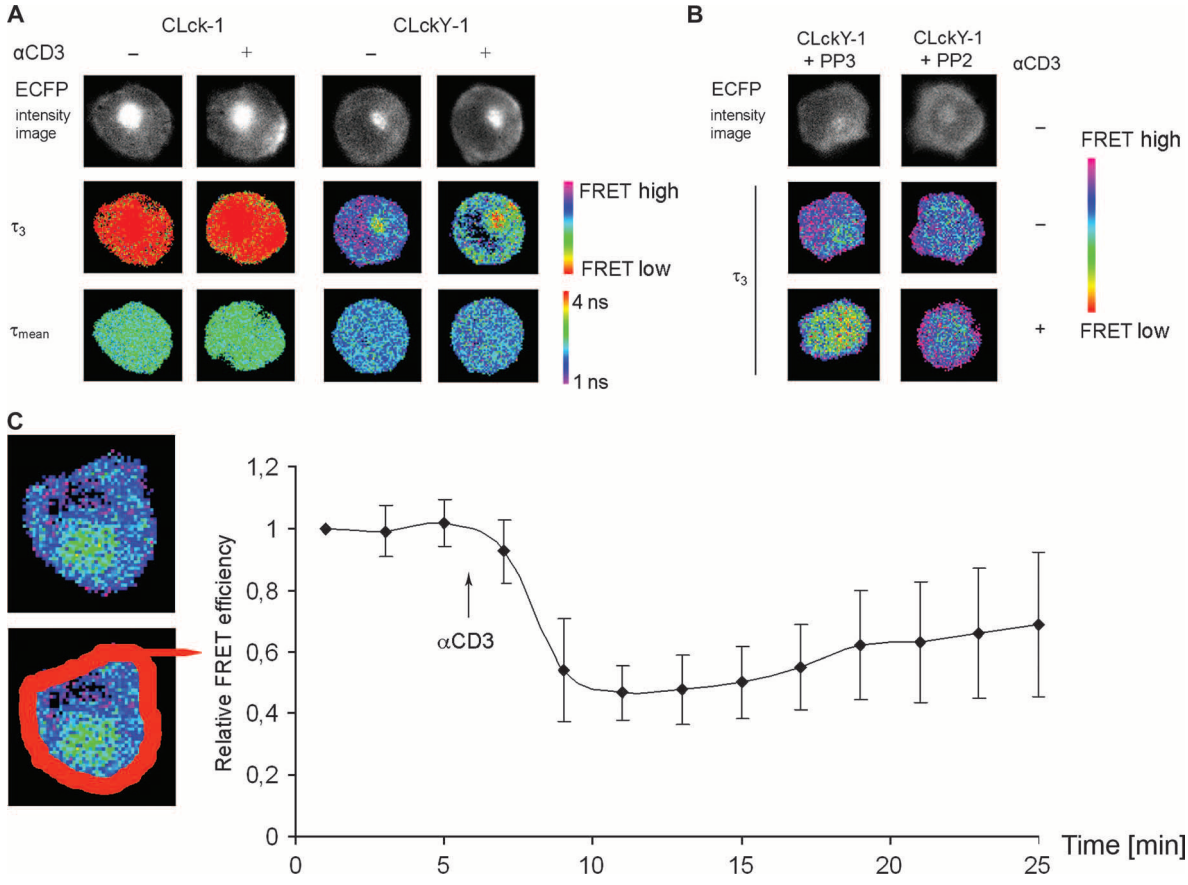

Fig. 3. Conformational changes in the Lck biosensor in response to stimulation of cells with anti-CD3 antibody. (**A** to **C**) Live JCam1.6 cells that had been transfected with plasmid encoding the biosensor (CLckY-1) or with a control plasmid lacking the FRET acceptor EYFP (CLck-1) were analyzed with the QA detector. After excitation at 420 nm, the spectral emissions of the FRET donor ECFP were detected at 465 to 485 nm. Data from at least three independent experiments were analyzed, and representative results are shown in (A) and (B). (A and B) ECFP intensity images captured by the QA detector are represented in the upper panels. (A to C) Pseudocolored images for the pre-exponential factors of τ_3 and τ_{mean} revealed the location of FRET events within the cells. Purple to blue pixels correspond to closed Lck molecules (high FRET), whereas yellow to red pixels indicate molecules with low FRET because of an open conformation of the Lck biosensor. (A) JCam1.6 cells transfected with plasmids encoding CLckY-1 or CLck-1 before and 7 min after stimulation with αCD3. (B) JCam1.6 cells transfected with plasmid encoding CLckY-1 were pretreated for 30 min with 10 μM PP2 or 10 μM PP3. Nonstimulated cells and cells stimulated with αCD3 for 7 min are depicted. (C) Time-resolved analysis of changes in the pre-exponential factor of τ_3 at the plasma membrane of JCam1.6 cells transfected with plasmid encoding CLckY-1 (n = 10 cells, from n = 3 independent experiments; data are means ± SD). The measured area in the lower micrograph is highlighted in red.

the total mean lifetime and therefore may remain undetected when conventional methods of FRET detection, such as intensity-based measurements or mean lifetime FLIM measurements, are applied.

The biosensor reports on the conformational dynamics of Lck at sites of TCR activation in Jurkat cells

Next, we investigated whether Lck underwent conformational change upon T cell activation. We expressed the biosensor or the donor-only tagged variants in JCam1.6 cells and measured the fluorescence lifetimes with the position-sensitive photomultiplier (QA detector) (*32*) to resolve the spatial distribution, as well as the three individual lifetimes of the biosensor (fig. S1). Both CLck-1 and CLckY-1 localized to two major areas, the plasma membrane and a cytoplasmic compartment that partially overlap with early endosomes but not with the endoplasmic reticulum or the Golgi apparatus (Fig. 3A and figs. S2 and S3). Similar subcellular distributions of Lck have been reported previously (*33*–*35*).

FLIM analysis focusing on τ_3 within the CLckY-1 biosensor detected a constitutively open Lck population (low FRET) at the plasma membrane of Jurkat cells and in the cytoplasmic compartment (Fig. 3A, right panels, middle row). Upon treatment with PP2, an inhibitor of SFKs, but not with the inactive analog PP3, these open CLckY-1 molecules became undetectable, and the biosensor assumed the closed conformation (Fig. 3B, middle panels). These data indicate that the open Lck molecules in unstimulated Jurkat cells were constitutively active, which confirmed previous data (*17*).

We then investigated whether Lck underwent conformational changes upon T cell activation. Stimulation with αCD3 induced a detectable decrease in the pre-exponential factors of τ_3 at the plasma membrane and in the cytoplasmic compartment of cells with the CLckY-1 biosensor (Fig. 3A, middle right panels), but not in cells with the ECFP-only variant CLck-1 (Fig. 3A, middle left panels). Opening of the biosensor at the plasma membrane was observed to last for at least 20 min (Figs. 3C and 4A). Again, the decrease in FRET upon T cell activation was completely lost when the cells were pretreated with PP2 (Fig. 3B, lower panels). Together, the behavior of τ_3 in αCD3-stimulated Jurkat cells showed that T cell activation induced an opening of the biosensor. This finding suggested that Lck became activated by a

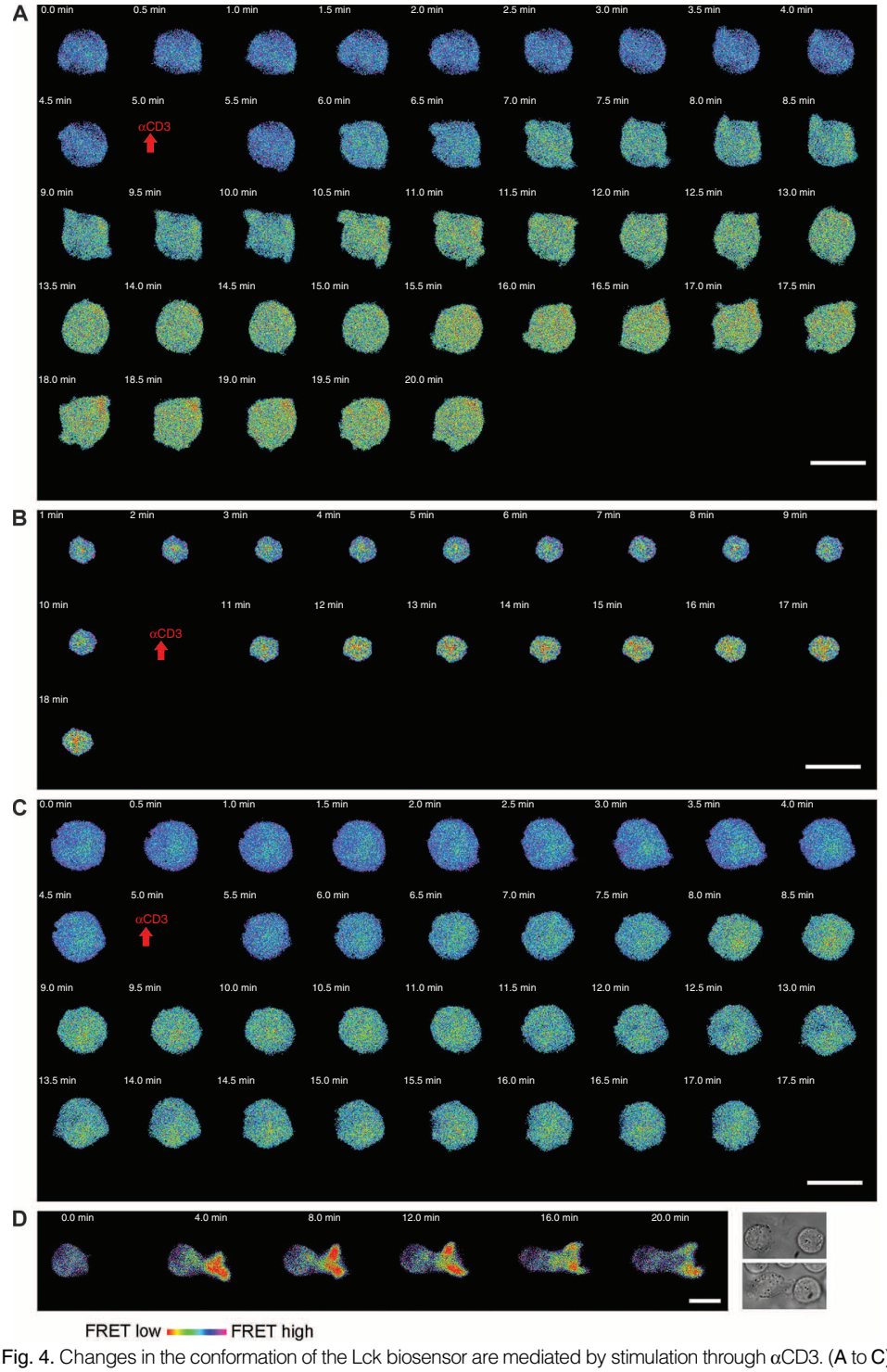

Fig. 4. Changes in the conformation of the Lck biosensor are mediated by stimulation through αCD3. (**A** to **C**) Pseudocolored FLIM images measured with the QA detector represent the pre-exponential factors of τ_3 in (A) JCam1.6 cells, (B) human T cells, and (C) Zap70-deficient P116 cells expressing CLckY-1. (**D**) In Jurkat cells stimulated with SEE-loaded Raji B cells (APCs), the Lck biosensor adopts an open conformation at the site of contact between the Jurkat cell and the APC. The transmitted light images show CLckY-1–expressing Jcam1.6 cells before and after contact with SEE-loaded Raji B cells. Representative images of cells are shown from 30 (A), 10 (B), 12 (C), and 10 (D) measurements from three independent experiments each. Scale bars, 10 μm.

conformational change immediately after stimulation of cells with αCD3. The constitutively open Lck molecules in unstimulated cells and the activation-induced decrease in FRET could only be observed by combining FLIM measurements with an analysis of the pre-exponential factors of τ_3, the characteristic lifetime of the subpopulation of the donor molecules involved in the FRET process. We did not detect alterations in the mean lifetime of the FRET signal in stimulated cells that had the CLckY-1 biosensor (Fig. 3A, lower panels). This observation corroborates the data of Paster *et al.* (*20*).

Table 1. Changes in T_{mean} and the pre-exponential factors of τ_3 of a JCam1.6 cell expressing the biosensor after TCR stimulation. The time range of 0 to 2 min was used as the reference point. n.d., not detectable.

Time points (min)	τ_{mean} (ns)	Change of τ_{mean} (%)	Change of fractional distribution of τ_3 (%)
0–2	2.82	—	—
7–9	2.82	n.d.	16
13–15	2.83	n.d.	20
18–20	2.84	n.d.	35

We then analyzed the tracks of TCR-mediated conformational changes in the Lck biosensor as visualized by FLIM over time after TCR stimulation (Fig. 4). Activation-induced opening of the Lck biosensor was observed in JCam1.6 cells (Fig. 4A) and in primary human T lymphocytes (Fig. 4B). The opening of the biosensor was already detectable just 1 min after application of the αCD3 antibody. Similarly, rapid opening of the biosensor was also observed in the ζ chain–associated protein kinase of 70 kD (Zap70)–deficient Jurkat variant P116 cells, which rules out the possibility that TCR-mediated opening of the biosensor in transfected JCam1.6 and primary T cells was a result of the binding of the SH2 domain of Lck to phosphorylated Zap70 (Fig. 4C).

To determine the relative fraction of the open biosensor molecules in unstimulated and activated T cells, we split the data stream into 2-min time windows. Photons collected during the first 2 min were defined as the baseline value. With this approach, we found that 16% of the biosensor molecules involved in FRET showed an open conformation before stimulation. After 5 min, the cell was stimulated with αCD3 antibody. Continuously recorded FLIM data were analyzed at the time points 0 to 2, 7 to 9, 13 to 15, and 18 to 20 min (Table 1), and the fractional intensities were calculated. This calculation showed that TCR stimulation induced a continuous decrease in the FRET signal (equivalent to opening of the Lck molecule) of an additional 20% of the biosensor molecules undergoing FRET at the plasma membrane (Table 1).

To visualize the conformational changes in the biosensor under more physiological conditions, we monitored the spatiotemporal changes in Lck conformation in a T cell activation model system in which the TCR was triggered by contact with antigen-presenting cells (APCs). We incubated superantigen (SEE)–loaded Raji B cells with Jurkat cells expressing the biosensor. Changes in FRET signals reported the rapid accumulation of the open, activated conformation of the Lck biosensor at the contact zone between both cell types (Fig. 4D). No changes in biosensor FRET occurred in conjugates of T cells with nonpulsed APCs (fig. S4), indicating that opening of the biosensor required engagement of the TCR.

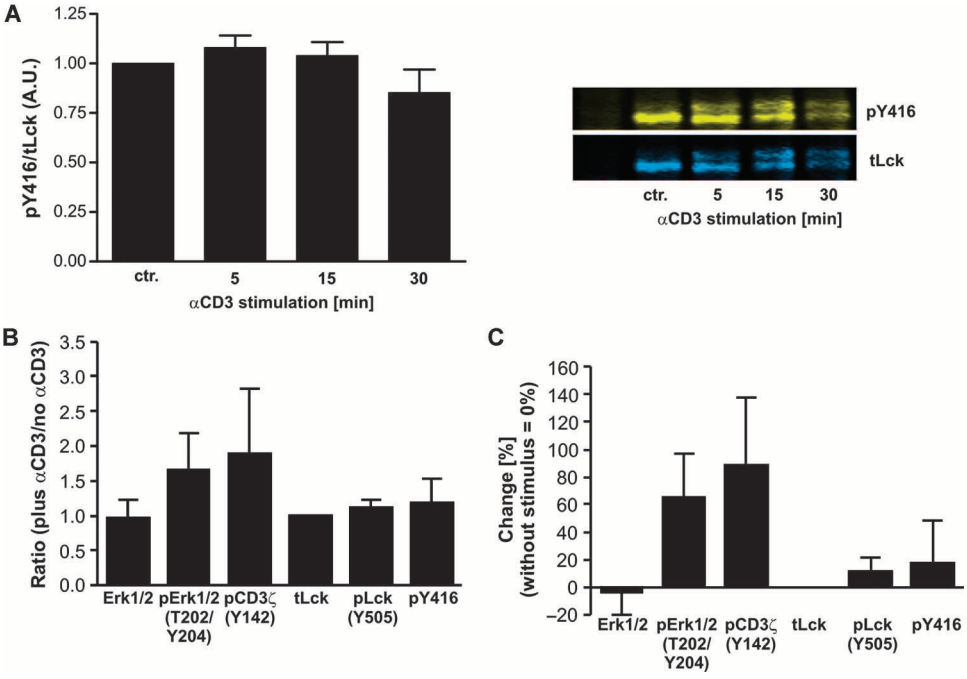

Fig. 5. Global analysis of Lck phosphorylation after T cell activation. (**A**) Lysates of unstimulated, control Jurkat cells (ctr.) and cells stimulated for the indicated times with αCD3-coated microbeads were subjected to immunoprecipitations. The Lck immunoprecipitates were analyzed in a dual fluorescence Western blot (right panel) with αLck (blue) and antibodies against Src family kinases containing $pTyr^{416}$, which label the corresponding $pTyr^{394}$ of Lck (yellow). The ratios of signals from tyrosine-phosphorylated Lck and total Lck protein were calculated from four independent experiments and are shown in the bar graph on the left as means ± SD. (**B** and **C**) MELK analysis: quantification of changes in signal intensities of the displayed signaling molecules after stimulation of Jurkat JE6.1 cells with αCD3 for 5 min. (B) Ratio of the signals of the indicated proteins between αCD3-stimulated and unstimulated Jurkat cells (mean ± SD). (C) Relative changes in the fluorescence signal ratios between stimulated and nonstimulated cells (mean ± 95% confidence interval). Data are combined from six independent experiments in which a total of 448 cells were analyzed.

The enzymatic activity of Lck is enhanced upon T cell activation

A fraction of Lck molecules underwent conformational changes upon T cell activation, in apparent disagreement with Nika *et al.*, who proposed that activation of T cells is not accompanied by increased pools of activated Lck. Consistent with this proposal, we observed that Lck in total cell lysates obtained from αCD3-stimulated primary human T cells showed no substantial increase in the Lck-activating Tyr^{394} phosphorylation (Fig. 5A). We obtained similar results when we examined the phosphorylation status of Lck by automated multidimensional fluorescence microscopy [multi-epitope ligand

cartography (MELK)], which enables simultaneous imaging of several signaling molecules within the same cell (Fig. 5, B and C). However, when we subjected Lck immunoprecipitated from resting or αCD3-stimulated human T lymphocytes or Jurkat cells to a classical in vitro kinase assay with radiolabeled adenosine 5′-triphosphate (ATP), we observed a 20% increase in Lck activity in four independent experiments with each cell type after 30 and 120 s of stimulation (Fig. 6). The increase in Lck phosphorylation was not a consequence of coimmunoprecipitation of Lck with Csk (fig. S5) and correlated well with our FLIM data, which showed that 20% of the biosensor molecules locally adopt an open active conformation at sites of TCR activation.

DISCUSSION

One of the first biochemical events after stimulation of the TCR is the phosphorylation of ITAMs within the TCR by the SFK Lck; however, very little is known about the regulation of Lck activity after T cell activation. With a FRET-based Lck biosensor and a new FLIM-based strategy, we assessed the intracellular conformation of Lck in unstimulated and TCR-stimulated Jurkat cells and primary human T lymphocytes. In unstimulated Jurkat cells, a fraction of the biosensor (and hence of Lck) was found in a constitutively open conformation. These open Lck molecules rapidly assumed a closed conformation when cells were treated with the SFK-specific inhibitor PP2. This suggests that the open fraction of Lck represents constitutively active Lck molecules, corroborating the data of Nika *et al*., who identified constitutively active forms of Lck in resting T cells (*17*). Mechanistically, PP2 induced a reduction in the extent of Tyr^{394} phosphorylation, which most likely was mediated by the transmembrane phosphatase CD45. Our FLIM measurements provide a direct demonstration of conformational changes in an SFK in live cells as a result of a change in its phosphorylation status. TCR activation induced the rapid opening of the Lck biosensor in T cells, including the Zap70-deficient P116 Jurkat variant cell line. This suggests that the binding of Lck to tyrosine-phosphorylated Zap70 through its SH2 domain (*36*) is not required for the conformational opening of Lck at sites of TCR activation.

Our FLIM and biochemical measurements conflict with reports that suggest that Lck changes neither its conformation nor its enzymatic activity upon T cell activation. Paster *et al.* did not detect changes in FRET efficiency, as a measure of conformational changes, with an Lck biosensor similar to the one that we used here (*20*). We attribute this discrepancy to the FRET detection technique that was used by Paster *et al*., namely, a fluorescence intensity–based method that monitors the integral of the mean fluorescence. Indeed, if considering the mean lifetimes of donor fluorescence, our results fit with those of Paster *et al*. This finding shows an advantage of our method, which focuses on the analysis of the subpopulation of donor molecules that is engaged in FRET. Antibody-based approaches led Nika *et al.* to propose that T cell activation does not increase the enzymatic activity of Lck (*17*). Similarly, we did not detect substantial alterations in Lck activity when we assessed its phosphorylation status in unstimulated and stimulated T cells in experiments with phosphorylation-specific antibodies. However, when we subjected Lck immunoprecipitates from primary T cells to in vitro kinase assays, we reproducibly found an ~20% increase in the amount of autophosphorylated Lck, which correlated with our biosensor data. We attribute the apparent discrepancy between the antibody-based approaches and the in vitro kinase assays to the higher sensitivity of the radioactive assays.

We would like to emphasize that our data do not exclude the possibility that, in addition to activation of Lck, additional changes

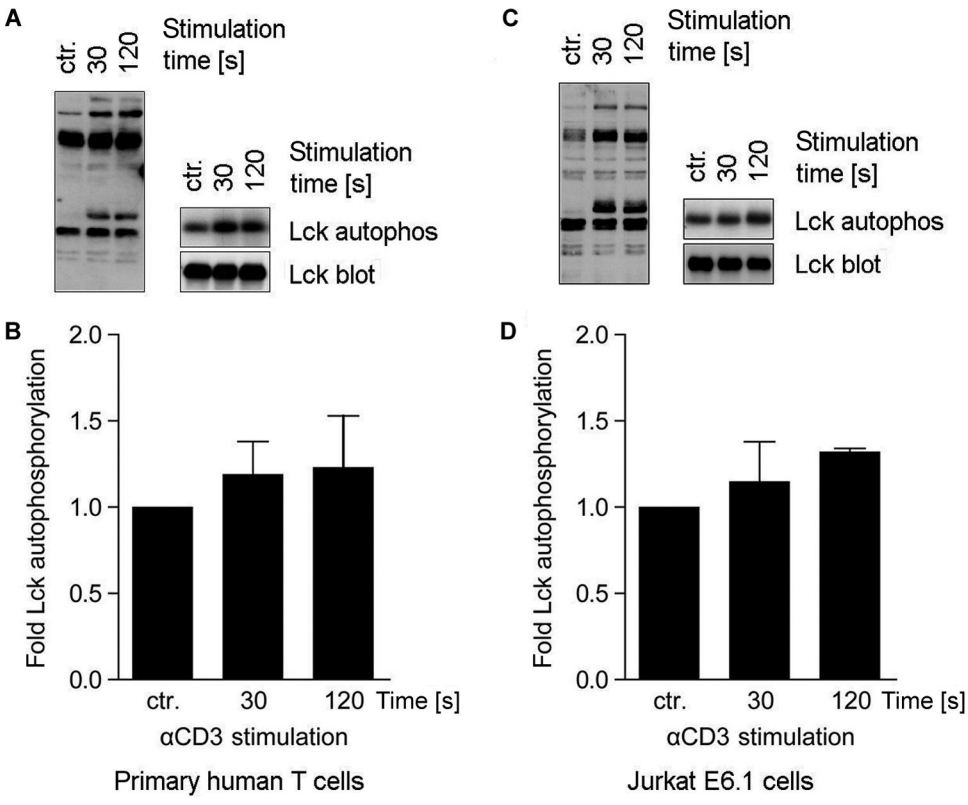

Fig. 6. Activation of Lck in primary human T cells and Jurkat E6.1 cells upon stimulation with αCD3. (A and B) Primary human T cells and (C and D) Jurkat cells were either left unstimulated as controls (ctr.) or stimulated with αCD3 for the indicated times. After lysis in buffer containing NP-40 and lauryl maltoside (LM), a fraction of the detergent lysate was subjected to SDS-PAGE and Western blotting analysis with the anti-pTyr antibody 4G10 (left panels of A and C). The remaining lysate was subjected to immunoprecipitation with antibody against Lck. Of the immunoprecipitated samples, 50% were subjected to SDS-PAGE and Western blotting analysis with anti-Lck antibody [right lower panels of (A) and (C)], whereas the remaining 50% were subjected to a classical in vitro kinase assay with radiolabeled ^{32}γ-ATP. After washing, the in vitro–labeled immunoprecipitates were subjected to SDS-PAGE, which was followed by autoradiography [right upper panels of (A) and (C)]. Data shown are a representative blot and autoradiogram from four independent experiments. (B and D) Densitometric analysis of autoradiographs of in vitro–labeled Lck immunoprecipitates obtained from unstimulated or αCD3-stimulated (B) primary human T cells or (D) Jurkat cells. The graphs show the means ± SD for the four independent experiments and indicate an increased autophosphorylation activity of Lck at 30 and 120 s after TCR activation of both cell types.

in the subcellular localization of Lck or enhanced substrate accessibility (for example, conformational changes in the TCR) contribute to ITAM phosphorylation after ligand binding. However, our data showed that a fraction of Lck adopted an open conformation and enhanced its activity after T cell activation and thus suggest that the highly conserved intramolecular regulatory mechanism of SFKs has evolved to fine-tune their activity at defined sites within T cells.

MATERIALS AND METHODS

Antibodies, cell culture, and transfection

The following antibodies were used in this study: horseradish peroxidase–conjugated mouse anti-phosphotyrosine (4G10, Millipore); mouse anti-Lck (clone 28), mouse anti-Csk, Alexa Fluor 488–conjugated mouse anti-Lck (clone 28), and Alexa Fluor 488–conjugated mouse anti-pCD3ζ (pY142, K25-407.69) (all from BD Transduction Laboratories); mouse anti-Lck (3A5, Santa Cruz Biotechnology Inc.); rabbit anti-Lck (Upstate); and rabbit anti–Src-pY416, rabbit anti-pLck (pY505), Alexa Fluor 488–conjugated mouse anti-pERK1/2 (E10), and Alexa Fluor 555–conjugated goat anti-rabbit Fab2 (all from Cell Signaling Technology). Secondary antibodies used for dual fluorescence analysis of Western blots were goat anti-rabbit IRDye 680LT and goat anti-rabbit IRDye 800CW and were obtained from LI-COR. The Jurkat cell line E6.1, the Lck-deficient variant cell line JCam1.6 (*24*, *37*), the Zap70-deficient variant Jurkat cell line P116, and the Raji B cell lymphoma cell line were obtained from the American Type Culture Collection. Cell lines were maintained in RPMI 1640 medium supplemented with 10% fetal calf serum (FCS; PAN Biotech), stable L-glutamine, penicillin (50 U/ml), and streptomycin (50 μg/ml) (Biochrom) in humidified 5% CO_2 at 37°C. Primary human T cells were isolated from healthy donors with the Pan T Cell Isolation Kit II and autoMACS (Miltenyi Biotec). The mouse anti-human CD3 monoclonal antibodies UCHT1 (eBioscience), C305 [immunoglobulin M (IgM), provided by A. Weiss, University of California San Francisco (UCSF)], and MEM92 (IgM, provided by V. Horejsi, Prague) were used to activate primary human T cells or Jurkat cells. JCam1.6 cells and P116 cells were transfected by electroporation as previously described (*38*). Briefly, 1.5×10^7 cells were transfected with 20 μg of the individual Lck-encoding plasmids or the FRET-positive control (*20*) and were analyzed 24 hours after transfection.

Fluorescence lifetime imaging microscopy

Reconstituted JCam1.6 cells (1×10^6/ml), in 1 ml of Krebs-Ringer solution [10 mM Hepes (pH 7.0), 140 mM NaCl, 4 mM KCl, 1 mM $MgCl_2$, 10 mM glucose, 1 mM $CaCl_2$], were plated on poly-L-lysine–coated glass-bottom culture disks (MatTek) for 10 min. The cells either were stimulated with soluble monoclonal antibody against human CD3ε (UCHT1, 5 μg/ml) for the indicated times or were mixed at a 1:1 ratio with Raji B cells that had been pulsed with SEE. Emission spectra (460 to 650 nm) and fluorescence lifetimes of the three pre-exponential factors of ECYFP and the different Lck constructs were determined with a microscopy system that enables time- and space-correlated single-photon counting. The imaging setup consisted of a frequency-doubled femtosecond laser (excitation wavelength, 420 nm), an inverted microscope, and two sensitive detectors: a microspectroscopic DL detector and a position-sensitive photomultiplier (QA imaging detector) (*28*, *31*, *39*, *40*). The DL detector was used to statistically analyze a very small area of the sample (with a diameter of 5 to 10 μm) and to resolve spectrally the corresponding fluorescence decays. Measurements with the QA imaging detector setup were performed to analyze the spatial distribution of the biosensors, as well as changes in their individual fluorescence lifetimes.

Analysis of FLIM data

In a multiexponential fluorescence system (for example, the ECFP-EYFP FRET pair), the intensity of the fluorescence signal decays as a sum of individual single lifetimes $I(t)$ is given by

$$I(t) = \sum_i \alpha_i \exp - t/\tau_i$$

where τ_i represents the individual decay times, and the pre-exponential factors α_i are the amplitudes of the components (indexed by i), for example, subpopulations of the fluorophore that are involved or not involved in FRET. The values of α_i and τ_i can be used to calculate the fractional distributions f_i of each of the decay times (*41*). Thus, the value of f_i represents the fractional intensities of the individual subpopulations of a mixture of fluorophores, for example, subpopulations of proteins that do or do not undergo FRET, such as ECFP.

$$f_i = (\alpha_i \tau_i)/(\sum_i \alpha_i \tau_i)$$

The values of f_i and α_i can be used to determine the mean fluorescence lifetime of each biosensor (*41*). To analyze the fluorescence decay $I(t)$, the data measured with both detectors were modeled by the convolution product of a multiexponential theoretical model with the instrument response function (IRF):

$$I(t) = \mathrm{IRF}(t) \otimes \sum_i \alpha_i \exp - t/\tau_i$$

where IRF is the measurement of the pulsed laser excitation obtained by acquiring the reflection of the laser beam. The data were analyzed by a Levenberg-Marquardt nonlinear, least-squares algorithm with the MATLAB software package, version R12.

Data acquired by the spectral (DL) detector were fitted with linked lifetimes along the wavelength band (460 to 650 nm). In this case, the intensity decay of the fluorescence signal can be described as (*41*)

$$I(\lambda, t) = \sum_i \alpha_i(\lambda) \exp - t/\tau_i$$

The wavelength-dependent pre-exponential factors $a_i(\lambda)$ of the individual lifetimes τ_i were plotted along different wavelengths, which resulted in generation of the DAS.

These spectra

$$I_i(\lambda) = \alpha_i(\lambda)\tau_i I(\lambda) \left[\sum_i \alpha_i(\lambda)\tau_i\right]^{-1}$$

represent the emission spectra of the individual components characterized by the individual lifetime τ_i (*41*). The comparison of the DAS of the individual lifetimes enables the identification of the fluorescent species (the donor and acceptor molecules) that are involved, or not, in FRET, as explained below:

Because FRET is a bimolecular process, the exited state population of the system can be described after excitation of the donor with a δ-shaped laser pulse:

$$\mathrm{d}D(t)/\mathrm{d}t = -(k_\mathrm{d} + k_\mathrm{t})D(t) \quad (1)$$

and

$$\mathrm{d}A(t)/\mathrm{d}t = D(t)k_\mathrm{t} - A(t)k_\mathrm{a} \quad (2)$$

where $D(t)$ is the concentration of the donor molecules in the exited state, $A(t)$ is the concentration of the exited acceptor molecules, k_d is the rate constant of relaxation of the donor molecules in the absence of the acceptor,

k_a is the acceptor de-excitation rate constant, and k_t is the rate constant of resonance energy transfer. The differential equations 1 and 2 describe the fluorescence decays of the donor and acceptor molecules and can be solved as follows (*42*):

$$D(t) = D_0 \exp - (k_d + k_t)t$$

$$A(t) = -D_0 k_t/(k_d + k_t - k_a)\exp - (k_d + k_t)t + D_0\ kt/(k_d + k_t - k_a)\ \exp - k_a t$$

D_0 represents the exited state population of the donor at time $t = 0$. The negative term in the function of the acceptor $A(t)$ reflects a rise component in the decay of the acceptor because of energy transfer (*42*, *43*) and results in a longer lifetime of the acceptor compared to its native lifetime. This can be detected as a negative term in the DAS in the wavelength range of the native acceptor emission wavelength (*41*). Therefore, negative terms in the DAS plot of the individual lifetimes of a multiexponential system (for example, a FRET pair consisting of fluorescent proteins) identify the subpopulation of molecules involved in the FRET process. Data collected by the QA detector were analyzed as previously described (*28*, *31*). To visualize the spatial distribution of different exited states (high or low FRET signals) of the fluorophores inside a cell, the pre-exponential factors of the lifetime τ_3, which characterizes the subpopulation of the donor molecules involved in the FRET process, were plotted as previously described (*32*). The resulting pseudocolor-coded maps show the distribution of the conformational changes of the biosensor.

Analysis of intracellular Ca^{2+} flux

JCam1.6 cells (0.3×10^6/ml) transfected with either plasmid encoding the Lck biosensor or the empty plasmid were loaded with Indo-1 AM (5 μg/ml) (Molecular Probes) for 45 min at 37°C in RPMI 1640 without phenol red (Invitrogen). After washing, cells were rested for 45 min at 37°C. Stimulation was initiated by adding 10 μl of C305 monoclonal antibody hybridoma supernatant per milliliter of cell suspension. Changes in intracellular Ca^{2+} were monitored with either a flow cytometer LSR I analyzer (BD Biosciences) or a confocal microscope Leica SP2 (Leica Microsystems Heidelberg). Cells were illuminated with the 364-nm line of an argon UV laser (for the confocal microscope) or the 325-nm laser line of a helium-cadmium laser (for the LSR flow cytometer). In both experimental settings, fluorescence emissions at 390 to 420 nm and 500 to 520 nm were detected simultaneously, and changes in the ratio of the two emission intensities were analyzed with ImageJ (confocal) or FlowJo (LSR) software, respectively. To demonstrate successful loading with the dye, we induced maximal Ca^{2+} release by adding calcium ionophore ionomycin (10 μg/ml) (Sigma-Aldrich).

Immunoprecipitations and in vitro kinase assays

To immunoprecipitate Lck (as shown in Fig. 5A), we left 5×10^6 Jurkat cells untreated or activated them with microbeads coated with anti-CD3 antibody. SuperAvidin-coated polystyrene microspheres (diameter, 10.14 μm; density, 1.6×10^7/ml; Bangs Laboratories Inc.) were incubated with the biotinylated αCD3ε monoclonal antibody UCHT1 (10 μg/ml) in phosphate-buffered saline (PBS) for 30 min at 37°C. αCD3-coated microbeads were washed twice with PBS and resuspended in RPMI 1640. Stimulation of Jurkat cells (at a cell-to-bead ratio of 2:1) was synchronized by centrifugation at 100*g* for 10 s. After the indicated times, cells were washed and lysed in buffer containing 1% LM (an *N*-dodecyl β-maltoside), 1% NP-40, 1 mM Na_3VO_4, 1 mM phenylmethylsulfonyl fluoride, 10 mM NaF, 10 mM EDTA, 50 mM tris-HCl (pH 7.5), and 150 mM NaCl. Detergent cell lysates were incubated overnight at 4°C with the anti-Lck monoclonal antibody 3A5 coupled to protein A–agarose (Santa Cruz Biotechnology Inc.). Samples were separated by 10% SDS–polyacrylamide gel electrophoresis (SDS-PAGE) and blotted onto nitrocellulose. For dual-color analysis, membranes were first incubated with rabbit antibody against pSrc-pY416, which corresponds to pY394 of Lck, and goat anti-rabbit IRDye 680LT, stripped for 20 min (in Restore PLUS Western Blot Stripping Buffer, Thermo Scientific) and then incubated with secondary antibody to exclude remaining anti–Src-pY416 binding. Membranes were subsequently incubated with rabbit antibody against Lck and goat anti-rabbit IRDye 800CW. Signal intensities were determined by scanning the membranes with an Odyssey infrared imager (LI-COR) and analyzing the data with the Odyssey application software. For in vitro kinase assays, freshly prepared human T lymphocytes (5×10^7 cells per sample) or Jurkat cells (2×10^7 cells per sample) were stimulated for 30 or 120 s with a 1:100 (v/v) dilution of ascites fluid of the αCD3 monoclonal antibody MEM92 (IgM, provided by V. Horejsi, Prague). In some experiments, the αCD3ε monoclonal antibody UCHT1 (10 μg/ml) was used to stimulate cells, yielding identical results. After stimulation, cells were lysed in lysis buffer supplemented with 1% NP-40 and 1% LM as detergents. Detergent lysates were subjected to immunoprecipitation with αLck antibody with 2 μg of polyclonal rabbit antibody (Upstate) used for each immunoprecipitation. After washing, the immunoprecipitates were split; 50% of the immunoprecipitates were used for Western blotting analysis, with the αLck antibody as a control, whereas the remaining 50% of the samples were resuspended in kinase buffer [20 mM tris-HCl (pH 7.5), 10 mM $MnCl_2$, 100 μM ATP, 10 μCi of $^{32}\gamma$-ATP (PerkinElmer; 3000 Ci/mmol)] and subjected to an in vitro kinase assay for 20 min at 30°C. After the kinase reaction was complete, the radiolabeled immunoprecipitates were washed four times in washing buffer [20 mM tris-HCl (pH 7.5), 20 mM EDTA, 150 mM $NaCl_2$] and subsequently subjected to SDS-PAGE and autoradiography.

Automated multidimensional fluorescence microscopy (MELK)

Jurkat cells (1×10^6/ml) were placed onto poly-L-lysine–coated cover slides and stimulated with the αCD3ε monoclonal antibody UCHT1 (5 μg/ml) or RPMI without FCS (as a negative control) at 37°C. After 5 min, the slides were transferred into ice-cold PBS to stop the stimulation. Cells were fixed with 2% paraformaldehyde (PFA; Santa Cruz Biotechnology Inc.) and permeabilized with 0.2% Triton X-100. After labeling and imaging of the first antibody set, the dye (Alexa Fluor 488) was bleached, and samples were then incubated with the next antibody. The appropriate working dilutions, incubation times, and positions within the MELK run were validated systematically with conditions suitable to MELK (*44*). Images were recorded with a toponome imaging cycler (TIC). The sample was placed on the stage of an inverted, wide-field fluorescence microscope (Leica DM IRE2, 63× oil lens with 1.40 numerical aperture). For each of the two conditions defined by application of individual droplets of cell solution, a suitable field of view was defined manually, and the corresponding XYZ positions and a transmitted light reference image were stored by the TIC Control software. A fully automated cyclic robotic process started with the incubation of the first fluorescent antibody (or tag). After a washing step, the fluorescence signals and a corresponding phase-contrast image were acquired by a cooled charge-coupled device camera (Apogee KX4, Apogee Instruments, 1× binning results in images of 2048 × 2048 pixels; final pixel size, 143 × 143 nm^2). To eliminate the specific signal of a given tag before the addition of the next, we performed a bleaching step. A post-bleaching fluorescence signal was recorded before the next incubation-imaging-bleaching cycle started with the next tag. These cycles were processed until all of the tags were applied to the sample.

The fluorescence and post-bleaching fluorescence images produced by each tag were automatically aligned pixel-wise with the corresponding phase-contrast images, reaching an alignment accuracy of 1 pixel. Fluorescence images were corrected for illumination faults with flat-field correction. Post-bleaching images were subtracted from the subsequent fluorescence tag images. Finally, cases of section artifacts were excluded as invalid by a mask-setting process. Regions of interest for T cells analyzed were defined manually, and the background-subtracted intensities for the individual tags were recorded.

Confocal imaging

Lck-deficient JCam1.6 cells expressing a biosensor were plated on poly-L-lysine–covered slides at room temperature for 5 min and immediately fixed for 10 min in PBS (pH 7.4) containing 1.5% PFA and 0.025% glutaraldehyde. Cells were permeabilized in PBS containing 0.2% Triton X-100 for 10 min, rinsed twice with PBS, and blocked with 1% bovine serum albumin in PBS (pH 7.4) for 10 min. Cells were incubated with primary antibodies including anti-Jurkat TCR monoclonal antibody C305 (IgM, provided by A. Weiss, UCSF) and antibodies against EEA1, Rab11, and Rab5 (all from BD Bioscience) for 1 hour, and cells were subsequently washed and blocked as described earlier. Specimens were then treated with a secondary antibody (DyLight 549, Dianova) for 1 hour. After washing three times with PBS, specimens were washed once in PBS (pH 8.9) and subsequently embedded. The specimens were analyzed with a confocal microscope (Leica SP2, Leica Microsystems Heidelberg). Sequential images were acquired in the corresponding wavelength channels to avoid bleed-through processes and were later merged with ImageJ software. For membrane staining, CellTracker (CM-Dil, Molecular Probes) was added to the plated cells, incubated for 5 to 10 min, washed with PBS, and fixed and scanned with a confocal microscope as described earlier.

SUPPLEMENTARY MATERIALS

www.sciencesignaling.org/cgi/content/full/6/263/ra13/DC1

Fig. S1. Two versus three lifetimes are needed to describe the fluorescence decay of an ECFP-EYFP FRET pair.

Fig. S2. Localization of the biosensor CLckY-1 at the plasma membrane.

Fig. S3. Localization of the biosensor in transfected Lck-deficient JCam1.6 cells.

Fig. S4. Conjugate formation between transfected JCam1.6 cells expressing CLckY-1 and mock-treated Raji B cells as measured with the QA detector in the FLIM setup.

Fig. S5. Lck does not coimmunoprecipitate with Csk.

REFERENCES AND NOTES

1. T. J. Molina, K. Kishihara, D. P. Siderovski, W. van Ewijk, A. Narendran, E. Timms, A. Wakeham, C. J. Paige, K. U. Hartmann, A. Veillette, D. Davidson, T. W. Mak, Profound block in thymocyte development in mice lacking p56^{lck}. *Nature* **357**, 161–164 (1992).
2. J. Lin, A. Weiss, T cell receptor signalling. *J. Cell Sci.* **114**, 243–244 (2001).
3. F. Sicheri, J. Kuriyan, Structures of Src-family tyrosine kinases. *Curr. Opin. Struct. Biol.* **7**, 777–785 (1997).
4. E. H. Palacios, A. Weiss, Function of the Src-family kinases, Lck and Fyn, in T-cell development and activation. *Oncogene* **23**, 7990–8000 (2004).
5. M. Bergman, T. Mustelin, C. Oetken, J. Partanen, N. A. Flint, K. E. Amrein, M. Autero, P. Burn, K. Alitalo, The human p50^{csk} tyrosine kinase phosphorylates p56^{lck} at Tyr-505 and down regulates its catalytic activity. *EMBO J.* **11**, 2919–2924 (1992).
6. M. Takeuchi, S. Kuramochi, N. Fusaki, S. Nada, J. Kawamura-Tsuzuku, S. Matsuda, K. Semba, K. Toyoshima, M. Okada, T. Yamamoto, Functional and physical interaction of protein-tyrosine kinases Fyn and Csk in the T-cell signaling system. *J. Biol. Chem.* **268**, 27413–27419 (1993).
7. W. Xu, S. C. Harrison, M. J. Eck, Three-dimensional structure of the tyrosine kinase c-Src. *Nature* **385**, 595–602 (1997).
8. M. J. Eck, S. K. Atwell, S. E. Shoelson, S. C. Harrison, Structure of the regulatory domains of the Src-family tyrosine kinase Lck. *Nature* **368**, 764–769 (1994).
9. H. L. Ostergaard, D. A. Shackelford, T. R. Hurley, P. Johnson, R. Hyman, B. M. Sefton, I. S. Trowbridge, Expression of CD45 alters phosphorylation of the *lck*-encoded tyrosine protein kinase in murine lymphoma T-cell lines. *Proc. Natl. Acad. Sci. U.S.A.* **86**, 8959–8963 (1989).
10. M. Shiroo, L. Goff, M. Biffen, E. Shivnan, D. Alexander, CD45 tyrosine phosphatase-activated p59^{fyn} couples the T cell antigen receptor to pathways of diacylglycerol production, protein kinase C activation and calcium influx. *EMBO J.* **11**, 4887–4897 (1992).
11. G. Hofmann, K. Schweimer, A. Kiessling, E. Hofinger, F. Bauer, S. Hoffmann, P. Rösch, I. D. Campbell, J. M. Werner, H. Sticht, Binding, domain orientation, and dynamics of the Lck SH3–SH2 domain pair and comparison with other Src-family kinases. *Biochemistry* **44**, 13043–13050 (2005).
12. A. D. Holdorf, J. M. Green, S. D. Levin, M. F. Denny, D. B. Straus, V. Link, P. S. Changelian, P. M. Allen, A. S. Shaw, Proline residues in CD28 and the Src homology (SH)3 domain of Lck are required for T cell costimulation. *J. Exp. Med.* **190**, 375–384 (1999).
13. W. Xu, A. Doshi, M. Lei, M. J. Eck, S. C. Harrison, Crystal structures of c-Src reveal features of its autoinhibitory mechanism. *Mol. Cell* **3**, 629–638 (1999).
14. J. S. Hardwick, B. M. Sefton, Activation of the Lck tyrosine protein kinase by hydrogen peroxide requires the phosphorylation of Tyr-394. *Proc. Natl. Acad. Sci. U.S.A.* **92**, 4527–4531 (1995).
15. A. Alonso, N. Bottini, S. Bruckner, S. Rahmouni, S. Williams, S. P. Schoenberger, T. Mustelin, Lck dephosphorylation at Tyr-394 and inhibition of T cell antigen receptor signaling by *Yersinia* phosphatase YopH. *J. Biol. Chem.* **279**, 4922–4928 (2004).
16. H. Xu, D. R. Littman, The kinase-dependent function of Lck in T-cell activation requires an intact site for tyrosine autophosphorylation. *Ann. N. Y. Acad. Sci.* **766**, 99–116 (1995).
17. K. Nika, C. Soldani, M. Salek, W. Paster, A. Gray, R. Etzensperger, L. Fugger, P. Polzella, V. Cerundolo, O. Dushek, T. Höfer, A. Viola, O. Acuto, Constitutively active Lck kinase in T cells drives antigen receptor signal transduction. *Immunity* **32**, 766–777 (2010).
18. Z. Ma, T. H. Finkel, T cell receptor triggering by force. *Trends Immunol.* **31**, 1–6 (2010).
19. P. A. van der Merwe, O. Dushek, Mechanisms for T cell receptor triggering. *Nat. Rev. Immunol.* **11**, 47–55 (2011).
20. W. Paster, C. Paar, P. Eckerstorfer, A. Jakober, K. Drbal, G. J. Schütz, A. Sonnleitner, H. Stockinger, Genetically encoded Förster resonance energy transfer sensors for the conformation of the Src family kinase Lck. *J. Immunol.* **182**, 2160–2167 (2009).
21. T. Zal, N. R. Gascoigne, Photobleaching-corrected FRET efficiency imaging of live cells. *Biophys. J.* **86**, 3923–3939 (2004).
22. P. I. Bastiaens, A. Squire, Fluorescence lifetime imaging microscopy: Spatial resolution of biochemical processes in the cell. *Trends Cell Biol.* **9**, 48–52 (1999).
23. F. S. Wouters, P. I. Bastiaens, Fluorescence lifetime imaging of receptor tyrosine kinase activity in cells. *Curr. Biol.* **9**, 1127–1130 (1999).
24. M. A. Goldsmith, A. Weiss, Isolation and characterization of a T-lymphocyte somatic mutant with altered signal transduction by the antigen receptor. *Proc. Natl. Acad. Sci. U.S.A.* **84**, 6879–6883 (1987).
25. A. J. Visser, S. P. Laptenok, N. V. Visser, A. van Hoek, D. J. Birch, J. C. Brochon, J. W. Borst, Time-resolved FRET fluorescence spectroscopy of visible fluorescent protein pairs. *Eur. Biophys. J.* **39**, 241–253 (2010).
26. J. W. Borst, S. P. Laptenok, A. H. Westphal, R. Kühnemuth, H. Hornen, N. V. Visser, S. Kalinin, J. Aker, A. van Hoek, C. A. Seidel, A. J. Visser, Structural changes of yellow Cameleon domains observed by quantitative FRET analysis and polarized fluorescence correlation spectroscopy. *Biophys. J.* **95**, 5399–5411 (2008).
27. S. Habuchi, M. Cotlet, J. Hofkens, G. Dirix, J. Michiels, J. Vanderleyden, V. Subramaniam, F. C. De Schryver, Resonance energy transfer in a calcium concentration-dependent cameleon protein. *Biophys. J.* **83**, 3499–3506 (2002).
28. M. Jose, D. K. Nair, C. Reissner, R. Hartig, W. Zuschratter, Photophysics of Clomeleon by FLIM: Discriminating excited state reactions along neuronal development. *Biophys. J.* **92**, 2237–2254 (2007).
29. S. P. Laptenok, J. W. Borst, K. M. Mullen, I. H. van Stokkum, A. J. Visser, H. van Amerongen, Global analysis of Förster resonance energy transfer in live cells measured by fluorescence lifetime imaging microscopy exploiting the rise time of acceptor fluorescence. *Phys. Chem. Chem. Phys.* **12**, 7593–7602 (2010).
30. M. Millington, G. J. Grindlay, K. Altenbach, R. K. Neely, W. Kolch, M. Bencina, N. D. Read, A. C. Jones, D. T. Dryden, S. W. Magennis, High-precision FLIM–FRET in fixed and living cells reveals heterogeneity in a simple CFP–YFP fusion protein. *Biophys. Chem.* **127**, 155–164 (2007).
31. D. K. Nair, M. Jose, T. Kuner, W. Zuschratter, R. Hartig, FRET-FLIM at nanometer spectral resolution from living cells. *Opt. Express* **14**, 12217–12229 (2006).
32. M. Vitali, F. Picazo, Y. Prokazov, A. Duci, E. Turbin, C. Götze, J. Llopis, R. Hartig, A. J. Visser, W. Zuschratter, Wide-field multi-parameter FLIM: Long-term minimal invasive observation of proteins in living cells. *PloS ONE* **6**, e15820 (2011).
33. O. M. Antón, L. Andrés-Delgado, N. Reglero-Real, A. Batista, M. A. Alonso, MAL protein controls protein sorting at the supramolecular activation cluster of human T lymphocytes. *J. Immunol.* **186**, 6345–6356 (2011).
34. I. A. Yudushkin, R. D. Vale, Imaging T-cell receptor activation reveals accumulation of tyrosine-phosphorylated CD3ζ in the endosomal compartment. *Proc. Natl. Acad. Sci. U.S.A.* **107**, 22128–22133 (2010).
35. S. C. Ley, M. Marsh, C. R. Bebbington, K. Proudfoot, P. Jordan, Distinct intracellular localization of Lck and Fyn protein tyrosine kinases in human T lymphocytes. *J. Cell Biol.* **125**, 639–649 (1994).

36. M. Pelosi, V. Di Bartolo, V. Mounier, D. Mège, J. M. Pascussi, E. Dufour, A. Blondel, O. Acuto, Tyrosine 319 in the interdomain B of ZAP-70 is a binding site for the Src homology 2 domain of Lck. *J. Biol. Chem.* **274**, 14229–14237 (1999).
37. D. B. Straus, A. Weiss, Genetic evidence for the involvement of the Lck tyrosine kinase in signal transduction through the T cell antigen receptor. *Cell* **70**, 585–593 (1992).
38. E. Bruyns, A. Marie-Cardine, H. Kirchgessner, K. Sagolla, A. Shevchenko, M. Mann, F. Autschbach, A. Bensussan, S. Meuer, B. Schraven, T cell receptor (TCR) interacting molecule (TRIM), a novel disulfide-linked dimer associated with the TCR–CD3–ζ complex, recruits intracellular signaling proteins to the plasma membrane. *J. Exp. Med.* **188**, 561–575 (1998).
39. K. Kemnitz, L. Pfeifer, R. Paul, F. Fink, A. Bergmann, Time- and space-correlated single-photon-counting spectroscopy. *SPIE Proc.* **2628**, 2–11 (1995).
40. K. Kemnitz, L. Pfeifer, R. Paul, M. Coppey-Moisan, Novel detectors for fluorescence lifetime imaging on the picosecond time scale. *J. Fluoresc.* **7**, 93–98 (1997).
41. J. Lakowicz, *Principles of Fluorescence Spectroscopy* (Springer, New York, ed. 3, 2006).
42. S. P. Laptenok, J. W. Borst, K. M. Mullen, I. H. M. van Stokkum, A. J. W. G. Visser, H. van Amerongen, Global analysis of Förster resonance energy transfer in live cells measured by fluorescence lifetime imaging microscopy exploiting the rise time of acceptor fluorescence. *Phys. Chem. Chem. Phys.* **12**, 7593–7602 (2010).
43. J. W. Borst, S. P. Laptenok, A. H. Westphal, R. Kühnemuth, H. Hornen, N. V. Visser, S. Kalinin, J. Aker, A. van Hoek, C. A. M. Seidel, A. J. W. G. Visser, Structural changes of Yellow Cameleon domains observed by quantitative FRET analysis and polarized fluorescence correlation spectroscopy. *Biophys. J.* **95**, 5399–5411 (2008).
44. W. Schubert, B. Bonnekoh, A. J. Pommer, L. Philipsen, R. Böckelmann, Y. Malykh, H. Gollnick, M. Friedenberger, M. Bode, A. W. Dress, Analyzing proteome topology and function by automated multidimensional fluorescence microscopy. *Nat. Biotechnol.* **24**, 1270–1278 (2006).

Acknowledgments: We thank T. Beyer for critically reading the manuscript and for the helpful discussions and J. Rudolph for performing densitometric analysis and preparing Fig. 6. **Funding:** This work was supported by collaborative research grants (SFB854, FOR521) from the German Research Society (DFG) to B.S., J.A.L., M.G., P.R., L.S., R.H., and W.Z., as well as a research grant from the State of Saxony-Anhalt (FKZ: XN0050KL/0206) to B.S. B.S. and J.A.L. are members of the SYBILLA consortium [EU 7FP] and the Magdeburg Center for Systems Biology (MaCS). Further support was provided by the Federal Ministry of Education and Research (BMBF), FKZ 13N10077, to W.Z., and the Austrian Science Fund through the EUROCORES Euromembrane program LIPIDPROD I0030 and the Erwin Schroedinger scholarship program to H.S. **Author contributions:** A.S., S.G., and R.H. performed the FLIM experiments; R.H., Y.P., and W.Z. designed and constructed the FLIM setup and analyzed the FLIM data; W.P. and H.S. provided the biosensor contructs; L.S. and M.P. performed the biochemical analysis of the Lck immunoprecipitates with the anti-Src family pY416 antibody in Fig. 5A; L.P. and P.R. analyzed the MELK data in Fig. 5, B and C; C.M. performed the functional analysis of Lck-reconstituted cells and the in vitro kinase assays in Fig. 6; and T.H., R.H., J.A.L., M.G., and B.S. designed the experiments and wrote the manuscript. **Competing interests:** The authors declare that they have no competing interests. **Data and materials availability:** Use of the plasmids encoding fluorescently tagged proteins requires a materials transfer agreement.

Submitted 13 September 2012
Accepted 31 January 2013
Final Publication 19 February 2013
10.1126/scisignal.2003607
Citation: A. Stirnweiss, R. Hartig, S. Gieseler, J. A. Lindquist, P. Reichardt, L. Philipsen, L. Simeoni, M. Poltorak, C. Merten, W. Zuschratter, Y. Prokazov, W. Paster, H. Stockinger, T. Harder, M. Gunzer, B. Schraven, T cell activation results in conformational changes in the Src family kinase Lck to induce its activation. *Sci. Signal.* **6**, ra13 (2013).

Appendix 07

Arndt B, Mateusz Poltorak, Bhavani S. Kowtharapu, **Peter Reichardt**, Lars Philipsen, Jonathan A. Lindquist, Burkhart Schraven and Luca Simeoni. Analysis of TCR activation kinetics in primary human T cells upon focal or soluble stimulation.
J Immunol Meth 2013; 387:276-83

IF: 2.2

Journal of Immunological Methods 387 (2013) 276–283

Contents lists available at SciVerse ScienceDirect

Journal of Immunological Methods

journal homepage: www.elsevier.com/locate/jim

Research paper

Analysis of TCR activation kinetics in primary human T cells upon focal or soluble stimulation

Boerge Arndt [a,1,2], Mateusz Poltorak [a,2], Bhavani S. Kowtharapu [a,2,3], Peter Reichardt [a], Lars Philipsen [a], Jonathan A. Lindquist [a], Burkhart Schraven [a,b], Luca Simeoni [a,*]

[a] Otto-von-Guericke University, Institute of Molecular and Clinical Immunology, Leipziger Str. 44, 39120 Magdeburg, Germany
[b] Department of Immune Control, Helmholtz Centre for Infection Research, Inhoffenstrasse 7, Braunschweig 38124, Germany

ARTICLE INFO

Article history:
Received 24 September 2012
Received in revised form 14 November 2012
Accepted 14 November 2012
Available online 22 November 2012

Keywords:
T-cell activation
Signaling signature
Antibody stimulation
Physiological stimuli
Erk dynamics
TCR-mediated signaling

ABSTRACT

Signaling through the TCR is crucial for the generation of different cellular responses including proliferation, differentiation, and apoptosis. A growing body of evidence indicates that differences in the magnitude and the duration of the signal are critical determinants in eliciting cellular responses. Here, we have analyzed signaling dynamics induced upon TCR ligation in primary human T cells. We used CD3 antibodies either cross-linked in solution (sAbs) or immobilized on microbeads (iAbs), two widely employed methods to stimulate T cells *in vitro*. We show that classical sAbs stimulation induces a transient and abortive response, whereas iAbs induce sustained TCR-mediated signaling, resulting in productive T-cell responses previously observed only in antigen-specific murine systems. In summary, our analysis documents TCR signaling kinetics and suggests that iAbs are better suited for studying TCR-mediated signaling as they mimic antigen specific systems.

1. Introduction

Triggering of the T cell receptor (TCR) by pathogens activates an intricate network of signaling cascades that are both temporally and spatially regulated. These signaling events will lead to transcriptional activation, proliferation, and differentiation of T cells that will ultimately culminate in an immune response. Defects in signal transduction may lead to either T-cell hyperresponsiveness or impaired T-cell activation, which results in autoimmunity or immunodeficiency, respectively. Thus, the study of how TCR signaling is initiated, propagated, and translated into a cellular response is important for the understanding not only of physiological processes, but also of the molecular mechanisms underlying human diseases.

To reproduce *in vitro* the signaling events occurring during physiological T-cell activation, immunologists need to pay particular attention in the choice of an appropriate stimulus. *In vivo*, T cells are activated upon contact with APCs expressing the agonistic peptide in the context of MHC-molecules. Therefore, the ideal method to activate T cells *in vitro* e.g. for biochemical analyses should mimic these conditions. Antigen-based systems, however, can only be used for the *in vitro* stimulation of monoclonal T-cell populations expressing a specific TCR, usually expressed on transgenic T cells, and are thus limited to mouse models.

Methods such as artificial antigen-presenting systems employing both cell-based and acellular technologies have been developed and are now being used to different extents in immunotherapy (Kim et al., 2004). However, to assess biochemical events during T-cell activation, soluble polyclonal stimuli such as agonistic antibodies against the TCR/CD3 complex, the co-receptors and/or the co-stimulatory molecules (i.e. CD4, CD28) are still largely used. For more than 30 years, this method has been extensively employed and indeed, has provided significant insight into the molecular

* Corresponding author. Tel.: +49 391 67 17894; fax: +49 391 6715852.
E-mail address: luca.simeoni@med.ovgu.de (L. Simeoni).
[1] Present address: Diabetes Centre, Department of Medicine Innenstadt, Ludwig-Maximilian University, 80336 Munich, Germany.
[2] B.A., M.P., and B.S.K. contributed equally to this work.
[3] Present address: Vectorology and Experimental Gene Therapy, University of Rostock, 18057 Rostock, Germany.

0022-1759/$ – see front matter © 2012 Elsevier B.V. All rights reserved.
http://dx.doi.org/10.1016/j.jim.2012.11.006

events occurring during T-cell activation. However, stimulations with soluble ligands have clear limitations, as they fail to reproduce the extra dimension of a cell–cell contact and, more importantly, they do not induce T-cell responses (Berg et al., 1998; Wang et al., 2008). Thus, it is questionable whether TCR signaling induced upon stimulation with soluble Abs mirrors the physiologic signaling cascade leading to productive T-cell responses. Moreover, it appears somehow surprising that, despite the availability of tools that trigger T-cell activation, mimic APCs, and induce proliferation, the analyses of intracellular signaling pathways are still mainly performed by applying soluble ligands.

Alternative method of T-cell stimulation is based on microbeads coated with the same antibodies against TCR complex is an efficient tool that can be used to expand T cells *ex vivo* especially for immunotherapeutic applications (Levine et al., 1997; Garlie et al., 1999; Trickett and Kwan, 2003). It is generally believed that sAbs and iAbs have different functional properties. However, a comprehensive functional and biochemical characterization of the two widely employed methods to stimulate human T cells *in vitro* has not yet been performed. Additionally, it has also not yet been analyzed which of the two stimuli more closely mimics physiological stimulation and hence is more suitable for signaling studies. Therefore, we performed a systematic analysis of the signaling signatures induced by Abs against the TCR complex either cross-linked in solution (sAbs) or immobilized on microbeads (iAbs). Our analysis documents signaling kinetics and functional responses of iAbs and shows that they are better suited than sAbs for studying TCR-mediated signaling.

2. Materials and methods

2.1. Human ethics

Approval for these studies involving the analysis of TCR-mediated signaling in human T cells was obtained from the Ethics Committee of the Medical Faculty at the Otto-von-Guericke University, Magdeburg, Germany with the permission number [107/09]. Informed consent was obtained in writing in accordance with the Declaration of Helsinki.

2.2. Cell purification

Peripheral blood mononuclear cells were isolated by Ficoll gradient (Biochrom) centrifugation of heparinized blood collected from healthy volunteers. Total population of human T cells or $CD4^+$ naïve and memory subpopulations were further purified by non-T cell depletion using specific T cell isolation kits (Miltenyi Biotec). The purity of T cells, determined by flow cytometry, was usually more than 96%.

OT-II TCR transgenic or wild type mouse T cells were isolated using a Pan T-cell Isolation Kit and AutoMacs magnetic separation system (Miltenyi Biotec). APCs were prepared as follows: T and NK cells were stained using FITC-labeled CD3, CD4, CD8, and NK1.1 mAbs (BD Biosciences). After staining, T and NK cells were depleted using anti-FITC microbeads on an AutoMacs magnetic separation system. The remaining splenic cell suspension was used as APCs.

2.3. T-cell stimulation

After isolation, human T cells were cultured overnight in RPMI 1640 medium containing 10% FCS (PAN Biotech) and 2 μg/ml Ciprobay (Bayer Schering Pharma). Successively, T cells were stimulated with either soluble or immobilized mAbs as follows. For soluble Ab stimulation, 2×10^6 cells were loaded with 10 μg/ml biotinylated anti-human CD3 (clone UCHT1, eBioscience) alone or in combination with 10 μg/ml biotinylated anti-human CD28 (clone CD28.2, eBioscience), and 10 μg/ml biotinylated anti-human CD4 (clone OKT4, eBioscience) mAbs as indicated in 100 μl RPMI 1640 and for 15 min on ice. After washing, receptors were cross-linked by adding 25 μg/ml NeutrAvidin™ (Pierce). For microbead stimulation, SuperAvidin™-coated polystyrene microspheres (Ø~10 μm, Bangs Laboratories) were coated with biotinylated CD3 alone or in combination with CD28 and CD4 mAbs as indicated (10 μg/ml each) for 30 min at 37 °C in PBS. Antibody-coated microbeads were washed twice with PBS, resuspended in RPMI 1640 and incubated with T cells in a 1:1 ratio. Stimulation of T cells was facilitated and synchronized by centrifugating samples for about 10 s at 1000 rpm. Biotinylated IgG_{2a} and IgG_1 mouse immunoglobulins (eBioscience) were used as a control. Stimulation with plate-bound antibodies was performed as follows. 10 μg/ml of CD3 and 10 μg/ml CD28 Abs were coated on U-bottomed 96-well plates for 2 h at 37 °C. After washing, 1×10^6 cells were added to the plates, rapidly centrifuged at 1000 rpm and incubated at 37 °C for the indicated time points.

Mouse T cells were stimulated with either soluble or immobilized βTCR×CD28 mAbs and processed as described above. For stimulations, 10 μg/ml of soluble or immobilized βTCR (clone H57-597, BD Biosciences) and CD28 (clone 37.51, BD Biosciences) mAbs were used. OT-II TCR transgenic T cells (1×10^6) were stimulated with (2×10^6) APCs that were either left unloaded or loaded with 5 μg/ml of $OVA_{323-339}$ for the indicated period of time.

2.4. Western blotting

T cells were lysed in buffer containing 1% lauryl maltoside (N-dodecyl β-maltoside), 1% NP-40, 1 mM Na_3VO_4, 1 mM PMSF, 10 mM NaF, 10 mM EDTA, 50 mM Tris pH 7.5, and 150 mM NaCl. Post-nuclear lysates were separated by SDS-PAGE and transferred onto nitrocellulose membranes. Membranes were probed with the indicated primary antibodies and the appropriate HRP-conjugated secondary antibodies (Dianova) and developed using the ECL detection system (Amersham Pharmacia). The following antibodies were used for Western blotting in this study: anti-phospho(p)-T^{202}/Y^{204} Erk1/2, anti-pY^{171}LAT, anti-pY^{783}PLC-γ1, anti-pS^{338}-c-Raf, anti-$pS^{217/221}$MEK1/2 (all from Cell Signaling Technology), and anti-β-actin (clone AC-15) (Sigma-Aldrich). For quantifications of the Western blots, the intensity of the detected bands was acquired using the Kodak Image Station 2000R and analysis was performed using 1D ImageQuant software (Kodak).

2.5. In vitro assays

Proliferation experiments were carried out in 96-well plates (Costar). T cells were labeled with 2.5 μM CFSE (Molecular

Probes) for 10 min at 37 °C. After washing, 2×10^5 cells were seeded in a total volume of 200 µl to each well and cultured in RPMI (supplemented with 10% FCS and antibiotics). Human T cells were either left unstimulated or were stimulated with soluble or immobilized CD3 alone, CD3×CD28, and CD3×CD28×CD4 mAbs as indicated above (see T-cell stimulation). Mouse T cells were either left unstimulated or stimulated with 10 µg/ml of soluble or immobilized βTCR (clone H57-597, BD Biosciences) and CD28 (clone 37.51, BD Biosciences) mAbs. T cells were cultured for 72 h at 37 °C, 5% CO_2. Proliferation was assessed by CFSE dilution using a FACS-Calibur and the CellQuest software (BD Biosciences) or BD LSRFortessa, FACSDiva Software 6.1.3 (BD Biosciences), and FlowJo 7.6.5 (Tree Star, Inc.).

To measure proliferation of lymph node cells isolated from OT-II transgenic mice 1×10^5 cells/well were cultured for 2 days in RPMI 1640 medium (supplemented with 10% FCS, antibiotics, 2-ME) in U-bottom 96-well plates (Costar) in the presence of 2×10^5 T cell-depleted irradiated splenocytes from wild-type mice loaded with increasing amount of $OVA_{323-339}$ peptide. Cells were pulsed with 1 µCi [^{3}H]-thymidine per well during the last 8 h and harvested using a PHD cell harvester (Inotech AG, Basel, Switzerland). Thymidine incorporation was measured by liquid scintillation counting.

To determine T-cell activation, human T cells were stimulated as described above. After 24 h, T cells were stained with either FITC- or PE-labeled mAbs against CD25 and CD69 (BD Biosciences), respectively. Cell associated fluorescence was analyzed by flow cytometry.

To quantify cell survival under different stimulation conditions, human T cells were stimulated with either soluble or immobilized mAbs as described above, and resuspended in RPMI supplemented with 10% FCS at a density of 1×10^6 cells/ml in a 24-well tissue culture plate. Cells were harvested after 24 h and the percentage of cells undergoing apoptosis were measured by flow cytometry using FITC-annexin V and propidium iodide (PI) (rh annexin V/FITC kit; Bender MedSystems) according to manufacturer's instructions.

To measure the antibody binding capacity, 1×10^6 microbeads were coated with either CD3 alone or in combination with CD28 and CD4 mAbs as described above. Subsequently, microbeads were washed and stained with FITC-conjugated anti-mouse antibody (Jackson ImmunoResearch Laboratories). Beads associated fluorescence was analyzed by flow cytometry.

2.6. T cell/microbead binding

Primary human T cells were mixed with the CD3×CD28 coated microbeads in a 1:1 ratio, rapidly centrifuged at 1000 rpm and incubated at 37 °C for the indicated time points in a 3 ml round-bottom tube. Subsequently, the samples were gently resuspended in 500 µl PBS and analyzed on a FACS Calibur. Microbeads coated with IgG_{2a} and IgG_1 were used as a control. T cell/microbead conjugates were also counted by using a hemocytometer. Single-cell imaging was done on a Leica microscope equipped with a 20× imaging system from Visitron Systems Imaging GmbH.

2.7. Florescence microscopy

Cell stimulation was performed as indicated above. Subsequently, cells were transferred to PLL-coated cover slides and allowed to settle down for 10 min at 4 °C before fixation with 2% para-formaldehyde. The samples were permeabilized with 0.2% TritonX100 for 10 min and blocked with 1% BSA for 30 min. Cell conjugates were stained with propidium iodide (Sigma Aldrich) and anti-pY^{142}CD3ζ-Alexa488 antibody (BD Pharmigen), and placed on the stage of an inverted wide-field fluorescence microscope (Leica DM IRE2; 63× oil lens NA 1.40). The fluorescent signals and the corresponding phase contrast image were acquired by a cooled charge-coupled device camera (Apogee KX4; Apogee Instruments, Roseville, CA, 2× binning). Fluorescence images were corrected for illumination faults using flat-field correction.

3. Results

3.1. iAbs induce activation and proliferation, whereas, sAbs result in T-cell unresponsiveness

It is generally accepted that soluble antibodies cannot induce productive T-cell responses. Indeed, we and others

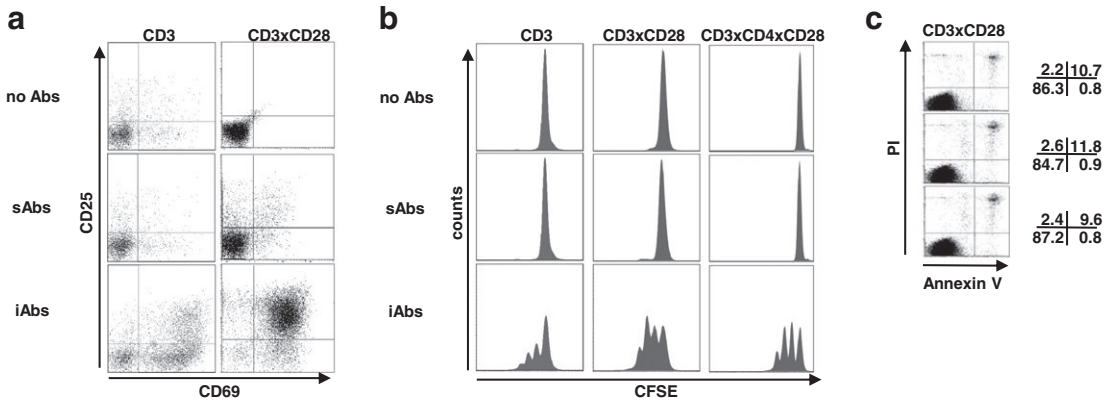

Fig. 1. Analysis of the functional effects of sAbs and iAbs. Purified human T cells were treated as indicated. (a) 24 h after stimulation, the activation of T cells was analyzed by staining with CD25 and CD69 and flow cytometry. (b) T cells were labeled with CFSE and stimulated as indicated. Proliferation was assessed after 72 h by analyzing CFSE content on a FACS Calibur. (c) T cells were stimulated as indicated for 24 h. Cell survival was assessed by FITC-annexin V and PI staining. One representative experiment of at least three independent experiments is shown. Numbers in c indicate the proportion of cells in each quadrant.

have demonstrated that OT-I transgenic T cells and cytotoxic T-lymphocyte clones are not activated and do not differentiate upon stimulation with antibodies cross-linked in suspension (Berg et al., 1998; Wang et al., 2008). Here, we have stimulated primary human T cells with either sAbs or iAbs and analyzed their functional responses. Fig. 1 shows that treatment of T cells with iAbs led to an expression of CD25 and CD69 and to a proliferative response. Conversely, treatment with sAbs (CD3 alone or in combination with CD28) failed to induce T-cell activation as indicated by the absence of CD69 and CD25 expression (Fig. 1a). In agreement with these data, proliferation assays revealed that T cells stimulated with sAbs (CD3 alone or in combination with CD28 and CD4) also did not proliferate (Fig. 1b).

To exclude the possibility that the lack of proliferation depends on the particular clone of antibody used for stimulation, we repeated the experiments depicted in Fig. 1 using two other CD3 mAbs of different Ig classes (OKT3 and MEM92). Moreover, we also tested different concentrations of soluble anti-CD3 (UCHT-1) (ranging from 0.1 μg/ml to 10 μg/ml) together with various concentrations of anti-CD28 (ranging from 0.1 μg/ml to 10 μg/ml) in different ratios in the presence or absence of anti-CD4. Under all conditions tested, human T cells did not proliferate in response to stimulation with cross-linked soluble Abs (Fig. 1b, Supplementary Fig. 1, and data not shown).

Finally, similar to human T cells, also the stimulation of mouse T cells with TCRβ×CD28 mAbs immobilized on microbeads resulted in proliferation, whereas, stimulation with the same antibodies cross-linked in suspension did not induce productive T-cell response (Supplementary Fig. 2). Similar stimulation conditions also failed to induce proliferation in OT-I transgenic T cells (Wang et al., 2008).

We have previously shown that cross-linked soluble CD3×CD8 antibodies induce apoptosis rather than proliferation in OT-I TCR transgenic $CD8^+$ mouse T cells (Wang et al., 2008). To analyze whether stimulation of human T cells with sAbs may also induce apoptosis, peripheral T cells were stimulated overnight and assayed for annexin V expression. Fig. 1c shows that, in contrast to mouse, stimulation of human T cells with sAbs did not induce apoptosis. Thus, despite the fact that sAbs are commonly used to activate proximal and distal TCR-mediated signaling pathways, they are unable to induce productive T-cell activation and proliferation.

3.2. iAbs efficiently stimulate T cells

To date, little is known about the signaling properties of mAbs coated to microbeads. We initially established a protocol to efficiently stimulate T cells with iAbs. For stimulation, we employed 10 μm microbeads that were coated with SuperAvidin. This gives the possibility to bind any biotin-labeled antibody or recombinant protein on the surface of the microbeads. For this investigation, we used biotinylated CD3ε and CD28 mAbs unless indicated otherwise. Microbeads were coated with 10 μg/ml biotinylated CD3 and CD28 mAbs. Microbeads loaded with non-relevant antibodies of the same isotype were used as control. To induce rapid and synchronous cell contact with the beads, we performed a brief centrifugation (5 s at 1000 rpm) in a small volume (100 μl). Aliquots of the samples were taken at regular time intervals and analyzed on a FACS Calibur. Fig. 2a shows that T cells and microbeads have clearly different physical parameters and can be easily visualized in FSC/SSC dot plots. The data also demonstrate that a significant number of cells associated with microbeads coated with CD3×CD28 Abs and appeared as a new population indicated in the gate R_{Tc+m} (Fig. 2b). Conversely, in the control samples the emergence of a new population in the R_{Tc+m} gate is not detected (Fig. 2b, upper panels), thus indicating that microbeads loaded with isotype controls do not bind to T cells. Successively, to quantify T cell-microbead association, we calculated the ratio R_a of the number of T cell/microbead conjugates (events in the R_{Tc+m} gate) to the total number of T cells (events in the R_{Tc} gate). We found that a high fraction of the cells was in contact with microbeads already after 5 min incubation, with R_a approximately 0.2 (Fig. 2c). After 15 min incubation, the proportion of T cells in contact with microbeads increased up to 50% ($R_a = 0.5$). Afterwards, the R_a slightly decreased and stabilized at values close to 0.3. A similar association rate between Jurkat T cells and CD3-coated micrometric particles has been recently described (Carpentier et al., 2009). To further address this issue and to check whether mechanical stress during flow cytometry measurements resulted in the disruption of T cell/bead conjugates, we performed additional analyses. We initially assessed cell/bead conjugates using light microscopy (Fig. 2d). We found that a high number of T cells rapidly established contact with iAbs. We next quantified cell/bead conjugates by manual counting in a hemocytometer. The data depicted in Fig. 2e show that around 50–70% of the cells conjugate with beads. As the proportion of T cell/microbead conjugates was slightly higher than this presented in Fig. 2c, this suggests that some contacts with beads were lost during flow cytometry. Collectively, these data demonstrate that a very high number of iAbs interact with T cells, thus ensuring a focal stimulation.

Additionally, we have analyzed formation of signaling microclusters in the T cell/bead contact zone by fluorescence microscopy. As shown in Supplementary Fig. 3, both physiological and iAbs stimulation induce the formation of signaling microclusters.

We next quantified the effectiveness of the stimulation by analyzing the proportion of cells displaying phosphorylated Erk1/2. The data presented in Fig. 2f confirmed that the cell/bead contact indeed resulted in T-cell stimulation as the proportions of T cells in contact with beads and those displaying intracellular phospho-Erk1/2 were similar. Similar proportions of activated T cells were also obtained upon stimulation with sAbs (Fig. 2g). Thus, the efficiency of iAbs and sAbs in stimulating T cells appears to be comparable.

Next, we have measured fluorescence of beads loaded with either CD3 alone or CD3×CD28 and CD3×CD4×CD28 to analyze binding capacity of microbeads. We have observed a consistent increase in the fluorescence of beads loaded with single vs. beads loaded with multiple mAbs. These data indicate that the coating with CD3 and CD3×CD28 mAbs are not sufficient to saturate the microbeads (Supplementary Fig. 4).

3.3. Sustained versus transient activation kinetics in TCR-mediated signaling induced by iAbs and sAbs, respectively

As sAbs and iAbs induce markedly different cellular outcomes, we next performed a comparative analysis of

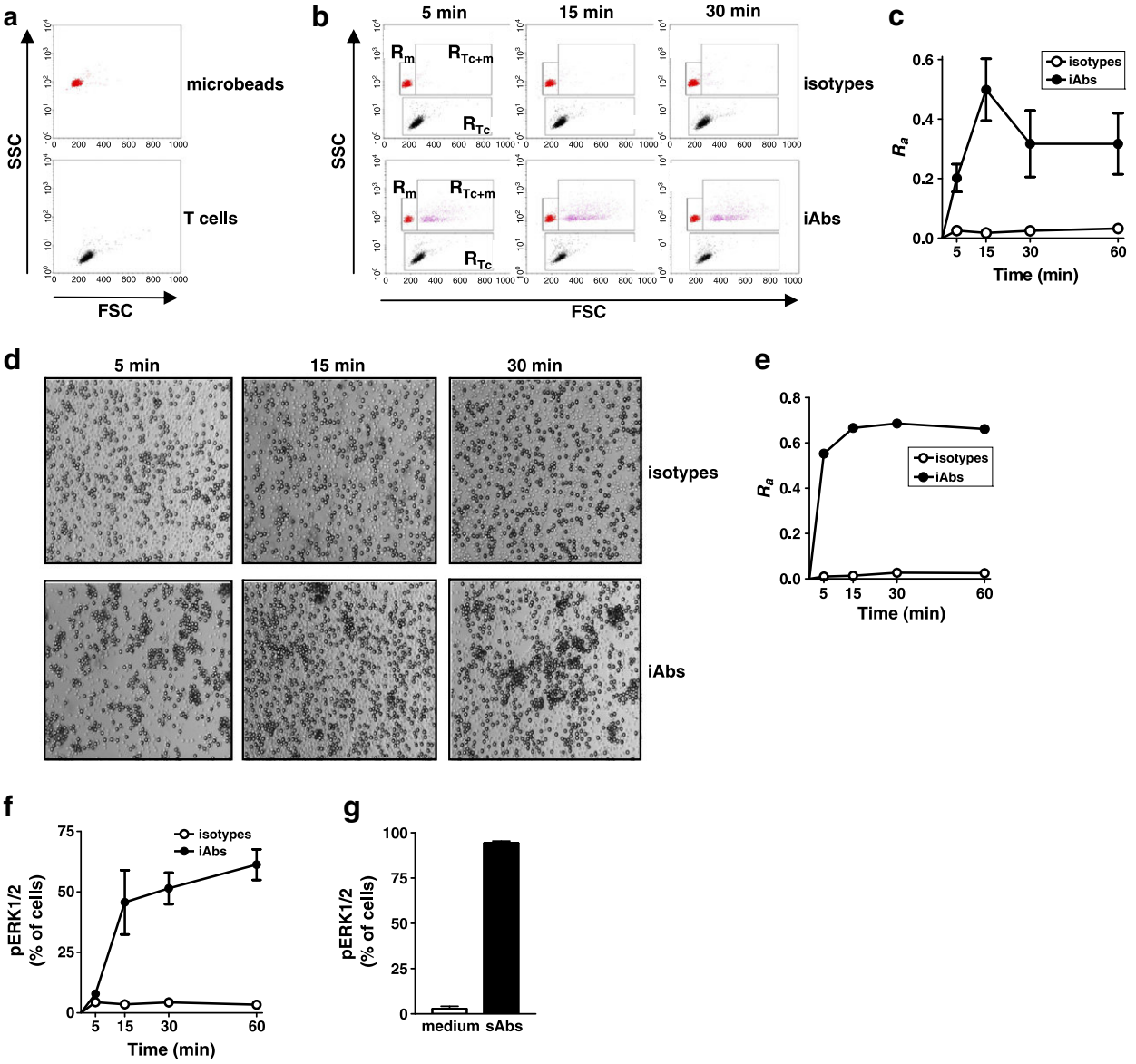

Fig. 2. Analyses of the T cell/microbead binding. (a) T cells and microbeads alone were analyzed by side scattering versus forward scattering dot plots. (b) Subsequently, T cells and microbeads loaded either with isotype controls (isotypes, upper panels) or CD3 × CD28 mAbs (iAbs, lower panels) were brought into contact for the indicated time periods. T cell/microbead conjugates (RTc + m) are clearly distinct from free T cells (RTc) and microbeads (Rm). (c) Statistical analysis of the ratio (R_a) between the numbers of T cell/microbead conjugates (events in the RTc + m gate) to the total number of unconjugated T cells (events in the RTc gate) is presented. (d) Transmission light images of T cells incubated with microbeads loaded either with isotype controls (isotypes, upper panels) or CD3xCD28 mAbs (iAbs, lower panels) are shown. (e) T cell/microbead conjugates were diluted and manually counted in a hemocytometer. The graph shows statistical analysis of the ratio (R_a) between the numbers of T cell/microbead conjugates to the total number of T cells from three independent experiments. Human T cells were purified and stimulated with beads loaded either with CD3xCD28 mAbs (iAbs) or isotype control (isotypes) for the indicated time points. (f) The level of pErk1/2 as marker of activation was measured by intracellular staining. Data represent the mean proportions of pErk1/2 positive cells ± SEM of 3 independent experiments. (g) Human T cells were purified and either left unstimulated (medium) or were treated with CD3 × CD28 mAbs cross-linked in solution (sAbs) for 2 min. The graph shows the mean proportions of pErk1/2 positive cells ± SEM from 3 independent experiments.

their signaling signatures in primary human T cells. We found that the magnitude and the duration of the signal induced by iAbs were strikingly different to those induced by sAbs (Fig. 3). Indeed, stimulation with sAbs (CD3 alone or in combination with CD28 or CD4) resulted in strong and transient activation of molecules involved in TCR-mediated proximal signaling, such as LAT and PLCγ1, whereas iAbs stimulation led to weaker but sustained phosphorylation (Fig. 3a). As an example of downstream pathway activated via the TCR, we investigated the phosphorylation levels of molecules in the Ras-Erk signaling cascade. Despite the fact that the magnitude of the phosphorylation of c-Raf, MEK1/2, and Erk1/2 appeared to be comparable in both types of stimulation, their activation was sustained upon iAbs treatment (Fig. 3a). Similar activation kinetics were also observed when purified mouse splenic T cells were stimulated with

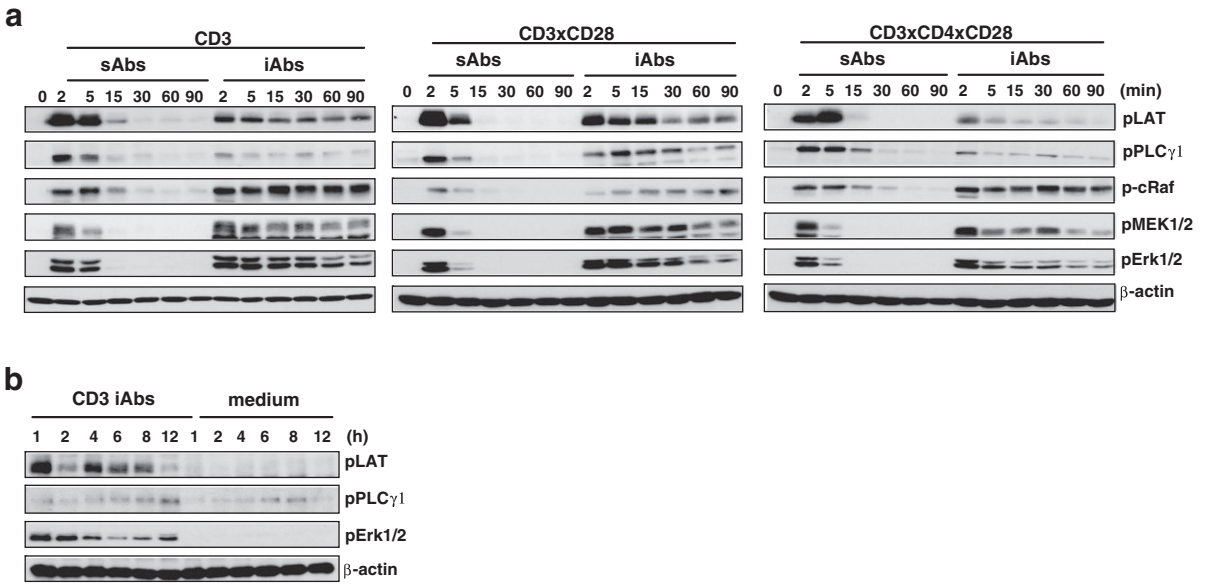

Fig. 3. sAbs induce transient, whereas, iAbs induce sustained signaling. (a,b) Purified human T cells were treated with either soluble (sAbs) or immobilized (iAbs) mAbs as indicated. Samples were analyzed by Western blotting using the indicated Abs. For each condition one representative immunoblot of at least 4 independent experiments is shown.

TCRβ × CD28 Abs immobilized on microbeads or cross-linked in solution (Supplementary Fig. 5), suggesting that TCR-mediated signaling induced by antibodies immobilized on beads is not dependent on the antibody clones used for stimulation.

Next, we compared activation kinetics of purified naïve and memory $CD4^+$ T cells upon stimulation with sAbs and iAbs. Similar to unfractionated T cells, both $CD4^+$ T-cell subsets displayed a transient activation upon sAbs stimulation, but sustained signaling upon treatment with iAbs (Supplementary Fig. 6). Thus, it appears that the signaling signatures of sAbs and iAbs are independent of the differentiation status of the cells.

Finally, we analyzed the signaling signatures induced by plate-bound antibodies, which also induce T-cell activation and proliferation. As shown in Supplementary Fig. 7, we found that plate-bound Abs have signaling kinetics similar to iAbs.

In summary, we show that stimulation with sAbs vs. iAbs induces different activation kinetics of both TCR proximal and distal signaling molecules. We believe that the duration of the signal may be the determinant factor for the generation of cellular responses.

3.4. Signaling dynamics induced by iAbs are similar to those induced by stimulation with APC

We next analyzed the signaling kinetics induced by physiological stimuli. We used $CD4^+$ T cells isolated from OT-II transgenic mice that were stimulated with APCs alone as control or with APCs loaded with the $OVA_{323–339}$ peptide. Stimulation with OVA-loaded APC proved to be effective method to generate productive response of OT-II transgenic T cells in the dose dependent manner (Fig. 4a). Fig. 4b shows that stimulation with peptide loaded APCs, but not with control APCs, induces sustained phosphorylation of LAT, PLCγ1, and Erk1/2 in OT-II transgenic T cells. These data further corroborate our previous observations showing that the stimulation of $CD8^+$ T cells from OT-I transgenic mice with physiological ligands also induced sustained phosphorylation of signaling molecules such as Erk1/2 and PLCγ-1 (Wang et al., 2008). It is important to note that, iAbs elicit effects that are comparable to those obtained with a physiological stimulation (Fig. 4 and (Wang et al., 2008)).

Collectively, these data show that stimulation of human T cells with immobilized Abs induces activation kinetics similar to those induced by physiological ligands in mouse TCR transgenic systems and that sustained activation of TCR signaling correlates with proliferation. In conclusion, it appears that iAbs mimic more closely physiological stimulation than sAbs and hence are better suited to study signaling correlating with productive T-cell responses.

4. Discussion

Current stimulation protocols to study T-cell signaling are mainly based on agonistic antibodies cross-linked in solution. This method has several advantages such as low costs, easy handling, high reproducibility, effective activation of signaling molecules, polyclonal activity and, most of all, it is well-characterized. However, despite its routine use to study signaling during T-cell activation, it is known that sAbs induce only a transient activation signal that results in an abortive response. Moreover, soluble antibodies do not reproduce the cell–cell contact induced by an APC and therefore fail to mimic at least one crucial event occurring during T-cell activation.

Here, we have analyzed whether Abs immobilized on microbeads, which mimic APCs and induce proliferation, represent an alternative and more suitable method to sAbs

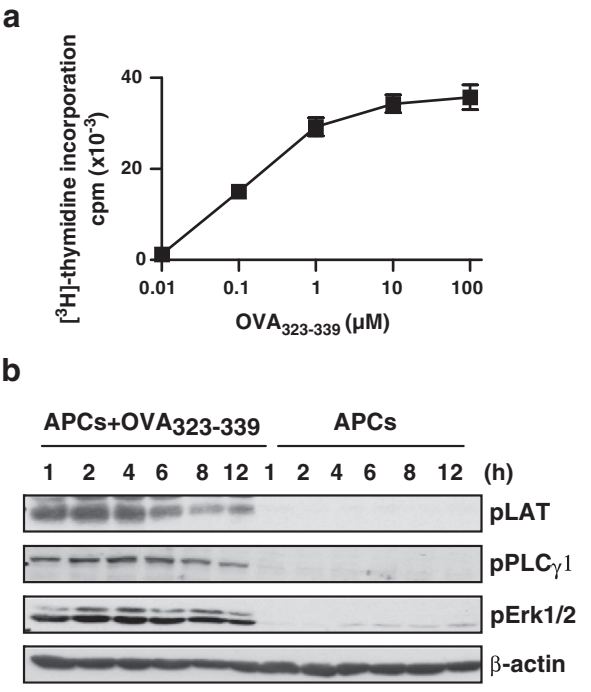

Fig. 4. OT-II transgenic T cells stimulated with OVA peptide present sustained activation dynamics. (a) Lymph node cells isolated from OT-II transgenic mice were stimulated in the presence of irradiated APCs pulsed with increasing amount of $OVA_{323–339}$ peptide. Proliferation was measured after 72 h. Data derive from 3 mice. (b) Purified mouse splenic OT-II transgenic T cells were stimulated with APCs either left unloaded or loaded with the agonist peptide $OVA_{323–339}$ for the indicated time points. Samples were analyzed by Western blotting using the Abs indicated.

for the stimulation of T cells for signaling studies. We further compared the kinetics of central signaling events induced by Abs immobilized on microbeads to those generated by Abs cross-linked in solution. We document profound signaling differences between these methods of stimulation.

One of the most important findings is that the sustained activation induced by iAbs recapitulated signaling events observed in antigen-specific systems. In fact, we show that T cells stimulated with APCs loaded with the OVA-peptide display similar activation kinetics as T cells stimulated with beads. Moreover, we have previously shown that H-$2K^b$ molecules loaded with the SIINFEKL peptide triggered prolonged activation of ZAP-70, LAT, PLCγ-1, and Erk1/2 and also induced proliferation in OT-I transgenic T cells (Wang et al., 2008).

In addition to the immobilization on beads, Abs can also be bound to cell culture plates. Similarly to iAbs, also plate-bound antibodies induce functional responses. Previous studies have shown that plate-bound, but not soluble CD3 Abs induce sustained TCR-mediated tyrosine phosphorylation and MAPK activation in murine CTL clones (Berg et al., 1998; Puente et al., 2000, 2006). However, the relevance of these studies is limited. They utilize $CD8^+$ T-cell clones, which were expanded in the presence of IL-2 and were stimulated with CD3 Abs alone in the absence of co-stimulation. Therefore, it is questionable whether these data also apply to primary human T cells. Conversely, in our studies we have provided an extensive biochemical characterization of signaling networks upon stimulation with either sAbs or iAbs in total human peripheral T cells as well as in naïve and memory $CD4^+$ T cells. To our knowledge similar studies describing the signaling properties of Abs immobilized either on beads or cell culture plates have not been performed. Despite the fact that both iAbs and plate-bound antibodies induce functional responses and likely similar signaling kinetics, antibodies immobilized on microbeads allow an easier handling of the samples during stimulation compared to plate-bound antibodies. Therefore, we believe that iAbs are a valid method of stimulation that allows easy and large scale biochemical analyses of TCR-mediated signaling events.

The availability of a method that mimics antigen-specific systems is of particular importance to study primary human T cells, which cannot be stimulated on a large scale by antigen-specific systems. Data from primary human T cells are still scarce and most of our knowledge on signaling in human T cells is based upon data obtained from the analysis of lymphoid cell lines that were stimulated with cross-linked soluble mAbs. Experiments employing primary human cells stimulated with more physiological systems are not only necessary to study the basis of T-cell function, but are also essential to understand the molecular mechanisms of human diseases such as autoimmunity and cancerogenesis.

In summary, our studies clearly show that iAbs are a valid alternative to sAbs for stimulation of T cells for signaling analysis. First, iAbs are easy and ready-to-use. Second, iAbs mimic signaling kinetics described in antigen-specific systems. Third, iAbs trigger signaling pathways correlating with T-cell activation and proliferation.

Acknowledgments

We are grateful to Tilo Bayer for critically reading the manuscript and helpful discussion and to Nicole Jüling, Ines Meinert, Stefanie Holze, and Guido Höbbel for their excellent technical assistance.

The work was supported by grants from the German Research Foundation (DFG), FOR-521 [SI861/1], GRK-1167 [TP12] and SFB-854 [TP19].

Appendix A. Supplementary data

Supplementary data to this article can be found online at http://dx.doi.org/10.1016/j.jim.2012.11.006.

References

Berg, N.N., Puente, L.G., Dawicki, W., Ostergaard, H.L., 1998. Sustained TCR signaling is required for mitogen-activated protein kinase activation and degranulation by cytotoxic T lymphocytes. J. Immunol. 161, 2919.

Carpentier, B., Pierobon, P., Hivroz, C., Henry, N., 2009. T-cell artificial focal triggering tools: linking surface interactions with cell response. PLoS One 4, e4784.

Garlie, N.K., LeFever, A.V., Siebenlist, R.E., Levine, B.L., June, C.H., Lum, L.G., 1999. T cells coactivated with immobilized anti-CD3 and anti-CD28 as potential immunotherapy for cancer. J. Immunother. 22, 336.

Kim, J.V., Latouche, J.B., Riviere, I., Sadelain, M., 2004. The ABCs of artificial antigen presentation. Nat. Biotechnol. 22, 403.

Levine, B.L., Bernstein, W.B., Connors, M., Craighead, N., Lindsten, T., Thompson, C.B., June, C.H., 1997. Effects of CD28 costimulation on long-term proliferation of CD4+ T cells in the absence of exogenous feeder cells. J. Immunol. 159, 5921.

Puente, L.G., Stone, J.C., Ostergaard, H.L., 2000. Evidence for protein kinase C-dependent and -independent activation of mitogen-activated protein kinase in T cells: potential role of additional diacylglycerol binding proteins. J. Immunol. 165, 6865.

Puente, L.G., He, J.S., Ostergaard, H.L., 2006. A novel PKC regulates ERK activation and degranulation of cytotoxic T lymphocytes: plasticity in PKC regulation of ERK. Eur. J. Immunol. 36, 1009.

Trickett, A., Kwan, Y.L., 2003. T cell stimulation and expansion using anti-CD3/CD28 beads. J. Immunol. Methods 275, 251.

Wang, X., Simeoni, L., Lindquist, J.A., Saez-Rodriguez, J., Ambach, A., Gilles, E.D., Kliche, S., Schraven, B., 2008. Dynamics of proximal signaling events after TCR/CD8-mediated induction of proliferation or apoptosis in mature CD8 + T cells. J. Immunol. 180, 6703.

Appendix 08

Schmidt Angelika, Nina Oberle, Eva-Maria Weiß, Diana Vobis, Stefan Frischbutter, Ria Baumgrass, Christine S. Falk, Mathias Haag, Britta Brügger, Hongying Lin, Georg W. Mayr, **Peter Reichardt**, Matthias Gunzer, Elisabeth Suri-Payer and Peter H. Krammer. Human regulatory T cells rapidly suppress T cel receptor-induced Ca2+s, NF-κB and NFAT signaling in conventional T cells
Sci Sign 2011;4(204):ra90.

IF: 7.6

IMMUNOLOGY

Human Regulatory T Cells Rapidly Suppress T Cell Receptor–Induced Ca^{2+}, NF-κB, and NFAT Signaling in Conventional T Cells

Angelika Schmidt,[1]* Nina Oberle,[1]* Eva-Maria Weiß,[1] Diana Vobis,[1] Stefan Frischbutter,[2] Ria Baumgrass,[2] Christine S. Falk,[3] Mathias Haag,[4] Britta Brügger,[4] Hongying Lin,[5] Georg W. Mayr,[5] Peter Reichardt,[6] Matthias Gunzer,[6] Elisabeth Suri-Payer,[1] Peter H. Krammer[1]†

$CD4^+CD25^{hi}Foxp3^+$ regulatory T cells (T_{regs}) are critical mediators of self-tolerance, which is crucial for the prevention of autoimmune disease, but T_{regs} can also inhibit antitumor immunity. T_{regs} inhibit the proliferation of $CD4^+CD25^-$ conventional T cells (T_{cons}), as well as the ability of these cells to produce effector cytokines; however, the molecular mechanism of suppression remains unclear. Here, we showed that human T_{regs} rapidly suppressed the release of calcium ions (Ca^{2+}) from intracellular stores in response to T cell receptor (TCR) activation in T_{cons}. The inhibition of Ca^{2+} signaling resulted in decreased dephosphorylation, and thus decreased activation, of the transcription factor nuclear factor of activated T cells 1 (NFAT1) and reduced the activation of nuclear factor κB (NF-κB). In contrast, Ca^{2+}-independent events in T_{cons}, such as TCR-proximal signaling and activation of the transcription factor activator protein 1 (AP-1), were not affected during coculture with T_{regs}. Despite suppressing intracellular Ca^{2+} mobilization, coculture with T_{regs} did not block the generation of inositol 1,4,5-trisphosphate in TCR-stimulated T_{cons}. The T_{reg}-induced suppression of the activity of NFAT and NF-κB and of the expression of the gene encoding the cytokine interleukin-2 was reversed in T_{cons} by increasing the concentration of intracellular Ca^{2+}. Our results elucidate a previously unrecognized and rapid mechanism of T_{reg}-mediated suppression. This increased understanding of T_{reg} function may be exploited to generate possible therapies for the treatment of autoimmune diseases and cancer.

INTRODUCTION

$CD4^+$ regulatory T cells (T_{regs}), which are characterized by high abundance of the surface marker CD25 and by the presence of the transcription factor Foxp3, play a pivotal role in the immune system and are involved in the prevention of autoimmune diseases and allergies (*1*). In addition to the beneficial functions of T_{regs} in graft-versus-host disease (GVHD) and in the prevention of organ pathology after infection, T_{regs} also lead to the unwanted dampening of immune responses, for example, in cancer (*2*). T_{regs} directly inhibit the proliferation of responder $CD4^+CD25^-$ conventional T cells (T_{cons}) and the production of effector cytokines by these cells (*3*). Some mechanisms of T_{reg}-mediated suppression have been described thus far (*4*, *5*). For example, adenosine 3′,5′-monophosphate (cAMP) inhibits the production of the cytokine interleukin-2 (IL-2) by murine T_{cons}. This study implied that cAMP was transferred from T_{regs} to T_{cons} to induce expression of the gene encoding the transcriptional repressor inducible cAMP early repressor (ICER), which in turn represses expression of the *Il2* gene encoding the cytokine IL-2 in T_{cons} (*6*). Various factors, such as location, inflammatory milieu, antigen load, cell number, and activation status of the responder cells, influence the mechanism of T_{reg}-mediated immune regulation in vivo (*4*). Furthermore, species differences regarding T_{reg} function have been found. For example, the immunosuppressive cytokine IL-35 is produced by murine T_{regs} but is not constitutively produced by human T_{regs} (*7*, *8*). Therefore, we sought to clarify the inhibitory mechanism(s) in vitro and investigated the direct suppression of primary human T_{cons} by T_{regs}.

We hypothesized that T_{regs} might disrupt a key component of T cell receptor (TCR) signaling and that such disruption could perturb the function of T_{cons}. Thus far, the influence of T_{regs} on signaling events in suppressed T_{cons} has not been investigated extensively. Stimulation of the TCR initially leads to the activation of the Src family kinase leukocyte-specific protein tyrosine kinase (Lck), which phosphorylates tyrosine residues in CD3, ζ chain–associated protein kinase of 70 kD (ZAP-70), and other substrates. This initiates signaling cascades that lead to the activation of transcription factors crucial for the expression of genes involved in T cell activation and proliferation. Central transcription factors that induce the expression of genes encoding cytokines are nuclear factor κB (NF-κB), nuclear factor of activated T cells (NFAT), and activator protein 1 (AP-1) (*9*). The AP-1 pathway depends on the activation of mitogen-activated protein kinases (MAPKs), such as extracellular signal–regulated kinase (ERK), c-Jun N-terminal kinase (JNK), and p38, which promote the synthesis, phosphorylation, and activation of the Fos and Jun proteins that together comprise the AP-1 transcription factor (*10*). Activation of both NF-κB and NFAT requires the activity of phospholipase C–γ1 (PLC-γ1), which generates the second messengers diacylglycerol (DAG) and inositol 1,4,5-trisphosphate (IP_3). DAG leads to activation of protein kinase C θ (PKCθ), which, in turn, activates the inhibitor of κB (IκB) kinase (IKK) complex, resulting in the phosphorylation and degradation of IκBα and the translocation of

[1]Division of Immunogenetics (D030), Tumor Immunology Program, German Cancer Research Center (DKFZ), 69120 Heidelberg, Germany. [2]Deutsches Rheuma-Forschungszentrum, a Leibniz Institute, 10117 Berlin, Germany. [3]Institute for Transplant Immunology, OE 8889, Hannover Medical School, 30625 Hanover, Germany. [4]Heidelberg University Biochemistry Center, 69120 Heidelberg, Germany. [5]Institut für Biochemie und Signaltransduktion, University Medical Center Hamburg-Eppendorf, 20246 Hamburg, Germany. [6]Institute of Molecular and Clinical Immunology, Otto-von-Guericke-University-Magdeburg, 39120 Magdeburg, Germany.
*These authors contributed equally to this work.
†To whom correspondence should be addressed. E-mail: P.Krammer@dkfz.de

the NF-κB p50:p65 heterodimer to the nucleus (*11*). IP_3 induces an increase in the concentration of cytoplasmic calcium (Ca^{2+}) and activation of the Ca^{2+}-dependent phosphatase calcineurin, which results in the rapid dephosphorylation and activation of NFAT, which is followed by its translocation to the nucleus (*12*). Ca^{2+} is critically involved not only in the activation of NFAT but also in the activation of NF-κB, because Ca^{2+} channel blockers, as well as other agents that prevent Ca^{2+} influx, inhibit the activation of NF-κB (*13*, *14*). Indeed, Ca^{2+} may lead to the activation of NF-κB signaling by inducing the degradation of IκBα (*15*, *16*). A previous study showed that murine T_{cons} deficient in both NFAT1 and NFAT4 are less susceptible to T_{reg}-mediated suppression than are their wild-type counterparts (*17*); however, TCR signaling and the subsequent activation of the transcription factors NFAT, NF-κB, and AP-1 in suppressed T_{cons} have not been analyzed so far.

We previously showed that suppression of the expression of cytokine-encoding genes by human T_{regs} is a rapid process (*18*). Here, we describe that this suppressive effect was persistent in T_{cons} even after the removal of T_{regs} from the coculture. To analyze this rapid suppression in more detail, we compared TCR signaling in suppressed and nonsuppressed T_{cons} by focusing on the signaling events immediately after TCR stimulation. We found that TCR-proximal signals as well as activation of PLC-γ1 were not altered in suppressed T_{cons}, whereas Ca^{2+}, NF-κB, and NFAT signaling pathways were strongly inhibited. An increase in intracellular Ca^{2+} concentrations in T_{cons} abrogated the T_{reg}-mediated suppression of NFAT and NF-κB activation as well as of the expression of *IL2*. These results suggest that suppression of Ca^{2+} signals appears to be a crucial event in the T_{reg}-mediated suppression of T_{cons}.

RESULTS

Suppression of T_{cons} is sustained upon removal of T_{regs}

To study T_{reg}-mediated suppression of T_{cons} in detail, we analyzed primary human responder T_{cons} from cocultures with T_{regs} (suppressed T_{cons}) and, as a control, responder T_{cons} from cocultures with T_{cons} (control T_{cons}) (Fig. 1A). The frequent human leukocyte antigen (HLA) serotype HLA-A2, which belongs to the major histocompatibility complex (MHC) class I proteins, was used as a cell surface marker to differentiate between the two populations of cells in the coculture. By the use of HLA-A2–disparate cells from HLA-A2–disparate donors in the coculture, we were able to reisolate pure populations of responder T_{cons} after coculture and, thus, to compare signaling in suppressed T_{cons} and control T_{cons}. All experiments were set up as described (Fig. 1A) with pre-activated T_{regs}, unless stated otherwise, and were controlled by determining the extent of inhibition of expression of *IL2* and *IFNg* [which encodes the proinflammatory cytokine interferon-γ (IFN-γ)] through measurement of the amounts of their mRNAs in suppressed T_{cons} and comparing them to those of control T_{cons}. As shown previously (*18*), we detected the inhibition of *IL2* and *IFNg* expression within 3 hours of TCR stimulation in suppressed T_{cons} (Fig. 1A). Within that time frame, either pre-activated or resting T_{regs} suppress cytokine mRNA production to a similar extent (*18*).

We were interested in how rapidly T_{regs} could exert suppression and whether T_{cons} remained suppressed after removal of the T_{regs}. Therefore, we used another coculture system (Fig. 1B), in which we cocultured T_{cons} with pre-activated T_{regs} (or with T_{cons} as control) for 10, 30, 45, and 60 min without TCR stimulation and tested whether this short coculture period was sufficient to suppress the T_{cons}. After the coculture period, T_{cons} were isolated on the basis of their distinct HLA-A2 and were stimulated separately, without T_{regs}, for 3 hours through the TCR to induce the expression of cytokine-encoding genes. We observed that *IL2* and *IFNg* expression in suppressed T_{cons} was inhibited compared to that in control T_{cons} after a coculture period of 30 to 45 min (Fig. 1B). Suppression of cytokine secretion by T_{cons} was retained upon removal of the T_{regs}, whereas inhibition of proliferation was not sustained (fig. S1). Even when the TCR stimulus was provided 24 hours after a short coculture period, the abundances of *IL2* and *IFNg* mRNAs were still reduced in suppressed T_{cons} compared to those in control T_{cons} (Fig. 1C). These results implied that T_{regs} altered the TCR signaling machinery of T_{cons} within 30 to 45 min of cell contact, which subsequently led to long-lasting suppression of cytokine gene expression in T_{cons} even in the absence of T_{regs}.

To analyze the suppression of cytokine gene expression in a more physiological setting, we performed cocultures in the presence of antigen-presenting cells (APCs). Costimulation with APCs and polyclonally stimulating antibody against CD3 (which mimics antigenic TCR stimulation) resulted in the production of lower amounts of cytokines than occurred in cells stimulated through cross-linked antibodies against CD3 and against the costimulatory receptor CD28; however, the extent of suppression of *IL2* mRNA generation was similar (fig. S2). Thus, the rapid T_{reg}-mediated suppression of cytokine-encoding gene expression in T_{cons} also occurred in the presence of APCs, which may be similar to the in vivo situation.

CTLA-4 is not involved in the rapid suppression of cytokine gene expression in T_{cons}

The presence of the inhibitory receptor cytotoxic T lymphocyte antigen 4 (CTLA-4) on the surface of murine T_{regs} contributes to the suppression of T_{cons} by decreasing the abundance of the costimulatory B7 molecules on APCs, thereby limiting the stimulatory capacity of the APCs (*19*–*21*). Mice with T_{regs} deficient in CTLA-4 suffer from autoimmune disease (*19*), suggesting that CTLA-4 is a key component of T_{reg}-mediated suppression. Because T_{regs} can suppress T_{cons} directly, we asked whether CTLA-4 was also important for T_{con} suppression in the absence of APCs and in the context of human cells, because CTLA-4 on T_{regs} may bind to B7 molecules that may be expressed on the surface of T_{cons}. First, we analyzed the kinetics of B7 expression on T_{cons} because it was reported that stimulation of the TCR for more than 24 hours can lead to the appearance of CD80 (B7.1) and CD86 (B7.2) on the surface of T cells (*22*). However, we could not detect CD80 before 24 hours of TCR stimulation, and we could not detect CD86 at any time point (fig. S3A). Thus, the involvement of CTLA-4 in the direct suppression of cytokine gene expression in T_{cons} through these ligands was unlikely.

We could also exclude a role for unknown CTLA-4 receptors (*23*) in the rapid suppression of cytokine gene expression because we detected no difference in the suppression of *IL2* and *IFNg* expression (as determined by measurement of mRNA abundance) in cocultures treated with a blocking antibody against CTLA-4 compared to that in cocultures incubated with isotype control antibodies (fig. S3B). In addition, in the presence of APCs, blocking CTLA-4 did not affect the rapid suppression of cytokine gene expression (fig. S3B). However, in proliferation assays containing APCs, suppression of proliferation was partly abrogated by blocking CTLA-4 (fig. S3C), as was shown similarly by others (*21*). Thus, we concluded that CTLA-4 was not involved in the T_{reg}-mediated rapid suppression of cytokine-encoding gene expression in human T_{cons} in the presence or absence of APCs. Because the rapid suppression of cytokine gene expression occurred to similar extents in the presence and absence of APCs (figs. S2 and S3), this suggested that the suppression of cytokine gene expression occurred through an APC-independent mechanism.

TCR-proximal signaling is not altered in suppressed T_{cons}

The observed rapid suppression of cytokine gene expression prompted us to investigate whether T_{regs} inhibited the activation of T_{cons} at the level of

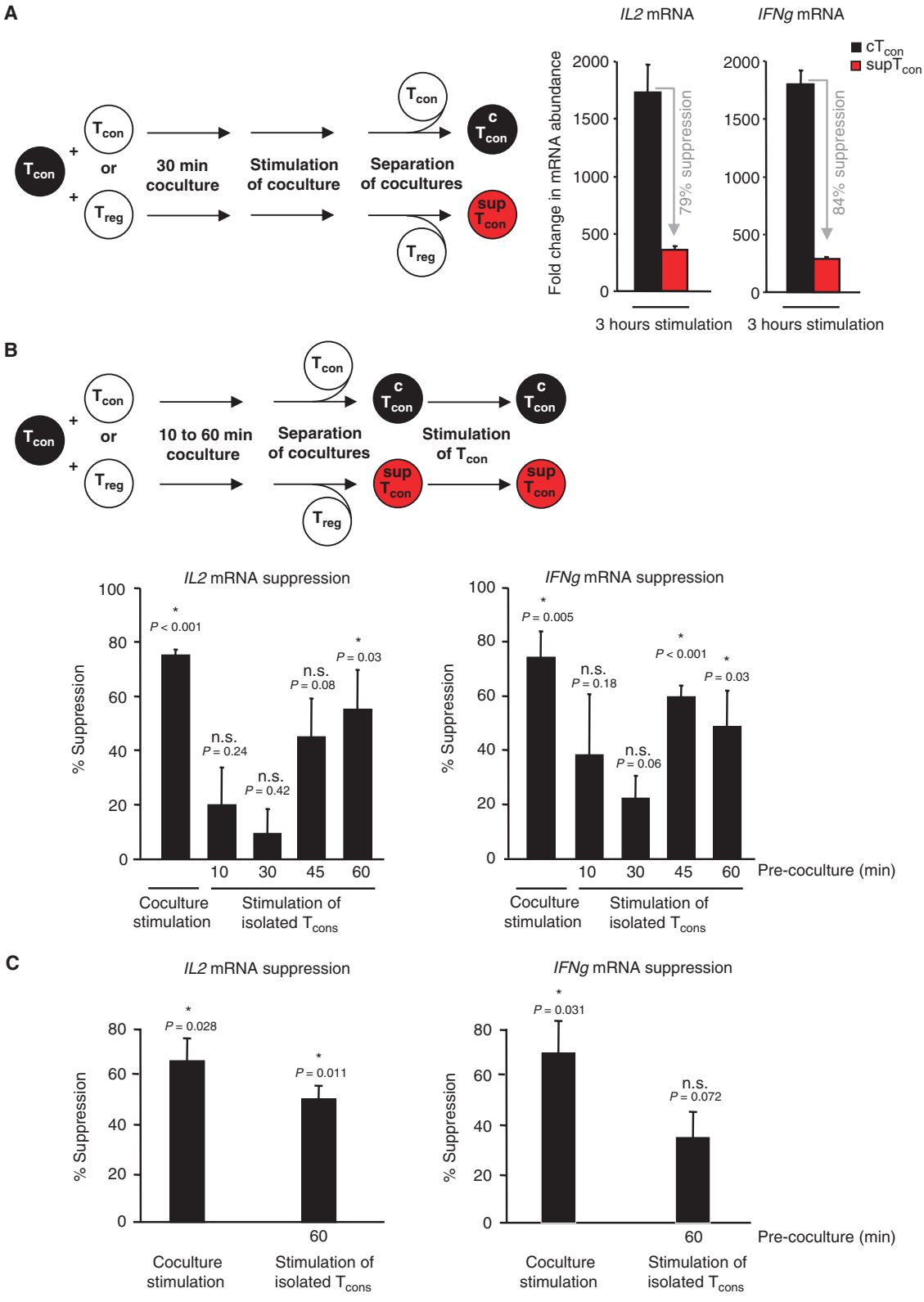

Fig. 1. Suppression of T_{cons} persists after the removal of T_{regs}. Quantitative reverse transcription–polymerase chain reaction (qRT-PCR) analysis of the abundances of *IL2* and *IFNg* mRNAs in HLA-A2$^-$ T_{cons}. (**A**) HLA-A2$^-$ T_{cons} were cocultured with pre-activated HLA-A2$^+$ T_{regs} ($supT_{con}$) or with HLA-A2$^+$ T_{cons} as a control (cT_{con}) at a 1:1 ratio and stimulated with cross-linked antibodies against CD3 and CD28 for 3 hours. HLA-A2$^-$ T_{cons} were then isolated and the abundances of *IL2* and *IFNg* mRNAs were analyzed. Results are presented as the fold change in the abundance of the indicated mRNA in stimulated suppressed T_{cons} or stimulated control T_{cons} compared to that in unstimulated T_{cons}, which was set to 1. Data are means ± SD of duplicate samples of a single donor and are representative of >20 donors. The percentages of reduction in the abundances of *IL2* and *IFNg* mRNAs in the suppressed T_{cons} compared to those in control T_{cons} are indicated in gray (% Suppression). (**B**) Cells were cocultured as described for (A) (coculture stimulation, left bars) or were cocultured for 10 to 60 min before undergoing stimulation of isolated responder T_{cons} ("pre-cocultured"). For the pre-cocultures, HLA-A2$^-$ T_{cons} were left unstimulated in the presence of pre-activated T_{regs} or T_{cons}, as a control, at a 1:1 ratio. HLA-A2$^-$ T_{cons} were then isolated and stimulated alone as described in (A), and the abundances of mRNAs for the indicated cytokines were measured. Shown are the percentages of suppression as described for (A). n.s., not significant. (**C**) Cocultures were established as described in (B), with the exception that after a pre-coculture period of 60 min, HLA-A2$^-$ T_{cons} were isolated and rested for 24 hours before they were stimulated. Data are the means ± SEM from four (B) or three (C) donors. Statistical significance of suppression was calculated with the Student's one-sample *t* test.

the TCR. If this were true, it would result in the immediate blockage of signaling pathways that lead to TCR-induced expression of cytokine-encoding genes. To explore whether T_{reg}-mediated suppression occurred at the TCR itself or at a TCR-proximal level, we set up cocultures as outlined earlier (Fig. 1A) and determined the extent of phosphorylation of CD3ε and ZAP-70. We found that the rapid tyrosine phosphorylation of CD3ε after TCR stimulation in control T_{cons} was not decreased in suppressed T_{cons} (fig. S4A). Similarly, we detected the rapid phosphorylation of ZAP-70 in both control T_{cons} and suppressed T_{cons} (fig. S4B). We then tested whether T_{reg}-mediated suppression affected the activation of PLC-γ1 downstream of ZAP-70, which represents the branching point at which the NF-κB and NFAT signaling pathways diverge. Flow cytometric and Western blotting analyses revealed that the extent of PLC-γ1 phosphorylation was similar in control T_{cons} and suppressed T_{cons} 5 min after TCR stimulation (fig. S4C). To further analyze PLC-γ activity, we determined the amounts of DAG by lipid mass spectrometry, and we found no difference in the amounts of DAG between control T_{cons} and suppressed T_{cons} (fig. S4D). Our results showed that the TCR-proximal signaling machinery was not affected during the rapid T_{reg}-mediated suppression of T_{cons}. Thus, we further investigated signaling events downstream of PLC-γ1.

NF-κB signaling is impaired in suppressed T_{cons}

To study the involvement of PKCθ in T_{reg}-mediated suppression, we set up cocultures as described earlier (Fig. 1A) and performed Western blotting analysis with phosphospecific antibodies. We detected no difference between control T_{cons} and suppressed T_{cons} in terms of the phosphorylation of PKCθ 5 and 25 min after TCR stimulation (Fig. 2A). PKCθ activates the IKK complex, which consists of IKKα, IKKβ, and IKKγ (*11*). Despite the phosphorylation of PLC-γ1 and PKCθ being unaffected in suppressed T_{cons}, we found that IKK phosphorylation was markedly inhibited in suppressed T_{cons} compared to that in control T_{cons} (Fig. 2B), which also occurred in the presence of APCs (fig. S2). Because the IKK complex directly affects the phosphorylation and subsequent degradation of IκBα (*24*), we were interested in determining whether the phosphorylation of IκBα was also diminished in these cells. Indeed, we found that the phosphorylation of IκBα was strongly inhibited in suppressed T_{cons} compared to that in control T_{cons} within 5 min of TCR stimulation (Fig. 2C).

In T cells, the classical NF-κB pathway depends mainly on the NF-κB heterodimer p50:p65, which translocates to the nucleus upon degradation of IκBα. Similarly to IKK and IκBα, the phosphorylation of p65 was almost completely blocked in suppressed T_{cons} 30 min after TCR stimulation, and it remained blocked until 2.5 hours after stimulation (Fig. 2D). Furthermore, we performed gene array analysis and compared the mRNA expression profiles of suppressed T_{cons} and control T_{cons} 3 hours after TCR stimulation. The expression of several NF-κB target genes (*25*), including *CCL22*, *ICAM1*, *IL2*, *IL8*, *TNF*, and *TNFAIP3*, was inhibited specifically in suppressed T_{cons} (Fig. 2E), confirming our Western blotting analysis that NF-κB signaling was impaired in these cells. Because T_{regs} need to be activated through the TCR to be suppressive (*26*, *27*), we pre-activated T_{regs} before their coculture with T_{cons}. However, to exclude any effects of the antibody against CD3 that was used for the pre-activation of the T_{regs}, we covalently coupled this antibody to plates that were used for the pre-activation of T_{regs} or, as a control, of T_{cons}. To minimize the production of the transcription factor Foxp3 in activated human T_{cons}, which may result in suppressive function (*28*, *29*), we also shortened the time for the pre-activation of T_{regs} and T_{cons}. In addition, we used T_{regs} that had not been pre-activated in our assays of cytokine mRNA suppression, because stimulation in coculture for several hours might have been sufficient for the T_{regs} to acquire suppressive function. With these controls, we only observed the suppression of NF-κB target genes and of IκBα phosphorylation in responder T_{cons} when they were cocultured with T_{regs} (fig. S5A). Thus, T_{regs} specifically and rapidly blocked the NF-κB pathway in suppressed T_{cons}.

Dephosphorylation of NFAT1 is inhibited in suppressed T_{cons}

In T cells, transcription of many activation-associated genes is dependent not only on NF-κB but also on the binding of the cooperative NFAT-Fos-Jun complex to DNA response elements, which results in T cell proliferation and the expression of cytokine-encoding genes. Therefore, we hypothesized that the transcription factors NFAT and AP-1 were additional possible targets in the T_{reg}-mediated suppression of T_{cons}. The NFAT family consists of five transcription factors, four of which (NFAT1 to NFAT4) are Ca^{2+}-dependent (*30*). In resting T cells, NFAT1 is the predominant isoform (*31*). TCR stimulation induces the activation of calcineurin, which dephosphorylates NFAT and thereby unmasks its nuclear localization sequence. This enables NFAT to translocate to the nucleus and induce the expression of cytokine-encoding genes in synergy with AP-1 and NF-κB (*32*).

We established cocultures and investigated the activation status of NFAT1 by Western blotting analysis by comparing the extent of NFAT1 dephosphorylation in control and suppressed T_{cons}. We observed a marked inhibition of NFAT1 dephosphorylation in suppressed T_{cons} after 5 min of TCR stimulation (Fig. 3A). We could not detect NFAT2 in human T cells after short-term stimulation. In addition, gene array analyses revealed significant inhibition of the expression of NFAT-dependent genes (*33*), such as *EGR2*, *IL2RA*, *CTLA4*, *IL3*, *IL4*, and *COX2*, in suppressed T_{cons} compared to that in control T_{cons} (Fig. 3B). As described earlier for NF-κB, only T_{regs} pre-activated with covalently plate-bound antibody against CD3, but not T_{cons} pre-activated in the same manner, suppressed NFAT1 dephosphorylation and the expression of NFAT target genes in responder T_{cons} (fig. S5B). Together, these findings showed that T_{regs} potently and rapidly suppressed TCR-induced NFAT1 activation in T_{cons}.

AP-1 signaling is not involved in T_{reg}-mediated suppression of cytokine gene expression

Because T_{reg}-mediated suppression of NF-κB and NFAT signaling pathways occurred downstream of TCR-proximal signaling events, the question remained whether T_{regs} acted through a general blockage of all transcription factors relevant for T cell activation, including AP-1. AP-1 is controlled mainly by phosphorylation of ERK, p38, and JNK and the subsequent activation of Fos and Jun (*34*). We found that ERK was activated similarly in control T_{cons} and suppressed T_{cons} after short-term TCR stimulation as assessed by Luminex analysis (Fig. 4A). Correspondingly, we observed no suppression of the phosphorylation of ERK in suppressed T_{cons} compared to that in control T_{cons}, as assessed by flow cytometry (fig. S6A). We monitored the activation status of p38 by Western blotting analysis with phosphospecific antibodies. We did not observe suppression of p38 phosphorylation in suppressed T_{cons} (Fig. 4B), which was confirmed by flow cytometric analysis (fig. S6B).

To test events further downstream in the AP-1 pathway, we investigated the phosphorylation of the transcription factor c-Jun, but we did not observe any inhibition of the phosphorylation of c-Jun in suppressed T_{cons} compared to that in control T_{cons} up to 60 min after TCR stimulation (Fig. 4C). These data are supported by analysis of the expression of representative AP-1 target genes (*35*), including *MMP9*, *MMP13*, *EGFR*, *FGF7*, *VEGF*, *CD69*, and *FYN*, which were not significantly changed in suppressed T_{cons} compared to that in control T_{cons} (Fig. 4D). Thus, in contrast to their potent inhibition of NF-κB and NFAT signaling pathways in T_{cons}, T_{regs} did not influence the early activation of AP-1 in T_{cons}.

Ca^{2+} signaling is abrogated in suppressed T_{cons}

Whereas NF-κB and NFAT signaling pathways rely on Ca^{2+} signals, AP-1 activation is largely Ca^{2+}-independent. The Ca^{2+}- and calmodulin-dependent phosphatase calcineurin dephosphorylates numerous sites in NFAT, which enables the nuclear translocation of NFAT and its subsequent binding to DNA target sequences. Furthermore, Ca^{2+} is involved in the activation of NF-κB, for example, by enhancing the degradation of IκBα (*15*, *16*). Because we observed the suppression of NF-κB and NFAT1 signaling, but not of TCR-proximal events or AP-1 signaling, we speculated that the inhibition of Ca^{2+} signaling might be the cause of T_{reg}-mediated suppression of T_{cons}. TCR-induced IP_3 stimulates the release of Ca^{2+} from intracellular stores into the cytoplasm (*36*). Depletion of Ca^{2+} stores is sensed by stromal interaction molecule 1 (STIM1), which resides in the endoplasmic reticulum membrane and contributes to the opening of Ca^{2+} release–activated Ca^{2+} (CRAC) channels and the influx of Ca^{2+} from the extracellular space. To measure Ca^{2+} signals, we loaded responder T_{cons} with the Ca^{2+}-sensitive

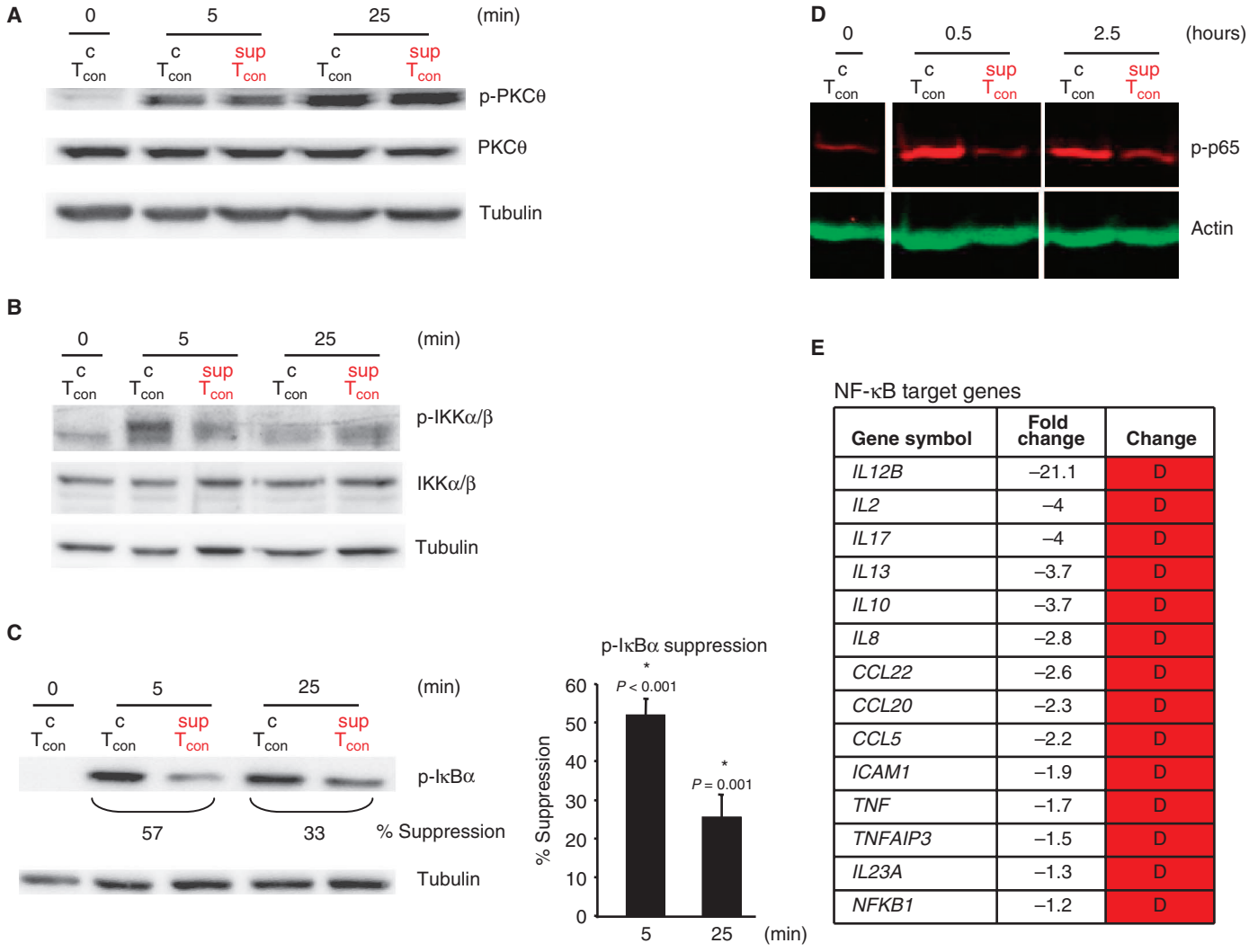

E

NF-κB target genes

Gene symbol	Fold change	Change
IL12B	–21.1	D
IL2	–4	D
IL17	–4	D
IL13	–3.7	D
IL10	–3.7	D
IL8	–2.8	D
CCL22	–2.6	D
CCL20	–2.3	D
CCL5	–2.2	D
ICAM1	–1.9	D
TNF	–1.7	D
TNFAIP3	–1.5	D
IL23A	–1.3	D
NFKB1	–1.2	D

Fig. 2. NF-κB signaling is inhibited in suppressed T_{cons}. (**A** to **C**) Western blotting analysis of the phosphorylation of (A) PKCθ (pT^{538}), (B) IKKα (pS^{180}) and IKKβ (pS^{181}), and (C) IκBα (pS^{32}) in HLA-$A2^-$ T_{cons}. Cocultures were established as described for Fig. 1A, and cells were stimulated for the indicated times. Suppressed T_{cons} or control T_{cons} were analyzed with phosphospecific antibodies (upper images in each panel). Blots were then incubated with antibodies against the indicated total proteins and with antibody against tubulin, which served as a loading control. Blots are from one experiment representative of 4 (A), 3 (B), or >12 (C) donors. The right panel in (C) shows the mean percentage suppression of IκBα phosphorylation ± SEM from 19 (5 min) or 12 (25 min) donors. Statistical significance of suppression was calculated with the Student's one-sample *t* test. (**D**) Western blotting analysis of the amount of phosphorylated p65 (p-p65). Suppressed T_{cons} (red) or control T_{cons} (black) were analyzed with fluorescently labeled antibodies against p-p65 (pS^{536}) and β-actin. One representative experiment from five different donors is shown. (**E**) NF-κB target genes obtained from gene array data. The gene expression patterns of control and suppressed T_{cons} were compared after 3 hours of TCR stimulation. D signifies genes whose expression was significantly decreased in suppressed T_{cons} compared to that in control T_{cons}. The array was performed with two different donors, and one donor is shown. T, threonine; S, serine.

ratiometric dye Indo-1 AM. To further distinguish responder T_{cons} from co-cultured T_{regs} (or T_{cons} in control assays), we labeled each cell population with different PKH dyes for general cell membrane labeling (Fig. 5A). Hence, we were able to specifically measure changes in Ca^{2+} concentrations only in responder T_{cons} even if they were conjugated with T_{regs} or, as a control, with T_{cons}. To enable the formation of cell pairs, we established cocultures at least 30 min before TCR-induced triggering of Ca^{2+} signals. In our flow cytometric analysis, by gating on T_{cons} that were not conjugated during the time of measurement, we observed an immediate increase in Ca^{2+} concentrations in the cytosol after TCR stimulation in control T_{cons}, and a partial inhibition of Ca^{2+} flux in suppressed T_{cons} (Fig. 5A, Q4 gate, lower left). By gating on PKH26 and PKH67 double-positive cell conjugates (Fig. 5A, Q2 gate), we detected an almost complete block of Ca^{2+} influx in suppressed T_{cons} (Fig. 5A, lower right). This result implied that, upon cell contact, T_{regs} entirely abrogated Ca^{2+} signals in T_{cons}. The partial inhibition of Ca^{2+} signals in the nonconjugated cell population might be ascribed to suppressed cells within the population that had contact with T_{regs} before the flow cytometric measurement.

Our analyses of cytokine gene expression and protein phosphorylation required the coculture of responder T_{cons} with T_{regs} (or T_{cons}, as a control) from different (HLA-A2–disparate) donors. Because of the staining protocol used for Ca^{2+} analyses, we were also able to analyze the suppression of Ca^{2+} signals in responder T_{cons} upon coculture with T_{regs} isolated from the same donor (autologous). We also observed suppression of Ca^{2+} signals when autologous T_{regs} were used (fig. S7A), and, thus, we can exclude the possibility that suppression is an artifact that resulted from coculture with T cells from a different donor. Because we observed suppression of NFAT1 and NF-κB signaling as well as *IL2* expression after a 30- to 45-min coculture period with T_{regs} before TCR stimulation (Fig. 1), we tested whether suppression of Ca^{2+} signaling also required similar conditions. Indeed, we found that for suppression of Ca^{2+} influx, it was necessary to coculture T_{regs} and T_{cons} for at least 30 min before TCR stimulation (fig. S7B); however, maximal conjugate formation was already reached after about 10 min of coculture (fig. S7C). Almost no conjugates formed between T_{cons} and control T_{cons} (fig. S7C). Because conjugates were strongly enriched in the population representing cell pairs according to their size (fig. S7D), they are unlikely to result from the transfer of PKH dyes from one cell to another.

We next tested whether the depletion of intracellular Ca^{2+} stores was blocked by T_{regs} or if suppression occurred later, at the level of influx of Ca^{2+} through the plasma membrane. To this end, cocultures were established and pre-cocultured as described earlier to enable formation of cell pairs. After this pre-coculture, cocultures were washed and resuspended in Ca^{2+}-free buffer to permit measurement of intracellular depletion of Ca^{2+} stores by flow cytometric analysis. We found that T_{regs} suppressed Ca^{2+} store depletion in T_{cons} during TCR stimulation in Ca^{2+}-free buffer (Fig. 5B). Unfortunately, because of the low number of conjugates formed in Ca^{2+}-free buffer, we could not analyze conjugates thoroughly with respect to Ca^{2+} store depletion. Because Ca^{2+} store depletion in T cells is mainly triggered through the binding of IP_3 to IP_3 receptors (IP3Rs), we investigated whether the amounts of IP_3 in suppressed T_{cons} were reduced compared to those in control T_{cons} because of either decreased IP_3 generation or altered inositol phosphate metabolism. Consistent with earlier analysis of PLC-γ1 phosphorylation and DAG generation, we detected no difference in the amount of IP_3 in responder T_{cons} cocultured with T_{regs} and that of responder T_{cons} cocultured with T_{cons} (Fig. 5C). Similarly,

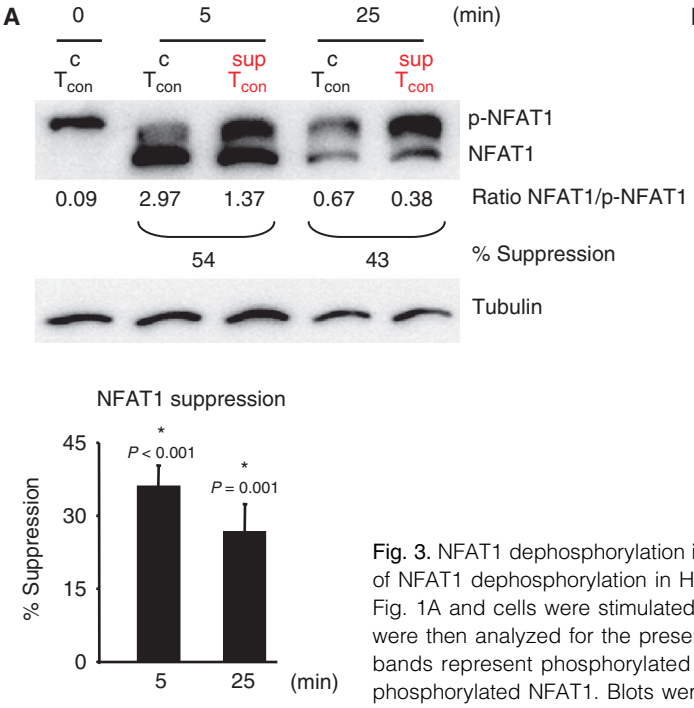

B NFAT target genes

Gene symbol	Fold change	Change
IL3	–59.7	D
IL4	–14.9	D
IL5	–9.2	D
IL2RA	–8	D
IL13	–3.7	D
EGR2	–2.5	D
FASLG	–2.5	D
CTLA4	–2.5	D
COX2	–1.2	D
CD5	–1.2	MD

Fig. 3. NFAT1 dephosphorylation is inhibited in suppressed T_{cons}. (**A**) Western blotting analysis of NFAT1 dephosphorylation in HLA-A2$^-$ T_{cons}. Cocultures were established as described for Fig. 1A and cells were stimulated for the indicated times. Suppressed T_{cons} and control T_{cons} were then analyzed for the presence of phosphorylated and total NFAT1 proteins. The upper bands represent phosphorylated NFAT1 (p-NFAT1), whereas the lower bands represent dephosphorylated NFAT1. Blots were then incubated with antibody against tubulin as a loading control. Data are from one donor representative of 11 (5 min) or 10 (25 min) donors. Lower graph shows the percentage suppression of NFAT1 dephosphorylation as determined by densitometric analysis of Western blots as shown in the upper panels. Data are the means ± SEM of 11 (5 min) or 10 (25 min) donors. Statistical significance of suppression was determined by Student's one-sample *t* test. (**B**) NFAT target genes obtained from gene array analysis as described for Fig. 2E. D, genes whose expression in suppressed T_{cons} was significantly decreased compared to that in control T_{cons}; MD, marginal decrease.

stimulation-induced quantities of IP_4 species were not reduced in suppressed T_{cons}, further implying that IP_3 metabolism was unchanged (Fig. 5C).

cAMP has been described as a suppressive molecule involved in the T_{reg}-mediated inhibition of murine T cells (*6*) and the suppression of Ca^{2+} signals in mast cells (*37*). However, we observed that the rapid suppression of Ca^{2+} signaling in T_{cons} was independent of cAMP, because a cAMP antagonist was unable to prevent suppression of Ca^{2+} influx in suppressed T_{cons} (fig. S8). Because Ca^{2+} signals were measured immediately after TCR stimulation, this time frame was likely too short to activate the suppressive potential of T_{regs}; thus, T_{regs} likely have to be pre-activated. To exclude potential effects of the antibody against CD3 that was used for pre-activation, we pre-activated T_{regs} or control T_{cons} with covalently plate-bound antibody against CD3. T_{regs} that were pre-activated in this way suppressed Ca^{2+} signals in responder T_{cons}, whereas pre-activated T_{cons} did not (fig. S9A). However, the suppressive capacity of T_{regs} was increased after pre-activation with soluble antibody against CD3. In addition, T_{regs} pre-activated with covalently plate-bound antibody against CD3 formed substantially more conjugates with responder T_{cons} than did T_{cons} that were pre-activated in the same way (fig. S9B).

Suppression of Ca^{2+} signaling causes the inhibition of NFAT and NF-κB signaling in T_{cons}

We hypothesized that suppression of Ca^{2+} signals might lead to inhibition of the activation of NFAT and NF-κB. To test the Ca^{2+} dependency of NFAT and NF-κB activation in our experimental system, we stimulated T_{cons} through the TCR in the presence of the Ca^{2+} chelator EGTA and investigated the phosphorylation status of various signaling molecules. As expected, we found that NFAT dephosphorylation was completely inhibited in the presence of EGTA, whereas the phosphorylation states of the TCR-proximal molecules ZAP-70 and PLC-γ1 were not affected (fig. S10). Phosphorylation of IκBα and IKK was also entirely inhibited in the presence of EGTA, whereas the phosphorylation of PKCθ was unchanged (fig. S10), supporting the notion that the suppression of Ca^{2+} signals caused the inhibition of NFAT and NF-κB activation in T_{cons} that are suppressed by T_{regs}.

To further support this idea, we investigated whether artificial depletion of Ca^{2+} stores in responder T_{cons} could abrogate the suppression of Ca^{2+}, NFAT, and NF-κB signaling. To this end, we performed experiments with the specific Ca^{2+} store–depleting agent thapsigargin. Alternatively, we used the Ca^{2+} ionophore ionomycin in concentrations (≤0.5 μM) that are described to selectively release Ca^{2+} from intracellular stores without

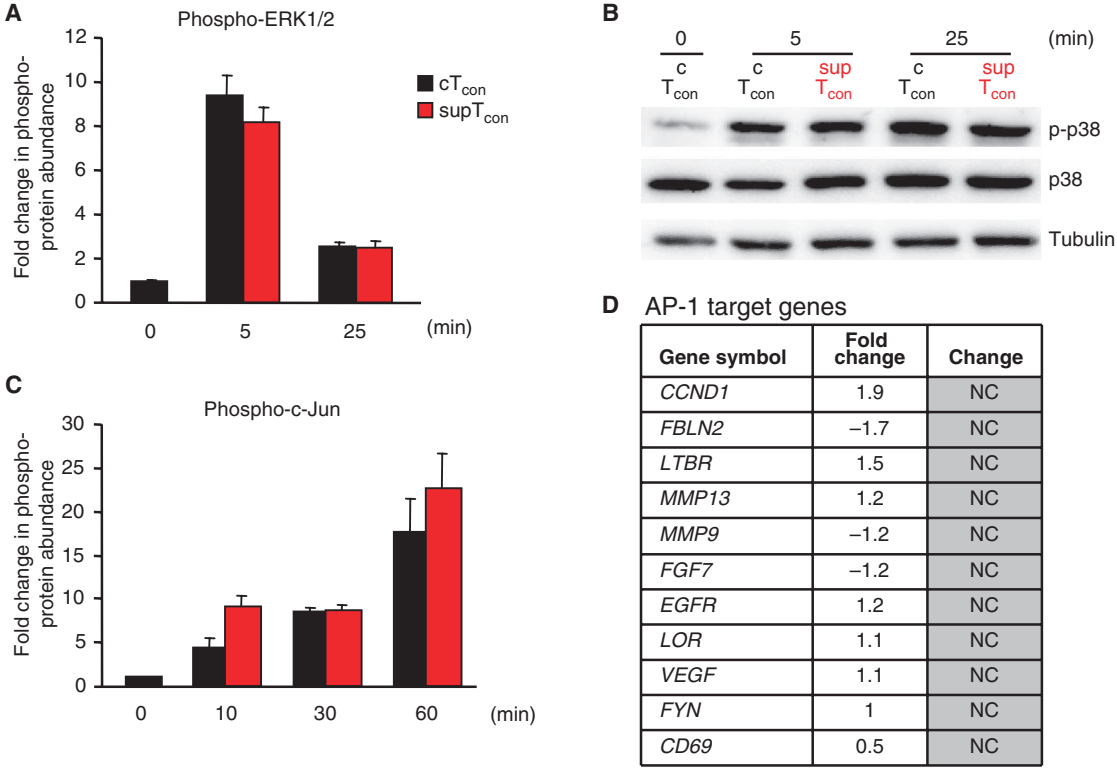

D AP-1 target genes

Gene symbol	Fold change	Change
CCND1	1.9	NC
FBLN2	–1.7	NC
LTBR	1.5	NC
MMP13	1.2	NC
MMP9	–1.2	NC
FGF7	–1.2	NC
EGFR	1.2	NC
LOR	1.1	NC
VEGF	1.1	NC
FYN	1	NC
CD69	0.5	NC

Fig. 4. AP-1 signaling is not involved in T_{reg}-mediated suppression of T_{cons}. (**A**) Luminex analysis of the phosphorylation of ERK1 and ERK2 (ERK1/2) in HLA-$A2^-$ T_{cons} after TCR activation. Cocultures were established as described for Fig. 1A, and cells were stimulated for the indicated times. Suppressed T_{cons} and control T_{cons} were analyzed for the extent of phosphorylation of ERK1/2 (pT^{185}/pY^{187}). Values were normalized to account for the amounts of total protein. Data are expressed as the fold change in the abundances of the indicated phosphorylated protein compared to those in unstimulated control T_{cons}, which were set at 1. Analyses were performed in duplicate, and mean fold change ± SD is shown. Data are from one donor representative of three different donors. (**B**) Western blotting analysis of the presence of p-p38 (pT^{180}/pY^{182}) in suppressed T_{cons} and control T_{cons}. Blots were analyzed with antibody against p-p38 and then incubated with antibodies against total p38 and tubulin. Data are from one experiment that is representative of five experiments. (**C**) Analysis of the phosphorylation of c-Jun (pS^{63}) as described for (A). Data are from one donor and are representative of five donors. (**D**) Analysis of the expression of AP-1 target genes obtained from gene array assays as described for Fig. 2E. NC, genes whose expression in suppressed T_{cons} was not significantly different from that in control T_{cons}; Y, tyrosine.

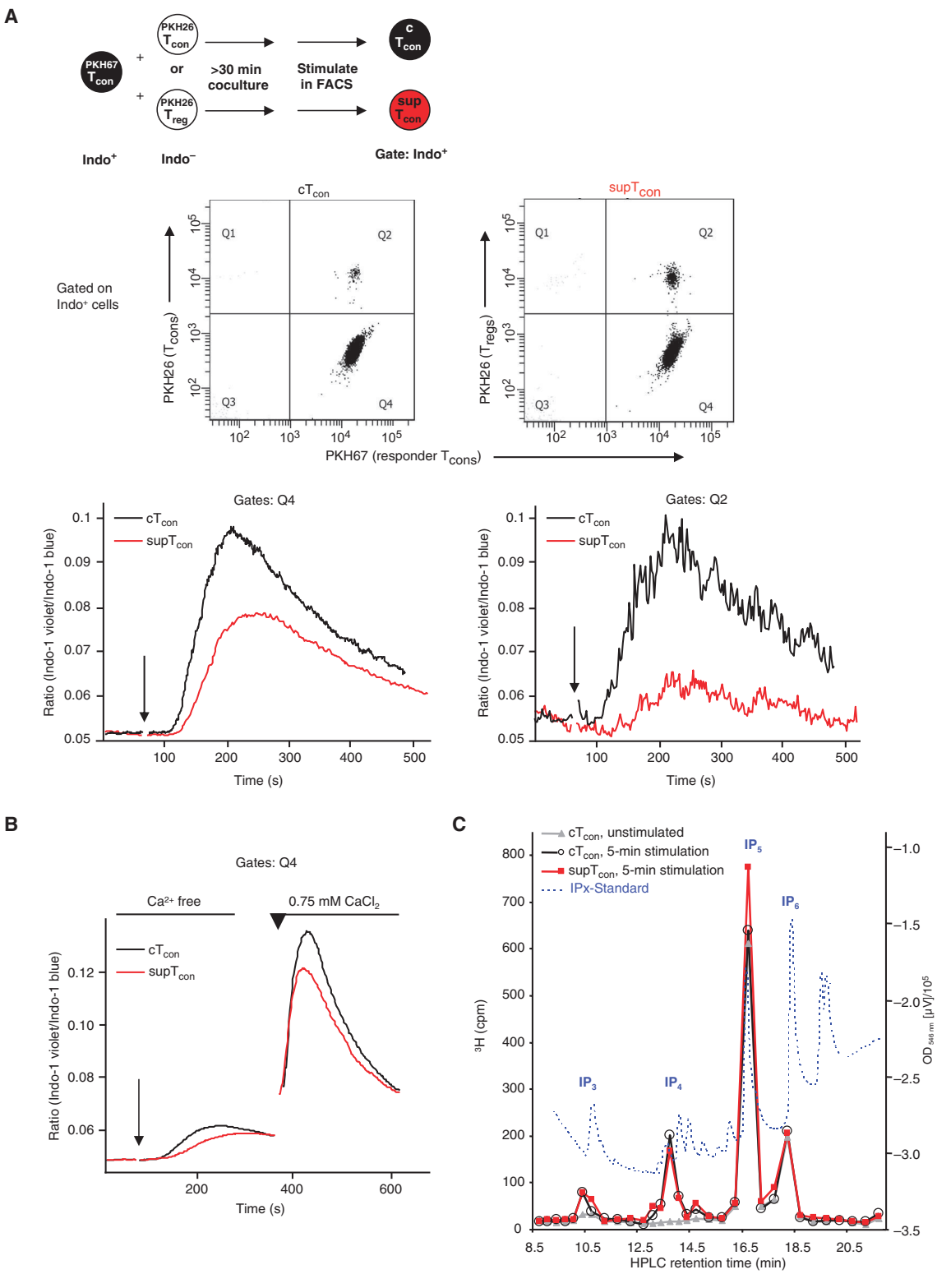

Fig. 5. Ca^{2+} signaling is abrogated in suppressed T_{cons} independently of IP_3. (**A**) T_{cons} were labeled with Indo-1 AM and PKH67 and cocultured with PKH26-labeled, pre-activated allogeneic T_{regs} ($supT_{con}$) or with allogeneic T_{cons} (cT_{con}) for at least 30 min. Cells were analyzed by flow cytometry and gated on Indo-loaded responder T_{cons}, as shown in the dot plots, and cells were then monitored for Ca^{2+} signaling as shown in the bottom panels depicting Ca^{2+} traces. After 1 min to establish a baseline, cross-linked antibodies against CD3 and CD28 were added to the cells (arrow) to stimulate Ca^{2+} signaling. The lower left panel shows Ca^{2+} influx in unconjugated T_{cons} (stained only with PKH67, from the Q4 gate in the upper dot plot), whereas the lower right panel shows Ca^{2+} influx in conjugated T_{cons} (PKH67- and PKH26-positive cells, from the Q2 gate in the upper dot plot). Data are from one donor and are representative of 20 donors. (**B**) Cells were labeled and cocultured as described for (A). Cocultured cells were then washed, resuspended in Ca^{2+}-free PBS, and analyzed for Ca^{2+} signaling. After 1 min, cross-linked antibodies against CD3 and CD28 were added to the cells (arrow), and then medium was added to provide a final extracellular concentration of Ca^{2+} of 0.75 mM (arrowhead). Ca^{2+} influx in unconjugated T_{cons} (from the Q4 gate) is shown. Data are from one donor representative of seven independent donors. (**C**) Responder T_{cons} were labeled with [^{3}H]inositol, cocultured with either unlabeled T_{cons} (cT_{con}) or unlabeled T_{regs} ($supT_{con}$), and then were stimulated for 5 min or were left unstimulated. Inositol phosphates were extracted from the cells and fractionated by HPLC, and the counts per minute (cpm) values were measured. Data are from one donor and are representative of five donors. OD, optical density.

increasing the Ca^{2+} permeability of the plasma membrane (*38*, *39*). Although suppression of Ca^{2+} store depletion was not complete in suppressed T_{cons} when Ca^{2+} amounts were compared to those in control T_{cons} (Fig. 5B), it was completely abrogated by addition of the Ca^{2+} store–depleting agent thapsigargin, further underlining that the observed partial reduction in Ca^{2+} signals was a result of suppression of Ca^{2+} store depletion (Fig. 6A). We also examined whether not only the suppression of Ca^{2+} store depletion (Fig. 6A) but also the suppression of Ca^{2+} signals in Ca^{2+}-containing medium was abrogated in the presence of thapsigargin. For this purpose, we added thapsigargin at the peak of Ca^{2+} influx when suppression already occurs, and indeed, we found that the addition of thapsigargin immediately resulted in an increase in intracellular Ca^{2+} concentrations in both suppressed and control T_{cons}, leading to nearly complete abrogation of suppression (Fig. 6, B and C).

To further examine whether suppression of Ca^{2+} signals caused inhibition of NFAT and NF-κB activation, we examined the phosphorylation of signaling molecules and the abundance of cytokine mRNAs in suppressed and control T_{cons} upon addition of thapsigargin and ionomycin, respectively. To treat only T_{cons} and not T_{regs} with thapsigargin or ionomycin, we set up cocultures similar to those described earlier (Fig. 1B): T_{cons} and T_{regs} were preincubated and then separated, after which responder T_{cons} were stimulated through the TCR in the absence or presence of thapsigargin or ionomycin (Fig. 6D). We found that suppression of NFAT1 activation was partially abrogated in the presence of thapsigargin and completely abrogated in the presence of ionomycin (Fig. 6D). In addition, suppression of the phosphorylation of IκBα was abrogated with both substances (Fig. 6D). Accordingly, suppression of *IL2* mRNA generation was reversed upon treatment with ionomycin (Fig. 6D). Thus, inhibition of Ca^{2+} signals largely contributed to T_{reg}-mediated suppression of NFAT and NF-κB signaling and, consequently, of cytokine gene expression. In conclusion, our results demonstrate that pre-activated T_{regs} need a short period (30 to 45 min) of coculture with T_{cons} to actively alter and suppress the signaling machinery of T_{cons}. Suppressed T_{cons} are unable to activate Ca^{2+}, NF-κB, or NFAT1 signaling pathways upon subsequent stimulation of their TCRs, which consequently prevents the expression of cytokine-encoding genes.

DISCUSSION

T_{regs} play an important role in the immune system because they can suppress different immune cells, including autoreactive T cells, and thereby prevent autoimmunity (*1*). Many groups have investigated the features of T_{regs}, but few data exist from studies of T_{reg}-mediated suppression mechanisms and signaling events in suppressed T cells. Most of the previous studies were conducted with mouse T cells; however, suppression mechanisms in mice and humans can differ (*4*). Therefore, research on the function of human T_{regs} is crucial, especially with regard to their clinical application.

We previously showed that inhibition of the expression of cytokine-encoding genes occurs rapidly in T_{cons} upon coculture with T_{regs} (*18*). In the current study, we demonstrated that suppression of the expression of cytokine-encoding genes persisted in T_{cons} even if the T_{regs} were removed before the T_{cons} were stimulated through the TCR. To be suppressed, T_{cons} had to have cell-cell contact with pre-activated T_{regs} for only 30 to 45 min. This suggests that T_{regs}, despite being present in lower numbers than those of T_{cons} in vivo, might have the capacity to suppress several T_{cons} in a sequential fashion.

In vivo, several immunosuppressive cytokines, such as transforming growth factor–β (TGF-β) and IL-10, are important for the prevention of inflammation of the colon and of experimental autoimmune encephalomyelitis (which is a mouse model similar to human multiple sclerosis), but they seem to be unnecessary for the prevention of other disorders, for example, autoimmune gastritis (*40*–*42*). Because various factors might contribute to T cell suppression in different microenvironments in vivo, it might be easier to clarify the inhibitory mechanisms in vitro. Therefore, many groups have investigated the direct suppression of T_{cons} by T_{regs} and have revealed a contact-dependent inhibitory mechanism that is independent of soluble cytokines (*43*, *44*). To date, several putative surface markers for T_{regs} have been described (*45*). For example, CTLA-4 is predominantly found on the surface of T_{regs} as well as on activated T cells, and CTLA-4 influences T_{reg}-mediated suppression in mice by limiting the stimulatory capacity of APCs (*19*–*21*). Our blocking experiments excluded a role for CTLA-4 in the rapid suppression of cytokine gene expression in human T_{cons} in the presence or absence of APCs, although CTLA-4 was involved in suppression of the proliferation of human T_{cons} in the presence of APCs. The receptor on T_{cons} that is recognized by T_{regs} remains elusive; however, our results indicate that triggering of this unknown receptor must lead to a suppressive signal within about 30 min.

We compared TCR signaling in control and suppressed T_{cons} and investigated the main signaling pathways that lead to the transcription of cytokine-encoding genes, namely, the AP-1, NF-κB, and NFAT pathways. We found no indication that the TCR itself or its associated proximal signaling molecules were involved in the suppression mechanism, because there was no change in the extent of phosphorylation of CD3ε, ZAP-70, or PLC-γ1 between control T_{cons} and suppressed T_{cons}, neither was there any difference in the generation of DAG and IP_3. Accordingly, we found no evidence of suppression of the AP-1 pathway by T_{regs}, as determined by analysis of the phosphorylation of ERK, p38, and c-Jun, as well as of the expression of AP-1 target genes in suppressed T_{cons} compared to control T_{cons}. However, we found that the NFAT1 and NF-κB pathways in suppressed T_{cons} were rapidly and markedly inhibited directly after TCR stimulation. We also detected the immediate suppression of Ca^{2+} release from intracellular stores in suppressed T_{cons}, which caused the reduced activation of NFAT and NF-κB and, consequently, the suppression of NFAT- and NF-κB–dependent expression of *IL2*.

As suggested by others (*46*), different mechanisms of suppression might be used by T_{regs} depending on, for example, the site of inflammation, the effector cell types, and the time point of suppression. In addition to suppression of the priming and proliferation of T_{cons} through the inhibition of APCs by T_{regs}, direct suppression of $CD8^+$ T cell effector function independently of repressed proliferation has been described (*47*), underscoring the in vivo relevance of direct suppression of T cells by T_{regs}. Our data suggest that at least two different mechanisms of suppression of human T_{cons} might operate. First, rapid suppression of Ca^{2+}, NFAT, and NF-κB signaling might result in inhibition of cytokine production, which is maintained upon removal of T_{regs} and seems to be independent of CTLA-4 and APCs. Second, suppression of the proliferation of human T_{cons} might require prolonged contact with T_{regs} and may be independent of Ca^{2+} signaling and the suppression of cytokine production. Consistent with this, mice with $CD4^+$ T cells that are doubly deficient in STIM1 and STIM2 display enhanced T cell proliferation compared to that of wild-type cells despite the lack of store-operated Ca^{2+} influx (*48*). In addition, a marked decrease in T_{reg} numbers contributes to lymphoproliferation in these mice. However, alternative modes of Ca^{2+} entry might compensate for the absence of STIM, for example, Ca_v calcium channels might operate when their inhibition by STIM1 is lacking (*49*, *50*).

Furthermore, NFAT might play multiple roles during the course of suppression. We showed that the suppression of NFAT signaling occurred within minutes of TCR stimulation, which, consequently, led to reduced NFAT-dependent gene expression. Nevertheless, NFAT may also actively contribute to the suppression of gene expression at later time points. In assays in which long-term suppression was assessed, such as by measuring

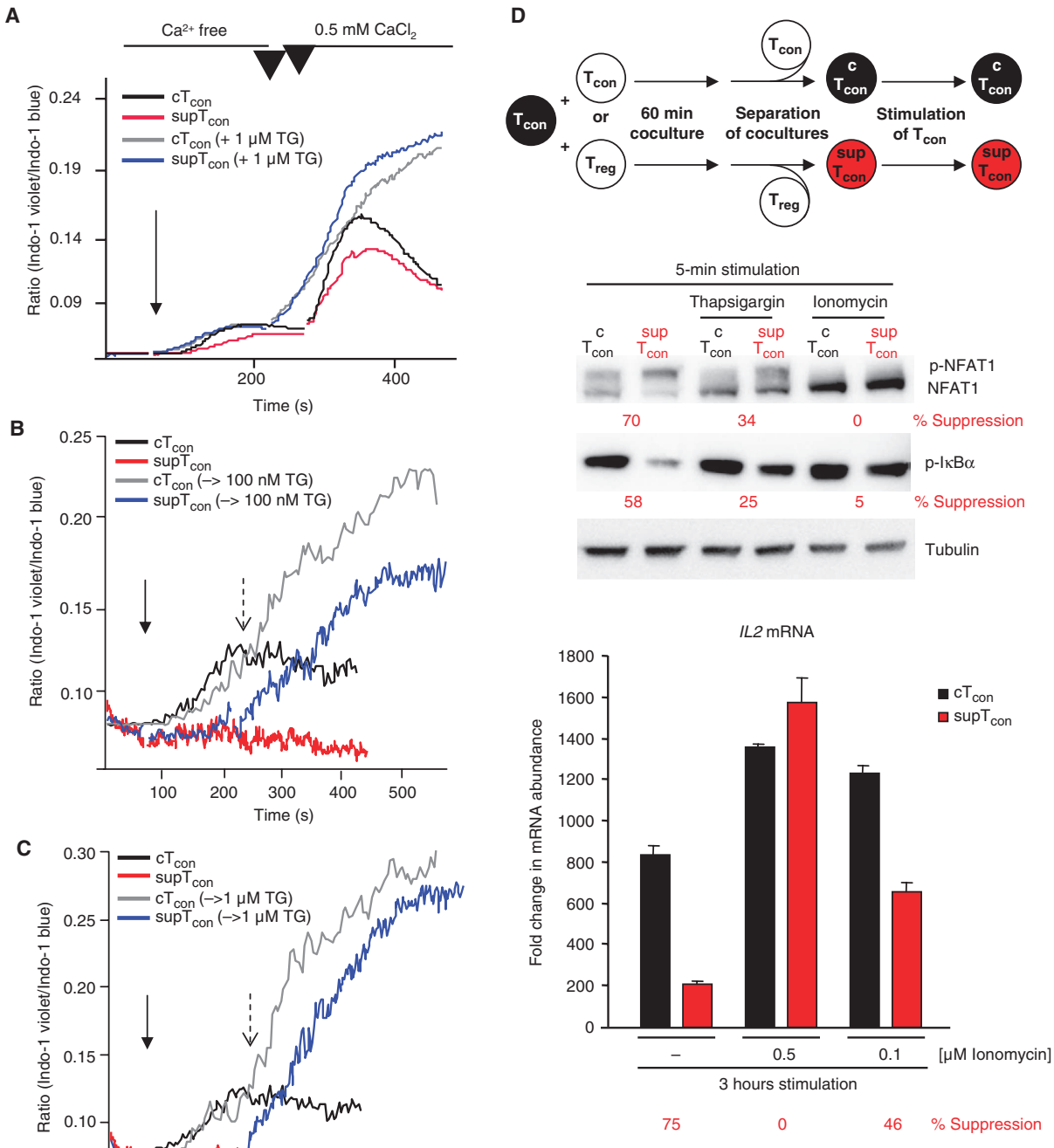

Fig. 6. Forced depletion of intracellular Ca^{2+} stores abrogates T_{reg}-mediated inhibition of Ca^{2+}, NFAT, and NF-κB signals in T_{cons}. (**A** to **C**) Cells were labeled and cocultured as described for Fig. 5. (A) Analysis in Ca^{2+}-free PBS. The arrow indicates the addition of cross-linked antibodies against CD3 and CD28 in the absence or presence of thapsigargin (TG, 1 μM). The arrowheads at the top of the graph indicate the addition of medium to obtain an extracellular Ca^{2+} concentration of 0.5 mM. (B and C) The arrow indicates the addition of cross-linked antibodies against CD3 and CD28. Dashed arrow indicates the addition of (B) 100 nM or (C) 1 μM thapsigargin. Ca^{2+} influx in conjugated T_{cons} is shown. Data are from a single donor representative of four (A) or three (B and C) donors. (**D**) HLA-$A2^-$ T_{cons} were cocultured with HLA-$A2^+$ T_{cons} (cT_{con}) or pre-activated HLA-$A2^+$ T_{regs} ($supT_{con}$) for 60 min, and then cell populations within the cocultures were separated on the basis of HLA-A2 expression. Middle panel shows Western blotting analysis of HLA-$A2^-$ T_{cons} stimulated with cross-linked antibodies against CD3 and CD28 in the absence or presence of ionomycin (500 nM) or thapsigargin (50 nM) for 5 min. Lower panel shows analysis of the abundance of *IL2* mRNA in HLA-$A2^-$ T_{cons} after 2 hours of stimulation with cross-linked antibodies against CD3 and CD28 in the absence or presence of ionomycin (100 and 500 nM). Relative mRNA amounts were normalized to those of *GAPDH* mRNA. Results are presented as the fold change in the abundance of *IL2* mRNA compared to that in unstimulated T_{cons}, which was set to 1. Data are the means ± SD of the analysis of duplicate samples from one donor by qRT-PCR and are representative of three donors.

proliferation or IL-2 production 18 hours after TCR stimulation, a study showed that murine T_{cons} doubly deficient in NFAT1 and NFAT4 are less susceptible to T_{reg}-mediated suppression than are wild-type T_{cons} (*17*). NFAT might form inhibitory complexes on the promoters of cytokine-encoding genes in conjunction with transcriptional repressors, as has been proposed for ICER-NFAT complexes (*51*) and in particular for NFAT2 (*52*). The amounts of ICER protein and mRNA are increased in suppressed mouse T_{cons} after 17 to 20 hours of stimulation compared to those in control T_{cons}, which correlates with an increase in the amount of cAMP in suppressed T_{cons} (*6*, *53*). In suppression assays with B7-deficient responder T cells, ICER fails to accumulate, but residual suppression is still detectable (*53*). This argues for additional suppressive mechanisms other than those mediated by CTLA-4, cAMP, and ICER. We did not detect accumulation of *ICER* mRNA or of mRNAs for other anergy-related genes in suppressed human T_{cons} up to 5 hours after TCR stimulation, whereas we found that the expression of cytokine-encoding genes was repressed earlier (*18*). Also, the passive diffusion of large amounts of cAMP through gap junctions from T_{regs} to T_{cons}, as has been proposed (*6*), seems unlikely within the short time period that we investigated.

The exact signaling events leading to the inhibition of Ca^{2+} release and NFAT1 and NF-κB activation in suppressed T_{cons} remain to be determined. We did not find any involvement of TCR-proximal signaling molecules, including PLC-γ1, which is crucial for Ca^{2+} influx and PKCθ activation. A report by Gri and colleagues showed the T_{reg}-mediated suppression of Ca^{2+} signals in murine mast cells in a PLC-γ2–independent fashion (*37*). However, suppression of Ca^{2+} signals in mast cells does not involve the suppression of depletion of Ca^{2+} stores, but rather involves a cAMP-dependent suppression of Ca^{2+} influx through the plasma membrane. We now describe a cAMP-independent, rapid suppression of Ca^{2+} store depletion in human T cells, which occurred downstream of PLC-γ1. Ca^{2+} store depletion was suppressed without alterations in PLC-γ1 activity. Because the amounts of IP_3 in suppressed T_{cons} were unaltered compared to those in control T_{cons}, it appears that IP_3 metabolism was unchanged. The exact mechanism through which T_{regs} inhibit store depletion therefore remains elusive. It might involve currently unknown modifications of the IP3R that could hinder its interaction with IP_3. Future studies will be needed to address these questions and to decipher the mechanism by which T_{regs} inhibit Ca^{2+} signals in T_{cons}. We propose that the suppression of Ca^{2+} signals leads to the suppression of both NFAT1 and NF-κB signaling because treatment of T_{cons} with ionomycin or thapsigargin relieved the suppression of NFAT1 and NF-κB activation. Suppression of *IL2* expression was completely abrogated upon treatment with ionomycin. This implies that inhibition of Ca^{2+} release is sufficient for the suppression of *IL2* expression.

In conclusion, we have elucidated the initial molecular processes that occur in primary human $CD4^+CD25^-$ T_{cons} upon suppression by $CD4^+CD25^+$ T_{regs}. Our data reveal that T_{regs} mediate an immediate block of NF-κB and NFAT signaling in T_{cons} through the inhibition of Ca^{2+} signals, which then leads to the suppression of cytokine gene expression. In cancer, suppression of effector T cells is deleterious, and breaking this suppressive state is highly desirable, whereas in autoimmunity, the suppression of autoreactive T cells is warranted. Thus, an understanding of the molecules and signaling pathways in T_{cons} that are affected upon suppression by T_{regs} is crucial for their future therapeutic manipulation.

MATERIALS AND METHODS

Preparation of T_{regs} and T_{cons}

Human peripheral blood leukocytes were purified from buffy coats by Biocoll (Biochrom) gradient centrifugation followed by adherence to plastic to deplete monocytes. Blood from $HLA\text{-}A2^+$ donors was used to isolate T_{regs} and T_{cons}, and blood from $HLA\text{-}A2^-$ donors was used to isolate responder T_{cons}. We first isolated $CD25^{high}$ cells with CD25-specific magnetic-activated cell sorting (MACS) beads (2 μl per 10^7 cells, Miltenyi). $CD4^+CD25^-$ T_{cons} were isolated from the $CD25^-$ fraction with the CD4 Isolation Kit II and were additionally depleted from the $CD25^+$ cells with CD25-specific MACS beads (6 μl per 10^7 cells). For some experiments, $CD4^+CD25^{high}$ T_{regs} were sorted on a FACS (fluorescence-activated cell sorting) Diva flow cytometer. T_{cons} were rested overnight in X-VIVO 15 medium (Lonza) supplemented with 1% GlutaMAX. T_{regs} were pre-activated overnight with antibody against CD3 (1 μg/ml) in X-VIVO 15 medium containing 1% GlutaMAX and IL-2 (50 U/ml), if not stated otherwise.

Coculture assays

$HLA\text{-}A2^+$ T_{regs} (using a pool of cells from several donors when we needed to obtain sufficient cell numbers) and $HLA\text{-}A2^+$ T_{cons} were incubated with fluorescein isothiocyanate (FITC)–conjugated antibody against HLA-A2 and FITC-specific microbeads (Miltenyi), whereas $HLA\text{-}A2^-$ T_{cons} were left untreated. Cocultures of $HLA\text{-}A2^-$ T_{cons} and either $HLA\text{-}A2^+$ T_{regs} or $HLA\text{-}A2^+$ T_{cons} as a control were set up in a 1:1 ratio. Cells were cultured for 30 to 60 min and then stimulated with soluble antibody against CD3 (0.2 μg/ml), antibody against CD28 (2 μg/ml), and goat antibody against mouse antibody as a cross-linker (2 μg/ml) for the indicated time periods at 37°C. Stimulation was then stopped, and the differing cell populations were separated on the basis of HLA-A2 expression by passing the cells over an LS column (Miltenyi) on ice. $HLA\text{-}A2^-$ T_{cons} (flowthrough from the column, >98% pure) were used for subsequent Western blotting, Luminex, and mRNA analyses. The suppressive capacity of T_{regs} was controlled in every assay by analyzing the abundances of *IL2* and *IFNg* mRNAs in the $HLA\text{-}A2^-$ T_{cons} after 2 to 3 hours of coculture with the T_{regs}. In some experiments, cell populations within cocultures were separated by MACS technology before stimulation of responder T_{cons}, which had been washed twice with X-VIVO medium to remove MACS buffer before stimulation. In some experiments, ionomycin (0.1 to 0.5 μM) or thapsigargin (0.05 to 1 μM) was added in addition to the stimulating antibodies.

RNA preparation and quantitative reverse transcription–polymerase chain reaction assays

Total RNA was isolated with the RNAqueous Micro Kit (Ambion), and complementary DNA (cDNA) was prepared with oligo$(dT)_{16}$ primers (Invitrogen). We quantified mRNAs by detection of incorporated SYBR Green with the ABI Prism 5700 sequence detector system (Applied Biosystems). The relative abundance of a given mRNA was determined by normalization to that of *GAPDH* mRNA, and the results are presented as the fold difference compared to the abundance of mRNA in unstimulated T_{cons}, which was set to 1. Primer sequences are listed in the Supplementary Methods.

Gene array analysis

$HLA\text{-}A2^+$ T_{regs} and $HLA\text{-}A2^+$ T_{cons} were incubated with FITC-conjugated antibody against HLA-A2 and FITC-specific microbeads. $HLA\text{-}A2^-$ T_{cons} were left unstimulated or were stimulated with antibody against CD3 (0.2 μg/ml) and antibody against CD28 (0.5 μg/ml) for 3 hours in the presence of $HLA\text{-}A2^+$ T_{regs} or $HLA\text{-}A2^+$ T_{cons} at a 1:1 ratio. After the stimulation period, cocultures were separated, RNA was isolated as described earlier, and gene array analysis (Affymetrix whole genome U133A 2.0.CHIP) was performed.

Western blotting analysis

Cocultures were established as described earlier, and cells were incubated for 30 to 60 min before stimulation. After separation of the individual populations in the coculture, responder T_{cons} were washed in tris-buffered

saline (TBS) and lysed in Beadlyte Cell Signaling Universal Lysis Buffer (Upstate) supplemented with complete protease inhibitors (Roche Applied Science) and PhosSTOP (Roche Applied Science). Proteins were denatured in SDS sample buffer, resolved by 8 to 12% SDS–polyacrylamide gel electrophoresis (SDS-PAGE), and transferred to Hybond nitrocellulose membranes (Amersham). After the membranes were blocked with 5% nonfat dry milk in TBS containing 0.1% (w/v) Tween 20 (TBST) and incubated with primary and horseradish peroxidase (HRP)–conjugated secondary antibodies, protein bands were developed with Immobilon Western Chemiluminescent HRP substrate (Millipore) in a Vilber Lourmat chemiluminescence acquisition system, and bands were quantified with Bio-1D software (Vilber Lourmat). For the detection of phosphorylated p65 by Western blotting analysis with fluorescently labeled secondary antibodies, cells were lysed by sonication for 1.5 min in sample buffer, Western blotting was performed as described earlier, and blots were scanned with the LI-COR Odyssey infrared imaging system.

Measurement of Ca^{2+} flux

T cells were incubated with the dyes PKH26 or PKH67 (1:200 in diluent C, 200 μl/10^6 cells, Sigma) for 5 min at 20°C, and the reaction was stopped with fetal bovine serum (FBS, Gibco). Cells were washed three times with X-VIVO 15 medium and left in X-VIVO 15 for 2 hours at 37°C. Responder T_{cons} were then labeled with Indo-1 AM (1 μM, Invitrogen) for 30 min at 37°C, washed, and resuspended in X-VIVO 15 medium. In some experiments, responder T_{cons} were incubated with the cAMP antagonist Rp-cAMPS (1 mM, Calbiochem) for 30 min at 37°C in X-VIVO 15 medium after incubation with PKH and Indo-1 and subsequently washed twice with medium before cocultures were established. T_{regs} or T_{cons} were cocultured in X-VIVO 15 medium supplemented with 0.5 mM $CaCl_2$ in a 1:1 ratio with allogeneic responder T_{cons} at 5×10^6 cells/ml for at least 30 min (if not stated otherwise) at 37°C to enable cell pairs to form. Ca^{2+} influx in X-VIVO 15 medium supplemented with 0.5 mM Ca^{2+} (final concentration, 2 mM) was induced after 1 min of measurement of basal Ca^{2+} flux by the addition of antibody against CD3 (0.2 μg/ml), antibody against CD28 (2 μg/ml), and cross-linking antibodies (2 μg/ml). In some experiments, thapsigargin was added. Measurements were performed on a FACS Diva or LSRII flow cytometer (BD Biosciences). For measurements of Ca^{2+} store depletion and Ca^{2+} influx through Ca^{2+} channels in the plasma membrane, cocultures were incubated for at least 30 min in X-VIVO 15 medium at 37°C to enable conjugate formation and then cells were washed twice with Ca^{2+}-free, phosphate-buffered saline (PBS) and immediately measured in PBS. After 1 min, Ca^{2+} store depletion was induced by the addition of antibodies against CD3 and CD28 and cross-linking antibodies, as described earlier, in PBS, and after further measurement, extracellular Ca^{2+} was added in X-VIVO 15 medium to a final concentration of 0.75 mM. Data were analyzed with the kinetics tool of FlowJo software and exported to PowerPoint to adjust baselines (Indo-1 ratio before stimulation) to equal levels for responder T_{cons} of one donor within one experiment. As an alternative to staining with PKH, responder T_{cons} were distinguished from allogeneic T_{cons} or T_{regs} by staining for surface HLA-A2, and Ca^{2+} measurements were performed as described above.

Inositol phosphate analysis

Responder T_{cons} were labeled with *myo*-[^{3}H]inositol (10 μCi/ml; Perkin Elmer) in inositol-free RPMI medium (Biomol) containing 10% dialyzed FBS (Sigma) for 48 to 50 hours. T_{cons} were then washed and resuspended in X-VIVO 15 medium for 12 hours. Cocultures were established with unlabeled T_{regs} or T_{cons} in a 1:1 ratio; the cells were incubated for 60 min at 37°C and then stimulated as described earlier. After stimulation, cocultures were washed with cold PBS, lysed in 10% trichloroacetic acid (TCA) supplemented with EDTA and sodium fluoride, and subjected to two rounds of freezing and thawing, and then the TCA was removed by diethyl ether extraction. The pH of the sample was adjusted to ~6, and samples were partially lyophilized, frozen, and shipped on dry ice. Inositol phosphate extracts were subjected to metal-dye detection high-performance liquid chromatography (MDD-HPLC), which was performed on a MiniQ PC 3.2/3 column (Pharmacia Biotech) with a Kontron system (BioTEK), as described previously (*54*), with slight modifications (see the Supplementary Methods). The radioactivity of [^{3}H]-labeled inositol phosphate isomers synthesized from *myo*-[^{3}H]inositol in the collected fractions was determined by liquid scintillation counting (Flo-Scint IV, Packard). The suppression of cytokine mRNA expression was controlled in parallel experiments with an aliquot of cells cultured under the same conditions, but with nonradioactive inositol. Before the analysis of mRNAs in responder T_{cons}, cell populations within the coculture were separated as described above.

Antibodies and reagents

Antibody against CD3 (OKT3) and antibody against CD28 (15E8) were purified from hybridoma supernatants. The cross-linking goat antibody against mouse antibody was obtained from Southern Biotechnology. Antibodies for the flow cytometric analysis of human HLA-A2, CD80, CD86, CTLA-4, PLC-γ1 (pY^{783}), p38 (pT^{180}/pY^{182}), and ERK1/2 (pT^{202}/pY^{204}) and the corresponding isotype control antibodies were purchased from BD Biosciences. Antibodies for the detection by Western blotting of IκBα (pS^{32}), IKKα (pS^{180})/β(pS^{181}), ZAP-70 (pY^{319})/Syk (pY^{352}), p65 (pS^{536}), and p38α were from Cell Signaling Technology; antibodies against ZAP-70, NFAT1, IκBα (c-21), PLC-γ1, and actin were from Santa Cruz Biotechnology; antibodies against PLC-γ1 (pY^{783}) and PKCθ (pT^{538}) were from BD Biosciences; antibody against tubulin was obtained from Sigma; and antibody against p38 (pT^{180}/pY^{182}) was from Promega. The HRP-conjugated antibodies against mouse immunoglobulin G (IgG), IgG1, IgG2a, IgG2b, or rabbit IgG were purchased from Santa Cruz Biotechnology. Alexa Fluor 680–conjugated antibody against rabbit IgG, Indo-1 AM, and thapsigargin were obtained from Invitrogen. PKH dyes, EGTA, and ionomycin were purchased from Sigma.

SUPPLEMENTARY MATERIALS

www.sciencesignaling.org/cgi/content/full/4/204/ra90/DC1

Methods

Fig. S1. Suppression of cytokine secretion is retained after removal of T_{regs}.

Fig. S2. T_{reg}-mediated rapid suppression of *IL2* expression in T_{cons} also occurs in the presence of APCs.

Fig. S3. CTLA-4 is not involved in the suppression of cytokine gene expression.

Fig. S4. Proximal TCR signaling is not altered in suppressed T_{cons}.

Fig. S5. Suppression of NFAT and NF-κB activation is independent of the antibody used to activate T_{regs}.

Fig. S6. Phosphorylation of ERK and p38 is not affected in suppressed T_{cons}.

Fig. S7. The block in Ca^{2+} influx in T_{cons} is not caused by allogeneic responses and requires 30 min of previous coculture with T_{regs}.

Fig. S8. Suppression of Ca^{2+} signaling is independent of cAMP.

Fig. S9. T_{regs}, but not T_{cons}, pre-activated with covalently plate-bound antibody against CD3 suppress Ca^{2+} signaling in responder T_{cons}.

Fig. S10. NFAT and NF-κB activation in T_{cons} is Ca^{2+}-dependent.

References

REFERENCES AND NOTES

1. S. Sakaguchi, Naturally arising CD4$^+$ regulatory T cells for immunologic self-tolerance and negative control of immune responses. *Annu. Rev. Immunol.* **22**, 531–562 (2004).
2. W. Zou, Regulatory T cells, tumour immunity and immunotherapy. *Nat. Rev. Immunol.* **6**, 295–307 (2006).
3. A. M. Thornton, E. M. Shevach, CD4$^+$CD25$^+$ immunoregulatory T cells suppress polyclonal T cell activation in vitro by inhibiting interleukin 2 production. *J. Exp. Med.* **188**, 287–296 (1998).

4. E. M. Shevach, Mechanisms of Foxp3$^+$ T regulatory cell-mediated suppression. *Immunity* **30**, 636–645 (2009).
5. S. Sakaguchi, K. Wing, Y. Onishi, P. Prieto-Martin, T. Yamaguchi, Regulatory T cells: How do they suppress immune responses? *Int. Immunol.* **21**, 1105–1111 (2009).
6. T. Bopp, C. Becker, M. Klein, S. Klein-Hessling, A. Palmetshofer, E. Serfling, V. Heib, M. Becker, J. Kubach, S. Schmitt, S. Stoll, H. Schild, M. S. Staege, M. Stassen, H. Jonuleit, E. Schmitt, Cyclic adenosine monophosphate is a key component of regulatory T cell–mediated suppression. *J. Exp. Med.* **204**, 1303–1310 (2007).
7. L. W. Collison, C. J. Workman, T. T. Kuo, K. Boyd, Y. Wang, K. M. Vignali, R. Cross, D. Sehy, R. S. Blumberg, D. A. Vignali, The inhibitory cytokine IL-35 contributes to regulatory T-cell function. *Nature* **450**, 566–569 (2007).
8. E. Bardel, F. Larousserie, P. Charlot-Rabiega, A. Coulomb-L'Hermine, O. Devergne, Human CD4$^+$ CD25$^+$ Foxp3$^+$ regulatory T cells do not constitutively express IL-35. *J. Immunol.* **181**, 6898–6905 (2008).
9. J. E. Smith-Garvin, G. A. Koretzky, M. S. Jordan, T cell activation. *Annu. Rev. Immunol.* **27**, 591–619 (2009).
10. C. Dong, R. J. Davis, R. A. Flavell, MAP kinases in the immune response. *Annu. Rev. Immunol.* **20**, 55–72 (2002).
11. S. Vallabhapurapu, M. Karin, Regulation and function of NF-κB transcription factors in the immune system. *Annu. Rev. Immunol.* **27**, 693–733 (2009).
12. I. Baine, B. T. Abe, F. Macian, Regulation of T-cell tolerance by calcium/NFAT signaling. *Immunol. Rev.* **231**, 225–240 (2009).
13. T. Kanno, U. Siebenlist, Activation of nuclear factor-κB via T cell receptor requires a Raf kinase and Ca^{2+} influx. Functional synergy between Raf and calcineurin. *J. Immunol.* **157**, 5277–5283 (1996).
14. M. Ouellet, B. Barbeau, M. J. Tremblay, p56^{lck}, ZAP-70, SLP-76, and calcium-regulated effectors are involved in NF-κB activation by bisperoxovanadium phosphotyrosyl phosphatase inhibitors in human T cells. *J. Biol. Chem.* **274**, 35029–35036 (1999).
15. R. E. Dolmetsch, R. S. Lewis, C. C. Goodnow, J. I. Healy, Differential activation of transcription factors induced by Ca^{2+} response amplitude and duration. *Nature* **386**, 855–858 (1997).
16. S. Feske, Calcium signalling in lymphocyte activation and disease. *Nat. Rev. Immunol.* **7**, 690–702 (2007).
17. T. Bopp, A. Palmetshofer, E. Serfling, V. Heib, S. Schmitt, C. Richter, M. Klein, H. Schild, E. Schmitt, M. Stassen, NFATc2 and NFATc3 transcription factors play a crucial role in suppression of CD4$^+$ T lymphocytes by CD4$^+$ CD25$^+$ regulatory T cells. *J. Exp. Med.* **201**, 181–187 (2005).
18. N. Oberle, N. Eberhardt, C. S. Falk, P. H. Krammer, E. Suri-Payer, Rapid suppression of cytokine transcription in human CD4$^+$CD25$^-$ T cells by CD4$^+$Foxp3$^+$ regulatory T cells: Independence of IL-2 consumption, TGF-β, and various inhibitors of TCR signaling. *J. Immunol.* **179**, 3578–3587 (2007).
19. K. Wing, Y. Onishi, P. Prieto-Martin, T. Yamaguchi, M. Miyara, Z. Fehervari, T. Nomura, S. Sakaguchi, CTLA-4 control over Foxp3$^+$ regulatory T cell function. *Science* **322**, 271–275 (2008).
20. R. H. Friedline, D. S. Brown, H. Nguyen, H. Kornfeld, J. Lee, Y. Zhang, M. Appleby, S. D. Der, J. Kang, C. A. Chambers, CD4$^+$ regulatory T cells require CTLA-4 for the maintenance of systemic tolerance. *J. Exp. Med.* **206**, 421–434 (2009).
21. C. Oderup, L. Cederbom, A. Makowska, C. M. Cilio, F. Ivars, Cytotoxic T lymphocyte antigen-4-dependent down-modulation of costimulatory molecules on dendritic cells in CD4$^+$ CD25$^+$ regulatory T-cell-mediated suppression. *Immunology* **118**, 240–249 (2006).
22. Z. W. Sun, Y. H. Qiu, Y. J. Shi, R. Tao, J. Chen, Y. Ge, Y. M. Hu, H. B. Ma, Q. Shi, X. G. Zhang, Time courses of B7 family molecules expressed on activated T-cells and their biological significance. *Cell. Immunol.* **236**, 146–153 (2005).
23. S. Chikuma, A. K. Abbas, J. A. Bluestone, B7-independent inhibition of T cells by CTLA-4. *J. Immunol.* **175**, 177–181 (2005).
24. S. Ghosh, M. Karin, Missing pieces in the NF-κB puzzle. *Cell* **109**, S81–S96 (2002).
25. T. D. Gilmore, Introduction to NF-κB: Players, pathways, perspectives. *Oncogene* **25**, 6680–6684 (2006).
26. A. M. Thornton, C. A. Piccirillo, E. M. Shevach, Activation requirements for the induction of CD4$^+$CD25$^+$ T cell suppressor function. *Eur. J. Immunol.* **34**, 366–376 (2004).
27. T. Takahashi, Y. Kuniyasu, M. Toda, N. Sakaguchi, M. Itoh, M. Iwata, J. Shimizu, S. Sakaguchi, Immunologic self-tolerance maintained by CD25$^+$CD4$^+$ naturally anergic and suppressive T cells: Induction of autoimmune disease by breaking their anergic/suppressive state. *Int. Immunol.* **10**, 1969–1980 (1998).
28. V. Pillai, S. B. Ortega, C. K. Wang, N. J. Karandikar, Transient regulatory T-cells: A state attained by all activated human T-cells. *Clin. Immunol.* **123**, 18–29 (2007).
29. M. R. Walker, D. J. Kasprowicz, V. H. Gersuk, A. Benard, M. Van Landeghen, J. H. Buckner, S. F. Ziegler, Induction of FoxP3 and acquisition of T regulatory activity by stimulated human CD4$^+$CD25$^-$ T cells. *J. Clin. Invest.* **112**, 1437–1443 (2003).
30. F. Macian, NFAT proteins: Key regulators of T-cell development and function. *Nat. Rev. Immunol.* **5**, 472–484 (2005).
31. F. Macían, F. García-Cózar, S. H. Im, H. F. Horton, M. C. Byrne, A. Rao, Transcriptional mechanisms underlying lymphocyte tolerance. *Cell* **109**, 719–731 (2002).
32. P. G. Hogan, L. Chen, J. Nardone, A. Rao, Transcriptional regulation by calcium, calcineurin, and NFAT. *Genes Dev.* **17**, 2205–2232 (2003).
33. F. Macían, C. López-Rodríguez, A. Rao, Partners in transcription: NFAT and AP-1. *Oncogene* **20**, 2476–2489 (2001).
34. Y. L. Zhang, C. Dong, MAP kinases in immune responses. *Cell. Mol. Immunol.* **2**, 20–27 (2005).
35. L. Florin, L. Hummerich, B. T. Dittrich, F. Kokocinski, G. Wrobel, S. Gack, M. Schorpp-Kistner, S. Werner, M. Hahn, P. Lichter, A. Szabowski, P. Angel, Identification of novel AP-1 target genes in fibroblasts regulated during cutaneous wound healing. *Oncogene* **23**, 7005–7017 (2004).
36. M. Oh-hora, A. Rao, Calcium signaling in lymphocytes. *Curr. Opin. Immunol.* **20**, 250–258 (2008).
37. G. Gri, S. Piconese, B. Frossi, V. Manfroi, S. Merluzzi, C. Tripodo, A. Viola, S. Odom, J. Rivera, M. P. Colombo, C. E. Pucillo, CD4$^+$CD25$^+$ regulatory T cells suppress mast cell degranulation and allergic responses through OX40-OX40L interaction. *Immunity* **29**, 771–781 (2008).
38. P. R. Albert, A. H. Tashjian Jr., Relationship of thyrotropin-releasing hormone-induced spike and plateau phases in cytosolic free Ca^{2+} concentrations to hormone secretion. Selective blockade using ionomycin and nifedipine. *J. Biol. Chem.* **259**, 15350–15363 (1984).
39. A. J. Morgan, R. Jacob, Ionomycin enhances Ca^{2+} influx by stimulating store-regulated cation entry and not by a direct action at the plasma membrane. *Biochem. J.* **300**, 665–672 (1994).
40. A. Izcue, J. L. Coombes, F. Powrie, Regulatory T cells suppress systemic and mucosal immune activation to control intestinal inflammation. *Immunol. Rev.* **212**, 256–271 (2006).
41. E. M. Shevach, R. S. McHugh, A. M. Thornton, C. Piccirillo, K. Natarajan, D. H. Margulies, Control of autoimmunity by regulatory T cells. *Adv. Exp. Med. Biol.* **490**, 21–32 (2001).
42. E. Suri-Payer, B. Fritzsching, Regulatory T cells in experimental autoimmune disease. *Springer Semin. Immunopathol.* **28**, 3–16 (2006).
43. C. Baecher-Allan, D. A. Hafler, Human regulatory T cells and their role in autoimmune disease. *Immunol. Rev.* **212**, 203–216 (2006).
44. C. A. Piccirillo, J. J. Letterio, A. M. Thornton, R. S. McHugh, M. Mamura, H. Mizuhara, E. M. Shevach, CD4$^+$CD25$^+$ regulatory T cells can mediate suppressor function in the absence of transforming growth factor β1 production and responsiveness. *J. Exp. Med.* **196**, 237–246 (2002).
45. K. Wing, S. Sakaguchi, Regulatory T cells exert checks and balances on self tolerance and autoimmunity. *Nat. Immunol.* **11**, 7–13 (2010).
46. Q. Tang, J. A. Bluestone, The Foxp3$^+$ regulatory T cell: A jack of all trades, master of regulation. *Nat. Immunol.* **9**, 239–244 (2008).
47. T. R. Mempel, M. J. Pittet, K. Khazaie, W. Weninger, R. Weissleder, H. von Boehmer, U. H. von Andrian, Regulatory T cells reversibly suppress cytotoxic T cell function independent of effector differentiation. *Immunity* **25**, 129–141 (2006).
48. M. Oh-hora, M. Yamashita, P. G. Hogan, S. Sharma, E. Lamperti, W. Chung, M. Prakriya, S. Feske, A. Rao, Dual functions for the endoplasmic reticulum calcium sensors STIM1 and STIM2 in T cell activation and tolerance. *Nat. Immunol.* **9**, 432–443 (2008).
49. C. Y. Park, A. Shcheglovitov, R. Dolmetsch, The CRAC channel activator STIM1 binds and inhibits L-type voltage-gated calcium channels. *Science* **330**, 101–105 (2010).
50. Y. Wang, X. Deng, S. Mancarella, E. Hendron, S. Eguchi, J. Soboloff, X. D. Tang, D. L. Gill, The calcium store sensor, STIM1, reciprocally controls Orai and $Ca_V1.2$ channels. *Science* **330**, 105–109 (2010).
51. J. Bodor, J. F. Habener, Role of transcriptional repressor ICER in cyclic AMP-mediated attenuation of cytokine gene expression in human thymocytes. *J. Biol. Chem.* **273**, 9544–9551 (1998).
52. M. Vaeth, T. Gogishvili, T. Bopp, M. Klein, F. Berberich-Siebelt, S. Gattenloehner, A. Avots, T. Sparwasser, N. Grebe, E. Schmitt, T. Hünig, E. Serfling, J. Bodor, Regulatory T cells facilitate the nuclear accumulation of inducible cAMP early repressor (ICER) and suppress nuclear factor of activated T cell c1 (NFATc1). *Proc. Natl. Acad. Sci. U.S.A.* **108**, 2480–2485 (2011).
53. J. Bodor, Z. Fehervari, B. Diamond, S. Sakaguchi, ICER/CREM-mediated transcriptional attenuation of IL-2 and its role in suppression by regulatory T cells. *Eur. J. Immunol.* **37**, 884–895 (2007).
54. K. Sauer, Y. H. Huang, H. Lin, M. Sandberg, G. W. Mayr, Phosphoinositide and inositol phosphate analysis in lymphocyte activation. *Curr. Protoc. Immunol.* **Chapter 11**, Unit11.1 (2009).

Acknowledgments: We thank U. Matiba for technical assistance; K. Hexel and S. Schmitt for cell sorting; C. Watzl and K. Kohl for help with the conjugate assay; F. T. Wieland for suggestions regarding DAG analyses; R. Arnold, K. Gülow, J. Hoffmann, M. Li-Weber, T. Mock, and H. Weyd for helpful discussions and critical reading of the manuscript; and J. Buer (Essen, Germany) and R. Geffers (Braunschweig, Germany) for performing gene

arrays. **Funding:** This research was supported by contract research "Forschungsprogramm Allergologie II" of the Baden-Württemberg Stiftung (P-LS-AL-18/2); the Alliance for Immunotherapy of the Helmholtz Society; SFB 405; CellNetworks (to B.B.); the German Research Foundation SFB 638 and TRR83 (to B.B. and M.H.); and a Ph.D. fellowship of the Helmholtz International Graduate School for Cancer Research at the Deutsches Krebsforschungszentrum (to A.S.). **Author contributions:** N.O. and A.S. designed, performed, and analyzed coculture assays, Western blotting, enzyme-linked immunosorbent assays, and RNA and proliferation assays and wrote the paper; A.S. designed, performed, and analyzed calcium measurements and coculture experiments for inositol phosphate extraction; N.O. and E.S.-P. designed, performed, and analyzed experiments involving detection of intracellular phosphoproteins by flow cytometry and gene array experiments; E.-M.W. provided assistance in the design, performance, and analysis of experiments; D.V. provided technical assistance; S.F., R.B., and N.O. designed, performed, and analyzed phosphorylated p65 by Western blotting; C.S.F., A.S., and E.S.-P. designed, performed, and analyzed Luminex experiments; M.H. and B.B. designed, performed, and analyzed lipid mass spectrometry; H.L. and G.W.M. designed, performed, and analyzed the HPLC analysis of inositol phosphates; P.R., M.G., and A.S. designed, performed, and analyzed experiments to set up the conditions for Ca^{2+} measurements; and E.S.-P. and P.H.K. designed and supervised the research and wrote the paper. **Competing interests:** The authors declare that they have no financial conflicts of interest.

Submitted 9 May 2011
Accepted 2 December 2011
Final Publication 20 December 2011
10.1126/scisignal.2002179
Citation: A. Schmidt, N. Oberle, E.-M. Weiß, D. Vobis, S. Frischbutter, R. Baumgrass, C. S. Falk, M. Haag, B. Brügger, H. Lin, G. W. Mayr, P. Reichardt, M. Gunzer, E. Suri-Payer, P. H. Krammer, Human regulatory T cells rapidly suppress T cell receptor–induced Ca^{2+}, NF-κB, and NFAT signaling in conventional T cells. *Sci. Signal.* **4**, ra90 (2011).

Appendix 09

Ocaña-Morgner C, **Reichardt P**, Chopin M, Braungart S, Wahren C, Gunzer M, Jessberger R. Sphingosine 1-Phosphate-Induced Motility and Endocytosis of Dendritic Cells Is Regulated by SWAP-70 through RhoA.
J Immunol. 2011;186(9):5345-55.

IF: 5.5

Sphingosine 1-Phosphate–Induced Motility and Endocytosis of Dendritic Cells Is Regulated by SWAP-70 through RhoA

Carlos Ocaña-Morgner,* Peter Reichardt,† Michaël Chopin,* Sarah Braungart,* Christine Wahren,* Matthias Gunzer,† and Rolf Jessberger*

The phospholipid mediator sphingosine 1-phosphate (S1P) enhances motility and endocytosis of mature dendritic cells (DCs). We show that in vitro migration of *Swap-70*$^{-/-}$ bone marrow-derived DCs (BMDCs) in response to S1P and S1P-induced upregulation of endocytosis are significantly reduced. S1P-stimulated movement of *Swap-70*$^{-/-}$ BMDCs, specifically retraction of their trailing edge, in a collagen three-dimensional environment is impaired. These in vitro observations correlate with delayed entry into lymphatic vessels and migration to lymph nodes of skin DCs in *Swap-70*$^{-/-}$ mice. Expression of S1P receptors ($S1P_{1–3}$) by wild-type and *Swap-70*$^{-/-}$ BMDCs is similar, but *Swap-70*$^{-/-}$ BMDCs fail to activate RhoA and to localize Rac1 and RhoA into areas of actin polymerization after S1P stimulus. The Rho-activating G protein $G\alpha_i$ interacts with SWAP-70, which also supports the localization of $G\alpha_{13}$ to membrane rafts in BMDCs. LPS-matured *Swap-70*$^{-/-}$ BMDCs contain significantly more active RhoA than wild-type DCs. Preinhibition of Rho activation restored migration to S1P, S1P-induced upregulation of endocytosis in mature *Swap-70*$^{-/-}$ BMDCs, and localization of $G\alpha_{13}$ to membrane rafts. These data demonstrate SWAP-70 as a novel regulator of S1P signaling necessary for DC motility and endocytosis. ***The Journal of Immunology*****, 2011, 186: 5345–5355.**

Uptake of Ag by dendritic cells (DCs) and their subsequent maturation and movements to lymphoid tissue to present to and activate T lymphocytes are key to initiate an adaptive immune response (1). Elucidating the mechanisms that regulate DC motility and Ag uptake is important also to design vaccination strategies and treatment of infections.

Sphingosine 1-phosphate (S1P) acts as a chemoattractant in the blood and lymph at concentrations in the hundred-nanomolar range (2). S1P promotes lymphocyte egress from lymphoid organs (3) and, as revealed through studies using S1P agonists and S1P receptor knockout mice, regulates migration of mature DCs from skin or lung to draining lymph nodes in vivo (4–8). S1P signals through G protein-coupled receptors (GPCRs) named $S1P_{1–5}$. These receptors execute different cellular functions through coupling to distinct heterotrimeric G proteins (α_i, α_q, or $\alpha_{12/13}$), resulting in activation of the small Rho GTPase family members Rac, RhoA, and/or Cdc42. Diversity in the expression of S1P receptors and in the response to S1P is seen among several cell types. The regulation of cell motility is a main function of these receptors (9, 10). In mature DCs, motility toward S1P is modulated by $S1P_1$ and $S1P_3$ (4, 5, 8, 11, 12). The in vitro observation that S1P induces upregulation of endocytosis in matured DCs suggests that S1P may promote the rapid removal of bacteria at sites of infection (11). $S1P_1$ activates Rac1 after coupling $G\alpha_I$, whereas $S1P_3$ activates Rac1 and RhoA after association with $G\alpha_i$ and $G\alpha_{12/13}$, respectively (10). The importance of S1P to control motility and endocytosis of mature DCs has clearly been demonstrated, but regulatory mechanisms that govern the S1P signaling pathways in DCs remain to be fully understood.

SWAP-70 is expressed in DCs and localizes to DC membranes at sites of cell–cell contact and of micropinosomes (13). Functionally, SWAP-70 supports surface localization of peptide-loaded MHC class II (MHC-II) on DCs (14). Maturation of DCs triggers massive cytoskeletal rearrangements mainly controlled by activation of Rho GTPases (15, 16), which also regulate DC migration (16–20). SWAP-70 loosely resembles proteins of the Dbl family of guanine nucleotide exchange factors for Rho GTPases, and it binds to F-actin and Rac (21, 22). We demonstrated that SWAP-70 preferentially interacts with active RhoA (RhoA-GTP) and Rac1 (Rac1-GTP) in lysates of stimulated DCs. Unlike naive wild-type (wt) bone marrow-derived DCs (BMDCs), naive *Swap-70*$^{-/-}$ DCs show constitutively active RhoA (14). On LPS stimulation, further Rho activation fails in *Swap-70*$^{-/-}$ DCs. Considering the function of SWAP-70 to regulate Rho GTPases, we hypothesized that SWAP-70 affects S1P receptor signaling required for migration of DCs.

In this study, we aimed at testing this hypothesis. We demonstrate the requirement for SWAP-70 in RhoA-dependent, S1P-dependent motility and endocytosis of DCs. *Swap-70*$^{-/-}$ BMDCs show deficient upregulation of motility and endocytosis in response to S1P. Migration to S1P is restored by re-expression of SWAP-70 in *Swap-70*$^{-/-}$ BMDCs. Analysis of Rho GTPase activation in mature *Swap-70*$^{-/-}$ BMDCs revealed that *Swap-70*$^{-/-}$ BMDCs fail to activate RhoA after an S1P stimulus. In BMDCs lysates, SWAP-70 was shown to interact with the proteins $G\alpha_i$. *Swap-70*$^{-/-}$ BMDCs also fail to localize the signaling protein $G\alpha_{13}$ required for RhoA activation to membrane rafts. These results thus highlight a novel pathway of S1P-induced DC functions.

*Faculty of Medicine Carl Gustav Carus, Institute of Physiological Chemistry, Dresden University of Technology, D-01307 Dresden, Germany; and †Institute of Molecular and Clinical Immunology, Otto von Guericke University Magdeburg, 39120 Magdeburg, Germany

Received for publication October 19, 2010. Accepted for publication February 18, 2011.

Address correspondence and reprint requests to Prof. Carlos Ocaña-Morgner and Prof. Rolf Jessberger, Institute of Physiological Chemistry, Faculty of Medicine Carl Gustav Carus, Dresden University of Technology, Fiedlerstrasse 42, MTZ, Dresden 01307, Germany. E-mail addresses: carlos.ocana-morgner@mailbox.tu-dresden.de and rolf.jessberger@mailbox.tu-dresden.de

The online version of this article contains supplemental material.

Abbreviations used in this article: BMDC, bone marrow-derived dendritic cell; DC, dendritic cell; 2D, two-dimensional; 3D, three-dimensional; GPCR, G protein-coupled receptor; MHC class II, MHC-II; S1P, sphingosine 1-phosphate; wt, wild-type.

www.jimmunol.org/cgi/doi/10.4049/jimmunol.1003461

Materials and Methods

Animals

Swap-70$^{-/-}$ and the isogenic wt 129vEMS mice were described before (14) and maintained at the Experimental Center of the Medizinisch-Theoretisches Zentrum of the Medical Faculty at the Dresden University of Technology according to approved animal welfare guidelines.

BMDC cultures

Primary cultures of immature DCs from *Swap-70*$^{-/-}$ and wt 129vEMS mice were obtained by differentiation of bone marrow-derived precursors as described previously (14). At days 10–11, 1 μg/ml LPS (Sigma-Aldrich; *Salmonella enterica*) was added overnight. For most of the experiments, CD11c$^+$ BMDCs were then purified from cultures using anti-CD11c Abs bound to magnetic beads (Miltenyi Biotec). For activation of Rho GTPases, BMDCs were activated with LPS and then starved from GM-CSF for 4 h before S1P stimulus.

Real time-PCR

Total BMDC RNA was prepared using the TRIzol method (Invitrogen) according to the manufacturer's instructions. RNA was reverse transcribed (SuperScript reverse transcriptase; Invitrogen). Expression of S1P1, S1P2, S1P3, and GAPDH was analyzed using a Rotor-Gene RG3000 (Qiagen) and the DNA Master Plus SYBR Green Kit (Roche). The relative gene expression was calculated by dividing by the expression of GAPDH. Samples were amplified in duplicate. S1P1, S1P2, and S1P3 primers used were previously described (23): S1P1 forward, 5′-GTGTAGACCCAGAGTC-CTGCG-3′; S1P1 reverse, 5′-AGCTTTTCCTTGGCTGGAGAG-3′; S1P2 forward, 5′-GGCCTAGCCAGTGCTCAGC-3′; S1P2 reverse, 5′-CCTTG-GTGTAATTGTAGTGTTCCAGA-3′; S1P3 forward, 5′-GGAGCCCCTA-GACGGGAGT-3′; S1P3 reverse, 5′-CCGACTGCGGGAAGAGTGT-3′. PCR product sizes were as follows: S1P1, 88 bp; S1P2, 118 bp; S1P3, 104 bp.

Flow cytometry

LPS-stimulated BMDCs were used to detect the expression of receptors $S1P_1$ and $S1P_3$ on the surface of the cells using an LSRII flow cytometer and FACSDiva software (BD Biosciences). Polyclonal Abs against $S1P_1$ and $S1P_3$ were used at a concentration of 4 μg/ml (Cayman Chemical). FITC-labeled goat anti-rabbit IgG (SouthernBiotech) was used as secondary Ab at a dilution of 1:250.

In vitro migration assay

Chemotaxis in response to chemoattractants was analyzed by measuring the number of cells migrating through a polycarbonate filter (8-μm pore size) in 24-well Transwell chambers (Costar). The upper chamber included 1–3 × 10^5 BMDCs in 100 μl chemotaxis medium (DMEM medium with 0.1% BSA and 10 mM HEPES), and the lower chamber contained 600 μl of the same medium with or without chemoattractants. After incubation for 3 h at 37°C, cells that migrated to the bottom chamber were stained with eFluor450 anti-CD11c (eBioscience) and analyzed for 1 min using LSRII flow cytometer and FACSDiva software (BD Biosciences). Numbers of CD11c$^+$ cells obtained in the lower chambers were divided by the number of CD11c$^+$ cells in the input samples and represented as percentage of input. In some experiments, cells were treated with 1 μg/ml exoenzyme C3 (cell-permeable form; Cytoskeleton) for 4 h before the migration assays. C3 was added or not to the upper chamber together with the cells.

DC retroviral infection

BMDCs were transfected by retroviral infection as described previously (14). Retrovirus was produced by transfecting Phoenix Eco 293T packaging cell line with SWAP-70–IRES–GFP or IRES-GFP. BMDCs were infected with retroviral supernatant at day 6. The plate was centrifuged at 1200 rpm at 24°C for 90 min and left overnight at 37°C. Virus was removed and DCs were reinfected with new retroviral supernatant. After 48 h of the second infection, CD11c$^+$ DCs were purified from cultures using anti-CD11c Abs bound to magnetic beads (Miltenyi Biotec) and activated overnight with LPS (1 μg/ml).

Time-lapse series of motile DC under an S1P concentration gradient

BMDCs were applied on a μ-slide for chemotaxis assay (ibidi) according to manufacturer's instructions. A total of 150 nM S1P was applied to create a concentration gradient. Time-lapse series of moving DCs were recorded every 2 min for 5 h on a Nikon live imaging station (Nikon) equipped with a 20× phase-contrast objective, automated X-Y-Z-stage, a climate chamber, and camera. Migration speed and directionality were analyzed with the Chemotaxis and Migration tool plug-in (ibidi) for ImageJ.

In vitro three-dimensional live cell imaging of DC morphology

Purified LPS-matured CD11c$^+$ BMDCs (3 × 10^5/ml) were kept in RPMI media (phenol red free; Invitrogen) containing 10% FCS and added to self-constructed imaging chambers with the glass bottom coated with a collagen mixture described previously for use in three-dimensional (3D) collagen matrices (24). Stimulation occurred with 100 nM S1P (Sigma). Imaging was performed on a CellR imaging workstation (Olympus, Hamburg, Germany) using an upright microscope stage (BX61) with a 60× (NA 0.9) water-coupled lens. Using an automated X-Y-Z-stage, we chose between 5 and 10 optical fields in each culture. Frame dimensions were 68 × 68 μm total. Images were taken every 20 s for up to 4 h with the transmitted light channel recorded. Images were processed with Virtualdub 1.8.6 and ImageJ 1.34s. For a total of 40 wt and *Swap70*$^{-/-}$ cells, mean dendrite length and number were quantified by measuring apparent dendrites at 5 consecutive time points with 240-sec interval for each cell.

Ear skin explant culture

Ears from wt or *Swap70*$^{-/-}$ animals were split into dorsal and ventral halves, and the cartilage-free half was cultured with medium in 24-well tissue culture plates for 24 or 48 h. Mechanical splitting of the ears is enough to trigger maturation of skin DCs (25). After incubation, ear halves were washed three times in PBS, fixed with methanol for 5 min, and incubated with PBS + 1% BSA before use for fluorescent labeling.

Confocal microscopy

For F-actin and Rho GTPases staining, LPS-matured BMDCs were left to adhere for 3 h on glass slides; then 50 nM S1P was added to the cells and left for 30 min. Cells were fixed with 3.7% paraformaldehyde in PBS for 10 min at room temperature. Cells were then blocked with 3% BSA in PBS and permeabilized with 1% Triton X-100 (Sigma) in PBS. Rac1 and RhoA staining was done with mAbs (Cytoskeleton) followed by Alexa Fluor 594-labeled Ab against mouse IgG (Invitrogen). Alexa Fluor 488-labeled phalloidin (Invitrogen) was used to visualize F-actin. Slides were mounted in Fluoromont-G (SouthernBiotech) and viewed using the Zeiss LSM 510 confocal microscopy system (Carl Zeiss). Imaging was performed using a 40×/1.3 differential interference contrast oil objective. Lasers of 488 and 561 nm were used for excitation of FITC and Alexa Fluor 594 respectively. Emissions wavelengths were separated by band passes 505–550 and >575 nm, respectively. Confocal sections of 1 μm/cell were taken. Colocalization of F-actin and Rho GTPases was quantified according to Ocaña-Morgner et al. (14). Forty cells were analyzed via ImageJ using the colocalization plug-in (ratio: 30%; threshold for each channel: 50). Nuclei were visualized with DAPI staining and an area around the cytoplasm of each cell in the colocalization image was analyzed for gray values representing the level of colocalization of two proteins (values close to the maximum of 256 represent strong colocalization). Profiles for each cell with a mean gray value per square micrometer were obtained, and the average of these mean values was plotted for Rac1–F-actin and RhoA–F-actin colocalization. Ears explant staining was done with goat polyclonal anti–LYVE-1 Abs (R&D Systems), FITC-labeled anti-murine Langerin/CD207 (Dendritics), FITC-labeled anti-CD86 (BD Biosciences), and Alexa 594-labeled anti-goat Abs (Invitrogen). The ear halves were mounted in Fluoromont-G (SouthernBiotech) and viewed using the Zeiss LSM 510 confocal microscopy system (Carl Zeiss). Imaging was performed using a 25×/0.8 differential interference contrast objective. Lasers of 488 and 561 nm were used for excitation of FITC and Alexa Fluor 594, respectively. Emissions wavelengths were separated by band passes 505–550 and >575 nm, respectively. Images were acquired using LSM 5Pas software (Carl Zeiss), analyzed by ImageJ (National Institutes of Health), and transferred to Photoshop 7.0 (Adobe Systems) to produce the final figures.

Skin FITC painting

Migration of skin DCs in foot pads was induced in vivo by applying 20 μl of 8 mg/ml FITC dissolved in a 50:50 (v/v) mixture of acetone and dibutylphthalate. After several time points, draining popliteal lymph node cell suspensions were analyzed for CD11c$^+$FITC$^+$ DCs by flow cytometry. Nondraining popliteal lymph nodes were used as control.

Endocytosis assay

LPS-mature BMDCs were incubated in DMEM with 0.5% BSA and 10 mM HEPES for 3 h at 37°C, then FITC-dextran (1 mg/ml) and S1P (100 nM)

were added together and left incubating for 5 min. Endocytosis was stopped by placing the cells on ice. DCs were then washed three times with cold PBS containing 0.1% NaN_3. Mean fluorescence intensity of FITC-dextran$^+$ cells was analyzed by flow cytometer. Incubation of DCs with FITC-dextran and S1P at 4˚C was used as negative control. In some experiments, cells were treated with 1 μg/ml exoenzyme C3 (cell-permeable form; Cytoskeleton) for 4 h before the migration assays. C3 was added or not to the lower chamber together with the chemoattractant.

Rho GTPases activity

The activities of Rho GTPases were analyzed using rhotekin-Rho– or PAK-rac/cdc42–binding domain agarose. Beads were subjected to SDS-PAGE and Western blotting with Abs against Rac1/2 (23A8; Upstate Biotechnology) and RhoA (119; Santa Cruz Biotechnology). Activity of Rho GTPases was quantified by densitometric analysis using ImageQuant software (Molecular Dynamics).

Purification of detergent-resistant membrane rafts

Membrane rafts were prepared by cell lysis of BMDCs followed by OptiPrep (Progen Biotechnik) gradient fractionation using ultracentrifugation as previously described (26). Five hundred-microliter fractions were collected from the top of the gradient. Protein concentration of each fraction was assayed by protein assay kit (Bio-Rad) based on the Bradford dye procedure. Fractions were analyzed individually by SDS-PAGE and Western blotting. Anti-caveolin 1 (Santa Cruz Biotechnology) and anti-transferrin receptor (Abcam) were used for positive and negative control of membrane rafts, respectively. Anti-$G\alpha_{12}$, anti-$G\alpha_{13}$, and anti-$G\alpha_I$ (all from Santa Cruz Biotechnology) were also used.

Immunoprecipitation

LPS-treated wt BMDCs were stimulated with 50 nM S1P for 30 min. A total of 2×10^7 DCs were incubated on ice for 10 min in hypertonic buffer (250 mM sucrose, 10 mM Na-HEPES pH 7.2, 2 mM $MgCl_2$, 10 mM NaF) that was freshly supplemented with a protease inhibitor mixture. Cells were lysed twice in a nitrogen cavitation apparatus at 1000 pounds per square inch for 7 min each. The soluble cell lysates were mixed with 1 μg polyclonal anti–SWAP-70. Cell lysates were rocked overnight at 4˚C. Protein G Sepharose beads were added and rocked for 1 h. The beads were washed three times with the hypertonic buffer and the precipitates analyzed by SDS-PAGE, followed by immunoblotting using anti–SWAP-70 or anti-Rho GTPase Abs.

Statistical analysis

For direct comparison of the activity of wt and *Swap70*$^{-/-}$ cells, statistical significance was determined with the Mann–Whitney *U* test for two-tailed data. The p values <0.05 were considered highly significant.

Results

Swap-70$^{-/-}$ *BMDCs are impaired in S1P-induced motility*

In mature DCs, motility is enhanced by S1P signaling mainly through $S1P_1$ and $S1P_3$ (8, 11, 12). Transwell chemotaxis assays showed that *Swap-70*$^{-/-}$ BMDCs are significantly reduced in their S1P-induced motility at every effective S1P concentration tested as compared with wt (Fig. 1*A*). This difference was observed for both BMDCs (Fig. 1*A*) and spleen-derived DCs (data not shown). Motility of immature DCs was not different from that seen without S1P and was similar in wt and *Swap-70*$^{-/-}$ BMDCs (data not shown). Motility tests using other chemoattractants, that is, CCL19 or CCL21, showed no difference in the response of *Swap-70*$^{-/-}$ or wt BMDCs (Fig. 1*A*), indicating specificity of SWAP-70 for S1P signaling. To confirm the SWAP-70 dependency of the S1P-mediated chemotactic response phenotype, we introduced a SWAP-70–IRES–GFP retroviral expression construct (14) into SWAP-70–deficient BMDCs. Expression of SWAP-70 in *Swap-70*$^{-/-}$ BMDCs restored their S1P response to levels comparable with wt cells (Fig. 1*B*). In wt BMDCs, expression of SWAP-70, as well as infection by the empty control vector itself, stimulated their migration when compared with mock-treated control cells. Transduction of DCs with retroviral vectors leads to some activation (27), which may be reflected in the improved capacity to migrate to S1P in wt BMDCs. Thus, activation is not sufficient to rescue the migration deficiency in *Swap-70*$^{-/-}$ BMDCs.

The speed of motility was also reduced in response to an S1P concentration gradient as seen by analysis of time-lapse movies of *Swap-70*$^{-/-}$ and wt BMDCs on two-dimensional (2D) surfaces (Fig. 1*C*, Supplementary Videos 1, 2). There was no difference between wt and *Swap-70*$^{-/-}$ BMDCs in response to CCL19 or CCL21 in these assays (not shown). Directionality toward S1P, however, was not affected in *Swap-70*$^{-/-}$ BMDCs (Fig. 1*C*). Analysis of individual cells in response to an S1P concentration gradient on 2D surfaces showed no significant difference in morphology (data not shown). The morphology of cells in response to S1P in a 3D environment was investigated next. In this study, motility is driven by cytoskeleton dynamics, that is, flow of actin polymerization at the cell front and actomyosin contractions of the trailing edge to propel the nucleus through narrow spaces (17). A deficiency in DCs to properly move through 3D environments, which to some extent reflect the interstitial space in the skin, was previously reported to result in deficient migration to lymph nodes (17, 18). Morphological analyses of wt cells showed a round cell body with the nucleus mostly close to the body center. Their dendrites were usually not very long and they spread around the entire cell body (circular dendrites) most of the time (Fig. 1*D*, Supplemental Video 3). *Swap-70*$^{-/-}$ BMDCs, in contrast, showed a more elongated morphology; the cell body was more stretched out and the nucleus often lagging behind. In addition, the dendrites of *Swap-70*$^{-/-}$ BMDCs were significantly longer when compared with wt BMDCs, whereas there was no difference in number of dendrites (Fig. 1*D*, Supplemental Video 4).

Delayed entry into lymphatic vessels and migration to lymph nodes of Swap-70$^{-/-}$ *DCs*

Recent studies indicate that S1P does not regulate migration of DCs from the periphery to lymph nodes under steady-state conditions (11, 28). However, this situation may change under local or systemic inflammatory conditions (8). In addition, S1P regulation of migration of DCs in vivo is indicated by studies with S1P agonists and S1P receptor knockout mice where S1P controls migration of mature DCs from skin, lung, or lamina propria to draining lymph nodes (4–8). The morphology of *Swap-70*$^{-/-}$ BMDCs on 3D collagen matrix indicated a defect in dragging the nucleus through small pores. This deficiency may reflect impaired migration of skin *Swap-70*$^{-/-}$ DCs through interstitial space likely resulting in impaired entry into lymphatic vessels in the skin (17). To test this, we studied entry of DCs into lymphatic vessels by analyzing the migration of DCs in the skin of ear explants. Mechanical splitting of ears into halves followed by incubation in medium at 37˚C triggered activation of DCs and their migration into lymphatic vessels, which were visualized by LYVE-1 staining (5). CD86 and Langerin were used as markers for skin DCs (5). We did not use MHC-II as a marker because of the MHC-II phenotype in *Swap-70*$^{-/-}$ BMDCs previously described (14). Vessel morphology and intervessel distance were the same in wt and *Swap-70*$^{-/-}$ ears. CD86$^+$- and Langerin$^+$- *Swap-70*$^{-/-}$ DCs showed significantly delayed entry into lymphatic vessels as compared with wt (Fig. 2*A*). Thus, *Swap-70*$^{-/-}$ DCs were impaired in their entry into skin lymphatic vessels in vivo. We also observed that Langerin$^+$ DCs generally entered lymphatic vessels later than the majority of CD86$^+$ cells. This probably is due to the fact that Langerin$^+$ DCs, which are mostly epidermal, are known to enter lymphatic nodes after dermal DCs (25, 29, 30). Entry of DCs into lymphatic vessels also depends on adhesion molecules on DCs that interact with ligands on lymphatic endothelial cells (31, 32). Lymphatic entry

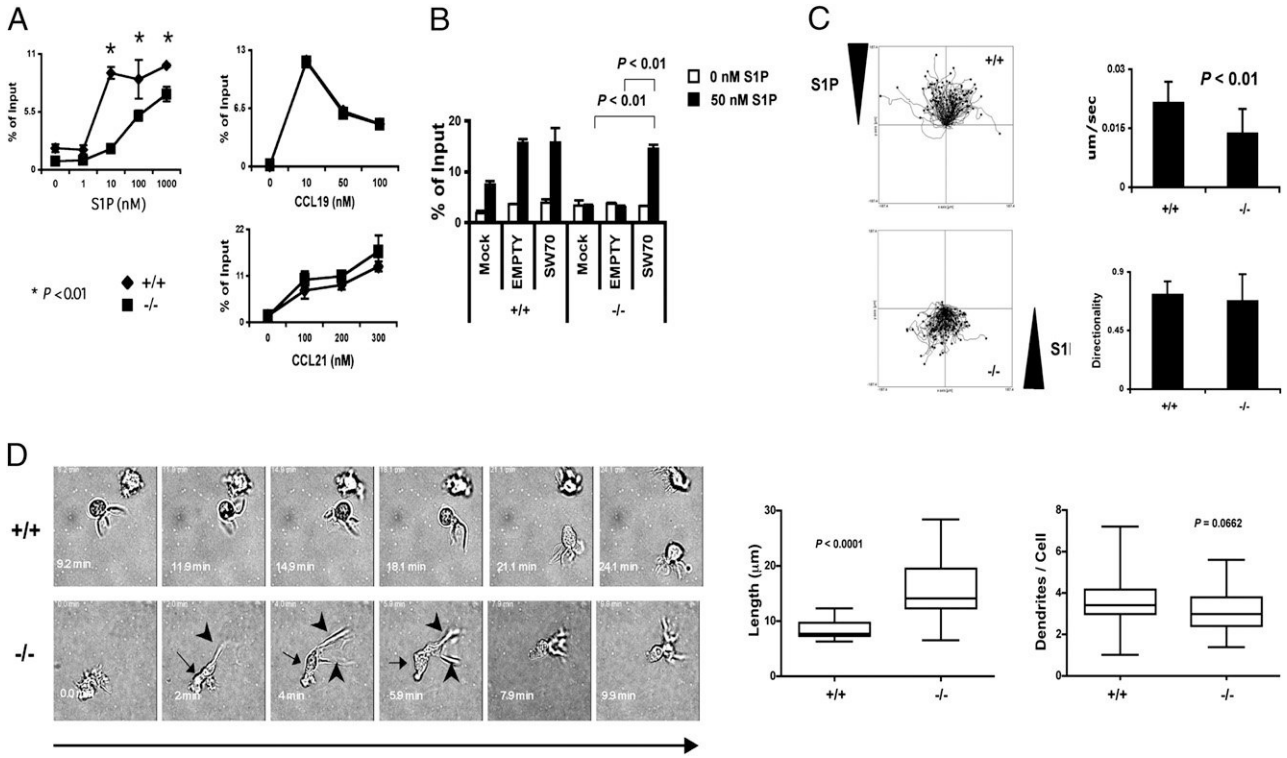

FIGURE 1. Impaired motility response to S1P by *Swap-70*$^{-/-}$ BMDCs. *A*, In vitro migration assays of LPS-activated *Swap-70*$^{-/-}$ and wt BMDCs in response to S1P (*top left panel*), CCL19 (*top right panel*), or CCL21 (*bottom left panel*). Migration is calculated as percentage of input after 3-h exposure to different concentrations of the chemoattractants in a Transwell system. Data are representative of at least 10 independent experiments. *B*, In vitro migration assays of LPS-activated *Swap-70*$^{-/-}$ and wt BMDCs in response to S1P after retroviral infection used for the expression of SWAP-70. Mock treatment and empty retroviral vector were used as control. Migration is calculated as percentage of input after 3-h exposure to 50 nM S1P in a Transwell system. *C*, Quantification of time series after live cell imaging in response to an S1P gradient using ibidi μ-slide shows velocity (μm/sec) and directionality. Images were taken every 2 min for up to 5 h. Videos were analyzed with the Chemotaxis and Migration tool plug-in (ibidi) for ImageJ. *D*, In vitro 3D live cell imaging of DC morphology. LPS-matured and MACS-purified CD11c$^+$ BMDCs (3×10^5/ml) were added to self-constructed imaging chambers with the glass bottom coated with a collagen mixture. Stimulation occurred with 100 nM S1P. Images were taken every 20 s for up to 4 h. *Swap-70*$^{-/-}$ BMDCs show a more elongated body shape with the nucleus dragging behind (arrows) and long dendrites (arrowheads). Dendrite length (*left panel*) and number (*right panel*) were determined for a total of 40 wt and *Swap70*$^{-/-}$ cells. Data are representative of at least three independent experiments.

defect in the skin may reflect an impairment of *Swap-70*$^{-/-}$ DCs to transmigrate through lymphatic endothelial cells. To address this, we tested the chemotactic response of wt and *Swap-70*$^{-/-}$ BMDCs to CCL19 in a modified Transwell system where the porous membranes were coated with the C3H/HeJ mouse endothelial line SVEC4-10 that is reported as lymphatic endothelial cells (33). Although the transmigration through the endothelial cells greatly improved the chemotactic response to CCL19 of wt cells, the magnitude of the *Swap-70*$^{-/-}$ BMDCs response was significantly lower (Supplemental Fig. 1*A*). We observed the same deficiency to transmigrate in *Swap-70*$^{-/-}$ BMDCs when S1P was used as chemoattractant (Supplemental Fig. 1*B*). SWAP-70–deficient B cells have impaired entry to lymph nodes from the blood (34). During this process, *Swap70*$^{-/-}$ B cells aberrantly regulated integrin-mediated adhesion to blood endothelial cells (34). To address the role of integrins in the transmigration defect of *Swap-70*$^{-/-}$ BMDCs, we performed the same experiments as in Supplemental Fig. 1*A* in the presence of different concentrations of either EDTA or a blocking Ab against integrin β_2, which has been reported to regulate transmigration of DCs (31, 32). Although EDTA and the anti-β_2 Ab had an immediate negative effect on wt BMDCs, it took concentrations of up to 1000× (EDTA) or 500× (anti-β_2) higher to have an effect on *Swap-70*$^{-/-}$ BMDCs (Supplemental Fig. 1*C*). A blocking Ab against VCAM did not have an effect on either wt or *Swap-70*$^{-/-}$ DCs. These results indicate defective integrin signaling in *Swap-70*$^{-/-}$ BMDCs, and future studies will be done to characterize the integrin-mediated adhesion to lymphatic endothelial cells in *Swap-70*$^{-/-}$ BMDCs.

Skin-resident DCs require $S1P_1$ for efficient migration into the draining lymph node (8). We analyzed in vivo migration of DCs by FITC painting of foot pads of *Swap-70*$^{-/-}$ and wt mice followed by analysis of FITC$^+$CD11c$^+$ cells in the draining lymph nodes after 24, 48, and 72 h. Although we observed a decrease in the percentage of FITC$^+$CD11c$^+$ cells in the draining lymph nodes of wt animals as time increases after painting, the percentage of cells in *Swap-70*$^{-/-}$ animals actually increased to reach similar levels as wt DCs at 24 h (Fig. 2*B*). The failure to migrate early to lymph nodes in *Swap-70*$^{-/-}$ mice was not due to reduced numbers of DCs in the skin of the animals, because microscopic analysis and cell isolation procedures did not reveal a difference between wt and *Swap-70*$^{-/-}$ mice in the number of skin DCs (Supplemental Fig. 1*D*, left panel, and data not shown). As already suggested by data shown in Fig. 2*A*, these results indicate delayed migration of skin-resident DCs to draining lymph nodes in *Swap-70*$^{-/-}$ mice. The assays used in this set of experiments represent inflammatory conditions (35), but under steady-state, *Swap-70*$^{-/-}$ animals also show significantly decreased percentage and total numbers of DCs in lymph nodes (Supplemental Fig. 1*D*, right panels); MHC-II$^-$ cells, considered quiescent resident cells (24), are not changed. This indicates a mechanism, controlled by SWAP-70, that is shared for migration of DCs under steady-state and inflammatory conditions, and shall be the subject of further studies.

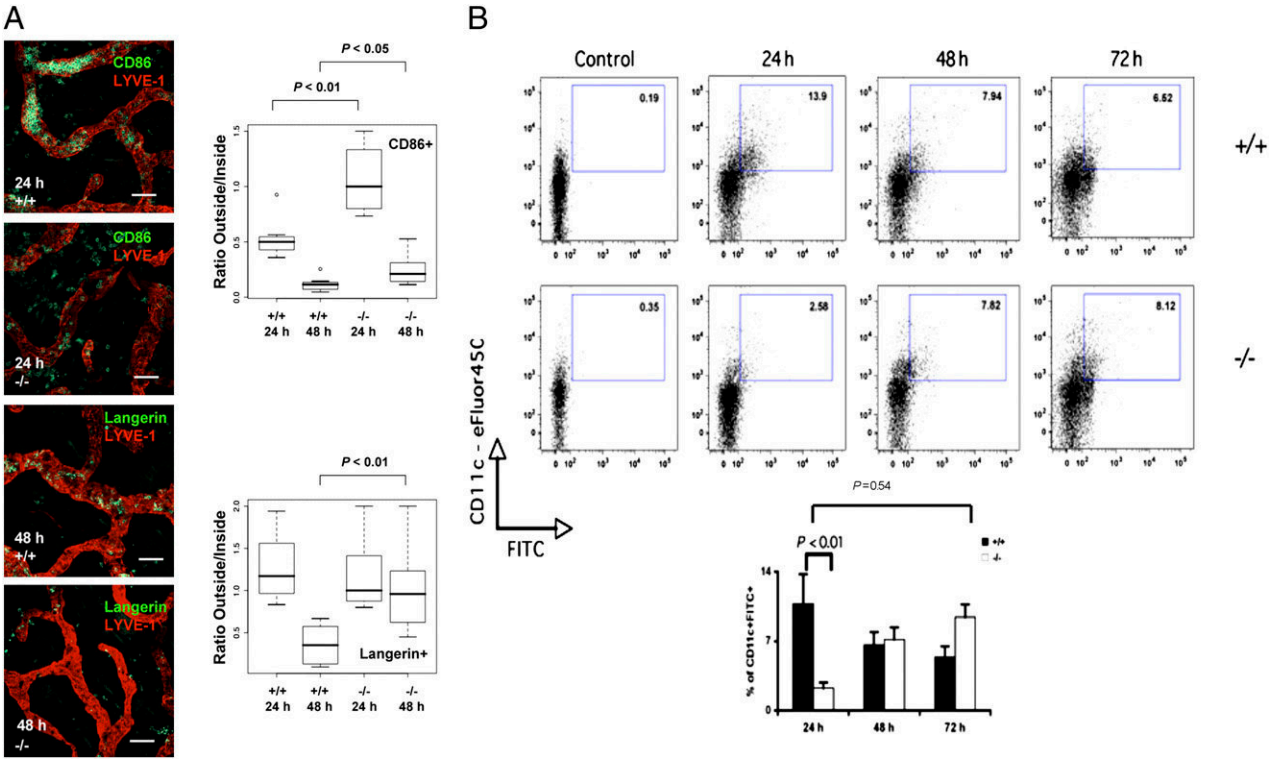

FIGURE 2. Delayed entry of *Swap-70*$^{-/-}$ DCs to lymphatic vessels and migration to lymph nodes. *A*, Confocal microscopy analysis of localization of CD86$^+$ and Langerin$^+$ cells outside or inside LYVE1$^+$ lymphatic vessels of ear explants after 24- or 48-h incubation at 37°C. CD86$^+$ and Langerin$^+$ cells were counted in each picture of ears, and the number of cells outside LYVE1$^+$ lymphatic vessels were plotted against the number of cells inside. Scale bars, 100 μm. *B*, FITC painting of foot pads. *Swap-70*$^{-/-}$ and wt animals were painting in one foot pad with 8 mg/ml FITC dissolved in a 50:50 (v/v) mixture of acetone and dibutylphthalate. After 24 h, draining popliteal lymph nodes were isolated and analyzed for CD11c$^+$FITC$^+$ DCs by flow cytometry. Popliteal lymph nodes from nonpainted foot pads were used as control. Data are representative of at least three independent experiments.

Expression of S1P receptors is unaltered in Swap-70$^{-/-}$ *BMDCs*

Using real-time PCR, we analyzed the expression of mRNA of the S1P receptors known to control DC motility and endocytosis in response to S1P, that is, $S1P_1$ and $S1P_3$ (11, 12), and of $S1P_2$. mRNA levels of these three receptors were not significantly different in *Swap-70*$^{-/-}$ or wt BMDCs at several time points after incubation with LPS (Table I). In agreement with previous reports, we observed upregulation of mRNA levels $S1P_1$ and $S1P_3$ and downregulation of $S1P_2$ (4, 8, 11). At the protein level, determination of expression of the receptors $S1P_1$ and $S1P_3$ by flow cytometry on the surface of LPS-stimulated *Swap-70*$^{-/-}$ or wt BMDCs did not show significant differences (Fig. 3). These results indicated that SWAP-70 might control signaling in response to S1P after binding to the receptors in mature DCs rather than receptor expression.

Defective S1P-induced endocytosis of Swap-70$^{-/-}$ *BMDCs*

In vitro, S1P enhances endocytosis in LPS-mature BMDCs, but not in immature BMDCs, through $S1P_3$ signaling (11, 36). This would constitute a mechanism thought to promote the rapid removal of pathogens at sites of infection (11, 36). To test this, we studied the effect of S1P on the endocytosis of LPS-matured BMDCs. After 5 min of exposure to S1P, endocytosis of FITC-dextran particles was significantly increased in wt BMDCs. In contrast, *Swap-70*$^{-/-}$ BMDCs failed entirely to enhance endocytosis of FITC-dextran (Fig. 4). Endocytosis is affected by the endosome transport inside cells that is mainly controlled by activation of RhoB (37, 38). We previously reported reduced expression of total RhoB during stimulus with LPS of *Swap-70*$^{-/-}$ BMDCs (14). However, the level of active RhoB-GTP remained the same in *Swap-70*$^{-/-}$ BMDCs after LPS addition (14). We excluded that the defect in S1P-induced endocytosis is due to failure to activate RhoB in

Table I. mRNA expression pattern of $S1P_1$, $S1P_2$, and $S1P_3$ in inactivated (LPS$^-$) and activated (LPS$^+$) DCs

BMDCs	$S1P_1$ (Mean ± SEM)	$S1P_2$ (Mean ± SEM)	$S1P_3$ (Mean ± SEM)
wt			
LPS$^-$	0.0009 ± 0.0001	0.0015 ± 0.0001	0.0001 ± 9.76E-05
LPS$^+$	0.0025 ± 0.0003	0.0008 ± 0.0002	0.0046 ± 0.0003
SWAP-70$^{-/-}$			
LPS$^-$	0.0009 ± 0.0001	0.0014 ± 0.0002	0.0002 ± 0.0001
LPS$^+$	0.0021 ± 0.0003	0.0007 ± 0.0002	0.0039 ± 0.0006

Real-time quantitative PCR analysis of wt and *SWAP-70*$^{-/-}$ BMDCs was performed as described in *Materials and Methods*. The amount of product for each PCR was normalized to GAPDH (mean ± SEM of a representative experiment).

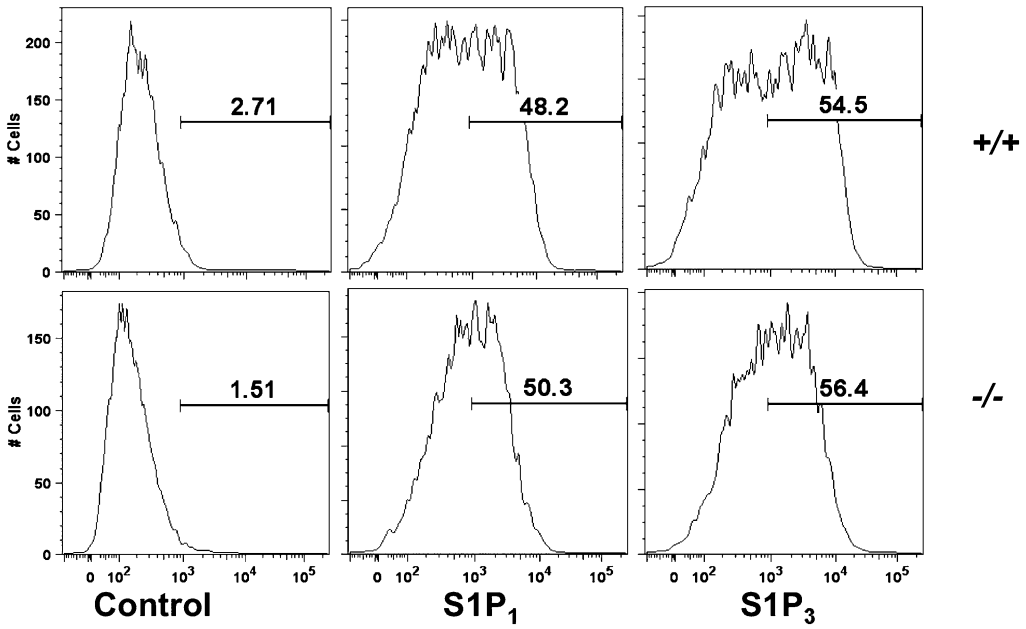

FIGURE 3. Expression of receptors $S1P_1$ and $S1P_3$ on the surface of LPS-stimulated wt (*top panels*) and *Swap-70*$^{-/-}$ BMDCs (*lower panels*). Secondary Ab anti-rabbit IgG was used as control. Data are representative of at least three independent experiments.

Swap-70$^{-/-}$ BMDCs because we do not observe any difference in the activation of RhoB after S1P stimulus in LPS-treated wt and *Swap-70*$^{-/-}$ BMDCs (data not shown). Furthermore, we did not find differences in endocytosis of immature wt and *Swap-70*$^{-/-}$ BMDCs (data not shown). These and the earlier data demonstrate an impaired S1P response in LPS-mature *Swap-70*$^{-/-}$ BMDCs that results in a failure to activate important functions, that is, motility and endocytosis.

SWAP-70 interacts with Gα$_I$ in BMDC extracts, and Swap-70$^{-/-}$ BMDCs fail to localize Gα$_{13}$ in membrane rafts

Previously, we reported interaction of SWAP-70 with the active forms of Rac1 and RhoA in BMDC lysates (14). This interaction may account for the proper activation and localization of these Rho GTPases after S1P stimulus. Failure of S1P signaling in *Swap-70*$^{-/-}$ DCs may also suggest interaction of SWAP-70 with other members upstream of Rho GTPases, for example, S1P receptors, G proteins, or both. We tested whether SWAP-70 interacts with S1P receptors and Gα proteins. We performed immunoprecipitation assays of cells after S1P stimulus. Lysates were obtained after incubation of cells with hypertonic buffer followed by lysis with nitrogen cavitation to preserve receptors complex that may form at the membrane, which otherwise would be disrupted in lysates prepared with detergents. We found that in wt BMDCs lysates, SWAP-70 interacts strongly with $G\alpha_I$ and, to a lesser level, with $G\alpha_{13}$ (Fig. 5*A*). We did not detect interaction with $S1P_3$ (Fig. 5*A*) or $S1P_1$ (data not shown). To test whether this interaction depends on intact membrane fragments where the proteins may associate, but not necessarily directly interact, we performed immunoprecipitation in detergent-containing lysis buffers. We observed interaction of SWAP-70 with $G\alpha_I$, but not with $G\alpha_{13}$, when the detergent NP-40 was used (Supplemental Fig. 2). However, this interaction disappeared when octyl glucoside was used, a detergent known to dissociate membranes and their associated proteins (39) (Supplemental Fig. 2). Together, these results show direct or membrane domain-mediated interactions of SWAP-70 with $G\alpha_I$ proteins.

S1P GPCRs and their signaling components, for example, Gα proteins, can be compartmentalized in membrane rafts and caveolae to initiate receptor-specific signal transduction (see Refs. 40, 41 for review). We analyzed the membrane localization of Gα proteins that are responsible for Rho GTPases activation after S1P stimulus (10). Fig. 5*B* shows that, in both immature wt BMDCs and *Swap-70*$^{-/-}$ BMDCs, $G\alpha_I$ and $G\alpha_{13}$ localized in membrane rafts/caveolae, which were identified by the use of caveolin 1. However, after LPS stimulus, $G\alpha_{13}$ disappeared from the membrane rafts/caveolae fractions of *Swap-70*$^{-/-}$ BMDCs, whereas it largely remained in the corresponding wt fractions. The same relocalization events happened in BMDCs stimulated by LPS and S1P. In wt BMDCs, a relatively large portion of $G\alpha_{13}$ localized to membrane rafts/caveolae (gradient fraction no. 2) compared with the portion of $G\alpha_{13}$ appearing in the heavy fractions (no. 5, 6). In addition, the Rac activator $G\alpha_i$ was lost from raft fractions in wt and *Swap-70*$^{-/-}$ BMDCs on LPS or LPS/S1P stimulation (Fig. 5*B*). Our initial data on failure of MHC-II localization into lipid

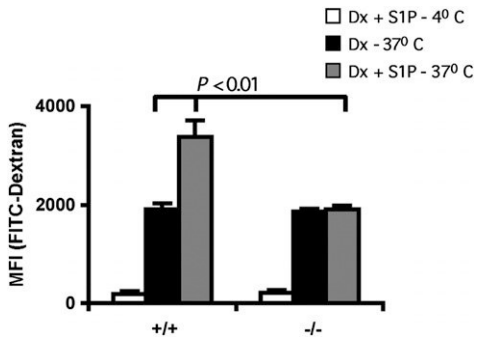

FIGURE 4. Deficient S1P-induced endocytosis of *Swap-70*$^{-/-}$ BMDCs. After serum starvation, LPS-matured BMDCs were incubated with 1 mg/ml FITC-dextran in the presence or absence of 100 nM S1P for 5 min at 37°C. After incubation, cells were analyzed by flow cytometry to determine the FITC mean fluorescence intensity (MFI). Incubation at 4°C was used as negative control. Data are representative of at least three independent experiments.

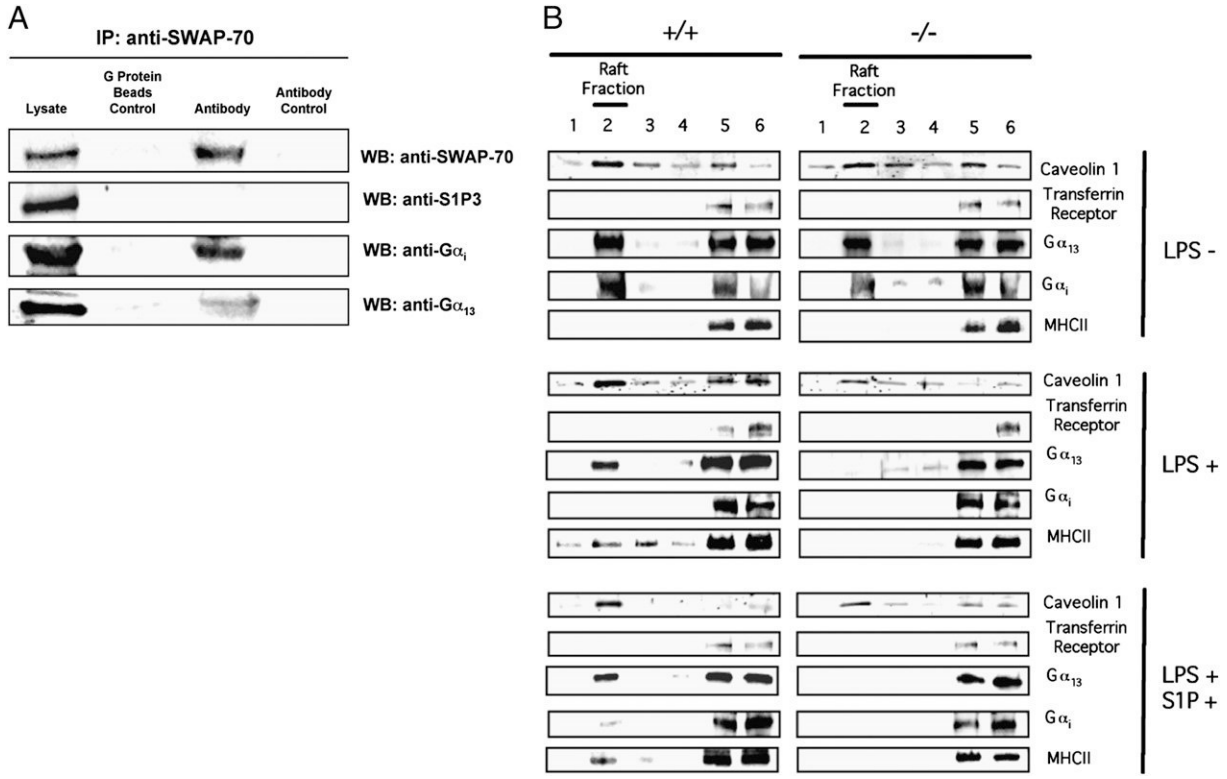

FIGURE 5. SWAP-70 interacts with $G\alpha_I$ in BMDC extracts and *Swap-70*$^{-/-}$ BMDCs fail to localize $G\alpha_{13}$ in membrane rafts. *A*, *Swap-70*$^{+/+}$ BMDCs lysates were immunoprecipitated with polyclonal anti–SWAP-70. Complexes were analyzed by Western blotting with anti–SWAP-70, anti-$S1P_3$, anti-$G\alpha_I$, and anti-$G\alpha_{13}$. *B*, Lysates of immature (LPS^-), LPS-matured (LPS^+), or LPS-S1P–matured (LSP^+S1P^+) BMDCs were subjected to OptiPrep gradient ultracentrifugation system. After centrifugation, six fractions were collected from the top of the tube, resolved by SDS-PAGE, and analyzed by Western blotting. Membranes were probed with polyclonal Ab against caveolin 1 for localization of membrane rafts and polyclonal Ab against transferring receptor as negative control.

rafts (14) were reproduced using additional markers such as caveolin 1 (Fig. 5*B*). Unlike in wt BMDCs, lipid raft formation is inefficient in *Swap-70*$^{-/-}$ BMDCs, as is formation of caveolin-positive membrane fractions. Thus, SWAP-70 is involved in control of formation of membrane domains like lipid rafts.

Swap-70$^{-/-}$ *BMDCs fail to activate RhoA and to localize Rac1 and RhoA to areas of F-actin on S1P treatment*

DC motility is enhanced by stimulation of $S1P_1$ and $S1P_3$ (5, 8, 11, 12), whereas endocytosis is mainly mediated through $S1P_3$ signaling (11). Previously, it was demonstrated that migration of mature DCs toward S1P depends on cytoskeleton-associated activation of Rho GTPases Rac1 and RhoA (4). $S1P_1$ activates Rac1, whereas $S1P_3$ activates Rac1 and RhoA (10). Thus, we studied the activation of Rac1 and RhoA in LPS-matured BMDCs after addition of S1P. *Swap-70*$^{-/-}$ BMDCs failed to activate RhoA and rather did not maintain its basal activation level (Fig. 6*A*). In contrast, activated Rac1 in *Swap-70*$^{-/-}$ BMDCs was not significantly different from wt BMDCs (Fig. 6*B*).

The role of RhoA activation in the chemotactic response to S1P of mature DCs was assayed using the exoenzyme C3 ADP-ribosyltransferase from *Clostridium botulinum*, which ADP-ribosylates and thus inactivates RhoA, but not Rac1 or Cdc42 (42). Although *Swap-70*$^{-/-}$ BMDCs were low in migration anyway, inactivation of RhoA during the transwell chemotaxis assays strongly inhibited migration to S1P of wt BMDCs (data not shown), indicating that RhoA plays an active role during migration to S1P in DCs in agreement with previous studies (4). In contrast, migration to CCL19 and CCL21 was not affected (data not shown), agreeing with previous data where RhoA inactivation with exoenzyme C3 did not inhibit CCR7-mediated migration of human DCs (43).

Rho GTPases colocalize with centers of actin polymerization as cells migrate in response to extracellular stimuli (44). Rho GTPases localize to F-actin structures that control migration in cells (45, 46). Colocalization analysis by confocal microscopy of Rac1 in F-actin areas in wt BMDCs on stimulation with S1P shows significantly more localization of the two proteins in the same areas (Fig. 6*C*), as shown by the levels of gray values representative of colocalization (Fig. 6*D*, 6*E*). There was a modest, albeit significant, increase in the level of localization of RhoA in F-actin areas in wt BMDCs after S1P stimulus (Fig. 6*C–E*). *Swap-70*$^{-/-}$ BMDCs fail to increase the level of localization of either Rac1 or RhoA with F-actin areas (Fig. 6*C–E*). In addition, the level of localization between RhoA and F-actin is significantly greater in *Swap-70*$^{-/-}$ BMDCs than in their wt counterparts before S1P stimulus (Fig. 6*D*, 6*E*). This agrees with the higher content of active RhoA, that is, RhoA-GTP, in unstimulated *Swap-70*$^{-/-}$ BMDCs (Fig. 6*A*). Taken together, these results show that *Swap-70*$^{-/-}$ BMDCs are impaired in their ability to properly activate and localize Rac1 and RhoA after S1P stimulus.

Preinhibition of RhoA restores S1P-induced motility, endocytosis, and localization of $G\alpha_{13}$ *in membrane rafts in Swap-70*$^{-/-}$ *BMDCs*

In nonactivated, immature *Swap-70*$^{-/-}$ BMDCs, RhoA is constitutively active, and this activation can be inhibited by pretreatment of the cells with exoenzyme C3 (14). In this study, we observed that in LPS-matured *Swap-70*$^{-/-}$ BMDCs, RhoA was also significantly more active than in wt BMDCs (Fig. 6*A*). We

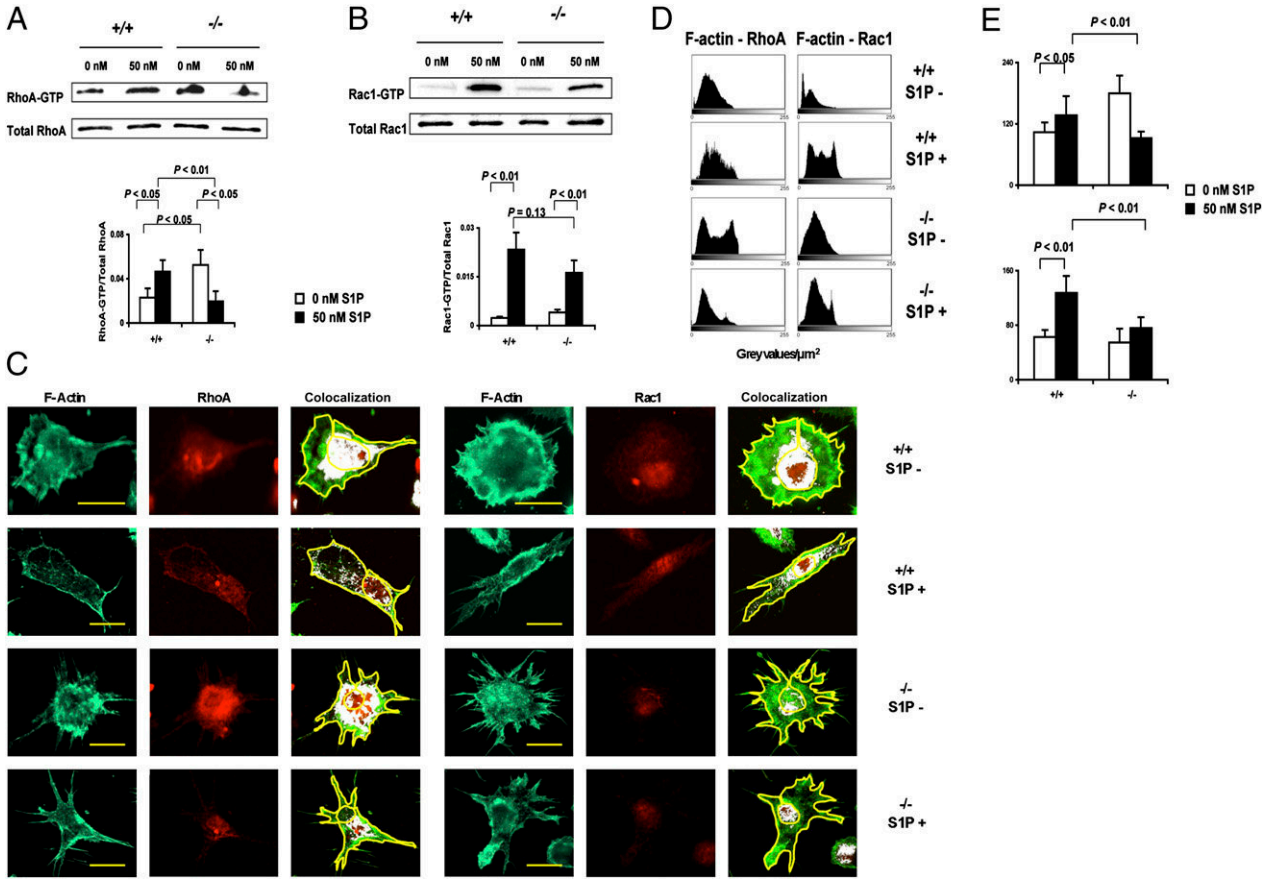

FIGURE 6. *Swap-70*$^{-/-}$ BMDCs fail to activate RhoA and to localize Rac1 and RhoA to areas of F-actin on S1P treatment. *A* and *B*, Activation of Rho GTPases in LPS-activated BMDCs after S1P stimulus was analyzed using (*A*) rhotekin-Rho–binding domain or (*B*) PAK-Rac/Cdc42–binding domain agarose beads. Beads were then subjected to SDS-PAGE and Western blotting. Activity of Rho GTPases was quantified by densitometric analysis and expressed as ratio of activated to total Rho GTPases. *C–E*, Localization of RhoA and Rac1 into F-actin areas in wt and *Swap-70*$^{-/-}$ BMDCs. *C*, Colocalization images show gray spots representing localization of the two proteins in F-actin areas. An area around the cytoplasm (yellow line) was drawn for quantification of gray values. Scale bars, 10 µm. *D*, Histograms show the distribution of gray values per square micrometer for the colocalization images used in *C*. *E*, Average of the mean gray values per square micrometer obtained from all of the histograms (40 for each staining) analyzed for RhoA (*upper panel*) and Rac1 (*lower panel*). Data are representative of at least 2 independent experiments, each with 40 cells measured.

preincubated LPS-matured BMDCs with exoenzyme C3 before performing S1P chemotaxis transwell and endocytosis assays. The cells were washed thoroughly before performance of the assays. Restoration of Rho GTPase activity is known to occur within 3 h after removal of the drug (42). Such treatment restored *Swap-70*$^{-/-}$ BMDC migration to S1P to levels close to wt cells (Fig. 7*A*). The same treatment inhibited to some degree migration of wt cells as well, indicating that there was some remaining inhibitory effect of the exoenzyme (Fig. 7*A*). Preinhibition of RhoA also restored the capacity of *Swap-70*$^{-/-}$ BMDCs to upregulate endocytosis after S1P triggering (Fig. 7*B*). In contrast, wt cells lost the ability to upregulate endocytosis, suggesting that RhoA activation was required for upregulation of S1P-mediated endocytosis (Fig. 7*B*). Moreover, localization of $G\alpha_{13}$ in membrane rafts in *Swap-70*$^{-/-}$ DCs was seen at the same level as in wt BMDCs when RhoA was preinhibited (Fig. 7*C*). Inactivation of RhoA by exoenzyme C3 before and during S1P stimulus in *Swap-70*$^{-/-}$ and wt BMDCs was tested by using pull-down assays with rhotekin-Rho–binding domain agarose (Supplemental Fig. 3). These results indicated that SWAP-70 ensures regulated and timely activation of RhoA in mature DCs, thereby allowing proper S1P signaling.

Discussion

S1P signaling through its receptors constitutes an important mechanism to enhance motility and endocytosis of mature DCs (4, 5, 8, 11, 12). In this article, we identify SWAP-70 as a new factor controlling S1P signaling in mature DCs. *Swap-70*$^{-/-}$ BMDCs showed deficient upregulation of motility and endocytosis in response to S1P. Migration to S1P was restored by re-expression of SWAP-70 in *Swap-70*$^{-/-}$ BMDCs. Morphological analysis in a 3D collagen matrix under S1P stimulus showed a deficiency of *Swap-70*$^{-/-}$ BMDCs to migrate through small pores. Reduced motility to S1P of *Swap-70*$^{-/-}$ BMDCs in 2D and 3D environments correlated with delayed entry into lymphatic vessels and migration to lymph nodes of skin *Swap-70*$^{-/-}$ DCs. Migration of mature DCs to S1P depends on the simultaneous activity of the GTPases Rac1 and RhoA (4), and our study shows that inhibition of RhoA activation abolished the upregulation of endocytosis in wt BMDCs. However, the analysis of Rho GTPase activation in mature *Swap-70*$^{-/-}$ BMDCs demonstrated that they contained a significantly greater level of active RhoA, and that they failed to upregulate active RhoA after an S1P stimulus. In this study, we found for the first time, to our knowledge, an interaction of SWAP-70 with the S1P signaling proteins $G\alpha_I$. These interactions may be direct, but as a membrane-solubilizing detergent dissociates them, the interaction may depend on the membrane; thus, SWAP-70 may colocalize with the G proteins in a membrane signaling cluster. This hypothesis fits to the observation that *Swap-70*$^{-/-}$ BMDCs failed to localize the signaling proteins $G\alpha_{13}$ required for RhoA activation to membrane rafts/caveolae. Together,

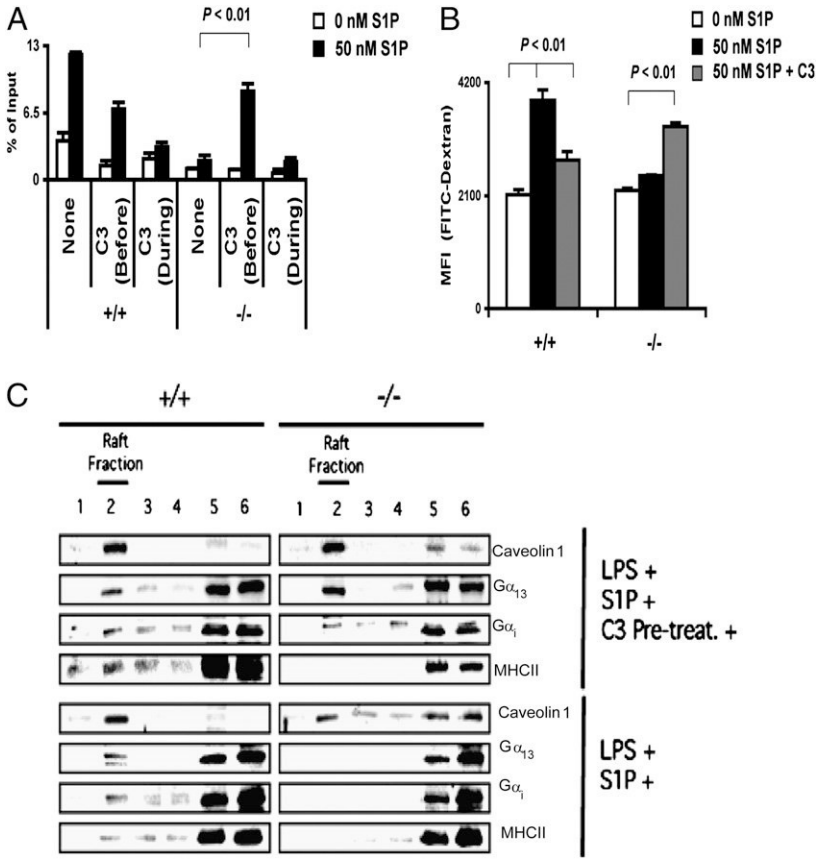

FIGURE 7. Preinhibition of RhoA activation increases the S1P-induced motility, endocytosis, and localization of $G\alpha_{13}$ in membrane rafts in *Swap-70*$^{-/-}$ BMDCs. *A*, LPS-activated *Swap-70*$^{-/-}$ and wt BMDCs were treated with exoenzyme C3 before or during in vitro migration in response to S1P. Migration is calculated as percentage of input after 3-h exposure to 50 nM S1P in a transwell system. *B*, LPS-activated *Swap-70*$^{-/-}$ and wt BMDCs were treated with 1 μg/ml exoenzyme C3 for 4 h before in vitro endocytosis in the presence or not of 100 nM S1P. Cells were analyzed by flow cytometry to determine the FITC mean fluorescence intensity (MFI). *C*, LPS-activated *Swap-70*$^{-/-}$ and wt BMDCs were treated or not with exoenzyme C3 for 4 h before S1P stimulus. Lysates of DCs were subjected to OptiPrep gradient ultracentrifugation system and analyzed as in Fig. 5*B*. Data are representative of at least three independent experiments.

these results indicate that a failure in RhoA activation by S1P accounts for the impaired upregulation of motility and endocytosis of *Swap-70*$^{-/-}$ BMDCs.

In vitro transwell assays showed that *Swap-70*$^{-/-}$ BMDCs migrate poorly to S1P. Video microscopic analyses of *Swap-70*$^{-/-}$ BMDCs revealed a significant decrease in migratory speed, but not in directionality, when compared with wt BMDCs in response to S1P. This indicates two different mechanisms controlling speed and directionality toward S1P, and that SWAP-70 regulates the former. In addition, this indicates that functional S1P receptors are expressed and locate on the surface of *Swap-70*$^{-/-}$ BMDCs, in agreement with their wt-like expression levels of S1PR mRNA and proteins. Interestingly, wt and *Swap-70*$^{-/-}$ BMDCs showed no difference in in vitro migration to CCL19 and CCL21. S1P and chemokines signal through GPCRs, which activate Rho GTPases necessary for the cytoskeletal rearrangements involved in migration of cells (10, 47). In DCs, signaling through CCR7 also activates RhoA, but this modulates only the migratory speed and not CCR7-dependent chemotaxis (43). We confirmed that inhibition of RhoA activation with exoenzyme C3 does not block CCR7-chemotaxis of BMDCs. In addition, *Swap-70*$^{-/-}$ BMDCs show no difference in migratory speed in response to CCL19 (data not shown) and behave like wt in transwell assays. Consistent with the previous notion (4) that RhoA activation by S1P or by chemokines are independent processes, we conclude that SWAP-70 plays a particular role in RhoA-dependent S1P signaling necessary for DC motility. We found that skin-derived DCs in ears of *Swap-70*$^{-/-}$ mice migrate poorly into dermal lymphatic vessels. *Swap-70*$^{-/-}$ BMDCs showed impaired transmigration through endothelial lymphatic cells in vitro in response to CCL19, which may account for the defect in entering to lymphatic vessels. However, this phenotype may also be caused by failure to activate RhoA and to localize Rac1 and RhoA to centers of actin polymerization after S1P stimulus because $S1P_1$ controls migration of skin-derived DCs to draining lymph nodes (8). Therefore, SWAP-70 may control S1P-dependent signaling and transmigration in skin-derived DCs, two processes that regulate DC migration to lymph nodes (8, 31, 32), an aspect that will be the subject of future studies.

Our previous studies showed interaction of RhoA and SWAP-70 in BMDC lysates, and that RhoA is already activated before arrival of an LPS stimulus in *Swap-70*$^{-/-}$ BMDCs, which suggests the control of RhoA activation by SWAP-70 (14). The abrogation of the preactivated state of RhoA in *Swap-70*$^{-/-}$ BMDCs by treatment with exoenzyme C3 before, but not during, a LPS stimulus restored upregulation of MHC-II on the surface of *Swap-70*$^{-/-}$ BMDCs (14). In this study, we detected a significant difference in the activation state of RhoA in LPS-matured wt and *Swap-70*$^{-/-}$ BMDCs before appearance of the S1P stimulus. Similar to the upregulation of MHC-II in *Swap-70*$^{-/-}$ BMDCs (14), treatment with the exoenzyme C3 before, but not during, the S1P stimulus restored migration to S1P and S1P-induced upregulation of endocytosis in *Swap-70*$^{-/-}$ BMDCs. Pretreatment with C3 also restored proper caveolin and G protein distribution to raft fractions. MHC-II is redistributed to the raft fraction only if the cells were not activated with LPS as described before (14). This indicates that SWAP-70 allows regulated and timely activation of RhoA, and thereby supports a proper response to S1P. SWAP-70 thus constitutes a novel element controlling S1P signaling in DCs.

Morphological analysis of BMDCs moving through pores in a 3D environment in response to S1P showed that wt cells have a rounded body shape and short dendrites that usually point to the direction of cell movement. In contrast, *Swap-70*$^{-/-}$ BMDCs showed an elongated morphology and long dendrites that pointed to different directions at the same time. The nucleus was often lagging behind the cell body. The analysis of *Swap-70*$^{-/-}$ BMDCs without S1P stimulus showed no morphological difference when

compared with wt cells (data not shown). DC movement in 3D environments is regulated by dynamic actin polymerization at the cell front and actomyosin contractions of the trailing edge to push the nucleus through narrow spaces (17). *Swap-70*$^{-/-}$ BMDCs required more time to move through the pores of the collagen matrix, and as a result, their dendrites are longer and the nucleus was often dragged behind. As a consequence, *Swap-70*$^{-/-}$ BMDCs may fail to retract the trailing edge on time. These observations are in agreement with the failure of *Swap-70*$^{-/-}$ BMDCs to activate RhoA on S1P stimulation, because this Rho GTPase is required for the contraction of the trailing edge of mature DCs moving in collagen matrix (17).

The inhibition of Rac1 through activation of RhoA impairs migration toward S1P in cells expressing only the $S1P_2$ receptor (48, 49). We deem it unlikely that the deficiency of *Swap-70*$^{-/-}$ BMDCs to migrate toward S1P results from deficient S1P signaling through $S1P_2$, because activation of Rac1 on S1P treatment is not significantly different between *Swap-70*$^{-/-}$ and wt BMDCs. However, localization of Rac1 to areas of actin polymerization after S1P stimulus is impaired in *Swap-70*$^{-/-}$ BMDCs. This failure may negatively affect $S1P_1$ signaling. In studies done with different cell lines, it has been concluded that $S1P_1$ only activates Rac1 by $G\alpha_i$ association, whereas $S1P_3$ activates both Rac1 and RhoA by coupling to $G\alpha_i$ and $G\alpha_{12/13}$, respectively (10). In BMDCs lysates, SWAP-70 interacts with Rac1, RhoA (14), and $G\alpha_I$ (this study). It is plausible to hypothesize that SWAP-70 acts at the level of interaction of G proteins with Rho GTPases during S1P signaling and, therefore, that its absence causes poor S1P-induced migration and endocytosis. At which level SWAP-70 regulates other G protein-dependent responses, for example, to chemokines, will be further studied. Both $G\alpha_{12}$ and $G\alpha_{13}$ localize to plasma membrane (50), and their compartmentalization into membrane rafts/caveolae can provide rapid and strong activation signaling (51, 52). In both immature wt and *Swap-70*$^{-/-}$ BMDCs, a fraction $G\alpha_{13}$, as well as the Rac1 activator $G\alpha_I$, localized into membrane rafts/caveolae. After LPS and S1P stimulus, $G\alpha_{13}$ is absent from membrane rafts/caveolae in *Swap-70*$^{-/-}$ BMDCs. Failure to localize $G\alpha_{13}$ to membrane rafts/caveolae may lead to poor activation of RhoA in LPS-matured *Swap-70*$^{-/-}$ BMDCs after S1P stimulus. In agreement with this, it has been demonstrated that membrane localization of $G\alpha_{13}$ is necessary to recruit p115-RhoGEF to the membrane for subsequent RhoA activation (53, 54). $G\alpha_I$ was observed to disappear from membrane rafts/caveolae in lysates from both wt and *Swap-70*$^{-/-}$ BMDCs after stimulation with LPS and S1P. This observation is reminiscent of the situation in smooth muscle cells where $G\alpha_I$ and $G\alpha_q$ redistribute to the cytosol after an agonist stimulus (55). This also suggests a mechanism of Rac1 activation different from that of RhoA.

Collectively, our results suggest that SWAP-70 contributes to proper, timely, and stable activation of RhoA in S1P signaling affecting motility and endocytosis in DCs. In addition, given that SWAP-70 interacts with $G\alpha_I$ and $G\alpha_{13}$, and that initial signaling through $G\alpha_{13}$ proteins may be negatively affected by a failure to localize in membrane rafts/caveolae, SWAP-70 is of considerable biological significance in S1P-induced functions of mature DCs.

Disclosures

The authors have no financial conflicts of interest.

References

1. Banchereau, J., F. Briere, C. Caux, J. Davoust, S. Lebecque, Y. J. Liu, B. Pulendran, and K. Palucka. 2000. Immunobiology of dendritic cells. *Annu. Rev. Immunol.* 18: 767–811.
2. Rosen, H., and E. J. Goetzl. 2005. Sphingosine 1-phosphate and its receptors: an autocrine and paracrine network. *Nat. Rev. Immunol.* 5: 560–570.
3. Pappu, R., S. R. Schwab, I. Cornelissen, J. P. Pereira, J. B. Regard, Y. Xu, E. Camerer, Y. W. Zheng, Y. Huang, J. G. Cyster, and S. R. Coughlin. 2007. Promotion of lymphocyte egress into blood and lymph by distinct sources of sphingosine-1-phosphate. *Science* 316: 295–298.
4. Czeloth, N., G. Bernhardt, F. Hofmann, H. Genth, and R. Förster. 2005. Sphingosine-1-phosphate mediates migration of mature dendritic cells. *J. Immunol.* 175: 2960–2967.
5. Gollmann, G., H. Neuwirt, C. H. Tripp, H. Mueller, G. Konwalinka, C. Heufler, N. Romani, and M. Tiefenthaler. 2008. Sphingosine-1-phosphate receptor type-1 agonism impairs blood dendritic cell chemotaxis and skin dendritic cell migration to lymph nodes under inflammatory conditions. *Int. Immunol.* 20: 911–923.
6. Idzko, M., H. Hammad, M. van Nimwegen, M. Kool, T. Müller, T. Soullié, M. A. Willart, D. Hijdra, H. C. Hoogsteden, and B. N. Lambrecht. 2006. Local application of FTY720 to the lung abrogates experimental asthma by altering dendritic cell function. *J. Clin. Invest.* 116: 2935–2944.
7. Alvarez, D., E. H. Vollmann, and U. H. von Andrian. 2008. Mechanisms and consequences of dendritic cell migration. *Immunity* 29: 325–342.
8. Rathinasamy, A., N. Czeloth, O. Pabst, R. Förster, and G. Bernhardt. 2010. The origin and maturity of dendritic cells determine the pattern of sphingosine 1-phosphate receptors expressed and required for efficient migration. *J. Immunol.* 185: 4072–4081.
9. Sanchez, T., and T. Hla. 2004. Structural and functional characteristics of S1P receptors. *J. Cell. Biochem.* 92: 913–922.
10. Taha, T. A., K. M. Argraves, and L. M. Obeid. 2004. Sphingosine-1-phosphate receptors: receptor specificity versus functional redundancy. *Biochim. Biophys. Acta* 1682: 48–55.
11. Maeda, Y., H. Matsuyuki, K. Shimano, H. Kataoka, K. Sugahara, and K. Chiba. 2007. Migration of CD4 T cells and dendritic cells toward sphingosine 1-phosphate (S1P) is mediated by different receptor subtypes: S1P regulates the functions of murine mature dendritic cells via S1P receptor type 3. *J. Immunol.* 178: 3437–3446.
12. Radeke, H. H., H. von Wenckstern, K. Stoidtner, B. Sauer, S. Hammer, and B. Kleuser. 2005. Overlapping signaling pathways of sphingosine 1-phosphate and TGF-beta in the murine Langerhans cell line XS52. *J. Immunol.* 174: 2778–2786.
13. Oberbanscheidt, P., S. Balkow, J. Kühnl, S. Grabbe, and M. Bähler. 2007. SWAP-70 associates transiently with macropinosomes. *Eur. J. Cell Biol.* 86: 13–24.
14. Ocana-Morgner, C., C. Wahren, and R. Jessberger. 2009. SWAP-70 regulates RhoA/RhoB-dependent MHCII surface localization in dendritic cells. *Blood* 113: 1474–1482.
15. Burns, S., S. J. Hardy, J. Buddle, K. L. Yong, G. E. Jones, and A. J. Thrasher. 2004. Maturation of DC is associated with changes in motile characteristics and adherence. *Cell Motil. Cytoskeleton* 57: 118–132.
16. Burns, S., A. J. Thrasher, M. P. Blundell, L. Machesky, and G. E. Jones. 2001. Configuration of human dendritic cell cytoskeleton by Rho GTPases, the WAS protein, and differentiation. *Blood* 98: 1142–1149.
17. Lämmermann, T., B. L. Bader, S. J. Monkley, T. Worbs, R. Wedlich-Söldner, K. Hirsch, M. Keller, R. Förster, D. R. Critchley, R. Fässler, and M. Sixt. 2008. Rapid leukocyte migration by integrin-independent flowing and squeezing. *Nature* 453: 51–55.
18. Lämmermann, T., J. Renkawitz, X. Wu, K. Hirsch, C. Brakebusch, and M. Sixt. 2009. Cdc42-dependent leading edge coordination is essential for interstitial dendritic cell migration. *Blood* 113: 5703–5710.
19. Quast, T., B. Tappertzhofen, C. Schild, J. Grell, N. Czeloth, R. Förster, R. Alon, L. Fraemohs, K. Dreck, C. Weber, et al. 2009. Cytohesin-1 controls the activation of RhoA and modulates integrin-dependent adhesion and migration of dendritic cells. *Blood* 113: 5801–5810.
20. Wang, Z., Y. Kumamoto, P. Wang, X. Gan, D. Lehmann, A. V. Smrcka, L. Cohn, A. Iwasaki, L. Li, and D. Wu. 2009. Regulation of immature dendritic cell migration by RhoA guanine nucleotide exchange factor Arhgef5. *J. Biol. Chem.* 284: 28599–28606.
21. Ihara, S., T. Oka, and Y. Fukui. 2006. Direct binding of SWAP-70 to non-muscle actin is required for membrane ruffling. *J. Cell Sci.* 119: 500–507.
22. Shinohara, M., Y. Terada, A. Iwamatsu, A. Shinohara, N. Mochizuki, M. Higuchi, Y. Gotoh, S. Ihara, S. Nagata, H. Itoh, et al. 2002. SWAP-70 is a guanine-nucleotide-exchange factor that mediates signalling of membrane ruffling. *Nature* 416: 759–763.
23. Matloubian, M., C. G. Lo, G. Cinamon, M. J. Lesneski, Y. Xu, V. Brinkmann, M. L. Allende, R. L. Proia, and J. G. Cyster. 2004. Lymphocyte egress from thymus and peripheral lymphoid organs is dependent on S1P receptor 1. *Nature* 427: 355–360.
24. Gunzer, M., A. Schäfer, S. Borgmann, S. Grabbe, K. S. Zänker, E. B. Bröcker, E. Kämpgen, and P. Friedl. 2000. Antigen presentation in extracellular matrix: interactions of T cells with dendritic cells are dynamic, short lived, and sequential. *Immunity* 13: 323–332.
25. Tripp, C. H., B. Haid, V. Flacher, M. Sixt, H. Peter, J. Farkas, R. Gschwentner, L. Sorokin, N. Romani, and P. Stoitzner. 2008. The lymph vessel network in mouse skin visualised with antibodies against the hyaluronan receptor LYVE-1. *Immunobiology* 213: 715–728.
26. Lingwood, D., and K. Simons. 2007. Detergent resistance as a tool in membrane research. *Nat. Protoc.* 2: 2159–2165.
27. Bowles, R., S. Patil, H. Pincas, and S. C. Sealfon. 2010. Validation of efficient high-throughput plasmid and siRNA transfection of human monocyte-derived dendritic cells without cell maturation. *J. Immunol. Methods* 363: 21–28.

28. Pham, T. H., P. Baluk, Y. Xu, I. Grigorova, A. J. Bankovich, R. Pappu, S. R. Coughlin, D. M. McDonald, S. R. Schwab, and J. G. Cyster. 2010. Lymphatic endothelial cell sphingosine kinase activity is required for lymphocyte egress and lymphatic patterning. *J. Exp. Med.* 207: 17–27.
29. Kissenpfennig, A., S. Henri, B. Dubois, C. Laplace-Builhé, P. Perrin, N. Romani, C. H. Tripp, P. Douillard, L. Leserman, D. Kaiserlian, et al. 2005. Dynamics and function of Langerhans cells in vivo: dermal dendritic cells colonize lymph node areas distinct from slower migrating Langerhans cells. *Immunity* 22: 643–654.
30. Shklovskaya, E., B. Roediger, and B. Fazekas de St Groth. 2008. Epidermal and dermal dendritic cells display differential activation and migratory behavior while sharing the ability to stimulate CD4+ T cell proliferation in vivo. *J. Immunol.* 181: 418–430.
31. Johnson, L. A., S. Clasper, A. P. Holt, P. F. Lalor, D. Baban, and D. G. Jackson. 2006. An inflammation-induced mechanism for leukocyte transmigration across lymphatic vessel endothelium. *J. Exp. Med.* 203: 2763–2777.
32. Johnson, L. A., and D. G. Jackson. 2010. Inflammation-induced secretion of CCL21 in lymphatic endothelium is a key regulator of integrin-mediated dendritic cell transmigration. *Int. Immunol.* 22: 839–849.
33. Ledgerwood, L. G., G. Lal, N. Zhang, A. Garin, S. J. Esses, F. Ginhoux, M. Merad, H. Peche, S. A. Lira, Y. Ding, et al. 2008. The sphingosine 1-phosphate receptor 1 causes tissue retention by inhibiting the entry of peripheral tissue T lymphocytes into afferent lymphatics. *Nat. Immunol.* 9: 42–53.
34. Pearce, G., V. Angeli, G. J. Randolph, T. Junt, U. von Andrian, H. J. Schnittler, and R. Jessberger. 2006. Signaling protein SWAP-70 is required for efficient B cell homing to lymphoid organs. *Nat. Immunol.* 7: 827–834.
35. Randolph, G. J., V. Angeli, and M. A. Swartz. 2005. Dendritic-cell trafficking to lymph nodes through lymphatic vessels. *Nat. Rev. Immunol.* 5: 617–628.
36. Yanagawa, Y., and K. Onoé. 2003. CCR7 ligands induce rapid endocytosis in mature dendritic cells with concomitant up-regulation of Cdc42 and Rac activities. *Blood* 101: 4923–4929.
37. Fernandez-Borja, M., L. Janssen, D. Verwoerd, P. Hordijk, and J. Neefjes. 2005. RhoB regulates endosome transport by promoting actin assembly on endosomal membranes through Dia1. *J. Cell Sci.* 118: 2661–2670.
38. Wallar, B. J., A. D. Deward, J. H. Resau, and A. S. Alberts. 2007. RhoB and the mammalian Diaphanous-related formin mDia2 in endosome trafficking. *Exp. Cell Res.* 313: 560–571.
39. Morandat, S., and K. El Kirat. 2007. Solubilization of supported lipid membranes by octyl glucoside observed by time-lapse atomic force microscopy. *Colloids Surf. B Biointerfaces* 55: 179–184.
40. Insel, P. A., B. P. Head, H. H. Patel, D. M. Roth, R. A. Bundey, and J. S. Swaney. 2005. Compartmentation of G-protein-coupled receptors and their signalling components in lipid rafts and caveolae. *Biochem. Soc. Trans.* 33: 1131–1134.
41. Patel, H. H., F. Murray, and P. A. Insel. 2008. Caveolae as organizers of pharmacologically relevant signal transduction molecules. *Annu. Rev. Pharmacol. Toxicol.* 48: 359–391.
42. Aktories, K., C. Wilde, and M. Vogelsgesang. 2004. Rho-modifying C3-like ADP-ribosyltransferases. *Rev. Physiol. Biochem. Pharmacol.* 152: 1–22.
43. Riol-Blanco, L., N. Sánchez-Sánchez, A. Torres, A. Tejedor, S. Narumiya, A. L. Corbí, P. Sánchez-Mateos, and J. L. Rodríguez-Fernández. 2005. The chemokine receptor CCR7 activates in dendritic cells two signaling modules that independently regulate chemotaxis and migratory speed. *J. Immunol.* 174: 4070–4080.
44. Raftopoulou, M., and A. Hall. 2004. Cell migration: Rho GTPases lead the way. *Dev. Biol.* 265: 23–32.
45. Albiges-Rizo, C., O. Destaing, B. Fourcade, E. Planus, and M. R. Block. 2009. Actin machinery and mechanosensitivity in invadopodia, podosomes and focal adhesions. *J. Cell Sci.* 122: 3037–3049.
46. Berdeaux, R. L., B. Díaz, L. Kim, and G. S. Martin. 2004. Active Rho is localized to podosomes induced by oncogenic Src and is required for their assembly and function. *J. Cell Biol.* 166: 317–323.
47. Thelen, M. 2001. Dancing to the tune of chemokines. *Nat. Immunol.* 2: 129–134.
48. Okamoto, H., N. Takuwa, T. Yokomizo, N. Sugimoto, S. Sakurada, H. Shigematsu, and Y. Takuwa. 2000. Inhibitory regulation of Rac activation, membrane ruffling, and cell migration by the G protein-coupled sphingosine-1-phosphate receptor EDG5 but not EDG1 or EDG3. *Mol. Cell. Biol.* 20: 9247–9261.
49. Sugimoto, N., N. Takuwa, H. Okamoto, S. Sakurada, and Y. Takuwa. 2003. Inhibitory and stimulatory regulation of Rac and cell motility by the G12/13-Rho and Gi pathways integrated downstream of a single G protein-coupled sphingosine-1-phosphate receptor isoform. *Mol. Cell. Biol.* 23: 1534–1545.
50. Veit, M., B. Nürnberg, K. Spicher, C. Harteneck, E. Ponimaskin, G. Schultz, and M. F. Schmidt. 1994. The alpha-subunits of G-proteins G12 and G13 are palmitoylated, but not amidically myristoylated. *FEBS Lett.* 339: 160–164.
51. Bhatnagar, A., D. J. Sheffler, W. K. Kroeze, B. Compton-Toth, and B. L. Roth. 2004. Caveolin-1 interacts with 5-HT2A serotonin receptors and profoundly modulates the signaling of selected Galphaq-coupled protein receptors. *J. Biol. Chem.* 279: 34614–34623.
52. Oh, P., and J. E. Schnitzer. 2001. Segregation of heterotrimeric G proteins in cell surface microdomains. G(q) binds caveolin to concentrate in caveolae, whereas G(i) and G(s) target lipid rafts by default. *Mol. Biol. Cell* 12: 685–698.
53. Bhattacharyya, R., J. Banerjee, K. Khalili, and P. B. Wedegaertner. 2009. Differences in Galpha12- and Galpha13-mediated plasma membrane recruitment of p115-RhoGEF. *Cell. Signal.* 21: 996–1006.
54. Bhattacharyya, R., and P. B. Wedegaertner. 2000. Galpha 13 requires palmitoylation for plasma membrane localization, Rho-dependent signaling, and promotion of p115-RhoGEF membrane binding. *J. Biol. Chem.* 275: 14992–14999.
55. Murthy, K. S., and G. M. Makhlouf. 2000. Heterologous desensitization mediated by G protein-specific binding to caveolin. *J. Biol. Chem.* 275: 30211–30219.

Appendix 10

Herroeder S, **Reichardt P**, Sassmann A, Zimmermann B, Hogg N, Hollmann MW, Fischer KD, Vogt S, Grosse R, Gunzer M, Offermanns S, Wettschureck N. G-proteins of the G12/G13 family shape immune functions by controlling CD4+ T-cell adhesiveness. **Immunity** 2009;30:708-20.

IF: 19.8

Please cite this article in press as: Herroeder et al., Guanine Nucleotide-Binding Proteins of the G_{12} Family Shape Immune Functions by Controlling $CD4^+$ T Cell Adhesiveness and Motility, Immunity (2009), doi:10.1016/j.immuni.2009.02.010

Immunity
Article

Guanine Nucleotide-Binding Proteins of the G_{12} Family Shape Immune Functions by Controlling $CD4^+$ T Cell Adhesiveness and Motility

Susanne Herroeder,[1,2,8] Peter Reichardt,[3] Antonia Sassmann,[1] Barbara Zimmermann,[1] Dagmar Jaeneke,[1] Jana Hoeckner,[1] Markus W. Hollmann,[4] Klaus-Dieter Fischer,[5] Stephan Vogt,[6] Robert Grosse,[1] Nancy Hogg,[7] Matthias Gunzer,[3] Stefan Offermanns,[1,9] and Nina Wettschureck[1,9,*]

[1]Institute of Pharmacology, University of Heidelberg, 69120 Heidelberg, Germany
[2]Department of Anesthesiology, University of Heidelberg, 69120 Heidelberg, Germany
[3]Institute of Molecular and Clinical Immunology, University of Magdeburg, 39120 Magdeburg, Germany
[4]Department of Anesthesiology, University of Amsterdam (AMC), 1105 DD Amsterdam, The Netherlands
[5]Institute of Biochemistry and Cell Biology and Department of Functional Genomics and Medical Toponomics, 39120 Magdeburg, Germany
[6]Department of Orthopaedic and Trauma Surgery, Technical University of Munich, 81675 Munich, Germany
[7]Leukocyte Adhesion Laboratory, Cancer Research UK, London Research Institute, WC2A 3PX London, UK
[8]Laboratory of Experimental Intensive Care & Anesthesiology (L.E.I.C.A.), Academic Medical Center Amsterdam, 1105 DD Amsterdam, The Netherlands
[9]Department of Pharmacology, Max-Planck-Institute for Heart and Lung Research, 61231 Bad Nauheim, Germany
*Correspondence: nina.wettschureck@pharma.uni-heidelberg.de
DOI 10.1016/j.immuni.2009.02.010

SUMMARY

Integrin-mediated adhesion plays a central role in T cell trafficking and activation. Genetic inactivation of the guanine nucleotide-binding (G) protein α-subunits $G\alpha_{12}$ and $G\alpha_{13}$ resulted in an increased activity of integrin leukocyte-function-antigen-1 in murine $CD4^+$ T cells. The interaction with allogeneic dendritic cells was enhanced, leading to an abnormal proliferative response in vitro. In vivo, T cell-specific inactivation of $G\alpha_{12}$ and $G\alpha_{13}$ caused lymphadenopathy due to increased lymph node entry and enhanced T cell proliferation, and the susceptibility toward T cell-mediated diseases was enhanced. Mechanistically, we show that in the absence of $G\alpha_{12}$ and $G\alpha_{13}$ the activity of the small GTPases Rac1 and Rap1 was increased, whereas signaling of the small GTPase RhoA was strongly reduced. Our data indicate that locally produced mediators signal through $G\alpha_{12}$- and $G\alpha_{13}$-coupled receptors to negatively regulate cell polarization and adhesiveness, thereby fine-tuning T cell trafficking, proliferation, and susceptibility toward T cell-mediated diseases.

INTRODUCTION

Integrin-mediated adhesion plays a central role in T cell functions. The integrin leukocyte-function-antigen-1 (LFA-1), for example, is crucial for the formation of the immunological synapse, the interface between antigen-loaded mature dendritic cells and naive T cells. LFA-1 also mediates firm adhesion to high endothelial venules, thereby allowing naive T cells to enter secondary lymphatic organs. In addition, LFA-1 has been implicated in the control of lymphocyte differentiation and proliferation, as well as in the regulation of T cell effector functions (Mor et al., 2007; Smith et al., 2007).

Given this multitude of LFA-1 functions, a precise understanding of the spatial and temporal control of the interaction between LFA-1 and its cellular counter-receptors, the intercellular adhesion molecules (ICAMs), is of great importance. In naive T cells, LFA-1 is tethered to components of the actin cytoskeleton and thereby held in the inactive state with the result that naive T cells are rounded and only mildly adhesive (Shimaoka et al., 2002; van Kooyk et al., 1999). Activation of LFA-1 occurs in response to a variety of extracellular signals, for example stimulation of cytokine receptors, the TCR-CD3 complex, or G protein-coupled receptors (GPCRs) (Kinashi, 2005). Best studied among the latter are the chemokine receptors, which have been shown to positively regulate LFA-1 through heterotrimeric G proteins of the G_i family (Laudanna and Alon, 2006; Laudanna et al., 2002). The intracellular signaling cascades mediating the effects of chemokines on integrin activation have been shown to involve several monomeric GTPases such as Rap1, Rac1, or RhoA (Mor et al., 2007). However, chemokine receptors are probably not the only GPCRs contributing to the regulation of integrin activity; T cells also express a variety of other GPCRs, such as lysophospholipid or prostanoid receptors, many of which have been implicated in the regulation of adhesiveness as well (Chun and Rosen, 2006; Matsuoka and Narumiya, 2007). In contrast to chemokine GPCRs, these receptors couple not only to G_i but also to other G protein families such as G_{12} (Riobo and Manning, 2005), but the role of this G protein family in the regulation of T cell in vivo functions has not been investigated so far.

The two members of the G_{12} family, G_{12} and G_{13}, are ubiquitously expressed and interact upon receptor-mediated activation with certain Rho guanine nucleotide exchange factors (RhoGEFs) (Fukuhara et al., 2001), which in turn mediate activation of the small GTPase RhoA. Because of the embryonic lethality of mice lacking the α-subunits of G_{12} and G_{13} ($G\alpha_{12}$ and $G\alpha_{13}$) (Gu et al., 2002; Offermanns et al., 1997), and because of the lack of specific inhibitors of these proteins, the relevance of this family in the adult organism has long been elusive. The

Please cite this article in press as: Herroeder et al., Guanine Nucleotide-Binding Proteins of the G_{12} Family Shape Immune Functions by Controlling CD4$^+$ T Cell Adhesiveness and Motility, Immunity (2009), doi:10.1016/j.immuni.2009.02.010

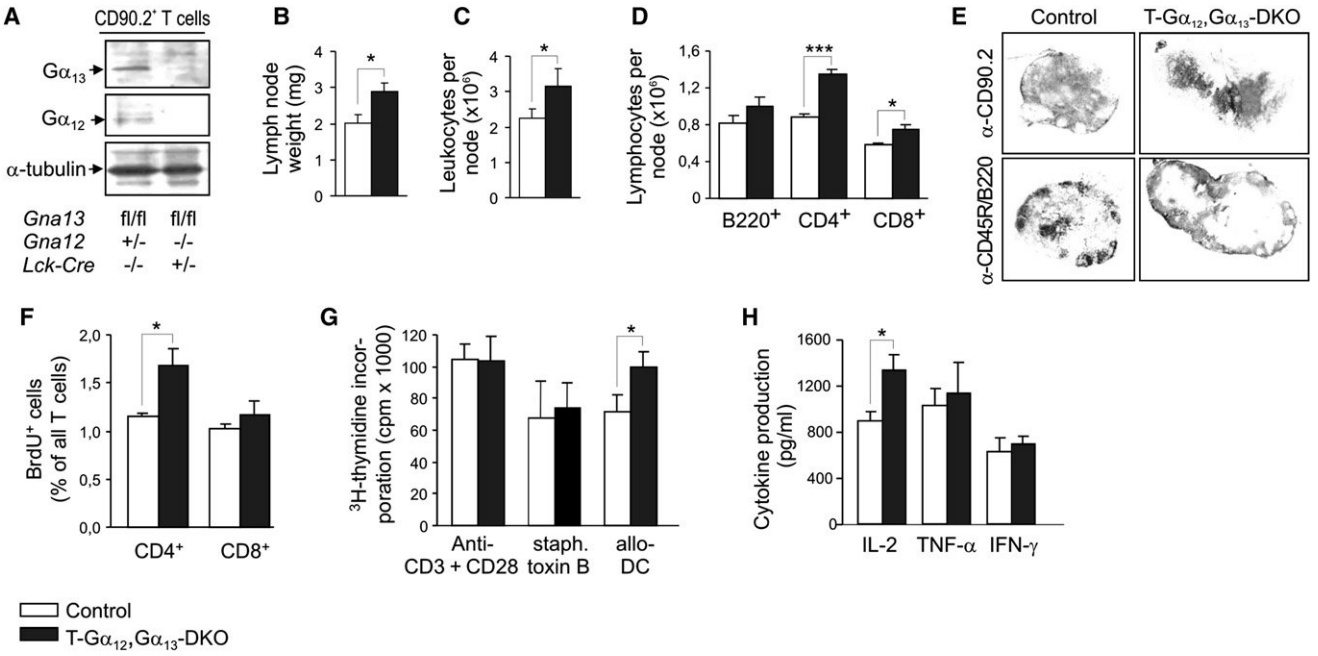

Figure 1. Lymphadenopathy in T-Gα_{12},Gα_{13} DKOs

(A) CD90.2$^+$ T cells were isolated from lymph nodes of controls (*Lck*Cre$^{-/-}$*Gna13*$^{fl/fl}$*Gna12*$^{+/-}$) and T-Gα_{12},Gα_{13} DKOs (*Lck*Cre$^{+/-}$*Gna13*$^{fl/fl}$*Gna12*$^{-/-}$) and subjected to immunoblotting with antibodies directed against Gα_{13}, Gα_{12} and α-tubulin as loading control.

(B) Weight of peripheral lymph nodes (n = 8).

(C) Leukocyte numbers per node (n = 8).

(D) Absolute numbers of CD45R/B220$^+$ B cells as well as CD4$^+$ and CD8$^+$ T cells per node (n = 10).

(E) Immunohistochemical staining of T cells and B cells in inguinal lymph nodes with antibodies against CD90.2 and CD45R/B220.

(F) Percentage of BrdU-positive T cells in lymph nodes 4 hr after intraperitoneal injection of BrdU as determined by intracellular flow cytometry (n = 6).

(G) In vitro proliferation of 2 × 10^5 CD4$^+$ T cells after 72 hr of culture with 5 × 10^4 CD11c$^+$ allo-DCs, after TCR crosslinking with immobilized CD3-CD28 antibodies, or after stimulation with staphylococcal enterotoxin B (10 ng/ml) (n = 6–10).

(H) The concentration of secreted cytokines was determined in the supernatant of cocultures between CD4$^+$ T cell and allo-DC after 72 hr (n = 8).

White bars represent the control; black bars represent the T-Gα_{12},Gα_{13} DKO. Data are displayed as mean ± SEM. *p < 0.05; ***p < 0.0005.

recent generation of tissue-specific Gα_{12},Gα_{13} double-deficient mice revealed important functions in platelets and B cells (Moers et al., 2003; Rieken et al., 2006a; Rieken et al., 2006b); the in vivo role of Gα_{12} and Gα_{13} in peripheral T cells, however, has not been addressed up to now. With the help of the Cre-loxP system, we generated T cell-specific Gα_{12},Gα_{13} double-deficient mice and show here that these proteins negatively regulate the activation state of integrin LFA-1, thereby modulating T cell trafficking and proliferation, as well as responses to foreign and self antigen.

RESULTS

Lymphadenopathy in T Cell-Specific Gα_{12},Gα_{13} Double-Deficient Mice

T cell-specific Gα_{12},Gα_{13} double-deficient mice were generated by intercrossing animals in which the gene coding for Gα_{13}, *Gna13*, was flanked by loxP sites (*Gna13*$^{fl/fl}$) with the T cell-specific *Lck*-Cre line (*Lck*Cre$^{+/-}$) and constitutively Gα_{12}-deficient (*Gna12*$^{-/-}$) mice (Gu et al., 2002; Hennet et al., 1995; Moers et al., 2003). As controls we used *Lck*Cre$^{-/-}$*Gna13*$^{fl/fl}$*Gna12*$^{+/-}$ littermates throughout the study. Immunoblots showed that Gα_{13} immunoreactivity was strongly reduced and that Gα_{12} was absent in extracts of isolated CD90.2$^+$ (Thy1.2) T cells (Figure 1A). T cell-specific Gα_{12},Gα_{13} double-deficient mice were born at expected frequencies and were viable and fertile, but showed an increased size and weight of axillary, cervical, and inguinal lymph nodes (Figure 1B). Mesenteric lymph nodes were enlarged as well, whereas Peyer's patches appeared normal (data not shown). The increased lymph node weight corresponded to increased cell numbers (Figure 1C), and flow cytometric analysis of lymphocyte subpopulations revealed that this was predominantly a result of an expansion of the CD4$^+$ T cell population (Figure 1D). The general organization into B cell follicles and T cell areas was not disturbed (Figure 1E). The relative numbers of CD4$^+$ regulatory T cells and CD4$^+$ memory-effector T cells within lymph nodes were not altered (data not shown). In addition to lymphadenopathy, T cell-specific Gα_{12},Gα_{13} double-deficient mice showed an increased thymic weight and cell number, with a proportionate increase in all subpopulations (Table S1 available online). There were no substantial differences with respect to the expression of TCRβ chain, CD3ε, CD69, or CD5 in the different thymic subpopulations (data not shown). The splenic weight and splenocyte numbers were increased, although not significantly (p = 0.08 and 0.27, respectively). The CD4$^+$ T cell population in the blood was increased (Table S1). Taken together, these results show that genetic inactivation of Gα_{12} and Gα_{13} in T cells resulted in an increased cell number especially of CD4$^+$ T cells in lymph nodes, blood, and the

Please cite this article in press as: Herroeder et al., Guanine Nucleotide-Binding Proteins of the G_{12} Family Shape Immune Functions by Controlling $CD4^+$ T Cell Adhesiveness and Motility, Immunity (2009), doi:10.1016/j.immuni.2009.02.010

thymus, suggesting that these G proteins have regulatory functions in $CD4^+$ T cell proliferation, apoptosis, or trafficking.

Proliferation Is Enhanced in $G\alpha_{12},G\alpha_{13}$ Double-Deficient $CD4^+$ T Cells

To study the causes of lymphadenopathy in T cell-specific $G\alpha_{12},G\alpha_{13}$ double-deficient mice, we investigated apoptosis and proliferation. Apoptosis, here determined as the percentage of Annexin V-positive T cells in freshly isolated lymph nodes, did not differ between the genotypes (data not shown). To assess basal T cell proliferation in lymph nodes, we determined the percentage of 5-bromo-2-deoxyuridine (BrdU) incorporating T cells 4 hr after intraperitoneal injection of BrdU. We found that lymph nodes from mutant mice contained more BrdU-positive $CD4^+$ T cells than those from control animals, whereas the proportion of BrdU-positive $CD8^+$ T cells was not increased (Figure 1F). We next determined in vitro proliferation by measuring the incorporation of [^{3}H]-thymidine into $CD4^+$ T cells after 72 hr of culture. Although there was no difference in the proliferation of unstimulated $CD4^+$ T cells, mutant cells showed an increased proliferation in response to allogeneic splenic $CD11c^+$ dendritic cells (allo-DCs) (Figure 1G). In contrast, the proliferative response induced by CD3-CD28 crosslinking, staphylococcal enterotoxin B, or phorbol-12-myristate-13-acetate (PMA) did not differ between the genotypes (Figure 1G and data not shown).

To test whether increased proliferation in response to allo-DCs was accompanied by altered cytokine production, we determined cytokine amounts in the supernatant of cocultures between $CD4^+$ T cell and allo-DCs by ELISA. The production of interleukin (IL)-2 was increased in mutant cells, whereas the production of tumor necrosis factor-α (TNFα) or interferon-γ (IFNγ) remained unchanged (Figure 1H). Taken together, these results indicate that $G\alpha_{12}$ and $G\alpha_{13}$ negatively regulate $CD4^+$ T cell proliferation in response to allogeneic dendritic cells.

$G\alpha_{12},G\alpha_{13}$ Double-Deficient $CD4^+$ T Cells Show Enhanced Interaction with Dendritic Cells

Because the G_{12} family is known to contribute to the regulation of cellular adhesiveness, we investigated whether the enhanced proliferation in response to allo-DCs was due to abnormal cell-cell interactions in mutant cells. Flow cytometric analysis of conjugate formation between fluorescently labeled $CD4^+$ T cells and allo-DCs revealed an increased interaction if the $CD4^+$ T cells were $G\alpha_{12},G\alpha_{13}$ deficient (Figure 2A). We next investigated the interaction between purified $CD4^+$ T cells and fluorescently labeled allo-DCs by live-cell imaging (Figure 2B and Movies S1 and S2). In mutant $CD4^+$ T cells, the proportion of cells with stable DC interactions ("stable" here defined as an interaction that lasted throughout a 10 min movie) was increased (Figure 2C and Movies S1 and S2), as well as the interaction between $CD4^+$ T cells themselves (Figure 2D). These data suggest an important role of $G\alpha_{12}$ and $G\alpha_{13}$ in the regulation of cellular interactions between $CD4^+$ T cells and allo-DCs.

LFA-1 Activity Is Increased in $G\alpha_{12},G\alpha_{13}$ Double-Deficient $CD4^+$ T Cells

To further investigate LFA-1 activity in mutant cells, we compared adhesiveness of control and $G\alpha_{12},G\alpha_{13}$ double-deficient $CD4^+$ T cells on ICAM-1- and VCAM-1 (vascular cell

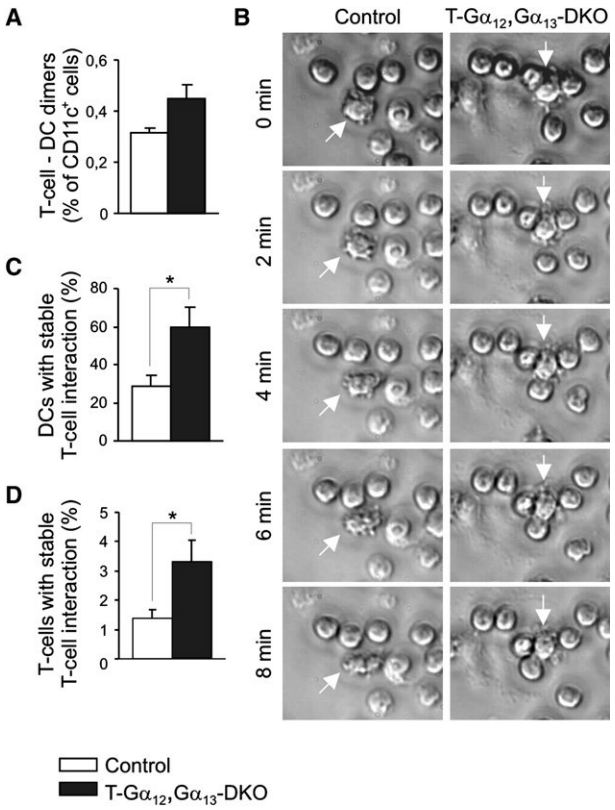

Figure 2. Cell-Cell Interactions of $G\alpha_{12},G\alpha_{13}$ double-deficient $CD4^+$ T Cells

(A) Flow cytometric analysis of dimer formation between CD4-PE-labeled T cells and CD11c-FITC-labeled allo-DCs (n = 8).

(B) Live-cell imaging of isolated $CD4^+$ T cells and CFSE-labeled allo-DCs. Time-lapse movies of 10 min duration were recorded and exemplary micrographs are depicted (magnification 40×). The microphotographs taken at 0 min are overlaid with the GFP fluorescence image for identification of CFSE-labeled DCs (marked by white arrows).

(C and D) Statistical evaluation of stable interactions between $CD4^+$ T cells and DCs (C) or between $CD4^+$ T cells (D).

White bars represent the control; black bars represent the T-$G\alpha_{12},G\alpha_{13}$ DKO. Data are displayed as mean ± SEM. *$p < 0.05$.

adhesion molecule-1)-coated plastic (Figure 3A). On ICAM-1, mutant cells showed a higher basal adhesion than control cells, whereas there was no difference with respect to basal adhesion on VCAM-1. Mutant cells also showed increased ICAM-1 adhesiveness after integrin activation by chemokines or Mg^{2+} and EGTA, whereas no differences were found in response to PMA or TCR crosslinking (data not shown). On VCAM-1, none of these integrin activators resulted in a substantial difference between the genotypes (Figure 3A and data not shown).

LFA-1 activation has been shown to involve two modalities, increased affinity and enhanced integrin clustering (Hogg et al., 2002; Laudanna et al., 2002). To assess LFA-1 affinity, we determined binding of soluble ICAM-1 to $CD4^+$ T cells in a flow cytometric assay and found that in mutant T cells, the proportion of cells that bound ICAM-1 was increased both under basal conditions and after stimulation with Mg^{2+} and EGTA, which are known to increase LFA-1 affinity (Figure 3B). We next investigated LFA-1 clustering by immunofluorescent staining of the

Please cite this article in press as: Herroeder et al., Guanine Nucleotide-Binding Proteins of the G_{12} Family Shape Immune Functions by Controlling $CD4^+$ T Cell Adhesiveness and Motility, Immunity (2009), doi:10.1016/j.immuni.2009.02.010

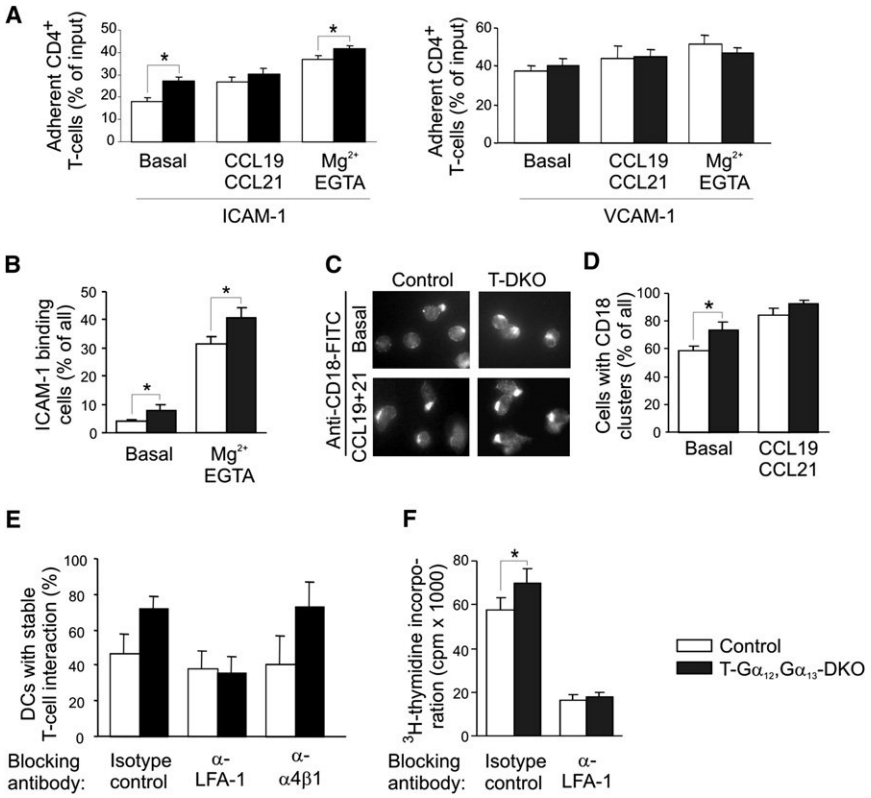

Figure 3. LFA-1 Activity in $G\alpha_{12},G\alpha_{13}$ double-deficient $CD4^+$ T Cells

(A) Adhesion of lymph node $CD4^+$ T cells to ICAM-1- or VCAM-1-coated plastic. The percentage of adherent $CD4^+$ T cells was determined by flow cytometry after 30 min of incubation under basal conditions as well as after stimulation with chemokines CCL19 and 21 (CCL19+21) or Mg^{2+}+EGTA. Data are expressed as percent of input (n = 8).

(B) Flow cytometric analysis of basal and Mg^{2+}+EGTA-induced binding of fluorescently labeled soluble ICAM-1 to $CD4^+$ T cells (n = 6).

(C and D) Basal and CCL19+21-induced LFA-1 clustering in $CD4^+$ T cells was determined by immunofluorescent staining with an CD18 antibody. (C) shows exemplary photomicrographs of CD18-stained cells (magnification 63×). (D) shows statistical evaluation of the percentage of cells showing CD18 clusters (n = 3).

(E) Effect of blocking antibodies directed against LFA-1, α4β1, or isotype control on T cell-DC interactions in live-cell imaging (n = 3).

(F) Effect of blocking antibodies directed against LFA-1 on $CD4^+$ T cell proliferation in response to DCs (n = 6).

White bars represent the control; black bars represent the T-$G\alpha_{12},G\alpha_{13}$ DKO. Data are displayed as mean ± SEM. *$p < 0.05$.

LFA-1 β-chain CD18 and found that the proportion of cells with clusters was increased in mutant $CD4^+$ T cells under basal conditions and, less prominently, after chemokine stimulation (Figures 3C and 3D). However, because LFA-1 clustering was shown to follow ligand binding (Kim et al., 2004), these findings might represent a direct consequence of increased affinity. To exclude that the observed differences were due to an increased surface expression of LFA-1, we analyzed expression of the α- and β-chains of LFA-1 by flow cytometry, but found no abnormalities (data not shown). In order to test whether increased LFA-1 activity in $G\alpha_{12},G\alpha_{13}$ double-deficient $CD4^+$ T cells altered integrin outside-in signaling, we studied phosphorylation of extracellular signal-regulated kinase (ERK) in response to Mn^{2+} and integrin crosslinking, but failed to detect differences between the genotypes. Also, ERK phosphorylation in response to TCR crosslinking or PMA was not altered (Figure S1).

To test whether increased interactions between mutant T cells and allo-DCs were indeed due to increased LFA-1 activity, we performed live-cell imaging in the presence of blocking antibodies directed against LFA-1. Whereas LFA-1 antibodies had only a minor effect on control $CD4^+$ T cells, they normalized enhanced interactions of $G\alpha_{12},G\alpha_{13}$ double-deficient $CD4^+$ T cells. In contrast, α4β1 antibodies had no effect on either control or mutant cells (Figure 3E). To further test whether increased LFA-1 activity also contributed to enhanced proliferation of $G\alpha_{12},G\alpha_{13}$ double-deficient $CD4^+$ T cells, we performed in vitro proliferation assays with allo-DCs in the presence of blocking antibodies directed against LFA-1. This treatment reduced proliferation in mutant cells to the degree found in control cells (Figure 3F), suggesting that deregulation of LFA-1 activity importantly contributes to hyperproliferation of mutant T cells. Taken together, these findings indicate that inactivation of $G\alpha_{12}$ and $G\alpha_{13}$ results in $CD4^+$ T cells in an increased affinity and avidity of LFA-1, which in turn leads to an increased interaction with antigen-presenting cells.

Polarization and Migration in the Absence of $G\alpha_{12}$ and $G\alpha_{13}$

In addition to increased LFA-1 avidity and affinity, morphological changes such as increased spreading might contribute to increased adhesiveness in the absence of $G\alpha_{12}$ and $G\alpha_{13}$. To investigate cell shape in vitro, we performed phalloidin stainings of polymerized actin in ICAM-1 adherent $CD4^+$ T cells. We found that the proportion of cells with firmly attached rear end and elongated tail was substantially increased in mutant cells (Figures 4A and 4B), as was the percentage of polarized cells (Figure 4C). To correlate these morphological changes with potential changes in migratory behavior, we performed time-lapse video microscopy of $CD4^+$ T cells on ICAM-1-coated plastic. The distance traveled by individual $CD4^+$ T cells was decreased in the absence of $G\alpha_{12},G\alpha_{13}$ (Figure 4D and Movies S3 and S4), whereas the proportion of motile cells did not differ between the genotypes (Figure 4E). We next investigated whether increased adhesiveness and polarization would affect transmigration through transwell inserts coated with ICAM-1 or bEND.3 endothelial cells. Under basal conditions, mutant cells showed reduced transmigration both through ICAM-1 and endothelial cells, although migration in response to chemokines CCL19 and CCL21 was not impaired (Figure 4F).

Please cite this article in press as: Herroeder et al., Guanine Nucleotide-Binding Proteins of the G_{12} Family Shape Immune Functions by Controlling $CD4^+$ T Cell Adhesiveness and Motility, Immunity (2009), doi:10.1016/j.immuni.2009.02.010

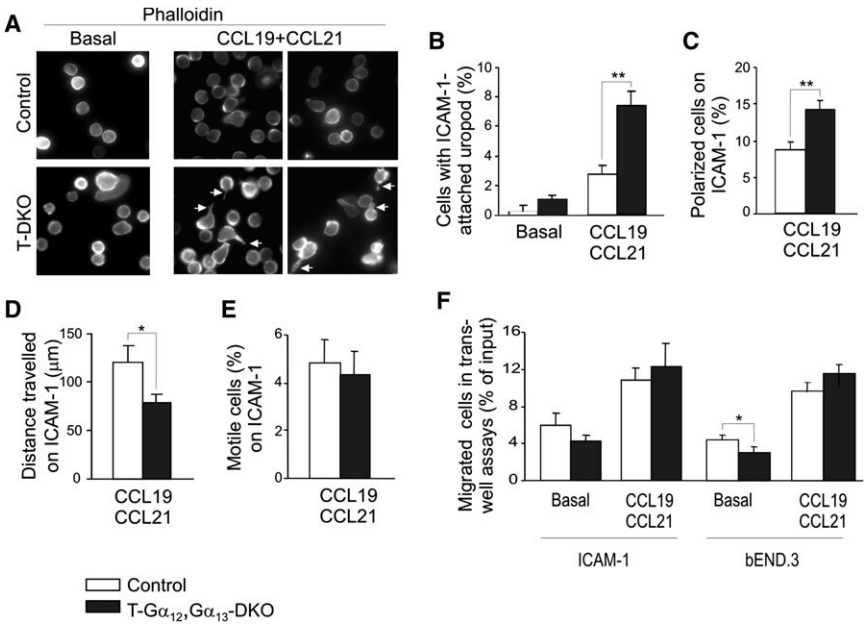

Figure 4. Migratory Behavior of Mutant $CD4^+$ T Cells

(A) Exemplary photomicrographs taken from phalloidin-stained $CD4^+$ T cells that have adhered for 20 min to ICAM-1-coated plastic in the absence (basal) or presence of CCL19+21 (magnification 63×).

(B) Statistical analysis of the percentage of cells with attached, elongated rear (n = 3).

(C) Percentage of $CD4^+$ T cells with a polarized phenotype (showing one or more F-actin positive pseudopods) (n = 3).

(D) The distance traveled by CCL19+21-stimulated $CD4^+$ T cells was determined on ICAM-1-coated plastic in time-lapse microscopy.

(E) Percentage of motile $CD4^+$ T cells (i.e., traveling more than one body length per 10 min) (n = 3).

(F) Percentage of $CD4^+$ T cells that have migrated through ICAM-1-coated transwells inserts (left) or inserts covered with a confluent monolayer of bEND.3 endothelial cells (right) during 3 hr of incubation without agonist in the lower chamber (basal) or in response to CCL19+21 (n = 5).

White bars represent the control; black bars represent the T-$G\alpha_{12}$,$G\alpha_{13}$ DKO. Data are displayed as mean ± SEM. *$p < 0.05$; **$p < 0.005$.

Enhanced Lymph Node Entry of Deficient $CD4^+$ T Cells

In addition to increased proliferation, LFA-1 hyperactivity in the absence of $G\alpha_{12}$ and $G\alpha_{13}$ might affect T cell trafficking into lymph nodes, thereby contributing to lymphadenopathy. To study whether increased adhesiveness to ICAM-1 altered T cell trafficking in vivo, we performed adoptive transfer experiments with fluorescently labeled purified $CD4^+$ T cells from control and mutant mice. Twenty-four hours after injection, significantly more mutant than control cells were found in cervical lymph nodes of the respective host (Figure 5A). Because this might be a result of altered entry and/or exit, we repeated these experiments at 2 hr after transfer and found that even at this time point, mutant $CD4^+$ T cells were overrepresented (Figure 5B). Also the entry of deficient $CD4^+$ T cells into the spleen was increased at two hours after transfer, whereas numbers of mutant cells in the blood were reduced (Figure 5B). Intravenous injection of LFA-1 antibodies into hosts 30 min prior to adoptive transfer normalized the increased entry of $G\alpha_{12}$,$G\alpha_{13}$ double-deficient $CD4^+$ T cells (Figure 5C), suggesting that increased LFA-1 activity, but not disinhibition of other integrins such as $\alpha4\beta1$, underlies enhanced entry.

To investigate in vivo whether increased adhesiveness of $G\alpha_{12}$,$G\alpha_{13}$ double-deficient $CD4^+$ T cells leads to a logjam of cells within the lymphatic vessels or to the opposite, a more efficient transendothelial migration, we performed two-photon intravital microscopy of inguinal lymph nodes 2 hr after adoptive transfer (Figures 5D and 5E). We determined the numbers of control and $G\alpha_{12}$,$G\alpha_{13}$ double-deficient $CD4^+$ T cells in (1) a vessel-rich zone, comprising mostly medulla, containing higher-order venules and high endothelial venules (HEV), and in (2) the T cell zone itself. Two hours after transfer, neither control nor mutant $CD4^+$ T cells were detected directly attached to HEV endothelium; all cells had transmigrated through the venule wall. Within the lymphatic tissue, the majority of cells had already proceeded to dense lymphatic tissues, i.e., to the proper T cell zones. A minority of $CD4^+$ T cells was found in the vessel rich zone, where $G\alpha_{12}$,$G\alpha_{13}$ double-deficient cells were overrepresented (Figure 5E). These findings indicate that enhanced transendothelial migration without persistent attachment to HEV is the main factor underlying the observed dominance of $G\alpha_{12}$,$G\alpha_{13}$ double-deficient $CD4^+$ T cells in the lymph node 2 hr after adoptive transfer.

To also address the question of potentially impaired lymph node egress, we studied transwell migration of $G\alpha_{12}$,$G\alpha_{13}$ double-deficient $CD4^+$ T cells in response to the GPCR agonist sphingosine 1-phosphate (S1P), which has been shown to regulate egress from lymph node or thymus through the $S1P_1$ receptor (Matloubian et al., 2004). However, neither with ICAM-1-coated nor with uncoated transwell inserts did we observe differences between the genotypes with respect to S1P-induced migration (Figure 5F and data not shown), and such a finding is in line with the assumption that $S1P_1$ is a predominantly G_i-coupled receptor (Chun and Rosen, 2006). To address the possibility of an egress impairment independent of S1P, we analyzed the percentage of dye-positive cells 24 hr after adoptive transfer in the cisterna chyli, which collects efferent lymph from the lower body. Also in cisterna chili lymph, mutant $CD4^+$ T cells were overrepresented, suggesting that the passage time through lymph nodes was not altered (Figure 5G). In summary, these results show that increased LFA-1-mediated adhesion in $G\alpha_{12}$,$G\alpha_{13}$ double-deficient $CD4^+$ T cells does not only result in an enhanced interaction with allo-DCs but also facilitates entry into lymph nodes.

Signaling Pathways Involved in $G\alpha_{12}$,$G\alpha_{13}$-Mediated Regulation of LFA-1

We next attempted to elucidate the molecular mechanisms underlying increased integrin activation and polarization in $G\alpha_{12}$,$G\alpha_{13}$ double-deficient $CD4^+$ T cells. Small GTPases such as Rap1, RhoA, and Rac1 are known to regulate integrin activity

Please cite this article in press as: Herroeder et al., Guanine Nucleotide-Binding Proteins of the G_{12} Family Shape Immune Functions by Controlling CD4$^+$ T Cell Adhesiveness and Motility, Immunity (2009), doi:10.1016/j.immuni.2009.02.010

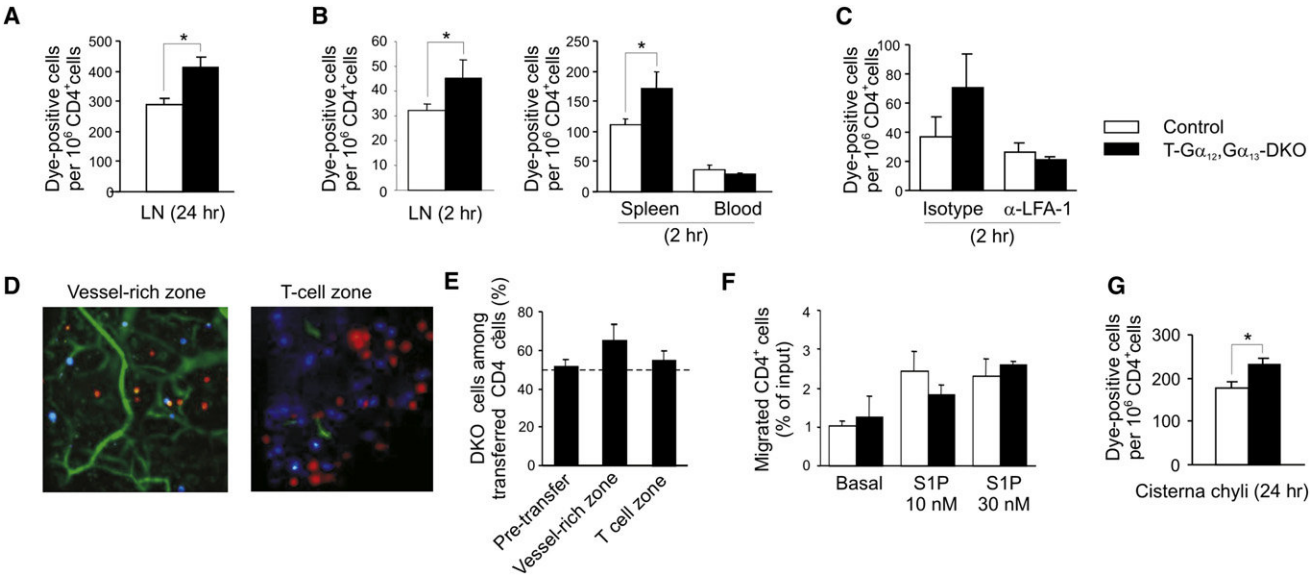

Figure 5. Lymph Node Homing In Vivo

(A–C) Differentially labeled CD4$^+$ T cells from control and mutant mice were mixed in a 1:1 ratio and injected intravenously into wild-type recipients (5 × 10^6 per mouse). After 24 (A) or 2 (B) hr, the proportion of labeled CD4$^+$ T cells was determined by flow cytometry (data are corrected for actual input ratio as determined by FACS). At 2 hr, spleen and blood were also investigated (n = 6–8). (C) shows the adoptive transfer into wild-type recipients pretreated with blocking LFA-1 antibodies or isotype control (n = 4).

(D and E) Intravital two-photon microscopy was used for analyzing the distribution of control versus $G\alpha_{12}$,$G\alpha_{13}$ double-deficient CD4$^+$ T cells in the inguinal lymph node 2 hr after adoptive transfer. (D) shows examples for the different areas studied (control cells in red, mutant cells in blue). (E) shows the statistical evaluation of the percentage $G\alpha_{12}$,$G\alpha_{13}$ double-deficient CD4$^+$ T cells found in the two respective image zones and in FACS analysis of the transferred population (n = 3).

(F) Migration of control and mutant CD4$^+$ T cells through uncoated transwell inserts in response to S1P.

(G) Proportion of dye-positive cells in cisterna chyli aspirates 24 hr after adoptive transfer.

White bars represent the control; black bars represent the T-$G\alpha_{12}$,$G\alpha_{13}$ DKO. Data are displayed as mean ± SEM. *$p < 0.05$.

and cell polarization in response to chemokines (Iden and Collard, 2008; Laudanna and Alon, 2006; Mor et al., 2007); we therefore studied the activation state of these signaling molecules in the absence of $G\alpha_{12}$ and $G\alpha_{13}$ (Figure 6). Both in control and $G\alpha_{12}$,$G\alpha_{13}$ double-deficient cells, active Rap1 was barely detectable in the basal state, but strongly increased 20 and 60 s after application of CCL19 and CCL21, and this increase was even more prominent in $G\alpha_{12}$,$G\alpha_{13}$ double-deficient cells (Figure 6A).

Although the potential interactions between the G_{12} family and Rap1 still need to be elucidated, the small GTPase RhoA is a well-known effector of G_{12} and G_{13}. We studied RhoA activation in response to stimulation of known G_{12},G_{13}-coupled receptors such as the TXA_2 receptor TP (Matsuoka and Narumiya, 2007) or LPA receptors (Chun and Rosen, 2006) and found that the TP agonist U46619, as well as LPA, induced a robust RhoA activation in control CD4$^+$ T cells, but not in $G\alpha_{12}$,$G\alpha_{13}$ double-deficient CD4$^+$ T cells (Figure 6B). Interestingly, also basal RhoA activity was reduced in $G\alpha_{12}$,$G\alpha_{13}$ double-deficient cells. Given that RhoA has been shown to negatively regulate Rac1 (Iden and Collard, 2008), we next studied basal and chemokine-induced Rac1 activation. We found that Rac1 activation was generally enhanced in mutant cells, most prominently at 60 s after stimulation, but also under basal conditions (Figure 6C). The G_{12},G_{13}-mediated signaling pathway obviously exerts an inhibitory effect on chemokine-induced Rac1 activation, and two different scenarios might underlie this finding: (1) CCR7 directly activates G_{12} and G_{13} in parallel with its main effector pathway G_i, or (2) the CCR7-G_i-Rac1 signaling cascade is modulated by other receptors than CCR7. To address the first possibility, we investigated whether CCL19 and CCL21 were able to induce RhoA activation in T cells and whether this depended on G_i and/or on G_{12} and G_{13} (Figure 6D). We found that CCL19+21 induced a mild RhoA activation in control T cells, but the response was weaker and slower than that induced by the TXA_2 analog U46619. Pretreatment with pertussis toxin, which ADP-ribosylates G_i and thereby uncouples it from receptors, did not affect U46619-induced RhoA activation but abrogated chemokine-induced RhoA activation. In $G\alpha_{12}$,$G\alpha_{13}$ double-deficient T cells, U46619-induced RhoA activation was clearly reduced, whereas RhoA activation in response to CCL19+21 was not changed compared to control cells (Figure 6D). These findings indicate that the mild RhoA activation observed after CCR7 stimulation is rather mediated through G proteins of the G_i family than the G_{12} family.

To investigate the potential involvement of other GPCRs in this context, we tested whether concomitant activation of the G_{12},G_{13}-RhoA pathway, for example in response to U46619, was able to quench chemokine-induced Rac1 activation in wild-type cells. We found that coapplication of U46619 with chemokines induced a strong RhoA activation within 20 s (Figure 6E) and that Rac1 activation was concomitantly reduced (Figure 6F). Of note, the quenching effect of U46619 on chemokine-induced Rac1 activation was abrogated in $G\alpha_{12}$,$G\alpha_{13}$ double-deficient

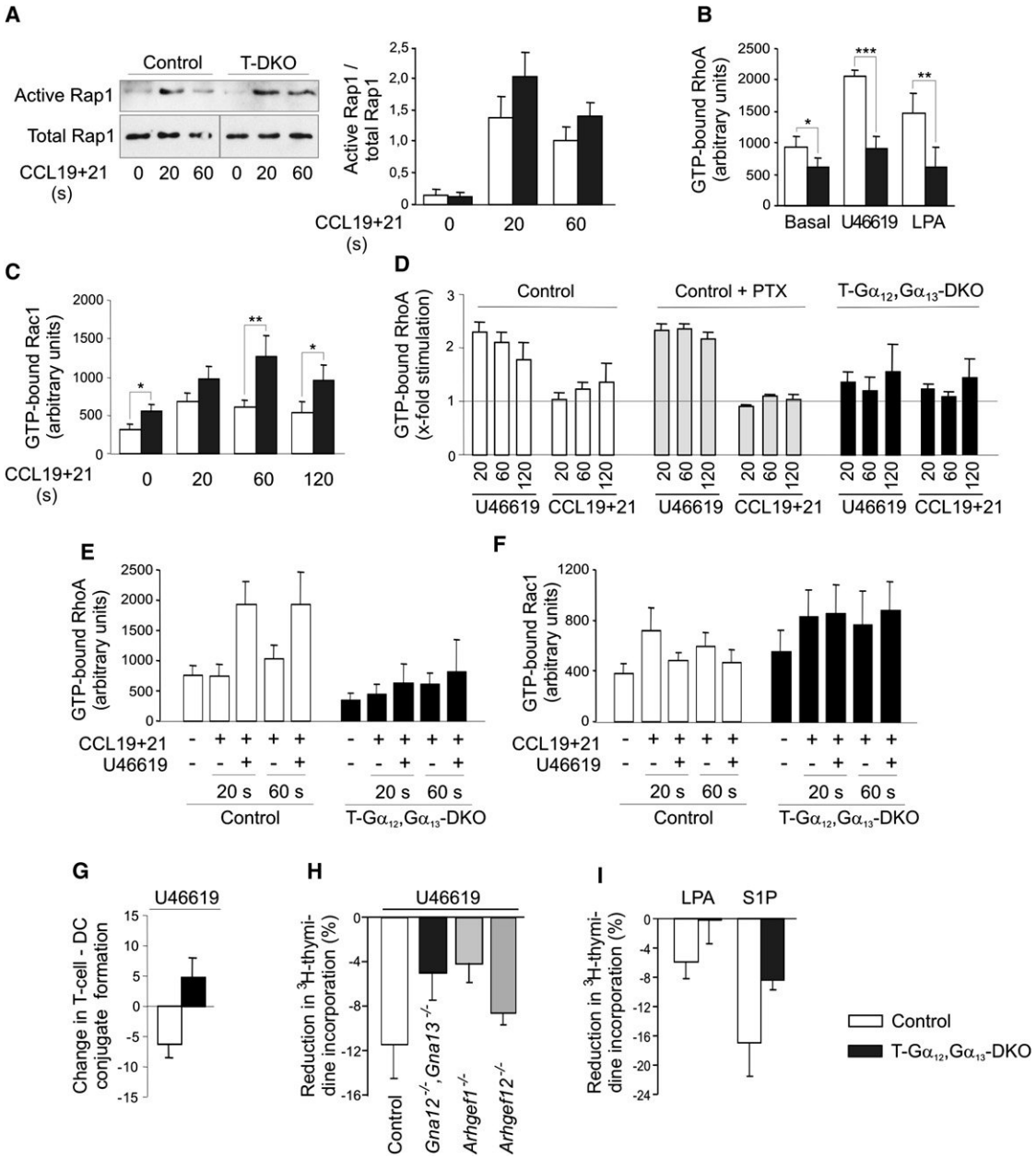

Figure 6. Signaling Pathways Involved in $G\alpha_{12},G\alpha_{13}$-Mediated Regulation of Adhesiveness and Polarization

(A) Basal and CCL19+21-induced Rap1 activation in control and $G\alpha_{12},G\alpha_{13}$ double-deficient T cells. The left panel shows exemplary immunoblots. The right panel shows the statistical evaluation of the densitometric quantification (n = 5).

(B) Amounts of active, GTP-bound RhoA under basal conditions and 1 min after stimulation with the TXA_2 analog U46619 or lysophosphatidic acid (LPA) (n = 6–10).

(C) Basal and CCL19+21-induced Rac1 activation in $CD4^+$ T cells (n = 6–10).

(D) Comparison of relative RhoA activation in response to U46619 and CCL19+21 in control T cells, pertussis toxin (PTX)-pretreated T cells, and $G\alpha_{12},G\alpha_{13}$ double-deficient T cells (n = 3).

(E and F) Effect of U46619 on CCL19+21-induced activation of RhoA (E) and Rac1 (F) (n = 4–6).

(G) Effect of U46619 on conjugate formation between control or mutant $CD4^+$ T cells and allo-DCs as determined by flow cytometry (n = 5).

(H) Effect of U46619 on allo-$CD11c^+$-induced proliferation in control $CD4^+$ T cells, as well as $CD4^+$ T cells deficient for $G\alpha_{12},G\alpha_{13}$ (*Gna12*$^{-/-}$,*Gna13*$^{-/-}$), Lsc (*Arhgef1*$^{-/-}$), or LARG (*Arhgef12*$^{-/-}$) (n = 3–5).

(I) Effect of LPA and S1P on allo-$CD11c^+$-induced proliferation in control and $G\alpha_{12},G\alpha_{13}$ double-deficient $CD4^+$ T cells (n = 3–5).

White bars represent the control; black bars represent the T-$G\alpha_{12},G\alpha_{13}$ DKO. s, seconds. Data are displayed as mean ± SEM. *$p < 0.05$.

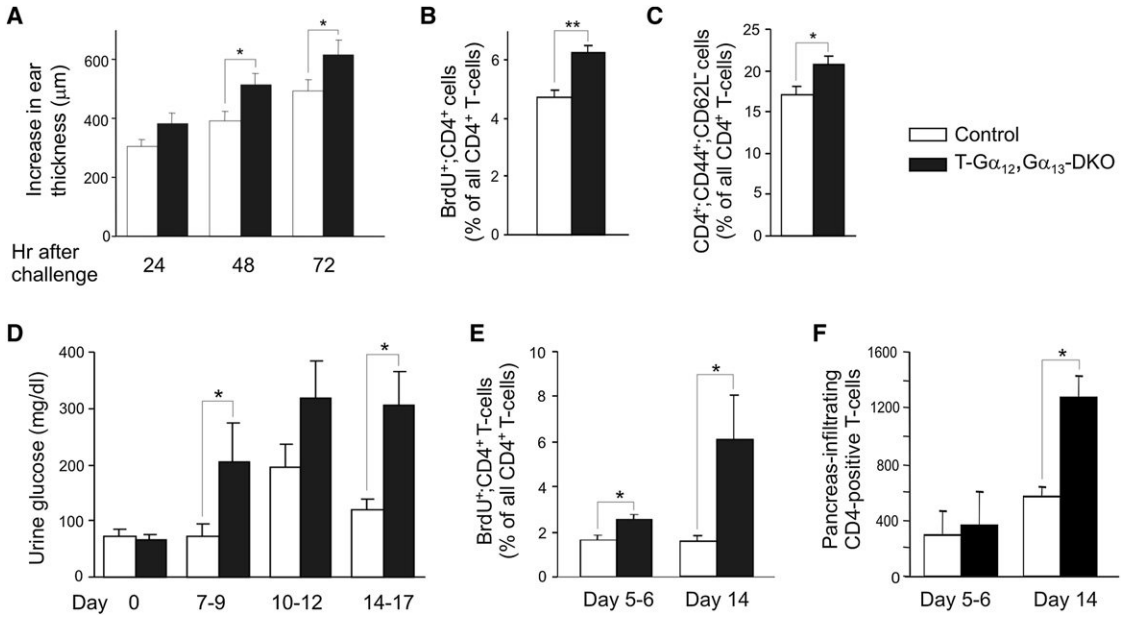

Figure 7. Immune Responses in T-G$\alpha_{12/13}$ DKOs

(A–C) Delayed type hypersensitivity. (A) shows an increase in ear thickness after sensitization and challenge with DNFB (n = 10). (B) and (C) show flow cytometric analysis of BrdU-positive $CD4^+$ T cells (B) and of $CD4^+$,$CD44^+$,$CD62L^-$ effector and memory T cells (C) in cervical lymph nodes 72 hr after challenge (n = 6). (D–F) MLD-STZ-induced diabetes mellitus. (D) shows urine glucose amounts at different time points after disease induction (n = 10). (E) shows flow cytometric analysis of BrdU-positive $CD4^+$ T cells in peripancreatic lymph nodes before onset of symptoms (days 5–6) and in the late phase of disease (day 14) (n = 4). (F) shows flow cytometric analysis of pancreatic infiltrates at days 5–6 and day 14 (n = 4–6). White bars represent the control; black bars represent the T-Gα_{12},Gα_{13} DKO. Data are displayed as mean ± SEM. *$p < 0.05$.

cells (Figure 6F), in which RhoA activation was strongly reduced (Figure 6E).

We next asked whether U46619-induced activation of the G_{12},G_{13}-RhoA-signaling cascade would also affect cell-cell interactions and, secondary to that, proliferation. We found that U46619 reduced dimer formation between control $CD4^+$ T cells and allo-DCs, whereas it moderately increased conjugate formation in Gα_{12},Gα_{13} double-deficient $CD4^+$ T cells (Figure 6G). Furthermore, U46619 reduced in vitro proliferation of control $CD4^+$ T cells, and this effect was impaired in mutant cells (Figure 6H). We next investigated the potential involvement of the G_{12},G_{13}-regulated RhoGEF proteins Lsc-p115RhoGEF (Lsc) and leukemia-associated RhoGEF (LARG) in this process and found that U46619-induced suppression of proliferation was reduced in Lsc-deficient cells as well (Figure 6H). Also, inactivation of LARG led to some reduction, although a less prominent one, suggesting that both LARG and Lsc contribute to the effects of Gα_{12},Gα_{13} on adhesiveness and proliferation, with a predominant role of Lsc (Figure 6H). Interestingly, lysophospholipids LPA and S1P also were able to reduce proliferation in response to allo-DCs in a Gα_{12},Gα_{13}-dependent manner (Figure 6I). Of note, the inhibitory effects of U46619, LPA, and S1P on proliferation are mild compared to the effect of LFA-blocking antibodies, showing that the G_{12},G_{13}-mediated signaling pathway only exerts a modulating role. Taken together, these results suggest that GPCRs such as the TXA_2 receptor, but also LPA and S1P receptor subtypes, negatively regulate cell adhesion and polarization through G_{12},G_{13}-mediated activation of RhoA, which in turn modulates chemokine-induced activation of Rac1, and, directly or indirectly, Rap1 (Figure S2). We hypothesize that TXA_2 or LPA regulate adhesiveness of $CD4^+$ T cells in an auto- or paracrine manner; in support of this hypothesis, we found that gentle washing of cells enhanced ICAM-1 adhesion, but not VCAM-1 adhesion (Figure S3).

Immune Functions In Vivo

Increased $CD4^+$ T cell proliferation and trafficking might alter responses to exogenous or endogenous antigens, resulting in abnormal immune responses or autoimmune disease. Neither routine histological analysis of internal organs nor staining for IgG deposition in the kidney of aged mice revealed signs of spontaneous autoimmune disease (data not shown), which led us to challenge T cell-specific Gα_{12},Gα_{13} double-deficient mice in two models of T cell-mediated pathology: contact hypersensitivity to dinitrofluorobenzene (DNFB) as a model for responses to foreign antigen (Kurimoto and Streilein, 1993) and low-dose streptozotocin-induced diabetes mellitus as a model of autoimmune disease (Like and Rossini, 1976).

During the sensitization phase of contact hypersensitivity, the hapten DNFB is applied to the abdominal skin from where it is transported to draining lymph nodes and presented by dendritic cells. The resulting activation of naive T cells and generation of effector cells leads during the elicitation phase (rechallenge with DNFB in the ear of the skin) to leukocyte recruitment to the ear, resulting in a Th1-cell-dependent local inflammation with consecutive swelling (Kurimoto and Streilein, 1993). We found that T cell-specific Gα_{12},Gα_{13} double-deficient mice showed increased ear swelling at 24, 48, and 72 hr after sensitization and challenge (Figure 7A), and histological analyses of ear

sections taken at 72 hr showed an increased leukocytic infiltration (data not shown). Basal ear thickness and histology did not differ between the genotypes (data not shown). $CD4^+$ T cells in cervical lymph nodes from mutant mice showed a higher proliferation rate than those of control mice (Figure 7B), and the proportion of T memory and effector cells was increased (Figure 7C).

In the second in vivo model, type I diabetes mellitus is induced by intraperitoneal administration of multiple low doses of streptozotocin (MLD-STZ), and the pathogenesis of this disease has been shown to involve an autoimmune-mediated destruction of pancreatic β-cells (Like and Rossini, 1976). We determined urine glucose levels every 72–96 hr starting from the seventh day after diabetes induction and found that in deficient mice diabetes development was both accelerated and aggravated (Figure 7D). Because this might be due to an increased proliferative response to an altered cytokine profile, or to increased entry into inflamed tissues, we investigated proliferation, cytokine production and number of infiltrating leukocytes before onset of symptoms (days 5–6) and at the height of disease (day 14). We found that peripancreatic lymph nodes were clearly enlarged already at day 5–6 (total cell number control mice: $9.8 \pm 3.4 \times 10^6$, mutant mice: $25.9 \pm 5.8 \times 10^6$); the $CD4^+$ T cells showed enhanced proliferation (Figure 7E) without substantial changes in the production of IFNγ, TNFα, or IL-4 (data not shown). The numbers of pancreas-infiltrating $CD4^+$ T cells, $CD8^+$ T cells, or $CD11b^+$ macrophages did not differ between the genotypes at days 5–6; at day 14, however, T cell-specific $G\alpha_{12}$,$G\alpha_{13}$ double-deficient mice showed increased numbers of pancreas-infiltrating $CD4^+$ T cells (Figure 7F and data not shown). Taken together, these findings show that the enhanced proliferative responses in T cell-specific $G\alpha_{12}$,$G\alpha_{13}$ double-deficient mice are associated with an increased susceptibility and severity of T cell-mediated diseases.

DISCUSSION

Whereas G_i-coupled chemokine receptors have in many studies been shown to importantly contribute to T cell trafficking or formation of the immunological synapse (Kinashi, 2005; Laudanna et al., 2002), the role of the G_{12} family in peripheral T cells is poorly understood. We report here that $G\alpha_{12}$,$G\alpha_{13}$ double-deficient $CD4^+$ T cells show an enhanced interaction with allo-DCs, thereby leading to abnormal proliferative responses in vitro. Together with an increased lymph node entry, this enhancement of proliferation most likely underlies the increased lymph node size observed in T cell-specific $G\alpha_{12}$,$G\alpha_{13}$ double-deficient mice in vivo. Our in vitro studies suggest an increased activity of integrin LFA-1 as an underlying mechanism, and this notion is strongly supported by the finding that blocking antibodies directed against LFA-1 normalized T-DC interactions and in vitro proliferation and increased lymph node entry of $G\alpha_{12}$,$G\alpha_{13}$ double-deficient T cells. Also the fact that hyperproliferation is only observed in response to adhesion-dependent stimulation by DCs, but not in response to direct stimulation of the T cell receptor (TCR), PMA, or superantigens, points to the important role of LFA-1 in this context.

The increased adhesiveness observed in the absence of $G\alpha_{12}$ and $G\alpha_{13}$, however, is moderate compared to that observed in a mouse line carrying a hyperactive LFA-1 mutant ($Itgal^{\Delta/\Delta}$) containing a five amino acid deletion in the membrane-proximal region of LFA-1 (Semmrich et al., 2005). $Itgal^{\Delta/\Delta}$ lymphocytes share with $G\alpha_{12}$,$G\alpha_{13}$ double-deficient cells in vitro phenotypes such as increased ICAM-1 adhesion, impaired transmigration, and tail retraction, but they differ considerably with respect to their in vivo phenotype. In vivo, $Itgal^{\Delta/\Delta}$ mice resemble LFA-1-deficient animals, with reduced lymph node and thymus sizes and impaired proliferative responses (Berlin-Rufenach et al., 1999; Schmits et al., 1996). These paradoxical findings are most likely due to the constitutive active nature of the $Itgal^{\Delta/\Delta}$ mutant, and this nature leads to irrevocable attachment to HEV or DCs and thereby prevents normal transmigration or activation. In $G\alpha_{12}$,$G\alpha_{13}$ double-deficient T cells, in contrast, negative regulation of LFA-1 through other mechanisms such as cbl-b (Zhang et al., 2003) or RhoH (Cherry et al., 2004) is still functional, leading to the observed moderate changes in trafficking and proliferation.

Our in vitro studies suggest that the inactivation of $G\alpha_{12}$ and $G\alpha_{13}$ results in an altered activation state of three small GTPases involved in the regulation of polarization and integrin-mediated adhesion: RhoA, Rac1, and Rap1. RhoA has been shown to regulate integrin activity in T cells both positively (Constantin et al., 2000; Giagulli et al., 2004) and negatively (Rodriguez-Fernandez et al., 2001; Smith et al., 2003); in addition, it has been involved in polarization (Iden and Collard, 2008; Mor et al., 2007). RhoA is probably the most important effector of $G\alpha_{12}$ and $G\alpha_{13}$, but it should be kept in mind that RhoA can also be activated by a variety of other signaling pathways such as integrins, receptor tyrosine kinases, plexins, or G_q and G_i family G proteins. RhoA activation in response to stimulation of G_{12},G_{13}-coupled receptors is mediated by three specific RhoGEF proteins, Lsc, LARG, and PDZ-RhoGEF (Fukuhara et al., 2001), and our data indicate that Lsc, and to a lesser extent also LARG, mediate the inhibitory effects of $G\alpha_{12}$ and $G\alpha_{13}$ on adhesion and proliferation. In line with these findings, Lsc-deficient mice share some phenotypical aspects with T cell-specific $G\alpha_{12}$,$G\alpha_{13}$ double-deficient mice, for example increased lymph node size and in vitro proliferation (Girkontaite et al., 2001) or impaired rear detachment from ICAM-1 (Rubtsov et al., 2005). An increased polarization was also observed in $G\alpha_{12}$,$G\alpha_{13}$ double-deficient B cells (Rieken et al., 2006b) or in neutrophils expressing dominant-negative forms of $G\alpha_{12}$ and $G\alpha_{13}$ (Xu et al., 2003). Xu et al. (2003) suggested that chemoattractant receptors might activate G_i- and G_{12},G_{13}-mediated signaling pathways in neutrophils in parallel, whereas our data suggest that G_{12},G_{13}-mediated quenching of chemokine-induced Rac1 activity involves receptors other than CCR7, for example, TP.

RhoA is known to antagonistically regulate Rac1, a small GTPase involved in the regulation of cellular morphology, polarization, and integrin signaling (Iden and Collard, 2008; Mor et al., 2007). We found that both basal and chemokine-induced Rac1 activation is increased in the absence of $G\alpha_{12}$ and $G\alpha_{13}$, possibly contributing to enhanced polarization and integrin-mediated adhesion of $G\alpha_{12}$,$G\alpha_{13}$ double-deficient T cells (D'Souza-Schorey et al., 1998; Garcia-Bernal et al., 2005). We furthermore show that chemokine-induced Rac1 activation in control $CD4^+$ T cells is dampened by concomitant simulation of the G_{12},G_{13}-RhoA pathway through the TP agonist U46619. Interestingly,

Please cite this article in press as: Herroeder et al., Guanine Nucleotide-Binding Proteins of the G_{12} Family Shape Immune Functions by Controlling $CD4^+$ T Cell Adhesiveness and Motility, Immunity (2009), doi:10.1016/j.immuni.2009.02.010

U46619 alone induces Rac1 activation through G proteins of the G_q family (Gratacap et al., 2001); it seems, however, that during combined application of U46619 and CCL19+21, the G_{12},G_{13}-RhoA mediated inhibition of Rac1 outweighs G_q-induced Rac1 activation. Importantly, stimulation of the G_{12},G_{13}-RhoA signaling cascade by U46619 does not only impede CCL19+21-induced Rac1 activation but also impacts on adhesiveness and, consecutively, on proliferation: U46619 is able to reduce conjugate formation between wild-type $CD4^+$ T cells and allo-DCs, resulting in reduced proliferation in vitro. Of note, the $G\alpha_{12}$,$G\alpha_{13}$-mediated modulation of adhesiveness and proliferation was not restricted to U46619, but was also observed in response to LPA and, to a lesser extent, S1P. We therefore hypothesize that local mediators such as S1P, LPA, and TXA_2 are released from lymphocytes or bystanding cells and modulate cell polarization and integrin-mediated adhesion in an auto- or paracrine manner. Lysophospholipids and TXA_2 are released from blood cells, macrophages, and dendritic cells (Chun and Rosen, 2006; Kabashima et al., 2003) and are therefore likely to contribute to the regulation of cell-cell interactions during lymph node entry or antigen presentation. Genetic inactivation of the TXA_2 receptor TP, for example, resulted in age-dependent lymphadenopathy and enhanced immune responses to foreign antigens (Kabashima et al., 2003). In line with an important role of $G\alpha_{12}$ and $G\alpha_{13}$ in the negative regulation of adhesiveness through auto- and paracrine factors, we found that gentle washing significantly increased ICAM-1 adhesiveness in control but not in $G\alpha_{12}$,$G\alpha_{13}$ double-deficient T cells.

The third GTPase that shows altered activation in the absence of $G\alpha_{12}$ and $G\alpha_{13}$ is Rap1, which has been shown to increase integrin-mediated adhesion (Katagiri et al., 2000; Sebzda et al., 2002), for example in response to chemokine receptor activation (Shimonaka et al., 2003). Whether increased chemokine-induced Rap1 activation in the absence of $G\alpha_{12}$ and $G\alpha_{13}$ is causally related to increased Rac1 and impaired RhoA activation is currently unclear. Crosstalk between Rac1 and Rap1 has been implicated in the regulation of cell migration, for example by localizing GEFs for Rap1 and Rac1 to the ruffling membrane (Arthur et al., 2004; Caloca et al., 2004), but the effects of $G\alpha_{12}$,$G\alpha_{13}$ on Rap1 and Rac1 might also be independent.

A fourth GTPase involved in the regulation of LFA-1 activity in lymphocytes is RhoH (Cherry et al., 2004). In contrast to other small GTPases, RhoH is GTPase deficient and therefore does not undergo the normal activation-inactivation cycle; instead, it was suggested to be regulated on the transcriptional level (Li et al., 2002). We investigated RhoH expression by RT-PCR but did not find altered expression in the absence of $G\alpha_{12}$ and $G\alpha_{13}$ (data not shown), suggesting that altered RhoH expression does not contribute to the phenotype of T cell-specific $G\alpha_{12}$,$G\alpha_{13}$ double-deficient mice.

Interestingly, whereas LFA-1 activity is clearly enhanced in $G\alpha_{12}$,$G\alpha_{13}$ double-deficient $CD4^+$ T cells, the activation state of integrin $\alpha4\beta1$ is not altered, suggesting that these integrins are differentially regulated. A differential regulation of $\alpha4\beta1$ and LFA-1 by small GTPases has been described in a rat monocytic cell line (Honing et al., 2004) and in human T cells (Ghandour et al., 2007); the underlying mechanisms, however, are unknown. It is also currently unclear why $G\alpha_{12}$,$G\alpha_{13}$ deficiency seems to affect $CD4^+$ T cells more prominently than $CD8^+$ T cells. Differences in the expression of G_{12} family G proteins or of G_{12},G_{13}-coupled receptors might explain these findings, but neither in literature (Chun and Rosen, 2006; Kabashima et al., 2003) nor in our own experiments did we find evidence for such differences. It might be speculated that not yet characterized G_{12},G_{13}-coupled receptors with cell type-specific expression are involved in the negative regulation of integrin activity.

The in vivo relevance of the G_{12},G_{13}-mediated negative regulation of LFA-1 is clearly documented by the finding that T cell-specific $G\alpha_{12}$,$G\alpha_{13}$ double-deficient mice show an increased susceptibility toward endogenous and exogenous antigens, resulting in increased severity of autoimmune diabetes and cutaneous hypersensitivity. Interestingly, except for the increased lymph node size, we did not detect signs of spontaneous autoimmune disease in T cell-specific $G\alpha_{12}$,$G\alpha_{13}$ double-deficient mice, suggesting that the regulatory effect of $G\alpha_{12}$ and $G\alpha_{13}$ is especially important under pathological conditions.

Taken together, our data show that heterotrimeric G proteins of the G_{12} family negatively regulate the activation state of integrin LFA-1, thereby fine-tuning T cell trafficking, proliferation, and susceptibility toward immune disease. We show that a variety of receptor systems such as lysophospholipid or prostanoid receptors converge on $G\alpha_{12}$ and $G\alpha_{13}$ to modulate activation of RhoA, Rac1, Rap1, and ultimately LFA-1, and it is well possible that other, yet unknown mediators contribute to this process. Therefore, a cell-type-specific manipulation of $G\alpha_{12}$ and $G\alpha_{13}$ or of downstream RhoGEF proteins might in the future prove useful to modulate T cell trafficking or the strength of the immunological synapse.

EXPERIMENTAL PROCEDURES

Animals and Cells

Mice were housed under specific pathogen-free conditions, and their genetic background was predominantly C57BL6/N (fifth generation backcross). Genotyping was performed as described previously (Moers et al., 2003). For generation of conditional LARG-deficient mice, please see Supplemental Experimental Procedures. Untouched lymph node $CD4^+$ T cells and splenic $CD11c^+$ dendritic cells were isolated with the mouse $CD4^+$ T cell isolation kit or mouse CD11c-Microbeads, respectively (Miltenyi, Bergisch-Gladbach, Germany). All animal experiments have been approved by local authorities.

Chemicals and Antibodies

U46619 was from Cayman (Ann Arbor, MI, USA); LPA and S1P were from Biomol (Hamburg, Germany), chemokines from PeproTech (London, UK); and STZ, DNFB, staphylococcal enterotoxin B, and α-tubulin antibodies were from Sigma-Aldrich (St. Louis, MO, USA). Endotoxin-free antibodies against LFA-1, VLA4, or isotype control were from the Cancer Research UK Monoclonal Antibody Unit, London. Antibodies against $G\alpha_{13}$, $G\alpha_{12}$, and LARG were from Santa Cruz Biotechnology (Santa Cruz, CA, USA). All other antibodies were from BD Biosciences (San Jose, CA, USA).

Flow Cytometry

All flow cytometric analyses were performed with a FACSCalibur flow cytometer and CellQuestPro Software (BD Biosciences). Apoptosis and proliferation were determined with the Annexin-V-FITC apoptosis kit and the FITC-BrdU flow kit, respectively; intracellular cytokine production was determined with the mouse intracellular cytokine staining kit (all BD Biosciences). For the flow cytometric analysis of conjugate formation, 1×10^5 PE-labeled $CD4^+$ T cells and 1×10^5 FITC-labeled $CD11c^+$ DCs were mixed, centrifuged for 1 min at 50 × g, and incubated for 20 min. After gentle resuspension, the proportion of CFSE-PE double-positive events was determined.

Live-Cell Imaging

For live-cell imaging, 10^5 unstained purified $CD4^+$ T cells from control or mutant mice were mixed with 2×10^4 CFSE-labeled $CD11c^+$ DCs in a droplet of 20 μl RPMI1640, 10 mM HEPES, and 10% FCS and allowed to attach to CELL STAR plastic dishes (Greiner Bio-One GmbH, Essen, Germany) for 20 min at 37°C and 5% CO_2. In some cases, 10 μg/ml LFA-1 antibodies, 10 μg/ml α4β1 antibodies, or 10 μg/ml isotype control were added to the mixture. Cell interactions were recorded for 10 min with a Leica DM IRE2 inverted fluorescence microscope and Leica FW4000 software at 37°C and 5% CO_2 (1 frame per 10 s). For statistical analysis, cell interactions were classified by an investigator blinded to genotype; an interaction was classified as stable if it lasted throughout a 10 min movie. In some cases, plates were coated with ICAM-1 (for coating, see Adhesion Assays) and the distance traveled by individual T cells was determined with the ImageJ program (NIH, Bethesda, MD, USA).

Adhesion Assays

Adhesion assays were carried out in 48-well plastic dishes as described previously (Rieken et al., 2006a), with minor modifications: for ICAM-1 coating, wells were coated with 50 μg/ml goat-anti-human-IgG-Fc antibody (Jackson ImmunoResearch, West Grove, PA, USA) at 4°C overnight, washed twice with PBS, and incubated with 2.5 μg/ml mouse ICAM-1-F_c (R&D Systems, Minneapolis, USA) in PBS for 2 hr. For VCAM-1 coating, wells were incubated for 1 hr at 37°C with 3 μg/ml hVCAM-1 (R&D Systems) in carbonate buffer. In some cases, chemokines CCL19 and 21 were added at final concentrations of 100 ng/ml during ICAM-1 and hVCAM-1 coating. Afterward, all wells were blocked with 0.5% bovine serum albumine (BSA) in PBS for 30 min before use. The volume per well was 100 μl in each step. For the adhesion assay, 5×10^5 lymph node cells were incubated in 100 μl RPMI1640 containing 10 mM HEPES and 0.5% FCS for 30 min at 37°C and 5% CO_2; in some cases, CCL19 and CCL21 (100 ng/ml final), Mg^{2+} (10 mM) and EGTA (1 mM), CD3-CD28 antibodies (5 μg/ml each), or PMA (5 ng/ml) were added. After discarding nonadherent cells, the plate was gently washed in PBS and adherent cells were subsequently detached in RPMI1640, 5 mM EDTA for 20 min on ice. Numbers of adherent $CD4^+$ T cells were determined after antibody staining by flow cytometry, and data are displayed as the proportion of adherent cells relative to cell input into the adhesion assay.

Soluble ICAM-1 Binding

Binding of ICAM-1 (10 μg/ml, R&D Systems) to $CD4^+$ T cells in the absence or presence of 10 mM Mg^{2+} and 1 mM EGTA was determined as described previously (Sebzda et al., 2002). In brief, freshly isolated lymph node cells (1×10^5 cells/ml) were resuspended in HEPES buffer (20 mM HEPES, 140 mM NaCl, and 2 g/l glucose) with 0.1% BSA at a concentration of 2×10^6 cells/ml. Lymphocyte aliquots of 50 μl (1×10^5 cells) were added to 96-well plates with or without 10 mM Mg^{2+} and 1 mM EGTA. Soluble murine ICAM-1–Fc (10 μg/ml, R&D Systems) was added to the cells. After 30 min incubation at 37°C, cells were washed twice in ice-cold PBS with 0.1% BSA and incubated with Fc-specific FITC-conjugated goat anti-human IgG (1:200; Jackson Immunoresearch, West Grove, PA, USA) and PerCP-conjugated anti-mouse CD4 antibody for 10 min on ice. We washed cells twice in PBS with 0.1% BSA to remove excess unbound antibodies and detected fluorescence by flow cytometry.

Migration Assays

For chemotaxis assays, lymph node cells were preincubated in RPMI1640 + 10 mM HEPES + 0.1% BSA for 30 min at 37°C and 5% CO_2 and then allowed to migrate through 5 μm pore size transwell inserts (Corning, Acton, MA, USA) at a density of 2×10^6 splenocytes/100 μl per well. The transwell inserts were uncoated, ICAM-1-coated (as described for Adhesion Assays), or seeded with 3×10^4 bEND.3 endothelial cells (from ATCC [Montesano et al., 1990]) 24 hr before the experiment. The lower wells contained either 600 μl RPMI1640 + 10 mM HEPES + 0.1% BSA alone or medium plus 100 ng/ml CCL19+21, or 1–100 nM S1P. After 3 hr of incubation at 37°C and 5% CO_2, transwell plates were kept on ice for 20 min and centrifuged at 180 × g for 3 min, inserts were discarded, and cells were stained for $CD4^+$ T cells and counted by flow cytometry. Cell numbers were expressed as a proportion of input. All experiments were done in triplicates.

Adoptive Transfer Experiments

Fluorescent labeling of cells with the Cell Trace CFSE Cell Proliferation Kit (50 νM CFSE final), CellTracker CM-DiI (5 mM final), or SNARF (500 nM final) (all Invitrogen, Karlsruhe, Germany) was performed according to the manufacturer's instructions. For adoptive transfer experiments, isolated $CD4^+$ T cells from mutant and control animals were labeled with CFSE and DiI, or SNARF, mixed in a 1:1 ratio, and injected intravenously (5×10^6 cells per mouse). In some cases, recipients were pretreated with 100 μg LFA-1 antibodies or isotype control. After 2 or 24 hr, the proportion of CFSE- and DiI-positive cells in cervical lymph nodes was analyzed by flow cytometry; in some cases we also analyzed cisterna chyli punctate. All data were corrected for the actual input ratio as determined by FACS.

RhoA, Rac1, and Rap1 Activation Assays

Amounts of GTP-bound RhoA or Rac1 were determined with RhoA or Rac1 G-LISA activation kits (Cytoskeleton, Denver, CO, USA), and Rap1 was detected with the EZ-Detect Rap1 activation kit (Pierce, Rockford, USA). For each measurement, 2×10^6 (RhoA) or 5×10^6 (Rac1, Rap1) T cells were used; in some cases, cells were pretreated with PTX 100 ng/ml. Agonist concentrations were 1 μM for U46618 and 100 ng/ml for chemokines.

Intravital Two-Photon Microscopy

Three-dimensional two-photon microscopy was performed with a MaiTai laser (Spectra-Physics, Darmstadt, Germany) running at 800 nm, a multibeam scanhead (LaVision Biotech, Bielefeld, Germany), and an Olympus BX51WI microscopic stage equipped with a XLUMPL ×20, NA 0.95 water dipping lens. Image detection was done with a cooled CCD-camera (Imager Intense, LaVision, Goettingen, Germany). RGB Z stacks of 300 × 300 μm images were recorded in typically 15 steps of 3 μm. Frames taken at two to three positions within each of the two imaging areas (vessel-rich zone [medulla, paracortex] and T cell zone) were analyzed (Sanna et al., 2006). Rendering of video sequences was performed with Volocity 4.3 (Improvision, Waltham, MA, USA). Cell tracking was done with computer-assisted manual tracking with CellTracker. Data were plotted with Prism 4 (GraphPad Software, San Diego, CA, USA). Swapping of dyes resulted in the same findings. For details, see Supplemental Experimental Procedures.

Animal Models

Delayed type hypersensitivity and MLD-STZ diabetes mellitus were induced in female (DTH) or male (MLD-STZ) mice aged 8–16 weeks as described previously (Kurimoto and Streilein, 1993; Like and Rossini, 1976). Urine glucose levels were determined with the glucose hexokinase method (Randox Laboratories, UK). For the flow cytometric quantification of pancreatic leukocyte infiltration, the peripancreatic lymph nodes were carefully removed; then pancreata were minced and digested for 10–15 min at 37°C under vigorous shaking in Krebs-Ringer solution containing 0.5 mg/ml Collagenase P (Roche Diagnostics, Mannheim, Germany). Leukocytes were then purified via Percoll and Lympholyte M gradients (Cedarlane, Burlington, Canada) according to the manufacturer's instructions and analyzed by flow cytometry.

In Vitro Proliferation Assays, Immunoblotting, and Immunohistochemistry

In vitro proliferation assays, immunoblotting, and immunohistochemistry were performed as described previously (Rieken et al., 2006a; Rieken et al., 2006b). For details, see Supplemental Experimental Procedures.

Statistics

Data are displayed as mean ± SEM. Comparisons between two groups were performed with unpaired t test. n indicates the number of animals per experimental group.

SUPPLEMENTAL DATA

Supplemental Data include Supplemental Experimental Procedures, one table, three figures, and four movies and can be found with this article online at http://www.cell.com/immunity/supplemental/S1074-7613(09)00183-6.

Please cite this article in press as: Herroeder et al., Guanine Nucleotide-Binding Proteins of the G_{12} Family Shape Immune Functions by Controlling $CD4^+$ T Cell Adhesiveness and Motility, Immunity (2009), doi:10.1016/j.immuni.2009.02.010

ACKNOWLEDGMENTS

We thank M. Bernhard, M. Hillesheim, and Y. Teschner for expert technical assistance; J. Marth for the LckCre line; and B. Arnold, R. Arnold, and B. Schraven for helpful advice. This work was funded by the collaborative research center 405 of the *Deutsche Forschungsgemeinschaft* and the *Young Investigator Award* of the Medical Faculty of the University of Heidelberg.

Received: July 8, 2008
Revised: January 9, 2009
Accepted: February 23, 2009
Published online: April 30, 2009

REFERENCES

Arthur, W.T., Quilliam, L.A., and Cooper, J.A. (2004). Rap1 promotes cell spreading by localizing Rac guanine nucleotide exchange factors. J. Cell Biol. *167*, 111–122.

Berlin-Rufenach, C., Otto, F., Mathies, M., Westermann, J., Owen, M.J., Hamann, A., and Hogg, N. (1999). Lymphocyte migration in lymphocyte function-associated antigen (LFA)-1-deficient mice. J. Exp. Med. *189*, 1467–1478.

Caloca, M.J., Zugaza, J.L., Vicente-Manzanares, M., Sanchez-Madrid, F., and Bustelo, X.R. (2004). F-actin-dependent translocation of the Rap1 GDP/GTP exchange factor RasGRP2. J. Biol. Chem. *279*, 20435–20446.

Cherry, L.K., Li, X., Schwab, P., Lim, B., and Klickstein, L.B. (2004). RhoH is required to maintain the integrin LFA-1 in a nonadhesive state on lymphocytes. Nat. Immunol. *5*, 961–967.

Chun, J., and Rosen, H. (2006). Lysophospholipid receptors as potential drug targets in tissue transplantation and autoimmune diseases. Curr. Pharm. Des. *12*, 161–171.

Constantin, G., Majeed, M., Giagulli, C., Piccio, L., Kim, J.Y., Butcher, E.C., and Laudanna, C. (2000). Chemokines trigger immediate beta2 integrin affinity and mobility changes: Differential regulation and roles in lymphocyte arrest under flow. Immunity *13*, 759–769.

D'Souza-Schorey, C., Boettner, B., and Van Aelst, L. (1998). Rac regulates integrin-mediated spreading and increased adhesion of T lymphocytes. Mol. Cell. Biol. *18*, 3936–3946.

Fukuhara, S., Chikumi, H., and Gutkind, J.S. (2001). RGS-containing RhoGEFs: The missing link between transforming G proteins and Rho? Oncogene *20*, 1661–1668.

Garcia-Bernal, D., Wright, N., Sotillo-Mallo, E., Nombela-Arrieta, C., Stein, J.V., Bustelo, X.R., and Teixido, J. (2005). Vav1 and Rac control chemokine-promoted T lymphocyte adhesion mediated by the integrin alpha4beta1. Mol. Biol. Cell *16*, 3223–3235.

Ghandour, H., Cullere, X., Alvarez, A., Luscinskas, F.W., and Mayadas, T.N. (2007). Essential role for Rap1 GTPase and its guanine exchange factor CalDAG-GEFI in LFA-1 but not VLA-4 integrin mediated human T-cell adhesion. Blood *110*, 3682–3690.

Giagulli, C., Scarpini, E., Ottoboni, L., Narumiya, S., Butcher, E.C., Constantin, G., and Laudanna, C. (2004). RhoA and zeta PKC control distinct modalities of LFA-1 activation by chemokines: Critical role of LFA-1 affinity triggering in lymphocyte in vivo homing. Immunity *20*, 25–35.

Girkontaite, I., Missy, K., Sakk, V., Harenberg, A., Tedford, K., Potzel, T., Pfeffer, K., and Fischer, K.D. (2001). Lsc is required for marginal zone B cells, regulation of lymphocyte motility and immune responses. Nat. Immunol. *2*, 855–862.

Gratacap, M.P., Payrastre, B., Nieswandt, B., and Offermanns, S. (2001). Differential regulation of Rho and Rac through heterotrimeric G-proteins and cyclic nucleotides. J. Biol. Chem. *276*, 47906–47913.

Gu, J.L., Muller, S., Mancino, V., Offermanns, S., and Simon, M.I. (2002). Interaction of G alpha(12) with G alpha(13) and G alpha(q) signaling pathways. Proc. Natl. Acad. Sci. USA *99*, 9352–9357.

Hennet, T., Hagen, F.K., Tabak, L.A., and Marth, J.D. (1995). T-cell-specific deletion of a polypeptide N-acetylgalactosaminyl-transferase gene by site-directed recombination. Proc. Natl. Acad. Sci. USA *92*, 12070–12074.

Hogg, N., Henderson, R., Leitinger, B., McDowall, A., Porter, J., and Stanley, P. (2002). Mechanisms contributing to the activity of integrins on leukocytes. Immunol. Rev. *186*, 164–171.

Honing, H., van den Berg, T.K., van der Pol, S.M., Dijkstra, C.D., van der Kammen, R.A., Collard, J.G., and de Vries, H.E. (2004). RhoA activation promotes transendothelial migration of monocytes via ROCK. J. Leukoc. Biol. *75*, 523–528.

Iden, S., and Collard, J.G. (2008). Crosstalk between small GTPases and polarity proteins in cell polarization. Nat. Rev. Mol. Cell Biol. *9*, 846–859.

Kabashima, K., Murata, T., Tanaka, H., Matsuoka, T., Sakata, D., Yoshida, N., Katagiri, K., Kinashi, T., Tanaka, T., Miyasaka, M., et al. (2003). Thromboxane A2 modulates interaction of dendritic cells and T cells and regulates acquired immunity. Nat. Immunol. *4*, 694–701.

Katagiri, K., Hattori, M., Minato, N., Irie, S., Takatsu, K., and Kinashi, T. (2000). Rap1 is a potent activation signal for leukocyte function-associated antigen 1 distinct from protein kinase C and phosphatidylinositol-3-OH kinase. Mol. Cell. Biol. *20*, 1956–1969.

Kim, M., Carman, C.V., Yang, W., Salas, A., and Springer, T.A. (2004). The primacy of affinity over clustering in regulation of adhesiveness of the integrin {alpha}Ł{beta}2. J. Cell Biol. *167*, 1241–1253.

Kinashi, T. (2005). Intracellular signalling controlling integrin activation in lymphocytes. Nat. Rev. Immunol. *5*, 546–559.

Kurimoto, I., and Streilein, J.W. (1993). Studies of contact hypersensitivity induction in mice with optimal sensitizing doses of hapten. J. Invest. Dermatol. *101*, 132–136.

Laudanna, C., and Alon, R. (2006). Right on the spot. Chemokine triggering of integrin-mediated arrest of rolling leukocytes. Thromb. Haemost. *95*, 5–11.

Laudanna, C., Kim, J.Y., Constantin, G., and Butcher, E. (2002). Rapid leukocyte integrin activation by chemokines. Immunol. Rev. *186*, 37–46.

Li, X., Bu, X., Lu, B., Avraham, H., Flavell, R.A., and Lim, B. (2002). The hematopoiesis-specific GTP-binding protein RhoH is GTPase deficient and modulates activities of other Rho GTPases by an inhibitory function. Mol. Cell. Biol. *22*, 1158–1171.

Like, A.A., and Rossini, A.A. (1976). Streptozotocin-induced pancreatic insulitis: New model of diabetes mellitus. Science *193*, 415–417.

Matloubian, M., Lo, C.G., Cinamon, G., Lesneski, M.J., Xu, Y., Brinkmann, V., Allende, M.L., Proia, R.L., and Cyster, J.G. (2004). Lymphocyte egress from thymus and peripheral lymphoid organs is dependent on S1P receptor 1. Nature *427*, 355–360.

Matsuoka, T., and Narumiya, S. (2007). Prostaglandin receptor signaling in disease. ScientificWorldJournal *7*, 1329–1347.

Moers, A., Nieswandt, B., Massberg, S., Wettschureck, N., Gruner, S., Konrad, I., Schulte, V., Aktas, B., Gratacap, M.P., Simon, M.I., et al. (2003). G13 is an essential mediator of platelet activation in hemostasis and thrombosis. Nat. Med. *9*, 1418–1422.

Montesano, R., Pepper, M.S., Mohle-Steinlein, U., Risau, W., Wagner, E.F., and Orci, L. (1990). Increased proteolytic activity is responsible for the aberrant morphogenetic behavior of endothelial cells expressing the middle T oncogene. Cell *62*, 435–445.

Mor, A., Dustin, M.L., and Philips, M.R. (2007). Small GTPases and LFA-1 reciprocally modulate adhesion and signaling. Immunol. Rev. *218*, 114–125.

Offermanns, S., Mancino, V., Revel, J.P., and Simon, M.I. (1997). Vascular system defects and impaired cell chemokinesis as a result of Galpha13 deficiency. Science *275*, 533–536.

Rieken, S., Herroeder, S., Sassmann, A., Wallenwein, B., Moers, A., Offermanns, S., and Wettschureck, N. (2006a). Lysophospholipids control integrin-dependent adhesion in splenic B cells through G(i) and G(12)/G(13) family G-proteins but not through G(q)/G(11). J. Biol. Chem. *281*, 36985–36992.

Rieken, S., Sassmann, A., Herroeder, S., Wallenwein, B., Moers, A., Offermanns, S., and Wettschureck, N. (2006b). G12/G13 family G proteins regulate marginal zone B cell maturation, migration, and polarization. J. Immunol. *177*, 2985–2993.

Riobo, N.A., and Manning, D.R. (2005). Receptors coupled to heterotrimeric G proteins of the G12 family. Trends Pharmacol. Sci. *26*, 146–154.

Rodriguez-Fernandez, J.L., Sanchez-Martin, L., Rey, M., Vicente-Manzanares, M., Narumiya, S., Teixido, J., Sanchez-Madrid, F., and Cabanas, C. (2001). Rho and Rho-associated kinase modulate the tyrosine kinase PYK2 in T-cells through regulation of the activity of the integrin LFA-1. J. Biol. Chem. *276*, 40518–40527.

Rubtsov, A., Strauch, P., Digiacomo, A., Hu, J., Pelanda, R., and Torres, R.M. (2005). Lsc regulates marginal-zone B cell migration and adhesion and is required for the IgM T-dependent antibody response. Immunity *23*, 527–538.

Sanna, M.G., Wang, S.K., Gonzalez-Cabrera, P.J., Don, A., Marsolais, D., Matheu, M.P., Wei, S.H., Parker, I., Jo, E., Cheng, W.C., et al. (2006). Enhancement of capillary leakage and restoration of lymphocyte egress by a chiral S1P1 antagonist in vivo. Nat. Chem. Biol. *2*, 434–441.

Schmits, R., Kundig, T.M., Baker, D.M., Shumaker, G., Simard, J.J., Duncan, G., Wakeham, A., Shahinian, A., van der Heiden, A., Bachmann, M.F., et al. (1996). LFA-1-deficient mice show normal CTL responses to virus but fail to reject immunogenic tumor. J. Exp. Med. *183*, 1415–1426.

Sebzda, E., Bracke, M., Tugal, T., Hogg, N., and Cantrell, D.A. (2002). Rap1A positively regulates T cells via integrin activation rather than inhibiting lymphocyte signaling. Nat. Immunol. *3*, 251–258.

Semmrich, M., Smith, A., Feterowski, C., Beer, S., Engelhardt, B., Busch, D.H., Bartsch, B., Laschinger, M., Hogg, N., Pfeffer, K., and Holzmann, B. (2005). Importance of integrin LFA-1 deactivation for the generation of immune responses. J. Exp. Med. *201*, 1987–1998.

Shimaoka, M., Takagi, J., and Springer, T.A. (2002). Conformational regulation of integrin structure and function. Annu. Rev. Biophys. Biomol. Struct. *31*, 485–516.

Shimonaka, M., Katagiri, K., Nakayama, T., Fujita, N., Tsuruo, T., Yoshie, O., and Kinashi, T. (2003). Rap1 translates chemokine signals to integrin activation, cell polarization, and motility across vascular endothelium under flow. J. Cell Biol. *161*, 417–427.

Smith, A., Bracke, M., Leitinger, B., Porter, J.C., and Hogg, N. (2003). LFA-1-induced T cell migration on ICAM-1 involves regulation of MLCK-mediated attachment and ROCK-dependent detachment. J. Cell Sci. *116*, 3123–3133.

Smith, A., Stanley, P., Jones, K., Svensson, L., McDowall, A., and Hogg, N. (2007). The role of the integrin LFA-1 in T-lymphocyte migration. Immunol. Rev. *218*, 135–146.

van Kooyk, Y., van Vliet, S.J., and Figdor, C.G. (1999). The actin cytoskeleton regulates LFA-1 ligand binding through avidity rather than affinity changes. J. Biol. Chem. *274*, 26869–26877.

Xu, J., Wang, F., Van Keymeulen, A., Herzmark, P., Straight, A., Kelly, K., Takuwa, Y., Sugimoto, N., Mitchison, T., and Bourne, H.R. (2003). Divergent signals and cytoskeletal assemblies regulate self-organizing polarity in neutrophils. Cell *114*, 201–214.

Zhang, W., Shao, Y., Fang, D., Huang, J., Jeon, M.S., and Liu, Y.C. (2003). Negative regulation of T cell antigen receptor-mediated Crk-L-C3G signaling and cell adhesion by Cbl-b. J. Biol. Chem. *278*, 23978–23983.

Appendix 11

Horn J, Wang X, **Reichardt P**, Stradal TE, Warnecke N, Simeoni L, Gunzer M, Yablonski D, Schraven B, Kliche S. Src homology 2-domain containing leukocyte-specific phosphoprotein of 76 kDa is mandatory for TCR-mediated inside-out signaling, but dispensable for CXCR4-mediated LFA-1 activation, adhesion, and migration of T cells. **J Immunol.** 2009 Nov 1;183(9):5756-67. Epub 2009 Oct 7.

IF: 5.5

Src Homology 2-Domain Containing Leukocyte-Specific Phosphoprotein of 76 kDa Is Mandatory for TCR-Mediated Inside-Out Signaling, but Dispensable for CXCR4-Mediated LFA-1 Activation, Adhesion, and Migration of T Cells[1]

Jessica Horn,[2]* Xiaoqian Wang,[2]* Peter Reichardt,* Theresia E. Stradal,† Nicole Warnecke,* Luca Simeoni,* Matthias Gunzer,* Deborah Yablonski,‡ Burkhart Schraven,[3]* and Stefanie Kliche[3]*

Engagement of the TCR or of chemokine receptors such as CXCR4 induces adhesion and migration of T cells via so-called inside-out signaling pathways. The molecular processes underlying inside-out signaling events are as yet not completely understood. In this study, we show that TCR- and CXCR4-mediated activation of integrins critically depends on the membrane recruitment of the adhesion- and degranulation-promoting adapter protein (ADAP)/Src kinase-associated phosphoprotein of 55 kDa (SKAP55)/Rap1-interacting adapter protein (RIAM)/Rap1 module. We further demonstrate that the Src homology 2 domain containing leukocyte-specific phosphoprotein of 76 kDa (SLP76) is crucial for TCR-mediated inside-out signaling and T cell/APC interaction. Besides facilitating membrane recruitment of ADAP, SKAP55, and RIAM, SLP76 regulates TCR-mediated inside-out signaling by controlling the activation of Rap1 as well as Rac-mediated actin polymerization. Surprisingly, however, SLP76 is not mandatory for CXCR4-mediated inside-out signaling. Indeed, both CXCR4-induced T cell adhesion and migration are not affected by loss of SLP76. Moreover, after CXCR4 stimulation, the ADAP/SKAP55/RIAM/Rap1 module is recruited to the plasma membrane independently of SLP76. Collectively, our data indicate a differential requirement for SLP76 in TCR- vs CXCR4-mediated inside-out signaling pathways regulating T cell adhesion and migration. *The Journal of Immunology,* **2009, 183: 5756–5767.**

Stimulation of T cells through the TCR activates a whole plethora of signaling pathways that collectively control activation, proliferation, and differentiation of T cells. One immediate consequence of TCR engagement is the formation of a multicomponent signaling complex close to the plasma membrane consisting of the Src homology 2-domain containing leukocyte-specific phosphoprotein of 76 kDa (SLP76),[4] the small adapter protein Gads, and the transmembrane adapter protein linker for activation of T cells (LAT) (1). In response to TCR engagement, LAT becomes phosphorylated on several tyrosine residues by the protein tyrosine kinase ZAP70 (1). This phosphorylation leads to recruitment of Gads. Through its constitutive association with Gads, SLP76 is also recruited to phosphorylated LAT (2). In the following, several other effector molecules assemble with the LAT/Gads/SLP76-signaling platform. These include phospholipase Cγ1 (PLCγ1), the nucleotide exchange factor Vav1, and the Tec family kinase IL-2-inducible T cell kinase (Itk) (1). Together these molecules coordinate TCR-mediated rises in intracellular calcium, up-regulation of CD69, and the activation of the Ras/ERK1/2 signaling pathway (1, 3).

The importance of SLP76 for TCR-mediated signaling events has been demonstrated in SLP76-deficient mice as well as in the SLP76-deficient Jurkat T cell line J14. Thus, loss of SLP76 in mice leads to a complete block at the double-negative 3 stage of thymic development and results in an almost complete loss of mature T cells (1). Moreover, loss of SLP76 in Jurkat T cells induces a complete failure of the TCR to induce rises in intracellular calcium, activation of the Ras/Raf/MAPK/ERK1/2 pathway, and up-regulation of CD69 expression (3).

Besides inducing the above-mentioned signaling events, TCR stimulation also leads to T cell adhesion, a process that is critical for the interaction between T cells and APCs. In T cells, the β_2 integrin LFA-1 ($\alpha_L\beta_2$) mediates adhesive events with APCs through binding to its ligand ICAM-1. LFA-1/ICAM-1 interactions are critical for T cell activation because they stabilize the interaction of T cells with APCs and the formation of the immunological synapse (IS) (4, 5).

*Institute of Molecular and Clinical Immunology, Otto-von-Guericke University, Magdeburg, Germany; †Signaling and Motility Group, Helmholtz Center for Infection Research, Braunschweig, Germany; and ‡Rappaport Faculty of Medicine and Technion-Israel Institute of Technology, Haifa, Israel

Received for publication March 3, 2009. Accepted for publication August 20, 2009.

The costs of publication of this article were defrayed in part by the payment of page charges. This article must therefore be hereby marked *advertisement* in accordance with 18 U.S.C. Section 1734 solely to indicate this fact.

[1] This work was supported by Deutsche Forschungsgemeinschaft Grants GRK1167 and KL-1295/5-1 (to B.S. and S.K.) and by German-Israeli Foundation for Scientific Research and Development Grant (to D.Y. and B.S.).

[2] J.H. and X.W. are first authors.

[3] Address correspondence and reprint requests to Drs. Stefanie Kliche or Burkhart Schraven, Institute of Molecular and Clinical Immunology, Otto-von-Guericke University, Leipziger Strasse 44, D-39120 Magdeburg, Germany. E-mail address: stefanie.kliche@med.ovgu.de

[4] Abbreviations used in this paper: SLP76, Src homology 2-domain containing leukocyte-specific phosphoprotein of 76 kDa; ADAP, adhesion- and degranulation-promoting adapter protein; IS, immunological synapse; Itk, IL-2-inducible T cell kinase; LAT, linker for activation of T cells; PFA, paraformaldehyde; PLCγ1, phospholipase Cγ1; RIAM, Rap1-interacting adapter protein; RNAi, RNA interference; SA, superantigen; sh, small hairpin RNA; siRNA, small interfering RNA; SKAP55, Src kinase-associated phosphoprotein of 55 kDa; TRITC, tetramethylrhodamine isothiocyanate.

www.jimmunol.org/cgi/doi/10.4049/jimmunol.0900649

Resting T cells are not adhesive because LFA-1 is presented in a closed, inactive conformation. Upon triggering of the TCR or of chemokine receptors (see below), a conformational change is induced within LFA-1 that augments its affinity for ICAM-1. In addition, clustering of LFA-1 molecules on the surface of T cells enhances avidity for ICAM-1 binding. The molecular events leading to integrin activation have collectively been termed inside-out signaling (6).

Gain-of-function and loss-of-function studies have demonstrated that additional signaling proteins are involved in TCR-mediated integrin activation. These include talin (6, 7), the Wiskott-Aldrich syndrome-Verprolin-homologous protein WAVE2 (8, 9), Rap1 (6, 10, 11), and its downstream targets regulator of adhesion and cell polarization enriched in lymphoid tissues or Rap1-interacting adapter protein (RIAM) (12–14), adhesion- and degranulation-promoting adapter protein (ADAP) (15, 16), and Src kinase-associated phosphoprotein of 55 kDa (SKAP55) (17, 18). Moreover, components of the LAT/Gads/SLP76 signaling platform are also critically involved in TCR-mediated activation of LFA-1. These include PLCγ1, Vav1, Itk, and ADAP (13, 19, 20). How exactly these molecules orchestrate TCR-mediated activation of integrins is not completely understood. However, we have recently shown that the formation of a signaling module consisting of ADAP/SKAP55 complex together with RIAM is required for plasma membrane targeting of Rap1 in response to TCR stimulation, and therefore for TCR-mediated activation of integrins (17, 21). In line with these data is the observation that ADAP- and SKAP55-deficient mouse T cells show a severe defect in integrin activation in response to TCR-mediated stimuli (15, 16, 18).

Currently, it is proposed that following T cell activation, tyrosine-phosphorylated ADAP binds to the Src homology 2 domain of SLP76, thereby leading to membrane recruitment of the ADAP/SKAP55/RIAM module and integrin activation. In line with this idea is the observation that disruption of the interaction between SLP76 and Gads blocks TCR-mediated adhesion to ICAM-1 (22). Furthermore, it was shown that mutation of those tyrosine residues within ADAP, which are believed to mediate the interaction between ADAP and SLP76, blocks TCR-mediated activation of LFA-1 (23). Thus, it appears as if SLP76 would also play a major role during TCR-mediated activation of integrins by facilitation membrane targeting of the ADAP/SKAP55/RIAM module. However, to date, an inducible interaction between endogenously expressed ADAP/SKAP55/RIAM module and SLP76 in response to TCR engagement has not been demonstrated biochemically. Hence, the molecular signaling events underlying the function of SLP76 for TCR-mediated integrin activation are not completely elucidated.

Importantly, integrins not only become activated after stimulation of the TCR, but also after triggering of chemokine receptors, such as CXCR4. Signaling via CXCR4 is induced by stromal cell-derived factor-1α (or CXCL12) and induces affinity and avidity regulation of LFA-1 (6). This process is important for firm T cell adhesion, T cell polarization, chemokinesis, and chemotaxis (24). Molecules involved in CXCR4-mediated integrin activation and/or chemotaxis are talin (25), Rap1 (6, 26, 27), and its downstream targets regulator of adhesion and cell polarization enriched in lymphoid tissues and *Mst*I (28–30), Itk (20), Vav1 (20, 31, 32), Rac (31), and members of the Wiskott-Aldrich syndrome protein family (33, 34). Moreover, we and others have shown that overexpression of ADAP enhances chemotaxis of T cells in response to CXCL12 (35, 36). These findings suggest an important role of ADAP for CXCR4-induced migration of T cells. However, the molecular basis of how ADAP is integrated into CXCR4 signaling is to date unclear. Based on its central role in TCR-mediated signaling processes, SLP76 would be an attractive candidate that could facilitate membrane targeting of ADAP after CXCR4 stimulation. Indeed, it was shown recently that SLP76 regulates CXCR4-induced Ca^{2+} flux and ERK1/2 phosphorylation (31). Conversely, we had demonstrated that disruption of the SLP76/Gads association, albeit impairing TCR-mediated signaling processes, does not affect CXCR4-induced Ca^{2+} flux and chemotaxis (22). Thus, it is unclear whether SLP76 is also important for CXCR4-mediated activation of integrins and chemotaxis.

In this study, we have addressed critical questions regarding the function of SLP76 during TCR vs CXCR4-mediated signaling. We show that SLP76 is indeed a critical regulator of TCR-mediated inside-out signaling events in T cells, and we demonstrate that SLP76 is mandatory for induction of TCR-mediated adhesion, affinity/avidity regulation of LFA-1, and the interaction between T cells and B cells. Furthermore, we show that SLP76 is required for TCR-induced Rap1 activation, Rac-mediated actin dynamics, and recruitment of both talin and the ADAP/SKAP55/RIAM/Rap1 module to the plasma membrane and to the IS. Surprisingly, however, SLP76 is not mandatory for CXCR4-mediated activation of LFA-1. In addition, SLP76 is dispensable for adhesion and migration of T cells in response to CXCL12. Finally, we demonstrate that the ADAP/SKAP55/RIAM/Rap1 module is crucial for T cell adhesion and migration in response to CXCR4 triggering, but is recruited to the plasma membrane independently of SLP76. Our findings show that SLP76 acts as a key player during TCR-mediated inside-out signaling, whereas the adapter protein appears to be dispensable for chemokine-dependent processes that regulate adhesion and migration of T cells.

Materials and Methods

Reagents and Abs

All tissue culture reagents were from Biochrom, and all chemicals were from Roth, unless mentioned otherwise. Staphylococcal enterotoxin B, D, and E were purchased from Toxin Technology, respectively. Indo-1 AM, Blue-7-amino-4-chloromethylcoumarin, DDAO-SE, and Alexa Fluor 633-phalloidin were bought from Molecular Probes. FITC or tetramethylrhodamine isothiocyanate (TRITC) phalloidin was from Sigma-Aldrich. PMA was purchased from Calbiochem. Glutathione-Sepharose beads were bought from Pharmacia. Protein A- and protein G-agarose beads were from Santa Cruz Biotechnology. The chemokine CXCL12 was bought from Tebu-bio, and the human Fc-tagged ICAM-1 was from R&D Systems. The anti-RIAM rat mAbs were raised against the bacterially expressed GST-tagged fragment of RIAM (1–420 aa), as previously described (37). Supernatants of secreting hybridomas were screened by Western blotting, immunofluorescence, and intracellular flow cytometry (FACS), and among the various clones tested, the mAb RIAM15B7E8 was selected. The mouse anti-CD3 mAb C305 (IgM) (38), OKT3 (ATCC), biotinylated UCHT-1 (NatuTec), or MEM92 (provided by V. Horejsi, Academy of Sciences of the Czech Republic, Czech Republic) was used for TCR stimulation of Jurkat T cells or human T cells. For protein surface expression analysis by FACS, the following mAbs were used: CD18 (MEM48), CD29 (MEM101A; both provided by V. Horejsi), CD184 (CXCR4; clone 12G5; BD Biosciences), MHC class I (clone W6/32; ATCC), KIM127 (provided by N. Hogg, Cancer Research U.K. London Research Institute, London, U.K.), APC-conjugated anti-CD69 (BD Bioscience), or FITC-conjugated MEM48 (Immunotools). The anti-SLP76 and anti-preimmune sheep serum (39), anti-SKAP55 rabbit serum (40), or anti-Gads rabbit serum (Upstate Biotechnology) was used for immunoprecipitation studies. The following Abs were used for immunoblot analysis and/or immunofluorescence in this study: anti-SKAP55 rat mAb (SK13B6) (17), anti-GST rat mAb (provided by C. Erk, Helmholtz-Zentrum für Infektionsforschung, Braunschweig, Germany), anti-β-actin mAb (Sigma-Aldrich), anti-phospho-ERK1/2 (T^{202}, Y^{204}) rabbit serum and anti-Vav rabbit serum (both from Cell Signaling Technology), anti-SLP76 mAb (Santa Cruz Biotechnology), anti-LAT mAb (BD Biosciences), anti-ADAP sheep serum (41), anti-phospho-SLP76 mAb (pY145; BD Biosiences), anti-phospho-LAT (pY171) rabbit serum and anti-phospho-ZAP70 (pY319) rabbit serum (both from Cell

Signaling Technology), anti-Rap1 rabbit serum (Santa Cruz Biotechnology), anti-Rap1 mAb and anti-Rac mAb (both from BD Biosciences), and anti-talin mAb (clone 8D4; Sigma-Aldrich). The following Abs were used for phospho-epitope staining by FACS: anti-phospho-ZAP70 (pY319)-Alexa Fluor 647, anti-phospho-PLCγ1 (pY783)-Alexa Fluor 647 (both from BD Biosciences), and anti-phospho-ERK1/2 (pT202, pY204; clone E10; Cell Signaling Technology). Streptavidin, HRP-labeled secondary Abs, and FITC-, Cy3-, APC-, and Cy5-conjugated secondary Abs were purchased from Dianova.

RNA interference (RNAi) of SLP76, ADAP, SKAP55, or RIAM and cDNA constructs

For small hairpin RNA (shRNA) of SLP76, the following oligonucleotides, shC (CCAAGTAATGTAGGATCAA; *Renilla*) and shSLP76 (CGAAGA GAGGAGGAGCATC; shSLP76), were cloned into pSuper (provided by T. Seufferlein (Universitätsklinik und Poliklinik für Innere Medizin I, Halle, Germany) and pCMS3-EGFP vector (provided by D. Billadeau (Mayo Clinic, Rochester, MN). For shRNA of ADAP and RIAM, the previously published oligonucleotides were cloned into the pCMS3 vector (12, 42). The pCMS3-EGFF construct for silencing of SKAP55 has been described (17). The pGEX PAK-PBD was provided by T. Seufferlein. The pGEX RalGDS-RBD was provided by J. Bos (University Medical Center, Utrecht, The Netherlands), and the pmCherry-C1 vector was purchased from BD Clontech.

Cell culture and transfection

Jurkat T cells (ATCC), B cells (Raji; ATCC), and SLP76-deficient/reconstituted Jurkat T cells (J14, J14-76-11, and J14-76-18) (3) were maintained in RPMI 1640 medium supplemented with 10% FBS (PAN) and stable L-glutamine at 37°C with 5% CO_2. Jurkat T cells (2×10^7) were transfected by electroporation, as previously described (17). Transfection with the pCMS3-EGFP vector into Jurkat T cells consistently yielded in an average of >80% GFP-expressing cell population. Primary human T cells were prepared from healthy donors by standard separation methods using AutoMACS (Miltenyi Biotec) maintained in RPMI 1640 medium containing 10% FBS, stable L-glutamine, and 1000 U/ml penicillin/streptomycin. Approval for these studies was obtained from the Ethics Committee of the Medical Faculty at the Otto-von-Guericke University. Informed consent was obtained in accordance with the Declaration of Helsinki. For electroporation of small interfering RNA (siRNA), human peripheral T cells (8×10^6) were washed in PBS containing Ca^{2+}/Mg^{2+} and resuspended in 200 μl of Opti-MEM (Invitrogen). siRNA smart pool against SLP76, ADAP (Dharmacon smart pools for SLP76 or ADAP), control siRNA (si*CONTROL* nontargeting smart pool from Dharmacon), Vav1.3 (31), siRNA for SLP76, or control siRNA *Renilla* (see above; all purchased from Invitrogen) was added, and after 3 min cells were transfected by electroporation (square-wave pulse, 1000 V, 0.5 ms, 2 pulses (pulse interval 5 s); Bio-Rad X-cell). The cells were then added to prewarmed cell culture medium, as described above, and cultured for 72 h before use. The knockdown efficiency of SLP76, ADAP, SKAP55, RIAM, or Vav1 was evaluated either by Western blotting or on a single-cell basis by intracellular flow cytometry.

Immunoprecipitation, Western blot analysis, isolation of cytosolic and plasma membrane fractions, and GTPase assays

Cell lysis and immunoprecipitation were performed, as previously described (17, 21). Equivalent amounts of protein (determined by Bradford assay (Roth)) were used in precipitation studies (500 μg of total protein from either Jurkat T cells or human primary T cells). Cell lysates (50 μg of total protein) or immune complexes were separated by SDS-PAGE and transferred to nitrocellulose. Western blots were conducted with the indicated Abs and developed with the appropriate HRP-conjugated secondary Abs and the Luminol detection system (Roth). Isolation of cytosolic and plasma membrane fractions has been described previously (17). GTPase activity of Rap1 or Rac activity was assessed, as previously described (17). Briefly, Jurkat T cells were either left untreated or stimulated for various time points with anti-CD3 mAb C305 or CXCL12 (100 ng/ml) and lysed. An aliquot of the lysate (10%) was used as loading control. Activated GTPases were precipitated using either glutathione-Sepharose conjugated with the GST-RalGDS fusion protein for Rap1 (RBD) or glutathione-Sepharose coupled with the GST fusion protein of the p21-binding domain of Pak (PBD) for Rac. Bound GTPases were quantified by Western blotting.

Flow cytometry, calcium release, and CD69 up-regulation

To analyze the cell surface expression of β_1 or β_2 integrin, CXCR4, TCR, and MHCI, cells were stained with the indicated Abs in combination with APC-conjugated goat anti-mouse IgG and analyzed using a FACSCalibur flow cytometer and CellQuestPro software (BD Biosciences). Soluble Fc-ICAM-1 binding of T cells after various stimuli was assessed, as previously described (43). Briefly, T cells suspended in binding puffer (HBSS containing 2% FBS) were either left untreated or stimulated with anti-CD3 mAb, CXCL12, or Mg^{2+}/EDTA for 5 min in the presence of 20 μg/ml human rFc-ICAM-1, and bound Fc-ICAM-1 was detected by flow cytometry. Intracellular staining by flow cytometry for SLP76, ADAP, SKAP55, or RIAM was performed, as previously described (44). The specificity of the staining for each serum or mAb was assessed using either SLP76-deficient/reconstituted Jurkat T cells or after loss of ADAP, SKAP55, or RIAM expression by vector-based shRNA in Jurkat T cells (please see supplemental Fig. 1).[5] To assess the F-actin content, T cells (1×10^5) were left untreated or stimulated with anti-CD3 mAbs or CXCL12, and reactions were stopped by adding PBS containing 4% paraformaldehyde (PFA), 2 μg/ml FITC- or Alexa Fluor 633-phalloidin, and 0.2% Triton X-100. After 15 min, cells were washed with 1% PFA in PBS and analyzed by flow cytometry. Measurement of TCR-induced calcium release and CD69 up-regulation have been previously described (17). Analysis of protein phosphorylation with phospho-specific Abs by flow cytometry was performed, as described (45).

Conjugate formation, adhesion, migration, and motility assays

Conjugate assays were performed, as described (21). Briefly, superantigen (SA) mixture of staphylococcal enterotoxin B-, D-, and E-pulsed and DDAO-SE-labeled Raji B cells were incubated with an equal number of Jurkat T cells or CFSE-loaded human T cells for 30 min at 37°C. Nonspecific aggregates were disrupted; cells were fixed with 1% PFA, and then analyzed by flow cytometry. The percentage of conjugates was defined as the number of double-positive events in the upper right quadrant. Adhesion assays were performed, as previously described (17). Briefly, Jurkat T cells or peripheral human T cells were stimulated with OKT3, PMA, or $MnCl_2$ for 30 min at 37°C before adhesion on Fc-ICAM-1-coated dishes. The bound total or GFP-expressing cell fraction was determined by counting four independent fields by microscopy using an ocular counting reticule. To assess CXCR4-mediated adhesion, peripheral human T cells were incubated for 10 min at 37°C on Fc-ICAM-1-coated dishes coimmobilized with or without CXCL12; subsequently, nonbound cells were removed by washing with HBSS and bound cells were counted, as described above. Chemotaxis assays were performed, as previously described, using Transwells (Costar) coated with fibronectin (35). After 2 h, the number of migrated cells into the lower chamber was counted and the percentage of GFP-expressing Jurkat T cells was determined by flow cytometry. For live cell imaging of either random or CXCL12-induced motility of T cells on Fc-ICAM-1, self-constructed imaging chambers (46) were coated with Fc-ICAM-1 in PBS at 4°C overnight. Immediately before imaging, cells were left untreated or stimulated with CXCL12 (100 ng/ml), and imaging was performed on a CellR imaging workstation (Olympus) using an upright microscope stage (BX61) with a ×20 lens. Using an automated X-Y-Z stage, at least two optical fields were chosen for each culture condition. Images were taken every 15–60 s for 2 h. At least 30 cells per observation field were analyzed. Tracking analysis of migrating cells to determine the velocity was done by computer-assisted cell tracking using the Software CellTracker (46).

Immunofluorescence microscopy

For B cell/T cell conjugates, SA- and Blue-7-amino-4-chloromethylcoumarin-loaded Raji B cells were incubated for 30 min at 37°C with human T cells on poly(L-lysine)-coated coverslips and fixed with 3.5% PFA in PBS for 10 min. Cells were permeabilized with 0.1% Triton X-100 in PBS, blocked with 5% horse serum in PBS, and incubated with the indicated Abs or phalloidin. Coverslips were mounted in Mowiol 488 and imaged with a LEICA TCS SP2 laser-scanning confocal system (Leica Microsystems) using a plan apochromatic oil emerging ×63 objective (NA 1.4). Figure constructions of images were performed in COREL Photopaint. For quantification of recruitment of proteins and F-actin at the contact zone or at the uropod, line scans (1 μm) were obtained. Fluorescence intensity was plotted as function of distance along this line, and the integrated areas under the curves representing the fluorescence intensity were calculated as ratio between the immunological synapse vs the uropod. Thirty conjugates were analyzed per experiment. To assess TCR-induced clustering of LFA-1, Jurkat T cells were incubated with biotinylated anti-UCHT-1 in the presence of streptavidin at 4°C. After washing, the cells were stimulated at 37°C for 30 min on poly(L-lysine)-coated slides, fixed with 3.5% PFA in PBS, and then blocked with 5% horse serum in PBS. The cells were stained

[5] The online version of this article contains supplemental material.

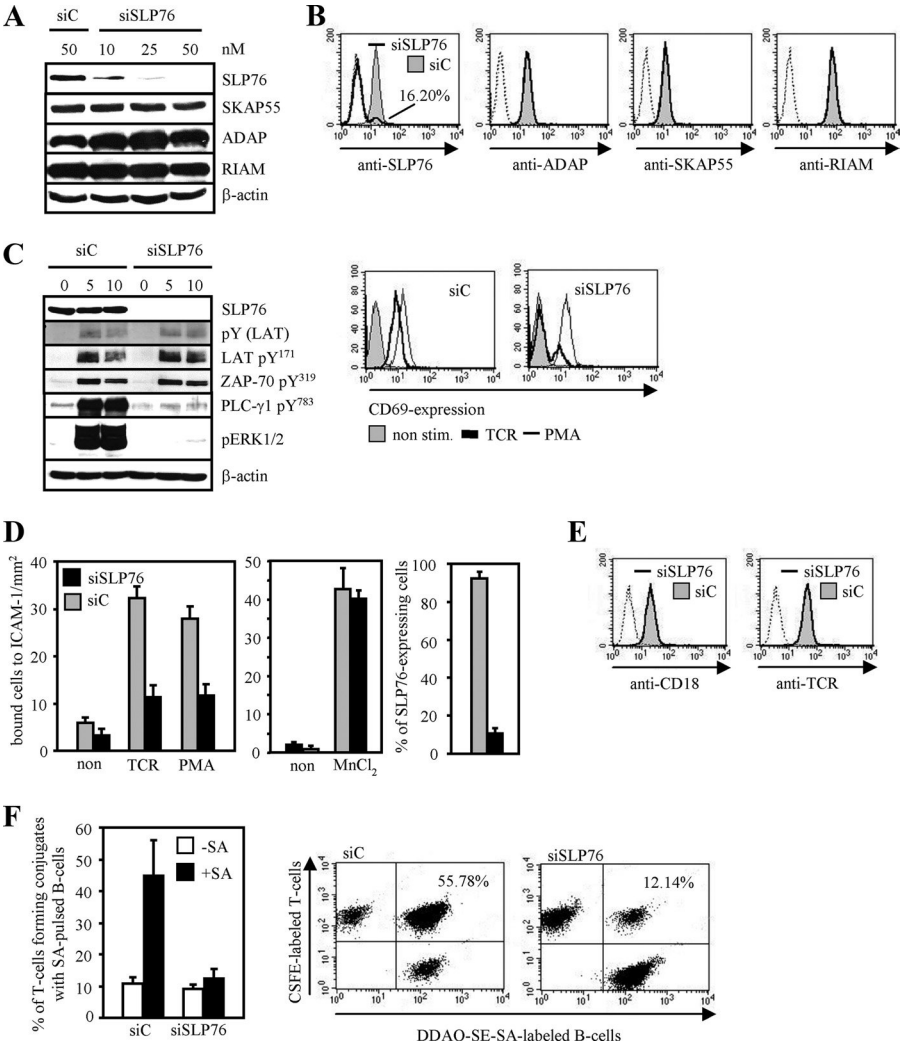

FIGURE 1. SLP76 is crucial for TCR-induced adhesion to ICAM-1 and conjugate formation. *A*, Purified human T cells were transfected with control siRNA (siC) or the indicated concentrations of siRNAs against SLP76 (siSLP76). After 72 h, whole-cell extracts were analyzed by Western blotting with the indicated Abs. *B*, In parallel, cells transfected with 50 nM siC or siSLP76 were analyzed by flow cytometry for the intracellular expression of SLP76, ADAP, SKAP55, and RIAM (black line). The preimmune sheep serum and the anti-GST mAb were used as isotype controls (dashed line). *C*, Human T cells transfected as described in *A* were left untreated or stimulated with anti-CD3 mAbs (TCR) for the indicated period of time. Lysates were analyzed by Western blotting using the indicated Abs. Moreover, the same transfectants were cultured on plate-bound anti-CD3 mAbs (TCR) or in the presence of PMA for 18 h, stained with anti-CD69 mAbs, and analyzed by flow cytometry. Data are representative of three individual experiments. Note that the total expression of LAT, ZAP70, PLCγ1, or ERK1/2 was not affected (data not shown). *D*, Human T cells transfected as described above were left untreated or stimulated with anti-CD3 mAb (TCR), PMA, or $MnCl_2$ for 30 min, and subsequently analyzed for their ability to adhere to Fc-ICAM-1. Suppression of SLP76 expression for each experiment was assessed by flow cytometry, and the percentage of SLP76-expressing cells was calculated. Data represent the mean and SE of three independently performed experiments. *E*, In parallel, transfectants were analyzed for the surface expression of CD18 or the TCR (black line), and control IgG were used as isotype controls (dashed line). One representative experiment of three is shown. *F*, Equal numbers of the same cells as described in *A* were stained with CFSE and incubated for 30 min without SA (−SA) or with SA-pulsed (+SA) DDAO-SE-labeled B cells. The percentage of conjugate formation was assessed by flow cytometry. Data represent the mean and SE of three independently performed experiments. Representative histograms of SA-pulsed DDAO-SE B cells conjugated with CFSE-stained T cells in the presence or absence of SLP76 are shown.

with FITC-conjugated anti-MEM48 and imaged, as described above. For each experiment, a minimum of at least 40 cells with LFA-1 polarized to one side of the cell was regarded as polarized, whereas those cells showing equal distribution of LFA-1 were considered not to be polarized. The percentage of polarized cells in each field was determined.

Results

Loss of SLP-76 impairs TCR-mediated activation of LFA-1 and T cell-APC conjugation

By using a small peptide that disrupts the constitutive interaction between SLP76 and Gads, we recently provided evidence that formation of the LAT/Gads/SLP76 signaling platform at the plasma membrane is required for TCR-mediated integrin activation (22). However, we formally could not exclude the possibility that the functional effects exerted by the Gads-binding fragment were not due to targeting the SLP76/Gads complex, but rather to disruption of a distinct signaling pathway that regulates intergrin activation in response to TCR stimulation. To assess this point more specifically, we reduced the expression of SLP76 in primary human T cells by RNAi. As shown in Fig. 1, *A* and *B*, SLP76 siRNA treatment lowered the expression levels of endogenous SLP76 up to 80%, whereas the expression levels of ADAP, SKAP55, and RIAM remained unaffected.

Previously, it had been reported that SLP76 is required for phosphorylation of PLCγ1, activation of ERK1/2, as well as for expression of CD69 upon TCR stimulation. To first address whether loss of SLP76 interferes with these SLP76-mediated functions also in primary human T cells, we analyzed the ability of SLP76-deficient human T cells to activate PLCγ1 and ERK1/2 in response to TCR stimulation by Western blotting and to up-regulate CD69 expression by flow cytometry. As shown in Fig. 1*C*, loss of SLP76 strongly attenuated TCR-mediated phosphorylation of PLCγ1 at Y^{783}, activation of ERK1/2, and up-regulation of CD69. As expected, more proximal signaling events such as the phosphorylation of ZAP70 at Y^{319} or tyrosine phosphorylation of LAT (either global or at Y^{171}) were not affected in the absence of SLP76 (Fig. 1*C*). Note that similar data were obtained, when we suppressed the expression of SLP76 by shRNA in Jurkat T cells (supplemental Fig. 2). Thus, with regard to well-established SLP76-regulated signaling processes, SLP76-deficient primary human T cells behave like their corresponding Jurkat T cell counterparts (3).

Using the siRNA approach, we next analyzed the capability of T cells to adhere to ICAM-1-coated dishes in response to various stimuli. As shown in Fig. 1*D* and supplemental Fig. 3*A*, control transfected human T cells and Jurkat T cells readily adhered to ICAM-1 upon TCR or PMA treatment. In contrast, loss of SLP76 substantially attenuated both PMA- and TCR-induced adhesion to ICAM-1 (*left panel*), whereas the cells showed no defect in their adhesiveness in response to Mn^{2+} (*middle panel*). The defect in TCR- or PMA-induced adhesion to ICAM-1 was not due to an altered expression of the β_2 integrin (or the TCR) as determined by flow cytometry (Fig. 1*E* and supplemental Fig. 3*B*).

Because the interaction of LFA-1 with ICAM-1 is important for the establishment and maintenance of T cell/APC interactions (5), we next analyzed whether SLP76 is required for conjugate formation between human T cells and SA-loaded B cells. Fig. 1*F* shows that in contrast to control transfected T cells, loss of SLP76 substantially blunted conjugate formation. Similarly, $SLP76^{low}$ Jurkat T cells failed to interact with SA-loaded B cells (supplemental Fig. 3*C*). Collectively, the experiments shown in Fig. 1 indicate that SLP76 is mandatory for both TCR-mediated adhesion to ICAM-1 and conjugate formation.

Loss of SLP76 attenuates TCR-mediated affinity/avidity regulation of LFA-1

TCR-mediated inside-out signaling alters both LFA-1 affinity (conformation) and avidity (clustering) (6). To determine the role of SLP76 for LFA-1 affinity modulation, we assessed the ability of soluble Fc-ICAM-1 to bind to SLP76-proficient and SLP76-deficient T cells after TCR stimulation by means of flow cytometry. Fig. 2*A* shows that knockdown of SLP76 in human T cells abrogates binding of soluble Fc-ICAM-1 after TCR stimulation (for Jurkat T cells, please see supplemental Fig. 3*D*). In contrast, both transfectants were able to bind similar amounts of Fc-ICAM-1 after treatment with Mg^{2+}/EDTA, which directly induces the high-affinity conformation of LFA-1.

Next, we investigated avidity regulation of LFA-1 by analyzing clustering of CD18 (the β2 chain of LFA-1) to the IS in response to TCR stimulation. Fig. 2*B* shows that localization of CD18 to the IS occurred readily in SLP76-expressing T cells after incubation with SA-pulsed B cells, whereas it was severely impaired in $SLP76^{low}$ T cells. In line with these data, $SLP76^{low}$ Jurkat T cells also displayed no typical clustering of CD18 upon cross-linking of the TCR (supplemental Fig. 3*E*). Taken together, SLP76 is required for both affinity and avidity regulation of LFA-1 after stimulation of the TCR.

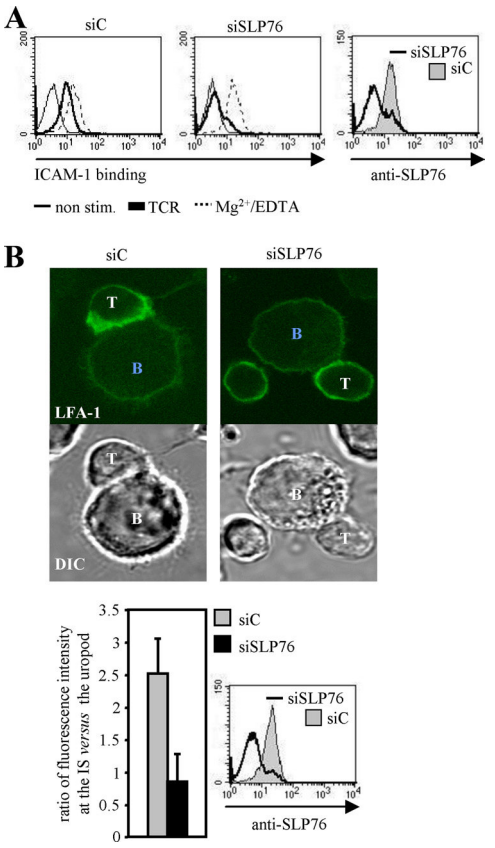

FIGURE 2. TCR-induced affinity/avidity regulation of LFA-1 depends on SLP76. *A*, Human T cells were transfected with either 50 nM control siRNA (siC) or siRNAs against SLP76 (siSLP76). After 72 h, cells were analyzed for their ability to bind soluble Fc-ICAM-1 in response to anti-CD3 mAb (TCR) or Mg^{2+}/EDTA stimulation for 5 min. Suppression of SLP76 expression was evaluated by flow cytometry. One representative experiment of three is shown. *B*, Human T cells transfected as described in *A* were allowed to form conjugates with SA-pulsed B cells for 30 min. Fixed cells were stained for the β2 subunit of LFA-1 (green) to determine IS localization of LFA-1. Fluorescence intensity of LFA-1 at the contact zone or the uropod was quantified and calculated as ratio of intensity at the IS vs the uropod. Knockdown efficiency of SLP76 expression was assessed by flow cytometry. Data present the average of three independently performed experiments.

TCR-mediated activation of Rac and actin dynamics require SLP76

Reorganization of the actin cytoskeleton is required for TCR-mediated integrin activation and conjugate formation (33, 34), and the small GTPase Rac is a major regulator regulating this process. In T cells, activation of Rac is mediated via the nucleotide exchange factor Vav1, which is recruited to and activated by SLP76 upon T cell activation (32). Therefore, it seemed likely that loss of SLP76 also leads to alterations in actin dynamics upon TCR stimulation. As depicted in Fig. 3, this is indeed the case. TCR-mediated activation of Rac (Fig. 3*A*), formation of F-actin (Fig. 3*B*), as well as accumulation of F-actin at the IS (Fig. 3*C*, *upper right panel*) are severely impaired in SLP76-deficient T cells. Note that similar data were obtained when the F-actin content after TCR triggering was assessed in $SLP76^{low}$ Jurkat T cells (data not shown). Hence, loss of SLP76 induces a failure to activate Rac and a defect in F-actin remodeling upon TCR stimulation.

Because the scaffolding protein talin links newly synthesized F-actin branches to LFA-1 and, hence, stabilizes the position of LFA-1 in the IS (7, 47), we also investigated whether SLP76 is required for targeting of talin to the IS after TCR stimulation.

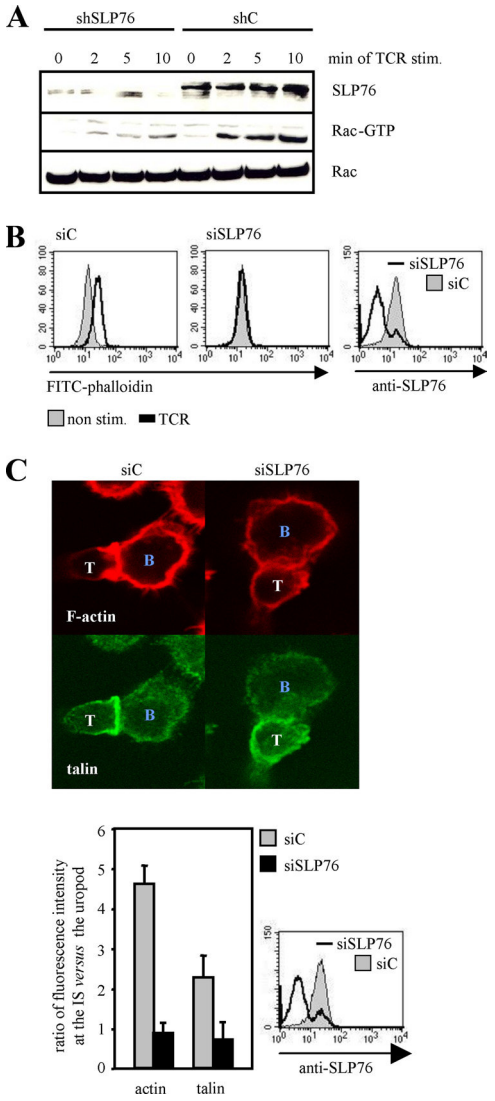

FIGURE 3. TCR-mediated actin remodeling, Rac activation, and recruitment of talin to the IS require the presence of SLP76. *A*, Jurkat T cells were transfected with either control vector (shC) or SLP76-suppression vector (shSLP76). After 48 h, cells were either left untreated or stimulated with anti-CD3 mAbs (TCR) for the indicated periods of time. GTP-loaded Rac was precipitated using the GST-PBD fusion protein. Precipitates and aliquots of whole-cell extracts were analyzed using the indicated Abs by means of Western blotting. One representative experiment of two is shown. *B*, Purified human T cells were transfected with either control siRNA (siC) or siRNA against SLP76 (siSLP76). After 72 h, cells were left untreated or stimulated with anti-CD3 mAbs (TCR) for 5 min and stained with FITC-coupled phalloidin. Reduction of SLP76 expression in human T cells was assessed by flow cytometry. Data are representative of three individual experiments. *C*, Human T cells transfected as described above were allowed to form conjugates with SA-loaded B cells for 30 min. Cells were fixed, permeabilized, and stained with TRITC-phalloidin (red) or talin (green). Fluorescence intensity of F-actin and talin at IS or uropod was quantified and calculated as ratio of intensity for the individual molecules at the IS vs the uropod. The knockdown efficiency of SLP76 was evaluated by flow cytometry. Data present the average results of three independent experiments.

Fig. 3*C* (*lower right panel*) shows that SLP76^{low} T cells also fail to target talin to the IS upon incubation with SA-pulsed B cells. Thus, SLP76 appears to also regulate LFA-1-dependent adhesion processes in activated T cells through its ability to recruit talin to the IS.

Activation of Rap1 and localization of the SKAP55/RIAM module to the IS depend on SLP76

Both the activation and the transport of Rap1 to the plasma membrane are known to regulate LFA-1 activation (6, 17, 48). Therefore, we next investigated whether loss of SLP76 affects TCR-mediated activation of Rap1. Fig. 4*A* demonstrates that control transfected cells exhibited strong activation of Rap1 within 2–10 min after TCR stimulation, whereas in SLP76^{low} Jurkat T cells, TCR-induced Rap1 was strongly suppressed. These results demonstrate that SLP76 is critically involved in Rap1 activation in response to TCR triggering.

We have recently shown that formation and membrane recruitment of a signaling module consisting of the cytosolic adapter proteins ADAP and SKAP55 and the Rap1 effector molecule RIAM (ADAP/SKAP55/RIAM module) regulate TCR-mediated LFA-1 activation through recruitment of Rap1 to the plasma membrane (17, 21). Moreover, an inducible association between SLP76 and ADAP following TCR stimulation had been suggested in several previous studies, but the question of whether SLP76 links the TCR via the ADAP/SKAP55/RIAM module to integrin activation has to date not been addressed directly. To clarify this point, we immunoprecipitated SLP76 from resting or TCR-stimulated T cells and subsequently analyzed the precipitates for coprecipitation of ADAP, SKAP55, RIAM, and Rap1 by means of Western blotting. Fig. 4*B* depicts that SLP76 inducibly associates with both the ADAP/SKAP55/RIAM complex and Rap1 upon TCR stimulation of Jurkat T cells (Fig. 4*B*, *left panel*) as well as of primary T cells (Fig. 4*B*, *right panel*). Analysis of SKAP55 immunoprecipitates that were prepared from either SLP76-proficient or SLP76-deficient T cells further revealed that Rap1 only associates with the ADAP/SKPAP55//RIAM module if SLP76 is present (Fig. 4*C*). Because only active Rap1 can interact with RIAM (12), this finding is most likely due to the attenuated activation of Rap1 in the absence of SLP76 (see Fig. 4*A*).

The immunoprecipitation data shown in Fig. 4, *B* and *C*, were further substantiated by cellular subfractionation experiments that showed that TCR-mediated plasma membrane recruitment of ADAP, SKAP55, RIAM, and Rap1 (Fig. 4*D*) and, consequently, targeting of SKAP55, RIAM, and Rap1 to the IS (Fig. 4*E*) were strongly impaired in SLP76^{low} T cells. In summary, the data shown in Fig. 4 indicate that SLP76 is required for both activation and plasma membrane/IS targeting through the ADAP/SKAP55/RIAM/Rap1 module of Rap1 after TCR triggering.

SLP76 is dispensable for CXCR4-mediated adhesion to ICAM-1 and affinity regulation of LFA-1

Similar to the TCR, triggering of the chemokine receptor CXCR4 leads to activation of LFA-1 and T cell adhesion to ICAM-1 (6). Above we have shown that SLP76 is mandatory for TCR-mediated integrin activation (Figs. 1 and 2). Therefore, we were interested to investigate whether SLP76 is also required for CXCR4-mediated adhesion. To assess this point, we down-regulated SLP76 expression by siRNA and subsequently analyzed the capability of SLP76^{low} T cells to adhere to ICAM-1 in response to CXCL12 in an adhesion assay. Surprisingly, these experiments revealed that SLP76^{low} T cells were as capable to adhere to Fc-ICAM-1 in response to CXCL12 as their SLP76^{high} counterparts (Fig. 5*A*). Similarly, neither the binding of soluble Fc-ICAM-1 (Fig. 5*B*) nor of the conformation-sensitive anti-LFA-1 mAb KIM127 (data not shown) was altered in SLP76^{low} T cells. Hence, we conclude that, in contrast to TCR stimulation, the presence of SLP76 is dispensable for T cell adhesion and affinity regulation in response to CXCL12 stimulation.

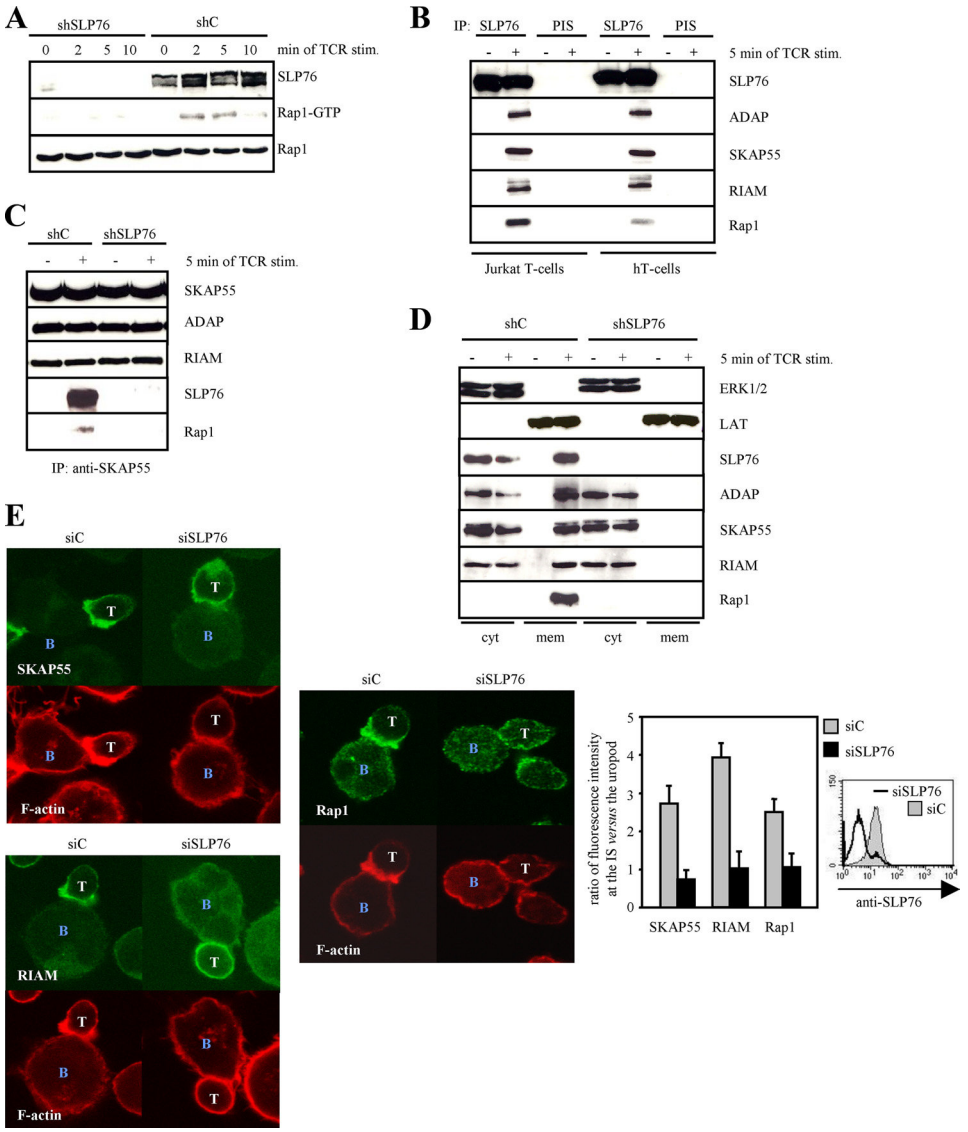

FIGURE 4. The inducible interaction between ADAP and SLP-76 is mandatory for the recruitment of SKAP55, RIAM, and Rap1 to the plasma membrane. *A*, Jurkat T cells were transfected with either control vector (shC) or SLP76-suppression vector (shSLP76). After 48 h, cells were either left untreated or stimulated with anti-CD3 mAbs (TCR) for the indicated periods of time. GTP-loaded Rap1 was precipitated using the GST-RalGDS-RBD fusion protein. Precipitates and aliquots of whole-cell extracts were analyzed with the indicated Abs by Western blotting. One representative experiment of three is shown. *B*, Jurkat T cells or human T cells (hT-cells) were left untreated or stimulated with anti-CD3 mAbs (+). Immunoprecipitations were performed using anti-SLP76 or preimmune sheep serum (anti-PIS), and precipitates were analyzed by Western blotting with the indicated Abs. One representative experiment of two is shown. *C*, Jurkat T cells were transfected as described in *A*. SKAP55 was immunoprecipitated from untreated or stimulated cells, and proteins interacting with SKAP55 were detected by Western blotting using the indicated Abs. Data are representative for two individual experiments. *D*, Jurkat T cells were transfected as described in *A*, and plasma membrane or cytosolic fractions were prepared from untreated (−) or TCR-stimulated cells (+). The individual fractions were analyzed by Western blotting using the indicated Abs. Fractionation efficiency was assessed by Western blotting using anti-LAT (plasma membrane) or anti-ERK1/2 (cytosol) Abs, respectively. One representative experiment of two is shown. *E*, Human T cells transfected with control siRNA (siC) or siRNA against SLP76 (siSLP76) were allowed to form conjugates with SA-loaded B cells for 30 min. Fixed and permeabilized cells were stained with mAbs to SKAP55, RIAM, or Rap1 (green) and TRITC-phalloidin (red). Fluorescence intensity of SKAP55, RIAM, or Rap1 at IS or uropod was quantified and calculated as ratio of intensity for the individual protein at the IS vs the uropod. Loss of SLP76 expression for each experiment was analyzed by flow cytometry. Data present the average results of three independently performed experiments.

SLP76 is dispensable for CXCR4-mediated Rac activation, actin dynamics, and migration

Similar to TCR stimulation, remodeling of the actin cytoskeleton through Rac is crucial for inducing T cell adhesion, polarization, and chemotaxis following CXCR4 stimulation (33). Our above findings led us to ask whether the presence of SLP76 might be dispensable for Rac activation in response to CXCL12 triggering. As shown in Fig. 6*A*, SLP76^{low} Jurkat T cells indeed display no obvious defect in CXCL12-mediated activation of Rac. Moreover, both SLP76^{high} and SLP76^{low} T cells revealed comparable levels of F-actin formation in response to CXCL12 (Fig. 6*B*). These data strongly suggest that SLP76 is indeed dispensable for signaling events that are critically involved in CXCR4-mediated activation of Rac and actin polymerization.

To prove whether expression of SLP76 is required for CXCR4-induced T cell chemokinesis, we determined the lateral locomotion of T cells by live cell imaging on Fc-ICAM-1-coated coverslips. As shown in Fig. 6*C*, both SLP76^{high} and SLP76^{low} T cells showed comparable basal and CXCL12-induced velocities. In contrast, and in line with previously published data (31), Vav1-deficient T cells displayed

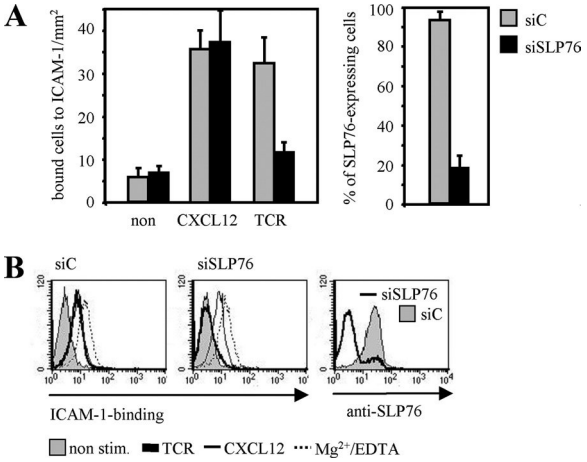

FIGURE 5. SLP76 is dispensable for CXCL12-mediated adhesion to ICAM-1, affinity maturation of LFA-1. *A*, Human T cells were transfected with control siRNA (siC) or siRNAs against SLP76 (siSLP76). Cells were left untreated or stimulated with immobilized CXCL12 (10 min) or anti-CD3 mAbs (TCR) for 30 min. Subsequently, cells were analyzed for their ability to adhere to Fc-ICAM-1. Suppression of SLP76 expression was assessed by flow cytometry, and the percentage of SLP76-expressing cells was calculated. Data represent the mean and SE of three independently performed experiments. *B*, Human T cells transfected as described in *A* were analyzed for their ability to bind soluble Fc-ICAM-1 upon anti-CD3 (TCR), CXCL12, or Mg^{2+}/EGTA (positive control) treatment for 5 min. Suppression of SLP76 expression was evaluated by flow cytometry. One individual experiment of three is shown.

a strongly reduced motility upon CXCR4 triggering (Fig. 6*C*). It is also important to note that nearly all $SPL76^{low}$ T cells displayed a polarized phenotype upon chemokine stimulation, whereas the majority of Vav1-depleted T cells remained a round, nonpolarized shape (Fig. 6*C*). Fig. 6*D* further demonstrates that the absence of SLP76 does not alter CXCR4-induced chemotaxis of human primary T cells in response to a CXCL12 gradient in vitro. In summary, it appears as if SLP76 is not mandatory for migratory steps triggered by CXCL12.

The ADAP/SKAP55/RIAM module is recruited to the plasma membrane independently of SLP76

Upon T cell activation, the Gads/SLP76 complex is recruited to phosphorylated LAT, thereby coupling the TCR to the intracellular signaling machinery (2, 49). Given the above data, we next investigated whether the LAT/Gads/SLP76 signaling platform would be assembled after CXCR4 stimulation. To test this, we stimulated human T cells for various periods of time with CXCL12 and subsequently analyzed global tyrosine phosphorylation of LAT by Western blotting. In contrast to TCR stimulation, phosphorylation of LAT was only very weakly induced upon CXCR4 triggering (Fig. 7*A*). Similar results were obtained when the phosphorylation status of LAT at Y^{171} (which is important for Gads binding) was assessed (Fig. 7*A*). These data suggested that the Gads/SLP76 complex might not associate with LAT following CXCR4 triggering. To investigate this point in more detail, we immunoprecipitated the Gads/SLP76 complex from untreated, TCR-stimulated, or CXCR4-triggered T cells. Fig. 7*B* shows that an inducible interaction among Gads/SLP76, LAT, and Vav1 was readily detectable after TCR stimulation. In contrast, neither LAT nor Vav1 was found to be associated with the Gads/SLP76 complex in

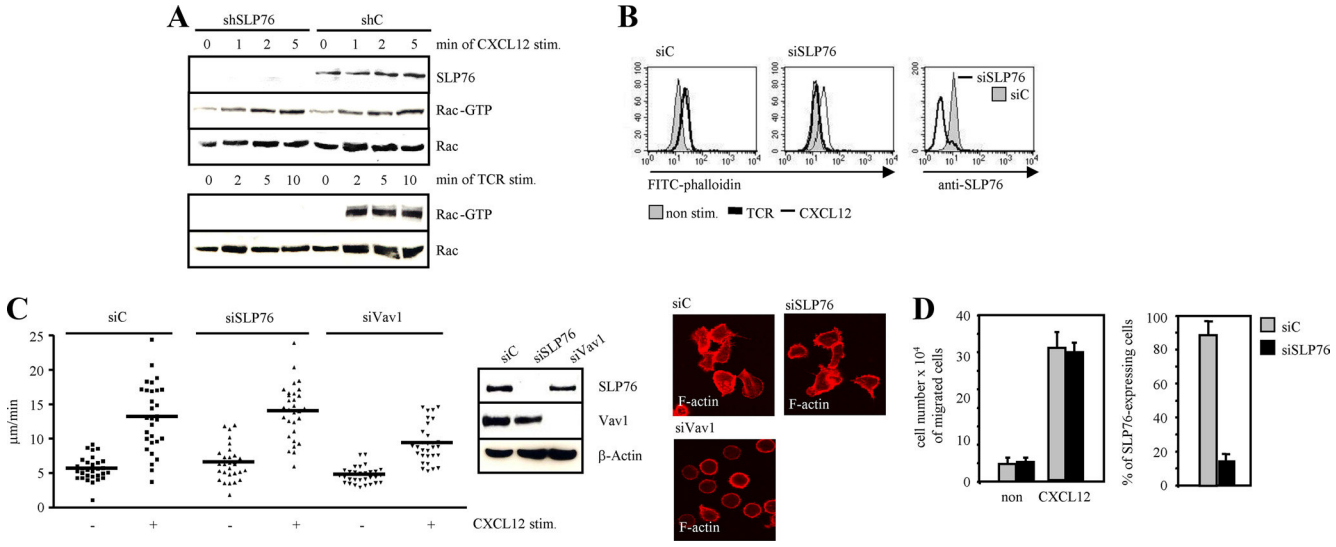

FIGURE 6. The presence of SLP76 is not required for Rac activation, actin polymerization, motility, and chemotaxis in response to CXCL12. *A*, Jurkat T cells were transfected with either control vector (shC) or SLP76-suppression vector (shSLP76). After 48 h, cells were either left untreated, or stimulated with CXCL12 or anti-CD3 mAbs (TCR) for the indicated time points. Activated Rac was precipitated using the GST-PBD fusion protein. Precipitates and aliquots of whole-cell extracts were analyzed by Western blotting using the indicated Abs. One representative experiment of three is shown. *B*, Human T cells were transfected with control siRNA (siC) or siRNA against SLP76 (siSLP76). After 72 h, cells were left untreated, stimulated with anti-CD3 mAbs (TCR, for 5 min) or CXCL12 for 1 min, and stained with FITC-coupled phalloidin. Reduction of SLP76 expression in human T cells was assessed by flow cytometry. Data are representative of three independent experiments. *C*, Human T cells were transfected with control siRNA (siC), siRNA against SLP76 (siSLP76), or siRNA against Vav1 (siVav1). After 72 h, motility of T cells in the absence or presence of CXCL12 was determined on Fc-ICAM-1-coated coverslips, as described in *Materials and Methods*. In parallel, transfectants were stimulated on Fc-ICAM-1-coated coverslips with CXCL12 for 30 min. Cells were fixed, permeabilized, and stained with TRITC-phalloidin. Whole-cell extracts were analyzed by Western blotting for the expression of SLP76, Vav1, and β-actin. One individual experiment of three is shown. *D*, Chemotaxis of human T cells transfected as described in *A* was addressed using a Transwell assay, as described in *Materials and Methods*. After 2 h, the number of migrated cells into the lower chamber was counted. Suppression of SLP76 expression was assessed by flow cytometry, and the percentage of SLP76-expressing cells was calculated. Data represent the mean and SE of three independently performed experiments.

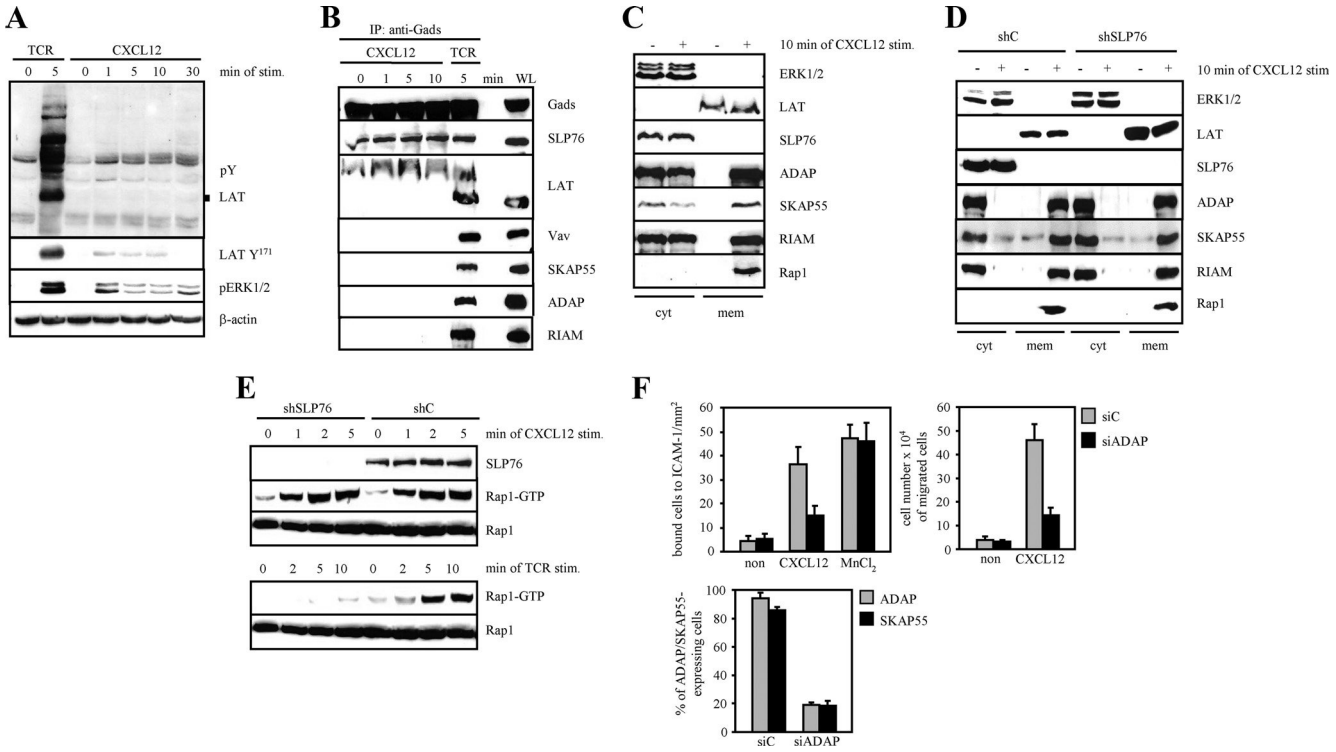

FIGURE 7. The SLP76/Gads complex is not associated with LAT or transported to the plasma membrane upon CXC12 stimulation. *A*, Human T cells were either left untreated, or stimulated with anti-CD3 mAbs (TCR) or CXCL12 for the indicated periods of time. Lysates were analyzed by Western blotting using the indicated Abs. *B*, The cell extracts as described in *A* were used for immunoprecipitation using anti-Gads Ab. Precipitates were analyzed by Western blotting using the indicated Abs. *C*, Plasma membrane or cytosolic fractions were prepared from untreated (−) or CXCR4-stimulated human T cells (+). The individual fractions were analyzed by Western blotting using the indicated Abs. Fractionation efficiency was assessed by Western blotting using anti-LAT (plasma membrane) or anti-ERK1/2 (cytosol) Abs, respectively. One representative experiment of two is shown. *D*, Jurkat T cells were transfected with either control vector (shC) or SLP76-suppression vector (shSLP76). After 48 h, plasma membrane or cytosolic fractions were prepared from untreated (−) or CXCR4-stimulated cells (+). The individual fractions were analyzed by Western blotting using the indicated Abs. Fractionation efficiency was assessed by Western blotting using anti-LAT (plasma membrane) or anti-ERK1/2 (cytosol) Abs, respectively. One representative experiment of two is shown. *E*, Jurkat T cells were transfected with either control vector (shC) or SLP76-suppression vector (shSLP76). After 48 h, cells were either left untreated, or stimulated with CXCL12 or anti-CD3 mAbs (TCR) for the indicated time points. GTP-loaded Rap1 was precipitated using the GST-RalGDS-RBD fusion protein. Precipitates and aliquots of whole-cell extracts were analyzed by Western blotting using the indicated Abs. One representative experiment of three is shown. *F*, Human T cells were transfected with control siRNA (siC) or siRNA against ADAP (siADAP). After 72 h, transfectants were left untreated or stimulated with CXCL12 (for 10 min) or $MnCl_2$ (for 30 min) and subsequently analyzed for their ability to adhere to Fc-ICAM-1. Chemotaxis of the same cells was analyzed using a Transwell assay, as described in *Materials and Methods*. After 2 h, the number of migrated cells into the lower chamber was determined. Suppression of ADAP and SKAP55 expression was determined by flow cytometry, and the percentage of ADAP/SKAP55-expressing cells was calculated. Note that loss of ADAP abrogates SKAP55 expression (17). Data represent the mean and SE of three independently performed experiments.

response to CXCL12 stimulation (Fig. 7*B*). These experiments indicate that the LAT/Gads/SLP76 signaling platform is not assembled in response to CXCL12 in T cells.

Above we have shown that the ADAP/SKAP55/RIAM module inducibly interacts with SLP76 upon TCR-mediated T cell activation, and that SLP76 is mandatory for membrane targeting of the ADAP/SKAP55/RIAM module and for activation of Rap1 (Fig. 4). In marked contrast, CXCL12 stimulation of T cells did not lead to an inducible interaction between the LAT/Gads/SLP76 complex and the ADAP/SKAP55/RIAM module (Fig. 7*B*). However, the ADAP/SKAP55/RIAM module (and also Rap1) was properly recruited to the plasma membrane in response to CXCR4 stimulation in both SLP76-proficient and -deficient T cells (Fig. 7, *C* and *D*). Moreover, $SLP76^{low}$ Jurkat T cells displayed no obvious defect in CXCL12-mediated activation of Rap1 (Fig. 7*E*). These data suggest that SLP76 is not required for CXCR4-mediated Rap1 activation and plasma membrane targeting of ADAP, SKAP55, RIAM, and Rap1.

To exclude the possibility that ADAP and SKAP55 themselves are dispensable for CXCR4-regulated adhesion and migration, we down-regulated ADAP expression in human T cells by siRNA and subsequently assessed both the adhesiveness and migratory capacity of these cells in response to CXCL12. Fig. 7*F* shows that loss of ADAP strongly attenuated CXCR4-induced adhesion and chemotaxis in human T cells. Similar data were obtained when we assessed CXCR4-induced migration of $ADAP^{low}$ Jurkat T cells or of T cells obtained from ADAP-deficient mice (data not shown). In summary, our data show that in contrast to TCR stimulation, SLP76 is not involved in membrane recruitment of the ADAP/SKAP55/RIAM module, the activation of Rac or Rap1, and the induction of adhesion or migration in response to CXCR4 stimulation.

Discussion

Together with the transmembrane adapter protein LAT, the cytosolic adapter protein SLP76 facilitates the formation of a signaling platform (LAT/Gads/SLP76) following TCR stimulation that leads to the activation of multiple intracellular signaling pathways (49). Our previous data suggested that the signaling pathways controlled by the Gads/SLP76 complex also include those regulating adhesion processes (22). In this study, we confirm this hypothesis by showing that suppression of SLP76 expression by RNAi in human T cells or the

Jurkat T cell line abrogates TCR-mediated conjugate formation, adhesion to ICAM-1, and affinity/avidity maturation of LFA-1. Consistent with previously published data (50, 51), we also found that loss of SLP76 attenuates adhesion to fibronectin (the ligand of β_1 integrins; VLA-4) in response to TCR stimulation (J. Horn and S. Kliche, unpublished data). Thus, SLP76 regulates TCR-induced inside-out signaling, leading to the activation of β_1 and β_2 integrins.

Reorganization of the actin cytoskeleton is critically involved in TCR-mediated integrin activation (33, 34). Moreover, it has previously been demonstrated that overexpression of SLP76 enhances F-actin formation in response to TCR stimulation (52). In addition to these overexpression data, we show in this study that loss of SLP76 attenuates TCR-mediated polymerization of F-actin. Together these findings suggest that SLP76 is one of the (if not the) central molecule that links the TCR to remodeling of the actin cytoskeleton.

The defect in actin dynamics most likely results from an abrogated activation of the small GTPase Rac. Activation of Rac depends on membrane recruitment and activation of the GEF Vav1 and the Tec kinase Itk (20, 32). Both Vav1 and Itk associate with SLP76 upon TCR stimulation, and both molecules are required for F-actin formation at the IS, activation of Rac, clustering of LFA-1, adhesion to ICAM-1, and conjugate formation (20, 32). In this scenario, the role of Vav1 is to generate sufficient pools of activated Rac to promote F-actin polymerization through activation of proteins of the Wiskott-Aldrich syndrome protein/Wiskott-Aldrich syndrome-Verprolin-homologues protein family (33, 34). Our data showing attenuated actin reorganization in SLP76^{low} cells are in line with a model in which loss of SLP76 blocks activation of Rac (and consequently signaling events downstream of Rac) by impairing the functions of Vav1 and Itk.

We are, however, aware that another group recently reported that TCR-mediated actin remodeling is not attenuated in the SLP76-deficient Jurkat T cell line J14 (53). In addition, no defect in Rac activation upon TCR stimulation was observed in this Jurkat variant (54). The reasons for these discrepant findings in SLP76-deficient Jurkat T cells vs SLP76^{low} human T cells are unclear at present. A possible explanation may come from compensatory mechanisms that developed in line J14 to escape the selection pressure that cannot develop in short-term manipulated T cells.

Besides the reorganization of the actin cytoskeleton, one critical regulator of TCR-mediated conjugate formation and inside-out signaling is the small GTPase Rap1 (6). Several studies have reported that Rap1 activation critically depends on the expression of PLCγ1 (13, 26, 55). PLCγ1 signaling to Rap1 occurs via the nucleotide exchange factor calcium and diacylglycerol-regulated guanine nucleotide exchange factor I that is activated by the second messengers calcium and diacylglycerol (which both are generated following phosphatidylinositol 4,5-bisphosphate hydrolysis by PLCγ1). Thus, a defect in PLCγ1 activation in SLP76-suppressed T cells (see Fig. 1*C* and supplemental Fig. 2, *C* and *D*) and consequently a failure to activate CalDAG-GEFI might be largely responsible for the attenuated activation of Rap1 after TCR triggering in the absence of SLP76. However, additional mechanisms controlled by SLP76 may also contribute to the block in Rap1 activation. For example, SLP76 is mandatory for activation and membrane targeting of protein kinase Cθ, which has recently been identified to control TCR-induced Rap1 activity by phosphorylation of Rap1-GEF2 (56, 57). Hence, loss of SLP76 might affect several signaling pathways that are critical for TCR-induced activation of Rap1.

We had previously shown that the ADAP/SKAP55/RIAM complex is required for plasma membrane targeting of Rap1. Moreover, we had demonstrated that this event is crucial for inside-out signaling and for the activation of integrins in response to TCR stimulation. However, loss of ADAP and/or SKAP55 selectively abrogated plasma membrane recruitment of Rap1, although TCR-mediated activation of Rap1 was not affected (17, 21). In contrast, the data presented in this study show that SLP76 is mandatory for both membrane targeting and activation of Rap1 after TCR triggering. The former event most likely involves the ADAP/SKAP55/RIAM module, whereas the activation of Rap1 might be regulated through the PLCγ1- or the protein kinase Cθ-signaling pathways that were discussed above. Hence, our data support a model in which plasma membrane targeting and activation of Rap1 are two interrelated, but distinctly controlled signaling events that are organized at the level of SLP76.

The activation of Rap1 and Rac as well as changes in F-actin dynamics are also mandatory for affinity modulation of LFA-1, T cell adhesion, and migration in response to CXCR4 stimulation (6, 58). Given the central role of SLP76 in TCR-mediated signaling, it was totally unexpected for us to find that loss of SLP76 did not affect these events after CXCR4 stimulation and that the SLP76/Gads complex was not recruited to LAT in response to CXCR4 stimulation. The latter observation is probably due to the fact that the tyrosine residue within LAT that is responsible for recruiting the Gads/SLP76 complex (Y^{171}) is not phosphorylated in response to CXCL12 triggering.

Our data also showed that SLP76 is not involved in the recruitment (and consequently the activation) of downstream effector molecules (e.g., Vav1) that are important for mediating adhesion and migration processes of T cells in response to CXCL12 triggering (58). Indeed, whereas Vav1-deficient T cells failed to polarize in response to CXCL12 stimulation, SLP76^{low} T cells showed no defect in this process. Moreover, CXCL12-induced lateral migration velocity and chemotaxis were unaffected in SLP76^{low} T cells. Hence, it appears as if SLP76 is dispensable for both adhesive and migratory processes in response to CXCL12 stimulation.

In line with the functional data, we found that membrane recruitment of the ADAP/SKAP55/RIAM module that is critical for CXCR4-mediated adhesion and migration of T cells was not affected by loss of SLP76. Although this finding strongly supports our above discussed hypothesis that membrane targeting of Rap1 and activation of this GTPase are distinct processes that are individually regulated by different signaling receptors, it opens the question as to which signaling molecule provides the molecular link between CXCR4 and the ADAP/SKAP55/RIAM module.

In this regard, it has recently been shown that the cytosolic adapter protein Shc is phosphorylated upon CXCR4 stimulation and assembles into a complex that includes Lck, ZAP70, Vav1, and LAT (59). Moreover, Shc-deficient Jurkat T cells show an attenuated migratory capacity and impaired F-actin dynamics upon CXCR4 stimulation, and mutation of critical tyrosine residues of Shc ($YY^{238/240}$ or Y^{317}) results in defective phosphorylation of Vav1 and Itk (59). Thus, Shc might be an attractive candidate to connect CXCR4 with the Vav1-Itk-dependent pathway of F-actin polymerization and T cell migration (59). It will be important to assess the role of Shc in CXCR4-induced inside-out signaling, adhesion, and Rap1 activation in future studies. Similarly, it needs to be analyzed whether, and if so how, LAT is involved in this process. Experiments are currently set up in our laboratory to assess these points. Nevertheless, our data collectively and surprisingly indicate that, in contrast to TCR signaling, SLP76 is not a key component connecting the chemokine receptor CXCR4 with the activation of integrins and the induction of T cell adhesion and migration.

Acknowledgments

We thank A. Weiss, V. Horejsi, J. Bos, T. Seufferlein, D. D. Billadeau, G. A. Koretzky, and N. Hogg for providing reagents, and K.-D. Fischer for critical reading of this manuscript. We are thankful to A. Ramonat, J. Hoppe, S. Holze, and N. Jüling for excellent technical assistance.

Disclosures

The authors have no financial conflict of interest.

References

1. Koretzky, G. A., F. Abtahian, and M. A. Silverman. 2006. SLP76 and SLP65: complex regulation of signalling in lymphocytes and beyond. *Nat. Rev. Immunol.* 6: 67–78.
2. Liu, S. K., N. Fang, G. A. Koretzky, and C. J. McGlade. 1999. The hematopoietic-specific adaptor protein gads functions in T-cell signaling via interactions with the SLP-76 and LAT adaptors. *Curr. Biol.* 9: 67–75.
3. Yablonski, D., M. R. Kuhne, T. Kadlecek, and A. Weiss. 1998. Uncoupling of nonreceptor tyrosine kinases from PLC-γ1 in an SLP-76-deficient T cell. *Science* 281: 413–416.
4. Grakoui, A., S. K. Bromley, C. Sumen, M. M. Davis, A. S. Shaw, P. M. Allen, and M. L. Dustin. 1999. The immunological synapse: a molecular machine controlling T cell activation. *Science* 285: 221–227.
5. Gunzer, M., C. Weishaupt, A. Hillmer, Y. Basoglu, P. Friedl, K. E. Dittmar, W. Kolanus, G. Varga, and S. Grabbe. 2004. A spectrum of biophysical interaction modes between T cells and different antigen-presenting cells during priming in 3-D collagen and in vivo. *Blood* 104: 2801–2809.
6. Kinashi, T. 2005. Intracellular signalling controlling integrin activation in lymphocytes. *Nat. Rev. Immunol.* 5: 546–559.
7. Kim, M., C. V. Carman, and T. A. Springer. 2003. Bidirectional transmembrane signaling by cytoplasmic domain separation in integrins. *Science* 301: 1720–1725.
8. Nolz, J. C., R. B. Medeiros, J. S. Mitchell, P. Zhu, B. D. Freedman, Y. Shimizu, and D. D. Billadeau. 2007. WAVE2 regulates high-affinity integrin binding by recruiting vinculin and talin to the immunological synapse. *Mol. Cell. Biol.* 27: 5986–6000.
9. Nolz, J. C., L. P. Nacusi, C. M. Segovis, R. B. Medeiros, J. S. Mitchell, Y. Shimizu, and D. D. Billadeau. 2008. The WAVE2 complex regulates T cell receptor signaling to integrins via Abl- and CrkL-C3G-mediated activation of Rap1. *J. Cell Biol.* 182: 1231–1244.
10. Duchniewicz, M., T. Zemojtel, M. Kolanczyk, S. Grossmann, J. S. Scheele, and F. J. Zwartkruis. 2006. Rap1A-deficient T and B cells show impaired integrin-mediated cell adhesion. *Mol. Cell. Biol.* 26: 643–653.
11. Sebzda, E., M. Bracke, T. Tugal, N. Hogg, and D. A. Cantrell. 2002. Rap1A positively regulates T cells via integrin activation rather than inhibiting lymphocyte signaling. *Nat. Immunol.* 3: 251–258.
12. Lafuente, E. M., A. A. van Puijenbroek, M. Krause, C. V. Carman, G. J. Freeman, A. Berezovskaya, E. Constantine, T. A. Springer, F. B. Gertler, and V. A. Boussiotis. 2004. RIAM, an Ena/VASP and Profilin ligand, interacts with Rap1-GTP and mediates Rap1-induced adhesion. *Dev. Cell* 7: 585–595.
13. Katagiri, K., M. Shimonaka, and T. Kinashi. 2004. Rap1-mediated lymphocyte function-associated antigen-1 activation by the T cell antigen receptor is dependent on phospholipase C-γ1. *J. Biol. Chem.* 279: 11875–11881.
14. Katagiri, K., M. Imamura, and T. Kinashi. 2006. Spatiotemporal regulation of the kinase Mst1 by binding protein RAPL is critical for lymphocyte polarity and adhesion. *Nat. Immunol.* 7: 919–928.
15. Griffiths, E. K., C. Krawczyk, Y. Y. Kong, M. Raab, S. J. Hyduk, D. Bouchard, V. S. Chan, I. Kozieradzki, A. J. Oliveira-Dos-Santos, A. Wakeham, et al. 2001. Positive regulation of T cell activation and integrin adhesion by the adapter Fyb/Slap. *Science* 293: 2260–2263.
16. Peterson, E. J., M. L. Woods, S. A. Dmowski, G. Derimanov, M. S. Jordan, J. N. Wu, P. S. Myung, Q. H. Liu, J. T. Pribila, B. D. Freedman, et al. 2001. Coupling of the TCR to integrin activation by Slap-130/Fyb. *Science* 293: 2263–2265.
17. Kliche, S., D. Breitling, M. Togni, R. Pusch, K. Heuer, X. Wang, C. Freund, A. Kasirer-Friede, G. Menasche, G. A. Koretzky, and B. Schraven. 2006. The ADAP/SKAP55 signaling module regulates T-cell receptor-mediated integrin activation through plasma membrane targeting of Rap1. *Mol. Cell. Biol.* 26: 7130–4144.
18. Wang, H., H. Liu, Y. Lu, M. Lovatt, B. Wei, and C. E. Rudd. 2007. Functional defects of SKAP-55-deficient T cells identify a regulatory role for the adaptor in LFA-1 adhesion. *Mol. Cell. Biol.* 27: 6863–6875.
19. Bezman, N. A., L. Lian, C. S. Abrams, L. F. Brass, M. L. Kahn, M. S. Jordan, and G. A. Koretzky. 2008. Requirements of SLP76 tyrosines in ITAM and integrin receptor signaling and in platelet function in vivo. *J. Exp. Med.* 205: 1775–1788.
20. Gomez-Rodriguez, J., J. A. Readinger, I. C. Viorritto, K. L. Mueller, R. A. Houghtling, and P. L. Schwartzberg. 2007. Tec kinases, actin, and cell adhesion. *Immunol. Rev.* 218: 45–64.
21. Menasche, G., S. Kliche, E. J. Chen, T. E. Stradal, B. Schraven, and G. Koretzky. 2007. RIAM links the ADAP/SKAP-55 signaling module to Rap1, facilitating T-cell-receptor-mediated integrin activation. *Mol. Cell. Biol.* 27: 4070–4081.
22. Jordan, M. S., J. S. Maltzman, S. Kliche, J. Shabason, J. E. Smith, A. Obstfeld, B. Schraven, and G. A. Koretzky. 2007. In vivo disruption of T cell development by expression of a dominant-negative polypeptide designed to abolish the SLP-76/Gads interaction. *Eur. J. Immunol.* 37: 2961–2972.
23. Wang, H., F. E. McCann, J. D. Gordan, X. Wu, M. Raab, T. H. Malik, D. M. Davis, and C. E. Rudd. 2004. ADAP-SLP-76 binding differentially regulates supramolecular activation cluster (SMAC) formation relative to T cell-APC conjugation. *J. Exp. Med.* 200: 1063–1074.
24. Campbell, D. J., C. H. Kim, and E. C. Butcher. 2003. Chemokines in the systemic organization of immunity. *Immunol. Rev.* 195: 58–71.
25. Smith, A., Y. R. Carrasco, P. Stanley, N. Kieffer, F. D. Batista, and N. Hogg. 2005. A talin-dependent LFA-1 focal zone is formed by rapidly migrating T lymphocytes. *J. Cell Biol.* 170: 141–151.
26. Ghandour, H., X. Cullere, A. Alvarez, F. W. Luscinskas, and T. N. Mayadas. 2007. Essential role for Rap1 GTPase and its guanine exchange factor CalDAG-GEFI in LFA-1 but not VLA-4 integrin mediated human T-cell adhesion. *Blood* 110: 3682–3690.
27. Shimonaka, M., K. Katagiri, T. Nakayama, N. Fujita, T. Tsuruo, O. Yoshie, and T. Kinashi. 2003. Rap1 translates chemokine signals to integrin activation, cell polarization, and motility across vascular endothelium under flow. *J. Cell Biol.* 161: 417–427.
28. Katagiri, K., T. Katakai, Y. Ebisuno, Y. Ueda, T. Okada, and T. Kinashi. 2009. Mst1 controls lymphocyte trafficking and interstitial motility within lymph nodes. *EMBO J.* 28: 1319–1331.
29. Katagiri, K., N. Ohnishi, K. Kabashima, T. Iyoda, N. Takeda, Y. Shinkai, K. Inaba, and T. Kinashi. 2004. Crucial functions of the Rap1 effector molecule RAPL in lymphocyte and dendritic cell trafficking. *Nat. Immunol.* 5: 1045–1051.
30. Miertzschke, M., P. Stanley, T. D. Bunney, F. Rodrigues-Lima, N. Hogg, and M. Katan. 2007. Characterization of interactions of adapter protein RAPL/Nore1B with RAP GTPases and their role in T cell migration. *J. Biol. Chem.* 282: 30629–30642.
31. Garcia-Bernal, D., N. Wright, E. Sotillo-Mallo, C. Nombela-Arrieta, J. V. Stein, X. R. Bustelo, and J. Teixido. 2005. Vav1 and Rac control chemokine-promoted T lymphocyte adhesion mediated by the integrin $\alpha_4\beta_1$. *Mol. Biol. Cell* 16: 3223–3235.
32. Tybulewicz, V. L. 2005. Vav-family proteins in T-cell signalling. *Curr. Opin. Immunol.* 17: 267–274.
33. Burkhardt, J. K., E. Carrizosa, and M. H. Shaffer. 2008. The actin cytoskeleton in T cell activation. *Annu. Rev. Immunol.* 26: 233–259.
34. Billadeau, D. D., J. C. Nolz, and T. S. Gomez. 2007. Regulation of T-cell activation by the cytoskeleton. *Nat. Rev. Immunol.* 7: 131–143.
35. Heuer, K., M. Sylvester, S. Kliche, R. Pusch, K. Thiemke, B. Schraven, and C. Freund. 2006. Lipid-binding hSH3 domains in immune cell adapter proteins. *J. Mol. Biol.* 361: 94–104.
36. Hunter, A. J., N. Ottoson, N. Boerth, G. A. Koretzky, and Y. Shimizu. 2000. Cutting edge: a novel function for the SLAP-130/FYB adapter protein in β_1 integrin signaling and T lymphocyte migration. *J. Immunol.* 164: 1143–1147.
37. Jenzora, A., B. Behrendt, J. V. Small, J. Wehland, and T. E. Stradal. 2005. PREL1 provides a link from Ras signalling to the actin cytoskeleton via Ena/VASP proteins. *FEBS Lett.* 579: 455–463.
38. Weiss, A., and J. D. Stobo. 1984. Requirement for the coexpression of T3 and the T cell antigen receptor on a malignant human T cell line. *J. Exp. Med.* 160: 1284–1299.
39. Motto, D. G., S. E. Ross, J. Wu, L. R. Hendricks-Taylor, and G. A. Koretzky. 1996. Implication of the GRB2-associated phosphoprotein SLP-76 in T cell receptor-mediated interleukin 2 production. *J. Exp. Med.* 183: 1937–1943.
40. Marie-Cardine, A., L. R. Hendricks-Taylor, N. J. Boerth, H. Zhao, B. Schraven, and G. A. Koretzky. 1998. Molecular interaction between the Fyn-associated protein SKAP55 and the SLP-76-associated phosphoprotein SLAP-130. *J. Biol. Chem.* 273: 25789–25795.
41. Musci, M. A., L. R. Hendricks-Taylor, D. G. Motto, M. Paskind, J. Kamens, C. W. Turck, and G. A. Koretzky. 1997. Molecular cloning of SLAP-130, an SLP-76-associated substrate of the T cell antigen receptor-stimulated protein tyrosine kinases. *J. Biol. Chem.* 272: 11674–11677.
42. Huang, Y., D. D. Norton, P. Precht, J. L. Martindale, J. K. Burkhardt, and R. L. Wange. 2005. Deficiency of ADAP/Fyb/SLAP-130 destabilizes SKAP55 in Jurkat T cells. *J. Biol. Chem.* 280: 23576–23583.
43. Li, Y. F., R. H. Tang, K. J. Puan, S. K. Law, and S. M. Tan. 2007. The cytosolic protein talin induces an intermediate affinity integrin $\alpha_L\beta_2$. *J. Biol. Chem.* 282: 24310–24319.
44. Dluzniewska, J., L. Zou, I. R. Harmon, M. T. Ellingson, and E. J. Peterson. 2007. Immature hematopoietic cells display selective requirements for adhesion- and degranulation-promoting adaptor protein in development and homeostasis. *Eur. J. Immunol.* 37: 3208–3219.
45. Krutzik, P. O., and G. P. Nolan. 2003. Intracellular phospho-protein staining techniques for flow cytometry: monitoring single cell signaling events. *Cytometry A* 55: 61–70.
46. Reichardt, P., F. Gunzer, and M. Gunzer. 2007. Analyzing the physicodynamics of immune cells in a three-dimensional collagen matrix. *Methods Mol. Biol.* 380: 253–269.
47. Liu, S., D. A. Calderwood, and M. H. Ginsberg. 2000. Integrin cytoplasmic domain-binding proteins. *J. Cell Sci.* 113: 3563–3571.
48. Bivona, T. G., H. H. Wiener, I. M. Ahearn, J. Silletti, V. K. Chiu, and M. R. Philips. 2004. Rap1 up-regulation and activation on plasma membrane regulates T cell adhesion. *J. Cell Biol.* 164: 461–470.
49. Singer, A. L., S. C. Bunnell, A. E. Obstfeld, M. S. Jordan, J. N. Wu, P. S. Myung, L. E. Samelson, and G. A. Koretzky. 2004. Roles of the proline-rich domain in SLP-76 subcellular localization and T cell function. *J. Biol. Chem.* 279: 15481–15490.

50. Epler, J. A., R. Liu, H. Chung, N. C. Ottoson, and Y. Shimizu. 2000. Regulation of β_1 integrin-mediated adhesion by T cell receptor signaling involves ZAP-70 but differs from signaling events that regulate transcriptional activity. *J. Immunol.* 165: 4941–4949.
51. Nguyen, K., N. R. Sylvain, and S. C. Bunnell. 2008. T cell costimulation via the integrin VLA-4 inhibits the actin-dependent centralization of signaling microclusters containing the adaptor SLP-76. *Immunity* 28: 810–821.
52. Bubeck Wardenburg, J., R. Pappu, J. Y. Bu, B. Mayer, J. Chernoff, D. Straus, and A. C. Chan. 1998. Regulation of PAK activation and the T cell cytoskeleton by the linker protein SLP-76. *Immunity* 9: 607–616.
53. Barda-Saad, M., A. Braiman, R. Titerence, S. C. Bunnell, V. A. Barr, and L. E. Samelson. 2005. Dynamic molecular interactions linking the T cell antigen receptor to the actin cytoskeleton. *Nat. Immunol.* 6: 80–89.
54. Ku, G. M., D. Yablonski, E. Manser, L. Lim, and A. Weiss. 2001. A PAK1-PIX-PKL complex is activated by the T-cell receptor independent of Nck, Slp-76 and LAT. *EMBO J.* 20: 457–465.
55. Peak, J. C., N. P. Jones, S. Hobbs, M. Katan, and S. A. Eccles. 2008. Phospholipase Cγ1 regulates the Rap GEF1-Rap1 signalling axis in the control of human prostate carcinoma cell adhesion. *Oncogene* 27: 2823–2832.
56. Herndon, T. M., X. C. Shan, G. C. Tsokos, and R. L. Wange. 2001. ZAP-70 and SLP-76 regulate protein kinase C-θ and NF-κB activation in response to engagement of CD3 and CD28. *J. Immunol.* 166: 5654–5664.
57. Letschka, T., V. Kollmann, C. Pfeifhofer-Obermair, C. Lutz-Nicoladoni, G. J. Obermair, F. Fresser, M. Leitges, N. Hermann-Kleiter, S. Kaminski, and G. Baier. 2008. PKC-θ selectively controls the adhesion-stimulating molecule Rap1. *Blood* 112: 4617–4627.
58. Patrussi, L., and C. T. Baldari. 2008. Intracellular mediators of CXCR4-dependent signaling in T cells. *Immunol. Lett.* 115: 75–82.
59. Patrussi, L., C. Ulivieri, O. M. Lucherini, S. R. Paccani, A. Gamberucci, L. Lanfrancone, P. G. Pelicci, and C. T. Baldari. 2007. p52Shc is required for CXCR4-dependent signaling and chemotaxis in T cells. *Blood* 110: 1730–1738.

Appendix 12

Jones DS, **Reichardt P**, Ford ML, Edwards LJ, Evavold BD. TCR antagonism by peptide requires high TCR expression.
J Immunol. 2008;181:1760-6.

IF: 5.5

TCR Antagonism by Peptide Requires High TCR Expression[1]

Daniel S. Jones, Peter Reichardt, Mandy L. Ford, Lindsay J. Edwards, and Brian D. Evavold[2]

Current models of T cell activation focus on the kinetics of TCR-ligand interactions as the central parameter governing T cell responsiveness. However, these kinetic parameters do not adequately predict all T cell behavior, particularly the response to antagonist ligands. Recent studies have demonstrated that TCR number is a critical parameter influencing the responses of $CD4^+$ T cells to weak agonist ligands, and receptor density represents an important means of regulating tissue responsiveness in other receptor ligand systems. To systematically address the impact of TCR expression on $CD8^+$ T cell responses, mAbs to the TCR α-chain and T cells expressing two TCR species were used as two different methods to manipulate the number of available TCRs on P14 and OT-I transgenic T cells. Both methods of TCR reduction demonstrated that the efficacy of antagonist peptides was significantly reduced on T cells bearing low numbers of available receptors. In addition, the ability of weak agonists to induce proliferation was critically dependent on the availability of high numbers of TCRs. Therefore, in this report we show that TCR density is a major determinant of $CD8^+$ T cell reactivity to weak agonist and antagonist ligands but not agonist ligands. ***The Journal of Immunology,*** **2008, 181: 1760–1766.**

Historically, the activation of T lymphocytes through the TCR has been considered remarkably Ag specific. However, more recent studies have identified variants of immunogenic peptides capable of dissociating the proliferative and effector functions of Ag-specific T cells (1–3). These observations have provided the rationale for a number of studies investigating the ability of peptides containing amino acid substitutions at TCR contact residues to mediate T cell activation. Such analog peptides, termed altered peptide ligands, can be categorized as agonists, weak agonists, or partial agonists according to their ability to stimulate various hierarchical T cell responses (3). In addition, antagonist ligands, which induce no measurable effector responses on their own, markedly inhibit T cell activation when presented concomitantly with agonist peptide (4).

Several reports have correlated peptide affinity for the TCR and/or MHC with ligand potency (5–7). As a result, current models have focused on the kinetics of TCR:ligand interactions as the pivotal factor in T cell activation, as well as the role of endogenous peptide:MHC (pMHC)[3] in potentiating T cell activation (8, 9). However, the relative contribution of TCR density to T cell responsiveness has received little attention (10–14), although receptor density represents an important mechanism regulating the sensitivity and rapidity of responses in other receptor-ligand systems. Although T cells typically express tens of thousands TCRs, T cell responses to agonist pMHC complexes require remarkably few TCR molecules (15, 16). These results draw into question the role of these excess Ag receptors. Our work has demonstrated that the ability of $CD4^+$ T cells to respond to weak ligands is critically dependent on high TCR expression (17, 18). Specifically, $CD4^+$ T cells with as few as 1500 available TCRs were capable of responding to agonist peptides, whereas measurable responses to several weak agonists required dramatically more TCRs (~20,000) (17). These data provided evidence supporting a spare receptor theory of T cell activation. According to the spare receptor theory, agonist ligands achieve maximal responses by engaging only a fraction of available receptors while the excess receptors, termed "receptor reserve", are required for the induction of responses by less potent ligands (19). The excess receptors provide a means for generating responses to ligands encompassing a range of affinities and potencies. In this study, we investigated the impact of TCR density on the recognition of ligands of varying potency by $CD8^+$ T cells. We demonstrate that the activation of $CD8^+$ T cells by weak agonist, but not agonist peptides, requires the existence of a receptor reserve. One challenge to any model of T cell activation is to describe the action of antagonist pMHC complexes. As such, we investigated whether the spare receptor theory of T cell activation accurately describes the interactions of TCR molecules with antagonist ligands. Our results demonstrate that high TCR density is required for effective T cell antagonism, indicating that TCR-mediated responses function according to a spare receptor model.

Materials and Methods

Mice

OT-I transgenic mice (20) and P14 transgenic mice (21) were purchased from The Jackson Laboratory. OT-I (Vα2Vβ5) and P14 (Vα2Vβ8) TCRs were visualized with PE-conjugated mAbs to Vβ5 (BD Pharmingen) and Vβ8 (BD Pharmingen), respectively (21, 22). OT-I and P14 mice were bred to generate P14 × OT-I dual transgenic mice bearing T cells expressing both TCRs. All mice were maintained according to federal guidelines by the Emory University Department of Animal Resources (Atlanta, GA).

Cell culture and reagents

Cell culture medium consisted of RPMI medium 1640 (Mediatech) supplemented with 10% FBS (Mediatech), 2 mM L-glutamine, 0.01 M HEPES buffer, 100 μg/ml gentamicin (Mediatech), and 2×10^{-5} M 2-ME (Sigma-Aldrich). All peptides were synthesized using Fmoc chemistry on a Symphony/Multiplex Peptide synthesizer (Rainin), purified by HPLC (purity > 90%) and analyzed by mass spectrometry at the Emory University Department of Chemistry Core Facility (Atlanta, GA). The OT-I agonist OVA257–264 (SIINFEKL) and antagonist E1 (EIINFEKL), as well as the P14 agonist lymphocytic choriomeningitis virus (LCMV) gp33–41 (KAVYNFATM), antagonist 36S (KAVSNFATM), and weak agonist rat

Department of Microbiology and Immunology, Emory University, Atlanta, GA 30322

Received for publication August 3, 2007. Accepted for publication May 21, 2008.

The costs of publication of this article were defrayed in part by the payment of page charges. This article must therefore be hereby marked *advertisement* in accordance with 18 U.S.C. Section 1734 solely to indicate this fact.

[1] This work was supported by National Institutes of Health Grant AI056017.

[2] Address correspondence and reprint requests to Dr. Brian D. Evavold, Department of Microbiology and Immunology, Emory University, 1510 Clifton Road, Atlanta, GA 30322. E-mail address: evavold@microbio.emory.edu

[3] Abbreviations used in this paper: pMHC, peptide:MHC interaction; LCMV, lymphocytic choriomeningitis virus; rDBM, rat dopamine β-mono-oxygenase.

A

α-Vα2 (μg/mL)	P14 TCR #	OT-I TCR #
0	21180	22599
0.06	18510	19967
0.12	16824	18165
0.23	13623	16158
0.47	11451	11876
0.94	7211	6718
1.88	4091	3079
3.75	1988	1825
7.5	1239	1295
15	803	960

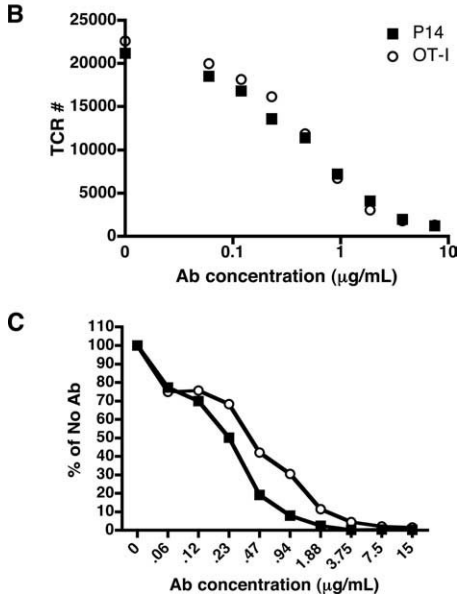

FIGURE 1. mAbs to Vα2 provide a range of densities of available TCRs and effectively inhibit TCR:pMHC interaction. *A*, To establish the relationship between Ab concentration and available TCR density, the number of unbound TCRs on P14 or OT-I T cells at each corresponding Ab concentration was determined by quantitative flow cytometry. α-Vα2, Anti-Vα2. *B*, The concentrations of Abs used resulted in a range of TCR densities, representing ~5–100% of original levels. The data indicated that the anti-Vα2 Abs were effective at masking both P14 (■) and OT-I (○) TCRs. *C*, P14 and OT-I T cells that had been incubated with various concentrations of anti-Vα2 mAbs were stained with gp33–41:D^b and SIIN FEKL:K^b MHC tetramers, respectively. Results demonstrated an inverse correlation between Ab concentration and tetramer binding, indicating that anti-Vα2 mAbs effectively mask the pMHC binding site of the TCR.

dopamine β-mono-oxygenase (rDBM) (KALYNYAPI) have all been previously described (23–25). The mAbs used included PerCP-conjugated anti-CD8α (BD Pharmingen), PE-conjugated anti-Vβ5 (clone MR9-4) (Pharmingen), PE-conjugated Vβ8 (clone F23.1) (BD Pharmingen), biotinylated and PE-conjugated anti-Vα2 (clone B20.1) (BD Pharmingen), and PE-conjugated anti-IFN-γ (clone XMG1.2) (BD Pharmingen). LCMV gp33–41:D^b and OVA257–264:K^b monomers were assembled at the Emory University Tetramer Core Facility (Atlanta, GA) and multimerized with PE- or allophycocyanin-conjugated streptavidin (Molecular Probes).

T cell proliferation assays

Proliferation of Ag-specific T cells was assessed by [^{3}H]thymidine incorporation (26). Briefly, transgenic splenocytes were incubated with varying concentrations of agonist peptides in HBSS for 2 h at 37°C. The cells were then washed to remove free peptide, and the splenocytes were cultured at 3×10^5 cells/well in a flat-bottom, 96-well plate. For antagonism assays, various concentrations of antagonist peptides were added to the appropriate wells. After 48 h, the cells were pulsed with 0.4 μCi of [^{3}H]thymidine for

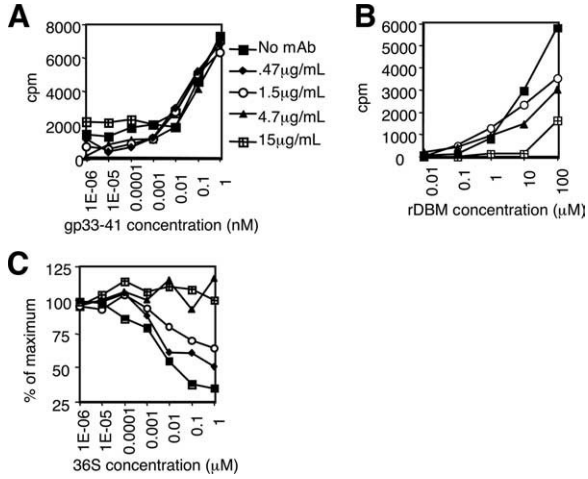

FIGURE 2. mAbs to Vα2 inhibited the function of P14 weak agonist and antagonist ligands but not agonist ligands. Naive P14 splenocytes were stimulated with the indicated concentrations of gp33–41 in the presence of anti-Vα2 mAbs. *A*, mAb treatment has no effect on agonist stimulation of proliferation. *B*, The stimulatory capacity of the weak agonist, rDBM was decreased by the addition of anti-Vα2 mAbs. *C*, The ability of the antagonist peptide (36S) to inhibit proliferation induced by stimulation with agonist (1 nM gp33–41) was decreased in the presence of increasing concentrations of anti-Vα2 mAbs.

18–24 h, at which time the cells were harvested and the cpm were counted on a Matrix 96 direct β-counter (Packard Instruments).

Intracellular cytokine production

Transgenic splenocytes were incubated with various peptides in HBSS for 2 h at 37°C, washed, resuspended in complete medium, and cultured in a

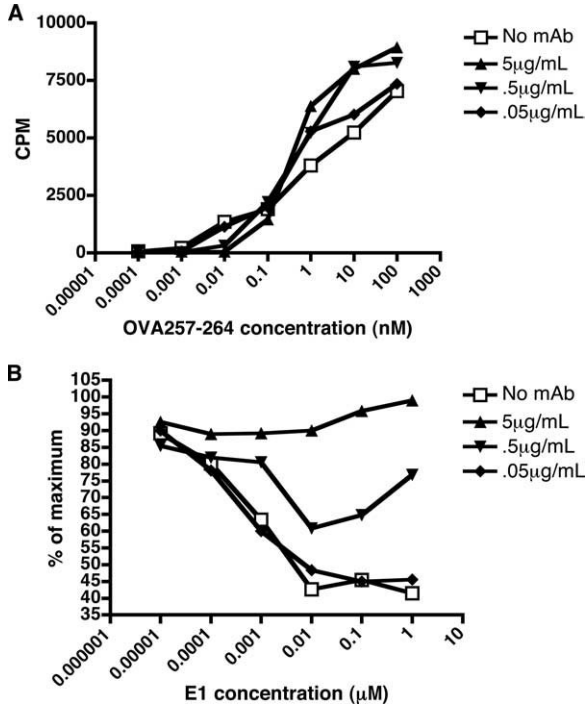

FIGURE 3. mAbs to Vα2 inhibited the function of an OT-I antagonist but not that of the agonist ligand. *A*, Treatment with anti-Vα2 mAbs had no effect on the agonist-induced stimulation of OT-I T cells as measured by the proliferation of naive OT-I splenocytes in response to the indicated concentrations of OVA257–264. *B*, The addition of anti-Vα2 mAbs decreased the effectiveness of the antagonist E1 at inhibiting agonist-induced (1 nM OVA257–264) proliferation.

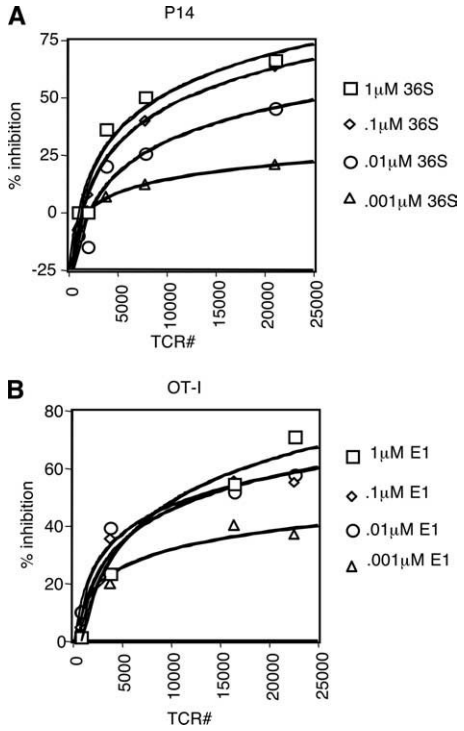

FIGURE 4. Antagonist peptide efficacy correlated with TCR density at all doses of antagonist ligand. The number of TCRs available at each dose of anti-Vα2 mAb was plotted against the corresponding observed percentage inhibition of agonist-induced proliferation. Regression analysis was conducted to determine the degree of correlation between TCR density and antagonist efficacy (solid lines). Antagonism assays conducted in the presence of neutralizing Abs to Vα2 revealed that the ability of both P14 (*A*) and OT-I (*B*) TCR antagonist to inhibit T cell activation correlated with TCR density ($r^2 = 0.9–1.0$). In addition, at a given TCR density the inhibition of both P14 (*A*) and OT-I (*B*) T cell proliferation was more effective at higher doses of antagonist peptide.

24-well plate (3×10^6 cells/well) with 50 U/ml IL-2 (26). At day 4, the live cells were collected by centrifugation over a Ficoll gradient (Mediatech). EL-4 thymoma cells were incubated with various peptides in HBSS for 2 h at 37°C, washed, resuspended in cell culture medium, and transferred to flat-bottom, 96-well plates (2×10^5 cells/well). For antagonist assays, the EL-4 APCs were incubated with continuous antagonist peptides before the addition of T cells. T cells (2×10^5 cells/well) were added to each experimental well with 50U/ml IL-2 and incubated for 6 h at 37°C. The cells were then transferred to round-bottom, 96-well plates, fixed, and permeabilized (Caltag Laboratories). IFN-γ production was detected intracellularly with PE-conjugated monoclonal rat anti-mouse IFN-γ Abs (BD Pharmingen). In these experiments, CD8 was visualized with PerCP-conjugated monoclonal rat anti-mouse CD8α Abs (BD Pharmingen).

Determination of TCR level and tetramer staining

Quantitative analyses of TCR expression were achieved using Quantum R-PE microbeads with 500–50,000 molecules of equivalent soluble fluorochrome (MESF) (Bangs Laboratories) and PE-conjugated anti-Vα2 (27). For tetramer staining, cells were incubated for 30 min on ice with 1 μg of tetramer per 1×10^6 cells. For Ab blockade of tetramer binding, cells were preincubated with indicated concentrations of Abs for 1 h at 37°C and then stained with tetramer as described. Flow cytometric data was collected on a BD FACSCalibur (BD Biosciences) and analyzed using FlowJo software (Tree Star).

Results

Manipulation of TCR density and effective blockade of the pMHC binding site using mAbs to the TCR α-chain

As an initial step in our investigation of the relationship between TCR density and T cell responsiveness, the number of available TCRs in the presence of various concentrations of mAbs to the TCR α-chain was determined by quantitative flow cytometry (Fig. 1) (27). P14 or OT-I transgenic splenocytes were incubated with 2-fold dilutions of anti-Vα2 (0.06–15 μg/ml) (Fig. 1*A*). The unoccupied TCRs were then visualized with R-PE-conjugated anti-Vα2 mAbs and quantitated using Quantum R-PE microbeads. Quantitative analyses verified that the doses of Abs chosen resulted in a range of TCR densities (Fig. 1*B*). To determine whether Abs to the TCR α-chain successfully inhibited the TCR:pMHC interaction, P14 and OT-I T cells were incubated with gp33–41:D^b and SIINFEKL/K^b tetramers, respectively, in the presence of anti-Vα2 Abs. Importantly, anti-Vα2 Abs

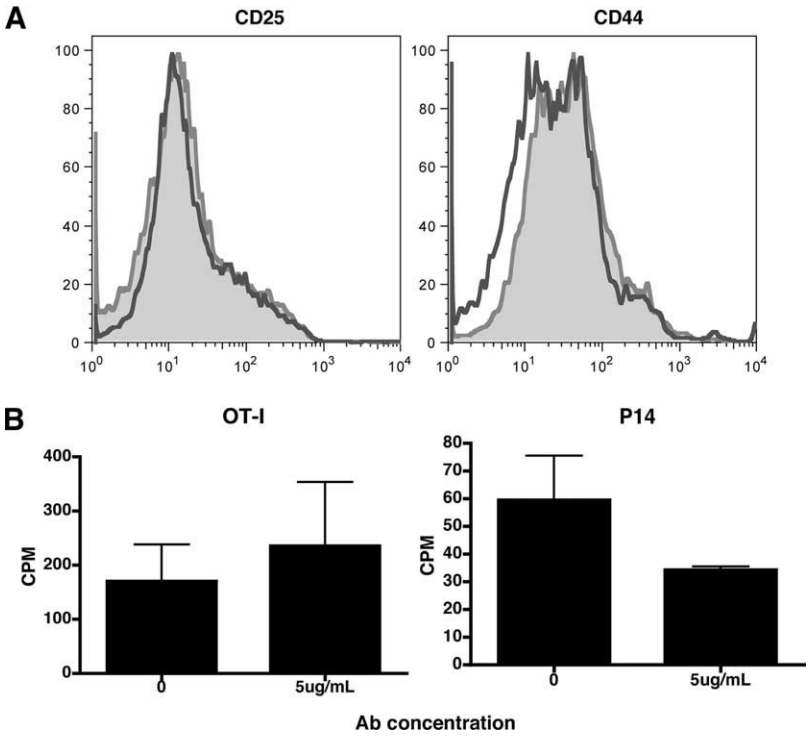

FIGURE 5. Anti-Vα2 Ab does not activate OT-I cells. *A*, OT-I splenocytes were stimulated for 48 h with 5 μg/ml anti-Vα2 Ab. Cells were stained for CD8, Vα2, CD25, and CD44. Histograms were gated on CD8$^+$ cells. The shaded histogram represents Ab-treated cells and the open histogram represents untreated cells. No significant difference in CD25 or CD44 up-regulation was detectable. *B*, Proliferation induced by the anti-Vα2 Ab was assessed by culturing cells for 48 h with the indicated concentration of Ab. [^{3}H]Thymidine was added and cells were cultured for an additional 18 h. Differences in proliferation were not statistically significant.

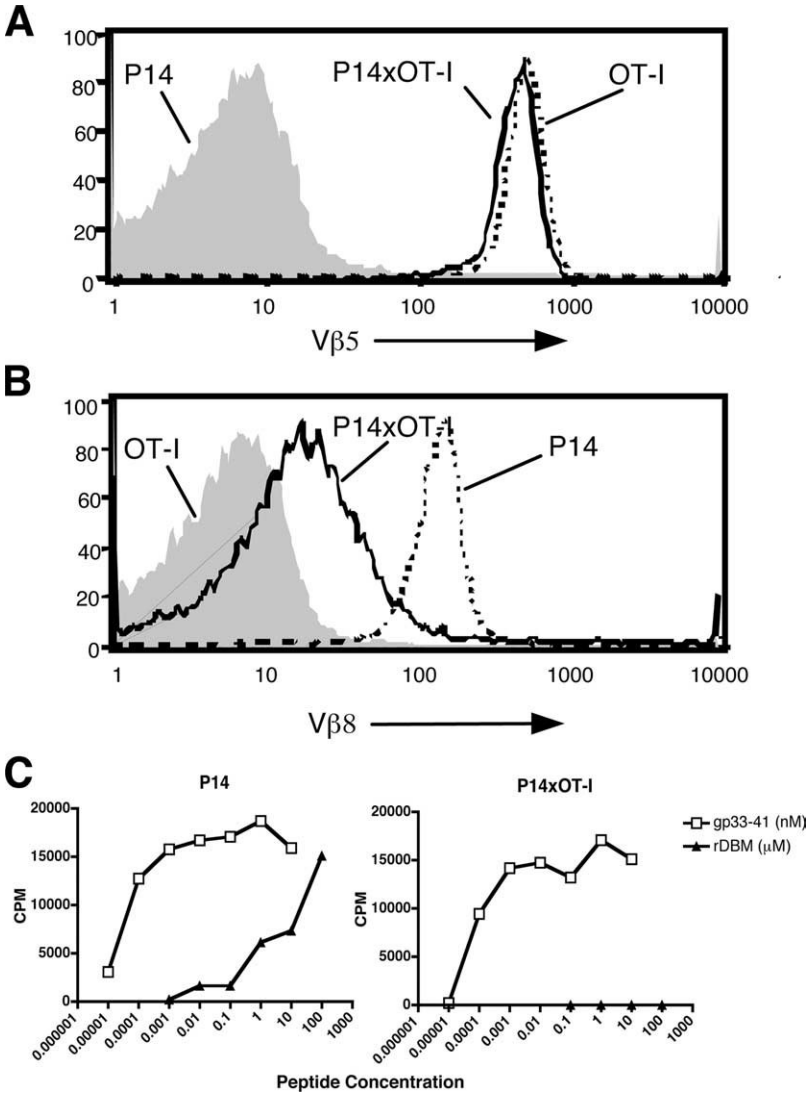

FIGURE 6. P14 × OT-I T cells expressed lower Vβ8 relative to cells from parental single transgenics, but Vβ5 levels were maintained at near parental levels. *A*, Levels of Vβ5 expression on P14 × OT-I T cells (solid line) was similar to those on cells from OT-I mice (dotted line). P14 cells were included as a negative control (shaded). *B*, Vβ8 expression is decreased on dual receptor cells (solid line) relative to P14 single transgenic cells (dotted line). OT-I cells were included as a negative control (shaded). *C*, P14 (*left panel*) and dual TCR cells (*right panel*) exhibited similar proliferative responses to agonist stimulation (□), but responses to the weak agonist rDBM (▲) were abrogated in the P14 × OT-I cells.

inhibited tetramer staining in a dose-dependent manner, demonstrating that treatment of T cells with these Abs effectively masks the pMHC binding site of the TCR (>98% inhibition; Fig. 1*C*). In addition, the minimal expression of TCR required for tetramer staining of these two T cell lines was identified. These data indicated that OT-I requires fewer TCR (~1825), as compared with the P14 T cell, which required 4000–7000 TCR for detectable tetramer staining. Thus, inhibition of tetramer binding using anti-Vα2 Abs demonstrated the effectiveness of Ab treatment for decreasing TCR density. These data also indicated differences in affinity of TCR for ligand, with the affinity of OT-I TCR for ligand being greater than that of P14 TCR.

TCR expression level is a critical parameter governing T cell responsiveness to suboptimal ligands

To assess whether agonist and weak agonist peptides exhibit differential requirements for TCR density, proliferation assays were conducted in the presence of various concentrations of mAbs to Vα2 (Fig. 2). P14 T cells were stimulated with either the agonist peptide gp33–41 (Fig. 2*A*) or the weak agonist peptide rDBM (Fig. 2*B*) in the presence of the indicated concentrations of anti-Vα2 Abs, resulting in a wide range of available TCR densities. Although the presence of high concentrations of anti-Vα2 reduced the number of available TCRs by >95%, this reduction in TCR density had little effect on agonist-induced proliferation of P14 T cells (Fig. 2*A*). In contrast, proliferation induced by the weak agonist rDBM was dramatically inhibited at low densities of available TCRs (Fig. 2*B*). Of note, biotinylated and R-PE-conjugated Abs proved the most effective at inhibiting T cell responses and tetramer staining, respectively, indicating a role for steric hindrance in their ability to inhibit pMHC binding. We have previously demonstrated that higher concentrations of this Ab (50 μg/ml) completely abrogate the ability of both P14 and OT-I T cells to bind to agonist pMHC (28). However, the concentrations used in our experiments are sufficient to alter the functional response to weak ligands.

Next, we used anti-Vα2 Abs to assess the role of TCR density in determining antagonist peptide efficacy. The impact of mAbs to Vα2 on the ability of 36S to antagonize the ex vivo proliferation of P14 T cells following stimulation with gp33–41 is shown in Fig. 2*C*. Decreasing the number of TCRs available for productive interactions with pMHC ligands drastically reduced the ability of 36S to inhibit agonist-induced proliferation of P14 T cells. The addition of 4.7 μg/ml anti-Vα2 resulted in the complete abrogation of TCR antagonism (Fig. 2*C*). Importantly, this observation was not unique to the P14 TCR, as similar results were obtained using OT-I (Vα2Vβ5) T cells (Fig. 3, *A* and *B*). The presence of 15 μg/ml anti-Vα2 resulted in the absolute loss of antagonist peptide function while maintaining the response of OT-I T cells to the

agonist peptide OVA257–264 (Fig. 3, *B* and *A*, respectively). In conjunction with the results in Fig. 1, these data highlight the disparate requirements for TCR density exhibited by agonist and antagonist ligands. Specifically, the efficacy of antagonist ligands for both the P14 and OT-I TCRs was negatively impacted by a ~60% reduction in TCR density, whereas the agonist-induced responses remained intact with <5% of the TCRs remaining. Thus, reducing the number of available TCRs selectively inhibits the function of suboptimal ligands while leaving agonist-induced responses intact. These results also indicate that antagonist ligands make use of the receptor reserve to inhibit T cell activation.

The correlation between antagonist peptide efficacy and TCR density is clearly illustrated in Fig. 4. Although the degree of maximal inhibition was dependent on the dose of the antagonist, the ability of both 36S and E1 to inhibit agonist-induced responses strongly correlated ($r^2 = 0.9–1.0$) with the number of available TCRs at all doses (Fig. 4, *A* and *B*, respectively). Strikingly, a precipitous decline in antagonist efficacy was observed at TCR densities below ~5000 TCR/cell at all concentrations of antagonist peptide tested (Fig. 4, *A* and *B*).

Anti-Vα2 Ab does not activate OT-I or P14 T cells

We verified that the clone of the anti-Vα2 Ab used in these studies (B20.1) was nonstimulatory by treating P14 or OT-I T cells with up to 15 μg/ml Ab. This concentration of Ab did not result in up-regulation of CD25 or CD44 (Fig. 5*A*) proliferation (Fig. 5*B*) or cytokine production (data not shown). Thus, we conclude that any potential activating properties of this Ab would not be detectable in our readouts of proliferation and cytokine production.

Differential expression of Vβ5 and Vβ8 on T cells isolated from P14 × OT-I dual transgenic mice results in limited responsiveness

Another means of reducing TCR expression is through the generation of T cells expressing two TCRs. This can be accomplished through the breeding of two TCR transgenic mice to yield mice bearing T cells that express both TCRs. As a result of the finite number of TCRs that can be expressed on the T cell surface, both TCRs cannot be present at parental levels. In this study, P14 TCR transgenic mice were bred to OT-I TCR transgenic mice to generate F1 progeny bearing dual receptor T cells (Fig. 6). Flow cytometric analyses indicated that while $CD8^+$ T cells from P14 × OT-I F1 mice expressed nearly equivalent levels of Vβ5 as those isolated from parental OT-I mice, the Vβ8 TCR was expressed at ~15% of parental P14 levels (Fig. 6, *A*, and *B*, respectively). This data revealed that the OT-I and P14 receptors represented ~85% and 15% of the TCRs at the cell surface, respectively (Fig. 6). Tetramer staining of the OT-I TCR was similar to that of the single transgenic. However, tetramer staining of the P14 receptor was undetectable, which is to be expected based on Fig. 1, as 15% of the receptors would be ~3000 P14 TCR. Thus, the conserved expression of the OT-I TCR and the reduced expression of the P14 TCR are significant features of this model.

Despite this skewing of receptor expression, $CD8^+$ T cells isolated from P14 × OT-I mice responded to both Ags in a dose-dependent manner as determined by [^{3}H]thymidine incorporation and intracellular staining for IFN-γ production (Fig. 7 and data not shown). Notably, although expression of the P14 TCR on P14 × OT-I T cells was reduced by ~85% relative to parental T cells, these cells remained remarkably sensitive to stimulation with the agonist gp33–41 as demonstrated by the similar dose-response curve exhibited by both single and dual receptor T cells (Fig. 6*C*, *left panel*). However, no proliferative response was observed when P14 × OT-I T cells were stimulated with the weak agonist, rDBM (Fig. 6*C*, *right panel*). Strikingly, these data indicate that while the response to agonist remains intact,

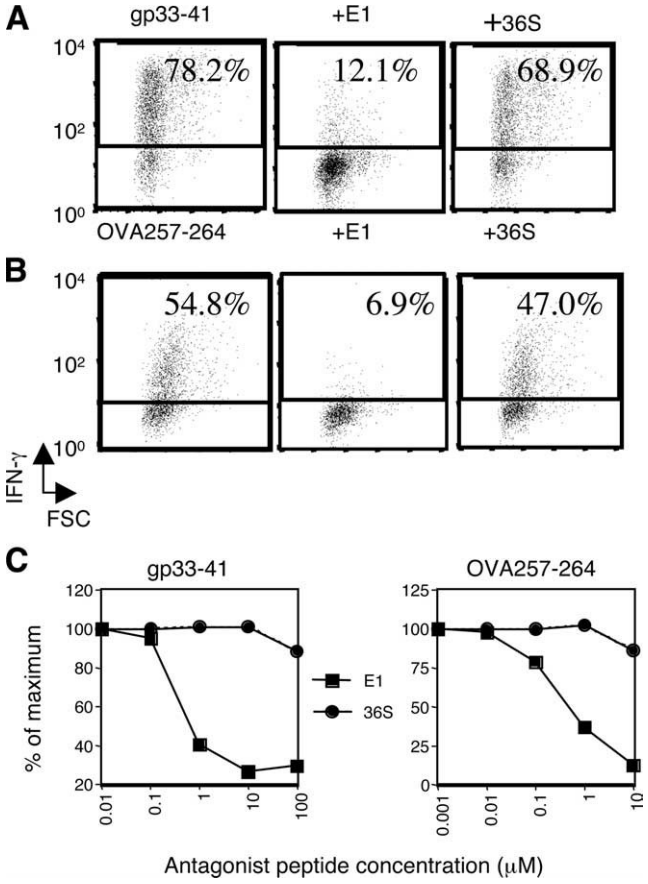

FIGURE 7. The OT-I antagonist (E1) but not the P14 antagonist (36S) potently inhibited the production of IFN-γ by P14 × OT-I dual receptor T cells through either TCR. P14 × OT-I T cells were cultured for 4 days with gp33–41, restimulated with either 1 nM gp33–41 (*A*, *left panel*), or 1 nM OVA257–264 (*B*, *left panel*) for 6 h and stained for the presence of intracellular IFN-γ. The addition of 10 μM E1 (*A* and *B*, *center panels*) but not 10 μM 36S (*A* and *B*, *right panels*) dramatically inhibited the responses of dual receptor T cells to either Ag. E1-mediated inhibition of both gp33–41 (*C*, *left panel*) and OVA257–264 (*C*, *right panel*) was dose dependent.

the reduced P14 TCR expression of P14 × OT-I T cells renders these cells at least 10,000-fold less sensitive than parental P14 T cells to stimulation with the weak agonist.

Cross-talk antagonism of IFN-γ production by $CD8^+$ P14 × OT-I dual receptor T cells

Dual TCR models have been used by a number of groups in an attempt to elucidate the mechanism of T cell antagonism. In such models, the presence of two independent TCR species minimizes or eliminates competition between agonist and antagonist pMHC complexes for available TCRs. Therefore, the ability of antagonist ligands for one TCR to inhibit the T cell responses induced via the second TCR, termed "cross-talk antagonism," would suggest that antagonists function either through the sequestration of intracellular molecules or the production of a negative signal. In these experiments, we examined whether antagonist peptides could inhibit IFN-γ production through either conventional or cross-talk antagonism (Fig. 7). This assay allowed us to assess the inhibition of T cell activation on a per cell basis. Antagonists for the P14 and OT-I TCRs were tested for their ability to inhibit P14 × OT-I T cell responses induced by either the P14 agonist LCMV gp33–41 or the OT-I agonist OVA257–264 (Fig. 7). The OT-I antagonist E1 potently reduced the number of cells producing IFN-γ in response

to OVA257–264 (>85%; Fig. 7*B*, compare *left* and *center panels*; Fig. 7*C*, *right panel*). Furthermore, the antagonist for the OT-I TCR (E1) reduced the response of P14 × OT-I T cells to the P14 agonist (gp33–41) by >80% (Fig. *A*, compare *left* and *center panels*; Fig. 7*C*, *left panel*). However, the P14 antagonist 36S was unable to significantly inhibit the agonist-induced responses provoked through either the P14 TCR or the dominantly expressed OT-I TCR (Fig. 7*C*). Therefore, while the 36S antagonist for P14 potently inhibited both the proliferation (Figs. 2*C* and 4*A*) and the production of IFN-γ (data not shown) by P14 single TCR-expressing T cells, minimal inhibition (~20%) of agonist-induced response in P14 × OT-I dual receptor T cells was observed (Fig. 7*C*) in concordance with the results from a previous study (29).

Discussion

According to the spare receptor theory, agonist ligands achieve maximal responses by engaging far fewer receptors than are required for the induction of responses by less potent ligands (19). Thus, receptor density represents an important mechanism for regulating cellular and, subsequently, tissue responsiveness. Our previous studies have shown that a spare receptor model accurately describes the responses of $CD4^+$ T cells to weak agonist peptides typified by altered peptide ligands or autoimmune Ags (17, 30). In this study we extend our original observations and demonstrate that this model also describes the responses of $CD8^+$ T cells to agonist and weak agonist as well as antagonist ligands. For both the P14 and OT-I systems, reducing the number of available TCRs drastically diminished both weak agonist and antagonist peptide potency while leaving responses to agonist ligands relatively unaffected (Figs. 2 and 3). It is possible that the antagonist peptides used in these experiments vary in potency. However, the data we have presented demonstrate a similar ability of E1 and 36S to antagonize their respective T cells (Figs. 2 and 3), allowing us to compare these two transgenic systems. These results suggest that high TCR density allows responsiveness to a wide variety of ligands. This ability to respond to suboptimal ligands has been shown to play a critical role in thymic selection (31, 32), and antagonist ligands have been shown to function as surrogate self-ligands in the promotion of the survival of naive $CD8^+$ T cells (33). The finding that T cell responses to weak ligands are absolutely dependent on TCR density implies that the ability to perceive self-ligands and subsequently survive is also dependent on TCR density. This requirement may represent an important selective pressure in the maintenance of high TCR density. However, this ability to respond to a variety of ligands due to the existence of a receptor reserve may also contribute to T cell cross-reactivity (34).

The mechanism by which antagonist peptides inhibit T cell activation remains incompletely understood, although commonly proposed mechanisms include competition for available TCRs (4, 35, 36), the sequestration of intracellular signaling intermediates (37), and the production of a qualitatively unique negative signal by TCRs engaged by antagonist ligands (38, 39). Dual TCR models have been used by a number of groups in an attempt to elucidate the mechanism of T cell antagonism, as there is minimal competition for TCRs in such dual receptor systems (26, 35, 36, 39). Initial studies using $CD8^+$ T cells failed to demonstrate cross-talk antagonism (29, 36), but another study and the data presented here report the opposite findings (29). In light of our current results, the establishment of TCR density as a critical parameter governing the efficacy of antagonist ligands provides new insights regarding the interpretation of these results from dual receptor models. In the initial studies in $CD8^+$ dual TCR models where cross-talk antagonism was not observed, the T cells displayed similar albeit equally reduced TCR expression levels (36). Our current data and our previous $CD4^+$ dual receptor model found substantial skewing of TCR expression such that one receptor was represented at near parental levels (26). Of interest, only antagonist ligands for the dominantly expressed receptor were capable of inhibiting T cell responses in *trans* (26).

The observation that the spare receptor theory accurately describes the action of TCR antagonists also provides correlative evidence for their ability to signal. Proponents of the competition model of TCR antagonism have suggested that, by virtue of their rapid dissociation rates, antagonist peptides interact with a large number of TCRs and thus merely prevent agonist complexes from triggering the number of TCRs required for activation (40). As such, the competition model predicts that as the number of available TCRs approaches the number required to support activation (~1500), antagonist pMHC complexes would need to sequester fewer TCRs to inhibit activation. Thus, whether considering either the total TCR population or the fraction of this population localized to the T cell:APC contact zone, a strict competition model predicts that antagonist peptides would be most effective at inhibiting the responses of Ag-specific T cells at low TCR density. Therefore, our observation that antagonist peptide efficacy is directly proportional to TCR density is inconsistent with the competition model of TCR antagonism. In contrast, if antagonist peptides function through the activation of intracellular signaling molecules, then the spare receptor theory predicts that sufficient TCR density is critical for the ability of antagonist ligands to produce a negative signal. The mediation of antagonism by a negative signal has been supported by the observation that the Src homology domain containing protein tyrosine phosphatase (SHP-1) is activated during T cell antagonism in $CD4^+$ T cells and is required for effective inhibition of T cell activation by antagonist pMHC ligands (41, 42).

Our data from both the single and dual TCR transgenic systems highlight the significance of TCR number in governing the potency of weak agonist and antagonist peptides. It is important that our observations were consistent in both model systems, as this limits the potential alternative explanations for our findings. The initial findings were made using Vα-specific Abs as a means to limit TCR access to pMHC Ag and were based on studies where mAbs have proven to be potent and effective competitors for binding at the cellular and purified protein levels (18, 43, 44). The high affinity interaction between TCR and Ab makes it unlikely that our data can be explained by the inability of the weak agonist and antagonist pMHC complexes to compete as effectively as agonist for TCR. The dual TCR system also eliminates this possibility. Similarly, the Ab treatment of the cells could alter the antagonists' effects by altering signal transduction pathways, TCR dimerization, or some other stereological aspect of TCR:pMHC interaction. Again, these potentially confounding effects were mitigated by using the dual TCR system. The dual TCR system alone may allow for alternative interpretations in that the presence of two different TCRs could affect engagement or clustering in some manner. However, the consistent inhibition of responses to weak ligands that we have observed in these complementary approaches suggests that the reduction of TCR and the spare receptor model of T cell activation are the most likely explanations for the data presented here.

Peptide:MHC tetramer staining was included to demonstrate specificity of the anti-Vα2 Ab in altering TCR density, but it also revealed several features related to Ag recognition by T cells. For example, fewer TCRs were needed to detect functional T cell responses (<800) as compared with tetramer staining (several thousand; Fig. 1 as compared with Figs. 2 and 3). This would suggest that although MHC tetramer staining is extremely valuable for assessing levels of response, it may also identify fewer Ag reactive

cells than are actually present if the T cells are of sufficiently low affinity or express low numbers of Ag-reactive TCRs. We made use of T cells with multiple TCRs to confirm the minimal TCR density required for response to weak ligands, but dual receptor cells can avoid allelic exclusion in the thymus and are normally found in the periphery (45). Thus, T cells with low specific density could contribute to a functional T cell response and yet be undetectable by a specific peptide:MHC tetramer.

A recent study demonstrated that the proliferation, but not the cytolytic function, of $CD8^+$ T cells is sensitive to cross-talk antagonism (29). In this study, we report that antagonist ligands for the OT-I TCR effectively inhibit IFN-γ production induced by the P14 agonist in the P14 $\times$ OT-I dual TCR model. Although Yang et al. proposed that antagonist ligands may inhibit cytolysis through a different mechanism than proliferation, another possible explanation is that both proliferation and cytokine production require de novo mRNA and protein synthesis (46, 47) and, therefore, the antagonist ligand may have a greater opportunity to interrupt the signaling cascade. In contrast, cytolysis results from the release of preformed granules (48), potentially rendering the process more difficult to inhibit. Although the dependence of antagonist peptide efficacy on TCR density supports the ability of antagonist ligands to induce a negative signal, an answer to the question of whether distinct mechanisms are active in the inhibition of different effector functions will require further investigation.

Disclosures

The authors have no financial conflict of interest.

References

1. Evavold, B. D., and P. M. Allen. 1991. Separation of IL-4 production from Th cell proliferation by an altered T cell receptor ligand. *Science* 252: 1308–1310.
2. Evavold, B. D., S. G. Williams, J. S. Chen, and P. M. Allen. 1991. T cell inducing determinants contain a hierarchy of residues contacting the T cell receptor. *Semin. Immunol.* 3: 225–229.
3. Evavold, B. D., J. Sloan-Lancaster, and P. M. Allen. 1993. Tickling the TCR: selective T-cell functions stimulated by altered peptide ligands. *Immunol. Today* 14: 602–609.
4. De Magistris, M. T., J. Alexander, M. Coggeshall, A. Altman, F. C. Gaeta, H. M. Grey, and A. Sette. 1992. Antigen analog-major histocompatibility complexes act as antagonists of the T cell receptor. *Cell* 68: 625–634.
5. Kersh, G. J., E. N. Kersh, D. H. Fremont, and P. M. Allen. 1998. High- and low-potency ligands with similar affinities for the TCR: the importance of kinetics in TCR signaling. *Immunity* 9: 817–826.
6. Alam, S. M., P. J. Travers, J. L. Wung, W. Nasholds, S. Redpath, S. C. Jameson, and N. R. Gascoigne. 1996. T-cell-receptor affinity and thymocyte positive selection [see comments]. *Nature* 381: 616–620.
7. Matsui, K., J. J. Boniface, P. Steffner, P. A. Reay, and M. M. Davis. 1994. Kinetics of T-cell receptor binding to peptide/I-Ek complexes: correlation of the dissociation rate with T-cell responsiveness. *Proc. Natl. Acad. Sci. USA* 91: 12862–12866.
8. Yachi, P. P., J. Ampudia, N. R. Gascoigne, and T. Zal. 2005. Nonstimulatory peptides contribute to antigen-induced CD8-T cell receptor interaction at the immunological synapse. *Nat. Immunol.* 6: 785–792.
9. Krogsgaard, M., and M. M. Davis. 2005. How T cells 'see' antigen. *Nat. Immunol.* 6: 239–245.
10. McKeithan, T. W. 1995. Kinetic proofreading in T-cell receptor signal transduction. *Proc. Natl. Acad. Sci. USA* 92: 5042–5046.
11. Rabinowitz, J. D., C. Beeson, D. S. Lyons, M. M. Davis, and H. M. McConnell. 1996. Kinetic discrimination in T-cell activation. *Proc. Natl. Acad. Sci. USA* 93: 1401–1405.
12. Valitutti, S., and A. Lanzavecchia. 1995. A serial triggering model of TcR activation. *The Immunologist* 3: 122–124.
13. Valitutti, S., S. Muller, M. Cella, E. Padovan, and A. Lanzavecchia. 1995. Serial triggering of many T-cell receptors by a few peptide-MHC complexes. *Nature* 375: 148–151.
14. Grakoui, A., S. K. Bromley, C. Sumen, M. M. Davis, A. S. Shaw, P. M. Allen, and M. L. Dustin. 1999. The immunological synapse: a molecular machine controlling T cell activation. *Science* 285: 221–227.
15. Labrecque, N., L. S. Whitfield, R. Obst, C. Waltzinger, C. Benoist, and D. Mathis. 2001. How much TCR does a T cell need? *Immunity* 15: 71–82.
16. Viola, A., and A. Lanzavecchia. 1996. T cell activation determined by T cell receptor number and tunable thresholds. *Science* 273: 104–106.
17. McNeil, L. K., and B. D. Evavold. 2002. Dissociation of peripheral T cell responses from thymocyte negative selection by weak agonists supports a spare receptor model of T cell activation. *Proc. Natl. Acad. Sci. USA* 99: 4520–4525.
18. McNeil, L. K., and B. D. Evavold. 2003. TCR reserve: a novel principle of CD4 T cell activation by weak ligands. *J. Immunol.* 170: 1224–1230.
19. Stephenson, R. P. 1956. A modification of receptor theory. *Br. J. Pharmacol.* 11: 379–393.
20. Hogquist, K. A., S. C. Jameson, and M. J. Bevan. 1994. The ligand for positive selection of T lymphocytes in the thymus. *Curr. Opin. Immunol.* 6: 273–278.
21. Pircher, H., K. Brduscha, U. Steinhoff, M. Kasai, T. Mizuochi, R. M. Zinkernagel, H. Hengartner, B. Kyewski, and K. P. Muller. 1993. Tolerance induction by clonal deletion of $CD4^+8^+$ thymocytes in vitro does not require dedicated antigen-presenting cells. *Eur. J. Immunol.* 23: 669–674.
22. Hogquist, K. A., A. J. Tomlinson, W. C. Kieper, M. A. McGargill, M. C. Hart, S. Naylor, and S. C. Jameson. 1997. Identification of a naturally occurring ligand for thymic positive selection. *Immunity* 6: 389–399.
23. Jameson, S. C., F. R. Carbone, and M. J. Bevan. 1993. Clone-specific T cell receptor antagonists of major histocompatibility complex class I-restricted cytotoxic T cells. *J. Exp. Med.* 177: 1541–1550.
24. Bachmann, M. F., D. E. Speiser, A. Zakarian, and P. S. Ohashi. 1998. Inhibition of TCR triggering by a spectrum of altered peptide ligands suggests the mechanism for TCR antagonism. *Eur. J. Immunol.* 28: 3110–3119.
25. Ohteki, T., A. Hessel, M. F. Bachmann, A. Zakarian, E. Sebzda, M. S. Tsao, K. McKall-Faienza, B. Odermatt, and P. S. Ohashi. 1999. Identification of a cross-reactive self ligand in virus-mediated autoimmunity. *Eur. J. Immunol.* 29: 2886–2896.
26. Robertson, J. M., and B. D. Evavold. 1999. Cutting edge: dueling TCRs: peptide antagonism of $CD4^+$ T cells with dual antigen specificities. *J. Immunol.* 163: 1750–1754.
27. Serke, S., A. van Lessen, and D. Huhn. 1998. Quantitative fluorescence flow cytometry: a comparison of the three techniques for direct and indirect immunofluorescence. *Cytometry* 33: 179–187.
28. Huang, J., L. J. Edwards, B. D. Evavold, and C. Zhu. 2007. Kinetics of MHC-CD8 interaction at the T cell membrane. *J. Immunol.* 179: 7653–7662.
29. Yang, W., and H. M. Grey. 2003. Study of the mechanism of TCR antagonism using dual-TCR-expressing T cells. *J. Immunol.* 170: 4532–4538.
30. Wasserman, H., and B. D. Evavold. 2008. Induction of anergy by antibody blockade of TCR in MOG-specific cells. *J. Immunol.* 180: 7259–7264.
31. Hogquist, K. A., S. C. Jameson, W. R. Heath, J. L. Howard, M. J. Bevan, and F. R. Carbone. 1994. T cell receptor antagonist peptides induce positive selection. *Cell* 76: 17–27.
32. Jameson, S. C., K. A. Hogquist, and M. J. Bevan. 1994. Specificity and flexibility in thymic selection. *Nature* 369: 750–752.
33. Goldrath, A. W., and M. J. Bevan. 1999. Low-affinity ligands for the TCR drive proliferation of mature $CD8^+$ T cells in lymphopenic hosts. *Immunity* 11: 183–190.
34. Ford, M. L., and B. D. Evavold. 2003. Regulation of polyclonal T cell responses by an MHC anchor-substituted variant of myelin oligodendrocyte glycoprotein 35–55. *J. Immunol.* 171: 1247–1254.
35. Stotz, S. H., L. Bolliger, F. R. Carbone, and E. Palmer. 1999. T cell receptor (TCR) antagonism without a negative signal: evidence from T cell hybridomas expressing two independent TCRs. *J. Exp. Med.* 189: 253–264.
36. Daniels, M. A., S. L. Schober, K. A. Hogquist, and S. C. Jameson. 1999. Cutting edge: A test of the dominant negative signal model for TCR antagonism. *J. Immunol.* 162: 3761–3764.
37. Torigoe, C., J. K. Inman, and H. Metzger. 1998. An unusual mechanism for ligand antagonism. *Science* 281: 568–572.
38. Sykulev, Y., Y. Vugmeyster, A. Brunmark, H. L. Ploegh, and H. N. Eisen. 1998. Peptide antagonism and T cell receptor interactions with peptide-MHC complexes. *Immunity* 9: 475–483.
39. Dittel, B. N., I. Stefanova, R. N. Germain, and C. A. Janeway, Jr. 1999. Cross-antagonism of a T cell clone expressing two distinct T cell receptors. *Immunity* 11: 289–298.
40. Viola, A., S. Linkert, and A. Lanzavecchia. 1997. A T cell receptor (TCR) antagonist competitively inhibits serial TCR triggering by low-affinity ligands, but does not affect triggering by high-affinity anti-CD3 antibodies. *Eur. J. Immunol.* 27: 3080–3083.
41. Stefanova, I., B. Hemmer, M. Vergelli, R. Martin, W. E. Biddison, and R. N. Germain. 2003. TCR ligand discrimination is enforced by competing ERK positive and SHP-1 negative feedback pathways. *Nat. Immunol.* 4: 248–254.
42. Kilgore, N. E., J. D. Carter, U. Lorenz, and B. D. Evavold. 2003. Cutting edge: dependence of TCR antagonism on Src homology 2 domain-containing protein tyrosine phosphatase activity. *J. Immunol.* 170: 4891–4895.
43. Matsui, K., J. J. Boniface, P. A. Reay, H. Schild, and B. Fazekas de St. Groth. 1991. Low affinity interaction of peptide-MHC complexes with T cell receptors. *Science* 254: 1788–1791.
44. Webb, S., and J. Sprent. 1987. Downregulation of T cell responses by antibodies to the T cell receptor. *J. Exp. Med.* 165: 584–589.
45. Padovan, E., G. Casorati, P. Dellabona, S. Meyer, M. Brockhaus, and A. Lanzavecchia. 1993. Expression of two T cell receptor α chains: dual receptor T cells. *Science* 262: 422–424.
46. Yang, J., T. L. Murphy, W. Ouyang, and K. M. Murphy. 1999. Induction of interferon-γ production in Th1 $CD4^+$ T cells: evidence for two distinct pathways for promoter activation. *Eur. J. Immunol.* 29: 548–555.
47. Germain, R. N., and I. Stefanova. 1999. The dynamics of T cell receptor signaling: complex orchestration and the key roles of tempo and cooperation. *Annu. Rev. Immunol.* 17: 467–522.
48. Esser, M. T., D. M. Haverstick, C. L. Fuller, C. A. Gullo, and V. L. Braciale. 1998. Ca^{2+} signaling modulates cytolytic T lymphocyte effector functions. *J. Exp. Med.* 187: 1057–1067.

Appendix 13

Waibler Z, Sender LY, Merten C, Hartig R, Kliche S, Gunzer M, **Reichardt P**, Kalinke U, Schraven B. Signaling signatures and functional properties of anti-human CD28 superagonistic antibodies.
PLoS ONE. 2008;3:e1708.

IF: 4.1

OPEN ACCESS Freely available online

PLoS one

Signaling Signatures and Functional Properties of Anti-Human CD28 Superagonistic Antibodies

Zoe Waibler[1☯], Linda Y. Sender[1☯], Camilla Merten[2], Roland Hartig[2], Stefanie Kliche[2], Matthias Gunzer[2], Peter Reichardt[2], Ulrich Kalinke[1*], Burkhart Schraven[2*]

1 Paul-Ehrlich-Institut, Langen, Germany, **2** Institute of Molecular and Clinical Immunology, Otto-von-Guericke-University, Magdeburg, Germany

Abstract

Superagonistic CD28 antibodies (CD28SAs) activate T lymphocytes without concomitant perturbation of the TCR/CD3-complex. In rodents these reagents induce the preferential expansion of regulatory T cells and can be used for the treatment of autoimmune diseases. Unexpectedly, the humanized CD28 superagonist TGN1412 caused severe and life threatening adverse effects during a recently conducted phase I clinical trail. The underlying molecular mechanisms are as yet unclear. We show that TGN1412 as well as the commercially available CD28 superagonist ANC28.1 induce a delayed but extremely sustained calcium response in human naïve and memory $CD4^+$ T cells but not in cynomolgus T lymphocytes. The sustained Ca^{++}-signal was associated with the activation of multiple intracellular signaling pathways and together these events culminated in the rapid de novo synthesis of high amounts of pro-inflammatory cytokines, most notably IFN-γ and TNF-α. Importantly, sustained transmembranous calcium flux, activation of Src-kinases as well as activation of PI3K were found to be absolutely required for CD28SA-mediated production of IFN-γ and IL-2. Collectively, our data suggest a molecular basis for the severe side effects caused by TGN1412 and impinge upon the relevance of non-human primates as preclinical models for reagents that are supposed to modify the function of human T cells.

Citation: Waibler Z, Sender LY, Merten C, Hartig R, Kliche S, et al (2008) Signaling Signatures and Functional Properties of Anti-Human CD28 Superagonistic Antibodies. PLoS ONE 3(3): e1708. doi:10.1371/journal.pone.0001708

Editor: Derya Unutmaz, New York University School of Medicine, United States of America

Received December 19, 2007; **Accepted** January 24, 2008; **Published** March 5, 2008

Funding: This work was supported by a grant from the German Research Foundation (DFG) to B.S. and to U.K. (SFB432, B15). The funders had no role in study design, data collection and analysis, decision to publish, or preparation of the manuscript.

Competing Interests: The authors have declared that no competing interests exist.

* E-mail: kalul@pei.de (UK); Burkhart.Schraven@med.ovgu.de (BS)

☯ These authors contributed equally to this work.

Introduction

According to the currently accepted model of T cell activation, two signals are required to fully activate resting naïve T lymphocytes. The primary signal is provided by the clonotypic T cell receptor (TCR) after recognition of antigen/MHC-complexes on the surface of antigen presenting cells. However, this signal by itself is not capable of fully activating T lymphocytes but has to be complemented by secondary signals which emerge from stimulation of so called co-stimulatory molecules [1,2]. In mouse and human T cells the dimeric transmembrane glycoprotein CD28 represents the most important co-stimulatory molecule. Under physiological conditions CD28-derived signals alone are not capable of inducing T cell activation, whereas simultaneous engagement of the TCR and CD28 (e.g. by its natural ligands CD80 and CD86 which are expressed on mature antigen presenting cells) leads to activation of resting T lymphocytes (reviewed in [3,4]).

Monoclonal antibodies (mAbs) directed to the extracellular domain of CD28 have been widely used during the last two decades to analyze CD28-mediated signaling pathways and to assess how CD28 facilitates activation and differentiation of murine, rat, and human T lymphocytes. Most recently a particular group of CD28 mAbs has been identified which is capable of activating T cells without the need for additional engagement of the TCR/CD3-complex [5–7]. These antibodies have collectively been termed mitogenic CD28 antibodies or CD28 superagonists. While conventional CD28 mAbs bind CD28 close to the binding site of the natural CD28 ligands, CD80 and CD86, CD28 superagonists bind to a laterally exposed loop within the extracellular domain of CD28 [8]. The particular binding topology of superagonistic CD28 antibodies (CD28SAs) might be responsible for their mitogenic potential.

A number of detailed biochemical studies in rat and mice addressed the question how CD28SA-mediated signaling is organized on the molecular level [5,6,8–13]. The emerged data can be summarized as follows: (i) the signaling capacity of CD28SAs depends on the expression of a functional TCR/CD3/ζ-complex; (ii) CD28SA-stimulation does not lead to detectable phosphorylation/activation of the TCRζ chain or the proximal TCR-effector molecules ZAP70 and LAT, but still induces phosphorylation of the adapter protein SLP76 and the nucleotide exchange factor Vav (likely via the Tec-family protein tyrosine kinases Itk or Rlk); (iii) CD28SA-stimulation activates PLCγ1 (phospholipase Cγ1) and induces calcium flux, and (iv) CD28SA-stimulation activates PKC θ (protein kinase C θ) as well as the transcription factors NF-κB, NF-ATc1, and GATA-3.

Studies in rat and mice have also shown that CD28 superagonists preferentially induce the expansion of regulatory T cells and therefore suggested that these antibodies can be used for the treatment of autoimmune diseases such as experimental autoimmune encephalomyelitis [13–20]. Based on the promising data in

rodents, it was hypothesized that CD28SAs might also be applicable for the treatment of human autoimmune disorders. However, when applied to healthy volunteers during a phase I clinical trial performed on March 13th, 2006 in London, UK, the humanized CD28 superagonist TGN1412 showed unexpected serious adverse events. These were associated with the induction of a cytokine storm, i.e. the release of high amounts of pro-inflammatory cytokines, most notably TNF-α and IFN-γ [21].

The molecular basis for the unexpected response upon treatment with the CD28 superagonist TGN1412 is as yet unclear. To shed light on this question, we here addressed membrane proximal signaling events in human T cells upon stimulation with two different CD28 superagonists. We show that, despite complete conservation of the CD28 extracellular and cytoplasmic domains, TGN1412 and a commercially available CD28SA, ANC28.1/5D10, induced a delayed but extremely sustained calcium response in human, but not in cynomolgus and rhesus monkey T cells. Biochemical analyses further revealed that both CD28SAs strongly activated a number of major T cell signaling pathways in human T cells. Together these signals culminate in the in vitro production of high amounts of IFN-γ, TNF-α, and other pro-inflammatory cytokines.

Our experiments contribute to the understanding of the particular pharmacologic properties of human CD28 superagonists and further suggest that currently available animal models do not necessarily correctly reproduce critical signaling mechanisms of human T cells.

Results

Mitogenicity of anti-human CD28 superagonist ANC28.1

By definition, CD28 superagonists induce polyclonal T cell activation in vitro without the need of concomitant stimulation of the TCR/CD3 complex [5,7]. We assessed the mitogenicity of a commercially available CD28 superagonist (ANC28.1). In contrast to stimulation of human T cells with the conventional CD28 antibody 248.23.2 [22], ANC28.1 was able to induce T cell proliferation without additional stimulation via CD3 (Fig. 1A), thus fulfilling the criteria of a CD28 superagonist. Note that ANC28.1 still exerted costimulatory properties as it strongly augmented the proliferative response of T cells stimulated with CD3 antibody (Fig. 1A).

Previously, several groups have assessed the signaling events induced by anti-rat or anti-mouse CD28 superagonistic antibodies [5,6,8,11–13]. In contrast, only few data are available regarding the signaling properties of anti-human CD28 superagonists. To explore the signaling properties of ANC28.1, phosphospecific western blots were performed (Fig. 1B). The transmembrane adapter protein LAT (Linker for Activation of T cells) represents a 35 kDa polypeptide that is essential for T cell activation [23,24]. Upon TCR-mediated phosphorylation of four critical tyrosine residues, LAT assembles a multi-component signaling complex consisting of the cytosolic adapter proteins Gads (Grb2-related adaptor downstream of Shc) and SLP76 (SH2 domain containing leucocyte specific phosphoprotein of 76 kDa), the Tec-family protein tyrosine kinase Itk (Inducible T-cell kinase), and PLCγ1 (Phospholipase Cγ1; reviewed in [25]). This complex is responsible for the rise in intracellular calcium upon stimulation of the TCR. We first employed a phosphospecific antibody that detects one of the major tyrosine phosphorylation sites within LAT, Y^{171}. As shown in Fig. 1B, upper panel, ANC28.1 induced a weak but clearly detectable phosphorylation of Y^{171}. Similar data were obtained when the phosphorylation status of Y^{136}, one of several additional phosphorylation sites of LAT, was assessed (data not shown). Hence, in contrast to rat T cells, anti-human CD28

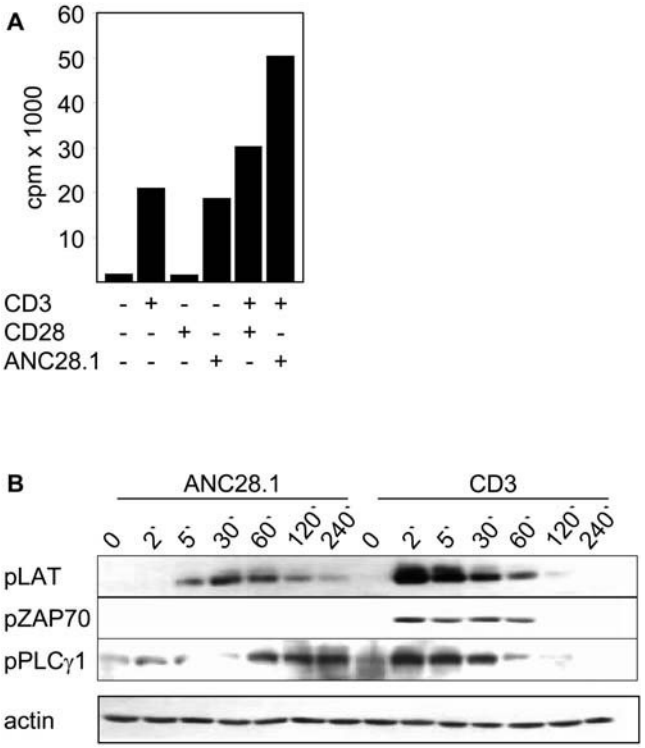

Figure 1. The CD28 superagonist ANC28.1 induces polyclonal T cell activation in vitro and leads to ZAP70 independent phosphorylation of LAT and PLCγ1. (A) 5×10^4 freshly prepared human T cells per well were seeded in 96-well plates and treated with the indicated combinations of antibodies or were incubated in medium as a control. 72 hours after stimulation, cultures were pulsed with ^{3}H-thymidine for 6 hours and harvested thereafter. Note that ANC28.1 only induces polyclonal T cell proliferation when applied in soluble form (in this case 10 μg/ml of soluble ANC28.1 were crosslinked in solution with 20 μg/ml of polyclonal goat-anti-mouse antiserum). All other stimulations (including stimulation of T cells with CD3ε mAb and ANC28.1; very right bar in Fig. 1A) were performed in wells that were pre-coated with polyclonal goat anti-mouse antiserum. Shown data are representative for at least 6 independently performed experiments. **(B)** 1×10^6 freshly prepared human T cells/lane were stimulated in solution with 10 μg/ml ANC28.1 followed by crosslinking with 20 μg/ml polyclonal goat anti-mouse antiserum for the indicated periods of time. As a control, cells were activated with a 1:50 v/v dilution of ascites fluid of CD3ε mAb MEM92 (IgM) or were left untreated. Cell lysates were processed for western blotting using the indicated phosphospecific antibodies (Y^{319} of ZAP70, Y^{171} of LAT, and Y^{783} of PLCγ1). Western blotting using an anti-actin antibody was performed as loading control.
doi:10.1371/journal.pone.0001708.g001

superagonist ANC28.1 induced a weak but clearly detectable phosphorylation of LAT. Interestingly and in line with previous data obtained in human and rat T cells [8,12], ANC28.1 stimulation did not result in a detectable phosphorylation (a sign for activation) of the protein tyrosine kinase ZAP70 which is believed to be primarily responsible for LAT phosphorylation upon TCR-stimulation (Fig. 1B, middle panel).

Upon engagement of the TCR/CD3-complex, phosphorylated LAT facilitates the activation of PLCγ1 which in turn generates the second messenger molecules IP3 (Inositol-tris-phosphate) and DAG (Diacyloglycerol; reviewed in [25]). To assess whether the moderate phosphorylation of LAT induced by ANC28.1 was sufficient to activate PLCγ1, we investigated the phosphorylation status of Y^{783} of PLCγ1 which correlates with its enzymatic activity [26]. The lower panel of Fig. 1B demonstrates that similar to rat T

cells [11] ANC28.1 induced a weaker and delayed but clearly sustained activation of PLCγ1 when compared to stimulation of human T cells with CD3 mAb. Thus, ANC28.1 induced a phosphorylation pattern that was different from the one obtained when human T cells were activated via CD3.

Sustained calcium flux upon T cell stimulation with superagonistic ANC28.1

The different activation kinetics of PLCγ1 produced by CD3 vs. CD28 superagonist ANC28.1 were translated into corresponding Ca^{++}-responses (Fig. 2A). Thus, independently of the concentrations used the CD3ε mAbs MEM92 (Fig. 2A, upper panel and Fig. S1) and OKT3 (Fig. S1 and [27]) induced a rapid, strong, and transient rise in intracellular Ca^{++} whereas the CD28SA-mediated Ca^{++}-signal started delayed and was of lower intensity (Fig. 2A, lower panel). Surprisingly, an extended analysis revealed that the CD28SA-mediated Ca^{++}-signal had an extremely sustained kinetics (Fig. 2A–2F) that lasted for more than six hours without significant decrease (Fig. S2).

The flow cytometric data obtained with Indo-1 labeled T cells were confirmed by live time video microscopy of T cells loaded with the calcium sensitive dye Fura2 (Movie S1 and Movie S2). Note that stimulation of the same cells with two conventional CD28 mAbs (CD28.2, Fig. 2A, middle panel and 248.23.2, data not shown) did not induce any detectable Ca^{++}-signal either with or without crosslinking.

Downmodulation of the TCR by treatment of T cells with the CD3ε mAb 2AD2A2 [28] (Fig. 2B, TCR^{dull} T cells) or pre-treatment of T cells with the Src-kinase inhibitor PP2 (Fig. 2C, lower panel) completely abrogated the ANC28.1-mediated calcium response, whereas pharmacologic inhibition of PI3K by Wortmannin had almost no effect (Fig. 2C, middle panel). Hence, similar to the situation in rat T cells [11,12] expression of a functional TCR and the activation of Src-kinases are required for ANC28.1-mediated calcium flux, whereas activation of PI3K appears to be dispensable. Further stimulation experiments in the presence of the calcium-chelator EGTA revealed that the ANC28.1-mediated Ca^{++}-signal required the presence of extracellular calcium ions (Fig. 2D).

Importantly, after inducing the expected peak (compare Fig. 2A, upper panel), addition of a conventional CD3 mAb to CD28SA-stimulated T cells abrogated the sustained Ca^{++}-flux (Fig. 2E). This might suggest that CD3 stimulation activates a negative feedback loop that is otherwise not activated upon CD28SA-stimulation.

We next assessed which T cell population preferentially responded to CD28SA stimulation. As expected from published work [29,30] ANC28.1 induced a stronger Ca^{++}-signal in $CD4^+$ T cells compared to $CD8^+$ T cells (Fig. 2F, left panels) whereas almost no differences were observed between $CD4^+/CD45RA^+$ naïve vs. $CD4^+/CD45RO^+$ memory T lymphocytes (Fig. 2F, right panels).

Induction of T cell proliferation and sustained calcium flux by CD28 superagonist TGN1412

To exclude the possibility that the induction of a sustained calcium signal was a particular property of ANC28.1, we repeated the experiment shown in Fig. 2A using the superagonistic CD28-specific antibody TGN1412. Fig. 3A depicts that TGN1412 generated a similarly shaped calcium signature as antibody ANC28.1 although it induced a calcium response only upon crosslinking. In addition, the magnitude of the calcium response elicited by TGN1412 was generally lower than that of ANC28.1. The weaker signaling properties of TGN1412 compared to the ANC28.1 were also reflected by a generally lower mitogenic potential of TGN1412 (Fig. 3B).

Intracellular signaling events induced by ANC28.1 and TGN1412

Given the sustained calcium response induced by ANC28.1 and TGN1412 we next investigated the consequences of CD28SA stimulation on downstream signaling events using reporter antibodies that monitor the activity of key signaling molecules involved in T cell activation. The first and third panels of Fig. 3C demonstrate that mAb ANC28.1 induced a delayed, strong, and sustained activation of all signaling events we investigated (Erk1/2, JNK, p38, AKT, GSK3β-1, NF-ATc1, and IκBα). Of note, ANC28.1 induced an even stronger activation of JNK, p38, AKT, and IκBα compared to CD3 mAb (second panel), whereas activation of Erk1/2 and dephosphorylation of the transcription factor NF-ATc1 were less pronounced. Similar results as for ANC28.1 were obtained when cells were stimulated with TGN1412 (Fig. 3C, right panel). However, in line with the lower magnitude of Ca^{++}-signaling and the weaker induction of a proliferative response, the phosphorylation signals induced by TGN1412 were generally less pronounced than those induced by ANC28.1. In multiple experiments, both ANC28.1 and TGN1412 induced a sharp initial rise of p38 phosphorylation which transiently dropped after 5 minutes of stimulation. The reason for this particular phosphorylation signature is yet unknown. Note that a conventional CD28 antibody only induced the known activation of the AKT and the JNK pathways (data not shown and [31]). In summary, both human CD28 superagonists not only produced a sustained induction of Ca^{++}-flux but also an activation of multiple intracellular signaling pathways.

In vitro cytokine production upon conventional vs. superagonistic human T cell stimulation

Within hours after administration of TGN1412 to six healthy individuals, clinical symptoms became apparent that were consistent with a massive cytokine storm mediated by the release of TH1- and TH2-specific cytokines [21]. In line with previous data obtained using TGN1412 [32] Fig. 4 shows that also in vitro human T cells respond upon ANC28.1- or TGN1412-mediated stimulation with a strong production of high amounts of the pro-inflammatory cytokines IFN-γ, TNF-α, IL-2, -4, -5, and anti-inflammatory IL-10. In all experiments we observed that at the chosen concentration, TGN1412 was a better inducer of IL-10 than ANC28.1. In contrast (and in agreement with the generally stronger signals elicited by ANC28.1), the amounts of TNF-α, IFN-γ, IL-2, and IL-4 were higher upon stimulation with ANC28.1. Nevertheless, at concentrations inducing similar levels of proliferation, both CD28 superagonists induced the synthesis of significantly higher levels of cytokines compared to conventional CD3/CD28 co-stimulation. Hence, the activation of multiple signaling pathways upon CD28SA-mediated T cell activation is translated into a corresponding in vitro cytokine response.

Fig. 5A depicts that similar to the situation in vivo, IFN-γ secretion occurred very rapidly after CD28SA stimulation. This allowed us to use pharmacological inhibitors to further dissect the molecular requirements leading to CD28SA-mediated IFN-γ production. Fig. 5B shows that incubation of T cells with cycloheximide, PP2, and Cyclosporin A (CSA) completely abrogated ANC28.1-mediated IFN-γ production. Hence, IFN-γ secretion upon CD28SA stimulation is due to de novo protein synthesis. Further, it requires activity of Src-kinases and involves the Calcineurin/NF-AT-mediated signaling pathway.

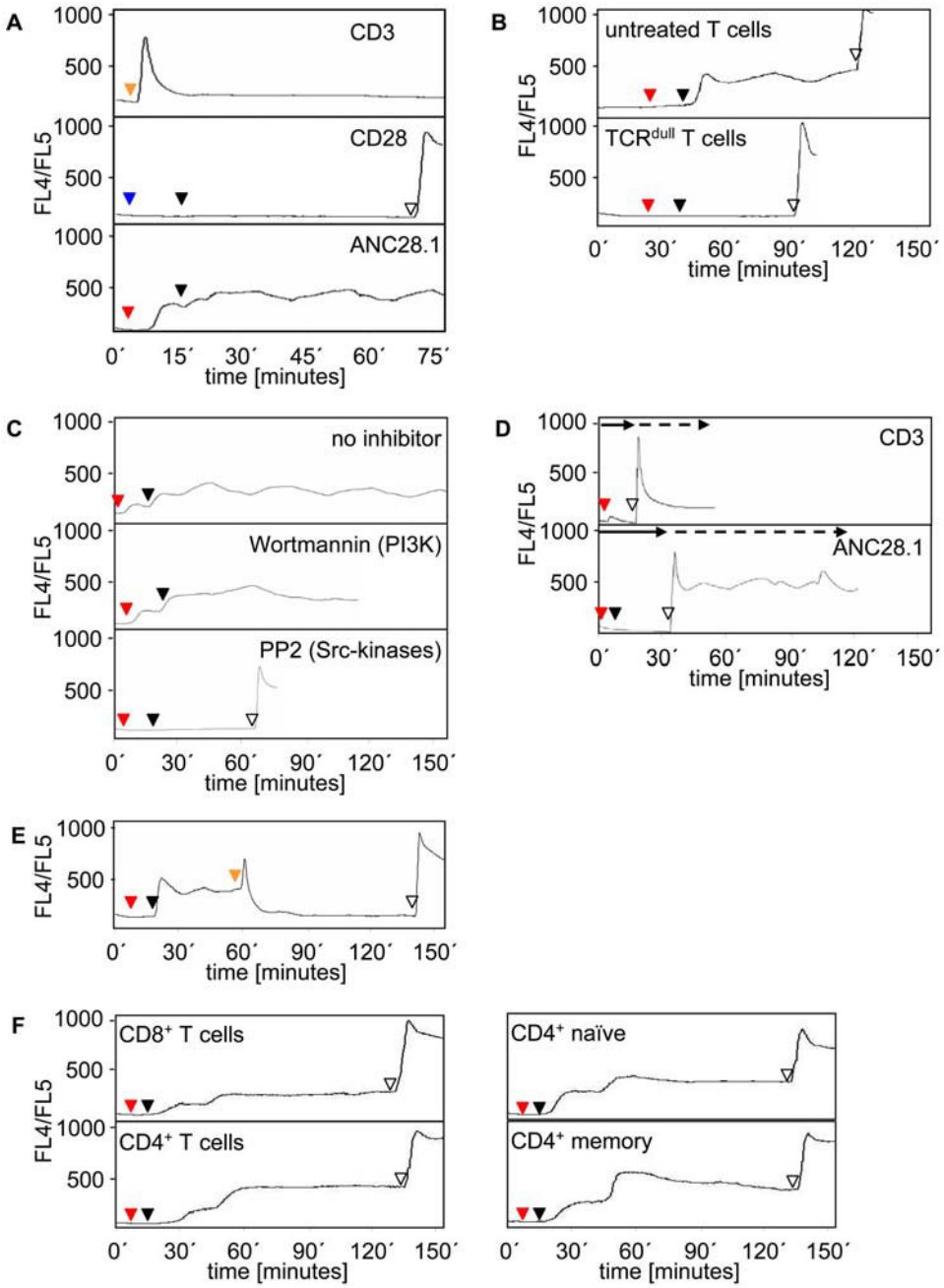

Figure 2. Induction of sustained calcium flux by human CD28 superagonistic antibody ANC28.1. (A) 1×10^6 freshly prepared Indo-1 loaded human T cells were stimulated with either a 1:50 v/v dilution of ascites fluid of CD3 mAb MEM92 (orange triangle), 10 μg/ml conventional CD28 mAb (CD28.2; blue triangle) followed by crosslinking with 20 μg/ml polyclonal goat anti-mouse antiserum (black triangle) or 10 μg/ml ANC28.1 (red triangle) followed by crosslinking with 20 μg/ml polyclonal goat anti-mouse antiserum (black triangle). Induction of the Ca^{++}-response was monitored for approximately 75 minutes. Note that using another conventional anti-CD28 mAb (248.23.2; with or without crosslinking) no Ca^{++}-flux was induced as well (data not shown). **(B)** Untreated (untreated T cells) or 2AD2A2 pre-treated (TCR^{dull} T cells) human T cells were stimulated with ANC28.1 (red triangles) and subsequently crosslinked (black triangles) as described in (A) and induction of the Ca^{++}-response was monitored for the indicated periods of time. To confirm proper loading of the cells with Indo-1, the Ca^{++}-ionophore Ionomycin (10 μg/ml) was added at the end of the experiment (unfilled triangle). **(C)** Cells were treated with ANC28.1 (red triangles) followed by crosslinking (black triangles) as described in (A) in the absence (no inhibitor) or presence of the PI3-kinase inhibitor Wortmannin (0.2 μM) or the Src-kinase inhibitor PP2 (10 μM). **(D)** CD3 (orange triangle) or ANC28.1 (red triangle) stimulation plus crosslinking (black triangle) was performed as described in (A) in culture medium that was supplemented with 1 mM EGTA to chelate extracellular Ca^{++} ions (solid arrow). At the indicated time points $CaCl_2$ was added at a final concentration of 2 mM (dashed arrow). **(E)** Cells were treated with ANC28.1 as described in Fig. 1A. Additionally, at about 1 h of Ca-flux, a 1:50 v/v dilution of ascites fluid of CD3 mAb MEM92 (orange triangle) was added. **(F)** $CD8^+$, $CD4^+$, $CD4^+/CD45RA^+$ naïve, and $CD4^+/CD45RO^+$ memory T lymphocytes were treated with ANC28.1 as described in (A) and induction of the Ca^{++}-response was monitored for approximately 150 minutes.
doi:10.1371/journal.pone.0001708.g002

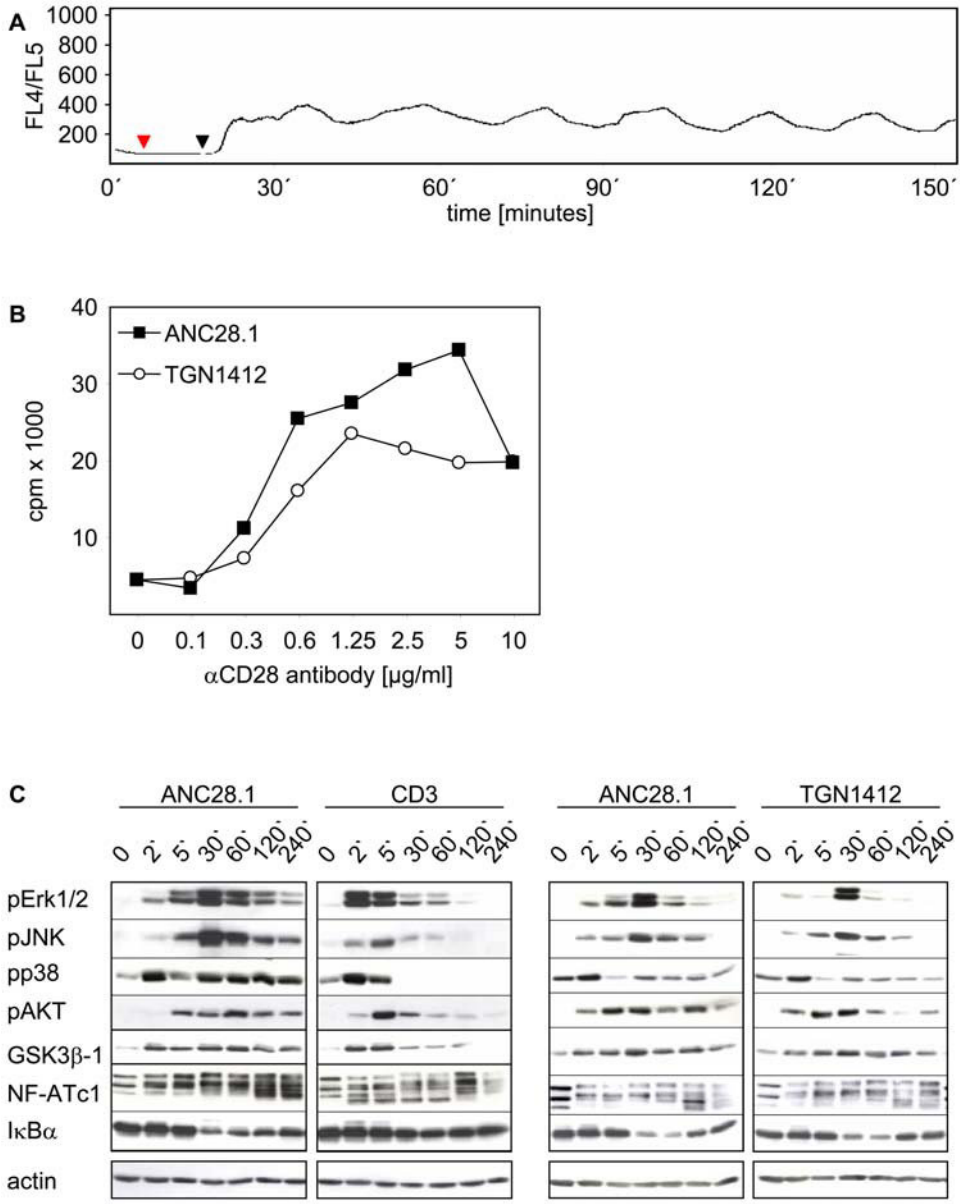

Figure 3. Sustained calcium flux, T cell proliferation, and T cell signaling upon TGN1412 treatment. (A) Freshly isolated human T cells were treated as described in Fig. 2 using the superagonistic CD28 specific mAb TGN1412 (10 μg/ml; red triangle). For crosslinking, 20 μg/ml of monoclonal mouse anti-human IgG_4 was used (black triangle) and induction of the Ca^{++}-response was monitored. **(B)** 5×10^4 freshly prepared human T-cells/96-well were stimulated with the indicated concentrations of ANC28.1 or TGN1412 or were left untreated as a control. For crosslinking of ANC28.1, a polyclonal goat anti-mouse antiserum was used and crosslinking of TGN1412 was performed as described in (A). Concentrations for crosslinking were the following: 0.1–1.25 μg/ml primary Ab+2.5 μg/ml crosslinker; 2.5 μg/ml primary Ab+5 μg/ml crosslinker; 5 μg/ml primary Ab+10 μg/ml crosslinker; 10 μg/ml primary Ab+20 μg/ml crosslinker. 72 hours after stimulation, cultures were pulsed with ^{3}H-thymidine for 6 hours, then harvested and proliferation analyzed by counts per minute [cpm]. **(C)** 1×10^6 freshly prepared human T cells/lane were left untreated or were stimulated with 10 μg/ml ANC28.1 (first and third panel) followed by crosslinking with 20 μg/ml polyclonal goat anti-mouse antiserum or with 10 μg/ml TGN1412 (right panel) followed by crosslinking as described in (A) for the indicated periods of time. As a control, cells were activated with a 1:50 dilution of ascites fluid of CD3 mAb MEM92 (second panel). Postnuclear lysates were processed for western blotting using the indicated phosphospecific antibodies. Western blotting using an anti-actin antibody was performed as loading control.
doi:10.1371/journal.pone.0001708.g003

Similar to cycloheximide treatment, depletion of extracellular calcium ions by EGTA completely abrogated IFN-γ production after ANC28.1 stimulation. This finding shows that transmembranous calcium flux is mandatory for CD28SA-mediated induction of cytokine synthesis. Note that addition of extracellular Ca^{++} ions to EGTA-treated cells completely restored the CD28SA-induced IFN-γ response (Fig. 5B), excluding toxic EGTA effects.

Above we showed that the PI3K inhibitor Wortmannin did not influence CD28SA-mediated calcium flux (Fig. 2C). Similarly, neither Wortmannin nor a second PI3K inhibitor, LY294002, influenced CD28SA-mediated phosphorylation of SLP76, Vav, Erk, JNK, p38, the degradation of IKK or the dephosphorylation of NF-ATc1 (Fig. 5C), whereas both inhibitors completely abrogated CD28SA-mediated phosphorylation of AKT (upper panel in Fig. 5C). These data corroborate a recent report showing

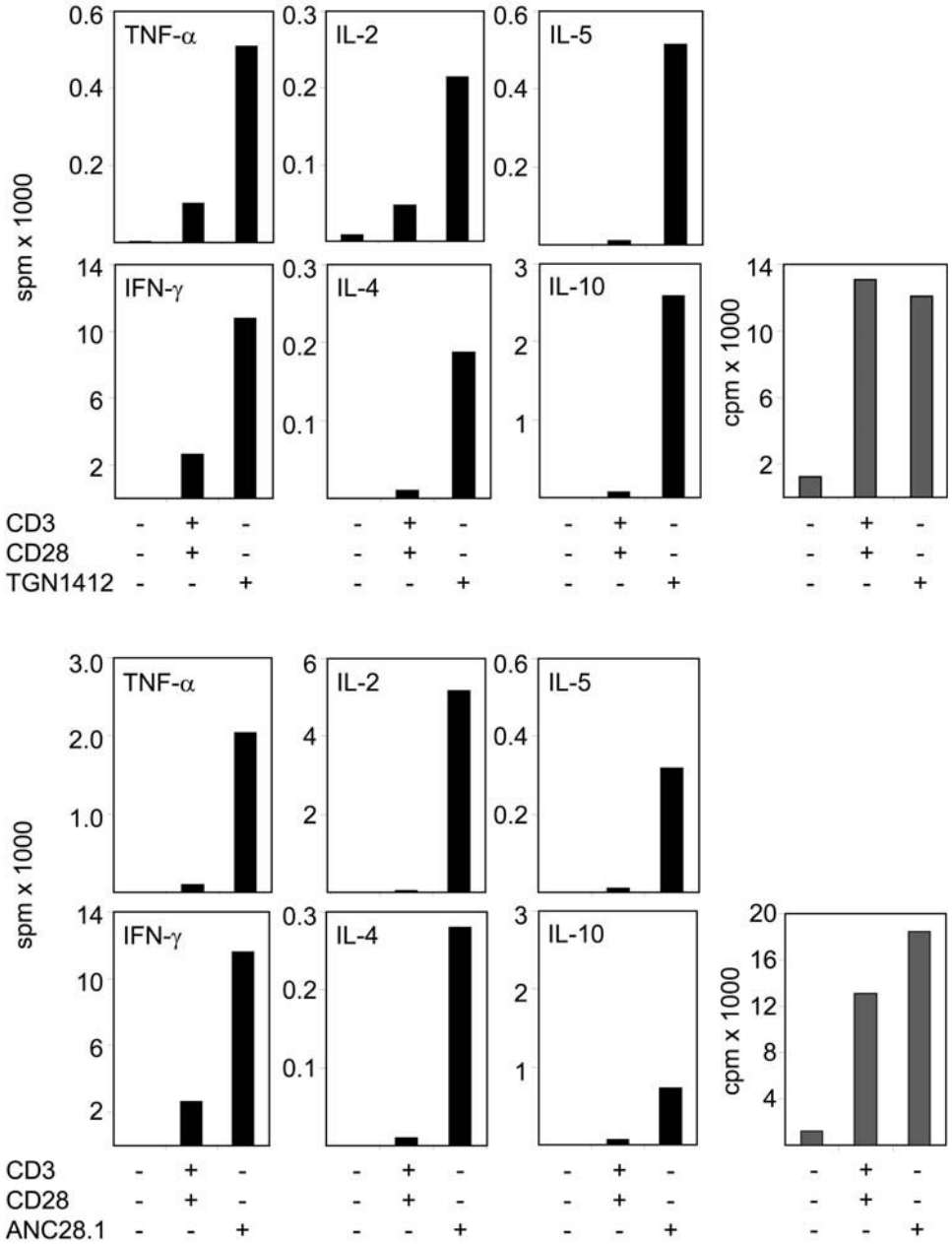

Figure 4. Cytokine production upon conventional and superagonistic CD28 stimulation of human T cells. 5×10^4 freshly prepared human T-cells/96-well were stimulated with the indicated combination of antibodies as described in Fig. 1A or were left untreated as controls. At 48 hours 50 µl culture supernatant was removed from each well. Supernatants obtained from 3 wells were pooled and cytokine content was determined using the Cytokine Bead Array from BD in signals per minute [spm] (black bars). Additionally, induction of T cell proliferation was monitored upon treatment with the indicated antibody combinations (gray bars). 72 hours after stimulation, cultures were pulsed with ^{3}H-thymidine for 6 hours, then harvested and proliferation analyzed by counts per minute [cpm]. Data represent the mean of 5 individual experiments.
doi:10.1371/journal.pone.0001708.g004

that CD28SAs still induce upregulation of CD69 in human T cells pretreated with Wortmannin or Ly294002 [33]. Surprisingly, both Wortmannin and Ly294002 induced an almost complete block of IFN-γ production after ANC28.1 stimulation (Fig. 5B). This suggests that PI3K or its downstream effector AKT [34,35] is mandatory (although not sufficient) for CD28SA-mediated IFN-γ production.

We next assessed the mechanisms underlying CD28SA-mediated IL-2 induction. This was of particular interest because a recent report suggested that in rat T cells CD28SA induced IL-2 production might not require PI3K activity [12]. Fig. 5D shows that, similar to IFN-γ production, CD28SA-mediated IL-2 synthesis by human T cells was sensitive to treatment with EGTA, cycloheximide, CSA, and PP2. Furthermore, Wortmannin and LY294002 abrogated CD28SA-mediated IL-2 synthesis. Hence, in contrast to rat T cells, activation of PI3K was also mandatory for CD28SA induced IL-2 production by human T lymphocytes.

We finally assessed whether the sustained Ca^{++} signaling that is induced by ANC28.1 and TGN1412 (see Figs. 2 and 3) is required for cytokine production upon CD28SA-stimulation. To achieve

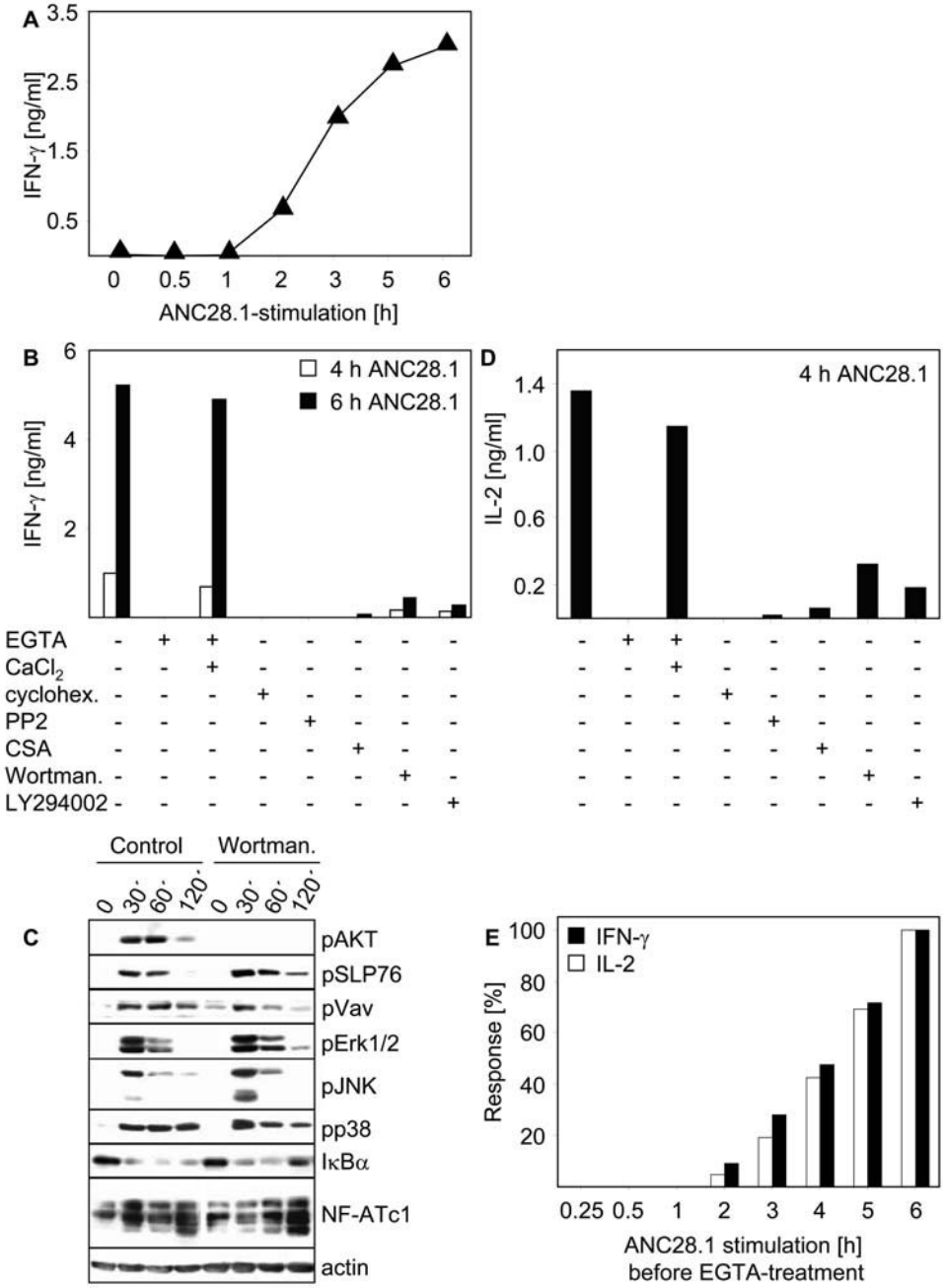

Figure 5. Analysis of the signaling pathways controlling CD28SA-mediated IFN-γ and IL-2 production. (A) Short term IFN-γ production upon CD28SA stimulation of T cells. 1×10^6 T cells/200 µl were activated by CD28SA ANC28.1 as described for Figs. 1–4. At the indicated time points 50 µl of the supernatants were removed, diluted 1:3 v/v, and the concentration of secreted IFN-γ was determined using a commercially available ELISA. **(B)** Molecular requirements determining CD28SA-mediated IFN-γ production. T cells were pretreated for 30 minutes with the indicated substances prior to stimulation with ANC28.1. EGTA was used at 1 mM, $CaCl_2$ at 2 mM, cycloheximide at 50 µg/ml, CSA at 150 ng/ml, PP2 at 10 µM, Wortmannin at 0.1 µM, and Ly294002 at 20 µM. At the indicated time points cytokine production was determined as described in (A). **(C)** 1×10^6 freshly prepared human T cells/lane were stimulated with 10 µg/ml ANC28.1 followed by crosslinking with 20 µg/ml polyclonal goat anti-mouse antiserum with or without Wortmannin treatment. Western blotting was conducted as described in Fig. 3. Note that identical results were obtained when T cells were pretreated with LY294002 (data not shown). **(D)** Molecular requirements determining CD28SA-mediated IL-2 production. T cells were pretreated for 30 minutes with the indicated substances prior to stimulation with ANC28.1 as described in (B). 4 h after stimulation 50 µl of the supernatants were removed, diluted 1:3 v/v, and the concentration of IL-2 was analyzed in supernatants by an ELISA. **(E)** CD28SA-mediated IFN-γ and IL-2 production requires sustained Ca^{++}-flux. T cells were stimulated with ANC28.1 as described above. At 15′, 30′, 1 h, 2 h, 3 h, 4 h, and 5 h Ca^{++}-flux was interrupted by addition of EGTA (1 mM) and the concentration of the cytokines in the supernatant was determined as described in (B) and (D). The concentrations of IL-2 and IFN-γ that were produced by ANC28.1-stimulated T cells following 6 hours of stimulation in the absence of EGTA were set to 100%. All data shown in Fig. 5 are representative for three independently performed experiments.
doi:10.1371/journal.pone.0001708.g005

this we inhibited transmembranous Ca^{++}-flux at different time points after stimulation with ANC28.1 by the addition of EGTA and subsequently determined the concentration of IFN-γ and IL-2 in the culture supernatants. Fig. 5E depicts that the amounts of IFN-γ and IL-2 secreted by CD28SA-stimulated T cells directly correlated with the duration of CD28-mediated transmembranous Ca^{++}-flux. Thus, sustained calcium flux is important for the strong production of IFN-γ and IL-2 upon CD28SA stimulation.

Lack of a TGN1412-mediated calcium response in monkey T cells

Before being used in the London phase I clinical trial, TGN1412 had been applied to rhesus and cynomolgus monkeys without showing obvious severe adverse effects [36]. Furthermore, it was debated whether the extracellular domains of *Macaca fascicularis* (cynomolgus), *Macaca mulatta* (rhesus), and *Homo sapiens* CD28 show subtle differences on the protein level [37] [38]. To clarify the latter question we sequenced CD28 cDNAs obtained from 14 individual rhesus and 11 cynomolgus monkeys and compared the deduced amino acid sequences with the protein sequence of human CD28. Notably, this approach corroborated that the CD28 extracellular domains (as well as the cytoplasmic tails) are completely conserved between the three species (Fig. S3). Interestingly, in all 25 monkeys investigated we observed three non-conservative amino acid exchanges in the transmembrane region (Fig. S3). Furthermore, one non-conservative amino acid exchange was found within the leader sequence of the non-human primates.

The complete conservation of the extracellular domains of CD28 across the investigated species was further reflected by similar TGN1412 binding of human $CD3^+$ and non-human primate $CD3^+$ T cells. A 1:1 mixture of $CD3^+$ human T cells (stained with an anti-CD3-APC antibody) and $CD3^+$ non-human primate T cells (stained with an anti-CD3-PE antibody) derived from cynomolgus (Fig. 6A, left panel) or rhesus (Fig. 6A, right panel) monkeys, respectively, was incubated with Alexa 488 labeled TGN1412 at graded concentrations. Similar decoration of T cells from both species with TGN1412 indicated similar binding capacities of human and non-human primate CD28 to the antibody. Moreover, FACS analyses revealed a similar ratio of $CD4^+$ vs. $CD8^+$ T cells in blood samples of human and non-human origin (Fig. 6B).

Interestingly, despite similar TGN1412 binding, identical extracellular CD28 domains of all three species, and a similar ratio of $CD4^+$ vs. $CD8^+$ T cells in blood samples of human and non-human origin (Fig. 6 and Fig. S3), TGN1412 only induced a very low calcium signal in rhesus or cynomolgus T cells (Fig. 6C). Similar results were obtained with ANC28.1 (data not shown). Note that the profound differences in the Ca^{++}-response between monkey and human T cells were also observed at higher concentrations of both antibodies (up to 20 μg/ml; not shown). Thus, despite comparable levels of CD28 expression and similar reactivity with TGN1412 only human T cells are capable of inducing a significant calcium response upon stimulation with CD28 superagonists.

Discussion

The data shown in this report clearly demonstrate that two superagonistic CD28 mAbs, TGN1412 and ANC28.1, generate a remarkably sustained Ca^{++}-response when applied to human T cells in vitro (Fig. 2 and 3). The prolonged Ca^{++}-signal is preceded by a sustained activation of PLCγ1 (Fig. 1) and is downstream correlated with an activation of a number of different signaling pathways (Fig. 3) that are involved in the activation and differentiation of T lymphocytes. Together, these signals culminate in the production of a variety of pro-inflammatory cytokines, most notably IFN-γ and TNF-α (Fig. 4).

The strong and sustained Ca^{++}-response elicited by the CD28SAs seems to be a particular property of the human system and it appears as if human T cells react more sensitive to CD28SA stimulation compared to rat and monkey T cells ([11] and Fig. 6). A sustained Ca^{++}-response following CD28SA-stimulation has previously been described for rat T cells [11]. However, due to the low on-rate or the weak accessibility of the CD28 epitope detected by CD28SAs, the induction of Ca^{++}-flux in rat T cells required antibody pre-incubation for several hours [11]. Similarly, the induction of proliferation by mitogenic rat CD28SA antibodies needs extensive crosslinking and we also observed that the binding of an anti-mouse CD28SA (D665) to the surface of murine T cells occurred with an extremely slow kinetics and was strongest upon overnight incubation on ice (data not shown).

In contrast, the binding of both TGN1412 and ANC28.1 to human T cells occurs rapidly and is almost indistinguishable from the binding of monoclonal antibodies directed to other cell surface receptors (data not shown). Hence, the binding of CD28SAs to human T cells occurs with much faster kinetics compared to mouse and rat CD28SAs. A faster on-rate (presumably combined with a slow off-rate) could explain why CD28SAs are capable of inducing sustained signaling in human T lymphocytes.

A number of previous studies had assessed the capability of conventional CD28 antibodies to induce Ca^{++}-flux in Jurkat T cells and primary human T cells. These studies suggested that CD28-mediated Ca^{++}-flux requires extracellular calcium ions and hence, is EGTA-sensitive [30]. However, they also suggested that CD28-mediated signals do not activate the PTK pathway [30], occur in the absence of TCR signals [30], do not lead to production of DAG [39], and also do not activate PKC. This appears not to be the case for the anti-human CD28SAs for the following reasons: (i) we show that (similar to rat T cells [12]) the Ca^{++}-signal produced by ANC28.1 required expression of a functional TCR (Fig. 2B); (ii) anti-human CD28SA signaling was Src protein tyrosine kinase dependent as it could be blocked by PP2 (Fig. 2C); (iii) anti-human CD28SA-mediated signaling induced the induction of the DAG-dependent Ras/Raf/Erk pathway (Fig. 3C), and (iv) it led to activation of the IKK/NF-κB pathway (Fig. 3C) which is dependent on activation of PKC. Hence, despite some similarities, the signaling properties of conventional anti-human CD28 antibodies fundamentally differ from those of CD28 superagonists.

In agreement with data obtained in rat T cells [12], ANC28.1 stimulation did not result in a detectable tyrosine phosphorylation of the protein tyrosine kinase ZAP70 (Fig. 1B, middle panel) although ZAP70 is believed to be primarily responsible for LAT phosphorylation upon TCR-stimulation. At present it is unclear which protein kinase is responsible for LAT phosphorylation upon CD28 superagonistic stimulation of human T cells. Attractive candidates include the two Tec-family protein tyrosine kinases Itk and Rlk [12].

An important question that needs to be addressed in the future is why the calcium-signal induced by human superagonistic CD28 mAbs has such a dramatically prolonged kinetics. It is obvious from our study that the potency of CD28SAs to activate PLCγ1 and to induce Ca^{++}-flux is lower than the potency of CD3 mAb. Thus, it is possible that the amount of IP3 generated upon triggering by CD28SAs suffices to activate membrane associated Ca^{++}-channels, but that the overall Ca^{++} influx is below the threshold that is needed to close the channels. In line with this idea

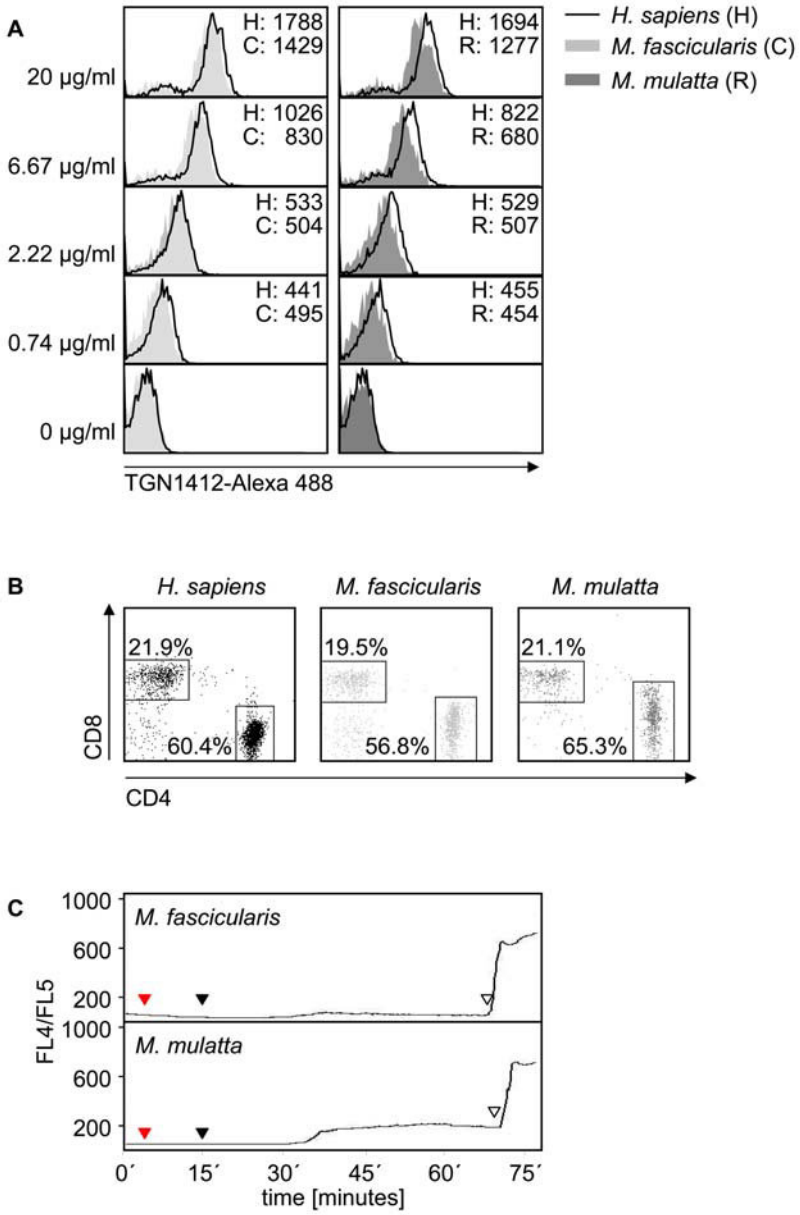

Figure 6. Despite similar TGN1412 binding, Macaca derived T cells show reduced calcium flux upon TGN1412 stimulation when compared to human T cells. (A) MACS purified $CD3^+$ human T cells (stained with an anti-CD3-APC antibody) and $CD3^+$ monkey T cells (stained with an anti-CD3-PE antibody) were mixed 1:1 and then incubated with graded concentrations of Alexa 488 labeled TGN1412. Binding of TGN1412-Alexa 488 was monitored by FACS analysis. Numbers given indicate the mean fluorescence intensity of samples. **(B)** Ratio of $CD4^+$ vs. $CD8^+$ T cells (gated on $CD3^+$ cells) of human and monkey blood samples was analyzed by FACS analyses. **(C)** 1×10^6 freshly isolated Indo-1 loaded *M. fascicularis* and *M. mulatta* T cells were treated as described in Fig. 2 using the superagonistic CD28 specific mAb TGN1412 (10 µg/ml; red triangle). For crosslinking, 20 µg/ml monoclonal mouse anti-human IgG_4 was used (black triangle) and induction of the Ca^{++}-response was monitored. To confirm viability of cells and proper loading with Indo-1, Ionomycin (10 µg/ml) was added at the end of the experiment (unfilled triangle).
doi:10.1371/journal.pone.0001708.g006

is our observation that the sustained calcium-response elicited by the CD28SAs can be stopped by administration of a CD3 mAb (Fig. 2E). However, further studies are required to elucidate the question how transmembrane flux is induced and maintained upon CD28SA-stimulation. Moreover, it will be important to determine the functional roles of the recently identified ORAI1 and STIM proteins in CD28SA-induced transmembrane Ca^{++}-flux [40].

Our data show that CD28SA-stimulation leads to a strong and very rapid production of cytokines in vitro (Figs. 4 and 5). Indeed, IFN-γ was detectable in the culture supernatant already 90–120 minutes after CD28SA stimulation (Fig. 5A). Inhibition of protein synthesis by cycloheximide completely abrogated IFN-γ secretion (Fig. 5B) which strongly suggests that this event is not due to a release of the cytokine from intracellular stores but rather due to de novo IFN-γ synthesis. Furthermore, the production of IFN-γ was dependent on CD28SA-mediated Ca^{++}-flux as pretreatment of the cells with EGTA completely blocked the response. Perhaps more importantly, our data show that the amounts of IFN-γ and IL-2 produced by CD28SA-treated cells directly depend on the

duration of transmembranous Ca^{++}-flux (Fig. 5E). Thus, it appears as if the large amounts of cytokines produced upon anti-human CD28SA-stimulation in vitro (and presumably also in vivo) are due to the sustained Ca^{++}-signal generated by the CD28 superagonistic antibodies.

With regard to the induction of IL-2 synthesis the signaling properties of CD28 superagonists again appear to differ from those of conventional CD28 mAbs. Based on studies using cholera-toxin, it was suggested that conventional CD28 antibodies activate two functionally unrelated signaling pathways [22]. One of these pathways was found to be cholera-toxin sensitive, initiated transmembranous Ca^{++}-flux, but did not influence IL-2 secretion whereas the other one was cholera-toxin insensitive and responsible for IL-2 production [22]. Both with regard to production of IL-2 and IFN-γ this mechanism does not hold true for signaling induced by CD28SAs. Indeed, we show that both the PTK/PLCγ/Ca^{++}-pathway and the PI3-kinase pathway must operate simultaneously in order to allow IL-2 and IFN-γ synthesis. Whether this also applies for the production of other cytokines upon CD28SA stimulation requires further analysis. Moreover, despite costimulatory capacity, the same antibody that was used by Nunes et al. to dissect signaling events upon CD28-stimulation in Jurkat T cells (mAb 248.23.2 [22]) did not generate a detectable Ca^{++} signal in primary human T cells (data not shown). These differences might be due to the different cells that were investigated or to different CD28 antibody preparations (ascites fluid in [22] vs. cell culture supernatant in our study).

It is important to note that the signaling pathways induced by CD28SAs also seem to differ between rat and human T cells. A recent report suggested that IL-2 production upon CD28SA-stimulation of rat T cells is primarily mediated via the SLP76/Vav-module and does not require activation of PI3K [12]. The latter assumption was based on the observation that anti-rat CD28 superagonists do not induce phosphorylation of AKT and that mutation of the PI3K binding site within the cytoplasmic domain of CD28 did not ablate CD28SA-mediated IL-2 production [12]. However, our data show that CD28-mediated IFN-γ and IL-2 production required both transmembranous Ca^{++}-flux and activation of PI3K (Fig. 5). Indeed, inhibition of PI3K blocked CD28SA-mediated IL-2 production in human T cells without influencing transmembranous Ca^{++}-flux, phosphorylation of SLP76, Vav, Erk, JNK, p38 as well as the activation of the transcription factors NF-AT and NF-κB. Together these data suggest that anti-human CD28SA signaling involves at least two major signaling modules, one that depends on activity of PI3K and a second one that requires transmembranous Ca^{++}-flux (note that treatment of T cells with EGTA did not substantially alter CD28SA-mediated activation of AKT (data not shown)). However, we certainly cannot exclude the possibility that CD28SA-stimulation activates a pool of PI3K that does not associate with CD28 upon CD28SA stimulation. Further, it will be important to investigate whether PI3K regulates the production of IL-2 and IFN-γ upon CD28SA stimulation in human T lymphocytes via its proposed downstream effector AKT [34,35].

Differences between human and rodent T cell activation are also underlined by experiments analyzing Ca^{++}-flux in $CD4^+$ and $CD8^+$ T cell subpopulations. It was shown previously that in mouse splenic T cells only $CD4^+$ but not $CD8^+$ T cells showed Ca^{++}-flux upon CD28 triggering [29] whereas within human PBMCs also $CD8^+$ cells were capable of Ca^{++}-release upon CD28 stimulation [30]. In agreement with data shown in this study (Fig. 2F) responses by $CD8^+$ T cells were less pronounced than those by $CD4^+$ T cells [30].

It is still unclear how CD28SAs precisely activate the multiple intracellular signaling pathways at the level of the plasma membrane. Initially we thought that this might be due to formation of large CD28 clusters on the T cell surface. However, in line with a recent report [33] we did not see obvious differences in CD28 cluster formation upon CD28SA vs. CD28 stimulation by confocal laserscanning microscopy (data not shown). However, we cannot exclude the possibility that the assembly or the dynamics of the recently identified microclusters [41] differs between CD28 vs. CD28SA stimulation. It will be important to assess this possibility in the future.

Although we observed that CD28SA stimulation led to the activation of many intracellular signaling pathways it is important to note that CD28SAs do not fully activate human T cells. For example, we did not observe an activation of β1- or β2-integrins upon CD28SA stimulation and we also did not see formation of F-actin or induction of cell migration by CD28SAs (data not shown). Why these cellular events are not initiated upon CD28SA stimulation is unclear at present. One reason might be that the thresholds that are required to activate these pathways are higher than those regulating cytokine production.

The amino acid sequence of the extracellular domains of rhesus and cynomolgus CD28 are identical with the one of human CD28 (Fig. S3 and see genebank entries 111144662 and 112817616 for *Macaca mulatta* and 110611295, 111144664, and 110611297 for *Macaca fascicularis* as well as ref. [42]). This was also reflected by similar decoration of CD28 on T cells of human, *Macaca mulatta*, and *Macaca fascicularis* origin with Alexa 488 labeled TGN1412 (Fig. 6A). Intriguingly however, monkey T cells did not show Ca^{++}-response upon CD28SA stimulation (Fig. 6C) as it was observed in human T cells. Unlike rodents, blood samples of non-human primates and humans show approximately 70% T cells in the lymphocyte gate and within the T cell population, non-human primates and humans show a similar ratio of $CD4^+$ vs. $CD8^+$ T cells (Fig. 6B and [43,44]). It is also important to note that the non-human primates used in this study are not kept under specific pathogen free (SPF) conditions although they are regularly screened for infections with pathogens. Thus, the observation that TGN1412 stimulation induced Ca^{++}-flux only in human but not in non-human primate T cells (Fig. 6C) can not be explained by significantly decreased numbers of $CD4^+$ T cells in non-human primates or by a more naïve activation state of the T cells due to SPF housing conditions.

Importantly, a recent study showed that chimpanzee T cells are also less responsive towards in vitro stimulation than human T cells and it was suggested that this might be due to loss of Siglec expression on human T cells [45]. Siglecs are inhibitory receptors that are related to CD33 and it appears as if their expression is lost on T cells during evolution from monkey to human [45]. Hence, the lack of Siglec expression might explain why human T cells react more sensitive upon CD28SA stimulation compared to Macaca T cells.

Alternatively, the number/size and/or distribution of lipid rafts might differ between monkey and human T lymphocytes. Finally, three non-conservative amino acid exchanges are present within the transmembrane regions of Macaca monkey and human CD28 which might influence the lateral interactions between CD28 and other signaling molecules within the plasma membrane. Clearly, these points need to be investigated in the future.

Collectively, our functional and biochemical data provide a first explanation for the severe adverse effects induced upon TGN1412 administration to human beings. Further, they show that in spite of absence of toxicity signals in the Macaca model that is broadly considered as the golden standard for preclinical tests, a detailed in

vitro analysis of human cells is still mandatory to reduce risks inherently related with first-in-man studies.

Materials and Methods

Animals

Macaca mulatta (rhesus monkey) and *Macaca fascicularis* (cynomolgus monkey) were kept under conventional conditions at the Central Animal Facility of the Paul-Ehrlich-Institut, Germany. The animals are regularly screened for infections according the recommendations of EUPRIM-Net including tuberculosis, alphaherpes virus, SIV, STLV, filovirus, and others. Experimental work was carried out in compliance with regulations of German animal welfare.

T cell purification

Peripheral blood mononuclear cells (PBMC) were isolated by Ficoll gradient (Biochrom) centrifugation of heparinized blood collected from healthy volunteers. Human T cells were further purified by non-T cell depletion using the Pan T cell isolation kit II (Miltenyi Biotec). For monkey T cell enrichment, monkey blood was Ficoll purified using individually adjusted Ficoll dilutions (between 95 and 100%). Then T cells were MACS purified using the Pan T cell isolation kit for non-human primates (Miltenyi Biotec). Human $CD8^+$, $CD4^+$, $CD4^+/CD45RA^+$ naïve, and $CD4^+/CD45RO^+$ memory T lymphocytes were purified using the $CD4^+/CD8^+$ T cell isolation kit and the $CD4^+$ naïve/memory T cell isolation kit (Miltenyi Biotec).

Antibodies

For the different applications the following antibodies were used: for cytokine release assays and proliferation assays the CD3ε monoclonal antibody OKT-3 (purchased from ATCC) was used as hybridoma supernatant. Stimulations for western blotting experiments and calcium release assays were performed using the CD3ε monoclonal antibody MEM92, kindly provided by Dr. Vaclav Horejsi, Prague Academy of Sciences, Prague, Czech Republic. For conventional co-stimulation, hybridoma supernatant of the CD28 monoclonal antibody 248.23.2 [22,46] or commercially available CD28.2 (Biosciences) was used. The superagonistic CD28 antibody ANC28.1/5D10 was obtained from Ancell (referred to as ANC28.1 throughout the text) and humanized superagonistic CD28 antibody TGN1412 was a gift from Thomas Hanke.

In vitro proliferation assays

96-well round-bottomed tissue culture plates (Costar) were coated with a 1:400 v/v dilution of polyclonal goat-anti-mouse antiserum (specific for IgG and IgM, 50 µl/well). Plates were then washed three times with phosphate buffered saline (Seromed) and either 100 µl of CD3ε mAb OKT-3 (1:2 v/v dilution of hybridoma culture supernatant), 100 µl of conventional CD28 mAb 248.23.2 (1:2 v/v dilution of hybridoma culture supernatant) or 100 µl of a 1:1 mixture of OKT-3 and 248.23.2 culture supernatants were added. For CD3xANC28.1 induced proliferation 100 µl of a 1:2 v/v dilution of hybridoma culture supernatant of CD3ε mAb OKT-3 were supplemented with 10 µg/ml of ANC28.1 were used. Alternatively, T cells were incubated with the indicated concentrations of ANC28.1 or TGN1412 and cross-linked with goat anti-mouse (IgG+IgM) polyclonal serum (Dianova) or purified mouse anti-human IgG_4 monoclonal antibody (BD Pharmingen), respectively. For T cell proliferation experiments, 5×10^4 T cells/well were added in a final volume of 200 µl. [3H]-thymidine (0.3 µCi/well; specific activity 50 Ci/mmol) was added for the last 8–10 hours of the three day incubation and cells were harvested using a PHD cell harvester. Thymidine incorporation was measured by liquid scintillation in counts per minute [cpm].

In vitro cytokine production

Cells were stimulated in vitro in triplicates as described for T cell proliferation. Approximately 48 hours after onset of the stimulation 50 µl of culture supernatant was removed from each well. Triplicate supernatants were pooled and 50 µl of each pool was then used in the TH1/TH2/Inflammatory Cytometric Bead Arrays (CBA) from Becton Dickenson according to the manufacturer's recommendation. Cytokine expression is shown in signals per minute [spm]. Data shown represent the mean of at least three individual experiments.

To determine the concentration of IFN-γ and IL-2 after short term stimulation of T cells, the cell suspension was adjusted to 1×10^5 T cells/200 µl. Cells were stimulated as described above for the indicated periods of time. Subsequently, 50 µl culture supernatant was removed and diluted 1:3 v/v in culture medium. The concentrations of IFN-γ and IL-2 were determined using the Quantikine ELISA system from R&D Systems according to the manufacturer's recommendation. To assess the molecular requirements for CD28SA-mediated IFN-γ and IL-2 production the following inhibitors were used: EGTA (1 mM), $CaCl_2$ (2 mM), cycloheximide (50 µg/ml; Sigma), CSA (150 ng/ml; Calbiochem), PP2 (10 µM; Calbiochem), Wortmannin (0.1 µM; Calbiochem), and Ly294002 (20 µM; Calbiochem).

Western blotting

T cells were lysed in buffer containing 1% lauryl maltoside (N-dodecyl β-maltoside), 1% NP-40, 1 mM Na_3VO_4, 1 mM PMSF, 10 mM NaF, 10 mM EDTA, 50 mM Tris pH 7.5, and 150 mM NaCl. Postnuclear lysates were separated by SDS-PAGE and transferred onto nitrocellulose membranes. Membranes were probed with the indicated primary antibodies and the appropriate HRP-conjugated secondary antibodies (Dianova) and developed using the ECL detection system (Amersham Pharmacia). The following antibodies were used for western blotting in this study: anti-pErk1/2 (Thr^{202}/Tyr^{234}), anti-pZAP70 (Y^{319}), anti-pLAT (Y^{171}), anti-pJNK ($Thr^{183/185}$), anti-pp38 ($Thr^{180/182}$), anti-IκBα, anti-AKT, and anti-GSK3β-1 (all from Cell signaling), anti-PLCγ1 (Y^{783}, Santa Cruz), anti-NF-ATc1 (Alexis/Axxora), anti-β-actin (Sigma), anti-pVav (Y^{174} Santa Cruz), and anti-pSLP76 (BD Biosciences).

Calcium measurements

Purified T cells (2×10^7 cells/ml) in RPMI medium (phenol-red free; Invitrogen) containing 10% FCS were loaded with 5 µg/ml Indo-1-AM (Molecular Probes) at 37°C for 45 min. After washing, cells were incubated in RPMI medium supplemented with 10% FCS (phenol-red free) at 37°C for an additional 45 min. The measurement was performed on a FACSort™ flow cytometer (Becton Dickinson). The kinetics of the data was analyzed with FlowJo software (TreeStar).

Sequencing

Blood was taken from 14 individuals *Macaca mulatta* (rhesus monkey) and 11 individuals *Macaca fascicularis* (cynomolgus monkey). The animals analyzed belong to different families and were from different origins to avoid inbreeding effects. RNA from blood cells was isolated using Paxgene RNA Blood Kit (Qiagen) in combination with Paxgene Blood RNA tubes (Preanalytix). RNA

was incubated with DNase I (Roche) for 15 min at 37°C and cDNA was prepared by using SuperScript II (Invitrogen) according to manufacturer's instructions. RT-PCR with RNA as template using GAPDH-specific primers confirmed the absence of genomic DNA within all samples and controls with no template confirmed specificity. Primers used for amplification were the following (sequences listed in 5′ to 3′ orientation): GAPDH: ACCACAGTCCATGCCATCAC and TCCACCACCCTGTTGCTGTA; CD28: CTCACACTTCGGGTTCCTCG and GGTCATTTCCTATCCAGAGC. RT-PCR fragments were sequenced both forward and reverse (MWG). Of note, there were individual differences in the nucleotide sequences not resulting in exchanged amino acids.

FACS Analysis

For FACS analysis TGN1412 was labeled using the Alexa Flour®488 monoclonal labeling kit (Invitrogen/Molecular Probes) according to the manufacturer's instructions. Human and monkey blood was stained with TGN1412-Alexa Flour®488 at the indicated concentrations in a total volume of 50 µl. Human and monkey cells were stained using the following antibodies: anti-CD3-PE, -APC or -FITC, anti-CD4-PE, anti-CD8-FITC or -PerCP (all from BD). After washing with FACS-buffer, samples were incubated with blood lysing buffer (BD Pharm Lyse™) for 2–3 hours at 4°C and washed again. Cells were analyzed via Flow cytometry (LSR™ II; BD) and evaluated with DIVA® software. One representative experiment out of three comparable experiments is shown.

Supporting Information

Figure S1
Found at: doi:10.1371/journal.pone.0001708.s001 (1.76 MB TIF)

Figure S2
Found at: doi:10.1371/journal.pone.0001708.s002 (3.22 MB TIF)

Figure S3
Found at: doi:10.1371/journal.pone.0001708.s003 (0.51 MB TIF)

Movie S1
Found at: doi:10.1371/journal.pone.0001708.s004 (4.45 MB MOV)

Movie S2
Found at: doi:10.1371/journal.pone.0001708.s005 (2.67 MB MOV)

Acknowledgments

We thank Stefanie Bauer, Carina Kruip, and Barbara Yutzy for expert technical assistance, Roland Plesker and his team for providing monkey blood, Oreste Acuto for reading the manuscript, and Thomas Hanke for the generous gift of the antibody TGN1412 and helpful discussion.

Author Contributions

Conceived and designed the experiments: UK BS ZW. Performed the experiments: RH SK ZW LS CM PR. Analyzed the data: UK BS ZW MG. Wrote the paper: UK BS ZW.

References

1. Schwartz RH (1992) Costimulation of T lymphocytes: the role of CD28, CTLA-4, and B7/BB1 in interleukin-2 production and immunotherapy. Cell 71: 1065–1068.
2. Sharpe AH, Abbas AK (2006) T-cell costimulation–biology, therapeutic potential, and challenges. N Engl J Med 355: 973–975.
3. Acuto O, Michel F (2003) CD28-mediated co-stimulation: a quantitative support for TCR signalling. Nat Rev Immunol 3: 939–951.
4. Rudd CE, Schneider H (2003) Unifying concepts in CD28, ICOS and CTLA4 co-receptor signalling. Nat Rev Immunol 3: 544–556.
5. Bischof A, Hara T, Lin CH, Beyers AD, Hunig T (2000) Autonomous induction of proliferation, JNK and NF-alphaB activation in primary resting T cells by mobilized CD28. Eur J Immunol 30: 876–882.
6. Rodriguez-Palmero M, Hara T, Thumbs A, Hunig T (1999) Triggering of T cell proliferation through CD28 induces GATA-3 and promotes T helper type 2 differentiation in vitro and in vivo. Eur J Immunol 29: 3914–3924.
7. Tacke M, Hanke G, Hanke T, Hunig T (1997) CD28-mediated induction of proliferation in resting T cells in vitro and in vivo without engagement of the T cell receptor: evidence for functionally distinct forms of CD28. Eur J Immunol 27: 239–247.
8. Luhder F, Huang Y, Dennehy KM, Guntermann C, Muller I, et al. (2003) Topological requirements and signaling properties of T cell-activating, anti-CD28 antibody superagonists. J Exp Med 197: 955–966.
9. Siefken R, Klein-Hessling S, Serfling E, Kurrle R, Schwinzer R (1998) A CD28-associated signaling pathway leading to cytokine gene transcription and T cell proliferation without TCR engagement. J Immunol 161: 1645–1651.
10. Michel F, Attal-Bonnefoy G, Mangino G, Mise-Omata S, Acuto O (2001) CD28 as a molecular amplifier extending TCR ligation and signaling capabilities. Immunity 15: 935–945.
11. Dennehy KM, Kerstan A, Bischof A, Park JH, Na SY, et al. (2003) Mitogenic signals through CD28 activate the protein kinase Ctheta-NF-kappaB pathway in primary peripheral T cells. Int Immunol 15: 655–663.
12. Dennehy KM, Elias F, Na SY, Fischer KD, Hunig T, et al. (2007) Mitogenic CD28 signals require the exchange factor Vav1 to enhance TCR signaling at the SLP-76-Vav-Itk signalosome. J Immunol 178: 1363–1371.
13. Hunig T, Dennehy K (2005) CD28 superagonists: mode of action and therapeutic potential. Immunol Lett 100: 21–28.
14. Beyersdorf N, Gaupp S, Balbach K, Schmidt J, Toyka KV, et al. (2005) Selective targeting of regulatory T cells with CD28 superagonists allows effective therapy of experimental autoimmune encephalomyelitis. J Exp Med 202: 445–455.
15. Beyersdorf N, Hanke T, Kerkau T, Hunig T (2005) Superagonistic anti-CD28 antibodies: potent activators of regulatory T cells for the therapy of autoimmune diseases. Ann Rheum Dis 64 Suppl 4: iv91–iv95.
16. Beyersdorf N, Hanke T, Kerkau T, Hunig T (2006) CD28 superagonists put a break on autoimmunity by preferentially activating CD4+CD25+ regulatory T cells. Autoimmun Rev 5: 40–45.
17. Beyersdorf N, Balbach K, Hunig T, Kerkau T (2006) Large-scale expansion of rat CD4+ CD25+ T(reg) cells in the absence of T-cell receptor stimulation. Immunology 119: 441–450.
18. Lin CH, Hunig T (2003) Efficient expansion of regulatory T cells in vitro and in vivo with a CD28 superagonist. Eur J Immunol 33: 626–638.
19. Rodriguez-Palmero M, Franch A, Castell M, Pelegri C, Perez-Cano FJ, et al. (2006) Effective treatment of adjuvant arthritis with a stimulatory CD28-specific monoclonal antibody. J Rheumatol 33: 110–118.
20. Schmidt J, Elflein K, Stienekemeier M, Rodriguez-Palmero M, Schneider C, et al. (2003) Treatment and prevention of experimental autoimmune neuritis with superagonistic CD28-specific monoclonal antibodies. J Neuroimmunol 140: 143–152.
21. Suntharalingam G, Perry MR, Ward S, Brett SJ, Castello-Cortes A, et al. (2006) Cytokine storm in a phase 1 trial of the anti-CD28 monoclonal antibody TGN1412. N Engl J Med 355: 1018–1028.
22. Nunes J, Bagnasco M, Lopez M, Lipcey C, Mawas C, et al. (1991) Dissociation between early and late events in T cell activation mediated through CD28 surface molecule. Mol Immunol 28: 427–435.
23. Zhang W, Sloan-Lancaster J, Kitchen J, Trible RP, Samelson LE (1998) LAT: the ZAP-70 tyrosine kinase substrate that links T cell receptor to cellular activation. Cell 92: 83–92.
24. Zhang W, Sommers CL, Burshtyn DN, Stebbins CC, DeJarnette JB, et al. (1999) Essential role of LAT in T cell development. Immunity 10: 323–332.
25. Horejsi V, Zhang W, Schraven B (2004) Transmembrane adaptor proteins: organizers of immunoreceptor signalling. Nat Rev Immunol 4: 603–616.
26. Poulin B, Sekiya F, Rhee SG (2005) Intramolecular interaction between phosphorylated tyrosine-783 and the C-terminal Src homology 2 domain activates phospholipase C-gamma1. Proc Natl Acad Sci U S A 102: 4276–4281.
27. Lewis RS (2001) Calcium signaling mechanisms in T lymphocytes. Annu Rev Immunol 19: 497–521.
28. Ross SE, Schraven B, Goldman FD, Crabtree J, Koretzky GA (1994) The association between CD45 and lck does not require CD4 or CD8 and is independent of T cell receptor stimulation. Biochem Biophys Res Commun 198: 88–96.
29. Abe R, Vandenberghe P, Craighead N, Smoot DS, Lee KP, et al. (1995) Distinct signal transduction in mouse CD4+ and CD8+ splenic T cells after CD28 receptor ligation. J Immunol 154: 985–997.
30. Ledbetter JA, Imboden JB, Schieven GL, Grosmaire LS, Rabinovitch PS, et al. (1990) CD28 ligation in T-cell activation: evidence for two signal transduction pathways. Blood 75: 1531–1539.

31. Saez-Rodriguez J, et al. (2007) A comprehensive logical model provides insights into T-cell signaling; submitted for publication.
32. Stebbings R, Findlay L, Edwards C, Eastwood D, Bird C, et al. (2007) "Cytokine storm" in the phase I trial of monoclonal antibody TGN1412: better understanding the causes to improve preclinical testing of immunotherapeutics. J Immunol 179: 3325–3331.
33. Sester U, Wabnitz GH, Kirchgessner H, Samstag Y (2007) Ras/PI3Kinase/cofilin-independent activation of human CD45RA(+) and CD45RO(+) T cells by superagonistic CD28 stimulation. Eur J Immunol 37: 2881–2891.
34. Kane LP, Andres PG, Howland KC, Abbas AK, Weiss A (2001) Akt provides the CD28 costimulatory signal for up-regulation of IL-2 and IFN-gamma but not TH2 cytokines. Nat Immunol 2: 37–44.
35. Okkenhaug K, Wu L, Garza KM, La RJ, Khoo W, et al. (2001) A point mutation in CD28 distinguishes proliferative signals from survival signals. Nat Immunol 2: 325–332.
36. Expert Scientific Group (2006) Expert Scientific Group on Phase One Clinical Trials: Final Report. (The Stationary Office, Norwich, United Kingdom, 2006). 1. ISBN-10 0 11 703722 2. http://www.dh.gov.uk/en/Consultations/Closedconsultations/DH_4139038:.
37. Kenter MJ, Cohen AF (2006) Establishing risk of human experimentation with drugs: lessons from TGN1412. Lancet 368: 1387–1391.
38. Hanke T (2006) Lessons from TGN1412. Lancet 368: 1569–1570.
39. Pantaleo G, Olive D, Harris D, Poggi A, Moretta L, et al. (1986) Signal transducing mechanisms involved in human T cell activation via surface T44 molecules. Comparison with signals transduced via the T cell receptor complex. Eur J Immunol 16: 1639–1642.
40. Feske S (2007) Calcium signalling in lymphocyte activation and disease. Nat Rev Immunol 7: 690–702.
41. Varma R, Campi G, Yokosuka T, Saito T, Dustin ML (2006) T cell receptor-proximal signals are sustained in peripheral microclusters and terminated in the central supramolecular activation cluster. Immunity 25: 117–127.
42. Gibbs RA, Rogers J, Katze MG, Bumgarner R, Weinstock GM, et al. (2007) Evolutionary and biomedical insights from the rhesus macaque genome. Science 316: 222–234.
43. Ibegbu C, Brodie-Hill A, Kourtis AP, Carter A, McClure H, et al. (2001) Use of human CD3 monoclonal antibody for accurate CD4+ and CD8+ lymphocyte determinations in macaques: phenotypic characterization of the CD3- CD8+ cell subset. J Med Primatol 30: 291–298.
44. Sopper S, Stahl-Hennig C, Demuth M, Johnston IC, Dorries R, et al. (1997) Lymphocyte subsets and expression of differentiation markers in blood and lymphoid organs of rhesus monkeys. Cytometry 29: 351–362.
45. Nguyen DH, Hurtado-Ziola N, Gagneux P, Varki A (2006) Loss of Siglec expression on T lymphocytes during human evolution. Proc Natl Acad Sci U S A 103: 7765–7770.
46. Kirchgessner H, Dietrich J, Scherer J, Isomaki P, Korinek V, et al. (2001) The transmembrane adaptor protein TRIM regulates T cell receptor (TCR) expression and TCR-mediated signaling via an association with the TCR zeta chain. J Exp Med 193: 1269–1284.

Appendix 14

Reichardt P, Dornbach B, Rong S, Beissert S, Gueler F, Loser K, Gunzer M. Naive B-cells generate regulatory T-cells in the presence of a mature immunologic synapse. **Blood**. 2007;110:1519-1529.

IF: 9.1

Blood. 2007 Sep 1;110(5):1519-29. Epub 2007 Mar 28.

Naive B cells generate regulatory T cells in the presence of a mature immunologic synapse.

Reichardt P, Dornbach B, Rong S, Beissert S, Gueler F, Loser K, Gunzer M.

Helmholtz Centre for Infection Research (HZI), Junior Research Group Immunodynamics, Braunschweig, Germany.

Abstract

Naive B cells are ineffective antigen-presenting cells and are considered unable to activate naive T cells. However, antigen-specific contact of these cells leads to stable cell pairs that remain associated over hours in vivo. The physiologic role of such pairs has not been evaluated. We show here that antigen-specific conjugates between naive B cells and naive T cells display a mature immunologic synapse in the contact zone that is absent in T-cell-dendritic-cell (DC) pairs. B cells induce substantial proliferation but, contrary to DCs, no loss of L-selectin in T cells. Surprisingly, while DC-triggered T cells develop into normal effector cells, B-cell stimulation over 72 hours induces regulatory T cells inhibiting priming of fresh T cells in a contact-dependent manner in vitro. In vivo, the regulatory T cells home to lymph nodes where they potently suppress immune responses such as in cutaneous hypersensitivity and ectopic allogeneic heart transplant rejection. Our finding might help to explain old observations on tolerance induction by B cells, identify the mature immunologic synapse as a central functional module of this process, and suggest the use of naive B-cell-primed regulatory T cells, "bTregs," as a useful approach for therapeutic intervention in adverse adaptive immune responses.

Comment in

Expert Rev Vaccines. 2007 Oct;6(5):667-71.

PMID: 17392507 [PubMed - indexed for MEDLINE]

Naive B cells generate regulatory T cells in the presence of a mature immunologic synapse

Peter Reichardt,[1] Bastian Dornbach,[1] Song Rong,[2] Stefan Beissert,[3] Faikah Gueler,[2] Karin Loser,[3] and Matthias Gunzer[1]

[1]Helmholtz Centre for Infection Research (HZI), Junior Research Group Immunodynamics, Braunschweig; [2] Department of Nephrology, Hannover Medical School, Hannover; and [3]Department of Dermatology and Interdisciplinary Center of Clinical Research (IZKF), University of Münster, Münster, Germany

Naive B cells are ineffective antigen-presenting cells and are considered unable to activate naive T cells. However, antigen-specific contact of these cells leads to stable cell pairs that remain associated over hours in vivo. The physiologic role of such pairs has not been evaluated. We show here that antigen-specific conjugates between naive B cells and naive T cells display a mature immunologic synapse in the contact zone that is absent in T-cell–dendritic-cell (DC) pairs. B cells induce substantial proliferation but, contrary to DCs, no loss of L-selectin in T cells. Surprisingly, while DC-triggered T cells develop into normal effector cells, B-cell stimulation over 72 hours induces regulatory T cells inhibiting priming of fresh T cells in a contact-dependent manner in vitro. In vivo, the regulatory T cells home to lymph nodes where they potently suppress immune responses such as in cutaneous hypersensitivity and ectopic allogeneic heart transplant rejection. Our finding might help to explain old observations on tolerance induction by B cells, identify the mature immunologic synapse as a central functional module of this process, and suggest the use of naive B-cell–primed regulatory T cells, "bTregs," as a useful approach for therapeutic intervention in adverse adaptive immune responses. (Blood. 2007;110:1519-1529)

Introduction

Naive B cells are poor antigen-presenting cells (APC) for naive T cells. In many systems, they have been dispensable for $CD4^+$ T-cell priming.[1,2] Yet antigen presentation by naive B cells is not an immunologic null event. Animals can be rendered tolerant toward antigens presented by naive B cells.[3] Indeed, evidence suggests that B cells can take part in antigen presentation via major histocompatibility complex (MHC) II molecules[4-7] and might even be required to reach full T-cell effector potential.[8]

We have previously shown that naive B cells, despite low efficiency on a per cell basis, when loaded with specific peptide antigen can induce antigen-specific proliferation in naive T cells.[9] However, the biophysics of the underlying T-B contact was very different from bona fide T-cell activation by dendritic cells (DCs).[10] While T-cell contacts to DCs were dynamic and sequential, contacts to B cells were mostly very stable in vitro and in vivo.[9,11] The functional significance of this discrepancy is not clear.

Information transfer between T cell and APC during cell-cell interaction is characterized by the formation of a supramolecular assembly of signaling and adhesion molecules termed immunologic synapse (IS).[12] Its exact function is still debated yet it is generally accepted as a T-cell activating structure.[13,14,14] A mature IS presents with a distinguished central part of the supramolecular activation cluster (c-SMAC) enriched in signaling molecules like T-cell receptor (TCR) and MHC, and a peripheral part (p-SMAC) enriched in adhesion molecules.[15] The formation of a mature IS takes between 30 to 60 minutes.[12] Encounters between DCs and T cells in early and late phases of immune responses, however, last only for several minutes.[16,17] This is too short to form a mature IS. In contrast, antigen-specific contacts to naive B cells invariably last several hours.[9] It is unclear whether a mature synapse can form under these circumstances.

Based on these arguments, we reasoned that the molecular organization of the IS between T cells and naive B cells might be different from the one found in T-DC pairs. We also wanted to test the potential consequences for the resulting activated $CD4^+$ T cells. To further evaluate the outcome of antigen-specific $CD4^+$ T-cell stimulation by naive B cells, we investigated the molecular structure of the underlying IS and the phenotype of $CD4^+$ T cells after in vitro contact with specific-antigen loaded naive B cells or DCs.

We present evidence that stimulation of naive T cells by naive B cells results in formation of a mature IS which is absent in DC–T-cell pairs. In addition, while DC stimulation generates classical effector T cells, naive B-cell–activated T cells show regulatory capacity in vitro and in vivo.

Materials and methods

Mice

DO11.10 mice carrying a transgenic TCR that recognizes a peptide of chicken ovalbumin (AA 323-339), pOVA, in context with $I\text{-}A^d$,[18] and OT-II mice carrying a TCR that recognizes the identical peptide in context with $I\text{-}A^b$ [19] were used as T-cell sources. C57BL/6 ($H\text{-}2^b$) and Balb/c ($H\text{-}2^d$) mice

Submitted October 23, 2006; accepted March 22, 2007. Prepublished online as *Blood* First Edition paper, March 28, 2007; DOI 10.1182/blood-2006-10-053793.

The publication costs of this article were defrayed in part by page charge payment. Therefore, and solely to indicate this fact, this article is hereby marked "advertisement" in accordance with 18 USC section 1734.

as sources of B cells and bone marrow DCs (bmDCs, DCs) were purchased from Harlan Germany. IL-10 KO mice were a kind gift from Werner Müller, Helmholtz Centre for Infection Research (HZI), Braunschweig, Germany. Animals were housed under specific pathogen-free conditions and treated according to institutional guidelines. All animal experiments were approved by the animal protection committee of the regional board of Braunschweig, Germany.

Cell preparation

Naive $CD4^+$ T cells from spleens of DO11.10 or OT-II mice were enriched by negative isolation via immunomagnetic depletion (Miltenyi, Bergisch-Gladbach, Germany) to purities of more than 90% and 80%, respectively (75%-85% TCR transgenic). Separation of naive splenic B cells from Balb/c or C57BL/6 mice resulted in purities between 90% to 95% B220/MHCII+/+cells. Pre-activated B cells were generated by coculture of naive B cells with T cells in a 1:1 to 1:2 (T:B) ratio. After 72 hours, pre-activated B cells were isolated as described above. BmDCs (DCs) were generated in 8-day cultures as described[20] and activated with 20ng/mL LPS (E.coli 0111, B4; Sigma, Deisenhofen, Germany) during the final 2 days of culture. Cell lines secreting murine granulocyte-macrophage colony-stimulating factor or IL-4 were kindly provided by Thomas Blankenstein, Max Delbrück Center for Molecular Medicine (MDC), Berlin. pOVA (10 μg/mL; Peptide Core facility, HZI, Braunschweig, Germany) was added to the cultures of B cells, and DCs overnight and for the final 4 hours, respectively, before use.

In vitro T-cell activation assays

Primary T-cell activation. Naive T cells (10^5) were cocultured in 96-well round bottom plates (Nunc, Roskilde, Denmark) with 10^4 mature, antigen-loaded DCs or 10^5 antigen-loaded B cells unless noted otherwise. The liquid medium used was RPMI-based and fetal calf serum (FCS) supplemented (Gibco, Los Angeles, CA). For some experiments, 3-D collagen gels were used.[10] Gels were digested by type VII collagenase (30 U/100mL gel for 30 minutes at 37°C; Sigma). For estimation of T-cell proliferation, naive T cells were stained with 5,6-carboxyfluorescein diacetate, succinimidyl ester (CFSE, 0.5 μM; Molecular Probes, Leiden, Netherlands). To obtain B-cell– and DC-primed T cells, cocultures underwent immunomagnetic depletion of non-$CD4^+$ cells after 72 hours. Naive T cells were CFSE-labeled and cocultured with DCs as described in "Cell preparation." Varying numbers of B-cell– (TofB) or DC (TofDC)–primed T cells were added to test their inhibitory effects on naive T cells, typically at a ratio of 1:1 (T primed: T naive). Readouts for proliferation or activation markers were taken at 72 hours by flow cytometry.

Transwell experiments

Transwell experiments were done in 24-well plates (Nunc) using 10^6 naive, CFSE-labeled $CD4^+$ T cells plus 10^5 antigen-loaded mature DCs. In addition, 10^6 TofDCs, TofBs, or naive T cells were either directly added or placed in transwell chambers (Millicell, 0.4 μm; Millipore, Billerica, MA) in the same well. Readouts for proliferation were taken at 72 hours by flow cytometry.

Adoptive transfer and flow cytometric determination of in vivo distribution of T cells

Primed T cells were dually stained with CFSE and with Cell Tracker Orange (CTO), 5-(and-6)-(((4-chloromethyl)benzoyl)amino) tetramethylrhodamine-mixed isomers (CMTMR; Molecular Probes), or carbocyanine (DiD, Vybrant DiD; Molecular Probes). T cells, 5×10^6 per type, were intravenously injected into tail veins. At indicated timepoints, mice were anesthesized with Isoflurane (Deltaselect, Pfullingen, Germany), bled by retroorbital venous puncture and killed to obtain spleen, Peyer Patches, and mesenteric, inguinal, popliteal, axillar, and cervical lymph nodes. Flow cytometric analysis of transferred cells was done based on the dual dye labeling.

Flow cytometry of surface activation marker and intracellular cytokines

The anti-CD11c was from Caltag (Burlingame, CA); antibodies against other surface markers came from BD Pharmingen (San Jose, CA); CCL19-huFc-Protein and anti-huFc were from eBioscience (San Diego, CA); anti-IL-2, anti-IL-4, IL-10, and IFNγ were from Invitrogen (Karlsruhe, Germany); the Fix&Perm Kits with Golgiplug from BD Pharmingen; anti-Foxp3 (FJK 16s) and staining kits were from eBioscience. Flow cytometry was performed on a BD Pharmingen FacsCalibur. Mean fluorescence intensity (MFI) was shown against the secondary antibody control.

ELISA

OptEIA kits (BD Pharmingen) were used for determining IL-2, IL-10, and IFNγ.

Immunohistology/confocal microscopy

Fixed cell pairs were generated by mixing DO11.10 T cells with pOVA loaded naive Balb/c B cells in a ratio of 1:1, with pre-activated B cells 1:5, and with mature DCs 1:5 (T cell: APC), in 96-well round bottom plates in FCS-supplemented RPMI-based media for 2 hours. Cells were transferred onto Poly-L-Lysine (Sigma)–coated cover slips, fixed with warm 4% paraformaldehyde and permeabilized with 0.1% Triton X-100 (Sigma) in PBS. Blocking with 5% horse serum in 1% bovine serum albumin (BSA, Sigma). Staining in 1% BSA using 2 U/mL Alexa-488-Phalloidin (Molecular Probes), 5 μg/mL biotinylated anti-DO11.10 TCR (KJ1.26, Caltag), and 5 μg/mL Streptavidin-Cy3 (Dianova, Hamburg, Germany). Samples were mounted in Mowiol (Calbiochem, Darmstadt, Germany) with 2.5 mg/mL N-Propylgallate (Sigma) as antifading reagent. Analysis was done with an Olympus FluoView1000 confocal microscope (Olympus, Hamburg, Germany) performing 3-D-reconstructions of z-stacks (mean width 0.2 μm/slice), scanning with 40 μs/Pixel using Kalman mode. Images were taken with a PLAPO 100×/TIRFM-SP, NA 1.45 oil immersion lens at room temperature. Reconstructions were made with the Olympus FluoView Software FV10-ASW, version 1.6 as well as with LSM Image Browser version 4.0 (Zeiss, Jena, Germany).

2-photon-microscopy of explanted lymph nodes

Naive T cells, TofBs, and B cells were labeled with 1 μM CFSE, CTO, or 7-amino-4-chloromethylcoumarin (CMAC, also called CTB, Cell Tracker Blue, Molecular Probes). Inversion of colors had no effect on results. TofBs (10^7) were injected intravenously into the tail veins of Balb/c mice 48 hours before imaging; 2×10^7 naive T cells and 3×10^7 naive B cells were applied 24 hours before imaging. Inguinal lymph nodes were removed and immediately subjected to imaging in pH-stabilized culture media constantly warmed to 37°C. Three-D 2-photon microscopy was performed with a MaiTai laser (Spectra-Physics, Darmstadt, Germany) running at 800 nm, a multibeam scanhead (LaVision Biotech, Bielefeld, Germany) and an Olympus BX51WI stage equipped with a XLUMPL 20×/0.95 NA water dipping lens. Image detection was made with a cooled CCD-camera (Imager Intense; LaVision, Goettingen, Germany). For estimation of TofB distribution, RGB z-stacks of 200×200 μm images were recorded in 48 steps of 3μm. A total of 932 cells were quantified in 14 extended focus projections within B follicles (> 90% B cells), in T-cell zones (> 80% T cells), and in mixed T-B areas, respectively.

Contact hypersensitivity

Mice were sensitized by painting 100 μL 2,4-dinitrofluorobenzene (DNFB) solution (Sigma; 0.5% in acetone/olive oil 4:1) on the shaved backs on day 0 as described.[21] On day 5, the left ear was challenged by applying 12 μL 0.3% DNFB, and the right ear was treated with acetone/olive oil alone. Ear swelling was measured in a blinded fashion with a spring-loaded micrometer (Mitutoyo, Hamburg, Germany) 48 hours after challenge (day 7). Contact hypersensitivity was determined as amount of swelling of the hapten-challenged ear compared with thickness of vehicle-treated ear and was expressed in μm (mean ± standard deviation [SD]). Mice that were ear-challenged without previous sensitization

served as negative controls. The immunoregulatory effect of adoptively transferred primed T cells was tested by intravenously transferring 0.5 to 5×10^6 MACS-separated DC–primed or B-cell–primed T cells at day 1 (for inhibition of priming) or at day 4 (for inhibition of challenge), or at d 10 (for inhibition of priming at later stage after transfer). In the latter case, mice received an (un)specific antigen boost at day 1. Control mice received media only. Each group consisted of 8 mice.

Allogeneic heart transplantation

Heterotopic vascularized heart transplantation was carried out according to the method of Corry et al.[22] Male C57BL/6 (H-2b) and female BALB/c (H-2d) were used as donors and recipients, respectively. Briefly, animals were anesthetized with isoflurane. The donor pulmonary artery was anastomosed to the recipient inferior vena cava and the donor ascending aorta was anastomosed to the recipient abdominal aorta. 2 experimental groups of 6 animals each were evaluated: Recipients of the control group were treated with saline and recipients of the TofB group received 5×10^6 cells via tail vein injection 24 hours prior to transplantation. No other immunosuppressive treatment was administered. Graft function was assessed by daily palpation. Rejection was defined as the lack of palpable cardiac contraction.

Statistical analysis

Survival analysis was performed using a Kaplan-Meier estimator as part of the statistical package in GraphPad Prism 4 (GraphPad Software, San Diego, CA). For all other statistics, Student *t* test was applied. Significance levels used are indicated in "Results."

Results

Naive B cells signal to naive T cells via a mature immunologic synapse

To study the molecular makeup of the interface between naive T cells and different APC, we established pairs of chicken ovalbumin-specific T cells[18] interacting with either naive splenic B cells or mature bmDCs, each loaded with specific peptide. Since the initial description of the mature immunologic synapse,[15] a large number of molecules were found to be characteristically located at c- and p-SMAC, respectively. The prototypic marker for c-SMAC is the TCR complex.[15] A more recent study shows that f-actin is highly enriched in p-SMAC.[23] Thus we chose to study the spatial distribution of f-actin and the peptide-specific TCR. T cells (Figure 1A,E,I) and naive B cells (Figure 1A) recruited the majority of their cortical actin cytoskeleton toward the contact zone, while DCs (Figure 1I) showed a very prominent actin scaffold that was not enhanced at the T-cell contact. While with T cells contacting naive B cells (Figure 1A) almost the entire TCR was located at the B-cell contact zone, surprisingly, the TCR in T cells contacting DCs remained scattered over the entire T-cell surface (Figure 1I). A three-dimensional reconstruction confirmed that in the contact plane to DCs no c-SMAC enrichment of TCR or p-SMAC enrichment of actin was detectable (Figure 1J,L). However, the contact zone to B cells presented as a structure with highly concentrated actin in the p-SMAC and the majority of TCR signal in the c-SMAC (Figure 1B-D). This pattern was consistently found in almost 90% of T naive B pairs, while more than 90% of the DC contacts did not show a mature IS (Figure 1M). To assess the impact of the activation state of the B cell, we also analyzed pairs of preactivated B cells and T cells (Figure 1E-H′). Preactivated B cells showed an intermediate phenotype of IS formation with heterogenous IS structures. In some cases this plasticity of IS phenotype could even be found on a single preactivated B cell contacting multiple naive T cells (Figure 1F-H and F'-H'). Quantitatively, the majority (80%) of preactivated B cells did not show a c-SMAC-(mature)–type of IS, while 20% did (Figure 1M). As parameter for the activation level we measured expression of the primary costimulatory molecules CD80 and CD86 and found an increase in CD86 in preactivated B-cells and an increase of

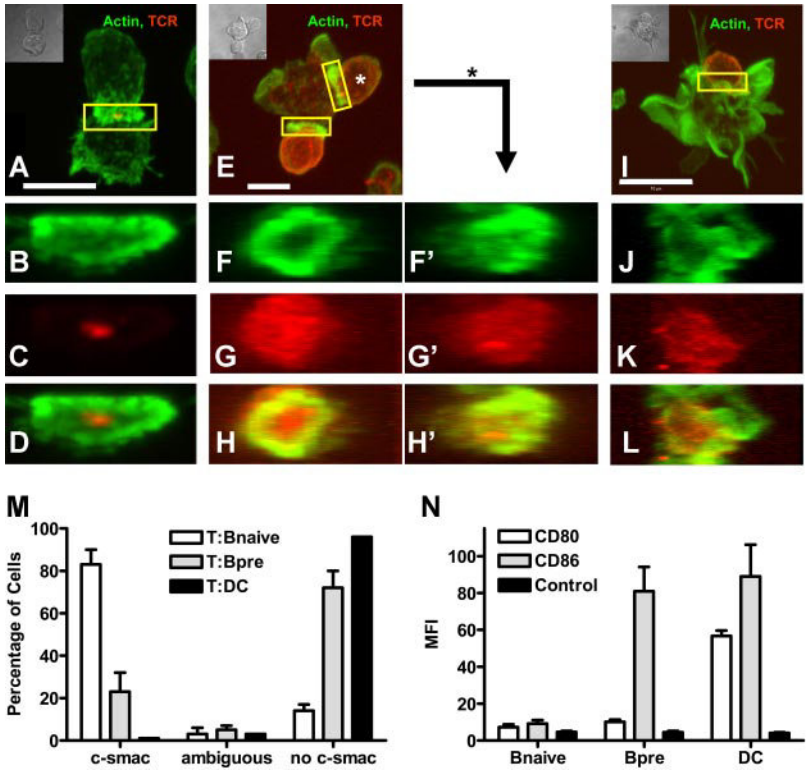

Figure 1. Naive B cells naive T cells form a mature immunologic synapse. Mature bmDC or naive or preactivated splenic B cells were loaded with pOVA. Cells were mixed with naive DO11.10 T cells and fixed after 120 minutes of interaction. Immunohistologic staining was performed for actin (green) and the clonotypic TCR (red). Individual pairs of T cells and naive B cells (A-D), T cells and preactivated B cells (E-H') or T cells and DC (I-L), respectively, were analyzed by 2-color confocal microscopy making Z-stacks over the entire range of a cell pair. T cells in contact with B cells have the entire TCR signal at the contact plane (A), while T cells attached to DC show TCR staining scattered over the body (I). T cells in contact with preactivated B cells show both accumulation of TCR and distribution over the whole T-cell surface (E). A three-dimensional reconstruction showing the en face view of the contact plane reveals no preferential accumulation of TCR in the contact with DC, see Actin-stain (J), TCR-stain (K), and merged image (L). In contrast, in T-cell–naive B-cell pairs the TCR signal is focused in the center of contact (B-D). Interactions with preactivated B cells show partially the formation of a mature IS (F-H'). Shown is a T-B interface resembling a mature IS, yet with substantially scattered TCR (T cell at 6 o'clock, F-H); and an interface between the same preactivated B cells interacting with a second T cell, showing almost no IS segregation (T cell at 2 o'clock, F'-H'). The scale bar defines 5 μm (A,E) and 10 μm (I), respectively. (M) Quantitative analysis of 300 random individual cell pairs for the distribution of TCR in the contact plane. (N) Mean Fluorescence Intensity (MFI) analysis of the expression of costimulatory molecules on APC. While naive splenic B cells show only a sparse expression of CD80 and CD86, CD86 is clearly up-regulated upon B-cell activation. DCs exhibit a high amount of CD80 as well as CD86 on their surface. (M,N) Bars represent mean plus or minus SD.

CD80 and CD86 in DCs compared with naive B cells (Figure 1N). IS formation in B-T pairs was antigen-specific as no IS formation was seen when B cells were left unloaded (data not shown). Taken together, naive B cells loaded with specific antigenic peptide engage naive T cells under formation of a mature IS.

CD4$^+$ T-cell stimulation by specific antigen-loaded naive B cells results in activated T cells with an unusual phenotype

We now asked whether the phenotype of activated CD4$^+$ T cells based on such diverse IS structures would differ. We therefore focused on naive B cells and mature DCs as these APC had shown the most extreme forms of IS structure (Figure 1). We first looked at the induction of T-cell proliferation and changes in characteristic activation markers. After 72 hours of in vitro stimulation with pOVA-loaded naive C57BL/6 B cells, TCR-transgenic OT-II T cells showed clear induction of proliferation (Figure 1A). When appropriate numbers of APC were used (B:T = 1:1; DC:T = 1:10), equivalent proliferation levels were reached. In addition, efficient and, within the type of APC, equivalent up-regulation of CD69 and CD44 (not shown) as well as CD25 (Figure 2A top row) was induced. Interestingly, under identical conditions, only DCs, but not B cells, induced down-regulation of CD62L in T cells driven into proliferation (Figure 2A bottom row). CD62L is a key molecule mediating T-cell entry into lymph nodes; its down-regulation is a hallmark for effective CD4$^+$ T-cell activation.[24] This effect was seen for all peptide concentrations tested, while DCs showed a similar behavior only at very low antigen concentrations in vitro (Figure 2B). Loading APCs with intact protein instead of peptide led to similar results (data not shown). As it was possible that the observed discrepancy between effective induction of proliferation and ineffective down-regulation of CD62L was an artifact of the two-dimensional liquid culture system, we looked at T-cell priming in a three-dimensional collagen matrix featuring a network of type I collagen fibres, the major component of the extracellular matrix. Cell behavior measured in this three-dimensional matrix closely resemble values observed in vivo.[9-11,25-27] Again, under conditions where equivalent and effective T-cell activation (based on CD69 levels) could be observed, DCs effectively down-regulated CD62L while B cells did not (Figure 2C). Next we wondered whether the induced phenotype of B cells was dominant over simultaneous DC stimulation. Thus, we looked at T-cell activation after contact with a mixture of B cells and DCs. As seen in Figure 2D, in the presence of 10% (compared with B cells) DCs, CD62L was down-regulated, indicating the dominance of T-cell activation by DCs over the one by B cells when both cell types were used as APC. This supremacy could be detected even at DC numbers as low as 1% (data not shown). The dominating role of DCs as APC in vivo has been demonstrated extensively.[28] In conclusion, exclusive stimulation of T cells by naive B cells results in activated T cells that retain high levels of CD62L.

In vivo, B-cell–stimulated T cells, TofBs, preferentially migrate to lymph nodes

Our result that naive B-cell–activated T cells, TofBs, did not down-regulate CD62L made us investigate possible implications of this finding in vivo. As CD62L mediates the entry of T cells into lymph nodes,[29] we reasoned that TofBs would predominantly migrate there. Indeed, when adoptively transferring intravenously

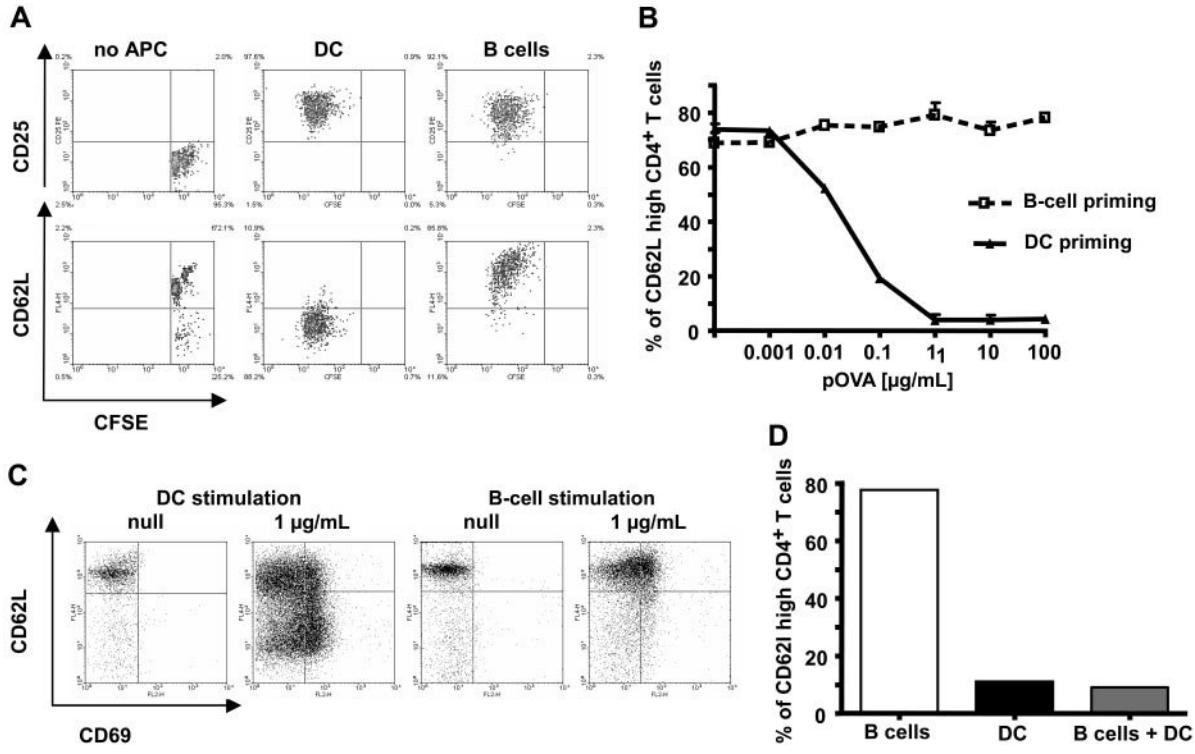

Figure 2. Antigen-specific T-cell activation by B cells leads to generation of T cells with aberrant phenotype. Naive splenic CD4$^+$ T cells were cocultured in vitro with mature DC or B cells, both loaded with specific antigenic peptide. After 72 hours, proliferation and expression of surface markers were determined by fluorescence-assisted cell sorting (FACS). (A) Specific antigenic peptide loaded B cells efficiently induce proliferation and up-regulation of CD25 in CD4$^+$ T cells. In contrast to DC, however, B cells fail to down-regulate CD62L. (B) B cells remain unable to down-regulate CD62L even at high antigen doses. (C) The failure to downmodulate CD62L levels by B cells is not restricted to a two-dimensional environment as it is also seen in a three-dimensional environment using a collagen matrix. (D) CD62L is down-regulated in cultures in which DC were added (10% of corresponding B-cell number). The data shown are representative of 3 to 5 independent experiments.

equal numbers (5×10^6) of dually stained TofBs or DC-primed T cells (TofDCs), respectively, TofBs clearly outnumbered transferred TofDCs in peripheral lymph nodes. In contrast, both populations were found at equal proportions in blood and spleen, where CD62L is not involved in the entry of cells[30] (Figure 3A-C). We also measured expression of CCR7, another important homing receptor for entry into lymph nodes. Using a monoclonal antibody as well as a CCL19-Fc fusion protein we found that TofBs retain CCR7 at levels similar to those in naive T cells (data not shown). However, as TofDCs showed comparable CCR7 expression, this molecule is unlikely to account for the differences in homing we observed.

To assess more precisely the localization of TofBs within the lymph node we used two-photon microscopy imaging studies. We found that adoptively transferred TofBs resided primarily in T-cell zones and were basically excluded from B-cell follicles (Figure 3D,E). Thus, B-cell–primed T cells migrate preferentially to the T-cell zones of peripheral lymph nodes where cell entry from the circulation is known to be mediated by CD62L.

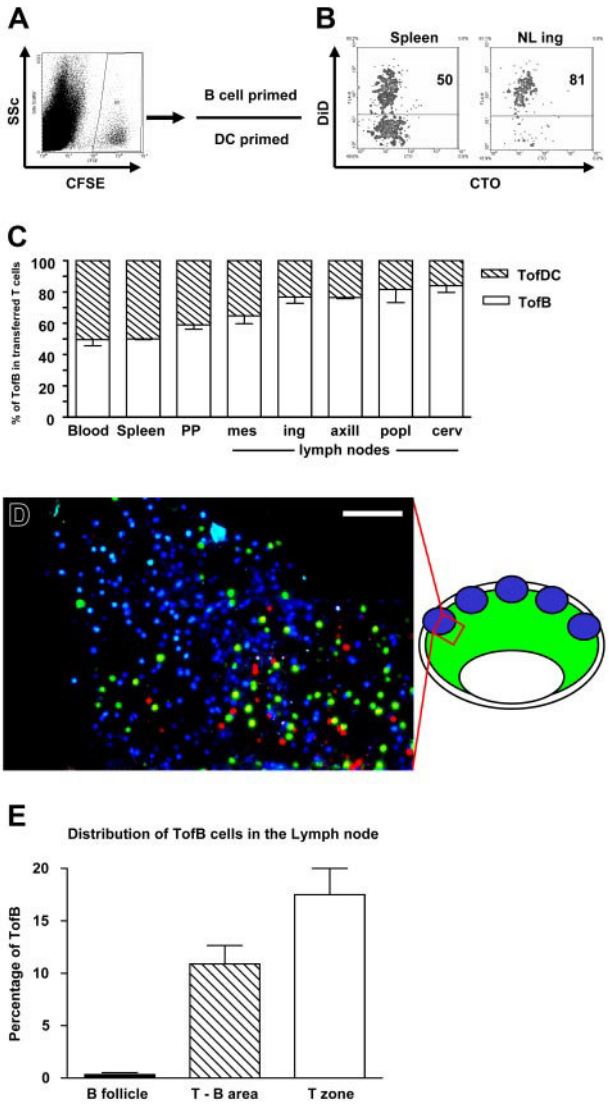

Figure 3. In vivo B-cell–primed T cells (TofB) preferentially migrate to lymph nodes. T cells primed by peptide-loaded DC and B cells were differentially labeled with live cell dyes. Equal numbers of TofDCs and TofBs were adoptively transferred intravenously, and distribution of the cells was determined 24 hours after transfer by organ removal and FACS analysis. (A) T cells for adoptive transfer were labeled with CFSE; TofDCs were additionally labeled with CTO and TofBs with DiD. (B) Upon organ analysis after transfer, equal numbers of TofDCs and TofBs as transferred can be found in the spleen, whereas in lymph nodes TofBs clearly dominate. (C) Distribution of the transferred T-cell populations in lymphatic organs 24 hours after transfer. When analysis was performed at day 7 after transfer, a similar pattern was observed (data not shown). The data shown are representative of at least 3 independent experiments. Within the lymph nodes, TofBs migrate to T-cell areas and are excluded from B-cell follicles. A simplified drawing illustrates lymph node architecture showing B-cell areas (blue), T-cell dominated areas [green], and the imaged area shown above (red rectangle) at the transition of the 2 zones. (D) An image stitched together of 6 individual extended focus projections of each 200 × 200 × 144 μm shows the transition from a B-cell follicle dominated by B cells (blue) to a mixed T-B zone containing mostly naive T cells (green). Note that TofBs (red) are found only in the T-cell area. Scale bar: 100 μm. (E) A quantification of TofB distribution analyzing 14 image stacks from within and outside B-cell follicles. TofBs clearly show T-cell homing behavior and localize within T-cell–dominated areas but are excluded from B-cell follicles. Bars represent mean plus or minus SD.

TofBs (but not TofDCs) regulate priming of naive T cells

The propensity of TofBs to home into lymph nodes might affect their involvement in immune responses. Classical $CD4^+$ T-cell activation results predominantly in short-lived effector cells that home to peripheral sites of infection/inflammation.[31-33] In addition, a fraction of activated cells turns into effector memory (EM) and central memory (CM) cells.[34] While EM are long-lived in peripheral organs, CM remain localized in central lymphatic tissue, most notably the spleen.[34] TofBs share a $CD4^+$ $CD62L^+$ phenotype with CM, yet do not preferentially home to the spleen (Figure 3). We also tested for a recently identified key memory T-cell marker, CD127 (IL-7 receptor alpha chain), which is important for cells of the $CD8^+$[35,36] and to some degree also of the $CD4^+$ lineage.[37,38] TofBs showed very low levels of CD127 on days 3 and 7 of the priming process (data not shown). Collectively, there was no evidence that TofBs belong to the memory T-cell lineage. Interestingly, there are reports that absence of expression of human CD127 correlates with a regulatory function.[39] Such regulatory T cells of natural occurrence (nTreg) are characterized by CD4, CD25 double positivity.[40] In addition, the subgroup of CD62Lhigh nTregs was shown to have regulatory activity in autoimmune processes.[41,42] Thus, we wanted to see whether the $CD4^+$/$CD25^+$/CD62Lhigh TofBs also show regulatory capacity.

The key activity of Tregs is the (down)regulation of an immune response, the inhibition of T-cell proliferation.[43] We therefore tested the effect of TofBs on fresh, naive T cells during priming by specific-antigen-loaded DCs in vitro. Indeed, TofBs inhibited almost completely the induced proliferation in naive T cells, whereas TofDCs did not (Figure 4A). The effect could be titrated and depended on the ratio of Treg versus T naive (Figure 4B). The inhibitory effect was seen upon priming by peptide but not by protein antigen (Figure 4C). The reason for the inability of protein to induce Tregs is most likely the well-known inherent incapability of B cells to take up and present complete protein. More than 100 times higher amounts of protein on a weight basis than peptide were necessary to induce T-cell proliferation in our system (data not shown). Thus, the great majority of T cells remain naive (based on low expression of CD69, CD25, CD44, and absence of CFSE-diluted proliferation, data not shown) after contact to B cells loaded with protein and, therefore, do not show regulatory capacity.

We also included pre-activated B cells in our studies and compared them with naive B cells and DCs in their capacity to induce regulatory T cells. We found that T cells generated by antigen-specific contact with pre-activated B cells (TofBpre) inhibit the proliferation of naive T cells in vitro to some degree, yet they do so clearly less than TofB(naive). In addition, TofBs retain considerably less CD62L than TofB(naive) (data not shown). Taken together and in accordance with our findings on IS formation

(Figure 1), TofBpre show an intermediate phenotype with characteristics between those found in TofB(naive) and TofDCs.

Taken together, we provide evidence that naive B-cell–primed T cells, TofBs, can suppress the proliferation of naive T cells in vitro.

B cells substantially induce IL-2 and IFNγ in CD4+ T cells following antigen-specific contact. B cells are the source of IL-10 found in T-B cocultures but the generation of regulatory T cells is IL-10 independent

To explore the mechanism by which TofBs exert their regulatory effect, we characterized the cytokine profile in T-APC-cocultures. In T-DC– and T-B–cocultures, substantial and approximately equivalent amounts of IL-2 and IFNγ were present (Figure 5A,B). When identical numbers of B cells and DCs were used in their respective cocultures, approximately half the amount (1415 pg/mL vs 720 pg/mL) of IL-2 was induced after B-cell contact (Figure 5A). Interestingly, we found much higher levels of IL-10 in the supernatants of T-B–cocultures than in supernatants of T-DC–cocultures (Figure 5B). This appeared noteworthy at this point as one regulatory T-cell subset (TR cells) is known to act via secretion of IL-10.[44,45] However, when tested at single cell level by intracellular cytokine staining, B cells were revealed as the source of IL-10 (Figure 5C,D). Previously, IL-10 produced by APC was found to be involved in induction of a tolerogenic T-cell phenotype.[46-48] However, subsequent testing in our study with B cells from IL-10 KO mice revealed that IL-10 was

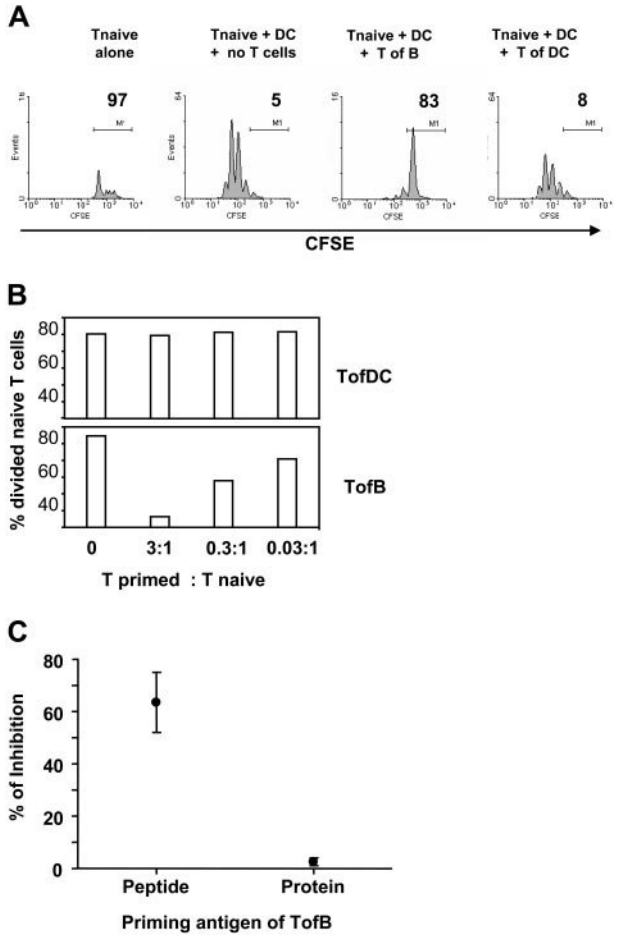

Figure 4. TofBs show regulatory capacity and suppress the proliferation of naive T-cells. Differentially primed T cells were added to in vitro cocultures of naive, CFSE-labeled CD4+ T cells and mature DCs loaded with antigenic pOVA. At 72 hours, proliferation of the naive T cells was determined by FACS. (A) Upon addition of TofBs but not of TofDCs, proliferation of naive T cells determined by CFSE-dilution is markedly inhibited. Equal numbers of cells (10^5) were used. No proliferation is observed when naive T cells are cultured in the absence of DCs. (B) The regulatory effect of TofBs can be titrated. When TofBs were added at a ratio of 3:1 to naive T cells, the effect was more pronounced. At a ratio of 0.03:1, minor effects can be seen. In contrast, TofDCs do not show inhibition even at a 3:1 ratio over naive T. (C) The inhibitory effect can only be observed after B-cell loading with specific peptide (pOVA) but not with complete protein (Ovalbumin). The data shown are representative of 2 (panel B) to 5 (panels A,C) independent experiments. Dots represent the mean plus or minus SD.

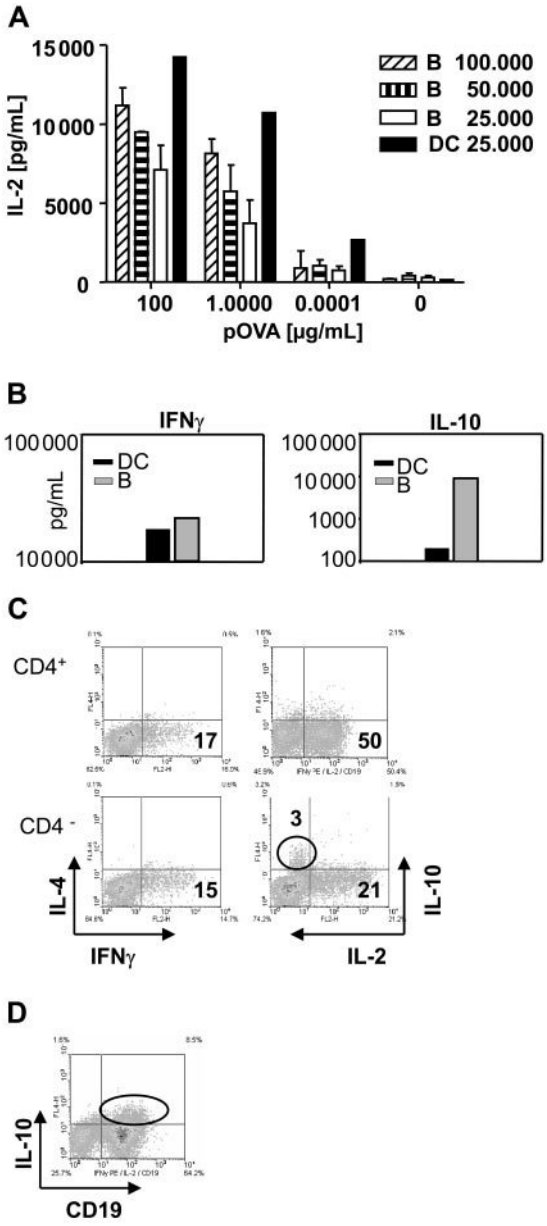

Figure 5. Cytokine profile during the activation of T cells by B cells shows substantial amounts of Th1 cytokines but also high levels of B-cell–derived IL-10. Supernatants were taken from DC–T-cell and from B-cell–T-cell cocultures and analyzed for cytokines by ELISA. Cells were analyzed for intracellular cytokines by FACS at 48 hours of culture. (A) B cells induce substantial amounts of IL-2 in supernatants of B-cell–T-cell cocultures, but DCs are at least twice as powerful on a per-cell basis. Bars represent mean plus or minus SD. (B) While equivalent amounts of IFNγ can be observed in supernatants of DC–T-cell and B-cell–T-cell cocultures, a marked increase in the amount of IL-10 is found in cultures containing B cells. (C) Intracellular cytokine staining reveals that IL-10 is produced by the CD4 negative population. The level of induced IL-4 is low for all cells. (D) Costaining with the specific B-cell marker CD19 identifies B cells as the source of IL-10. The data shown are representative of 3 independent experiments.

dispensable for the generation of TofBs with regulatory phenotype (data not shown). Thus, B-cell priming leads to substantial induction of Th1 cytokines in T cells. B cells are the source of concomitantly found IL-10 but the mechanism of induction of T cells with regulatory phenotype is IL-10 independent.

The mechanism of regulation by TofBs requires close cell-cell proximity and is independent of Foxp3

Naturally occurring, "classic," $CD4^+$ $CD25^+$ Tregs were shown to mainly act independently of soluble mediators such as cytokines and to depend on very close cell-cell interactions as recently reviewed.[49] It was possible that TofBs also required the proximity of interacting cells for proliferation inhibition. We tested this hypothesis by using a Transwell membrane assay. This assay tests whether for a given effect cells need to be in close proximity, either because direct cell-cell contact is necessary or because potentially required soluble messengers are released in limited amounts and work only at short distances. Indeed, regulation by TofBs requires naive T cells to be in close proximity (Figure 6A). A molecular marker for classical $CD4^+$ $CD25^+$ Tregs is the transcription factor

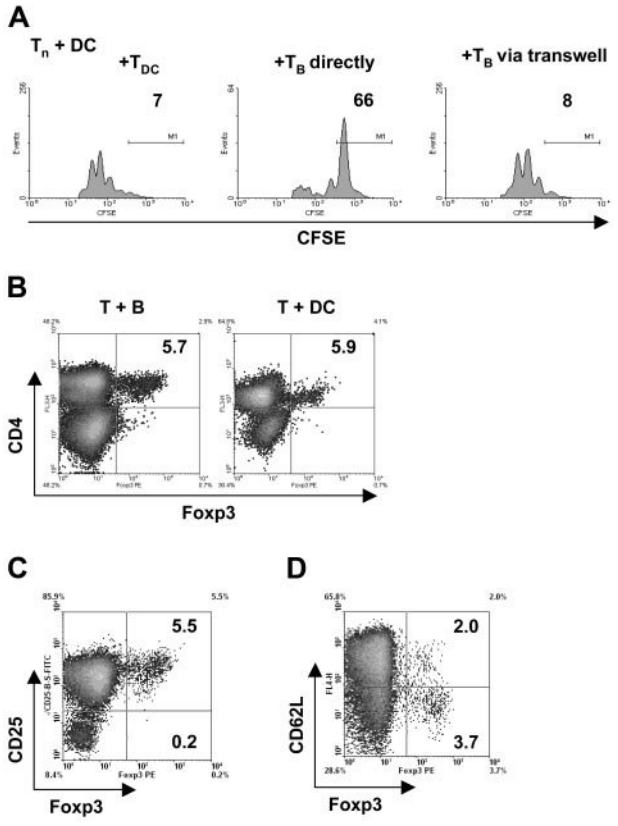

Figure 6. The generation of T cells with regulatory capacity requires immediate vicinity of cells but is independent of Foxp3. (A) To in vitro cocultures of naive, CFSE-labeled $CD4^+$ T cells and mature DC loaded with antigenic peptide (pOVA 323-339), TofDC or TofB were added directly and via a semipermeable transwell membrane. At 72 hours, proliferation of the naive T cells was determined by FACS. Close cell contact is needed for exertion of the regulatory effect of TofB, as separation from naive T cells plus DC via a transwell membrane abrogates the effect. (B-D) The level of the transcription factor Foxp3 was determined via intracellular staining and FACS after 72 hours of cocultures of naive splenic $CD4^+$ T cells with peptide-loaded mature DC or B cells, respectively. (B) Preferential induction of $Foxp3^+$ T cells could not be observed after B-cell contact; equally low numbers were found in Tof B and TofDC. (C) The $Foxp3^+$ T cells are also $CD25^+$. Depicted is the result for the $CD4^+$ TofB population only. (D) The positivity of Foxp3 is independent of the CD62L level. Depicted is the result for the $CD4^+$ TofB population only. The data shown are representative of at least 3 independent experiments.

Foxp3.[50] If TofBs use identical mechanisms as these Tregs, a great part of TofBs in contrast to TofDCs should be $Foxp3^+$. We found, however, that this was not the case. Only 5% of TofBs were $Foxp3^+$, the same amount as within TofDCs (Figure 6B). This proportion was also unchanged from naive T cells (not shown). $Foxp3^+$ cells resided exclusively in the $CD4^+$ $CD25^+$ population (Figure 6C) but no correlation was seen with expression of CD62L (Figure 6D). Most of the $Foxp3^+$ Tregs were CD62L low. In conclusion, B-cell priming of T cells does not lead to an increased frequency of $Foxp3^+$ Tregs. Therefore, we believe that TofBs act via pathways different from the ones of classical Tregs and do not require increased expression of Foxp3 yet need close cell-cell proximity.

TofBs inhibit priming of T cells during immune responses in vivo

Having demonstrated immunoinhibitory effects in vitro we then tested the effects of TofBs in vivo. First, we used a hapten hypersensitivity assay, where TofB were added to recipients at different timepoints to dampen an immune response elicited by priming and challenge with DNFB. The resulting inflammatory response was significantly reduced when TofBs were added to recipients shortly before priming (Figure 7B). In contrast, when TofBs were added shortly before challenge, no effect was seen (Figure 7A). This discrepancy complies with our finding that TofBs migrate preferentially to lymph nodes where they are most effective during priming. Thus, we could show that TofBs mediate immunoregulation during the priming phase of immune responses in vivo.

We then tested whether TofBs maintain their function over a longer time span and whether function at later timepoints requires specific antigen restimulation. To this end we extended the hapten hypersensitivity assay, injecting TofBs 10 days before sensitization. Without specific restimulation, TofBs were not able to suppress priming at day 0. However, the cells were still present and functional as application of specific antigen at day –1 re-activated suppressor function (Figure 7C). Thus, TofBs are present at least 10 days after intravenous transfer but only regulate upon specific antigenic restimulation.

Finally, we wanted to test TofBs in a model of ectopic allogeneic heart transplantation. Based on our observation that TofBs preferentially home to lymph nodes, we expected them to work most efficiently when applied before initiation of immune response, before an immune challenge occurs. Indeed, TofBs were able to successfully suppress rejection and prolong functioning of transplanted allogeneic hearts significantly (Figure 7D). Thus, TofBs are able to suppress solid organ transplant rejection in vivo.

Discussion

The outcome of interactions between resting B lymphocytes and naive T cells has always spurred a controversial discussion.[51] Initially, contacts were believed to be nonproductive in vivo.[1] Later, evidence accumulated that B cells can induce tolerance.[3,52] Under some circumstances, B cells were even found to be effective T-cell activators.[53] It is known that naive B cells show a lesser number of MHC-II and coactivation molecules on their surface than DCs,[54] and Figure 1N. In that sense, B cells may be similar to immature DCs, which can also induce T-cell tolerance.[55-57] However, to our knowledge this is the first report that tolerization after B-cell contact can be mediated, at least in

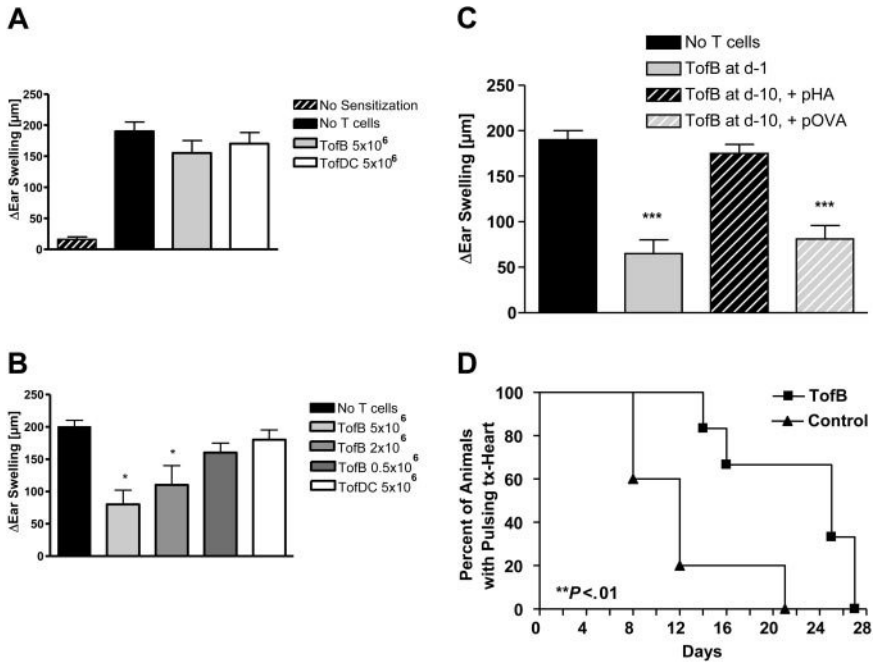

Figure 7. TofBs inhibit priming of T cells during immune responses in vivo. (A-C) In a hapten hypersensitivity assay, Balb/C mice were sensitized against DNFB by epicutaneous application on the back. Ears were challenged with DNFB 5 days later and ear swelling was measured 48 hours after challenge. T cells primed by different APCs loaded with T-cell antigen–specific, hapten-unrelated, peptide (pOVA) were intravenously applied at different time points to modulate ear swelling. Ear swelling response is expressed as the difference (μm, mean ± SD) between the thickness of the challenged ear and the vehicle-treated ear. *, *P* less than.05; ***, *P* less than .005 versus positive control. (A) Adoptive transfer of primed TofDCs, and TofBs at 24 hours before challenge. Transferred cells were unable to modulate the ear swelling induced by the challenge. (B) In contrast, when T cells were transferred before priming (at d −1), a specific inhibitory effect of TofBs could be seen. The transfer of TofBs but not of TofDCs resulted in a decreased immune response post challenge. (C) TofBs are functioning at 10 days after transfer yet require specific antigen restimulation. The suppressive effect shown after transfer at d −1 (as in panel B) is lost when cells were transferred already at d −10 before priming. However, when hapten priming and specific antigen restimulation (pOVA) occurred together, TofBs were rescued to suppress. In contrast, the application of an unspecific control antigen (pHA; Hemagglutinin peptide) had no effect. (D) In ectopic allogeneic heart transplantation in the mouse model, TofBs effectively inhibit organ rejection. At d −1 before ectopic transplantation of C57BL/6 donor hearts, Balb/c recipients of the treatment group were injected with TofBs, while the control group received only a saline injection. No other immunosuppressive treatment was administered. Graft function was assessed by daily palpation. Rejection was defined as the lack of palpable cardiac contraction. **, *P* less than.01 vs. control group.

part, by the de novo generation of T cells with regulatory phenotype. Such pathways have hitherto been discussed for immature dendritic cells[58,59] and recent reports have suggested a similar mechanism for human macrophages.[60]

What triggers the differential response of T cells toward these distinct APC? The result of T-cell priming is defined at the level of earliest interactions.[61,62] Thus, individual IS structures might be decisive for this process. We demonstrate formation of a mature IS between a naive B cell and an antigen-specific T cell and its absence in T-DC pairs. This appears surprising at first glance as naive B cells are very ineffective antigen presenters and synapses are generally considered structures leading to effector T-cell generation.[63] However, many studies demonstrating presence of mature IS actually used B cells as APC.[15,64,65] In contrast, a thorough analysis of singular T-DC interactions revealed the predominance of multifocal structures without a typical p-SMAC–c-SMAC appearance.[66] The function of theses structures is usually judged by the measurement of T-cell proliferation.[12] Our data show that T-cell proliferation alone is not sufficient to characterize the phenotype of a T cell. Only analysis of proliferated T cells in secondary coculture assay allowed us to identify a regulatory role of these cells.

The function of the synapse, especially of the c-SMAC, is intensely debated.[67] As it was shown that phospho-tyrosine levels are low to absent in c-SMAC,[68] the current concept considers c-SMAC as an area of TCR internalization and signal termination.[14] Signaling in p-SMAC is constantly maintained in microclusters that are then transported to c-SMAC.[69,70] Such microclusters might also be present in T-B synapses because B cells can induce long-lasting Ca^{2+} signaling in T cells.[9] As shown here, this could be the basis for deviation of T-cell effector function to a phenotype with regulatory properties. Thus, synapses formed between naive B cells and naive T cells may be the prototype of a novel type of IS, the regulatory synapse.

We show that inhibition of T-cell proliferation by TofBs is cell contact–dependent or at least requires close cell-cell interactions. In addition we show that most TofBs localize in T-cell zones of lymph nodes. This suggests interactions between TofBs and T cells or DCs in the T-cell zone being the mode of action in vivo. Contacts of Tregs with T-DC clusters impacting on recruitment of signaling molecules in involved naive T cells have been demonstrated before.[71] However, the intrinsic molecular mechanism of how Tregs can mediate cell-contact inhibition is insufficiently defined. Many independent pathways seem to exist, none of which can alone account for all aspects of regulation. Signaling molecules like CTLA-4 and Cbl-b as well as immunosuppressive cytokines such as IL-10, TGF beta and more may have important roles (for recent reviews see Miyara and Sakaguchi[72] and Graca et al[73]). TGF beta may be especially important during peripheral generation of Treg, most notably $CD4^+$ $CD25^+$ $Foxp3^+$ T cells.[74,75] The Forkhead box transcription factor Foxp3 is considered to be the most specific intracellular marker for naturally occurring (n)Tregs.[76] Thus, it was unexpected that TofBs did not show enhanced Foxp3 expression. However, the group of Treg phenotypes is expanding.[77] In fact, also Foxp3 independent Tregs have been described.[45,78]

The most obvious molecular T-cell marker differentially regulated by B cells and DCs, respectively, in this study, was CD62L, L-Selectin. This molecule is down-regulated on lymphocytes within 30 minutes after activation[79] by cleavage near the cell

surface by a member of the A Disintegrin and Metalloprotease (ADAM) family ADAM-17.[80] However, other sheddases or additional factors may be required.[81] Whether B cells activate sheddases differently than DCs is not clear. Spatial distribution of Tregs was shown to be of great importance for their role in immune responses.[82-84] Likewise, manipulation of molecules involved in lymphocyte homing and trafficking greatly affects lymphocyte function.[83] In that respect, it is important that our data provide a model correlating the level of CD62L and, thus, the entry into peripheral lymphatic organs with the regulatory function in vivo.

Our demonstration that antigen presentation by naive B cells induces Tregs might help to explain older findings on induction of specific tolerance in vivo against antigens presented by naive B cells.[3,85] Our data might also shed light on results from a recent study where prolonged subcutaneous infusion of low peptide doses transformed mature T cells into $CD4^+$ 25^+ suppressors.[86] In accordance with our data, this approach proved effective in inducing tolerance prospectively (priming phase), but it was open whether ongoing immune responses could be suppressed (challenge phase). Involvement of B-cell antigen presentation to generate Tregs in both systems seems to be an attractive model to explain their mode of action. Indeed, Matzinger has suggested that B cells, by virtue of their large quantities, may indeed participate in T-cell priming in a tolerizing manner.[85] In light of our data, this might be a consequence of de novo generation of Tregs. Such processes may play a role in vivo as B-cell–deficient individuals tend to develop autoaggressive phenomena.[87,88] Interestingly, T cells specifically activated in vivo show substantial proliferation yet remain CD62L high in up to 50% of the proliferating cells (unpublished observations). This could be interpreted as result of DC-triggering low antigen doses or as B-cell participation in T-cell priming. It is tempting to speculate that a fraction of these in vivo activated T cells is regulatory as well.

More importantly, even if physiologic relevance of naive B-cell triggered T-cell activation in vivo may be limited facing overwhelming competition by professional APC, the process described by us can have important clinical implications. As we show, B cells with their specific way of inducing T-cell activation may prove powerful for cell-based immunosuppression. Currently, DCs are the main focus of strategies against alloreactivity, transplant rejection, autoimmune diseases and allergy.[89-94] However, generation of DCs for therapeutic applications requires sophisticated handling, is expensive, time-consuming, and difficult to standardize.[92] In that respect, B cells may be a better option for obtaining defined APC. Indeed, genetically modified B cells have been used to tolerize animals against epitopes of pathophysiologic relevance.[95] Our model provides a more direct approach without the need for transgenic manipulation. It can be envisioned that the use of B-cell primed regulatory T cells, TofBs or "bTregs," may be a new way of significantly improving current cell-based therapies.

Acknowledgments

We thank Dunja Bruder, Markus Gereke, and Wiebke Hansen for help with initial experiments. We thank Werner Müller and Andreas Lengeling for providing IL-10 deficient animals. Jiong Tian is gratefully acknowledged for passing microsurgical expertise to S.R. Peter H. Krammer, Burkhart Schraven, Waldemar Kolanus and Jan Buer are acknowledged for critical reading of the manuscript.

This study was supported by the Deutsche Forschungsgemeinschaft (SPP 1160 (GU 769/1–1 and GU 769/1–2) to M.G.), by the European Union (FP6, Nest, 043243, Mamocell) to M.G., by the Interdisciplinary Center of Clinical Research (IZKF) grant Lo2/017/07 to K.L., and by the fund Innovative Medical Research (IMF) of the University of Münster Medical School grant Lo11/06 03 to K.L

Authorship

P.R., B.D., S.R., F.G., S.B., and K.L. performed experiments and analyzed data; M.G. conceived the study; and P.R. and M.G. wrote the paper.

Conflict-of-interest disclosure: The authors declare no competing financial interests.

Correspondence: Matthias Gunzer, PhD, Helmholtz Centre for Infection Research, Junior Research Group Immunodynamics, Inhoffenstraße 7, D-38124 Braunschweig, Germany; e-mail: mgunzer@helmholtz-hzi.de.

References

1. Lassila O, Vainio O, Matzinger P. Can B cells turn on virgin T cells? Nature. 1988;334:253-255.
2. Epstein MM, Di RF, Jankovic D, Sher A, Matzinger P. Successful T cell priming in B cell-deficient mice. J Exp Med. 1995;182:915-922.
3. Fuchs EJ, Matzinger P. B cells turn off virgin but not memory T cells. Science. 1992;258:1156-1159.
4. Germain RN, Jenkins MK. In vivo antigen presentation. Curr Opin Immunol. 2004;16:120-125.
5. Byersdorfer CA, Dipaolo RJ, Petzold SJ, Unanue ER. Following immunization antigen becomes concentrated in a limited number of APCs including B cells. J Immunol. 2004;173:6627-6634.
6. Zhong G, Reis e Sousa C, Germain RN. Antigen-unspecific B cells and lymphoid dendritic cells both show extensive surface expression of processed antigen-major histocompatibility complex class II complexes after soluble protein exposure in vivo or in vitro. J Exp Med. 1997; 186:673-682.
7. Rodriguez-Pinto D, Moreno J. B cells can prime naive CD4(+) T cells in vivo in the absence of other professional antigen-presenting cells in a CD154-CD40-dependent manner. Eur J Immunol. 2005;35:1097-1105.
8. Crawford A, Macleod M, Schumacher T, Corlett L, Gray D. Primary T cell expansion and differentiation in vivo requires antigen presentation by B cells. J Immunol. 2006;176:3498-3506.
9. Gunzer M, Weishaupt C, Hillmer A, et al. A spectrum of biophysical interaction modes between T cells and different antigen presenting cells during priming in 3-D collagen and in vivo. Blood. 2004; 104:2801-2809.
10. Gunzer M, Schäfer A, Borgmann S, et al. Antigen presentation in extracellular matrix: interactions of T cells with dendritic cells are dynamic, short lived, and sequential. Immunity. 2000;13:323-332.
11. Okada T, Miller MJ, Parker I, et al. Antigen-engaged B Cells undergo chemotaxis toward the T Zone and form motile conjugates with helper T Cells. PLoS Biol. 2005;3:e150.
12. Grakoui A, Bromley SK, Sumen C, et al. The immunological synapse: a molecular machine controlling T cell activation. Science. 1999;285:221-227.
13. Dustin ML, Bromley SK, Davis MM, Zhu C. Identification of self through two-dimensional chemistry and synapses. Annu Rev Cell Dev Biol. 2001;17: 133-157.
14. Lee KH, Dinner AR, Tu C, et al. The immunological synapse balances T Cell receptor signaling and degradation. Science 2003;302:1218-1222.
15. Monks CR, Freiberg BA, Kupfer H, Sciaky N, Kupfer A. Three-dimensional segregation of supramolecular activation clusters in T cells. Nature. 1998;395:82-86.
16. Mempel TR, Henrickson SE, von Andrian UH. T-cell priming by dendritic cells in lymph nodes occurs in three distinct phases. Nature. 2004;427: 154-159.
17. Miller MJ, Safrina O, Parker I, Cahalan MD. Imaging the single cell dynamics of CD4+ T cell activation by dendritic cells in lymph nodes. J Exp Med. 2004;200:847-856.
18. Murphy KM, Heimberger AB, Loh DY. Induction by antigen of intrathymic apoptosis of $CD4^+CD8^+TCR^{lo}$ thymocytes in vivo. Science. 1990;250:1720-1723.
19. Barnden MJ, Allison J, Heath WR, Carbone FR. Defective TCR expression in transgenic mice

constructed using cDNA-based alpha- and beta-chain genes under the control of heterologous regulatory elements. Immunol Cell Biol. 1998;76: 34-40.

20. Labeur MS, Roters B, Pers B, et al. Generation of tumor immunity by bone marrow-derived dendritic cells correlates with dendritic cell maturation stage. J Immunol. 1999;162:168-175.
21. Gunzer M, Riemann H, Basoglu Y, et al. Systemic administration of a TLR7 ligand leads to transient immune incompetence due to peripheral blood leukocyte depletion. Blood. 2005;106:2424-2432.
22. Corry RJ, Winn HJ, Russell PS. Primarily vascularized allografts of hearts in mice. The role of H-2D, H-2K, and non-H-2 antigens in rejection. Transplantation. 1973;16:343-350.
23. Barda-Saad M, Braiman A, Titerence R, et al. Dynamic molecular interactions linking the T cell antigen receptor to the actin cytoskeleton. Nat Immunol. 2005;6:80-89.
24. Jung TM, Gallatin WM, Weissman IL, Dailey MO. Down-regulation of homing receptors after T cell activation. J Immunol. 1988;141:4110-4117.
25. Friedl P, Noble PB, Zänker KS. Lymphocyte migration in three-dimensional collagen gels. Comparison of three quantitative methods for analysing cell trajectories. J Immunol Meth. 1993;165: 157-165.
26. Huang NN, Han SB, Hwang IY, Kehrl JH. B cells productively engage soluble antigen-pulsed dendritic cells: visualization of live-cell dynamics of B cell-dendritic cell interactions. J Immunol. 2005; 175:7125-7134.
27. Miller MJ, Wei SH, Parker I, Cahalan MD. Two-photon imaging of lymphocyte motility and antigen response in intact lymph node. Science. 2002;296:1869-1873.
28. Banchereau J, Steinman RM. Dendritic cells and the control of immunity. Nature. 1998;392:245-254.
29. Warnock RA, Askari S, Butcher EC, von Andrian UH. Molecular mechanisms of lymphocyte homing to peripheral lymph nodes. J Exp Med. 1998; 187:205-216.
30. Nolte MA, Hamann A, Kraal G, Mebius RE. The strict regulation of lymphocyte migration to splenic white pulp does not involve common homing receptors. Immunology. 2002;106:299-307.
31. Hwang JM, Yamanouchi J, Santamaria P, Kubes P. A critical temporal window for selectin-dependent CD4+ lymphocyte homing and initiation of late-phase inflammation in contact sensitivity. J Exp Med. 2004;199:1223-1234.
32. Galkina E, Tanousis K, Preece G, et al. L-selectin shedding does not regulate constitutive T cell trafficking but controls the migration pathways of antigen-activated T lymphocytes. J Exp Med. 2003; 198:1323-1335.
33. von Andrian UH, Mempel TR. Homing and cellular traffic in lymph nodes. Nat Rev Immunol. 2003;3:867-878.
34. Sallusto F, Lenig D, Förster R, Lipp M, Lanzavecchia A. Two subsets of memory T lymphocyes with distinct homing potentials and effector functions. Nature. 1999;401:708-712.
35. Kaech SM, Tan JT, Wherry EJ, et al. Selective expression of the interleukin 7 receptor identifies effector CD8 T cells that give rise to long-lived memory cells. Nat Immunol. 2003;4:1191-1198.
36. Huster KM, Busch V, Schiemann M, et al. Selective expression of IL-7 receptor on memory T cells identifies early CD40L-dependent generation of distinct CD8+ memory T cell subsets. Proc Natl Acad Sci U.S.A. 2004;101:5610-5615
37. Lenz DC, Kurz SK, Lemmens E, et al. IL-7 regulates basal homeostatic proliferation of antiviral CD4+T cell memory. Proc Natl Acad Sci U.S.A. 2004;101:9357-9362.
38. Wojciechowski S, Jordan MB, Zhu Y, et al. Bim mediates apoptosis of CD127(lo) effector T cells and limits T cell memory. Eur J Immunol. 2006; 36:1694-1706.
39. Seddiki N, Santner-Nanan B, Martinson J, et al. Expression of interleukin (IL)-2 and IL-7 receptors discriminates between human regulatory and activated T cells. J Exp Med. 2006;203:1693-1700.
40. Sakaguchi S. Regulatory T cells: key controllers of immunologic self-tolerance. Cell. 2000;101: 455-458.
41. Ermann J, Hoffmann P, Edinger M, et al. Only the CD62L+ subpopulation of CD4+CD25+ regulatory T cells protects from lethal acute GVHD. Blood. 2005;105:2220-2226.
42. Szanya V, Ermann J, Taylor C, Holness C, Fathman CG. The subpopulation of CD4+CD25+ splenocytes that delays adoptive transfer of diabetes expresses L-selectin and high levels of CCR7. J Immunol. 2002;169:2461-2465.
43. von Boehmer H. Dynamics of suppressor T cells: in vivo veritas. J Exp Med. 2003;198:845-849.
44. Vieira PL, Christensen JR, Minaee S, et al. IL-10-secreting regulatory T cells do not express Foxp3 but have comparable regulatory function to naturally occurring CD4+CD25+ regulatory T cells. J Immunol. 2004;172:5986-5993.
45. Groux H, O'Garra A, Bigler M, et al. A CD4+ T-cell subset inhibits antigen-specific T-cell responses and prevents colitis. Nature. 1997;389: 737-742.
46. Akbari O, DeKruyff RH, Umetsu DT. Pulmonary dendritic cells producing IL-10 mediate tolerance induced by respiratory exposure to antigen. Nat Immunol. 2001;2:725-731.
47. Fillatreau S, Sweenie CH, McGeachy MJ, Gray D, Anderton SM. B cells regulate autoimmunity by provision of IL-10. Nat Immunol. 2002;3:944-950.
48. Levings MK, Sangregorio R, Galbiati F, et al. IFN-alpha and IL-10 induce the differentiation of human type 1 T regulatory cells. J Immunol. 2001; 166:5530-5539.
49. Shevach EM. CD4+ CD25+ suppressor T cells: more questions than answers. Nat Rev Immunol. 2002;2:389-400.
50. Hori S, Nomura T, Sakaguchi S. Control of regulatory T Cell development by the transcription factor FOXP3. Science 2003;299:1057-1061.
51. Ashwell JD. Are B lymphocytes the principal antigen-presenting cells in vivo? J Immunol. 1988; 140:3697-3700.
52. Eynon EE, Parker DC. Small B cells as antigen-presenting cells in the induction of tolerance to soluble protein antigens. J Exp Med. 1992;175: 131-138.
53. Raimondi G, Zanoni I, Citterio S, Ricciardi-Castagnoli P, Granucci F. Induction of peripheral T cell tolerance by antigen-presenting B cells. I. Relevance of antigen presentation persistence. J Immunol. 2006;176:4012-4020.
54. Delon J, Bercovici N, Raposo G, Liblau R, Trautmann A. Antigen-dependent and -independent Ca^{2+} responses triggered in T cells by dendritic cells compared with B cells. J Exp Med. 1998; 188:1473-1484.
55. Reis e Sousa C. Dendritic cells in a mature age. Nat Rev Immunol. 2006;6:476-483.
56. Roncarolo MG, Levings MK, Traversari C. Differentiation of T regulatory cells by immature dendritic cells. J Exp Med. 2001;193:F5-F9.
57. Jonuleit H, Schmitt E, Schuler G, Knop J, Enk AH. Induction of interleukin 10-producing, non-proliferating CD4(+) T cells with regulatory properties by repetitive stimulation with allogeneic immature human dendritic cells. J Exp Med. 2000; 192:1213-1222.
58. Dhodapkar MV, Steinman RM, Krasovsky J, Munz C, Bhardwaj N. Antigen-specific inhibition of effector T cell function in humans after injection of immature dendritic cells. J Exp Med. 2001;193: 233-238.
59. Steinman RM, Hawiger D, Nussenzweig MC. Tolerogenic dendritic cells. Annu Rev Immunol. 2003;21:685-711.
60. Hoves S, Krause SW, Schutz C, et al. Monocyte-derived human macrophages mediate anergy in allogeneic T cells and induce regulatory T cells. J Immunol. 2006;177:2691-2698.
61. Richter A, Lohning M, Radbruch A. Instruction for cytokine expression in T helper lymphocytes in relation to proliferation and cell cycle progression. J Exp Med. 1999;190:1439-1450.
62. Maldonado RA, Irvine DJ, Schreiber R, Glimcher LH. A role for the immunological synapse in lineage commitment of CD4 lymphocytes. Nature. 2004;431:527-532.
63. Dustin ML. A dynamic view of the immunological synapse. Semin Immunol 2005;17:400-410.
64. Li QJ, Dinner AR, Qi S, et al. CD4 enhances T cell sensitivity to antigen by coordinating Lck accumulation at the immunological synapse. Nat Immunol. 2004;5:791-799.
65. Serrador JM, Cabrero JR, Sancho D, et al. HDAC6 Deacetylase activity links the tubulin cytoskeleton with immune synapse organization. Immunity. 2004;20:417-428.
66. Brossard C, Feuillet V, Schmitt A, et al. Multifocal structure of the T cell - dendritic cell synapse. Eur J Immunol. 2005;35:1741-1753.
67. Friedl P, den Boer AT, Gunzer M. Tuning immune responses: diversity and adaption of the immunological synapse. Nat Rev Immunol. 2005;5:532-545.
68. Lee KH, Holdorf AD, Dustin ML, et al. T Cell receptor signaling precedes immunological synapse formation. Science. 2002;295:1539-1542.
69. Yokosuka T, Sakata-Sogawa K, Kobayashi W, et al. Newly generated T cell receptor microclusters initiate and sustain T cell activation by recruitment of Zap70 and SLP-76. Nat Immunol. 2005;6: 1253-1262.
70. Campi G, Varma R, Dustin ML. Actin and agonist MHC-peptide complex-dependent T cell receptor microclusters as scaffolds for signaling. J Exp Med. 2005;202:1031-1036.
71. Sumoza-Toledo A, Eaton AD, Sarukhan A. Regulatory T cells inhibit protein kinase C theta recruitment to the immune synapse of naive T cells with the same antigen specificity. J Immunol. 2006; 176:5779-5787.
72. Miyara M, Sakaguchi S. Natural regulatory T cells: mechanisms of suppression. Trends Mol Med 2007;13:108-116.
73. Graca L, Chen TC, Le MA, et al. Dominant tolerance: activation thresholds for peripheral generation of regulatory T cells. Trends Immunol. 2005; 26:130-135.
74. Chen W, Jin W, Hardegen N, et al. Conversion of peripheral CD4+. J Exp Med. 2003;198:1875-1886.
75. Floess S, Freyer J, Siewert C, et al. Epigenetic control of the foxp3 locus in regulatory T cells. PLoS Biol. 2007;5:e38.
76. Sakaguchi S. Naturally arising Foxp3-expressing CD25+CD4+ regulatory T cells in immunological tolerance to self and non-self. Nat Immunol. 2005;6:345-352.
77. Shevach EM. From vanilla to 28 flavors: multiple varieties of T regulatory cells. Immunity. 2006;25: 195-201.
78. MacKenzie DA, Schartner J, Lin J, et al. GRAIL is upregulated in CD4+CD25+ T regulatory cells and is sufficient for conversion of T cells to a regulatory phenotype. J Biol Chem. 2007
79. Jung TM, Dailey MO. Rapid modulation of homing receptors (gp90MEL-14) induced by activators of protein kinase C. Receptor shedding due to accelerated proteolytic cleavage at the cell surface. J Immunol. 1990;144:3130-3136.

80. Black RA, Rauch CT, Kozlosky CJ, et al. A metalloproteinase disintegrin that releases tumour-necrosis factor-alpha from cells. Nature. 1997;385:729-733.

81. Smalley DM, Ley K. L-selectin: mechanisms and physiological significance of ectodomain cleavage. J Cell Mol Med. 2005;9:255-266.

82. Siegmund K, Feuerer M, Siewert C, et al. Migration matters: regulatory T-cell compartmentalization determines suppressive activity in vivo. Blood. 2005;106:3097-3104.

83. Brinkmann V, Pinschewer DD, Feng L, Chen S. FTY720: altered lymphocyte traffic results in allograft protection. Transplantation. 2001;72:764-769.

84. Ochando JC, Yopp AC, Yang Y, et al. Lymph node occupancy is required for the peripheral development of alloantigen-specific Foxp3 regulatory T Cells. J Immunol. 2005;174:6993-7005.

85. Matzinger P. Tolerance, danger, and the extended family. Annu Rev Immunol. 1994;12:991-1045.

86. Apostolou I, von Boehmer H. In vivo instruction of suppressor commitment in naive T cells. J Exp Med. 2004;199:1401-1408.

87. Knoechel B, Lohr J, Kahn E, Abbas AK. The link between lymphocyte deficiency and autoimmunity: roles of endogenous T and B lymphocytes in tolerance. J Immunol. 2005;175:21-26.

88. Mizoguchi A, Bhan AK. A case for regulatory B cells. J Immunol. 2006;176:705-710.

89. Kuipers H, Lambrecht BN. Modification of dendritic cell function as a tool to prevent and treat allergic asthma. Vaccine. 2005;23:4577-4588.

90. Banchereau J, Palucka AK. Dendritic cells as therapeutic vaccines against cancer. Nat Rev Immunol. 2005;5:296-306.

91. Bayry J, Thirion M, Delignat S, et al. Dendritic cells and autoimmunity. Autoimmun Rev. 2004;3:183-187.

92. Gunzer M, Janich S, Varga G, Grabbe S. Dendritic cells and tumor immunity. Semin Immunol. 2001;13:291-302.

93. McCurry KR, Colvin BL, Zahorchak AF, Thomson AW. Regulatory dendritic cell therapy in organ transplantation. Transpl Int. 2006;19:525-538.

94. Yamazaki S, Inaba K, Tarbell KV, Steinman RM. Dendritic cells expand antigen-specific Foxp3+ CD25+ CD4+ regulatory T cells including suppressors of alloreactivity. Immunol Rev. 2006;212:314-329.

95. Lei TC, Scott DW. Induction of tolerance to factor VIII inhibitors by gene therapy with immunodominant A2 and C2 domains presented by B cells as Ig fusion proteins. Blood. 2005;105:4865-4870.

Appendix 15

Reichardt P+, Müller D, Posselt U, Vorberg B, Diez U, Schlink U, Reuter W, Borte M. Fatty acids in colostrum from mothers of children at high risk of atopy in relation to clinical and laboratory signs of allergy in the first year of life.
Allergy.2004;59(4):394-400.
+Corresponding author

IF: 5.9

Allergy 2004: 59: 394–400
Printed in UK. All rights reserved

ALLERGY

Original article

Fatty acids in colostrum from mothers of children at high risk of atopy in relation to clinical and laboratory signs of allergy in the first year of life

Background: It remains controversial whether fatty acid (FA) composition of breast milk relates to development of atopy in the infant. This study evaluates FA in colostrum from mothers of children at high risk of atopy in association with atopy at the age of 1 year.
Methods: The FA of colostrum were analyzed for 218 children (60 with low birth weight between 1500 and 2500 g, 84 with a history of maternal atopy, and 74 with an elevated cord blood immunoglobulin (Ig)E of >0.9 IU/ml). Total lipids were extracted, methylated and separated by gas–liquid chromatography. Laboratory screening for allergic sensitization and clinical examination took place within the Leipzig Allergy Risk Children's Study (LARS).
Results: Low birth weight was correlated with low percentage levels of 20:2n-6, 22:2n-6, and 22:3n-3 ($r = 0.14$, $P < 0.05$; $r = 0.14$, $P < 0.05$ and $r = 0.20$, $P < 0.01$, respectively) and low gestational age at birth was correlated with low 22:3n-3 ($r = 0.15$, $P < 0.05$). There was no association between FA and atopic eczema at the age of 1 year. However, high linoleic acid (LA, 18:2n-6) was linked to high specific IgE against cow's milk protein ($P < 0.05$), and low docosapentaenoic acid (DPA, 22:5n-3) was associated with elevated total serum IgE ($P < 0.05$) at the age of 1 year, respectively.
Conclusions: The polyunsaturated fatty acid composition of colostrum in a high risk newborn population shows associations with atopic sensitization at the age of 1 year and may be predictive for later atopic disease.

P. Reichardt[1], D. Müller[1], U. Posselt[2], B. Vorberg[3], U. Diez[4], U. Schlink[4], W. Reuter[2], M. Borte[1], The Leipzig Allergy Risk Children's Study Group
[1]Children's Hospital, University of Leipzig; [2]Clinic of Internal Medicine IV, Department of Lipid Metabolism, University of Leipzig; [3]Institute of Laboratory Medicine, Clinical Chemistry and Molecular Diagnostics, University of Leipzig; [4]Department of Human Exposure Research and Epidemiology, Centre for Environmental Research Leipzig-Halle, Leipzig, Germany

Key words: atopy; breast milk; low birth weight infants; polyunsaturated fatty acids.

Peter Reichardt
Department of Microbiology and Immunology
Emory University
1510 Clifton Road
#3128 Rollins Research Center
30322 Atlanta, GA
USA

Accepted for publication 23 September 2003

The relationship between fatty aids (FA), in particular long chain polyunsaturated fatty acids (long chain PUFA, LCP) and atopy has been heavily investigated since the first observation of increased levels of linoleic acid (LA, 18:2n-6) and lower levels of its long chain metabolites in the plasma of patients with eczema (1). A number of LCP are involved in inflammatory responses, where most member of the n-6 PUFA series such as AA (20:4n-6) and its metabolites leukotriene B_4 and prostaglandin E_2 show proinflammatory capacity (2). In contrast, the n-3 series, e.g. eicosapentaenoic acid (EPA, 20:5n-3) and docosahexaenoic acid (DHA, 22:6n-3), are mostly referred to as suppressing the inflammatory response (3). The parent PUFA, LA (18:2n-6) and alpha-linolenic acid (LNA, 18:3n-3), respectively, compete for the same enzyme systems, desaturases and elongases. Linoleic acid and LNA are essential and have to be provided with the diet. Thus, the nutritional intake influences PUFA composition of the body, where small changes between the n-3 and n-6 series can have important effects on physiological processes and may influence the development of allergy (4).

The major nutritional source for newborns is breast milk. It is still controversial whether the FA composition of breast milk may relate to the development of atopy in the child. Breast milk that was given to atopic children has been reported to higher LA (5) or lower n-6 LCP (6) than milk given to healthy children, but other studies found instead decreased n-3 LCP (7, 8).

In our study, we investigated the FA composition of colostrum in a population of 218 newborns at high risk of atopy: (1) low birth weight (LBW) infants (<2500 g), (2) newborns of atopic mothers, and (3) newborns with elevated cord blood immunoglobulin (Ig)E (>0.9 IU/ml). The main aim of this study was to investigate links between the FA composition of colostrum and signs of atopy in the child. We analyzed our data in association with the development of clinical atopy and allergic

sensitization in the first year of life, as followed-up within the Leipzig Allergy Risk Children's Study (LARS). By choosing a high-risk population we aimed to increase sensitivity of analysis because of an expected higher percentage rate of atopic individuals. Additionally, we wanted to see whether these risk factors would be differentially reflected in the colostral FA composition. Finally, by choosing colostrum for analysis we wanted to explore, whether possible alterations in breast milk composition might be visible at this early, well-defined timepoint of lactation.

Material and methods

Patients and general experimental design

Between March 1995 and March 1996, 429 LBW neonates (birth weight between 1500 and 2500 g and without neonatal intensive care) and neonates with elevated cord blood IgE >0.9 kU/l or double positive family atopy history were selected from a full 1 year birth cohort ($n = 3540$) within the LARS study. The response rate was 47.9% (429 of 895 with these criteria). Two hundred and eighteen of these 429 mothers additionally agreed on providing breast milk samples for FA analysis. They also answered a nutritional questionnaire to ensure comparable diet. Vegetarian mothers were allowed to enter the study. Only three mothers declared to have been on a vegetarian diet, and all of those reported to have consumed cow's milk products. No mother declared to be on a predominantly fish diet or on other 'exotic' diets, what would have led to her exclusion from the study.

The corresponding 218 children were grouped into one of three risk groups according to modified criteria from LARS, and as such included in the study described here. Group 1 consisted of 60 of these 218 children (27.5%) who had a LBW (1500 < b.w. < 2500 g). Forty-one of these 60 LBW newborns (68%) were also premature (<37 completed gestational weeks). Group 2 was formed of 84 newborns (38.5%) with a history of maternal atopy. Group 3 included 74 newborns (34%) showing an elevated total IgE in cord blood (>0.9 kU/l; Pharmacia CAP System, Pharmacia, Feucht, Germany). The mean birth weights (±SD) for groups 1–3 were 2218 ± 247 g, 3483 ± 422 g, and 3452 ± 453 g, respectively. The mean gestational age at birth (mean ± SD) for groups 1–3 were 36.1 ± 2.3, 39.3 ± 1.2, and 39.5 ± 1.1 weeks, respectively.

The grouping was performed hierarchically in the sequence given, i.e. all LBW newborns were grouped into group 1 (irrespective of additional risks such as maternal atopy or high IgE), then all non-LBW with maternal atopy went into group 2 (irrespective of IgE-level), followed by non-LBW, nonmaternal atopy newborns with elevated IgE in group 3.

Clinical and laboratory evaluation of atopy

At the age of 6 weeks and at the age of 1 year, parents responded to questionnaires on signs of allergy in the children, and infants underwent a medical examination by an experienced pediatrician (U.D.). A clinical endpoint under the pediatrician's judgment was atopic dermatitis diagnosed according to Sampson's criteria (9). Blood samples were taken at the age of 1 year in an outpatient department of the children's hospital specifically designed for the follow-up of the study. Among other parameters tested, determination of total IgE, and specific IgE as well as radioallergosorbent test (RAST) against a battery of antigens (milk protein, egg white, egg yolk, grass, birch, aspergillus, candida, *Dermatophagoides pteronyssinus, D. farinae*, cat) were performed as described previously (10). Total and specific IgE were measured from the same blood sample and simultaneously, without prescreening for total IgE. All antibodies and kits were provided by Pharmacia, Feucht, Germany. Laboratory analyses were performed without knowledge of the clinical evaluation of the patient. Signs of atopy were compared with PUFA in colostrum of children with 5 months or more of exclusive breast-feeding in order to ensure a possible maximal effect of breast milk while still having enough children for statistical valid analysis (analyses for 4 months, 3 months and irrespective of duration of breast-feeding were also done, but did not reveal additional statistical associations with FA, data not shown). The 5 months children group had been of special interest, as in a previous study of LARS investigating other aspects of this cohort, a correlation between breast-feeding for at least 5 months and the frequency of eczema at the age of 1 year had been found for children with elevated cord blood IgE (11).

Breast milk sampling

Between day two and five after birth, 2–7 ml samples of midstream colostrum were collected in duplicates into sterile plastic collecting jars and stored at −20°C until analysis. The mothers were instructed to collect the milk in the early morning, at the first meal.

Preanalytical treatment of samples

The principles of analysis have been described previously (12) and received modifications in incubation temperature and period for best results with the given samples. Briefly, a 0.2 ml sample of milk was mixed with 5 ml of methanol : acetyl chloride (50 : 1, v/v) and incubated for 90 min at 70°C. The process of ester formation was stopped by adding sodium bicarbonate. After adding hexane and vortexing, the upper phase, containing the FA methyl esters was removed, purified by centrifugation and diluted with hexane before analysis.

Analysis by gas chromatography

Fatty acid methyl esters were separated and quantitated using a Hewlett Packard (HP) 5890 series II chromatograph (HP Co., Avondale, PA) with a HP INNO WAX (30 m × 0.32 mm × 25 μm) column coated with cross-linked polyethylenglycole and quantitated by a 3396A HP integrator with a split ratio of 1 : 32. Helium gas was used as carrier gas (5.7 ml/min). Identification of FA of carbon chain length C10–24 occurred by comparison with commercially available standards (Supelco Inc. and Sigma Chemical Co., St Louis, MO). The level of each FA was expressed as weight percent of total lipid.

Statistical analysis

Data were analyzed with the statistical package SPSS 9.0 (Chicago, IL). Nonparametric analyses were performed as FA had been recorded as weight percentages of total weight. Nonparametric ANOVA (Kruskal–Wallis *H*-test) was performed in the three group comparison of the risk population (The Kruskal–Wallis ANOVA by Ranks test assumes that the variable under consideration is continuous and that it was measured on at least an ordinal (rank

order) scale. The test assesses the hypothesis that the different samples in the comparison were drawn from the same distribution of from distributions with the same median. Thus, the interpretation of the Kruskal–Wallis test is basically identical to that of the parametric one-way ANOVA, except that it is based on ranks rather than on means. Mann–Whitney's U test (a nonparametric rank sum test) was performed for pairwise comparisons between FA and with clinical and laboratory expression of allergy. Spearman's Rank correlation was employed for comparison of FA with birth weight and gestational age at births. Individual Spearman's correlation coefficients r are listed. Differences were considered statistically significant if $P < 0.05$.

Ethical considerations

Participation in the study was voluntary. Informed consent was obtained from the parents of all children. The study was approved by the Ethics Committee of the University of Leipzig.

Results

Table 1 compares the FA composition of colostrum in 218 mothers of children at high risk of atopic disease.

Table 1. Fatty acid composition (% wt/wt; median, interquartile range IR) of colostrum in mothers of children at high risk of atopic disease

	All risk groups ($n = 218$)		Low birth weight (1550–2500 g) ($n = 60$)		Atopic mother ($n = 84$)		Elevated cord blood immunoglobulin E (>0.9 IU/l) ($n = 74$)	
Fatty acid	Median	IR	Median	IR	Median	IR	Median	IR
10:0	0.17	0.15	0.18	0.28	0.18	0.15	0.16	0.14
12:0	1.55	1.01	1.70	1.54	1.51	1.01	1.49	0.89
14:0	4.14	1.76	4.22	2.12	4.13	1.94	3.99	1.46
14:1n-5	0.14	0.06	0.13	0.08	0.14	0.06	0.14	0.05
15:0	0.34	0.12	0.33	0.15	0.35	0.12	0.33	0.12
16:0	22.72	2.49	22.59	3.08	22.75	2.72	22.75	2.61
16:1n-7	2.30	0.67	2.29	0.69	2.24	0.64	2.34	0.75
18:0	8.34	1.59	8.20	1.70	8.37	1.94	8.29	1.41
18:1n-9c	38.38	3.78	38.62	4.52	38.39	3.93	37.97	3.38
18:1n-9t	1.70	0.44	1.68	0.54	1.70	0.41	1.71	0.40
18:2n-6	9.34	2.86	9.31	2.79	9.15	3.41	9.68	2.44
18:3n-9	0.11	0.06	0.10	0.06	0.10	0.06	0.12	0.08
18:3n-6	0.05	0.07	0.05	0.09	0.05	0.07	0.04	0.06
18:3n-3	0.80	0.25	0.78	0.29	0.79	0.21	0.81	0.23
18:4n-3	0.41	0.14	0.42	0.14	0.41	0.13	0.41	0.21
20:0	0.31	0.09	0.31	0.10	0.30	0.10	0.30	0.08
20:1n-9	1.16	0.29	1.12	0.38	1.18	0.29	1.15	0.28
20:2n-6	0.67	0.26	0.61	0.28	0.72	0.23	0.69	0.33
20:3n-6	0.63	0.24	0.65	0.26	0.61	0.22	0.62	0.26
20:4n-6	0.83	0.24	0.82	0.28	0.84	0.21	0.85	0.20
20:3n-3	0.12	0.04	0.12	0.03	0.12	0.04	0.13	0.04
20:5n-3	0.11	0.05	0.11	0.05	0.11	0.05	0.10	0.05
22:0	0.18	0.12	0.17	0.12	0.19	0.12	0.18	0.12
22:1n-9	0.24	0.07	0.24	0.08	0.25	0.08	0.24	0.09
22:2n-6	0.12	0.06	0.11	0.07	0.13	0.06	0.12	0.07
22:4n-6	0.36	0.19	0.34	0.19	0.36	0.18	0.36	0.21
22:3n-3	0.10	0.05	0.08	0.04	0.10	0.04	0.10	0.06
22:5n-3	0.34	0.14	0.31	0.14	0.33	0.14	0.34	0.15
22:6n-3	0.75	0.26	0.71	0.28	0.76	0.26	0.76	0.20
24:1n-9	0.26	0.17	0.24	0.15	0.28	0.16	0.26	0.18
Total n-6	12.05	3.00	11.87	2.78	11.87	3.25	12.24	3.03
LCP n-6	2.63	0.72	2.54	0.64	2.67	0.67	2.68	0.86
LA/n-6 LCP	3.53	1.40	3.45	1.37	3.49	1.62	3.65	1.23
Total n-3	2.69	0.49	2.70	0.51	2.70	0.52	2.66	0.59
LCP n-3	1.41	0.48	1.40	0.48	1.41	0.54	1.42	0.42
LNA/n-3LCP	0.57	0.25	0.56	0.29	0.57	0.30	0.60	0.22
SAFA	38.07	5.41	38.12	6.70	38.59	5.33	37.77	4.62
MUFA	44.28	4.00	44.43	5.30	44.11	4.02	44.14	3.50
PUFA	14.88	3.17	14.72	3.14	14.79	3.44	15.10	3.32
P/S-ratio	0.39	0.13	0.38	0.14	0.39	0.12	0.41	0.13
n-6/n-3	4.54	1.34	4.46	1.26	4.58	1.47	4.60	1.08
n-6 LCP/n-3 LCP	1.85	0.44	1.87	0.52	1.84	0.40	1.85	0.38

wt, weight; SAFA, saturated fatty acids; MUFA, monounsaturated fatty acids; PUFA, Polyunsaturated fatty acids; P/S, PUFA/SAFA; LCP, long chain PUFA.
No statistical differences (nonparamatic ANOVA of Kruskal–Wallis).

When the three risk groups, each defined by a single risk factor, were compared, no differences were seen. Neither the saturated FA, nor monounsaturates or n-6 series or n-3 series of polyunsaturates in each group showed statistically significant deviations. Furthermore, when a group was formed of all atopic mothers (group 2 + atopic mothers in group 1) and compared against the remaining (all nonatopic) mothers, also no associations with the FA status of colostrums were detected.

While the group comparisons did not reveal differences, correlation analyses with birth weight (irrespective of the arbitrary threshold of 2500 g defining LBW) and gestational age at birth did. Low birth weight was shown to be correlated with low 20:2n-6, 22:2n-6, and 22:3n-3 ($r = 0.142$, $P < 0.05$; $r = 0.136$, $P < 0.05$; and $r = 0.196$, $P < 0.01$, respectively). Low gestational age at birth (which as expected correlated by itself with LBW, $r = 0.558$, $P < 0.001$) correlated with low 22:3n-3 ($r = 0.147$, $P < 0.05$).

We also compared the breast milk of the three mothers who declared to have been on a vegetarian diet with that of their nonvegetarian counterparts. The breast milk did not differ significantly within the respective groups and in the total risk population, respectively.

Table 2 shows the results of the comparison of FA with clinical expression of allergy (atopic eczema) at the age of 1 year. Of the initial 218 children 164 were seen at the age of 1 year. Results are demonstrated for the 78 children exclusively breast-fed for at least the first 5 months. These 78 children consisted of 11 children (14%) of group 1, 36 children (46%) of group 2, and 31 children (40%) of group 3. The data demonstrate that there were no differences between the weight percentages of PUFA in colostrum of children expressing atopic eczema or obstructive bronchitis compared with clinically healthy infants at the age of 1 year.

Table 3 comparatively lists the colostral PUFA for the children with and without allergic sensitization at the age of 1 year. Statistically significant differences between the groups are marked. Here, the parent FA of the n-6 series of polyunsaturates, LA, was higher among mothers with children bearing specific IgE against cow's milk ($P < 0.05$). This effect also leads to a higher amount of total n-6 series of PUFA ($P < 0.01$), an elevated ratio of LA to LNA ($P < 0.05$), and an elevated ratio of n-6/n-3 PUFA ($P < 0.05$). No changes were seen among the long chain derivatives of LA, AA and dihomo-gamma-linoleic acid (DHGLA, 20:3n-6) in relation to specific IgE. In contrast, DPA (22:5n-3) was found to be decreased ($P < 0.05$) in the breast milk of mothers of children with elevated total IgE in serum at the age of 1 year. Other members of the n-3 series including EPA and DHA were found unchanged. Data are presented for children with 5 months or more of exclusive breast-feeding for possible maximal effect of breast milk. Analyses of 4 months, 3 months, and irrespective of duration disclosed no additional statistical differences.

Table 2. Parent fatty acids and polyunsaturated fatty acids (% wt/wt; median, interquartile range IR) in colostrum of children at high risk of allergy and expression of atopic eczema at the age of 1 year. Results are shown for children exclusively breast-fed for at least the first 5 months

	Atopic eczema at the age of 1 year			
	Yes ($n = 17$)		No ($n = 60$)	
	Median	IR	Median	IR
Omega (n)-6				
18:2n-6	8.81	3.16	9.10	2.78
20:2n-6	0.63	0.29	0.63	0.24
20:3n-6	0.56	0.20	0.63	0.22
20:4n-6	0.81	0.21	0.84	0.19
22:2n-6	0.12	0.04	0.12	0.06
22:4n-6	0.38	0.18	0.36	0.19
Total n-6	11.26	4.18	12.02	2.93
n-6 LCP	2.69	0.62	2.61	0.78
18:2n-6/n-6 LCP	3.35	1.63	3.43	1.26
Omega (n)-3				
18:3n-3	0.74	0.35	0.80	0.22
20:3n-3	0.13	0.04	0.12	0.04
20:5n-3	0.11	0.06	0.10	0.04
22:3n-3	0.10	0.05	0.10	0.06
22:5n-3	0.34	0.16	0.34	0.16
22:6n-3	0.72	0.27	0.79	0.31
Total n-3	2.77	0.36	2.73	0.45
n-3 LCP	1.42	0.63	1.41	0.55
18:3n-3/n-3 LCP	0.45	0.40	0.57	0.24
18:2n-6/18:3n-3	11.02	5.19	11.46	2.46
Total n-6/total n-3	4.12	1.55	4.53	1.29

wt, weight; LCP, long chain polyunsaturated fatty acids.
No statistical differences (Mann–Whitney's *U*-test).

Analyses of other specific IgE tested showed no associations between FA and sensitization. Fourteen children (of the 78 children exclusively breast-fed for at least 5 months) were tested CAP positive against egg white, and seven against egg yolk. Sensitization against respiratory allergens was considerably lower as expected: grass (two children), birch (two), cat (one), aspergillus (one), candida (one), *D. pteronyssinus* (1), *D. farinae* (none). For all of these antigens, analyses of breast-feeding periods of 4 months, 3 months, and irrespective of duration showed no statistical association with the FA investigated (data not shown).

Discussion

Our data demonstrate an association between the PUFA composition of colostrum of mothers of children at high risk of atopy and an increased rate of atopic sensitization in the child. High percentage levels of LA (18:2n-6), and resulting higher LA/LNA ratio and higher total n-6/n-3 ratio were correlated with high specific IgE against cow's milk protein, and low levels of 22:5n-3 and low total n-3 were associated with elevated serum total IgE at the age of 1 year.

Table 3. Parent fatty acids and polyunsaturated fatty acids (% wt/wt; median, interquartile range IR) in colostrum of children at high risk of allergy and signs of allergic sensitization at the age of 1 year. Results are shown for children exclusively breast-fed for at least the first 5 months

	Elevated total IgE in serum (>34 IU/ml)				Specific IgE against cow's milk in serum (CAP > 0)			
	Yes ($n = 31$)		No ($n = 32$)		Yes ($n = 8$)		No ($n = 54$)	
	Median	IR	Median	IR	Median	IR	Median	IR
Omega (n)-6								
C 18:2n-6	9.12	3.49	9.28	2.79	11.11*	8.73	8.07*	2.64
C20:2n-6	0.62	0.24	0.66	0.26	0.73	0.37	0.62	0.21
C 20:3n-6	0.60	0.20	0.67	0.21	0.75	0.22	0.61	0.22
C 20:4n-6	0.82	0.18	0.86	0.18	0.84	0.26	0.83	0.16
C22:2n-6	0.12	0.06	0.13	0.05	0.14	0.08	0.12	0.06
C22:4n-6	0.35	0.16	0.36	0.19	0.36	0.12	0.35	0.18
Total n-6	11.64	2.41	12.21	2.89	13.57**	9.19	11.55**	2.56
n-6 LCP	2.51	0.78	2.65	0.73	2.93	0.90	2.60	0.60
C 18:2n-6/n-6 LCP	3.82	1.46	3.38	1.17	4.32	2.49	3.41	1.14
Omega (n)-3								
C 18:3n-3	0.75	0.28	0.81	0.26	0.91	0.49	0.78	0.27
C 20:3n-3	0.12	0.04	0.12	0.04	0.11	0.09	0.12	0.04
C 20:5n-3	0.10	0.04	0.11	0.04	0.10	0.04	0.11	0.05
C 22:3n-3	0.10	0.0	0.10	0.06	0.10	0.06	0.10	0.06
C 22:5n-3	0.31*	0.11	0.38*	0.18	0.32	0.11	0.35	0.14
C 22:6n-3	0.74	0.26	0.86	0.36	0.74	0.35	0.77	0.28
Total n-3	2.66*	0.42	2.88*	0.41	2.75	0.45	2.75	0.46
n-3 LCP	1.29	0.56	1.60	0.61	1.33	0.58	1.46	0.54
C 18:3n-3/n-3 LCP	0.62	0.30	0.48	0.22	0.61	0.29	0.56	0.26
C 18:2n-6/C 18:3n-3	11.77	4.62	11.27	2.46	14.54*	4.27	11.12*	2.48
Total n-6/total n-3	4.62	1.51	4.21	1.15	5.63*	2.06	4.16*	1.20

* $P < 0.05$; ** $P < 0.01$ (Mann–Whitney's *U*-test).
LCP, long chain polyunsaturated fatty acids; IgE, immunoglobulin E.

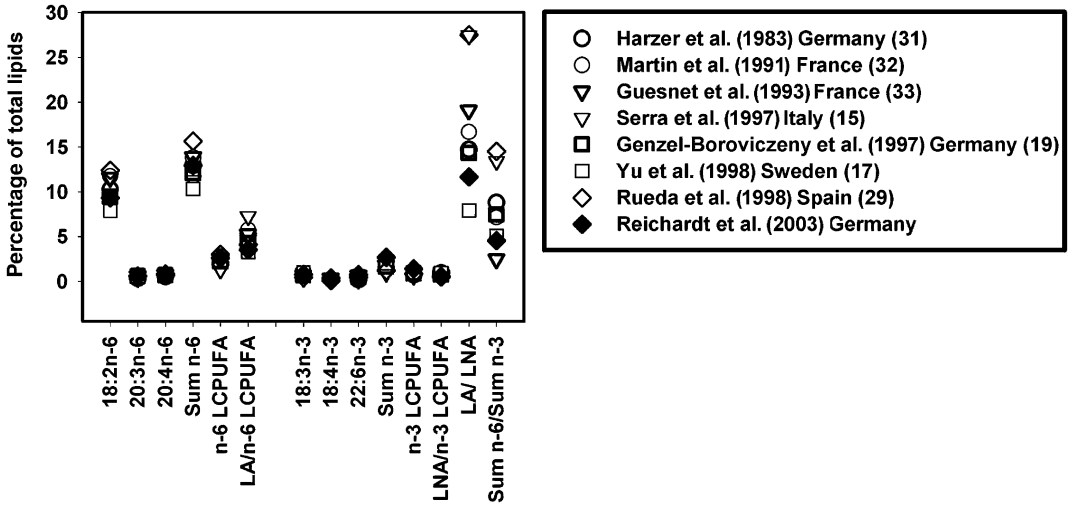

Figure 1. Percentages of characteristic polyunsaturated fatty acids (PUFA) and PUFA ratios as determined in our study compared to results from studies of colostrum of healthy Caucasian women in developed (Western) central European countries on a normal, nonmediterranean diet.

Our observation resembles data from previous studies of breast milk, where high LA and low n-3 LCP (6), low n-3 LCP plus low total n-3 (7), and low total n-3 and high n-6/n-3 ratio (because of both higher n-6 and lower n-3) (8) were linked to atopic development in children. Studies in serum phospholipids also found higher LA (13–15), lower n-3 LCP (33) or both (8, 16) in atopic compared with healthy individuals. Many of these studies also

found decreased n-6 LCP. In fact, for many years research was more focused on disturbances in the n-6 series. The concomitant increase of LA and decrease of n-6 LCP gave rise to the idea of an abnormal metabolism in atopic individuals, namely of an impaired conversion of the C18 precursors into their LCP products because of enzymatic deficiencies (16, 17). However, this hypothesis is not unquestioned (14). Recently, the importance of disturbances in the n-3 series for the development of atopy has been stressed (7, 8). In one report, only the composition of n-3 LCP was related to atopic development in children (18). 22:5n-3, which we found connected to elevated serum IgE is the metabolic linker between 20:3n-5 (EPA) and 22:6n-3 (DHA) both of which have reportedly anti-inflammatory capacity (3).

The varying results in previous studies regarding PUFA in breast milk in relation to atopy may have one reason in the fact that the percentage of LCP in breast milk varies substantially throughout lactation. The PUFA metabolites were found to be highest in colostrum and to decrease later (12, 19). Thereby, the decline of n-3-PUFA during lactation occurs more rapidly than of n-6-PUFA (17), what has to be considered in analysis. In our study, we chose colostrum for several reasons. First, sampling breast milk at one convenient and well-defined timepoint minimizes errors because of varying composition of breast milk during the time course of lactation. Secondly, some studies investigating breast milk in the context of atopy were able to observe differences at earlier timepoints, which disappeared later through lactation (7, 17). Thirdly, because of the higher percentual contents of PUFA metabolites in colostrum, possible differences can be more apparent and increase the reliability of detection. This can be of importance, as many of the characteristic PUFA are available in only low quantities.

Our observation of associations between PUFA in colostrum and atopic sensitization but not clinical atopy at the age of 1 year can likely be explained by the early timepoint of clinical analysis. While clinical symptoms for atopy, e.g. atopic dermatitis, start often before the age of 1 year (9), many and more specific symptoms will become apparent only later. However, there is evidence that exposure to environmental antigens, modulated by genetic susceptibility, can result in allergic sensitization very early (22). As sensitization generally preceeds manifestation of atopy, our finding of associations with atopic sensitization may point to a possible development of allergy later in life. It would therefore be of interest to follow-up the children included for a longer time. In this regard, is it somewhat disappointing that there was no association between FA and IgE specific to hen's egg protein, as the presence of such antibodies in the first year of life is reportedly predictive for allergic sensitization against other antigens later in life (23). However, we observed sensitization against cow's milk protein, which can also be associated with a higher incidence of asthma later in childhood (24).

A secondary result of our study was that the FA composition of colostrum did not differ between the three individual risk groups when compared with each other. In fact, the composition seemed to closely match values obtained in studies of colostrum of healthy Caucasian women in developed (Western) central European countries on a normal, nonmediterranean diet (see Fig. 1). Maternal nutrition is a key influence factor for the composition of breast milk is (20). We had all women included in our study fill in a nutritional questionnaire to exclude 'exotic diets'. Breast milk of the three vegetarians in our study was not statistically different from nonvegetarians. It is known that vegetarian diet can lead to increased levels of LA, and LNA as well as to reduced levels of DHA (21). While we have no solid explanation for the lack of difference in our study, it is possible that the low number of participating vegetarians and the fact that all three reported to have consumed cow's milk products may have masked some differences.

Our data suggest that the risk factors 'elevated cord blood IgE' in the child and 'atopic mother' were not reflected in the colostral FA composition. A number of studies observed lower LA in the milk of atopic mothers (7, 25), but others did not (8, 26). It is possible that some deviations will only reveal in mature milk, while being masked in colostrum or early transitional milk (7, 18).

Our data correlating birth weight and gestational age at birth with LCP levels in breast milk confirm previous reports (19, 27). However, other studies were unable to find differences when preterm and term breast milk was compared (28, 29). The selection of an appropriate time point of investigation may again be of importance for the results.

In conclusion, our data show that links between the FA status of breast milk and atopic sensitization in children can be observed as early as during the first few days of lactation, in colostrum. Apart from the advantage of using a well-defined and convenient timepoint, it seems worthwhile to speculate on the future importance of detecting FA deficiencies early after birth. Future studies will need to further our understanding of defects in metabolic pathways of FA related to atopic disease. They also might reveal specific deficiencies in subgroups of individuals/families at high risk of atopy. It is possible to envision that some of these patients might profit from an early individual supplementation of nutrition by specific LCP, an approach currently recommended only for nutritional purposes for very LBW infants (30).

Acknowledgments

Participating families are thanked for their valuable contribution to the study. LARS was kindly supported by the Ministry of Science and Arts of Saxony, Germany, Grant No. 4-7531.50-03-UFZ/701, and 4-7541.83-UFZ/404c.

References

1. Hansen AE. Reduced plasma essential fatty acid levels in patients with eczema. Am J Dis Child 1937;**53**:933–946.
2. Ohtsuka Y, Yamashiro Y, Shimizu T, Nagata S, Igarashi J, Shinohara K et al. Reducing cell membrane n-6 fatty acids attenuates mucosal damage in food-sensitive enteropathy in mice. Pediatr Res 1997;**42**:835–839.
3. Calder PC. Fat chance of immunomodulation. Immunol Today 1998;**19**:244–247.
4. Kankaanpää P, Sütas Y, Salminen S, Lichtenstein A, Isolauri E. Dietary fatty acids and allergy. Ann Med 1999;**31**:282–287
5. Wright S, Bolton C. Breast milk fatty acids in mothers of children with atopic eczema. Br J Nutr 1989;**62**:693–697.
6. Businco L, Ioppi M, Morse NL, Nisini R, Wright S. Breast milk from mothers of children with newly developed atopic eczema has low levels of long chain polyunsaturated fatty acids. J Allergy Clin Immunol 1993;**91**:1134–1139.
7. Duchén K, Casas R, Fageras-Bottcher M, Yu G, Björkstén B. Human milk polyunsaturated long-chain fatty acids and secretory immunoglobulin A antibodies and early childhood allergy. Pediatr Allergy Immunol 2000;**11**:29–39.
8. Kankaanpää P, Nurmela K, Erkkilä A, Kalliomäki M, Holmberg-Marttila D, Salminen S et al. Polyunsaturated fatty acids in maternal diet, breast milk, and serum lipid fatty acids of infants in relation to atopy. Allergy 2001;**56**: 633–638.
9. Sampson HA. Pathogenesis of eczema. Clin Exp Allergy 1990;**20**:459–467.
10. Lehmann I, Rehwagen M, Diez U, Seiffart A, Rolle-Kampczyk U, Richter M et al. Enhanced *in vivo* IgE production and T cell polarization toward the type 2 phenotype in association with indoor exposure to VOC: results of the LARS study. Int J Hyg Environ Health 2001;**204**:211–221
11. Wetzig H, Schulz R, Diez U, Herbarth O, Viehweg B, Borte M. Associations between duration of breastfeeding, sensitization to hens' eggs and eczema infantum in one and two year old children at high risk of atopy. Int J Environ Health 2000;**203**:17–21.
12. Gibson RA, Kneebone GM. Fatty acid composition of human colostrum and mature breast milk. Am J Clin Nutr 1981;**34**:252–257.
13. Oliwiecki S, Burton JL, Elle K, Horrobin DF. Levels of essential and other fatty acids in plasma and red cell phospholipids from normal controls and patients with atopic eczema. Acta Derm Venereol (Stockh) 1990;**71**:224–228.
14. Leichsenring M, Kochsiek U, Paul K. n-6-fatty acids in plasma lipids of children with atopic bronchial asthma. Pediatr Allergy Immunol 1995;**6**: 209–212.
15. Serra G, Marletta A, Bonacci W, Campone F, Bertini I, Lantieri PB et al. Fatty acid composition of human milk in Italy. Biol Neonate 1997;**72**:1–8.
16. Manku MS, Horobin DF, Morse NL, Wright S, Burton JL. Essential fatty acids in the plasma phospholipids of patients with atopic eczema. Br J Dermatol 1984;**110**:643–648.
17. Yu G, Duchén K, Björkstén B. Fatty acid composition in colostrum and mature milk from non-atopic and atopic mothers during the first 6 months of lactation. Acta Paediatr 1998;**87**: 729–736.
18. Duchén K, Yu G, Björkstén B. Atopic sensitization during the first year of life in relation to long chain polyunsaturated fatty acid levels in human milk. Pediatr Res 1998;**44**:478–484.
19. Genzel-Boroviczény O, Wahle J, Koletzko B. Fatty acid composition of human milk during the 1st month after term and preterm delivery. Eur J Pediatr 1997;**156**:142–147.
20. Koletzko B, Thiel I, Abiodun PO. The fatty acid composition of human milk in Europe and Africa. J Pediatr 1992;**120**:S62–70.
21. Sanders TA, Reddy S. The influence of a vegetarian diet on the fatty acid composition of human milk and the essential fatty acid status of the infant. J Pediatr 1992;**120**:S71–77.
22. Martinez FD, Wright AL, Taussig LM, Holberg CJ, Halonene M, Morgan WJ. Asthma and wheezing in the first six years of life. N Engl J Med 1995;**332**:133–138.
23. Nickel R, Kulig M, Forster J, Bergmann R, Bauer CP, Lau S et al. Sensitization to hen's egg at the age of twelve months is predictive for allergic sensitization to common indoor and outdoor allergens at the age of three years. J Allergy Clin Immunol 1997;**99**:613–617.
24. Host A, Halken S, Jacobsen HP, Christensen AE, Herskind AM, Plesner K. Clinical course of cow's milk protein allergy/intolerance and atopic diseases in childhood. Pediatr Allergy Immunol 2002;**13** (S15):23–28.
25. Thijs C, Houwelingen A, Poorterman I, Mordant A, van den Brandt P. Essential fatty acids in breast milk of atopic mothers: comparison with non-atopic mothers, and effect of borage oil supplementation. Eur J Clin Nutr 2000;**54**:234–238.
26. Schroten H, Schöls K, Melnik B, von Kries R, Wahn V, Biggemann B. Breast milk of atopic mothers provide their infants with normal amounts of omega-6-fatty acids. Pediatr Allergy Immunol 1992;**3**:140–143.
27. Beijers RJ, Schaafsma A. Long-chain polyunsaturated fatty acid content in Dutch preterm breast milk; differences in the concentrations of docosahexaenoic acid and arachidonic acid due to length of gestation. Early Hum Dev 1996;**44**:215–223.
28. Bitman J, Wood L, Hamosh M, Hamosh P, Mehta NR. Comparison of the lipid composition of breast milk from mothers of term and preterm infants. Am J Clin Nutr 1983;**38**:300–312.
29. Rueda R, Ramirez M, Garcia-Salmerón JL, Maldonado J, Gil A. Gestational age and origin of human milk influence total lipid and fatty acid contents. Ann Nutr Metab 1998;**42**: 12–22.
30. ESPGAN Committee on Nutrition. Comment on the composition of cow's milk based follow-up formulas. Acta Paediatr Scand 1990;**79**:250–254.
31. Harzer G, Haug M, Dieterich I, Gentner PR. Changing patterns of human milk lipids in the course of the lactation and during the day. Am J Clin Nutr 1983;**37**:612–621.
32. Martin JC, Niyongabo T, Moreau L, Antoine JM, Lanson M, Berger C et al. Essential fatty acid composition of human colostrum triglycerides: its relationship with adipose tissue composition. Am J Clin Nutr 1991;**54**:829–835.
33. Guesnet P, Antoine JM, Rochette de Lempdes JB, Galent A, Durand G. Polyunsaturated fatty acid composition of human milk in France: changes during the course of lactation and regional differences. Eur J Clin Nutr 1993;**47**: 700–710.

Appendix 16

Reichardt P, Schreiber A, Wichmann G, Metzner G, Efer J, Raabe F. Identification and quantification of *in vitro* adduct formation between protein reactive xenobiotics and a lysine-containing model peptide.
Environ Toxicol.2003;18:29-36.

IF: 2.6

Identification and Quantification of *in vitro* Adduct Formation Between Protein Reactive Xenobiotics and a Lysine-Containing Model Peptide

Peter Reichardt,[1] André Schreiber,[2] Gunnar Wichmann,[3] Gerhard Metzner,[4] Juergen Efer,[2] Ferdinand Raabe[4]

[1]Children's Hospital of the University of Leipzig, Oststrasse 21–25, 04317 Leipzig, Germany.

[2]Department of Chemistry, Institute of Analytical Chemistry, University of Leipzig, Linnéstrasse 3, 04103 Leipzig, Germany

[3]UFZ Centre for Environmental Research Leipzig-Halle, Department of Human Exposure Research and Epidemiology, Permoserstrasse 15, 04318 Leipzig, Germany

[4]Institute of Clinical Immunology and Transfusion Medicine, University of Leipzig, Max-Buerger-Center, Johannisallee 30, 04103 Leipzig, Germany

Received 30 August 2002; revised 23 September 2002; accepted 13 October 2002

ABSTRACT: Formation of *in vitro* adducts between different classes of xenobiotics and the lysine-containing peptide Lys-Tyr was monitored by high-performance liquid chromatography and electrospray ionization mass spectrometry. The molecular structures of the main resulting products could be sensitively analyzed by mass spectrometry (flow injection analysis), enabling the detection of characteristic binding formations. Aldehydes such as formaldehyde, acetaldehyde, and benzaldehyde were shown to form stable linkages to lysine amino groups via Schiff bases. Other electrophilic substances (e.g., toluene-2,4-diisocyanate, 2,4-dinitro-1-fluorobenzene, 2,4,6-trinitrobenzene sulfonic acid, dansyl chloride, and phthalic acid anhydride) also formed covalent adducts with lysine residues. The reactivity of the compounds was quantified by measuring the amount of peptide that remained unchanged after incubation for a certain period with the xenobiotic. Although reactivity levels within this group of aldehydes varied only to a small extent, as would be expected, extreme differences were seen among the structurally heterogeneous group of nonaldehyde xenobiotics. These results support the hypothesis that simple chemical reactions may lead to the adduction of nucleophilic macromolecules such as peptides or proteins. Such reactions, in particular, Schiff base formation of aldehydes, have previously been shown to be capable of specifically interfering with costimulatory signaling on T cells. Our results suggest that electrophilic xenobiotics of other classes may also inherit the capacity to exert similar effects. Forming covalent linkage to peptides may represent a possible molecular mechanism of electrophilic xenobiotics *in vivo,* yielding immunotoxic effects. The model utilized in this study is appropriate for monitoring the adduction of xenobiotics to basic peptides and for analyzing the resulting molecular structures. Environ Toxicol 18: 29–36, 2003.

Keywords: xenobiotics; peptides; proteins; lysine; adducts; mass spectrometry; immunotoxic effects

INTRODUCTION

Environmental pollutants are increasingly made responsible for the rise in immunologically determined diseases such as allergies and autoimmunities (Peterson and Saxon, 1996; Davies et al., 1998). Electrophilic xenobiotics are an important group of pollutants. The *in vivo* adduction of nucleophilic macromolecules such as DNA, proteins, and peptides can be one of several molecular mechanisms for such influences on the immune system (Luster et al., 1987; Hess and Rieder, 1997). In proteins, the main nucleophilic reaction partners involved are mercapto and basic amino groups.

Correspondence to: Ferdinand Raabe; e-mail: raabef@medizin.uni-leipzig.de.

Published online in Wiley InterScience (www.interscience.wiley.com). DOI 10.1002/tox.10097

The ϵ-amino group of the lysine residue belongs to the most commonly involved and characteristic groups for protein–xenobiotic interaction *in vivo* because of its high basicity and degree of ionization (Braun et al., 1995; Hazen et al., 1997). Mass spectrometry was used in a recent study to reveal the amino groups of peptides that frequently interact via Schiff bases with adduct partners (Boutaud et al., 1999). The existence of Schiff base–forming ligands seems to be a universal principle of molecular interaction between proteins and an essential part of antigen presentation on (murine) T cells (Gao and Rhodes, 1990). Aldehydes, which form Schiff bases with amino groups of lysine residues, have been shown to specifically interact with the immune system, binding to the T-cell surface and interfering with clofilium-sensitive sodium and potassium channels also involved in costimulatory signaling (Rhodes, 1989). Hence, aldehydes may provide a costimulatory signal to the cell, thus favoring an immune response and directing it toward a Th1 answer (Shearer, 1995; Rhodes et al., 1995). Much less has been learned about the reactions of other electrophilic xenobiotics with proteins under physiological conditions. In this article we report on a study that demonstrated that xenobiotics of different chemical classes may bind effectively and stably to lysine-containing peptides upon *in vitro* incubation under physiological conditions. Characterization of a selection of main adducts by mass spectrometry is presented, as well as an approach for quantifying the impact on the molecular structure of the peptide.

MATERIALS AND METHODS

Peptide and Xenobiotics

The peptide used, H—lysine-tyrosine—OH, salt, with a molecular weight of 369.4 was supplied by Bachem (Heidelberg, Germany). The xenobiotic acetonitrile (ACN), C_2H_3N, 75-05-8, came from Merck (Darmstadt, Germany) and the xenobiotic dansyl chloride (DC), $C_{12}H_{12}ClNO_2S$, 605-65-2, from Molecular Probes (Eugene, OR). Sigma (Deisenhofen, Germany) was the supplier for the following xenobiotics: acetaldehyde (AA), C_2H_4O, CAS (Chemical Abstract Service) 75-07-0; benzaldehyde (BA), C_7H_6O, 100-52-7; 2,4-dinitro-1-fluorobenzene (DNFB), $C_6H_3FN_2O_4$, 70-34-8; formaldehyde (FO), CH_2O, 50-00-0; glutaraldehyde (GA), pentane-1,5-dial, $C_5H_8O_2$, 111-30-8; phthalic acid anhydride (PA), $C_8H_4O_3$, 85-44-9; toluene-2,4-diisocyanate (TDI), 4-methyl-m-phenylene diisocyanate, $C_9H_6N_2O_2$, 584-84-9; trifluoroacetic anhydride (TFAA), C_4F_603, 407-25-0; and 2,4,6-trinitrobenzene sulfonic acid (TNBS), $C_6H_3N_3O_9S$, 2508-19-29.

Instrumentation

High-performance liquid chromatography (HPLC) was performed using a Bischoff (Leonberg, Germany) HPLC system consisting of two compact pumps (19-95) and a Knauer dynamic mixer (19-93), in combination with reversed-phase columns [Nucleosil 5 C18 (Grom Analytic, Herrenberg-Kayh, Germany); 5 C18, 5 C18 PAH, C18 MPN (Macherey-Nagel, Dueren, Germany); Adsorbosphere C18 3, C18 5 (Alltech, San Jose, CA); Nucleosil 300-5 C 8, 300-7 C6H5, 300-5 C 4 (Macherey-Nagel, Dueren, Germany)]; mixed-mode columns [C18 Anion 100 A 5U, 150 × 4.6 (Alltech, San Jose, CA)]; and gel permeation columns [125 Bio-Sil (Biorad, Hercules, CA), Macrosphere GPC 100, Macrosphere GPC 60 (Alltech, San Jose, CA)]. The eluent (flow rate of 1 mL/min) was 0.1% TFA in water with a linear gradient to 0.1% TFA in CH_3CN/H_2O (various ratios), sodium phosphate buffer in water with a linear gradient to sodium phosphate buffer in methanol/H_2O (various ratios), and sulfonic acid buffer in water with a linear gradient to methanol/H_2O (various ratios), respectively. The eluate was monitored at 220 and 280 nm with a Bio-Dimension UV-vis monitor (Bio-Rad, Hercules, CA) and at 250/350, 325/392, and 335/515 nm (excitation/emission) with an 8450 fluorescence HPLC monitor (Bischoff, Leonberg, Germany). Flow injection analysis–mass spectrometry (FIA-MS) was performed on an API mass spectrometer [Applied Biosystems/MDS Sciex API 100 LC-MS System (Concord, Ontario, Canada)]. Samples were applied through a Rheodyne 7125 injection valve equipped with a 20-μL sample loop. Conditions for mass spectrometry are given in the relevant entries. Reaction vials (1.8 mL) and corresponding microvials were obtained from CRS (Fairbanks, AL) and Bischoff (Leonberg, Germany).

Incubation of Lys-Tyr with Xenobiotics

For subsequent MS analysis, to 20 μL of a 100 mM peptide solution (0.1*M* phosphate buffer, pH 7.4) were added 5 μL of a solution of a 1*M* xenobiotic in H_2O (glutaraldehyde) and CH_3CN (all other xenobiotics), respectively. After incubation for varying time spans according to the protocol (15 min standardized for concentration dependency and 15 min up to 4 days for kinetic studies) at 37°C in the dark, 75 μL of 0.1*M* phosphate buffer (pH 7.4) was added to the reaction solution. The mixture was then centrifuged, immediately after which MS analysis was done. For subsequent HPLC analysis incubation was performed as described above except that the initial concentration of xenobiotics varied from 10 μM to 1 M. After incubation and centrifugation, samples were placed in a cooled (4°C) autosampling chamber to do immediate HPLC analysis.

FIA-MS Analysis of Adducts

The peptide and possible adducts were analyzed by FIA-MS on an API mass spectrometer. The native peptide Lys-Tyr was detected by collision-induced dissociation (CID) of a

$[M + H]^+$ ion at *m/z* 310. For adduct formation with the intact peptide, in our experiments the resulting adducts could be detected at higher mass-to-charge ratios (*m/z*), ranging from 336 to 793. The operating conditions of the mass spectrometer were: scan range, *m/z* 100–500 (for fragmentation) and *m/z* 300–800; scan time, 2 s; cone voltage, 30 V: injection volume, 20 μL (2 μL of sample + 18 μL of eluent [CH_3CN, 2 mM of ammonium acetate in H_2O; 3:1 (v/v)]; flow rate of injection, 0.4 mL/min).

HPLC Analysis and Quantification of Peptide Adduct Formation

To do this analysis, 20 μL of the sample solution (50 μL for gel permeation columns) was injected and eluted with one of the elution systems described above. Retention times and peak areas of native and added peptides were determined by UV- and fluorescence monitoring as described above.

Mathematical Description of Total Peptide Turnover after Incubation with Xenobiotic

To assess the total changes that occurred in the molecular structure of the peptide after incubation with the xenobiotic, we introduced the factor of reactivity (FR), defined as the amount of xenobiotic necessary to allow a reaction with 50% of the peptide in a given solution. The peptide was deemed unchanged when its retention time in HPLC did not change (±1%) and/or its mass-to-charge ratio remained the same as before incubation. FR summarizes the effects of specific adduct formation, changes in tertiary structure, ionization, degradation, and other factors associated with the xenobiotic. It provides a simple tool for estimating how much the molecular structure of the peptide is affected by the reactive agent. For FR the concentration of a xenobiotic at which the amount of unchanged peptide is 50% is termed the concentration (*x*) of this xenobiotic [eq. (1)], making FR defined as the quotient of the concentration of the peptide in the solution and concentration (*x*) [eq. (2)]. Thus, FR is calculated as the inverse of the relative amount of xenobiotic necessary to transform 50% of the peptide into an adduct (mM/mM).

$$\frac{m_{\text{Peptide}}^{\text{Xeno}(x)}}{m_{\text{Peptide}}^{\text{Xeno}(0)}} = 50\% \quad (1)$$

$$\text{FR}^{50} = \frac{[\text{Peptide}]}{[\text{Xeno}(x)]} \quad (2)$$

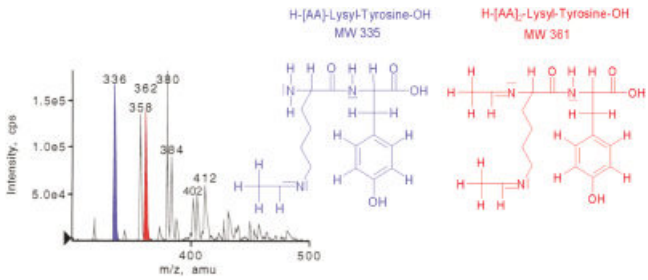

Fig. 1. Mass spectrum of molecular ion $[M + H]^+$ of Lys-Tyr after incubation with acetaldehyde. A spectrum of new products is shown. Two genuine adducts can be observed: the 1:1 adduct at 336 (blue) and the 2:1 adduct at 362 (red). All other peaks are formed by sodium and potassium clusters of the former adducts. [Color figure can be viewed in the online issue, which is available at www.interscience.wiley.com.]

RESULTS

Identification of Specific Xenobiotic Peptide Adducts

The structures identified in our experiments confirmed the results of previous studies on *in vitro* and *in vivo* adduct formation of xenobiotics as, for example, AA, BA, FO, and DNFB. In addition, new insights were gained about the reactions of a number of other substances, such as DC, PA, TDI, TFAA, and TNBS. In general, most xenobiotics were shown to react via covalent linkage to the ϵ-amino group of the lysine residue. The specific adducts that resulted were predominantly in a ratio of 1:1. For AA and PA, 2:1 adducts, in which two xenobiotic molecules were bound to one peptide molecule, using both α- and ϵ-amino groups of lysine, also could be demonstrated. We first directed our attention toward identification of the adducts of a number of aldehydes to Lys-Tyr. In a first attempt, AA was incubated with the peptide. Two genuine adducts could be shown, representing a 1:1 adduct and a 2:1 adduct, resulting from Schiff base formation between the hydroxyl group of AA and the amino group or groups of the lysine residue (Fig. 1). To sustain the hypothesis that binding occurs mainly via the ϵ-amino group of lysine, we investigated which amino acid of Lys-Tyr AA actually binds to upon adduct formation. After the peptide was incubated with AA, cone voltage was raised to 70 V during MS analysis, resulting in partial fragmentation of the peptide. Subsequently, we analyzed adduct formation of other aldehydes. It was found that BA and FO also form Schiff bases when binding to Lys-Tyr (not shown). However, although a 1:1 adduct occurred in quantities similar to that with AA, a 2:1 adduct could not be detected in significant amounts (data not shown).

We then turned our attention to the analysis of adducts with protein reactive xenobiotics of other classes. DNFB (Fig. 2), PA (Fig. 3), and TDI (Fig. 4) also form C—N bindings with the ϵ-amino group. Of note is that PA also

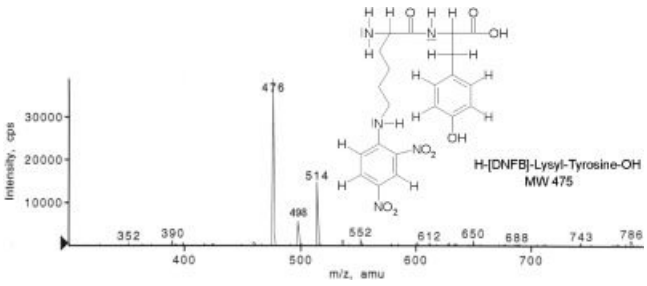

Fig. 2. Mass spectrum of molecular ion $[M + H]^+$ after incubation of Lys-Tyr with 2,4-dinitro-1-fluorobenzene (DNFB). One genuine adduct appears at 476.

leads to a 2:1 adduct and that TDI reacts in an even more complicated manner, including the formation of a 1:2 adduct (1 TDI + 2 Lys-Tyr). The common principle of TDI reactions is the derivatization of isocyanate groups into urea derivatives on reaction with the ϵ-amino group of lysine residues (Fig. 4). DC reacts with the amino group differently, forming a sulfonamide bond (Fig. 5). TNBS forms a number of different adducts with the amino group, some of which can be explained by trinitrophenylation of amino groups and conjugation of the complete molecules of the partners (not shown). In contrast to all the other xenobiotics investigated, TFAA did not lead to any observable specific adducts when the peptide was incubated with it (not shown).

Localization of Adduction of Acetaldehyde to Lys-Tyr at the Single Amino Acid Level by Adduct Fragmentation

To investigate whether the adduction of xenobiotics, which was suspected to occur by binding to Lys-Tyr via the formation of Schiff bases, indeed occurs at the amino acid

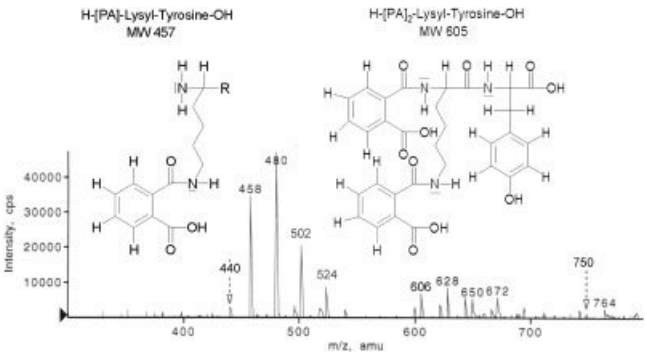

Fig. 3. Mass spectrum of molecular ion $[M + H]^+$ after incubation of Lys-Tyr with phthalic anhydride (PA). A spectrum of new products is shown. The adduct at 458 results from a decomposing of the furan ring. It is followed by the adduct's sodium clusters (480, 502, 524). Adduction of another molecule PA results in the 2:1 adduct (606), again followed by its sodium clusters (628, 650, 672). Phthalimide (440) and a corresponding product (750) are only marginally available (see text).

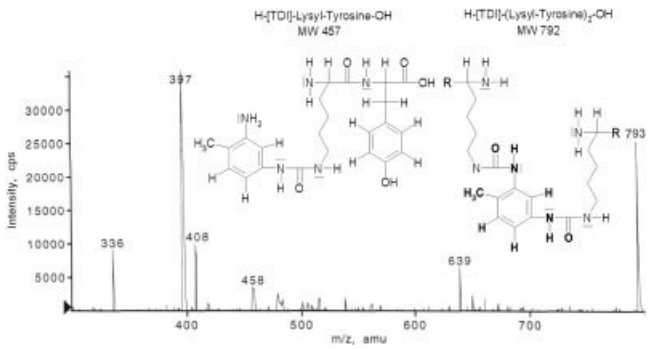

Fig. 4. Mass spectrum of molecular ion $[M + H]^+$ after incubation of Lys-Tyr with toluene-2,4-diisocyanate (TDI). The adduct at 458 is the result of adduction of the ϵ-amino group of Lys-Tyr, possibly to the sterically favored p-isocyanate group of TDI. When the second isocyanate group also reacts with a peptide molecule, the toluyl-diurea bipeptide results (793). The peak at 397 may be interpreted as the double-charged toluyl-di-urea bipeptide (1:2 adduct) and the peak at 408 as its sodium cluster. The product at 336 possibly results from the adduction of an intermittently formed carboxy amino acid to an amino group of Lys-Tyr. The identity of the peak at *m/z* 639 could not be unraveled.

lysine and not tyrosine, we changed the parameters of the mass spectrometry such that the adduct formed was disrupted so that fragments could be analyzed. The results confirmed our hypothesis that adduction was to the amino acid lysine under release of H_2O, whereas no binding to tyrosine could be observed (not shown).

Quantification of Adduct Formation by HPLC and Mass Spectrometry

After the detection of specific adduct formation, the turnover of the peptide in association with the incubation with xenobiotics was quantified using the factor of reactivity (FR). FR values for all chemicals investigated were calculated. The results are presented in Table I.

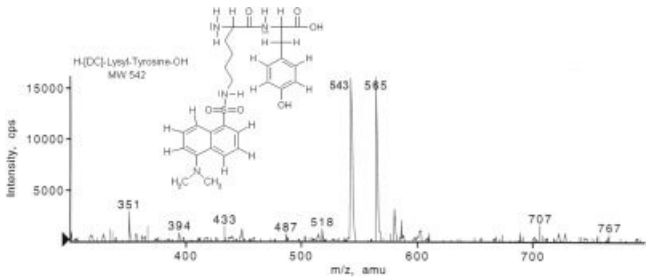

Fig. 5. Mass spectrum of molecular ion $[M + H]^+$ of Lys-Tyr after incubation with dansyl chloride (DC). One genuine adduct results at 543 from the binding of the sulfur atom to the ϵ-amino acid of the peptide.

TABLE I. Factors of reactivity (FR) in *in vitro* adduct formation between selected xenobiotics and the peptide lysine-tyrosine

Xenobiotics	Factor of Reactivity (FR) [mM/mM]
Acetonitrile (ACN)	$4.22*10^{-5} \pm 0.91*10^{-5}$
Acetaldehyde (AA)	0.164 ± 0.037
Benzaldehyde (BA)	0.406 ± 0.084
Formaldehyde (FO)	0.509 ± 0.032
Glutaraldehyde (GA)	0.575 ± 0.046
Trifluoroacetic anhydride (TFAA)	0.019 ± 0.001
Trinitrobenzene sulfonic acid (TNBS)	0.030 ± 0.06
2,4-Dinitro-1-fluorobenzene (DNFB)	0.077 ± 0.041
Dansyl chloride (DC)	0.713 ± 0.348
Phthalic acid anhydride (PA)	1.061 ± 0.057
Toluene-2,4-diisocyanate (TDI)	2.620 ± 0.663

DISCUSSION

To develop sensitive methods for the detection and quantification of protein–xenobiotic adducts formed under near-physiological *in vitro* conditions, we initiated a study of a range of protein reactive and immunotoxic compounds binding to a model peptide containing one of the most characteristic groups for protein–xenobiotic interaction, the ϵ-amino group of the lysine residue. Reactions of electrophilic xenobiotics with the ϵ-amino group of the lysine residue are especially favored *in vivo* because of the high basicity of this group. By binding to lysine residues, electrophilic organic compounds such as products of lipid peroxidation (alkenals) have been shown to change the molecular structure of proteins and to alter their function (Baker et al., 1999). In addition, E-amino groups have been shown to be involved in a number of immunological signaling processes (Chen et al., 1997). We chose a dipeptide to minimize the steric hindrances and dipole effects that are known to influence the binding characteristics of proteins (Chen et al., 1999). Tyrosine was used as the second amino acid, as its aromatic ring is easily detectable in UV light. Because of its much lower reactivity, it would be expected that reactions would mainly occur at the lysine residue, a hypothesis that was confirmed in our experiments. Among the xenobiotics investigated, Schiff base–forming aldehydes represented a main group, as Schiff bases have been detected to play an important role in immunological signal cascade in T cells (Rhodes, 1989; Rhodes et al., 1995). Compared with various aldehydes, where xenobiotics of other classes are known to be protein reactive and to have immunotoxic capacity. As we hypothesized, all xenobiotics investigated in the *in vitro* system, except for TFAA, were shown to undergo simple chemical reactions with the amino group of the peptide, mainly forming 1:1 adducts. The structural analyses that were done in our experiments enabled some new insights into possible reactions occurring under physiological conditions and confirmed the available reports on reaction mechanisms. In detail, AA is well known to react with amino-containing compounds in an aqueous environment, forming Schiff bases (Braun et al., 1995, 1997). Basically, the same is true for the other aldehydes investigated. BA may cause costimulation (Chen and Rhodes, 1996), FO–albuminadducts may result in production of specific anti-adduct IgG (Kim et al., 1999), and GA may cause allergic sensitization (Dearman et al., 1999). For all aldehydes investigated, our results confirmed the formation of Schiff bases with the ϵ-amino group of lysine, mainly leading to 1:1 adducts under the chosen conditions. In contrast to nonaldehydes, reactivities differed only little within the aldehyde group. This might be because of an identical binding type. Among the nonaldehydes, DNFB, which is used as a model hapten for contact sensitization (Manetz and Meade, 1999), reacts with amino groups of peptides, forming highly immunogenic dinitrophenylpeptides. Our experiments confirmed the formation of adducts via dinitrophenylation of amino groups. For PA, which can cause sensitization *in vivo* (Yokota et al., 1998), we observed adduct formation via decomposing of the furan ring. Under the conditions chosen, this phenomenon has not yet been described to our knowledge. Of further interest was the marginal availability of phthalimide (*m/z* 440), an intermediate product of this reaction frequently formed in conditions used in technical chemistry. It is possible that its formation, which occurs under release of H_2O, is only a minor reaction path under physiological conditions. This possibility is supported by the probable product of a reaction of phthalimide itself, an adduct formed after reaction of the second carboxyl group of phthalic acid with a second molecule of the peptide, also being hardly detectable (*m/z* 750). TDI, one of the major causes of occupational asthma (Aul et al., 1999), is known to convert in aqueous solutions into urea and aromatic diamines (Seel et al., 1999). In our system, along with direct adduct formation with the peptide, TDI also underwent changes in which the peptide was only secondarily involved. Isocyanates react in water solutions immediately to carboxy amino acids (carbamino acids). These unstable compounds dissolve into primary amine and CO_2 or may further react to become stable final products. Such a reaction could explain the product at 336, which possibly was formed after the adduction of a carboxy amino acid to an amino group of Lys-Tyr. The identity of the peak at *m/z* 639 could not be unraveled. When investigating TFAA, surprisingly, there were no specific adducts to be observed. TFAA was investigated as being a very reactive trifluoroacetylating substance. Microsomal peptides trifluoroacetylated by metabolites of halothane, a volatile anesthetic, trigger halothane hepatitis (Clarke et al., 1995). A possible explanation for the

apparently low peptide reactivity is the sufficient nucleophilic capacity of the surrounding H_2O to react with TFAA because of the extremely high reactivity of the molecule. Thus, TFAA was turned completely into a poorly reactive trifluoroacetic acid, leaving the peptide unchanged. This shows that high structural activity may not necessarily be connected with a high rate of adduct formation under physiological conditions. It has been found that in a group of electrophilic xenobiotics those with medium chemical reactivity showed the highest mutagenicity (Eder and Kutt, 1989). The molecular basis of adduct formation by TNBS, a model hapten for hapten-associated colitis (Neurath et al., 1996), is trinitrophenylation of the ϵ-amino groups of lysine (von Bonin et al., 1992), a process, that we also observed in our reaction system. In addition, we found adducts whose structures could not be elucidated. The main product at 338 and smaller products possibly represent fragments of TNBS, resulting from hydrolytic processes, and conjugates of these fragments.

The quantification of peptide reactivity of xenobiotics by determination of the amount of specific adducts did not seem very promising, as adducts may be unstable, fragmented, or clustered with a number of ions, thus making quantification of specific adducts difficult. Therefore, we instead determined the amount of peptide with apparently unchanged molecular structure remaining after a specific duration of incubation. For this purpose, we introduced a factor of reactivity (FR). The advantage of this mathematical approach is enabling the recording of the summarized effect of all factors that lead to a structural change in the peptide recognizable in HPLC or MS. Thus, exact knowledge about the kinetics of major and minor reaction pathways that may occur in parallel and are mostly unknown is not necessary.

The quantification of reactivity using the FR showed that peptide conversion occurred with a reaction kinetic higher than first grade. This would be expected, as, according to the concentrations used in our system, the velocity of adduct formation depended on the concentration of both the peptide and the xenobiotic. When comparing the FRs of the substances, it was evident that among aldehydes reactivities varied only to a small degree. GA, the most reactive compound in this group, was only 3.5 times more reactive than AA, the least reactive aldehyde. In contrast, extreme differences were seen in the group of nonaldehydes. ACN, the organic solvent used for all lipophilic compounds, was, as expected, by far the least reactive chemical. TFAA, the second least reactive xenobiotic, was both 1000 times more reactive than ACN and 100 times less reactive than the xenobiotic with the highest factor of reactivity, TDI. These enormous differences may be linked to the structural heterogeneity within this group. However, when substances were compared according to their principle of binding, no substantial differences were noted. Schiff base–forming xenobiotics (AA, BA, FO, GA) in general were equally potent whether they were substances forming similar C—N bindings (PA, TDI, TFAA) or substances using other binding forms (DC, DNFB, TNBS). As it is known that Schiff base–forming aldehydes may help provide costimulatory signals and that the type of costimulatory signal may influence functional priming of T lymphocytes (Rhodes, 1989; Rhodes et al., 1995; Shanafelt et al., 1995), it seemed interesting to look at whether substances known to lead to a predominantly Th1-driven immune response *in vivo* (AA, BA, FO, DNFB, TNBS; Dearman et al., 1996) would show a generally different reactivity from those inducing a Th2 response (PA, TDI; Kapsenberg, 1996). In our experiments, we did not observe such differences. We speculate that although specific reactivity toward amino groups is necessary for initiating potentially costimulatory signals, the grade of this reactivity may not be reflected in the functional quality of the signal (Th1 vs. Th2). It is obvious that our *in vitro* results carry a number of limitations and only incompletely reflect the *in vivo* protein reactivity of a substance. In particular *in vivo* groups other than ϵ-amino groups may also become targets of an electrophilic attack of xenobiotics, and some highly reactive chemicals may only arise as a result of metabolizing processes. In addition, the covalent protein binding of xenobiotics *in vivo* frequently shows a substance-specific affinity for certain tissue- or organ-specific proteins, and regional specificity for binding xenobiotics may occur within macromolecules (Brunmark et al., 1997). Thus, quantification of binding to such specific proteins in some cases may correlate better with toxicity than the total protein-binding capacity (Cohen et al., 1997).

Our results demonstrate that simple chemical reactions may lead to the adduction of peptides, proteins, or other macromolecules by protein-reactive xenobiotics. Such reactions may represent a possible molecular effector mechanism of protein-reactive xenobiotics *in vivo*. Thus, they may influence the immunotoxic properties of chemical agents. We believe that knowledge of the molecular structures of adduct formation between protein-reactive xenobiotics and macromolecules may contribute substantially to the risk assessment of potentially hazardous and immunotoxic xenobiotics and may enhance understanding of influencing receptor systems, translator proteins, and DNA enhancer sequences. We therefore suggest the inclusion of appropriate methods into a careful evaluation of the (immuno)toxic properties of a substance that will cover not only reactivity to DNA but also to other macromolecules. Although determination of the adducts to structural proteins for dosimetry and risk assessment is well established (Bartsch, 2000), relatively few attempts have been made to measure protein reactivity and adduct formation (Wass and Belin, 1990). In our opinion, the model utilized in our study may be appro-

priate for monitoring certain aspects of *in vitro* adduction of xenobiotics to basic peptides and for investigating the resulting molecular structures.

REFERENCES

Aul DJ, Bhaumik A, Kennedy AL, Brown WE, Lesage J, Malo JL. 1999. Specific IgG response to monomeric and polymeric diphenylmethane diisocyanate conjugates in subjects with respiratory reactions to isocyanates. J Allergy Clin Immunol 103: 749–755.

Baker AG, Wiesler D, Novotny MV. 1999. Tandem mass spectrometry of model peptides modified with trans-2-hexenal, a product of lipid peroxidation. J Am Soc Mass Spectrom 10:613–624.

Bartsch H. 2000. Studies on biomarkers in cancer etiology and prevention: a summary and challenge of 20 years of interdisciplinary research. Mutat Res 462:255–279.

Boutaud O, Brame CJ, Salomon RG, Roberts LJ 2nd, Oates JA. 1999. Characterization of the lysyl adducts formed from prostaglandin H2 via the levuglandin pathway. Biochemistry 38: 9389–9396.

Braun KP, Cody RB Jr, Jones DR, Peterson CM. 1995. A structural assignment for a stable acetaldehyde–lysine adduct. J Biol Chem 270:11263–11266.

Braun KP, Pavlovich JG, Jones DR, Peterson CM. 1997. Stable acetaldehyde adducts: structural characterization of acetaldehyde adducts of human hemoglobin *N*-terminal beta-globin chain peptides. Alcohol Clin Exp Res 21:40–43.

Brunmark P, Harriman S, Skipper SL, Wishnok JS, Amin S, Tannenbaum SR. 1997. Identification of subdomain IB in human serum albumin as a major binding site for polycyclic aromatic hydrocarbon epoxides. Chem Res Toxicol 10:880–886.

Chen H, Rhodes J. 1996. Schiff base forming drugs: mechanisms of immune potentiation and therapeutic potential. J Mol Med 74:497–505.

Chen H, Hall S, Heffernan B, Thompson NT, Rogers MV, Rhodes J. 1997. Convergence of Schiff base costimulatory signaling and TCR signaling at the level of mitogen-activated protein kinase ERK2. J Immunol 159:2274–2281.

Chen X, Anderson VE, Chen YH. 1999. Isotope edited product ion assignment by alpha-N labeling of peptides with [2H3(50%)]2,4-dinitrofluorobenzene. J Am Soc Mass Spectrom 10:448–452.

Cohen SD, Pumford NR, Khairallah EA, Boekelheide K, Pohl LR, Amouzadeh HR, Hinson JA. 1997. Selective protein covalent binding and target organ toxicity. Toxicol Appl Pharmacol 143:1–12.

Clarke JB, Thomas C, Chen M, Hastings KL, Gandolfi AJ. 1995. Halogenated anesthetics form liver adducts and antigens that cross-react with halothane-induced antibodies. Int Arch Allergy Immunol 108:24–32.

Davies RJ, Rusznak C, Devalia JL. 1998. Why is allergy increasing?—environmental factors. Clin Exp Allergy 28 Suppl 6:8–14.

Dearman RJ, Basketter DA, Kimber I. 1996. Characterization of chemical allergens as a function of divergent cytokine secretion profiles induced in mice. Toxicol Appl Pharmacol 138:308–316.

Dearman RJ, Basketter DA, Evans P, Kimber I. 1999. Comparison of cytokine secretion profiles provoked in mice by glutaraldehyde and formaldehyde. Clin Exp Allergy 29:124–132.

Eder E, Kutt W. 1989. The dependence of the mutagenicity of methanesulphonic acid esters in S. typhimurium TA100 on the alkylation mechanisms. Chem Biol Interact 69:45–69.

Gao XM, Rhodes J. 1990. An essential role for constitutive Schiff base–forming ligands in antigen presentation to murine T cell clones. J Immunol 144:2883–2890.

Hazen SL, Gaut JP, Hsu FF, Crowley JR, D'Avignon A, Heinecke JW. 1997. p-Hydroxyphenylacetaldehyde, the major product of L-tyrosine oxidation by the myeloperoxidase-H_2O_2-chloride system of phagocytes, covalently modifies epsilon-amino groups of protein lysine residues. J Biol Chem 272:16990–16991708.

Hess DA, Rieder MJ. 1997. The role of reactive drug metabolites in immune-mediated adverse drug reactions. Ann Pharmacother 31:1378–1387.

Kapsenberg ML. 1996. Chemicals and proteins as allergens and adjuvants. Toxicol Lett 86:79–83.

Kim H, Kim YD, Cho SH. 1999. Formaldehyde exposure levels and serum antibodies to formaldehyde–human serum albumin of Korean medical students. Arch Environ Health 54:115–118.

Luster MI, Blank JA, Dean JH. 1987. Molecular and cellular basis of chemically induced immunotoxicity. Annu Rev Pharmacol Toxicol 27:23–49.

Manetz TS, Meade BJ. 1999. Development of a flow cytometry assay for the identification and differentiation of chemicals with the potential to elicit irritation, IgE-mediated, or T cell–mediated hypersensitivity responses. Toxicol Sci 48:206–217.

Neurath MF, Fuss I, Kelsall BL, Presky DH, Waegell W, Strober W. 1996. Experimental granulomatous colitis in mice is abrogated by induction of TGF-beta-mediated oral tolerance. J Exp Med 183:2605–2616.

Peterson B, Saxon A. 1996. Global increases in allergic respiratory disease: the possible role of diesel exhaust particles. Ann Allergy Asthma Immunol 77:263–268.

Rhodes J. 1989. Evidence for an intercellular covalent reaction essential in antigen-specific T cell activation. J Immunol 143: 1482–1489.

Rhodes J, Chen H, Hall SR, Beesley JE, Jenkins DC, Collins P, Zheng B. 1995. Therapeutic potentiation of the immune system by costimulatory Schiff-base-forming drugs. Nature 377:71–75.

Seel K, Walber U, Herbold B, Kopp R. 1999. Chemical behaviour of seven aromatic diisocyanates (toluenediisocyanates and diphenylmethanediisocyanates) under *in vitro* conditions in relationship to their test results in the Salmonella/microsome test. Mutat Res 438:109–123.

Shanafelt MC, Soderberg C, Allsup A, Adelman D, Peltz G, Lahesmaa R. 1995. Costimulatory signals can selectively modulate cytokine production by subsets of CD4+ T cells. J Immunol 154:1684–1690.

Shearer GM. 1995. Redirecting T-cell function. Nature 377:16–18.

von Bonin A, Ortmann B, Martin S, Weltzien HU. 1992. Peptide-conjugated hapten groups are the major antigenic determinants for trinitrophenyl-specific cytotoxic T cells. Int Immunol 4:869–874.

Wass U, Belin L. 1990. An *in vitro* method for predicting sensitizing properties of inhaled chemicals. Scand J Work Environ Health 16:208–214.

Yokota K, Yamaguchi K, Takeshita T, Morimoto K. 1998. The association between serum levels of Th cytokines and rhinoconjunctivitis caused by methyltetrahydrophthalic anhydride. Allergy 53:803–807.

Appendix 17

Reichardt P+, Lehmann I, Sierig G, Borte M. Analysis of T-cell receptor V-beta 2 in peripheral blood lymphocytes as a diagnostic marker for Kawasaki disease. **Infection**.2002;30:360-4.
+Corresponding author

IF: 2.4

Analysis of T-Cell Receptor V-Beta 2 in Peripheral Blood Lymphocytes as a Diagnostic Marker for Kawasaki Disease

P. Reichardt, I. Lehmann, G. Sierig, M. Borte

Abstract

Background: Kawasaki disease (KD) is the most frequent cause of acquired heart disease in children, yet there are no specific diagnostic markers for it. There is controversy whether and by what mechanism selective expansion of T-cell subsets occurs and whether this phenomenon might be helpful for early diagnosis.

Patients and Methods: To obtain age-related normal values of V-beta 2^+ T-lymphocytes in healthy children and to investigate expansion in KD, we measured expression in 228 children. Peripheral $CD3^+$ cells were stained with monoclonal antibodies to V-beta 2.1 and the percentage of V-beta 2^+ T-cells was analyzed using flow cytometry.

Results: In a control group of 184 healthy subjects (0 to 17 years; median age 6.0 years) we found age-related changes. Levels were highest from 0–2 years (9.02 ± 2.80%) and declined towards adolescence (7.56 ± 2.42% in 11–15 year olds) ($p < 0.001$). Results were compared with 24 patients with acute febrile diseases of origin other than KD and with 20 patients with presumed diagnosis KD at admission. Interestingly, while all seven patients whose clinical picture retrospectively confirmed KD showed elevated levels, none of the other children, including none of the patients with initially suspected but not clinically confirmed KD, had levels higher than normal, with the exception of two teenage girls with toxic shock syndrome, a classical superantigen-mediated disease.

Conclusion: When compared with appropriate age-matched controls, estimation of V-beta 2^+ T-cells might be a valuable tool when making diagnostic decisions suspecting KD.

Infection 2002; 30: 360–364
DOI 10.1007/s15010-002-3063-4

Introduction

Kawasaki disease (KD) is an acute systemic vasculitis of infancy and early childhood characterized by prolonged fever, conjunctivitis, inflammation of the oropharynx, rash, erythematous induration of the distal extremities and cervical lymphadenopathy [1, 2]. When untreated, coronary artery abnormalities can develop in up to 25% of patients [3, 4]. High-dose iv immunglobulins (IVIG) are the single therapeutic option shown to significantly reduce this risk to less than 5% [5–7], but administration must occur within the first 10 days after onset of fever for efficacy [8]. Thus, early recognition and prompt treatment is critical for successful outcome.

Diagnosis mainly relies on clinical signs and symptoms [9], as there is so far no specific and reliable diagnostic test for KD. Unfortunately, the initial clinical picture resembles a variety of other illnesses and can be incomplete, making early detection of disease difficult.

While there is increasing evidence for an infectious etiology of KD, the responsible agents and pathomechanisms leading to KD remain unknown. The intense search for a specific laboratory parameter allowing early diagnosis of KD has not yet been very successful. A variety of immunologic abnormalities demonstrating an inflammatory response have been observed in patients with KD, including increased serum levels of cytokines, such as IL-1, IL-2, IL-6, tumor necrosis factor-alpha, interferon-gamma and soluble IL-2 receptors [10–14]. However, these changes are of low specificity. A number of reports observed a selective expansion of specific V-beta chain bearing subsets of T-cells in KD and this has widely been interpreted as being suggestive for the involvement of superantigens (SAs) in the pathogenesis of the disease [15–20]. T-cells are a major target of SAs, which can polyclonally activate up to 20% of T-cells [21]. They thereby generate a severe immune response with liberation of large amounts of cytokines and activation of effector cells that is thought to be the main cause for tissue destruction in SA-

P. Reichardt *(corresponding author)*
Dept. of Microbiology and Immunology, Emory University, R3128 Rollins Research Center, 1510 Clifton Road, 30322 Atlanta, GA, USA;
Phone. (+1/404) 727-1546, Fax -3659, e-mail: preicha@emory.edu
Irina Lehmann
Environmental Research Center, Section Exposure Epidemiology, Leipzig, Germany
G. Sierig
University Clinic of Pediatric Cardiology, Cardiac Center, Leipzig, Germany
M. Borte
Children's Hospital of the University of Leipzig, Germany

Received: April 4, 2002 • Revision accepted: August 19, 2002

mediated diseases [22]. SAs omit binding to the antigen-specific binding site at the T-cell receptor (TCR) but interact directly with specific variable V-beta chains of TCR [23]. There is evidence that this might lead to selective proliferation of particular V-beta fractions of T-cells such as V-beta 2 [24, 25], V-beta 3 [26], V-beta 6 [27], V-beta 7 [28] and V-beta 8 [26, 29] and V-beta 11 [26].

For KD, V-beta 2+ T-cells are of special importance, as different bacterial toxins reported to be involved in the pathogenesis of KD are potent activators of this subset. Toxins found in KD are predominantly toxic shock syndrome (TSS) toxin-1 (TSST-1) of *Staphylococcus aureus* and to a lesser extent a number of exotoxins produced from Group A streptococci, all believed to predominantly stimulate V-beta 2+ T-cells [24, 30, 31]. Indeed, in all studies observing selective expansion of T-cells in KD, V-beta 2 was involved with some studies also showing elevation of other subsets [15–20, 32, 33]. However, changes were generally only minor, and a number of studies failed to see any specific elevation in KD [34–36]. While each of these studies had its own control group, one problem in making a general evaluation of the parameter might be the lack of appropriate age-matched healthy controls in children.

The purpose of our study was to obtain age-related normal values in healthy children and to further investigate the existence of selective expansion of V-beta 2+ T-lymphocytes in KD in order to examine if the determination of the level of TCR V-beta 2+ T-cells in peripheral blood can be a helpful tool for early detection of patients with KD.

Patients and Methods

Patients and General Experimental Design

All patients enrolled in this study were admitted to the Children's Hospital of the University of Leipzig. The control group for age- and sex-matched normal values in healthy children consisted of 184 children between 0 and 17 years (median age 6.0 years; 94 male and 90 female subjects) undergoing corrective surgery or medical checkup. Patients qualified for this group, when free of febrile diseases for at least 4 weeks before examination and not under the influence of any treatment.

A second group of patients served as a disease control group. It included 24 patients (median age 7.5 years; 11 male and 13 female patients) with febrile illness of known origin other than KD. The diagnoses were anaphylactoid purpura in six, rotavirus enteritis in five, febrile seizure in one, paravertebral abscess in one, burn injuries in two, febrile complications after abdominal surgery in seven and TSS in two patients (isolation of *S. aureus* in both patients, diagnostic criteria according to [37]).

In a third group, patients with presumed diagnosis of KD at admission were included in a prospective manner. The group consisted of 20 patients (median age 2.5 years; 12 male and eight female patients). The diagnosis KD was finally made when the clinical criteria in accordance with the international consensus statement [9] were fulfilled. In detail, prolonged fever of unknown origin (temperature of more than 38.5 °C for more than 5 days) had to be present together with four of the following criteria: bilateral nonpurulent conjunctivitis, mucosal inflammation of the oropharynx, erythematous induration of the peripheral extremities, polymorphous rash, and nonsuppurative cervical lymphadenopathy. In addition, the diagnosis KD required that the illness could not be explained by other diseases known to mimic KD.

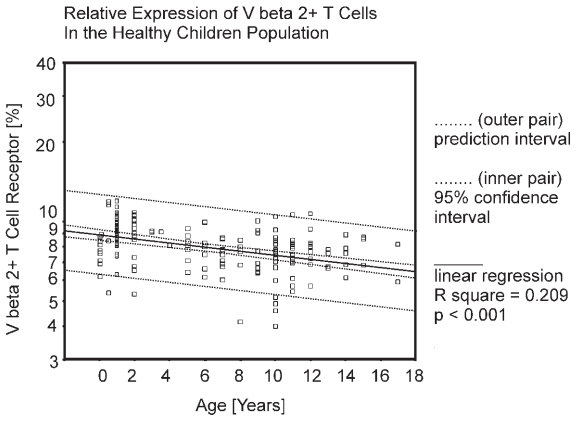

Figure 1. Correlation between age and TCR V-beta 2.1 expression of peripheral T-cells in healthy or clinically inconspicuous children. The amount of TCR V-beta 2.1+ T-lymphocytes was determined by flow cytometry and expressed as a percentage of total T(CD3+)-cells.

The study was approved by the Research Ethics Committee of the University of Leipzig. Written informed consent was obtained from the parents of all patients before entry into the study.

Collection of EDTA Blood Samples

Peripheral blood (0.5 ml in EDTA) was obtained by peripheral venipuncture and was stored at room temperature for a maximum of 12 h until staining and analysis by fluorescent-activated cell sorter (FACS).

Two-Color Staining of T-Cells from Peripheral Blood

V-beta 2+ T-cells were determined using fluorescence-conjugated monoclonal antibody (mAb). The whole blood samples of each patient were divided into two aliquots of 100 µl for staining. To one aliquot of 100 µl whole blood, 10 µl anti-TCR V-beta 2.1 (FITC, Clone E22E7, COULTER-Immunotech) and 10 µl of anti-CD3 (PE, Clone UCHT; COULTER-Immunotech) were added. To the other aliquot of the pair, 10 µl anti-CD3 alone was added as control. Incubation proceeded for 20 min at room temperature. Cells were fixed in PBS/1% formaldehyde and erythrocytes were lysed using FACS lysing solution (Becton Dickinson) for 10 min at room temperature. Cells were washed twice, resuspended in 250 µl PBS/1% formaldehyde and immediately analyzed by FACS.

Determination of TCR V-Beta 2+ Expression of T-Cells by Flow Cytometry

Samples were examined on an FACScan cytometer (Becton Dickinson) using CellQuest software; 10,000 events were collected. Forward and sideward scatter were used to gate on lymphocytes. The percentage of T-cells bearing the TCR V-beta 2 was expressed as the percentage of total T(CD3+)-cells.

Statistics

Means and variances were calculated for each measured patient as well as for the different patient groups and age-groups, respec-

tively. Statistical comparisons were made based on a 95% overall CI. Data were analyzed and plotted with the statistical package SPSS 9.0, using the Mann-Whitney rank sum test. Z scores (standard scores) of V-beta 2 values comparing data to the corresponding age-groups in the normal child population were calculated for all KD patients.

Results

In the control group of 184 healthy subjects (0 to 17 years; median age 6.0 years) we obtained a wide range for normal V-beta 2.1 expression on peripheral T-cells. Levels were found to be highest in newborns and toddlers while declining towards adolescence (Figure 1). When being divided into four age-groups, ranges for TCR V-beta 2 expression were significantly higher in the younger age-groups. In the group of children ranging from 0–2 years and in the group of 3–6 years levels were higher than in every older age-group, respectively (Table 1). No differences between females and males were found (data not shown); accordingly, the data are presented as pooled values.

In the disease control group of 24 patients with febrile diseases other than (suspected) KD, the rates of TCR V-beta 2+ T-cells were not higher than predicted from our data from age-matched controls in the healthy child population (Figure 2), with the exception of two teenage girls with TSS who showed elevated levels (19.0%, and 21.9%, respectively).

In the group of 20 patients initially suspected to have KD, retrospectively only seven fulfilled the diagnostic criteria of KD, while in the 13 others the diagnosis had to be dropped. In seven of the 13, an infection of the upper respiratory tract was diagnosed. Fever in these patients dropped after less than 5 days (without administration of IVIG) and not more than three KD criteria were fulfilled. In particular, none of these children showed a polymorphous rash, while all showed some of the oropharyngeal or cervical affections. Two children suffered pneumonia, as proved by X-ray. In one of them, high levels of antibodies to influenza A virus were detected, suggesting influenza pneumonia. One child was diagnosed as having an intraabdominal infection after *Salmonella* spp. was isolated. One child had a multisystemic vasculitis. He showed sustained fever and rash, but lacked conjunctivitis, mucosal inflammation of oropharynx and cervical lymphadenopathy. One patient showed fever and a suspicious rash, the latter being later recognized as severe contact dermatitis possibly accompanied by an infection of the upper respiratory tract at that time. One patient turned out to have erythema exsudativum multiforme. Strikingly, while none of the 13 patients in whom the presumed diagnosis KD had to be dropped showed elevated levels of TCR V-beta 2+ T-cells compared to the healthy child population, all seven patients with clinically proven KD had levels which were higher than the expected age-related normal range (12.9% [z-score 2.77], 12.9% [4.21], 13.0% [2.84], 13.8% [3.41], 14.1% [5.29], 14.3% [3.77] and 33.5% [17.49], respectively) (Figure 2). Samples were taken on the day of admission, corresponding to day 3 (two patients), day 4 (two patients), day 5 (two patients) and day 6 (one patient) after onset of fever, respectively. There was no correlation between levels of V-beta 2 expression and day after onset of fever (data not shown). In all seven patients and in the two patients with TSS, levels later declined and were found to be normal at follow-up less than 4 weeks after onset of disease (data not shown).

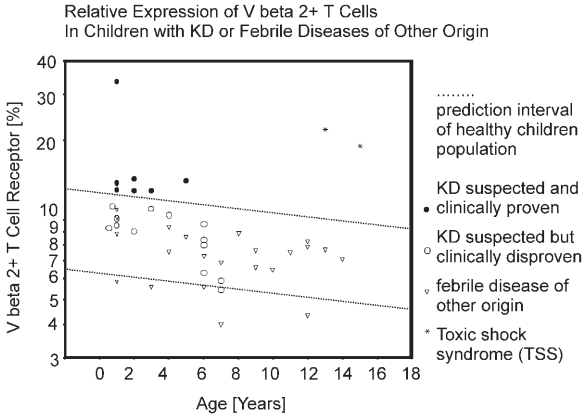

Figure 2. TCR V-beta 2.1 expression in patients with suspected KD and in children with other acute febrile diseases. While all patients with clinically proven KD showed elevated V-beta 2+ levels (black dots), patients who did not fulfill criteria for KD in the course of disease showed normal values (white dots). Also, no patient with other febrile diseases suspected at admission showed elevated levels (white triangles), with the exception of the two patients diagnosed with toxic shock syndrome (asterix).

Table 1
Ranges of a normal child population of TCR V-beta 2+ T-cell expression (% of total T-cells) in diverse age-groups (median ± 2 SD).

Age (years)	Age-group	No. of patients	Median ± 2 SD	Statistical significance of differences between age-groups
0–2	1	78	9.02 ± 2.80	$p < 0.001$ 1 vs 3; 1 vs. 4, $p < 0.01$ 1 vs 2
3–6	2	19	8.18 ± 2.24	$p < 0.01$ 2 vs 1; 2 vs. 3, $p < 0.05$ 2 vs 4
7–10	3	47	7.23 ± 2.86	$p < 0.001$ 3 vs 1, $p < 0.01$ 3 vs 2
11–15	4	38	7.56 ± 2.42	$p < 0.001$ 4 vs 1, $p < 0.05$ 4 vs 2

Discussion

Our results provide data about normal values of V-beta 2+ T-cells in the healthy child population. We were able to show that the level of V-beta 2 expression significantly differs with the age of the subject during childhood and adolescence.

Such age-related differences can be crucial for correct interpretation of data, as differences between V-beta 2 expression in patients and controls seem to be narrow in most cases. Furthermore, when comparing our data with those from children with infectious diseases, among them KD, we observed elevated V-beta 2^+ T-cells in all of our patients with KD and in two patients with TSS, but not in patients with other febrile diseases. Our data suggest elevated levels of V-beta 2^+ T-cells in SA-driven diseases such as KD and TSS.

Conflicting data have been reported regarding expanded T-cell populations in KD. Elevated levels of V-beta 2^+ and to a lesser extent V-beta 6^+ and V-beta 8.1^+ T-cells were shown in a number of reports in the peripheral blood during the acute phase of KD compared with age-matched normal children and patients with other febrile illnesses [15–17, 20]. The observed elevated levels returned to normal in convalescence. The pathogenetical impact of elevated T-cell fractions, however, is not fully understood. Some reports describe V-beta 2 changes but suggest no involvement of these cells in disease pathogenesis [15]. In contrast, other authors were not able to confirm abnormal usage of any V-beta family neither acutely nor during convalescence [34–36]. One reason for the failure of detection of selective enhancement of T-cell populations in KD might be the dynamic nature of the disease process. Specific T-cells may already have been transferred into inflamed tissue when analysis in blood samples is performed [19, 33]. In our study, in all KD patients V-beta 2 was determined relatively early, between day 3 and 6 after onset of disease. In addition, the fate of the stimulated T-cells varies depending on a number of factors and can range from sustained expansion to apoptosis and clonal deletion [24]. Finally, studies in mice indicate that SAs also use major histocompatitbility complex (MHC)-independent pathways which may lead to different immune responses [38]. Besides, the participation of conventional infectious antigens in KD, which might even be responsible for the observed clonal expansions of T-cells in the acute phase of KD, is still discussed [30, 39]. In our study, apart from the KD patients, two patients with TSS showed elevated V-beta 2 levels. TSS is considered a classical SA-mediated disease, which shows great clinical similarity to KD. TSST-1, the leading SA associated with KD, is also responsible for the majority of cases of TSS [40]. TSS may even belong to the same pathophysiological entity as KD [41]. Thus, while elevation of V-beta 2 may not be specific for KD, it may well point to the existence of a potentially lethal SA-triggered immune response such as KD and TSS. Furthermore, given the characteristic age range of KD, we believe that determination of V-beta 2 can provide valuable help to the clinician suspecting KD.

We conclude that the analysis of TCR V-beta 2^+ T-cells in peripheral blood may be a useful laboratory tool for early diagnosis of KD when carefully compared to appropriate age-matched control values.

References

1. Kawasaki T: Acute febrile mucocutaneous syndrome with lymphoid involvement with specific desquamation of the fingers and toes in children [in Japanese]. Arerugi 1967;16:178–222.
2. Shulman ST, De Inocencio J, Hirsch R: Kawasaki disease. Pediatr Clin N Am 1995; 42: 1205–1222.
3. Fujiwara H, Hamashima Y: Pathology of the heart in Kawasaki's disease. Pediatrics 1978; 1: 100–107.
4. Kato H, Sugimura T, Akagi T, Sato N, Hashino K, Maeno Y, Kazue T, Eto G, Yamakawa R: Long term consequences of Kawasaki disease. A 10-21 year follow-up study of 594 patients. Circulation 1996; 94: 1379–1385.
5. Furusho K, Kamiya T, Nakano H, Kiyosawa N, Shinomiya K, Hayashidera T, Tamura T, Hirose O, Manabe Y, Yokoyama T: High-dose intravenous gammaglobulin for Kawasaki disease. Lancet 1984; 2: 1055–1058.
6. Newburger JW, Takahaski M, Burns JC, Beiser AS, Chung KJ, Duffy CE: The treatment of Kawasaki syndrome with intravenous gamma globulin. N Engl J Med 1986; 31: 341–346.
7. Terai M, Shulman ST: Prevalence of coronary artery abnormalities in Kawasaki disease is highly dependent on gamma globulin dose but independent of salicylate dose. J Pediatr 1997; 131: 888–893.
8. Durongpisitkul K, Gururaj VJ, Park JM, Martin CF: The prevention of coronary artery aneurysm in Kawasaki disease: a meta-analysis on the efficacy of aspirin and immunoglobulin treatment. Pediatrics 1995; 96: 1057–1061.
9. Third International Kawasaki Disease Symposium, Tokyo, Japan, Dec 1988. Ped Inf Dis J 1989; 8: 663.
10. Furukawa S, Matsubara T, Yone K, Hirano Y, Okumara K, Yabuta K: Kawasaki disease differs from anaphylactoid purpura and measles with regard to tumor necrosis factor-alpha and interleukin 6 in serum. Eur J Pediatr 1992; 51: 44–47.
11. Leung DY, Cotran RS, Kuret-Jones E, Burns JC, Newburger JW, Pober JS: Endothelial cell activation and high interleukin-1 secretion in the pathogenesis of acute Kawasaki disease. Lancet 1989; 2: 1298–1302.
12. Lin CY, Lin CC, Hwang B, Chiang BN: The changes of interleukin 2, tumor necrosis factor and gamma-interferon production among patients with Kawasaki disease. Eur J Pediatr 1991; 150: 179–182.
13. Lin CY, Lin CC, Hwang B, Chiang BN: Cytokines predict coronary aneurysm formation in Kawasaki disease patients. Eur J Pediatr 1993; 152: 309–312.
14. Matsubara T, Furukawa S, Yabuta K: Serum levels of tumor necrosis factor, interleukin 2 receptor and interferon-gamma in Kawasaki disease involved coronary-artery lesions. Clin Immunol Immunopathol 1990; 56: 29–36.
15. Abe J, Kotzin BL, Meissner C, Melish ME, Takahashi M, Fulton D, Romagne F, Malissen B, Leung DY: Characterization of T-cell-repertoire changes in acute Kawasaki disease. J Exp Med 1993; 177: 791–796.
16. Abe J, Kotzin BL, Jujo K, Melish ME, Golde MP, Kohsaka T, Leung DY: Selective expansion of T-cell expressing T-cell receptor variable regions V beta 2 and V beta 8 in Kawasaki disease. Proc Natl Acad Sci USA 1992; 89: 4066–4070.
17. Curtis N, Zheng R, Lamb JR, Levin M: Evidence for a superantigen mediated process in Kawasaki disease. Arch Dis Child 1995; 72: 308–311.
18. Leung DY, Travers JB, Giorno R, Norris DA, Skinner R, Aelion J, Kazemi LV, Kim MH, Trumble AE, Kotb M: Evidence for a streptococcal superantigen-driven process in acute guttate psoriasis. J Clin Invest 1995; 96: 2106–2112.

19. Yamashiro Y, Nagata S, Oguchi S, Shimizu T: Selective increase of V-beta 2+ T-cells in the small intestinal mucosa in Kawasaki disease. Pediatr Res 1996; 39: 264–266.
20. Yoshioka T, Matsutani T, Iwagami S, Toyosaki-Maeda T, Yutsudo T, Tsuruta Y, Suzuki H, Uemura S, Takeuchi T, Koike M, Suzuki R: Polyclonal expansion of TCRBV2- and TCRBV6-bearing T cells in patients with Kawasaki disease. Immunology 1999; 96: 465–472.
21. Li H, Llera A, Malchiodi AE, Mariuzza RA: The structural basis of T cell activation by superantigens. Ann Rev Immunol 1999;17: 435–466.
22. Marrack P, Kappler J: The staphylococcal enterotoxins and their relatives. Science 1990; 248: 705–711.
23. Fraser JD: High-affinity binding of staphylococcal enterotoxins A and B to HLA-DR. Nature 1989; 339: 221–223.
24. Mingari MC, Cambiaggi A, Vitale C, Schiavetti F, Bellomo R, Poggi A: Effect of superantigens on human thymocytes: selective proliferation of V-beta 2+ cells in response to toxic shock syndrome toxin-1 and their deletion upon secondary stimulation. Int Immunol 1996; 8: 203–209.
25. Choi Y, Lafferty JA, Clements JR, Todd JK, Gelfand EW, Kappler J, Marrack P, Kotzin BL: Selective expansion of T-cells expressing Vß2 in toxic shock syndrome. J Exp Med 1990; 172: 981–984.
26. Shu S, Krinock RA, Matsumura T, Sussman JJ, Fox BA, Chang AE, Terman DS: Stimulation of tumor-draining lymph node cells with superantigenic staphylococcal toxins leads to the generation of tumor-specific effector T cells. J Immunol 1994; 152: 1277–1288.
27. Lafon M, Scott-Algara D, Marche PN, Cazenave PA, Jouvin-Marche E: Neonatal deletion and selective expansion of mouse T cells by exposure to rabies virus nucleocapsid superantigen. J Exp Med 1994; 180: 1207–1215.
28. Conrad B, Weidmann E, Trucco G, Rudert WA, Behboo R, Ricordi C, Rodriquez-Rilo H, Finegold D, Trucco M: Evidence for superantigen involvement in insulin-dependent diabetes mellitus aetiology. Nature 1994; 371: 351–355.
29. Galelli A., Delcourt M, Wagner MC, Peumans W, Truffa-Bachi P: Selective expansion followed by profound deletion of mature V beta 8.3+ T cells in vivo after exposure to the superantigenic lectin Urtica dioica agglutinin. J Immunol 1995; 154: 2600–2611.
30. Choi IH, Chwae YJ, Shim WS, KIM DS, Kwon DH, Kim JD, Kim SJ: Clonal expansion of CD8+ T cells in Kawasaka disease. J Immunol 1997; 159: 481–486.
31. Leung DY, Meissner C, Fulton DR, Murray DL, Kotzin BL, Schlievert PM: Toxic shock syndrome toxin-secreting *Staphylococcus aureus* in Kawasaki syndrome. Lancet 1993. 342: 1385–1388.
32. Jason J, Montana E, Donald JF, Seidman M, Inge KL, Campbell R: Kawasaki disease and the T-cell antigen receptor. Hum Immunol 1998; 59: 29–38.
33. Leung DY, Giorno RC, Kazemi LV, Flynn PA, Busse JB: Evidence for superantigen involvement in cardiovascular injury due to Kawasaki syndrome. J Immunol 1995; 155: 5018–5021.
34. Mancia L, Wahlstrom J, Schiller B, Chini L, Elinder G, D'Argenio P, Gigliotto D, Wigzell H, Rossi P, Grunewald J: Characterization of the T-cell receptor V-beta repertoire in Kawasaki disease. Scand J Immunol 1998; 48: 443–449.
35. Pietra BA, De Inocencio J, Giannini EH, Hirsch R: TCR V-beta family repertoire and T cell activation markers in Kawasaki disease. J Immunol 1994; 153: 1881–1888.
36. Sakaguchi M, Kato H, Nishiyori A, Sagawa K, Itoh K: Characterization of CD4+ T helper cells in patients with Kawasaki disease (KD): preferential production of tumour necrosis factor-alpha (TNF-alpha) by V-beta 2- or V-beta 8- CD4+ T helper cells. Clin Exp Immunol 1995; 99: 276–282.
37. CDC: Case definitions for infectious conditions under public health surveillance. MMWR 1997; 46: 39–40.
38. Avery AC, Markowitz JS, Grusby MY, Glimcher LH, Cantor H: Activation of T-cells by superantigen in class II-negative mice. J Immunol 1994; 153: 4853–4861.
39. Rowley AH, Eckerley CA, Jack HM, Shulman ST, Baker SC: IgA plasma cells in vascular tissue of patients with Kawasaki syndrome. J Immunol 1997; 159: 5946–5955.
40. Parsonnet J: Nonmenstrual toxic shock syndrome: new insights into diagnosis, pathogenesis, and treatment. Curr Clin Top Infect Dis 1996; 16: 1–20.
41. Meissner HC, Leung DY: Superantigens, conventional antigens and the etiology of Kawasaki syndrome. Pediatr Infect Dis J 2000; 19: 91–94.

Appendix 18

Reichardt, P+; Dähnert, I.; Tiller, G.; Häusler, H.-J. Possible activation of an intra-myocardial inflammatory process (S. aureus) after treatment with infliximab in a boy with Crohn's disease.
European Journal of Pediatrics.2002;161:281-3.
+Corresponding author

IF: 1.9

Eur J Pediatr (2002) 161: 281–283
DOI 10.1007/s00431-002-0925-9

ORIGINAL PAPER

Peter Reichardt · Ingo Dähnert · Gabriele Tiller
Hans-Jürgen Häusler

Possible activation of an intramyocardial inflammatory process (*Staphylococcus aureus*) after treatment with infliximab in a boy with Crohn disease

Received: 13 November 2001 / Accepted: 16 January 2002 / Published online: 8 March 2002

Abstract In an 11-year old boy with Crohn disease, long-term therapy with prednisolone was decided to be augmented by infliximab, a monoclonal antibody to tumour necrosis factor alpha. The patient, who was in a stable clinical condition with low signs of inflammation at that time, deteriorated 3 days after the first dose of 200 mg infliximab with fever, nausea, myalgia and signs of cardiac failure. Echocardiography demonstrated destruction of the aortic valve with third grade insufficiency. In the blood culture, a susceptible strain of *Staphylococcus aureus* was isolated. Antibiotic therapy resulted in rapid improvement, but the aortic valve had to be replaced by a homograft due to massive insufficiency. At surgery, there were no signs of endocarditic vegetations, the aortic ring and the right coronary aortic cusp had been destroyed by a massive intramyocardial abscess, leading from close beneath the aortic ring in the direction of the right atrium. The size of the process suggested chronic infection or reinfection after several weeks. As clinical and laboratory signs as well as echocardiographic changes pointed to a dramatic flare-up shortly after the administration of infliximab, we suggest that this chronic inflammatory process was activated by infliximab. *Conclusion:* when using infliximab, special awareness of potential risks is necessary in patients with chronic infections or in a state of immunodeficiency.

P. Reichardt (✉)
Children's Hospital, University of Leipzig,
Oststrasse 21-25, 04317 Leipzig, Germany

I. Dähnert · H-J. Häusler
University's Clinic of Paediatric Cardiology,
Herzzentrum Leipzig, Leipzig, Germany

G. Tiller
Children's Hospital Chemnitz, Chemnitz, Germany

Present address: P. Reichardt
Emory University, Department of Microbiology
and Immunology, R3128 Rollins Research Center,
1510 Clifton Road, 30322 Atlanta, GA, USA,
Tel.: +1-404-7271546, Fax: +1-404-7273659,
e-mail: preicha@emory.edu

Keywords Anti-tumour necrosis factor alpha · Crohn disease · Infection · Myocard

Abbreviation *TNF* tumour necrosis factor

Introduction

Infliximab, a monoclonal antibody to tumour necrosis factor (TNF) alpha, is a new immunosuppressive drug. Showing remarkable effectiveness, the drug is increasingly being used in refractory cases of rheumatoid arthritis [8,14] and Crohn disease [3, 4, 7, 11, 16]. While side-effects consist mainly of local and systemic hypersensitivity reactions, an increased susceptibility to infections is also known. Invasive fungal infections associated with infliximab therapy have been reported [17] and there is evidence suggesting increased susceptibility to certain severe bacterial infections [9].

We report on an 11-year-old boy with Crohn disease, who 3 days after the first administration of infliximab, developed fever, signs of cardiac failure and a *Staphylococcus aureus* sepsis. Upon surgery, an intramyocardial para-aortic abscess was found suggesting a chronic infection, possibly activated by infliximab. The aim of this case report is to highlight the potential risks associated with the use of this powerful immunomodulating drug.

Case report

In an 11-year-old boy treated for 1 year with azathioprine and prednisolone for Crohn disease, therapy was intensified with infliximab. At that time, the patient was in good clinical condition. Laboratory studies showed good control of inflammatory activity with leucocytes falling, bands, CRP and body temperature all returning to normal values before administration of infliximab. Three days after the first dose of infliximab (200 mg, concomitantly azathioprine 1×50 mg and prednisolone 3×20 mg at 32 kg body weight) the patient deteriorated with high fever, signs of heart failure, and erythematous lesions on the fingers and toes resembling Osler nodules (Fig. 1). Laboratory studies revealed a sharp rise in

Fig. 1. Painful pin-point sized erythematous lesions with haemorrhagic periphery resembling Osler nodules on the toes (and fingers) of a patient with Crohn disease and intramyocardial para-aortic abscess due to *S. aureus* infection

activity of systemic inflammation (Fig. 2). Echocardiography suggested endocarditis, a therapy with ceftazidime and gentamicin was started and the patient was transferred to our cardiology unit. Echocardiography showed a third degree aortic insufficiency (ejection fraction 0.37, fractional shortening 0.18) and a destruction of the aortic valve with the right coronary cusp being totally disrupted and floating in the bloodstream (Fig. 3). Haematological data were as follows: leucocytes 24,800/µl, haematocrit 0.47, thrombocytes 313,000/µl, IgG 6.89 g/l, IgA 2.46 g/l, IgM 3.21 g/l, creatinine 44 µmol/l, BUN 3.0 mmol/l. In two blood cultures a highly susceptible *S. aureus* strain was isolated. After 21 days of antibiotic treatment with cefuroxime and gentamicin, replacement of the highly insufficient aortic valve was performed. Upon surgery, a large para-aortic intramyocardial abscess was detected, reaching from close beneath the destroyed right aortic cusp in the direction of the right atrium. The abscess cavity was drained and primarily closed and the aortic root including the valve was replaced by an aortic homograft. Histologically, the myocard showed an increased amount of lymphocytes and macrophages, probably reflecting the inflammatory process. Post-operatively, the homograft appeared competent and laboratory signs of inflammation completely normalised within a week. The patient is currently in good clinical condition with a competent aortic valve and stable Crohn disease.

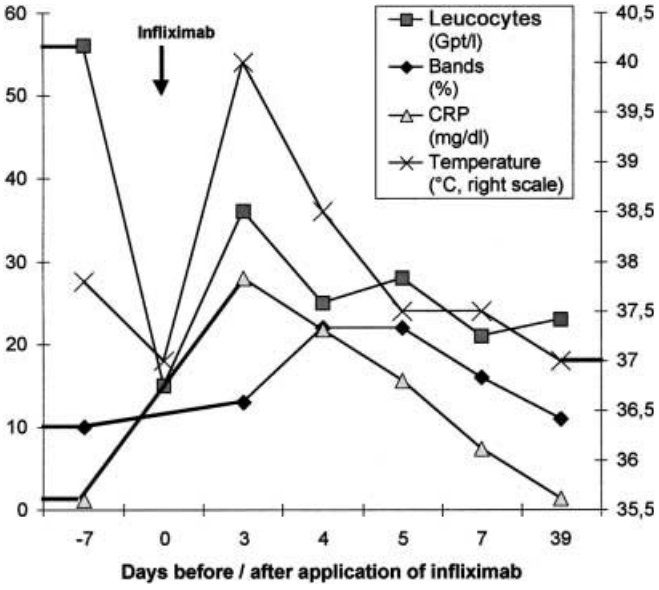

Fig. 2. Course of systemic inflammation after administration of infliximab in a patient with intramyocardial para-aortic abscess and Crohn disease

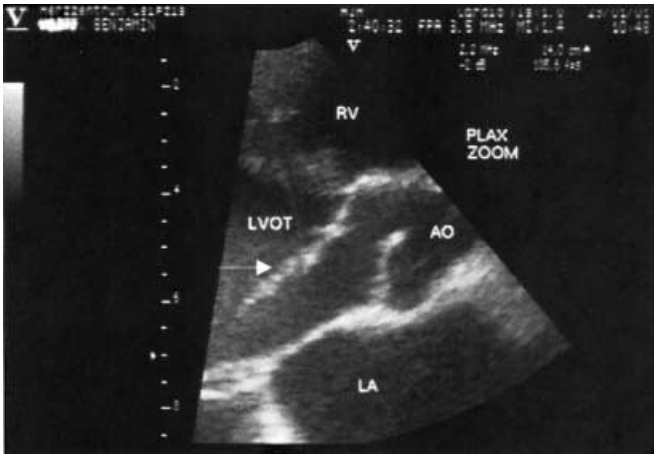

Fig. 3. Echocardiography of a patient with intramyocardial para-aortic abscess and Crohn disease. The *arrow* shows the disrupted right coronary aortic cusp appearing as filamentous structure floating in the bloodstream. The left ventricle shows enlargment (left ventricular enddiastolic diameter 62 mm), possibly secondary to the severely insufficient aortic valve. The left ventricular function was heavily diminished (fractional shortening 0,18; ejection fraction 0.37)

Discussion

Our patient presented with Crohn disease, *S.aureus* sepsis and a large intramyocardial para-aortic abscess which led to the destruction of the aortic valve. Due to the close time lag between the administration of infliximab and the deterioration of the patient we believe that the activation of the inflammatory process had been favoured by the drug.

Experience with infliximab is still limited, especially in patients with immunosuppression and chronic infections [1]. Concerns have been raised about the safety of the drug because of its immunomodulating potential [14]. Patients with Crohn disease do carry additional risks as they are more susceptible to bacterial infections possibly due to their disturbed mucosal barrier and to concomitant immunosuppressive therapy [6, 18]. In addition, Crohn disease itself may lead to vasculitic changes of the aorta [5, 10, 15], which might have further favoured the development of the intramyocardial abscess in our patient. The size of the abscess suggested its persistence for several weeks, however, it gained only destructive activity shortly after infliximab was given. The lesions detected on echocardiography had not been present at routine echocardiography the previous week, with exception of a first degree aortic insufficiency. Furthermore, according to laboratory studies, inflammatory activity in our patient was low before administration of infliximab. What may have further contributed to the precipitation of the systemic

infection with *S. aureus* is the fact that 3 days before administration of infliximab, the dosage of prednisolone had been increased (from 1×10 mg to 3×20 mg) and that the patient received a total of 6.25 mg infliximab per kg body weight. While most studies suggest an initial dose of 5 mg/kg, safety in doses up to 20 mg/kg body weight has been demonstrated [12,13]. However, adverse events may be elevated when higher doses are administered [2]. As others [9,17], we express our concern that infliximab may bear the potential for serious side-effects such as invasive infections. In order to minimise the chance of such complications, we suggest that upon the use of infliximab, possible co-infections must be carefully excluded. In children with Crohn disease, we suggest that an initial dose of 5 mg/kg should not be surpassed and that, if possible, doses of concomitant immunosuppressive drugs should not be simultaneously increased. When using infliximab, extreme care should be taken in patients in whom additional risks such as immunodeficiency or chronic infections may exist.

References

1. Campbell S, Ghosh S (2001) Infliximab therapy for Crohn's disease in the presence of chronic hepatitis C infection. Eur J Gastroenterol Hepatol 13: 191–192
2. Centocor (2001) Remicade (infliximab) – clinical alert: congestive heart failure. The FDA safety information and adverse event reporting program, October 23
3. Cohen RD, Tsang JF, Hanauer SB (2000) Infliximab in Crohn's disease: first anniversary clinical experience. Am J Gastroenterol 95: 3469–3477
4. Farrell RJ, Shah SA, Lodhavia PJ, Alshali M, Falchuk KR, Michetti P, Peppercorn MA (2000) Clinical experience with infliximab therapy in 100 patients with Crohn's disease. Am J Gastroenterol 95: 3490–3497
5. Hilario MO, Terreri MT, Prismich G, Len C, Kihara EN, Goldenberg J, Sole D (1998) Association of ankylosing spondylitis, Crohn's disease and Takayasu's arteritis in a child. Clin Exp Rheumatol 16: 92–94
6. Kreuzpaintner G, Horstkotte D, Heyll A, Losse B, Strohmeyer G (1992) Increased risk of bacterial endocarditis in inflammatory bowel disease. Am J Med 92: 391–395
7. Kugathasan S, Werlin SL, Martinez A, Rivera MT, Heikenen JB, Binion DG (2000) Prolonged duration of response to infliximab in early but not late pediatric Crohn's disease. Am J Gastroenterol 95: 3189–3194
8. Markham A, Lamb HM (2000) Infliximab: a review of its use in the management of rheumatoid arthritis. Drugs 59: 1341–1359
9. Morelli J, Wilson FA (2000) Does administration of infliximab increase susceptibility to listeriosis? Am J Gastroenterol 95: 841–842
10. Morita Y, Yamamura M, Suwaki K, Mima A, Ishizu T, Hirohata M, Kashihara N, Makino H, Ota Z (1996) Takayasu's arteritis associated with ulcerative colitis; genetic factors in this association. Intern Med 35: 574–578
11. Present DH, Rutgeerts P, Targan S, Hanauer SB, Mayer L, van Hogezand RA, Podolsky DK, Sands BE, Braakman T, DeWoody KL, Schauble TF, van Deventer SJ (1999) Infliximab for the treatment of fistulas in patients with Crohn's disease. N Engl J Med 349: 1398–1405
12. Rutgeerts P, D'Haens G, Targan S, Vasiliauskas E, Hanauer SB, Present DH, Mayer L, Van Hogezand RA, Braakman T, DeWoody KL, Schaible TF, Van Deventer SJ (1999) Efficacy and safety of retreatment with anti-tumor necrosis factor antibody (infliximab) to maintain remission in Crohn's disease. Gastroenterology 117: 761–769
13. Sands BE, Tremaine WJ, Sandborn WJ, Rutgeerts PJ, Hanauer SB, Mayer L, Targan SR, Podolsky DK (2001) Infliximab in the treatment of severe, steroid-refractory ulcerative colitis: a pilot study. Inflamm Bowel Dis 7: 83–88
14. Seymour HE, Worsley A, Smith JM, Thomas SH (2001) Anti-TNF agents for rheumatoid arthritis. Br J Clin Pharamacol 51: 201–208
15. Sharma BK, Jain S, Sagar S (1996) Systemic manifestations of Takayasu arteritis: the expanding spectrum. Int J Cardiol 54: S149–S154
16. Targan SR, Hanauer SB, van Deventer SJ, Mayer L, Present DH, Braakman T, DeWoody KL, Schaible TF, Rutgeerts PJ (1997) A short-term study of chimeric monoclonal antibody cA2 to tumor necrosis factor alpha for Crohn's disease. Crohn's Disease cA2 Study Group. N Engl J Med 337: 1029–1035
17. Warris A, Bjorneklett A, Gaustad P (2001) Invasive pulmonary aspergillosis associated with infliximab therapy. N Engl J Med 344: 1009–1010
18. Wong JS (1989) Infective endocarditis in Crohn's disease. Br Heart J 62: 163–164

Appendix 19

Reichardt P+, Apel TW, Domula M, Tröbs RB, Krause I, Bierbach U, Neumann HP, Kiess W. J Recurrent polytopic chromaffin paragangliomas in a 9-year-old boy resulting from a novel germline mutation in the von Hippel-Lindau gene.
J Pediatr Hematol Oncol. 2002: 24:145-8.
+Corresponding author

IF: 0.9

Recurrent Polytopic Chromaffin Paragangliomas in a 9-Year-Old Boy Resulting From a Novel Germline Mutation in the von Hippel–Lindau Gene

Peter Reichardt, M.D., Thomas W. Apel, M.D., Manfred Domula, M.D., Ralf-Bodo Tröbs, M.D., Ingrid Krause, M.D., Uta Bierbach, M.D., Hartmut P. H. Neumann, M.D., and Wieland Kiess, M.D.

Abstract: Pheochromocytomas are frequently associated with inherited cancer syndromes such as von Hippel–Lindau disease (VHL). Retinal angioma and hemangioblastomas of the central nervous system are hallmarks of VHL, but its clinical variety is remarkably broad. Pheochromocytomas as the sole or first manifestation of VHL are rare but have been observed. In this case report, the authors describe an unusual case of initial collapse, seizures, and hypertensive crisis in a child who later was found to have multiple extraadrenal pheochromocytomas. Molecular diagnostics revealed a novel point mutation in the *VHL* gene (*VHL* nt. 406 T→G). Only 7 months after the first lesions had been removed, a new paraganglioma developed in the contralateral periadrenal region. When encountering pheochromocytomas in children, the clinician should be aware that an associated tumor syndrome might be present, and appropriate molecular screening should be initiated. Molecular genetics aid in the clinical decision-making and clinical management of individual patients with pheochromocytoma.

Key Words: von Hippel–Lindau disease—*VHL* gene—Pheochromocytoma—Paraganglioma.

Pheochromocytomas are catecholamine-secreting neuroendocrine tumors arising from chromaffin cells in the adrenal medulla (1). Extraadrenal forms associated with ganglia of the autonomic nervous system are called paragangliomas. Excessive secretion of epinephrine and norepinephrine can lead to severe hypertensive crisis and heart failure. Pheochromocytomas can be part of three inherited tumor syndromes: multiple endocrine neoplasia II, neurofibromatosis type 1, and von Hippel–Lindau disease (VHL) (2). Pheochromocytomas, even when apparently sporadic, are in 10% to 20% part of VHL (3,4). Bilateral adrenal and extraadrenal forms, which tend to be more frequent in children than in adults (5), have an even higher risk of being associated with an hereditary syndrome (6).

von Hippel–Lindau disease is rare, with an estimated incidence of 1 in 40,000 (7,8). The clinical variety of VHL is remarkably broad. Retinal angiomas and cerebellar hemangioblastomas, renal cell carcinomas, pancreatic cysts, and pheochromocytomas are predominantly observed; cystadenomas of the epididymis, islet cell tumors, and tumors of the inner ear are found more rarely (9). Pheochromocytomas or paragangliomas as single manifestations of VHL are uncommon, but familial pheochromocytomas caused by *VHL* mutations have been described (10,11).

von Hippel–Lindau disease is an autosomal, dominant, inherited disease. The *VHL* susceptibility gene, a tumor suppressor gene, is located on chromosome 3p and has been identified and characterized (12). The VHL protein is fairly ubiquitously expressed (13). As part of a protein complex with elongin C and elongin B (14), the VHL protein is involved in angiogenesis, formation of extracellular matrix, regulation of cell cycles, and ubiquitin-mediated proteolysis (15). Nearly 300 mutations in the *VHL* gene are known, a large proportion of which interfere with the elongin-binding site (16). Loss of elongin-binding capacity of the VHL protein may lead to substrate accumulation and up-regulation of hypoxia-inducible factors such as vascular endothelial growth factor (17).

In this case report, we describe an unusual case of severe hypertensive crisis in a child in whom consecutively developing adrenal and thoracic paragangliomas were found. On molecular analysis, a novel mutation in the *VHL* gene was found. The aim of this case report is to stress the importance of screening for inherited diseases in patients with pheochromocytomas and to increase awareness of the presence of VHL in children.

CASE REPORT

A 9-year-old boy was admitted to the hospital with generalized seizures necessitating mechanical ventilation and with marked hypertension (maximum systolic blood pressure 190 mmHg). Heart rate was 110 bpm, respiratory rate was 20, and body temperature was 37.5°C. Physical examination revealed no other internal and no focal neurologic abnormalities. No café-au-lait-spots were present. Echocardiography showed muscular hypertrophy of the left ven-

Submitted for publication July 19, 2002; accepted January 1, 2001.

From the Intensive Care Unit (P.R.) and the Department of Hematology and Oncology (M.D., U.B., W.K.), Children's Hospital of the University of Leipzig, Leipzig, Germany; Department of Internal Medicine IV (T.W.A., H.B.H.N.), Hospital of the Albert Ludwigs University, Freiburg, Germany; Department of Pediatric Surgery (R.-B.T.), University of Leipzig, Leipzig, Germany; and Department of Pediatric Hematology (I.K.), Children's Hospital of the Klinikum Chemnitz, Chemnitz, Germany.

Address correspondence and reprint requests to Peter Reichardt, M.D., Intensive Care Unit, Children's Hospital of the University of Leipzig, Oststr. 21–25, 04317 Leipzig, Germany. E-mail: reichp@medizin.uni-leipzig.de.

tricle. A radiograph of the thorax revealed a round paramediastinal mass at the left side at the level of the fourth thoracic vertebra. The patient, whose condition had quickly stabilized with an intravenous nifedipine infusion, was transferred to the oncology department, with a presumed diagnosis of neuroblastoma, for further evaluation. Magnetic resonance imaging confirmed a thoracic structure of 2 × 2 × 3 cm (Fig. 1). A second tumor was seen in the abdomen, a structure of 2 × 3 × 5 cm in the right suprarenal region (Fig. 2). No structural changes in other abdominal organs were noted. Magnetic resonance imaging of the head showed no cerebral lesions. On metaiodobenzylguanidine scintigraphy, the suprarenal tumor showed selective enhancement, whereas the intrathoracic tumor remained silent. Technetium Tc 99 scintigraphy of the skeleton revealed no osseous metastasis. Bone marrow aspiration proved to be cytomorphologically negative for tumor cell metastasis. On ophthalmologic examination, a beginning fundus hypertonicus was found, but no angiomatosis of the retina was present. Laboratory investigations showed increased levels of neuron-specific enolase and chromogranin A (15 ng/mL and 153 μg/L, respectively). A diagnostic clue for a catecholamine-secreting tumor was the determination of catecholamines and metabolites measured in plasma and urine. Norepinephrine was markedly increased in plasma at 3390 ng/L (normal 0–600). Both norepinephrine and vanillylmandelic acid were increased in urine at 1,156 μg/24 hours (0–105) and 17 mg/24 hours (0–8.0), respectively.

Because the laboratory parameters and clinical course made the lesions highly suspicious for pheochromocytomas, they were excised. The abdominal lesion was removed first.

FIG. 1. Magnetic resonance imaging of a patient with a thoracic paraganglioma (arrow) in the left paravertebral region at the level of the fourth thoracic vertebra.

FIG. 2. Magnetic resonance imaging of a patient with an abdominal pheochromocytoma in the right periadrenal region. Arrow 1 indicates the pheochromocytoma; arrow 2 shows a normal paraadrenal gland left with no signs of the later-developing tumor.

It presented as two separate tumors apart from the adrenal gland. The tumors were completely excised, sparing the adrenal gland. Four weeks later, the thoracic tumor was removed. All three tumors were classified histologically as pigmented paragangliomas showing positivity for neuron-specific enolase, chromogranin A, and synaptophysin.

To exclude multiple endocrine neoplasia II, DNA of peripheral blood cells was tested. There was no amplification of N-*myc* and there was no amplification or mutation in the RET-protooncogene on chromosome 10. Analyzed were exon 10 (for codon 609, 611, 618, 620), exon 11 (for codon 630, 634), exon 13 (for codon 768, 790, 791), exon 14 (for codon 803), exon 15 (for codon 883, 891), and exon 16 (for codon 918). Molecular DNA analysis of the *VHL* gene was performed as previously described (6). For sequence analysis, aberrant DNA bands from the single-strand conformation polymorphism were cut out of the gel and reamplified, and the double strand was sequenced. Aberrant bands were confirmed by a second DNA sample extracted from newly drawn blood. This procedure revealed a novel point mutation in exon 1. At position 406, thymine was replaced by guanine (406 T→G), which resulted in codon 65 in a change of the amino acid serine to alanine (Fig. 3). This mutation was absent in the mother. Paternal DNA was not available for study.

The patient's blood pressure returned to normal and antihypertensive therapy could be stopped 9 days after surgery. Catecholamine and metabolite levels decreased into normal ranges. Postoperative imaging excluded residual tu-

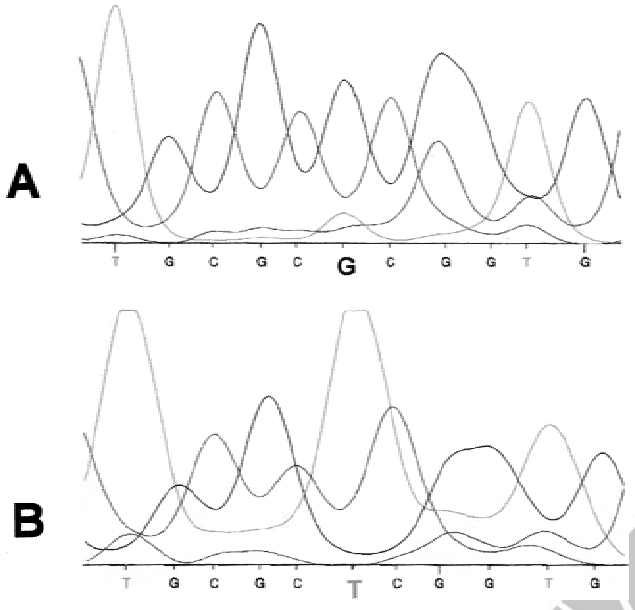

FIG. 3. Automated sequence analysis of exon 1 of the VHL gene of a patient with mutation in the VHL gene **(A)** and his mother **(B):** The aberrant DNA band found in the SSCP (single-strand conformation polymorphism) of the patient shows the mutation with a G at nucleotide position 406 **(A),** whereas the band of the patient's mother shows the wildtype (wt) sequence **(B).** Note that the minor T peak in A results from a little amount of the patient wt allel in the sequencing probe preparation.

mor or new tumor manifestations. The patient was released from hospital in good condition but was soon lost to follow-up as a result of poor compliance. Seven months later, he returned with tachycardia, vomiting, and hypertension. Norepinephrine was again increased at 2,025 ng/L in serum and 525 μg/24 hours in urine. Scintigraphy with metaiodobenzylguanidine and magnetic resonance imaging showed a new tumor of 2 × 2 × 2 cm in the left periadrenal region. Detailed imaging excluded other tumor manifestations. During surgery, three distinct paragangliomas were found localized in the proximity of the adrenal gland. The tumors were removed, again sparing the adrenal gland. Levels of catecholamines were normal on day 10 after surgery.

As of this writing, 16 months after his first admission to the hospital, the patient is in good health. Improved compliance seems to ensure regular follow-up. Visits every 4 to 6 weeks with 24-hour ambulatory blood pressure recording will ensure close contact with the family. In addition, every 3 months, catecholamine metabolites are measured in urine and sonography of the abdomen is performed. Radiologic imaging of the thorax and abdomen and ophthalmologic controls are performed once per year.

DISCUSSION

Our patient had multiple extraadrenal pheochromocytomas as result of a novel germline mutation in the *VHL* gene. Of further interest is the rapid occurrence of a third tumor, which was not detectable at excision of the first two lesions 7 months before.

The diagnosis of paragangliomas in our patient was based on radiologic imaging, metaiodobenzylguanidine scintigraphy, measurement of catecholamine metabolites, and histologic examination of the excised tumors. Whereas pheochromocytomas usually appear alone in or close to the adrenal medulla, they are bilateral in 5% to 10% of patients and occur extraadrenally in 15% to 20% of the cells associated with the ganglia of the autonomic nervous system (5). Only 5% of reported pheochromocytomas occur in children, but extraadrenal forms seem to be more frequent, appearing in up to 30%. In particular, a thoracic location of pheochromocytomas producing catecholamines, so-called functioning paragangliomas, is suspicious for the presence of underlying VHL (6).

von Hippel–Lindau disease was diagnosed by detection of a previously unknown germline mutation in the *VHL* gene (*VHL* nt. 406 T→G). Apart from the paragangliomas, no other tumor manifestations were found. Whereas classic VHL manifests with retinal angiomas and hemangioblastomas of the central nervous system, the affected organs and the age of onset vary greatly. Some patients show only mild anomalies; others suffer from a severe disease. Pheochromocytomas as part of VHL are so well recognized that they are used to subclassify the disease. von Hippel–Lindau disease without pheochromocytoma is classified as type 1 (7). Manifestations with pheochromocytoma are further divided into 2A (without renal cell carcinoma) and 2B (with pheochromocytoma and renal cell carcinoma). Some authors additionally suggest classifying cases of pheochromocytoma as the sole manifestation of VHL as separate subtype (2C disease) (18).

There is a noticeable genotype–phenotype correlation in VHL. Patients with pheochromocytomas show almost exclusively missense mutations in the *VHL* gene. Patients without pheochromocytomas mainly show deletions, splice-site mutations, or nonsense mutations in the *VHL* gene (19). Indeed, the mutation we describe is a missense mutation. Although the mutation is unique in the literature, germline mutations of neighboring codons have been associated with primary pheochromocytomas (4). The inheritance of VHL is autosomal dominant, but spontaneous de novo mutations are also possible. Our patient is living with his mother, who was proven to have no germline mutation in the *VHL* gene. There is no contact with the father. The patient has 10 siblings, but all from a different father. In none of the siblings was a tumor or other severe disease known, and none was willing to be analyzed for the given mutation. We therefore cannot definitely differentiate between an inherited or a de novo mutation in our patient. Screening for germline mutation of the *VHL* gene should be performed in any patient with pheochromocytoma in childhood, even when only a single tumor is present because more than 20% of patients with apparently sporadic pheochromocytomas may be carriers of familial disorders (3). Gene testing for VHL has

been performed successfully in families at risk and persons with symptoms suspicious for the disease (20,21). In familial forms, with the recent use of more powerful diagnostic methods, germline mutations in up to 100% of affected families can be detected (22).

When a mutation is found in a patient, genetic screening of the family and genetic counseling are indicated. Patients and family members showing a mutation must be included in a clinical screening program, with radiologic imaging of the head and spinal cord and eye examinations. Regular and prolonged follow-up is essential. Tumors at other locations may become apparent after years. Successful treatment requires timely detection, often before symptoms occur, especially in the case of eye lesions and renal carcinoma. Follow-up procedures must be designed individually according to the associated clinical picture. In our opinion, a complete follow-up program for VHL in childhood should include the measurement of blood pressure at least every 3 months, measurement of catecholamines and metabolites in urine every 6 months, and ophthalmologic examinations and magnetic resonance imaging studies less than 6 months after surgery and afterward once per year.

REFERENCES

1. Bravo EL. Evolving concepts in the pathophysiology, diagnosis, and treatment of pheochromocytoma. *Endocrinol Rev* 1994;5:356–68.
2. Woodward ER, Eng C, McMahon R, et al. Genetic predisposition to pheochromocytoma: analysis of candidate genes GDNF, RET and VHL. *Hum Mol Genet* 1997;6:1051–6.
3. Neumann HPH, Berger DP, Sigmund G, et al. Pheochromocytomas, multiple endocrine neoplasia type 2, and von Hippel-Lindau disease. *N Engl J Med* 1993;329:1531–8.
4. van der Harst E, de Krijger RR, Dinjens WN, et al. Germline mutations in the VHL gene in patients presenting with phaeochromocytomas. *Int J Cancer* 1998; 77:337–40.
5. Whalen RK, Althausen AF, Daniels GH. Extra-adrenal pheochromocytoma. *J Urol* 1992;147:1–10.
6. Bender BU, Altehöfer C, Januszewicz A, et al. Functioning thoracic paraganglioma: association with Von Hippel-Lindau-Syndrome. *J Clin Endocrinol Metab* 1997;82:3356–60.
7. Neumann HPH, Wiestler OD. Clustering of features of von Hippel-Lindau syndrome: evidence for a complex genetic locus. *Lancet* 1991;337:1052–4.
8. Maher ER, Iselius L, Yates JR, et al. Von Hippel-Lindau disease: a genetic study. *J Med Genet* 1991;28:443–7.
9. Friedrich CA. von Hippel-Lindau syndrome. A pleomorphic condition. *Cancer* 1999;86:2478–82.
10. Gross DJ, Avishai N, Meiner V, et al. Familial pheochromocytoma associated with a novel mutation in the von Hippel-Lindau gene. *J Clin Endocrinol Metab* 1996;81:147–9.
11. Mulvihill JJ, Ferrell RE, Carty SE, et al. Familial pheochromocytoma due to mutant von Hippel-Lindau disease gene. *Arch Intern Med* 1997;157:1390–1.
12. Latif F, Tory K, Gnarra J, et al. Identification of the von Hippel-Lindau tumour suppressor gene. *Science* 1993;260:1317–20.
13. Sakashita N, Takey M, Kishida T, et al. Expression of von Hippel-Lindau protein in normal and pathological human tissues. *Histochem J* 1999;31:133–44.
14. Stebbins CE, Kaelin WG, Pavletich NP. Structure of the VHL-Elongin C-Elongin B complex: implications for tumor suppressor function. *Science* 1999; 284:455–61.
15. Ohh M, Kaelin W. The Von Hippel Lindau tumor suppressor protein. New perspectives. *Mol Med Today* 1999;5:257–63.
16. Zbar B, Kaelin W, Maher E, et al. Third International Meeting on von Hippel-Lindau disease. *Cancer Res* 1999;59:2251–3.
17. Maxwell PH, Wiesener MS, Chang GW, et al. The tumor suppressor protein VHL targets hypoxia-inducible factors for oxygen-dependent proteolysis. *Nature* 1999;399:271–5.
18. Maher ER, Kaelin WG. von Hippel-Lindau disease. *Medicine* 1997;76:381–97.
19. Zbar B, Kishida T, Chen F, et al. Germline mutations in the VHL gene in families from North America, Europe, and Japan. *Hum Mutat* 1996;8:348–57.
20. Glavac D, Neumann HP, Wittke C, et al. Mutations in the VHL tumour suppressor gene and associated lesions in families with von Hippel-Lindau disease from central Europe *Hum Genet* 1996;98:271–80.
21. Atuk NO, Stolle C, Owen JA Jr, et al. Pheochromocytoma in von Hippel-Lindau disease: clinical presentation and mutation analysis in a large, multigenerational kindred. *J Clin Endocrinol Metab* 1998;83:117–20.
22. Pack SD, Zbar B, Pak E, et al. Constitutional von Hippel-Lindau (VHL) gene deletions detected in VHL families by fluorescence in situ hybridization. *Cancer Res* 1999;59:5560–4.

Appendix 20

Reichardt, P+, W. Handrick, A. Linke, R. Schille, W. Kiess. Leukocytopenia, thrombocytopenia and fever related to piperacillin/tazobactam treatment - a retrospective analysis in 38 children with cystic fibrosis.
Infection.1999;27:355-6

IF: 2.4

Leukocytopenia, Thrombocytopenia and Fever Related to Piperacillin/Tazobactam Treatment – A Retrospective Analysis in 38 Children with Cystic Fibrosis

P. Reichardt, W. Handrick, A. Linke, R. Schille, W. Kiess

Summary

Bone marrow suppression is an important adverse reaction to most betalactam antibiotics. Recently it was suggested that piperacillin/tazobactam (PT) also may cause bone marrow toxicity. We retrospectively analyzed 100 IV antibiotic treatment courses (mean duration 12.5 days) in 38 patients (median age 14 years) with cystic fibrosis (CF) who were treated in our hospital. Of the patients receiving PT (84%), 6 patients (18.75% of PT-treated patients, 10.3% of PT treatment courses) developed fever, malaise and headache during treatment without signs of acute infection. In one patient definite thrombocytopenia and neutropenia, in two others a milder decrease in leukocyte and thrombocyte counts was observed after the onset of fever. The events were time- and dose-dependent occurring between day 11 and 15 of treatment. Treatment courses lasted longer (14.2 vs 11.3 days; $p < 0.05$) and patients had received a higher cumulative dose of PT (4919 ± 1975 mg/kg b.w. vs 3161 ± 1635 mg/kg; $p < 0.02$, Student's t-test) in the affected group than in the unaffected group. After discontinuation of PT, fever subsided within 24 h and blood cell counts normalized. We hypothesize that these fever episodes and changes of blood parameters are related to PT therapy.

Key Words

Betalactams · Penicillins · Piperacillin/tazobactam · Adverse event · Leukocytes · Thrombocytopenia · Neutropenia

Infection 1999;27:355–356

Introduction

Betalactam antibiotics can cause neutropenia and thrombocytopenia as a result of bone marrow suppression. Hematologic complications during treatment with betalactams have been first described in 1946 [1]. Lately, neutropenia has also been observed in association with betalactam/betalactamase inhibitors, which may cause dose-dependent, reversible maturation arrest of bone marrow precursor cells. Neutropenia occurs in 1–4% of patients treated with betalactam antibiotics [2, 3]. With longer durations of treatment and higher doses, this rate may rise to 27.5% [2, 4]. Relatively little is known about hematological adverse events associated with the use of piperacillin/tazobactam (PT). One study did not show any clinically significant hematological adverse effects of PT [5]. However, PT was only given for short time periods in these studies. In contrast, more recent reports demonstrated substantial hematological adverse events associated with PT when treatment lasted more than 10 days [6, 7].

Over the course of several years, we observed the development of fever without signs of acute infection in a number of cystic fibrosis (CF) patients who were treated with intravenous antibiotics. We therefore hypothesized that these febrile episodes might have been at least in part drug induced.

Patients and Methods

We retrospectively analyzed the data of all 38 patients with cystic fibrosis who were treated with intravenous antibiotics between December 1996 and June 1998. Patients were between 2 and 22 years old (median age 14 years). All had chronic pulmonary infection with *P. aeruginosa*, 31 simultaneously with *S. aureus*. Drug-related fever was suspected when febrile patients did not show any other clinical signs of acute systemic or local infection, and laboratory parameters including blood cultures did not indicate the presence of infection or inflammation. The diagnosis of drug-related fever was further supported by the observation of spontaneous normalization of the temperature within 24 h after discontinuation of the drug. Onset and duration of fever (rectal temperature of ≥ 38.5 °C) was recorded as were the results of hematological and chemical blood tests as well as type, dose and duration of antibiotic treatment and other therapeutic measures.

P. Reichardt *(corresponding author)*, **W. Handrick, A. Linke, R. Schille, W. Kiess**
Children's University Hospital, University of Leipzig, Oststr. 21–25, D-04317 Leipzig, Germany,
Phone +49 0341 9726065, Fax +49 341-9726039,
e-mail: reichp@medizin.uni-leipzig.de

Received: February 8, 1999 • Accepted: September 17, 1999

Results

During the study period, 38 CF patients received a total of 100 treatment courses of parenteral antibiotics (mean duration 12.5 days). Ten different antibiotics were used in 11 combinations. PT was the most frequently used antibiotic, representing 57 treatment courses in 32 patients (84%). In 40 courses it was combined with gentamicin, in 17 with amikacin. The occurrence of fever was only observed in the PT group. It affected 6 patients (18.75% of PT patients, 10.3% of PT treatment courses) and included 4 patients also receiving gentamicin or amikacin (2 patients each). In some patients malaise and/or headache were additional symptoms. Fever was neither observed in patients treated with aminoglycosides, which were given in combination with drugs other than PT, nor with any other antibiotic or concomitant drug. This was also the case for 33 treatment episodes with ceftazidime, the second most frequently used antibiotic.

Onset of fever occurred between day 11 and 15 of treatment (mean 13.3 days). Two patients were switched to ceftazidime or meropenem, in the 4 remaining patients antibiotic therapy was stopped. Fever subsided in all cases within 24 h after discontinuation of PT. In 3 of the 6 febrile patients, a complete blood count was done after onset of fever. These patients showed a decrease in leukocyte and thrombocyte counts. One of them developed definite thrombocytopenia (< 150,000) and neutropenia (< 1000). Recovery of blood cells was recorded as early as 4 days after discontinuation of PT in one patient. At follow-up (2–18 weeks after onset), complete remission was observed in all cases. Anemia did not occur in any of these cases, nor was any significant change in liver enzymes noted. Patients received between 191 and 672 mg PT per kg daily (mean 288 ± 91 mg/kg/day). The induction of fever and hematological changes appeared to be dose dependent. While no significant difference was seen between the daily dose per kg (355 ± 164 in febrile patients vs 281 ± 77 mg/kg in patients without fever; $p = 0.059$), all patients developing fever received at least 240 mg PT/kg/day, treatment courses lasted longer (mean 14.2 vs 11.3 days; $p < 0.05$), and patients received a higher cumulative PT dose during the course (mean 4919 ± 1975 mg/kg vs 3161 ± 1635 mg/kg; $p < 0.02$, Student's t-test).

Discussion

Hematological side effects of PT have been reported to be rare (< 1%) and are mostly mild [8]. However, life-threatening neutropenia due to PT may occur [6]. Fever due to PT was seen in 5–24% of CF patients [7, 9]. Whether the rate of adverse events in CF patients is generally higher than in other patients is unclear [10], as is the question whether penicillin-induced neutropenia is more frequent in children than in adults [11].

Six of our 32 PT-treated patients (18.75% of PT-treated patients and 10.3% of PT treatment courses) developed an episode of fever. We conclude that PT may be associated with febrile reactions at a rate comparable to that seen with piperacillin alone. No other antibiotic used in our CF patients during the study period was associated with similar reactions. Blood cell counts were done in 3 of the 6 affected patients after onset of fever. All showed a decrease in leukocyte and thrombocyte counts during the febrile episode. Hematological changes were completely reversible. This is consistent with other reports [2, 6, 8]. Fever occurred between the 11th and 15th day of treatment. This corresponds to the finding that hematological adverse reactions involving PT occur rarely before day 10 of treatment [8]. The dose dependency of hematological complications, which are usually mediated through reversible maturation arrest of precursor cells in the bone marrow, has been demonstrated before [8]. However, sudden falls of cell counts as seen in one of our patients can only partially be explained by cumulative toxicity. Immunologically mediated processes may play an additional role. Such processes may be responsible for the development of thrombocytopenia following treatment with betalactams [12, 13]. No difference in sex, age or body weight was seen between patients with fever and those without. However, marrow suppression in underweight adults receiving the unadjusted adult dose has been observed [8]. In conclusion, in CF patients treated with PT, particular attention should be paid to the potential for hematologic side effects.

References

1. Spain DM, Clark TB: A case of agranulocytosis occurring during the course of penicillin therapy. Ann Intern Med 1946; 25: 732–733.
2. Eich G, Neftel A: Haematological side effects of anti-infective therapy: agranulocytosis caused by β-lactam antibiotics, vancomycin and amodiaquine. Infection 1991; 19 (suppl 1): S33–S37.
3. Olaison L, Alestig K: A prospective study of neutropenia induced by high doses of betalactam antibiotics. J Antimicrob Chemother 1990; 25: 449–453.
4. Parry MF: Toxic and adverse reactions encountered with new beta-lactam antibiotics. Bull N Y Acad Med 1984; 60: 358–368.
5. Kuye O, Teal J, DeVries VG, Morrow CA, Tally FP: Safety profile of piperacillin/tazobactam in phase I and phase III clinical studies. J Antimicrob Chemother 1993; 31 (suppl A): 113–124.
6. Gerber L, Wing EJ: Life-threatening neutropenia secondary to piperacillin/tazobactam therapy. Clin Infect Dis 1995; 21: 1047–1048.
7. Mallon P, Murphy P, Elborn S: Fever associated with intravenous antibiotics in adults with cystic fibrosis. Lancet 1997; 350: 1676–1677.
8. Ruiz-Irastorza G, Barreiro G, Aguirre C: Reversible bone marrow depresssion by high-dose piperacillin/tazobactam. Br J Haematol 1996; 95: 611–612.
9. Brock PG, Maryanne A: Adverse reactions to piperacillin in cystic fibrosis. Lancet 1984; 1: 1070–1071.
10. Strandvik B: Adverse reactions to piperacillin in patients with cystic fibrosis. Lancet 1984; 1: 1362.
11. Iwai N, Nakamura H, Miyazu M: Pharmacokinetic, bacteriological and clinical evaluation of tazobactam/piperacillin in pediatrics. Jpn J Antibiot 1998; 51: 346–361.
12. Pérez-Vázquez A, Pastor JM, Riancho JA: Immune thrombocytopenia caused by piperacillin/tazobactam. Clin Infect Dis 1998; 27: 650–651.
13. Neftel KA, Wälti M, Spengler H, von Felten A, Weitzman SA, Bürgi H, de Weck AL: Neutropenia after penicillins: toxic or immune-mediated? Klin Wochenschr 1981; 59: 877–888.